FEUP Universidade do Porto
Faculdade de Engenharia

DETERMINISTIC AND PROBABILISTIC METHODS FOR STRUCTURAL SEISMIC SAFETY ASSESSMENT

Xavier Das Neves Romão

A dissertation presented to the Faculty of Engineering of the University of Porto
for the degree of Doctor in Civil Engineering.
Supervisors: Aníbal Guimarães da Costa (Full Professor); Raimundo Moreno Delgado (Full Professor).

Visível ou invisível, a estrutura de tudo é tudo.
(kindly written by José Luís Peixoto for this dissertation, 2012)

All things are subject to interpretation;
whichever interpretation prevails at a given time is a function of power and not truth.
(Friedrich Nietzsche, 1844-1900)

Acknowledgments

It has been a long and rewarding journey, longer than envisioned, filled with twists and setbacks, excitement and frustration, both academically as on a more personal level. It has been a journey that was only made possible due to the influence of many. In the next few lines, I would like to express my sincere gratitude to those who have contributed in any way to the completion of this thesis.

First of all, I would like to acknowledge my sincere gratitude to my supervisors, Prof. Aníbal Costa and Prof. Raimundo Delgado, for believing in me since the early ages of my academic career, more than twelve years ago. I also want to thank them for persuading me to change the initial topic of my research and take part in the LessLoss research project which presented me with new challenges that ultimately led to the development of this dissertation.

To Prof. Aníbal Costa I would also like to gratefully and sincerely thank for his support, guidance, knowledge and friendship throughout the years, and for the opportunity to take part in many side-projects that contributed to my professional growth.

To Prof. Raimundo Delgado I would also like to express my deepest gratitude for his support and guidance, while giving me the freedom to pursue independent work and explore things on my own. I am also deeply grateful to him for the long discussions that helped me to solve many technical details of the work, for the insightful comments and constructive criticisms, and for helping me to view and think outside the box in many occasions.

I would like to thank also colleagues and friends from the Civil Engineering Department and the Construction Institute of the Faculty of Engineering of the University of Porto (FEUP). Among those, I would like to thank Miguel Castro for the fruitful discussions about earthquake engineering and for the many ideas for future research. I am also especially grateful to Lau for the friendship, the unending encouragement and the many discussions about losses. This journey would have been intensely isolating and a great deal more demanding had it not been for your support and for the numerous side projects and tasks that you challenged me with and that helped me keep my sanity. For their support, a special word of thanks also goes to my colleagues from the Structural Division, namely António Arêde, João Guedes and Nelson Vila Pouca. For his help and guidance with some statistical issues over the course of this work, I would like to thank Rui Gonçalves. For the many talks, her friendship and encouragement, and for bridging the gap between mathematicians and engineers, I would also like to thank Isabel Ribeiro. To those who are still completing their own journey and to those who, inevitably, came and went over the years, namely Alexandre Costa, Bruno Silva, Cristina Costa, Filipe Neves, Hugo Rodrigues, Pedro Quintela, Sandra Nunes, Tiago Ilharco and Valter Lopes, I would like to thank their companionship. Finally, I would also like to thank Nuno Pereira for the help in

editing some chapters and especially for picking up the things that I left behind to start his own PhD journey.

From the LessLoss team, I would also like to express my gratitude to Prof. Paolo Pinto, Prof. Paolo Franchin and Prof. Alessio Lupoi from the University of Rome "Sapienza" for sharing their experience and knowledge during the project. Your work was instrumental for my research.

My thanks are also due to Dr. Alexandra Carvalho, from the National Laboratory for Civil Engineering (LNEC), for providing me with the most recent Portuguese seismic hazard data.

I also thank the Portuguese Foundation for Science and Technology for supporting part of this research through the grant SFRH/BD/32820/2007.

Much of the research in this thesis is based on the work of many others before me. A great deal of time was spent consulting, reading, scrutinizing the research of others from many fields. My deepest thank goes to the http://www.abcdfree.com/ community for their collaborative help in providing many of the publications that I required over the years.

I am also grateful to the secretaries in the Civil Engineering Department, especially Mrs. Vitória, Marta and Joana, for assisting me in many different ways, and to Manuel for his help in formatting a large part of the final text and developing some of the figures.

I would also like to thank José Luís Peixoto for finding the time throughout the mists of his busy agenda to write a citation for this dissertation.

To Lena, I want to thank for her support over many years, right from the beginning and, despite the hardship of times we both endured, for remaining my dearest friend.

To my close and oldest friends Ani, Bela and Ricardo, I want to express my gratitude for their unconditional friendship and support, especially during more difficult times.

To my parents, I must thank for their unconditional encouragement and support, allowing me to be as ambitious as I wanted.

Finally, to everyone who kept asking over and over again "When will you get it done? Next week? Next month? When?" while I was thinking to myself "I just whish I could hit you… with a (sharp) stick… many times over", thank you for believing in me.

January 1st, 2012

… for wanting to know me
… for letting me know you
… for being everything
… for everything

Abstract

The proposed thesis addresses several topics in the field of seismic risk assessment of structures. The main objective is to propose probabilistic methods for the seismic risk assessment of existing buildings which can be used in the research and development of codified procedures addressing this type of structures.

In light of this wide-scope objective, a preliminary analysis is carried out to characterize how the seismic safety assessment of existing structures is addressed within the scope of the Eurocodes. In this context, the seismic safety assessment methodology defined by Eurocode 8 – Part 3 (EC8-3) is analysed and discussed. Based on the limitations identified in the chord rotation demand quantification procedure defined by EC8-3, a study is made to analyse several alternative proposals for its quantification. Moreover, the definition of the Confidence Factor and its role in the safety analysis is another aspect of the EC8-3 features that is addressed with more detail. Based on the interpretation of the code procedures, a statistical framework is proposed to reflect the uncertainty of the material properties required for the safety analysis in the definition of the Confidence Factor.

The analysis of the code procedures also emphasises the need for adequate methods to validate the results obtained by the EC8-3 safety assessment methodology. Such need asks for the development of a suitable probabilistic framework aiming to assess the reliability of the code procedures and calibrate parameters they involve. In this context, the remaining research presented in the thesis introduces several contributions to such probabilistic framework involving the development and enhancement of methods for the probabilistic performance assessment of structures.

The aspects of the probabilistic performance assessment addressed in the proposed thesis are the adequate characterization of probabilistic models for the structural demand of building response under earthquakes, the seismic risk assessment of building components, and the seismic risk and loss assessment of building systems, combining both component-level and system-level criteria. With respect to the characterization of probabilistic models for the structural demand of building response parameters, an in-depth analysis of the common assumption that structural demand conditional to a seismic intensity level follows a lognormal distribution is performed using adequate statistical methods. Having established the type of statistical distribution of the demand parameters, an extensive study is also performed to address the characterization of the parameters of such distributions using robust estimation methods. In the context of the seismic risk assessment of building components, methodologies defining analytical closed form expressions for the risk and the exceedance probability of structural component limit states are developed. The proposed procedures use a strategy similar to that of the well known SAC-FEMA method, but extend that approach by introducing different functional forms to represent the earthquake hazard and by addressing the issue of force-based limit states.

Finally, a probabilistic methodology is proposed to analyse the seismic performance of existing buildings using global metrics to determine if the behaviour conforms to a given limit state. The considered performance metrics are the probability of occurrence of the limit state, the corresponding loss associated to the repair of the building, and the corresponding number and type of mechanisms that occur. Based on these latter parameters, a number of possible scenarios corresponding to the limit state occurrence are established, which can then be combined to obtain a global performance value representing the expected loss over a given reference period of time.

The topics addressed throughout the thesis are illustrated with several application examples involving reinforced concrete structures. These structures were selected in order to include both regular and irregular structures of different heights, as well as non-seismically designed structures and structures designed according to modern seismic design methods.

Resumo

O objectivo principal desta dissertação consiste na proposta de metodologias probabilísticas para a avaliação do risco sísmico de edifícios existentes que possam ser utilizadas no desenvolvimento de procedimentos regulamentares dirigidos para este tipo de estruturas. Neste âmbito, foram abordadas e analisadas várias temáticas no contexto da avaliação do risco sísmico de estruturas tendo sido, nomeadamente, caracterizada a forma como a avaliação da segurança sísmica de estruturas existentes é tratada no âmbito dos Eurocódigos.

Neste contexto, foi analisada a metodologia de avaliação da segurança sísmica proposta na Parte 3 do Eurocódigo 8 (EC8-3), sendo discutidas algumas das suas limitações. Assim, o procedimento proposto pelo EC8-3 para a quantificação da rotação da corda de elementos estruturais foi analisado num estudo mais detalhado em que foram discutidas diferentes alternativas para a sua determinação. Paralelamente, o Factor de Confiança e o seu papel na avaliação da segurança foram igualmente analisados com maior detalhe. Para tal, foi estabelecido um enquadramento de base estatística para a definição do Factor de Confiança, o qual reflecte a incerteza das propriedades materiais que têm de ser determinadas para proceder à avaliação da segurança sísmica.

A análise dos procedimentos regulamentares salientou a necessidade de existirem métodos adequados que permitam validar os resultados obtidos pela metodologia de avaliação da segurança sísmica do EC8-3. Assim, conclui-se que é necessário estabelecer um enquadramento de base probabilística que permita avaliar a fiabilidade dos procedimentos regulamentares e calibrar os parâmetros envolvidos. Neste contexto, a presente dissertação apresenta, ainda, diversas contribuições para o estabelecimento duma formulação probabilística da avaliação da segurança sísmica, nomeadamente ao nível do desenvolvimento e do refinamento de métodos probabilísticos para avaliação do desempenho estrutural. Os conceitos abordados envolvem a caracterização probabilística da resposta estrutural de edifícios sujeitos à acção sísmica, métodos para a avaliação do risco sísmico de elementos estruturais e métodos para a avaliação do risco sísmico e das correspondentes perdas económicas em edifícios. A caracterização de modelos probabilísticos para a resposta estrutural de edifícios foi tratada em detalhe utilizando métodos estatísticos adequados, sendo analisada a legitimidade da hipótese generalizadamente assumida relativa à distribuição da resposta estrutural obtida para um determinado nível da acção sísmica seguir uma distribuição lognormal. Após estabelecer o tipo de distribuição estatística da resposta estrutural, foi realizado um estudo alargado que abordou a caracterização dos parâmetros das referidas distribuições estatísticas utilizando métodos de estatística robusta. No contexto dos métodos para a avaliação do risco sísmico de elementos estruturais foram abordadas diversas metodologias analíticas que permitiram o desenvolvimento de expressões para a avaliação do risco e da probabilidade de ocorrência de diferentes estados limite. Os procedimentos propostos foram desenvolvidos

com base na formulação do método SAC-FEMA, sendo alargada a aplicabilidade desta abordagem com a introdução de expressões alternativas para a representação da perigosidade sísmica e ao estabelecer propostas especificamente dirigidas para estados limite definidos em termos de esforços. Finalmente, é proposta uma metodologia probabilística para a avaliação do desempenho de edifícios existentes através da utilização de indicadores globais que determinam se o comportamento da estrutura verifica as condições de segurança associadas ao estado limite em análise. Os indicadores globais considerados são a probabilidade de ocorrência do estado limite, as perdas económicas associadas à reparação do edifício e o número e o tipo de mecanismos locais que ocorrem. Com base nestes parâmetros, é então possível definir diversos cenários que correspondem à ocorrência do estado limite em análise, os quais, posteriormente, podem ser combinados para obter um indicador global do desempenho do edifício.

Os diferentes assuntos abordados ao longo da dissertação são ilustrados com recurso a várias aplicações que envolvem estruturas de betão armado. As estruturas envolvidas neste estudo foram seleccionadas de modo a incluir estruturas regulares e irregulares de diferentes alturas, e estruturas com e sem dimensionamento sísmico.

Table of Contents

Chapter 1
Introduction

1.1 General overview

Earthquakes are, without a doubt, among the most impressive and powerful natural phenomena striking the Earth. The burst of energy released by major earthquakes is so large that it can lead to a redistribution of the Earth's mass with significant implications on the planetary dynamics (Chao *et al.*, 1996). For example, the energy released by the 2004 magnitude M_W 9.1 Sumatra earthquake - equivalent to more than 63 million Hiroshima atomic bombs (USGS, 2009) - was found to have shortened the length of a day by 6.8 microseconds and to have shifted the Earth's figure axis (the axis about which the mass of the Earth is balanced) by about 7 centimetres (NASA, 2011). Similar effects were also observed after the more recent 2010 magnitude M_W 8.8 Chile earthquake - the day length was shortened by 1.26 microseconds and the Earth's figure axis was shifted by about 8 centimetres - and the 2011 magnitude M_W 9.0 Tohoku earthquake in Japan - the day length was shortened by 1.8 microseconds and the Earth's figure axis was shifted by about 17 centimetres, (NASA, 2011). Although changes in the Earth's rotation also occur due to several other natural phenomena, e.g. due to seasonal shifts in ocean currents, atmospheric jet streams or solar and lunar tides (Stephenson, 2003), and do not have any impacts on our daily lives, those produced by earthquakes are still significant enough to be accounted for in fields such as astronomy, geography and space navigation.

Aside from these facts, the energy released from earthquakes is best known for its destructive power that generates, in many cases, extensive human and economic losses spread across large areas. In order to have an idea about the extent of the areas devastated by earthquakes, Fig. 1.1 presents several visual comparisons involving data obtained from recent earthquakes and records associated to other natural and man-made disasters. As can be observed, the scale of the affected areas by some of these earthquakes is overwhelming

when compared to that of the other examples. However, the size of the areas devastated does not reflect entirely the scale of the global consequences of these disastrous events.

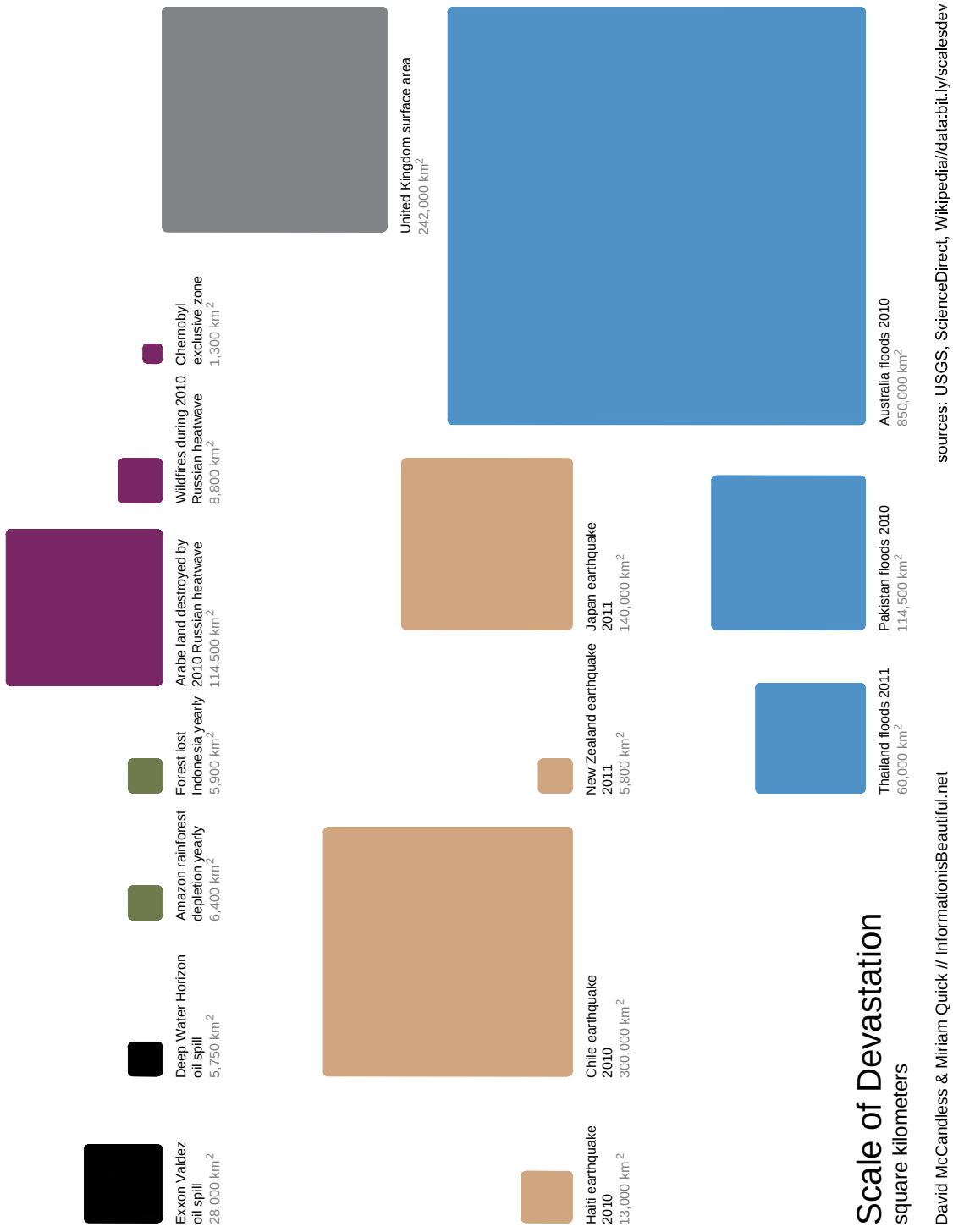

Figure 1.1. Areas affected by recent earthquakes compared to that of other natural and man-made disasters (adapted from http://www.informationisbeautiful.net/).

To obtain a more general perspective about the considerable impact of some of these events, Fig. 1.2 presents visual comparisons of the estimated economical loss (in billions of

US$), the number of people that were affected and the number of fatalities associated to the four earthquakes, the 2010 Australian floods and the Chernobyl nuclear accident that are referred in Fig. 1.1. To complement this analysis, Fig. 1.2 also presents the extent of the areas devastated by these six events previously presented in Fig. 1.1.

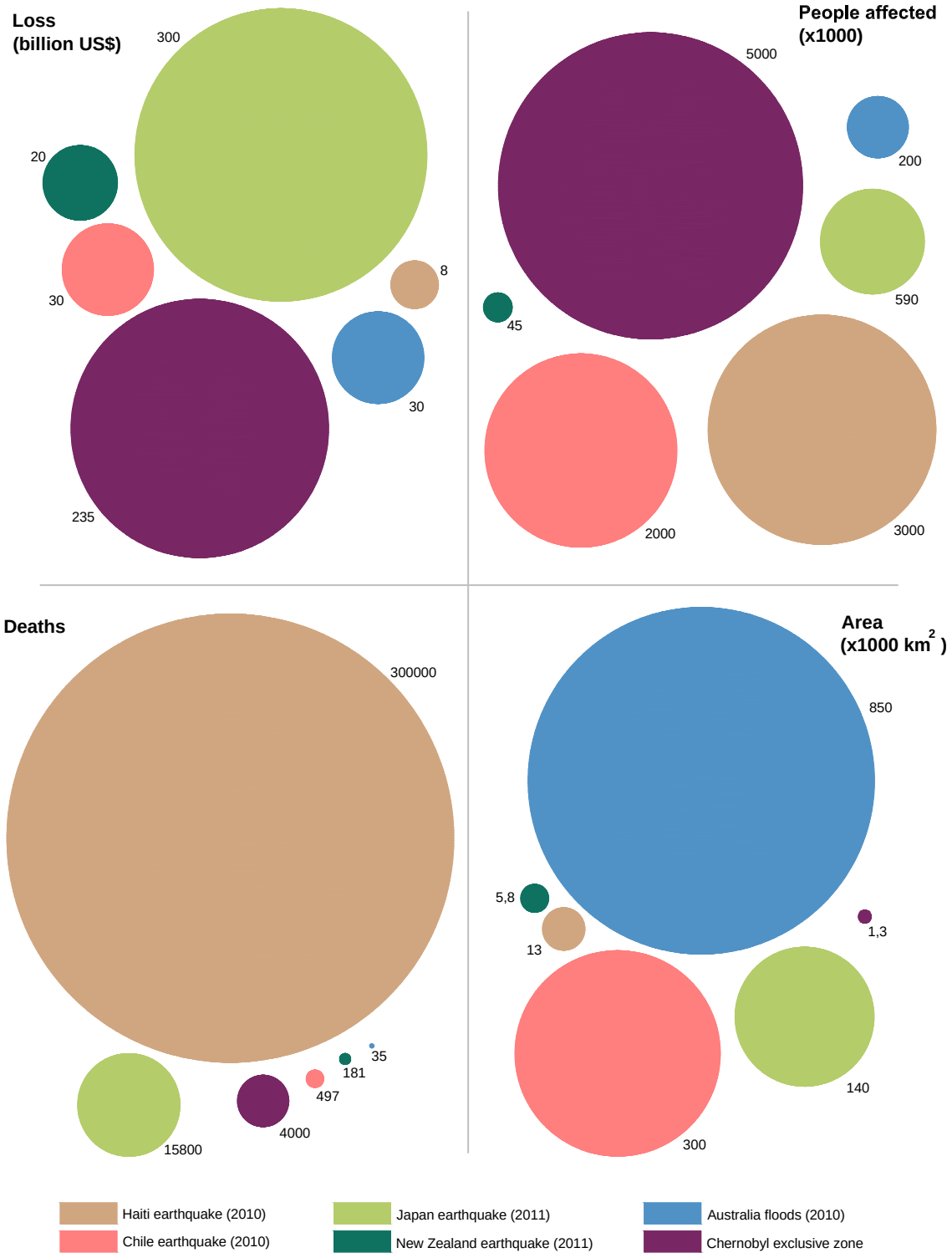

Figure 1.2. Comparison of the economical loss, number of people affected, number of fatalities and devastated areas for the four earthquakes, the 2010 Australian floods and the Chernobyl nuclear accident referred in Fig. 1.1 (Source: http://bit.ly/vNO350)

With respect to the Japan 2011 earthquake, it is noted that over 90% of the fatalities resulted from drowning as a consequence of the tsunami. In what concerns the Chernobyl nuclear accident, the number of people affected is that of residents of the Belarus, the Russian Federation and the Ukraine territories that were contaminated by the Chernobyl fallout, the 235 billion US$ loss refers to losses over thirty years for Belarus alone, and the 4000 fatalities are estimated over a period of more than twenty years (IAEA, 2006).

By analysing the data presented in Fig. 1.2, it can be seen that earthquakes can be far more deadly than other disasters and that the value of their immediate economic losses can also be seen to be considerably large. Although earthquake ground shaking has a number of damaging effects that involve, for example, different types of soil failure (e.g. landslides, liquefaction, surface fault rupture or general settlements) and tsunamis, a significant part of the human losses (injuries and fatalities) can be associated to one main factor: the existence of man-made structures and infra-structures lacking appropriate seismic design that will, inevitably, exhibit inadequate behaviour when subjected to earthquakes. When focussing on the behaviour of buildings only, the importance of this factor can clearly be observed when analysing the reasons for the fatalities of the 2010 Haiti and Chile earthquakes. The severe death toll of the Haiti earthquake has been largely credited to a lack of adequate earthquake-resistant design practice and to the poor quality of a large part of the building inventory (ARUP, 2010; Eberhard *et al.*, 2010). On the other hand, the low number of deaths (when compared to the number of people affected) resulting from the 2010 Chile earthquake can be seen to be a consequence of the relatively good performance of modern earthquake-resistant structures, which can then be attributed to the adequacy of building codes and standards adopted in that country (Elnashai *et al.*, 2010; Kato *et al.*, 2010; Rojas *et al.*, 2010). Still, a significant number of non-engineered masonry and adobe constructions suffered extensive damage and collapsed as a result of that earthquake (RMS, 2010; Tanner and Carboni, 2011). A similar analysis can be made for the outcomes of the New Zealand earthquake of 2011. Findings for this event also show that modern earthquake-resistant structures were seen to exhibit adequate seismic behaviour, while unprepared constructions (e.g. unreinforced masonry buildings) did not (Chouw *et al.*, 2011; Clifton *et al.*, 2011; EERI, 2011). Analyses of this sort have also been made for other earthquakes (Spence and So, 2009; Pomonis *et al.*, 2011) and the results have shown that vulnerable housing is the main cause of human casualties and injuries. In light of these findings, and as frightening as this prospect might be, it has to be acknowledged that Nick Ambraseys' 1968 observation on the fact that "*earthquakes don't kill people, buildings do*" (Bilham, 2006) is as valid today as it was then, if modern earthquake-resistant design practices are not considered.

Another aspect of the data in Fig. 1.2 that must be highlighted is the considerably large value of earthquake related losses. Two factors can be seen to be related to such large amounts of economical losses: the extent of the area that is affected by the earthquake and its level of development. To illustrate further the extent of earthquake related economic losses, Fig. 1.3 presents maps displaying worldwide earthquake related economic losses for

some of the earthquakes with magnitude M_W higher than 6.0 that occurred between 1985 and March 2011 and that involved losses over one billion US$, according to data found in NGDC (2011) and Ferreira, (2012). The map of Fig. 1.3a) represents thirty events, where some of them are identified, while Fig. 1.3b) does not represent the events with the three largest losses (the 2011 Tohoku, Japan, earthquake, the 1995 Kobe, Japan, earthquake and the 2008 Sichuan, China, earthquake) to have a more detailed view of the remaining events. It should be noted that, although the number of earthquakes with magnitude M_W higher than 6.0 during the considered time period is 604, reliable data about the economic losses they have caused could only be obtained for 133 events (NGDC, 2011). Therefore, the true representation of worldwide earthquake losses over one billion US$ could be far more significant than that of Fig. 1.3. The data in Fig. 1.3a) represents a total loss close to 835 billion US$ (i.e. about 75% of the European Union budget for the period 2007-2013) and the three largest losses represent 70% of this total loss.

As can be observed by these numbers, earthquake related economic losses can be of overwhelming and economically disruptive proportions. Moreover, in earthquakes where the main cause of damage is due to ground shaking (i.e. in cases where secondary effects such as tsunamis were not felt), the share of such losses which corresponds to direct losses to the building stock can also be seen to be significant. For example, in the case of the 1994 Northridge earthquake, the global estimated losses are about 40 billion US$ and more than 60% are estimated to be losses to the building stock (Wu and Lindell, 2004). Similarly, the building stock losses from the 1995 Kobe earthquake are also close to 60% of the global estimated losses which, in this case, are 131 billion US$ (Otani, 1999). Likewise, the 1999 Athens earthquake caused over 2.5 billion US$ (*fib*, 2006) in losses to the building stock which are close to 60% of the 4.5 billion US$ of global estimated losses (Gurenko, 2011).

Although limited, the presented data indicates that more recent structures designed according to modern earthquake resistant design codes have been able to reduce the risk to human life. However, the large monetary losses resulting from many recent earthquakes indicate that the issue of economical losses is not adequately addressed by such earthquake resistant practice. Moreover, the human and monetary losses resulting from the inadequate seismic behaviour of older sub-standard constructions emphasize the need to develop adequate procedures addressing the seismic safety assessment and strengthening of these existing structures.

With the intention of answering these needs, the past fifteen years have witnessed the development and the wide dissemination of the performance-based earthquake engineering (PBEE) philosophy which is a conceptual framework that involves the design, assessment and construction of engineered structures. The fundamental principles inherent to PBEE aim to improve the adequate quantification of the behaviour of structures subjected to earthquake loading in order to predict their performance with sufficient confidence and to contribute for the development of more effective seismic risk mitigation measures. The development of the PBEE concept was triggered by several reasons (Krawinkler, 1997).

Among those, acknowledging that seismic risk in urban areas was increasing and reaching unacceptably high socio-economic levels was decisive. This awareness is a consequence of the analysis of the effects of significant earthquakes that occurred since the 1980s (Bertero and Bertero, 2004), with special emphasis on the effects of the 1989 Loma Prieta, USA, the 1994 Northridge, USA, and the 1995 Kobe, Japan, earthquakes. The unexpected large monetary losses resulting from these events were paramount for the considerable changes that earthquake engineering practice and research have been undergoing from then on.

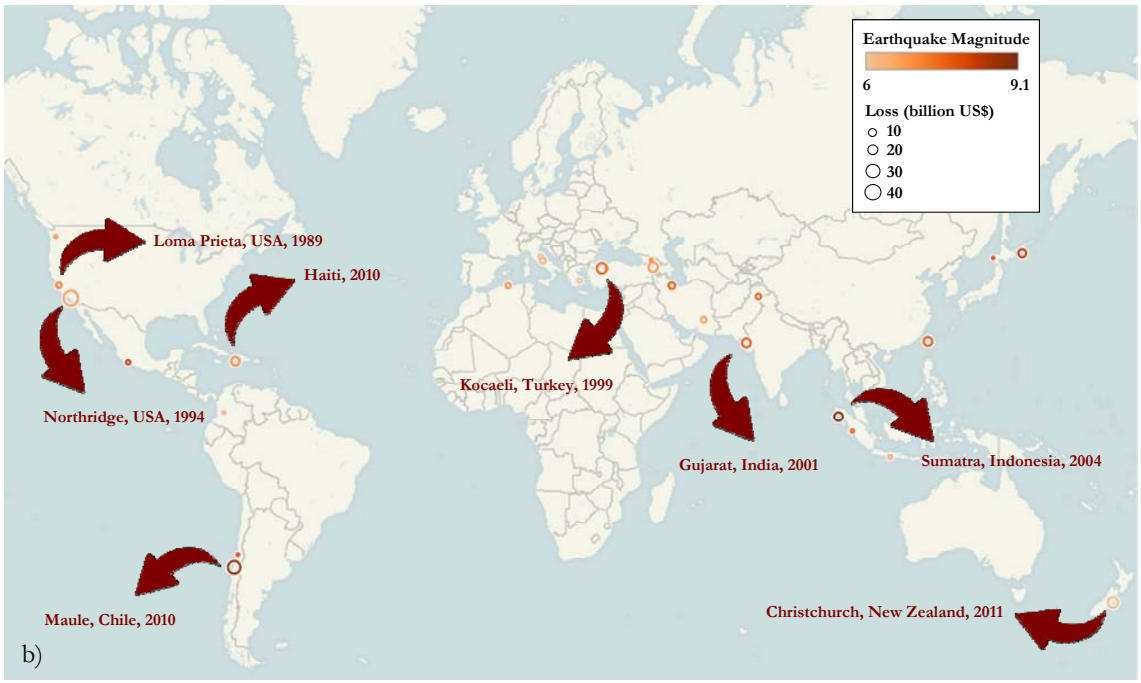

Figure 1.3. Earthquake related economic losses for earthquakes with magnitude M_W higher than 6.0 that occurred between 1985 and March 2011 and that involved losses over one billion US for the full range of the losses (a), and removing the events with the three largest losses (b), NGDC (2011) and Ferreira (2012).

In order to reverse the progression of seismic risk, it was acknowledged that new structures should be designed using more reliable seismic standards and code provisions that should reflect the more up-to-date research-based knowledge about earthquake occurrences, ground motions and structural response characteristics. However, it is noted that a number of these developments did not target the issues and the potential risk associated with existing constructions.

It is agreed by earthquake engineering experts, public authorities and general public alike that the assessment of the seismic safety and performance of the built environment is a matter of high priority. The current widespread interest in methodologies addressing the assessment and the retrofit of existing constructions reflects the global perception that such constructions are exposed to inadequate levels of seismic risk. The need for rational and cost effective interventions on the built environment has led to the development of several normative documents and guidelines addressing specifically the seismic performance assessment of existing buildings over the past fifteen years (ATC 40, 1996; FEMA 273, 1997; FEMA 274, 1997; FEMA 310, 1998; FEMA 356, 2000; BRI, 2001a; BRI, 2001b; ASCE, 2003; OPCM 3274, 2003; EC8-3, 2005; OPCM 3431, 2005; NZSEE, 2006; ASCE, 2007; NTC, 2008; ATC, 2009). In the context of the Eurocodes, Part 3 of Eurocode 8 (EC8-3) (EC8-3, 2005) was developed specifically to address this matter. Most of the referred documents include modelling, analysis and verification procedures that are more detailed and lengthy than those commonly used in the design of new structures. Hence, extensive practical application of such procedures must be carried out to observe their adequacy and to determine if some of them need to be re-examined or modified. In the case of EC8-3, as noted by Franchin *et al.* (2010), the document should be seen as an experimental one that will be subjected to further progress in the near future based on the results of applications and studies regarding the procedures involved. However, few comparative applications of the code procedures (Chrysostomou, 2005; Mpampatsikos *et al.*, 2008a; Masi *et al*, 2008; Elefante, 2009) and a reduced number of critical discussions addressing some of the key features of EC8-3 (Pinto and Franchin, 2008; Franchin *et al.*, 2010; Jalayer *et al.*, 2011) have appeared until now. Therefore, research addressing the evaluation and validation of the code safety assessment procedures is needed, both in terms of their practical applicability and reliability.

In addition to these standards and guidelines, the research promoted by the introduction of the PBEE concept, namely towards the development of methodologies for seismic risk reduction, also led to considerable advancements in the use and dissemination of probabilistic approaches in earthquake engineering. One of the key outcomes of these advancements was the development of the formal probabilistic framework for risk and/or loss assessment defined by the Pacific Earthquake Engineering Research (PEER) Center (Cornell and Krawinkler, 2000). The PEER framework involves several stages such as quantifying the earthquake hazard, characterizing the structural response and predicting the expected damage to the construction and to its contents, as well as the resulting

consequences (financial losses, fatalities, and business interruption). Each stage of the framework is addressed in probabilistic terms and can be handled separately, based on the fundamental assumption that each stage is independent from the others. Although some aspects of the framework might require conceptual adjustments (Kiureghian, 2005), and aside from the fact that the independence of the stages should be carefully analysed in some cases (Baker, 2005), the PEER framework has the merits of introducing several simplifications in the way seismic risk was addressed in the past, and of establishing a common language for the widespread dissemination of the many concepts involved. Furthermore, it should be noted that, over the past decade, the development of this framework has led to a considerable increase in research addressing the several stages of this probabilistic approach.

One of the most recent outcomes of this research was the methodology developed by the Applied Technology Council in the ATC-63 project (Deierlein *et al.*, 2008; Kircher and Heintz, 2008; ATC, 2009) for the quantification of building performance and the analysis of response parameters to be used in seismic design. The methodology embodies incremental dynamic analysis (Vamvatsikos and Cornell, 2002) and probabilistic methods to evaluate seismic fragility margins of the building system against collapse and to calibrate appropriate values of design-related parameters such as the behaviour factor and other parameters affecting the response of the building.

1.2 Objectives and Scope

The main objective of the thesis is to propose probabilistic methods for the seismic risk assessment of existing buildings which can be used in the research and development of codified procedures addressing this type of structures. In light of this wide-scope objective, a preliminary analysis is required to characterize how the seismic safety assessment of existing structures is addressed in the scope of the Eurocodes. Within this context, the seismic safety assessment methodology defined by EC8-3 is analysed and some of the procedures proposed therein are discussed. Based on the findings of this analysis, issues that require additional research are identified and proposals are made to address some of them, namely for the chord rotation demand quantification and for the characterization of the Confidence Factor.

The analysis of the code procedures combined with the reduced number of existing studies addressing the application of such procedures emphasises the need for an adequate validation of the results obtained by the EC8-3 safety assessment methodology. Such condition asks for the development of a suitable probabilistic framework aiming to assess the reliability of the code procedures and to calibrate parameters they involve. Therefore, several contributions are presented in the thesis towards the definition of such probabilistic framework. The aspects of the probabilistic methodologies addressed in the thesis are key

features of the seismic risk assessment process and involve both proposals for new approaches as well as for the enhancement of existing ones. An important probabilistic performance assessment feature that is analysed herein is the adequate characterization of probabilistic models for the structural demand of building response under earthquakes. Based on the findings of this analysis, methodologies with different levels of detail and complexity are proposed for seismic risk assessment. At first, several methodologies are proposed for the seismic risk assessment of building components for different levels of performance. Such approaches are best suited for a component-by-component analysis which can be used to calibrate code procedures that are essentially based on component-level safety verifications. Finally, a methodology is proposed for the seismic risk and loss assessment of building systems for multiple performance levels, combining component-level and system-level criteria. By involving a more general approach to characterize building performance, this methodology can be used to analyse the adequacy of the system-level risk and of the loss that can be expected when applying the code procedures for seismic safety assessment.

1.3 Thesis Outline

The present thesis analyses a wide variety of topics under the common theme of seismic safety assessment. The topics are addressed over ten chapters that can be divided into two parts. The first part, comprising Chapters 2 to 4, addresses the EC8-3 procedures for the seismic safety assessment of existing structures. The second part, which consists of Chapters 5 to 9, addresses several matters in the context of probabilistic seismic demand characterization and probabilistic seismic risk assessment. The topics addressed throughout the chapters are illustrated with a number of application examples involving reinforced concrete structures. These structures were selected in order to include both regular and irregular structures of different heights, as well as non-seismically designed structures and structures designed according to modern seismic design methods.

Chapter 2 provides a general overview of the seismic safety assessment methodology defined by EC8-3 and discusses several issues and limitations related to the code procedure for chord rotation demand quantification. Upon these findings, a study is made to analyse several alternative proposals for its quantification. Given the significance of the shear-span in the referred study, a sensitivity analysis of the EC8-3 limit state capacity models with respect to this parameter is also carried out to examine the importance of its accurate quantification. Results and findings of this chapter were published in Romão *et al.* (2010a).

Chapter 3 presents an application study of the EC8-3 seismic safety assessment methodology. Besides testing the applicability of some of the code procedures, the study also aims to assess the possibility of establishing conclusions regarding the consistency and reliability of the safety levels that are obtained when using the EC8-3 methodology. Based

on the application of the deterministic procedure, the study aims to determine if the considered methods of analysis lead to similar safety results and to identify the factors that may affect these results. To reach these objectives, the application of the EC8-3 procedure is complemented with a probabilistic approach to obtain the fragility values corresponding to the deterministically assessed safety levels. Results and findings of this chapter were published in Romão *et al.* (2010b).

Chapter 4 discusses the definition of the Confidence Factor and its role in the EC8-3 seismic safety assessment methodology. Following a detailed interpretation of the code survey procedures associated to the characterization of the Confidence Factor, a statistical framework is proposed to reflect the uncertainty involved in the evaluation of the material properties required for the safety analysis in the definition of the Confidence Factor. Results and findings of this chapter were submitted for publication in Romão *et al.* (2012a).

Chapters 5 to 7 involve the adequate characterization of probabilistic models for structural demand under earthquake loading. Chapter 5 presents an in-depth analysis of the common assumption that structural demand conditional to a seismic intensity follows a lognormal distribution using adequate statistical methods. In addition to this analysis, the normal distribution hypothesis is also addressed. The statistical methods considered in this analysis were selected based on results of an extensive statistical study previously carried out that is presented in Appendix A. Results and findings of Chapter 5 were published in Romão *et al.* (2011) while those of Appendix A were published in Romão *et al.* (2010c).

Having established the type of statistical distribution of the demand parameters, an extensive study was then performed to address the characterization of the parameters of such distributions. In this context, Chapter 6 addresses the statistical characterization of the central value of structural demand under earthquake loading using estimation methods from the field of robust statistics. These methods were selected for their ability to account for the occurrence of anomalous data (i.e. outliers). Results and findings of this chapter were published in Romão *et al.* (2012b).

In order to complement the study presented in Chapter 6, Chapter 7 addresses the statistical characterization of the dispersion of structural demand under earthquake loading also using estimation methods from the field of robust statistics. Results and findings of this chapter were published in Romão *et al.* (2012c).

Chapter 8 presents several methodologies for the seismic risk assessment of building components. Two approaches are presented, termed Methodology 1 and Methodology 2, which involve the analytical definition of closed form expressions for the quantification of limit state exceedance probabilities at the structural component level. The procedures use a strategy similar to that of the method presented by Cornell *et al.* (2000), but extend that approach by introducing different functional forms to represent the earthquake hazard and by addressing the issue of force-based limit states probabilities. Methodologies 1 and 2 differ mainly on the hypotheses made to represent the earthquake hazard and on the level of mathematical tractability that can be achieved based on these hypotheses. Results and

findings of Chapter 8 associated to the development of Methodology 1 were published in Romão *et al.* (2008). Additional insights on the theoretical background of Methodologies 1 and 2 were also published in Delgado *et al.* (2010).

Finally, Chapter 9 proposes a probabilistic methodology for the seismic performance assessment of buildings systems. The proposed methodology analyses the seismic safety of a building using global performance metrics to determine if its behaviour conforms to a given limit state. The considered performance metrics are the probability of occurrence of the limit state, the corresponding expected loss associated to the repair of the building, and the corresponding number and type of mechanisms that are developed and that establish a possible scenario for the occurrence of that limit state.

The final chapter presents a summary of the main conclusions and findings of the previous chapters, alongside proposals and recommendations for future research on some of the topics addressed in this thesis.

Chapter 2
Practical aspects of demand and capacity evaluation in the context of EC8-3

2.1 Introduction

The current widespread interest in methodologies addressing the assessment and the retrofit of existing constructions reflects the global perception that such constructions are exposed to inadequate levels of seismic risk. The need for rational and cost effective interventions on the built environment led to the development of several normative documents and guidelines specifically addressing the seismic performance assessment of existing buildings (ATC 40, 1996; FEMA 273, 1997; FEMA 274, 1997; FEMA 310, 1998; FEMA 356, 2000; BRI, 2001a; BRI, 2001b; ASCE, 2003; OPCM 3274, 2003; EC8-3, 2005; OPCM 3431, 2005; NZSEE, 2006; ASCE, 2007; NTC, 2008; ATC, 2009). Most of these documents include modelling, analysis and verification procedures that are more detailed and lengthy than those commonly considered in the design of new structures. Hence, extensive practical application of such procedures must be carried out to observe their adequacy and to determine if some of them need to be re-examined or modified.

As previously referred, part of the present thesis addresses the procedures proposed in Part 3 of Eurocode 8 (EC8-3) (EC8-3, 2005) for structural safety assessment. In this context, some of the procedures associated to the seismic safety assessment of reinforced concrete (RC) structures are analysed herein and in the following two chapters. As seen in the following, the chord rotation demand plays an important role in the EC8-3 safety assessment procedure. Since there are several issues regarding its evaluation, as will be shown in later sections, the present chapter proposes a detailed study of its quantification. Given the significance of the shear-span in the referred study, a sensitivity analysis of the EC8-3 limit state capacity models with respect to this parameter is also carried out to examine the importance of its accurate quantification.

2.2 Brief outline of the EC8-3 procedures for seismic safety assessment of existing structures

Before presenting the study proposed in the current chapter, a brief overview of the more important aspects of the EC8-3 procedure for seismic safety assessment of existing structures is presented in the following to provide some context.

In global terms, the methodology proposed by EC8-3 for seismic safety assessment of existing structures involves a sequence of four levels of decision and analysis. The first level corresponds to the selection of the limit states that are going to be considered for a given structural performance assessment problem. EC8-3 defines three limit states that represent fundamental performance requirements of the structure, where each one is associated to a corresponding damage state. These limit states are the Near-Collapse (NC), the Significant Damage (SD) and the Damage Limitation (DL) limit states. The limit state of NC refers to a state of the structure that is close to its actual collapse, and corresponds to the full exploitation of the deformation capacity of the structural elements, while the definition of the SD limit state is roughly equivalent to what is called Ultimate limit state (or no-collapse) in the design of new buildings. The limit state of DL corresponds to a situation of light structural damage without significant yield of the members. The return periods of the design seismic action indicated in EC8-3 as appropriate for the three limit states and for buildings of ordinary importance are 2475, 475 and 225 years, respectively. However, each country may assign different values to the return periods in its National Annex.

The second decision level is associated to an important distinctive feature of existing structures when compared to new ones: the fact that their material properties may be known with varying degrees of accuracy, depending on the situation. This fact raises the questions of how to define quantitatively the available knowledge and how to account for such knowledge in the assessment. For this purpose, EC8-3 establishes three Knowledge Levels (KL), for which a number of survey procedures with different degrees of detail must be performed in order to achieve the required knowledge. By selecting a certain KL to be achieved and performing the referred survey procedures, EC8-3 assigns to the assessment problem a parameter called Confidence Factor that reflects the existing KL and will play the role of a partial safety factor in the subsequent safety verification stage. For the three KLs, denoted by KL1, KL2 and KL3 in increasing order of comprehensiveness, EC8-3 recommends Confidence Factor values of 1.35, 1.2 and 1.0, respectively. Further details are presented in Chapter 4 where a study addressing this specific topic is presented.

The third level of the EC8-3 procedure involves selecting the structural analysis method that will be used to perform the assessment. In terms of the admissible analysis methods, options range from linear to nonlinear methods, either static or dynamic. The admissibility of a given method of analysis depends also on the available KL. For example, if the available information can only meet the KL1 conditions, EC8-3 only allows the use

of linear analysis. Still, to be able to use linear methods for structural assessment, besides the requirements defined for new structures in Part 1 of Eurocode 8 (EC8-1) (EC8-1, 2004), an additional condition must also be met. This condition states that for the method to be applicable, the ratio ρ between the bending moment demand D and the corresponding capacity C must be sufficiently uniform across all the primary resisting elements of the structure, i.e. the ratio $\rho_{\max}/\rho_{\min}$ must not exceed a value in the range between 2 and 3 (considering only values $\rho \geq 1$) (EC8-3, 2005). The assumption underlying this approach is that if the structure goes into the inelastic range with an approximately uniform distribution of inelastic demands (expressed in terms of the D/C ratios), the structural response, in terms of displacements, is found to be acceptably accurate. This is an extension of the equal displacement rule, approximately valid for a single-degree-of-freedom oscillator, to a whole building, hence the condition that geometry, stiffness and mass distributions have to be regular. When linear analysis is not applicable, the alternative is to use nonlinear analysis, either static (pushover) or dynamic.

In terms of the pushover analysis, there are no conditions of applicability related to structural regularity in elevation. However, a spatial structural model is requested for the case of in-plan non-regular buildings. To use pushover analysis, EC8-3, by referring to what is defined in EC8-1, requests the use of at least two lateral force patterns: a uniform one (i.e. corresponding to a rigid translational mode) and a modal one (i.e. corresponding to the inertia forces pattern from the first mode in the direction under consideration). The structural element safety verifications are then carried out for the most unfavourable result. Each pushover analysis yields a capacity curve, i.e. a curve relating the lateral force resultant (the base shear) with the displacement at the top of the structure, that must be computed for a maximum displacement equal to 150% of the target displacement d_t. The target displacement represents the seismic demand and is obtained from the ordinate of the elastic displacement response spectrum at the effective period T^* of the structure. This latter is evaluated using the stiffness of the bi-linearized capacity curve and the modal mass. The value of d_t is assumed to be equal to the elastic response displacement if $T^* \geq T_C$, where T_C is the period that separates the constant acceleration from the constant velocity branches of the spectrum, while for $T^* \leq T_C$ a correction factor is applied (EC8-1, 2004).

When nonlinear dynamic analysis is selected, besides the additional complexity of the mathematical model of the structure, the major issues arise in terms of defining the seismic action. For this purpose, EC8-3, by referring also to specific rules defined in EC8-1, allows the consideration of either artificial or recorded accelerograms, in a minimum of three accelerograms. Structural demand must be assessed for all accelerograms and member safety verifications are then carried out for the most unfavourable result. In cases where at least seven accelerograms are considered, member safety verifications can be carried out for the average demand. In addition to defining a number of required accelerograms to be

used for seismic safety assessment, EC8-1 also specifies the following additional conditions these accelerograms should comply with:

- The mean of the zero period spectral response acceleration values (calculated from the individual accelerograms) must not be smaller than the value of $a_g \cdot S$ for the site in question, where a_g is the design ground motion acceleration, hereon termed peak ground acceleration (PGA), on type A soil and *S* is the soil factor.

- In the range of periods between $0.2T_1$ and $2T_1$, where T_1 is the fundamental period of the structure in the direction where the accelerogram will be applied, no value of the mean 5% damping elastic spectrum, calculated from all accelerograms, should be less than 90% of the corresponding value of the 5% damping elastic response spectrum.

As also noted by Iervolino *et al.* (2008), based on these conditions, it appears to be easier to meet these spectrum requirements using artificial spectral-matching accelerograms or by numerically altering real recorded ones to reduce the spectral mismatch of the time series, e.g. see Hancock *et al.* (2006).

The fourth and final level of analysis of the EC8-3 methodology corresponds to the safety verification stage where the conformity of each structural mechanism is checked involving procedures which depend on the nature of the mechanisms. In this context, it is appropriate to distinguish the two cases of linear and nonlinear methods of analysis. When linear analysis is used, the action effects (the demand *D*) on ductile and brittle mechanisms must be evaluated differently according to a capacity design philosophy aiming to check the occurrence of undesirable failure mechanisms. The demand on ductile mechanisms is the chord rotation at the member ends which is obtained directly from the analysis. On the contrary, demand in brittle mechanisms is obtained by means of equilibrium conditions, considering the actions transmitted by the relevant ductile components. These actions are those from the analysis, if the ductile element satisfies the condition $\rho \leq 1$ (i.e. if the element remains below yielding). On the other hand, if $\rho > 1$, these actions are to equal the capacity of the element, evaluated with mean values of the material properties multiplied by the Confidence Factor. From the capacity side, ductile mechanisms are checked in terms of deformations, and the capacity values for the different limit states are obtained from given expressions computed using mean values of the mechanical properties divided by the Confidence Factor. On the other hand, brittle mechanisms are checked in terms of strength, and the values of the capacities are obtained from given expressions computed using mean values of the mechanical properties divided by both the usual partial safety factor and by the Confidence Factor. If a nonlinear method of analysis is used instead, the only difference is that demand for both ductile and brittle mechanisms is directly obtained from the analysis (to be carried out using mean values of the mechanical properties).

2.3 Review of the chord rotation demand quantification

The previous review of the procedure for seismic safety assessment established by EC8-3 emphasizes the important role of the member chord rotation demand. Therefore, its quantification according to EC8-3 is examined in the following along with several alternatives. The need for these alternative formulations is demonstrated by presenting example situations where the EC8-3 proposal is difficult to apply. The effectiveness of the proposed approaches is assessed by comparing their performance with that of the EC8-3 procedure in cases where the application of the latter is straightforward. The comparisons are performed for a RC example structure that is analysed using nonlinear static and nonlinear dynamic methods, and for earthquake intensity levels associated to the three previously referred limit states. Several recommendations for the chord rotation demand evaluation are then defined based on the results of the application.

2.3.1 The Exact Integral Method (EIM)

The quantification of the chord rotation θ at a given section A of a structural member, θ_A, involves the consideration of a second cross section B within the member. According to CEB (1996), θ_A is the angle between the chord connecting the centroid of the two sections and the tangent to the member axis at section A. In analytical terms, θ_A can be written as:

$$\theta_A = \int_{x_A}^{x_B} \phi(x) \left(\frac{x_B - x}{x_B - x_A} \right) dx \tag{2.1}$$

where x_A and x_B are the abscissas of the two sections and $\phi(x)$ represents the curvature evolution between sections A and B. EC8-3 proposes a similar definition, specifying section B as that corresponding to the point of contraflexure. Considering this definition of section B, the chord rotations θ_1 and θ_2 of the two member ends, which are the sections of interest according to EC8-3, are:

$$\theta_1 = \int_{0}^{x_{L_s}} \phi(x) \left(\frac{x_{L_s} - x}{x_{L_s}} \right) dx \tag{2.2}$$

$$\theta_2 = \int_{x_{L_s}}^{L} \phi(x) \left(\frac{x_{L_s} - x}{L - x_{L_s}} \right) dx \tag{2.3}$$

where x_{L_s} is the abscissa of the point of contraflexure, and the abscissas of the two member ends are equal to zero and to the member length L, respectively. Details leading to Eq. (2.3), which is not directly obtained from Eq. (2.1), are found in CEB (1996).

2.3.2 The Exact Geometrical Method (EGM)

Alternatively, the chord rotation at a given section A can also be defined, in a more geometrically related fashion, as the member deflection at the abscissa x_B (section B) with respect to the tangent to the member axis at section A, divided by x_B. Again, considering the definition of the sections according to EC8-3, chord rotation θ_1, for example, can be defined as the member deflection at x_{L_s} with respect to the tangent to the member axis at the corresponding member end, δ_1, divided by x_{L_s}. Considering the simple case of Fig. 2.1a) which represents a member with only transversal displacements at the member ends, i.e. the simplified interpretation of the deformation of a column, θ_1 is obtained by:

$$\tan(\theta_1) = \delta_1 / x^* \tag{2.4}$$

Since $x^* = x_{L_s}$, in this case, and under the hypothesis that θ_1 is small, the following simplification can be made to Eq. (2.4):

$$\tan(\theta_1) \approx \theta_1 \Rightarrow \theta_1 = \delta_1 / x_{L_s} \tag{2.5}$$

In a more general case where both the rotation and the transversal deformation of the member ends are present, Fig. 2.1b), θ_1 is still obtained by Eq. (2.4), which, also under the hypothesis that θ_1 is small, now leads to the following simplifications:

$$\left.\begin{array}{l} \tan(\theta_1) \approx \theta_1 \\ x^* \approx x_{L_s} \end{array}\right\} \theta_1 = \delta_1 / x_{L_s} \tag{2.6}$$

Since calculating δ_1 may not be simple, θ_1 is defined by the following equivalent approach:

$$\theta_1 = \theta_{1a} - \theta_{1b} \tag{2.7}$$

where θ_{1a} represents the contribution of the deflection at x_{L_s} with respect to the initial member configuration and θ_{1b} corresponds to the nodal rotation, considering clockwise rotations to be positive. Similarly, θ_2 is defined by:

$$\theta_2 = \theta_{2a} - \theta_{2b} \tag{2.8}$$

where θ_{2a} and θ_{2b} have the meaning of θ_{1a} and θ_{1b}, respectively. In addition to the cases of Figs. 2.1a) and b), Fig. 2.1c) presents another example of chord rotation quantification that will be addressed in the next Section.

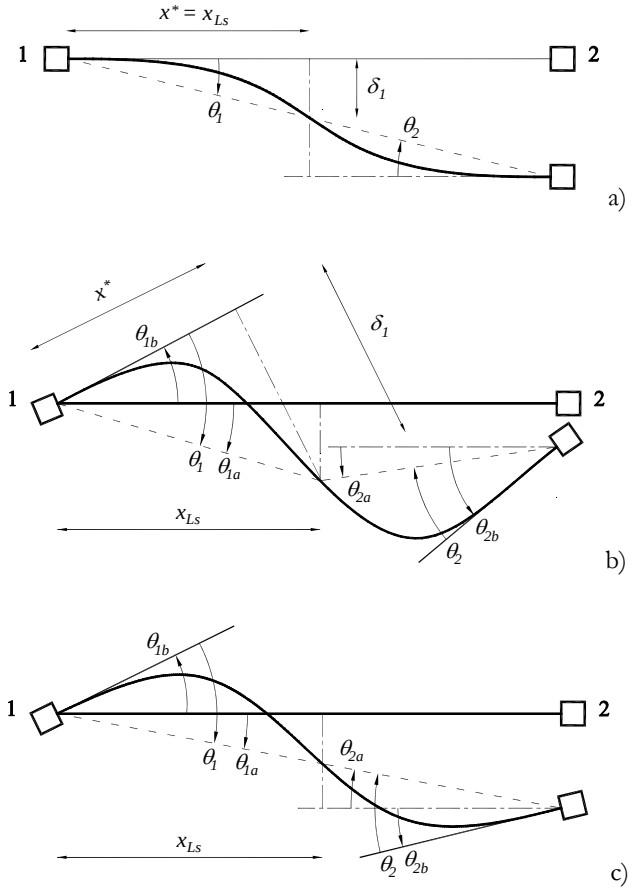

Figure 2.1. Examples of the chord rotation definition.

Although the approaches defined by Eqs. (2.2) and (2.3) are equivalent to those defined by Eqs. (2.7) and (2.8), there are several situations where their application is not straightforward. In this context, attention is first drawn to the EC8-3 definition of the point of contraflexure based on the moment-shear ratio M/V at the end section, usually identified as the shear-span L_s. It is known that x_{L_s} and L_s will only coincide under certain conditions, namely if the member under analysis is not subjected to any transversal loading, i.e. for the case of a typical frame column. In beams, which are usually subjected to gravity loading, the approximation of x_{L_s} by L_s may produce acceptable results under some conditions, e.g. when the influence of the gravity loads is small when compared to that of the earthquake loading. In situations where the level of gravity loading is significant, two points of contraflexure, with abscissas $x_{L_s 1}$ and $x_{L_s 2}$, may occur within the member length, instead of only one. In such cases, the value of x_{L_s} associated to Eqs. (2.2), (2.3), (2.7) and (2.8) must be replaced by that of $x_{L_s 1}$, for the case of θ_1, and by that of $x_{L_s 2}$, for the case of θ_2.

Further difficulties may arise in the quantification of the chord rotation in cases where there is no point of contraflexure within the member span. For example, by

considering the bending moment diagrams represented in Figs. 2.2a) and b), typically found in columns, the value of x_{L_s} (the abscissa that would correspond to a moment equal to zero) can be negative or larger than the member length. The case represented in Fig. 2.2c) is another possibility which may occur in short beams. In this case, x_{L_s} is undefined. Under such conditions, the quantification of the chord rotation following the EC8-3 procedure (i.e. where x_{L_s} is based on M/V) may lead to inadequate results.

From this discussion, the adequate evaluation of the chord rotation can be seen to depend on a suitable definition for x_{L_s}. The alternative approaches proposed in the next Section aim to overcome the observed difficulties.

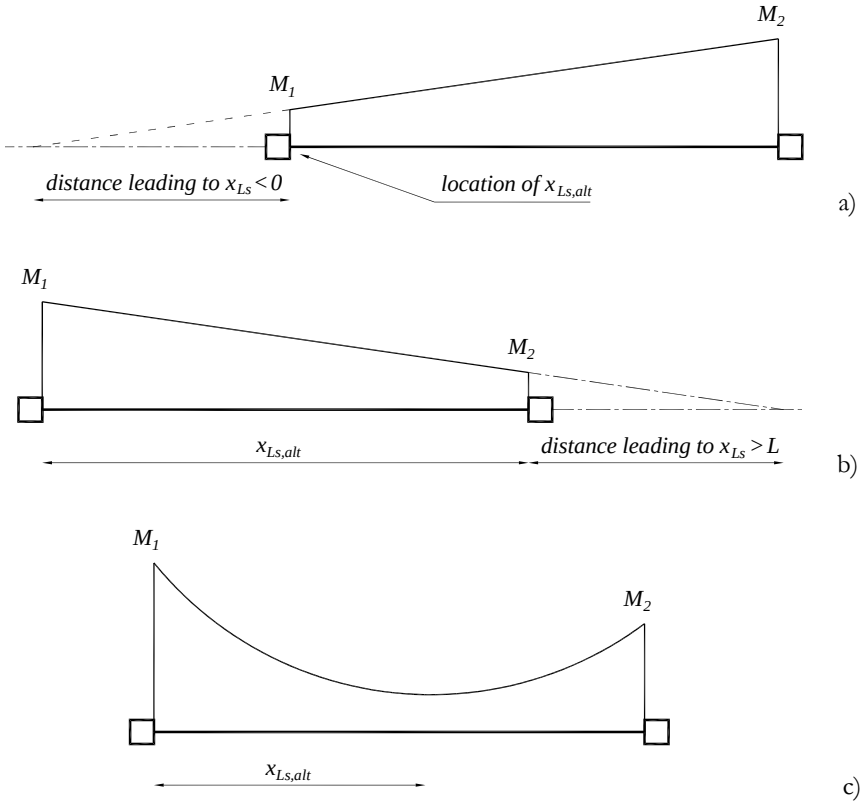

Figure 2.2. Examples of moment diagrams causing difficulties in the chord rotation evaluation.

2.4 Alternative approaches for chord rotation demand

Two alternative approaches are presented in the following for an adequate evaluation of the chord rotation. The first approach defines alternative interpretations for the value of x_{L_s} enabling the application of Eqs. (2.2), (2.3), (2.7) and (2.8) in the presence of the previously observed difficulties. The second approach defines alternative chord rotation evaluation methods which do not require the quantification of x_{L_s}. Following the definition of the several methods for chord rotation quantification, an example application is presented in Section 2.5 in order to assess their relative performance.

2.4.1 Alternative interpretations for x_{L_s}

From a theoretical point of view, the chord rotation quantification according to EC8-3 is undefined for the cases represented in Fig. 2.2. Subsequently, the proposed approximations only aim to circumvent the issues of numerical applicability of the EC8-3 safety assessment procedure arising in such cases, providing reasonable values of θ. Nonetheless, it is noted that such alternative values of x_{L_s} imply that Eqs. (2.2) and (2.3) may no longer yield the results of Eqs. (2.7) and (2.8), respectively.

When the point of contraflexure is undefined, the proposed alternative value of x_{L_s} is that corresponding to the distance between the end section under consideration and the section of minimum moment (in terms of absolute value). For columns this means that, for the situations of Figs. 2.2a) and b), the member safety assessment in terms of deformation is only relevant at the section with the higher absolute bending moment (section 2 for the case of Fig. 2.2a) and section 1 for that of Fig. 2.2b), identified as $x_{L_s,alt}$ in both cases). This hypothesis reflects the assumption that column geometry and reinforcement are constant along the member, as it is commonly found. In this situation, the value of x_{L_s} reflects the entire length of the member, with respect to the end section of interest. Hence x_{L_s} is equal to zero, for the case of Fig. 2.2a), and equal to L, for the case of Fig. 2.2b) (considering that x_{L_s} is measured from left to right). The application of this proposal with Eqs. (2.2) and (2.3) does not require any additional conditioning. On the other hand, the application of Eqs. (2.7) and (2.8) requires that only the expression of the relevant end section is evaluated. For beams, Fig. 2.2c), and since both end sections are significant in this case, the proposed alternative defines x_{L_s} as the abscissa $x_{L_s,alt}$ corresponding to that of the section closer to having a zero moment, i.e. closer to being a point of contraflexure. In this case, the application of this approximation with Eqs. (2.2), (2.3), (2.7) and (2.8) does not require any additional conditioning.

2.4.2 Evaluation of the chord rotation without quantifying x_{L_s}

The following three alternative approximate methods are proposed for the evaluation of the chord rotation without requiring the quantification of x_{L_s}.

2.4.2.1 The Approximate Geometrical Method that considers member Drift and nodal Rotations for beams and columns (AGM-DR)

This first method is adapted from the displacement-deformation relationship under large displacements proposed in Filippou and Fenves (2004) for frame elements. In the

chord rotation example represented in Fig. 2.1c), it can be seen that $\theta_{1a} = \theta_{2a}$. In this situation, this component of the chord rotation can be obtained without evaluating $\varkappa_{L_s}$ by:

$$\theta_{1a} = \theta_{2a} = d_y / L \tag{2.9}$$

where d_y represents the relative transversal displacement of sections 1 and 2, neglecting the contribution of the axial deformation of the member (Filippou and Fenves, 2004). Assuming these approximations for θ_{1a} and θ_{2a}, Eqs. (2.7) and (2.8) can be applied without further difficulties.

2.4.2.2 The Approximate Integral Method (AIM)

The second alternative method is especially suited for structures modelled by nonlinear frame elements with plastic hinges (lumped plasticity) where the nonlinear behaviour is defined by moment-curvature relations. In this type of modelling approach, the curvature demand is usually considered to be uniform along the plastic hinge length L_{pl} and equal to a value that can be obtained, for example, by the midpoint integration rule. Assuming that the most important contribution to the chord rotation comes from the plastic hinge deformation, the values of θ_1 and θ_2 can be approximately obtained by:

$$\theta_1 = \phi_1 \cdot L_{pl,1} \; ; \; \theta_2 = \phi_2 \cdot L_{pl,2} \tag{2.10}$$

where ϕ_1 and ϕ_2 represent the constant curvature of the two member ends, and $L_{pl,1}$ and $L_{pl,2}$ are their corresponding plastic hinge lengths.

2.4.2.3 The Approximate Geometrical Method that considers member Drift for columns and nodal Rotations for beams (AGM-D_cR_b)

The third method is a variant of the AGM-DR (application of Eqs. (2.7) and (2.8) considering Eq. (2.9)) combined with the assumptions proposed in the study presented by Mpampatsikos *et al.* (2008a). For the case of typical columns under seismic loading, this study states that the contribution to the chord rotation demand coming from θ_{1a} and θ_{2a}, Eqs. (2.7) and (2.8), is more significant than that coming from θ_{1b} and θ_{2b}, respectively. Hence the study suggests that, for simplicity, the chord rotation demand of column end sections could be obtained by θ_{1a} and θ_{2a} only. Furthermore, since, according to AGM-DR, the quantification of these components is approximated by Eq. (2.9), the third method proposed considers Eq. (2.9) for the evaluation of the chord rotation demand in columns. It is noted that this approximation implies that both column ends have the same chord rotation demand. For the case of beams, the third approach follows the suggestion

proposed by Mpampatsikos *et al.* (2008a). Therefore, the contribution of components θ_{1a} and θ_{2a} of Eqs. (2.7) and (2.8) is neglected and the chord rotation of beam end sections is approximated by the corresponding nodal rotations, i.e. components θ_{1b} and θ_{2b}.

2.5 Example application: the ICONS frame

2.5.1 General description

The ICONS frame is a four-storey, three-bay RC frame designed and built at the Joint Research Center in Ispra, Italy, for pseudo-dynamic testing (Carvalho *et al.*, 1999). The structure is representative of the design and construction common practice until the late 1970's in southern European countries and was designed for vertical loads only. The reinforcement details were specified in accordance to the normative available and to the construction practice at that time. The elevation view of the structure is presented in Fig. 2.3. For additional information concerning the frame characteristics and cross section reinforcement details, the reader is referred to Carvalho *et al.* (1999).

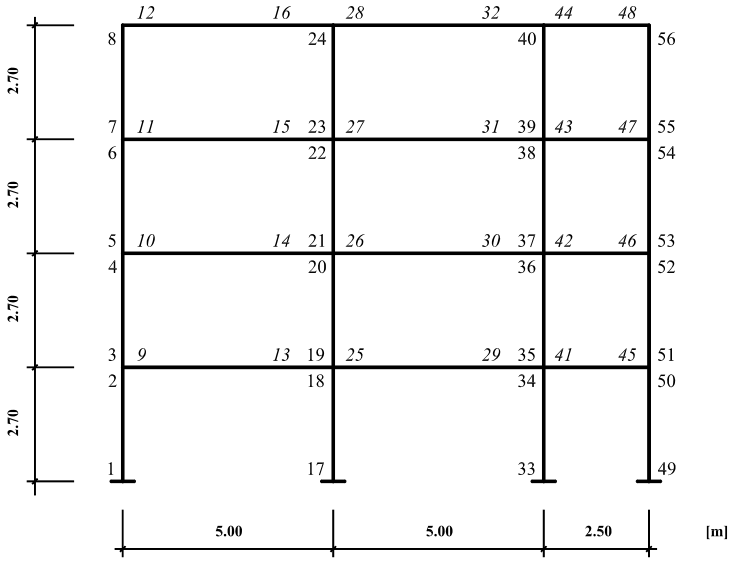

Figure 2.3. Elevation view of the ICONS frame.

2.5.2 Numerical modelling

The nonlinear response analysis of the frame under earthquake loading was carried out using a computer programme developed during previous research studies (Varum, 1997; Romão, 2002; Rodrigues, 2005) which include the simulation of several experimental tests performed on the ICONS frame (Rocha *et al.*, 2004). This computer programme is a two-dimensional analysis platform for the study of the nonlinear response of multi-storey

RC buildings. Column and beam elements are modelled as member-type nonlinear macro-models with three zones: one internal zone with linear elastic behaviour and two plastic hinges, located at the member ends, where inelastic flexural behaviour is considered. Control sections are located at each member end according to the numbering presented in Fig. 2.3 (numbers in italic refer to end sections of beams). Nonlinear analyses are carried out considering an event-to-event strategy with modification of the structure's stiffness matrix at each event and using the standard Newmark integration method for the dynamic analyses. Prior to a dynamic or pushover analysis, a nonlinear static analysis is carried out for the gravity loads acting on the structure, the results of which become the initial conditions for the subsequent analysis.

Since the purpose of this application example is not to represent the actual behaviour of the original ICONS frame, some simplifications were considered. Based on the original mechanical material properties of the ICONS frame, concrete of class C16/20 and steel of class S235 were selected, considering the mean values of the relevant structural material properties. The inelastic behaviour of the plastic hinges is represented by moment-curvature relations. Trilinear skeleton curves associated with monotonic loading and with an initial slope reflecting the secant-to-yield stiffness were obtained following the work presented in Arêde and Pinto (1996). Both asymmetric bending for beams and axial load effects for columns were considered. In beams, the elastic behaviour of the internal macro-model region was defined in order to reflect the cracked stiffness of the central part of the members when their bottom reinforcement is under tension. Slab participation to the beam tension flange was not considered. To assess the influence of the confined concrete characteristics, separate analyses were carried out for the two different models that can be considered according to EC8-3. The first model is defined in Part 1 of Eurocode 2 (EC2-1, 2004), referred hereon as the "EC2-1 model", and the second is defined in EC8-3, referred hereon as the "EC8-3 model". Details on these models can be found in EC2-1 (2004) and EC8-3 (2005), and are omitted here for the sake of brevity.

Hysteretic flexural behaviour of the members was modelled by the piecewise linear hysteretic Costa-Costa model (Costa and Costa, 1987; CEB, 1996) which is a generalized Takeda-type model. Stiffness degradation and pinching effects were considered in the hysteretic behaviour of the structural members. With respect to the considered plastic hinge length, although EC8-3 proposes expressions for its evaluation as a function of the selected confined concrete model, their consideration for the analyses is not straightforward since they depend on the shear-span (point of contraflexure) which is not known beforehand. Hence, L_{pl} values were considered equal to the depth of the member cross section for beams and equal to half of the depth of the member cross section for columns. For limit states leading to higher levels of inelastic demand, i.e. the limit states of SD and NC, most damping is due to hysteretic dissipation. Hence, viscous damping was not considered for these limit states. On the other hand, for the limit state of DL, for

which lower levels of inelastic demand are expected, viscous damping was accounted for. In this case, damping was assumed to be of Rayleigh type and the damping parameters were calculated for the first and second mode periods of the structure and considering a fraction of critical damping equal to 3% for both periods. Periods were obtained assuming the mass of the structure to be distributed on the beams and the stiffness of the members to be defined by their secant-to-yield stiffness. Gravity loading was defined for each structure according to the values set in Carvalho *et al.* (1999).

According to EC8-3, the safety assessment for the limit state of DL in terms of deformations must be carried out with a numerical model where the stiffness of the members is taken as the average effective (secant-to-yield) stiffness K_{eff} given by

$$K_{eff} = \frac{1}{4}\left(\frac{M_{y,1}^{+}}{3\theta_{y,1}^{+}} L_{s,1}^{+} + \frac{M_{y,1}^{-}}{3\theta_{y,1}^{-}} L_{s,1}^{-} + \frac{M_{y,2}^{+}}{3\theta_{y,2}^{+}} L_{s,2}^{+} + \frac{M_{y,2}^{-}}{3\theta_{y,2}^{-}} L_{s,2}^{-} \right) \tag{2.11}$$

where M_y is the yield moment, the indexes 1 and 2 refer to the two end sections of the member and the apexes + and – refer to positive and negative bending, respectively. For the particular case of a column with the same top and bottom reinforcement at both ends, i.e. $M_{y,1}^{+} = M_{y,1}^{-} = M_{y,2}^{+} = M_{y,2}^{-} = M_y$ and $\theta_{y,1}^{+} = \theta_{y,1}^{-} = \theta_{y,2}^{+} = \theta_{y,2}^{-} = \theta_y$, subjected to an antisymmetric moment distribution, i.e. $L_{s,1}^{+} = L_{s,1}^{-} = L_{s,2}^{+} = L_{s,2}^{-} = L_s$, Eq. (2.11) reduces to the well known expression $M_y L_s / \left(3\theta_y\right)$. In a more general situation, and given that L_s may be taken as $L/2$ (EC8-3, 2005), Eq. (2.11) can be simplified into:

$$K_{eff} = \frac{L}{24} \sum_{i=1}^{4} \frac{M_{y,i}}{\theta_{DL,i}} \tag{2.12}$$

where θ_{DL} is the yield chord rotation defined by (EC8-3, 2005):

$$\theta_{DL} = \phi_y \cdot \frac{L_s}{3} + 0.0013 \cdot \left(1 + 1.5 \frac{h}{L_s} \right) + 0.13 \cdot \phi_y \cdot \frac{d_b \cdot f_y}{\sqrt{f_c}} \tag{2.13}$$

in which ϕ_y is the yield curvature of the section, L_s is the shear span taken constant and equal to half of the member length, h is the section depth, d_b is the mean diameter of the tension reinforcement, f_y is the estimated steel yield strength and f_c is the estimated value of the concrete compressive strength. In columns, the consideration of K_{eff} according to Eq. (2.12) presents no difficulties, assuming that top and bottom reinforcement are equal in both end sections and considering that the axial load N necessary for the computation of M_y can be set to the value obtained for the gravity loads only. This axial load value is assumed to be a good approximation to the average value of N that a column may experience under earthquake loading (Mpampatsikos *et al.*, 2008a). On the other hand, the application of Eq. (2.12) in beams may lead to inadequate structural behaviour results.

Since, in beams, the top and bottom reinforcement of a given end section may be different, the corresponding values of M_y and θ_y may lead to considerably different values of positive and negative bending secant-to-yield stiffnesses. The consideration of Eq. (2.12) in this situation can then result in a value of K_{eff} that is excessively low to adequately represent the behaviour of the member. In a limit situation, this K_{eff} value may lead to the yielding of the member under the vertical loading alone. Hence, the plastic hinges of beams were modelled with different average values of K_{eff} for positive and negative bending. The behaviour of the internal macro-model region was defined as referred previously.

Finally, one aspect of the numerical implementation of the EIM and the EGM defined by Eqs. (2.2), (2.3), (2.7) and (2.8) is additionally noted. In order to observe the influence of the simplifications introduced by the AIM in the quantification of the chord rotation, the application of the EIM requires a more rigorous characterization of the curvature demand along the members, namely for situations where x_{L_s} is small or falls within L_{pl}. Hence, an approach defining a more detailed evolution of the curvatures along L_{pl} was selected for the EIM. Such evolution was represented by the incremental step-by-step recording of the curvature, in agreement with the moment distribution, in a number of points *np* along L_{pl}. For the case of the EGM, the step-by-step recording of the displacements in a number of points *np* along L_{pl} was also necessary to account for the cases where x_{L_s} falls within L_{pl}. A sensitivity study was carried out to determine a value of *np* leading to stable results of the chord rotation demand. Several tests were made with *np* values of 5, 10, 20 and 30. Results obtained with the EGM were rather insensitive to the selected value of *np* for the computation of the displacements along L_{pl}. Hence, an *np* value of 10 was selected. On the other hand, results obtained with the EIM were seen to be more sensitive to the value of *np*. In situations where x_{L_s} is small or falls within L_{pl}, as the *np* value goes from 5 to 30, the proximity of the results obtained with the EIM and those obtained with the EGM increases. Although an *np* value of 30 does not lead to the exact values obtained with the EGM in some cases, it was considered to yield results with sufficient accuracy.

2.5.3 Seismic demand

Seismic demand was set for Zone 1 of the Italian territory considering a soil of type B. According to OPCM 3274 (2003), the PGAs defined for the different limit states are 0.14*g*, 0.35*g* and 0.525*g* for the limit states of DL, SD and NC, respectively. Depending on the selected analysis method, the effective seismic demand was defined in different ways. When pushover analysis was considered, the effective seismic demand was characterized by

a set of target displacements defined for each PGA value and for each force pattern. Pushover analysis of the frames was performed using the uniform and the modal force patterns previously referred. When nonlinear dynamic analysis was considered, two different sets of accelerograms were used to evaluate the structural demand. The first set is made of seven artificial spectrum-compatible accelerograms with fifteen seconds for each limit state. These accelerograms were computed in order to meet the spectral-matching requirements defined by EC8-3. Figure 2.4a) shows the response spectra of the seven artificial accelerograms for the limit state of SD and their average response spectrum against the EC8-1 elastic response spectrum with ± 10% bounding limits. The second set has also seven records and corresponds to one of the unscaled real ground motion sets compatible with the EC8-3 spectral matching criteria proposed by Iervolino *et al.* (2008). As for the first set, Fig. 2.4b) presents the response spectra for this set, hereon termed the ReLUIS set, for the limit state of NC along with the average response spectrum, the EC8-1 elastic response spectrum and the ± 10% bounding limits. Since the original ground motion set is defined for the PGA corresponding to the limit state of SD, a scaling factor equal to $0.525g/0.35g$ was considered for this case.

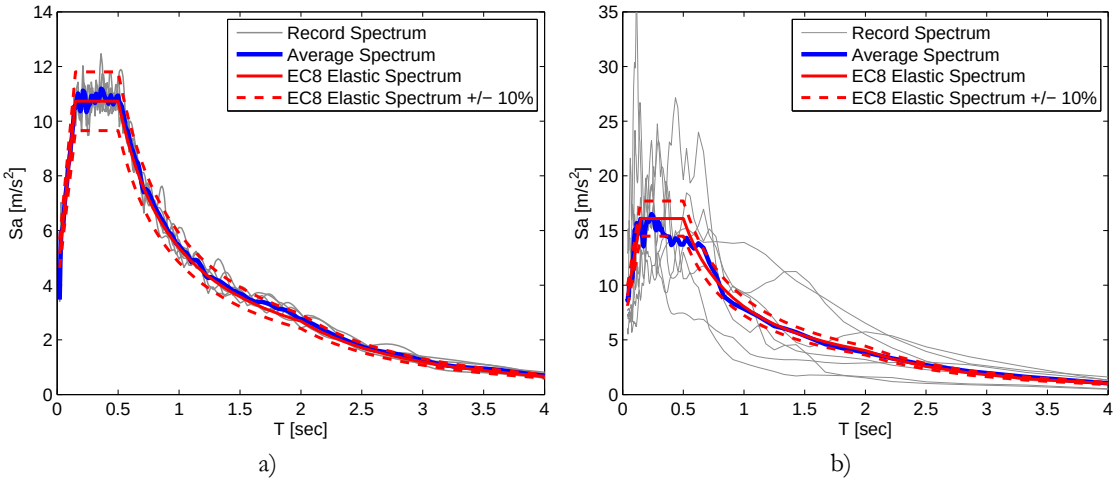

Figure 2.4. Response spectra of the artificial records for the limit state of SD (a), and of the ReLUIS records for the limit state of NC (b), along with the average spectra and the EC8 elastic response spectrum +/- 10%.

2.6 Structural analysis results

2.6.1 Initial considerations

The general trends and conclusions that were observed from the detailed comparison of the several methods for chord rotation quantification are presented herein, along with representative figures illustrating the more important findings. For the sake of brevity, only a sample of the results is shown. For the purpose of the presentation of the results, the considered chord rotation quantification methods (CRQMs) are termed according to the following:

- EGM - the chord rotation obtained using Eqs. (2.7) and (2.8), considering the alternatives proposed in Section 2.3.1 when necessary;
- EIM - the chord rotation obtained using Eqs. (2.2) and (2.3), considering the alternatives proposed in Section 2.3.1 when necessary;
- AGM-DR - the chord rotation obtained using Eqs. (2.7) and (2.8) combined with Eq. (2.9);
- AIM - the chord rotation obtained using Eq. (2.10);
- AGM-D_cR_b - the chord rotation obtained by the proposals of Section 2.4.2.3;
- EGM-APC - the chord rotation obtained using Eqs. (2.7) and (2.8), considering an Approximate abscissa for the Point of Contraflexure defined by M/V;
- EIM-APC - the chord rotation obtained using Eqs. (2.2) and (2.3), considering an Approximate abscissa for the Point of Contraflexure defined by M/V.

The performance assessment of the different CRQMs was carried out for the control sections identified in Fig. 2.3 and for the limit states of DL, SD and NC, based on the results of pushover and nonlinear dynamic analyses, the latter considering both artificial and real earthquake records. In cases where the alternative proposals of Section 2.3.1 are not required, this assessment involves comparisons between the approximate (i.e. those defined in Section 2.4.2) and the exact CRQMs (EGM and EIM) to determine the best approximate approach. Otherwise, the results of the previous comparison are used to determine the validity of the alternative proposals of Section 2.3.1 and to confirm the performance of the approximate approaches. In these comparisons, distinction is made between beam and column sections and between positive and negative chord rotations (positive chord rotations are considered to be those associated to clockwise rotations). The presented chord rotation values represent the maxima obtained for each section during the analysis under consideration. For the case of nonlinear dynamic analysis, comparisons were made for each record and also considering the average demand of a given set of records. It is recalled that the latter is the recommended demand measure to be used in the safety assessment according to EC8-3 for record sets of the considered size. In addition to the section level comparisons, a global efficiency measure, defined by the mean squared error (MSE), was also computed for the approximate methods of a given analysis case. As stated previously, both the EC2-1 and the EC8-3 confined concrete models were considered in the analyses. Since no significant differences were found between the results of both modelling approaches, the presented results are those obtained considering the EC8-3 confinement model, unless stated otherwise.

2.6.2 Presentation and discussion of the results

To demonstrate the occurrence of the problematic situations illustrated in Fig. 2.2, Fig. 2.5 presents the frame bending moment diagrams obtained from the pushover analysis with the modal loading pattern (from left-to-right), for the limit state of NC and for the load-step in which the corresponding target displacement is reached. The highlighted column and beam diagrams exhibit the referred x_{L_s} definition issues. Similar moment configurations were also obtained from the dynamic analyses.

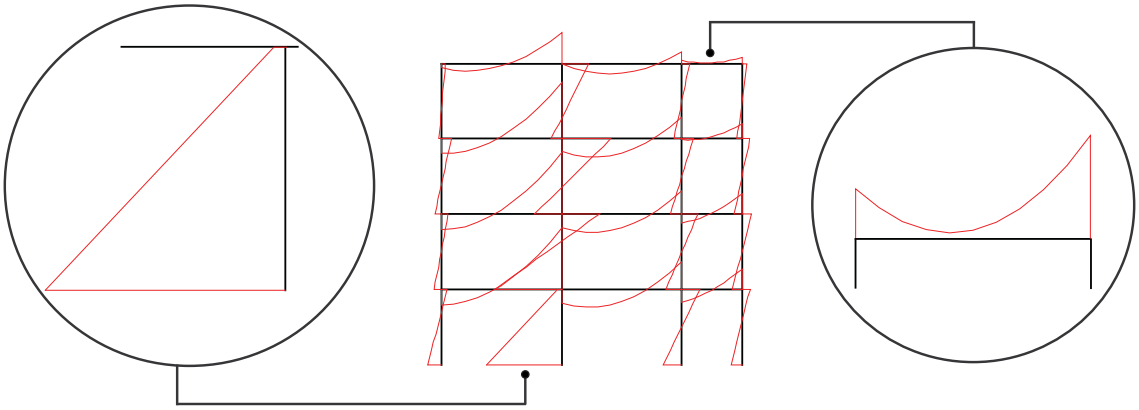

Figure 2.5. Example of a bending moment diagram obtained from pushover analysis illustrating the difficulties for chord rotation evaluation.

The performance of the EGM, the EIM, the AGM-DR, the AIM and the AGM-D_cR_b obtained from pushover analyses is illustrated in Figs. 2.6 and 2.7, for the limit state of NC under the modal loading pattern and for the limit state of DL under the uniform loading pattern, respectively. By examining Fig. 2.6, the results of the column sections obtained with the EGM, the EIM, the AGM-DR and the AIM are seen to show a good agreement. On the other hand, the results of the AGM-D_cR_b can be seen to deviate from those of the remaining methods in some of the sections, exceeding significantly the chord rotation values in such cases. Similar findings were observed in other pushover analysis results associated to limit states involving larger earthquake intensities (i.e. the SD and the NC). In beam sections, all methods are in good agreement. When observing Fig. 2.7, the results of column sections indicate that the AGM-DR performs well when compared to the EGM and the EIM, while the AIM and the AGM-D_cR_b have the tendency to, respectively, underestimate and overestimate the chord rotation. For the beam sections, the AGM-DR and the AGM-D_cR_b show a good performance when compared to the EGM and the EIM. On the other hand, the AIM tends to underestimate the chord rotation in some cases. Comparable trends were observed in the remaining pushover analysis results associated to the limit state of DL. From these analyses, it was also observed that the EGM and the EIM results are in good agreement for members where x_{L_s} definition issues were

identified. However, such situation was not always observed in the results obtained from nonlinear dynamic analyses, as shown further ahead in this Section.

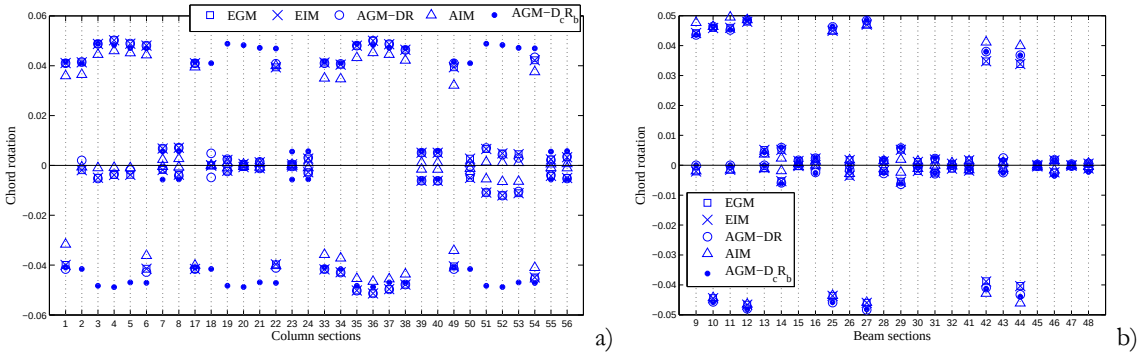

Figure 2.6. Performance of several CRQMs for the limit state of NC considering pushover analysis with modal loading pattern, for column (a) and beam (b) sections.

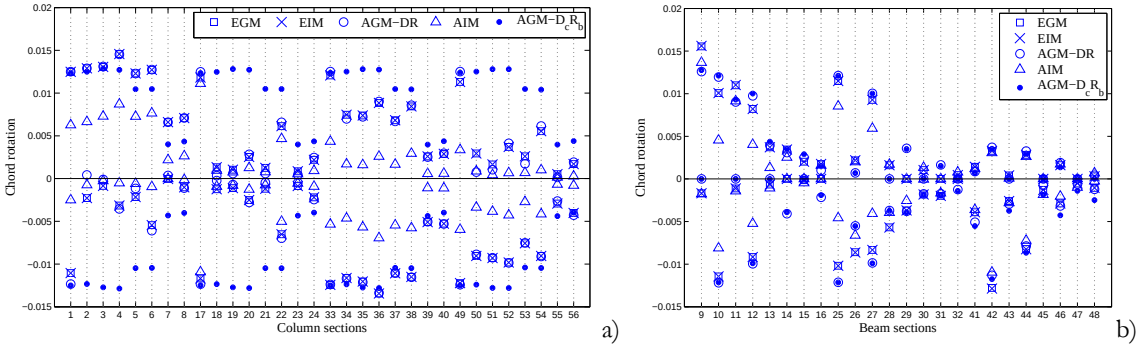

Figure 2.7. Performance of several CRQMs for the limit state of DL considering pushover analysis with the uniform loading pattern, for column (a) and beam (b) sections.

The performance of the EGM, the EIM, the AGM-DR, the AIM and the AGM-D$_c$R$_b$ obtained from nonlinear dynamic analyses is illustrated in Figs. 2.8 and 2.9, for the limit state of NC and one of the artificial records, and for the limit state of DL and one of the ReLUIS records, respectively. The results obtained for these cases exhibit general trends similar to those obtained for the pushover analyses. By examining the results of each record, those obtained for the limit states of SD and NC indicate that, in some of the column sections, the AGM-D$_c$R$_b$ also yields results with larger deviations from those of the remaining methods, while, in beams, all methods continue to exhibit a general good agreement. For the case of the limit state of DL, the results obtained for column sections indicate that, on average, the AGM-DR performs best, while the AIM and the AGM-D$_c$R$_b$ seem to under- and overestimate, respectively, the values of the EGM and the EIM. In beams, the AGM-DR and the AGM-D$_c$R$_b$ show a good performance, while the AIM presents results with larger deviations from those of the remaining methods, underestimating the chord rotation demand. After analysing the results of the AGM-DR, the AIM and the AGM-D$_c$R$_b$, the following can be noted about their performance:

- the AGM-DR performs well, both in column and in beam sections;
- the AIM underestimates the chord rotation for the limit state of DL since a significant part of the member rotation is neglected by considering the plastic hinge contribution only;
- the AGM-D_cR_b overestimates the chord rotation in columns because the nodal rotation contribution is not considered by this approach. On the other hand, its good performance in beams indicates that the gravity loading influence can be neglected without a significant loss of accuracy.

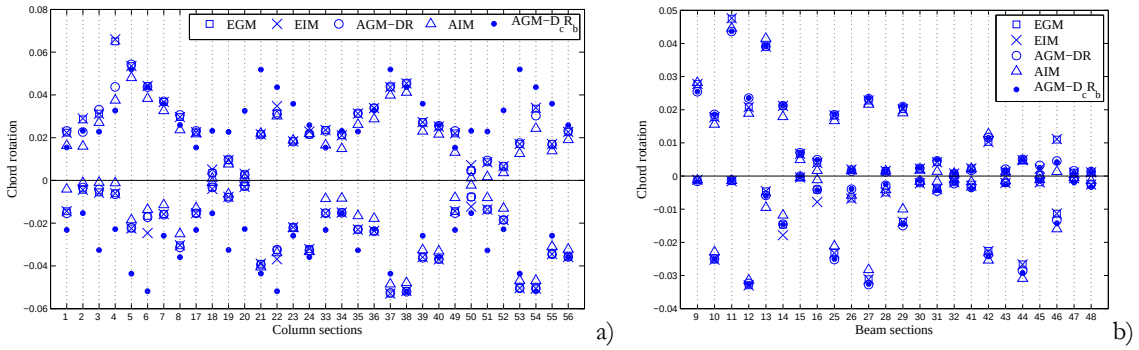

Figure 2.8. Performance of several CRQMs for the limit state of NC considering one of the artificial records, for column (a) and beam (b) sections.

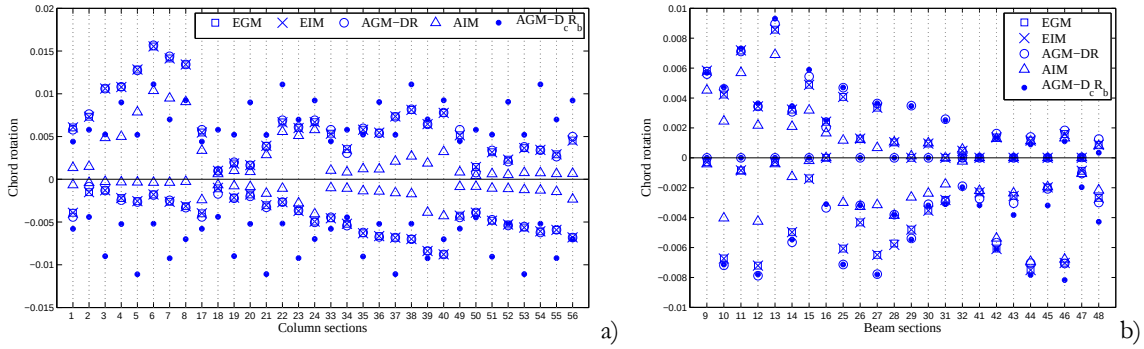

Figure 2.9. Performance of several CRQMs for the limit state of DL considering one of the ReLUIS records, for column (a) and beam (b) sections.

Even though x_{L_s} definition issues occur frequently during the dynamic analyses, particularly in columns, the corresponding results indicate that the maxima of the demand are seldom governed by such issues. With respect to these cases, it is emphasized that, in general, the EGM and the EIM may not yield similar results for columns, while for beams their results are much closer. It is noted that sections for which results of the EGM and the EIM differ correspond to situations where one of the two following conditions occurred:

- a x_{L_s} definition issue occurred and led, simultaneously, to maximum demand for at least one of the CRQMs;
- a small x_{L_s} occurred and led, simultaneously, to maximum demand for at least one of the CRQMs due to the numerical issues referred in Section 2.5.2.

To illustrate these conditions, reference is made to column section 50 of Fig. 2.8a) for which the EGM and the EIM are seen to yield different results for both positive and negative chord rotation demands. For the negative chord rotation, a small x_{L_s} occurred and led to maximum demand for the EIM while for the positive one, a x_{L_s} definition issue occurred and led to maximum demand also for the EIM. In both cases, the chord rotation demand obtained by the EGM is not governed by the same condition. The differences in the results of sections 6 and 22 of Fig. 2.8a) are also due to the occurrence of small x_{L_s} values that led to maximum demand for the EIM. It should be emphasized that the occurrence of such conditions for a given section does not necessarily implies differences between the results of the EGM and the EIM. For example, positive demand of sections 2 and 4 of Fig. 2.8a) are governed by the occurrence of a small x_{L_s} for the EGM and the EIM, and the results of both methods exhibit negligible differences. Moreover, the negative demand of section 17 of Fig. 2.8a) is governed by a x_{L_s} definition issue for the EGM and the EIM and, again, both approaches led to the same results. Based on these observations and on its lower sensitivity to numerical issues, the EGM is seen to yield more accurate results when x_{L_s} definition issues or small x_{L_s} values occur.

With respect to the average chord rotation demand based on the nonlinear dynamic analysis results, the observed trends are similar to those identified from the analysis of each record individually. For these cases, Figs. 2.10 and 2.11 illustrate the performance of the EGM, the EIM, the AGM-DR, the AIM and the AGM-D_cR_b for the limit state of DL, considering the ReLUIS records, and for the limit state of SD, considering the artificial records, respectively.

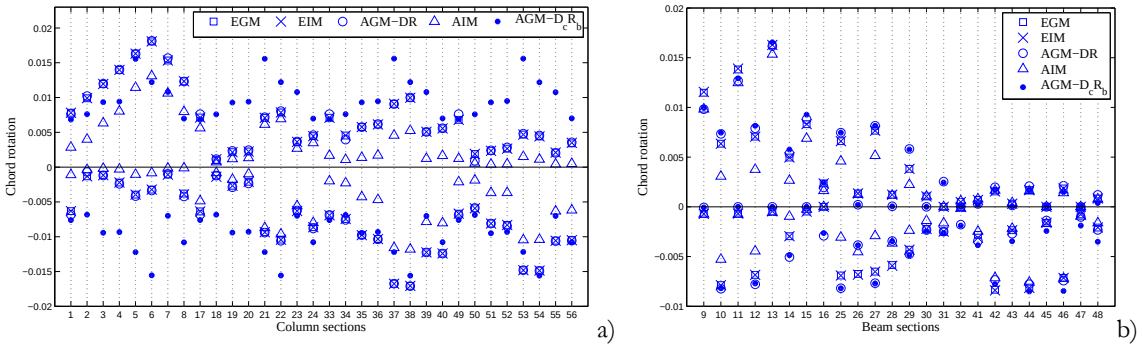

Figure 2.10. Performance of several CRQMs for the limit state of DL considering the average results from the ReLUIS records, for column (a) and beam (b) sections.

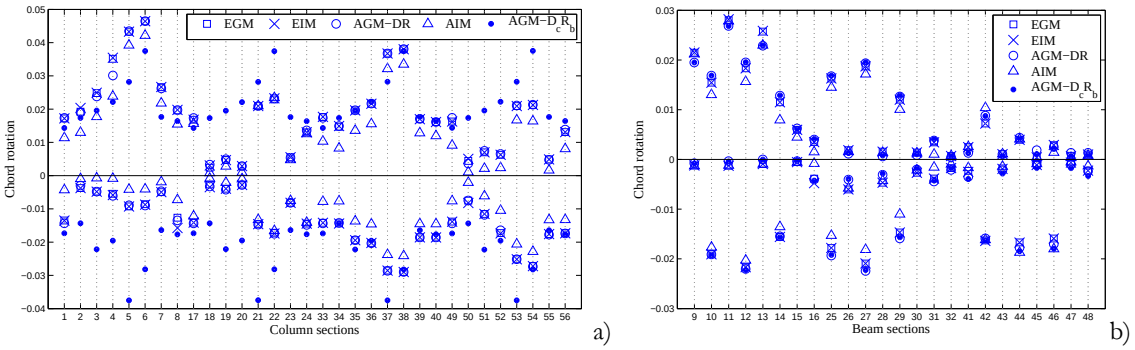

Figure 2.11. Performance of several CRQMs for the limit state of SD considering the average results from the artificial records, for column (a) and beam (b) sections.

As previously referred, given the performance variability of the different approximate CRQMs from section to section, the MSE was computed for each analysis case in order to obtain a global efficiency measure of the methods. Separate MSE values were calculated for column and beam sections as well as for positive and negative chord rotation values. The MSE values were defined by:

$$\mathrm{MSE}_{CRQM_i} = \frac{1}{ns}\sum_{j=1}^{ns}\left(CRQM_{i,j} - EGM_j\right)^2 \tag{2.14}$$

where *ns* represents the number of sections, $CRQM_{i,j}$ is the value of the AGM-DR, the AIM and the AGM-D_cR_b obtained for section *j* when *i* is 1, 2 or 3, respectively, and EGM_j is the value of the EGM obtained for section *j*. Given the aforementioned, the EGM is considered as the reference method for the calculation of the MSE values. In order to illustrate the MSE values that were obtained, Figs. 2.12 to 2.15 present several examples that include different types of analysis, different limit states and MSE values for both positive and negative chord rotations. Figure 2.12 presents MSE values (in log scale) for two limit states and pushover analysis cases. Figures 2.13 and 2.14 present MSE values (in log scale) obtained for the seven artificial records and for the limit states of NC and DL, respectively. Figure 2.15 presents MSE values (in log scale) for all the limit states and for the two record sets, based on the average chord rotation demand. The analysis of these results shows that, in beams, MSE values exhibit a somewhat stable variability across the analysis types, the limit states and the ground motion records. On the other hand, the MSE values of the columns become larger as the limit state intensity increases and the record-to-record variability seems to be more important for the limit state of DL. In the overall, the MSE values confirm the conclusions obtained from the section-by-section analysis.

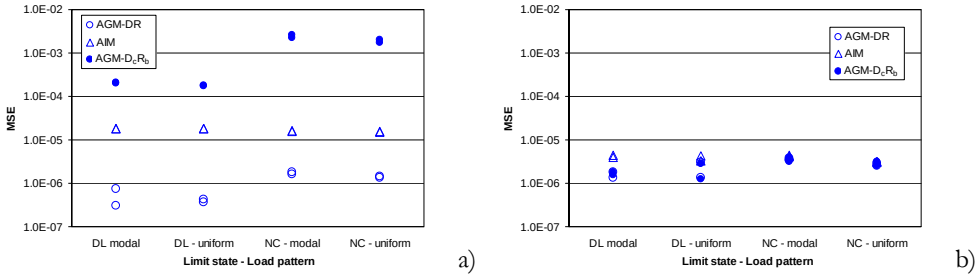

Figure 2.12. Mean squared error (MSE) values, Eq. (2.14), of the alternative CRQMs for two limit states and the pushover analysis cases, for column (a) and beam (b) sections.

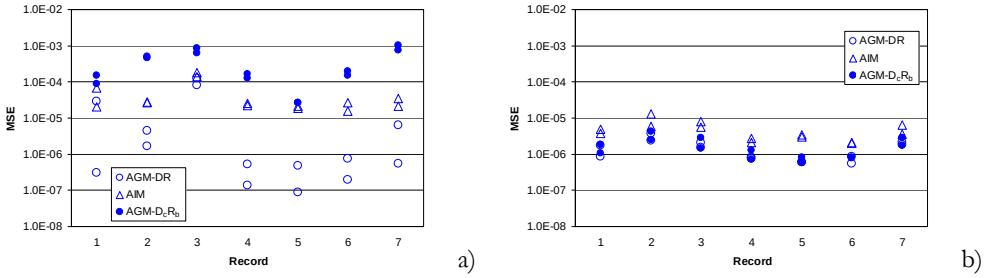

Figure 2.13. Mean squared error (MSE) values, Eq. (2.14), of the alternative CRQMs for the limit state of NC from the seven ReLUIS records, for column (a) and beam (b) sections.

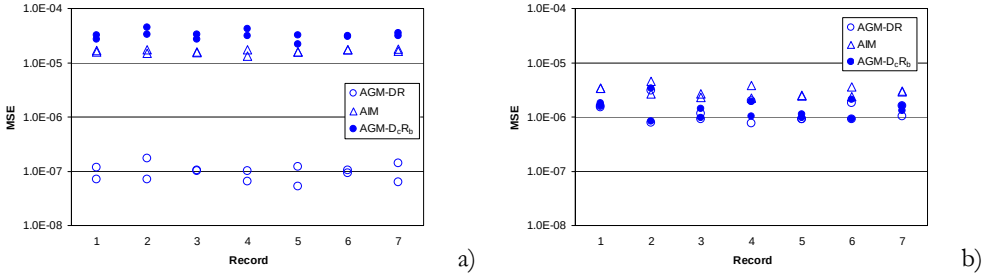

Figure 2.14. Mean squared error (MSE) values, Eq. (2.14), of the alternative CRQMs for the limit state of DL from the seven artificial records, for column (a) and beam (b) sections.

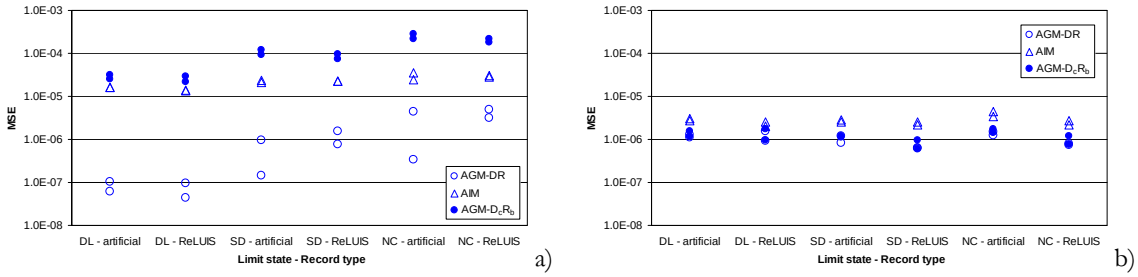

Figure 2.15. Mean squared error (MSE) values, Eq. (2.14), of the alternative CRQMs for all the limit states, for the two record sets based on the average chord rotation demand, for column (a) and beam (b) sections.

With respect to the comparison of the performance of the EGM-APC and the EIM-APC with that of the EGM and the EIM, it is referred that x_{L_s} values of the EGM-APC and the EIM-APC were computed separately for each member end by:

$$x_{Ls,1} = -M_1/V_1 \;;\; x_{Ls,2} = M_2/V_2 \tag{2.15}$$

where M_1, M_2, V_1 and V_2 are the member end bending moments and shear forces. The considered convention assumes that clockwise moments and upward shear forces are positive. Moreover, if any of the obtained x_{L_s} values was larger than L, the considered x_{L_s} value was considered to be L. If the x_{L_s} value was negative for a given section, the chord rotation was not computed for that section. In order to illustrate the results obtained, Fig. 2.16 presents the performance of the EGM, the EIM, the EGM-APC and the EIM-APC for the limit state of DL and one of the ReLUIS records. As expected, chord rotation demand in columns is not affected by the way x_{L_s} is computed, as long as the aforementioned exceptions are considered for larger than L and negative x_{L_s} values. On the other hand, the situation is different for beam sections. There are considerable differences in the positive demand of some of the member left-end sections (e.g. sections 9 and 11) and in the negative demand of some of the right-end sections (e.g. sections 10 and 12). To understand the reason for such situation, Fig. 2.17 presents the moment diagrams of common cases in columns and beams. Each diagram includes the bending moments and the shear forces with their considered signs and the location of the true x_{L_s}. It can be seen that when applying Eq. (2.15) to the cases of Figs. 2.17a) and b), adequate x_{L_s} values are obtained. On the other hand, for the cases of Figs. 2.17c) and d), a negative value is obtained for one of the sections (the left-end section for Fig. 2.17c) and the right-end section for Fig. 2.17d)). Problems arise in beams due to the presence of vertical loads that lead to shear forces of the same sign at both member ends. Since the direct consideration of Eq. (2.15) is not appropriate for beams, an alternative method was considered instead. For a given section *i* of a beam, the proposed alternative considers that when $x_{L_s,i}$ is negative, its value should be replaced in the chord rotation calculations by $L - x_{L_s,j}$, where $x_{L_s,j}$ represents the x_{L_s} value of the other end section. After repeating the analyses of Fig. 2.16 considering this alternative, the chord rotations of the several CRQMs are now in good agreement, as can be seen from Fig. 2.18. Nonetheless, there are still some differences between the results of the EGM and the EIM and those of the EGM-APC and the EIM-APC. These are due to the approximate values of x_{L_s} given by Eq. (2.15).

Finally, in order to illustrate the range of differences that can be expected by selecting the EC2-1 confined concrete model instead of the EC8-3 model, Fig. 2.19 presents the demand obtained with the EGM considering both models, for the limit state of NC and one artificial record. The presented results correspond to one of the cases where the influence of the confinement model is more significant. In the remaining analysis cases, the agreement between both modelling approaches is better.

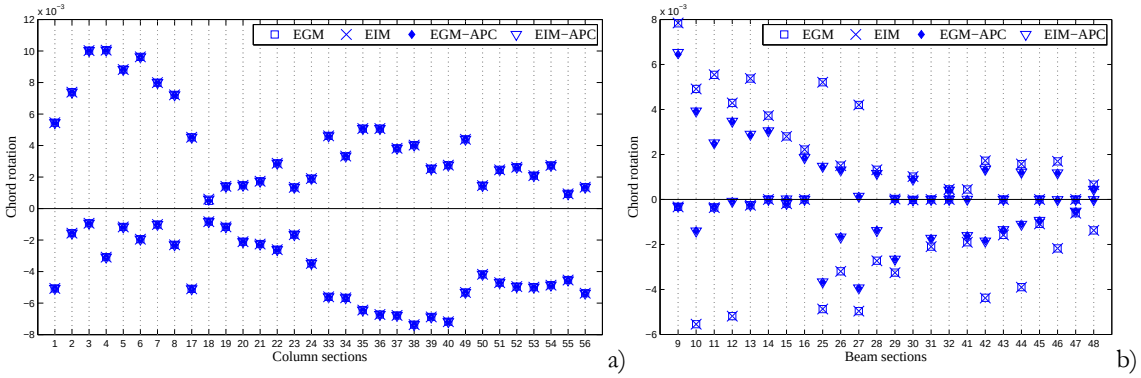

Figure 2.16. Performance of the EGM, the EIM, the EGM-APC and the EIM-APC for the limit state of DL considering one of the ReLUIS records, for column (a) and beam (b) sections.

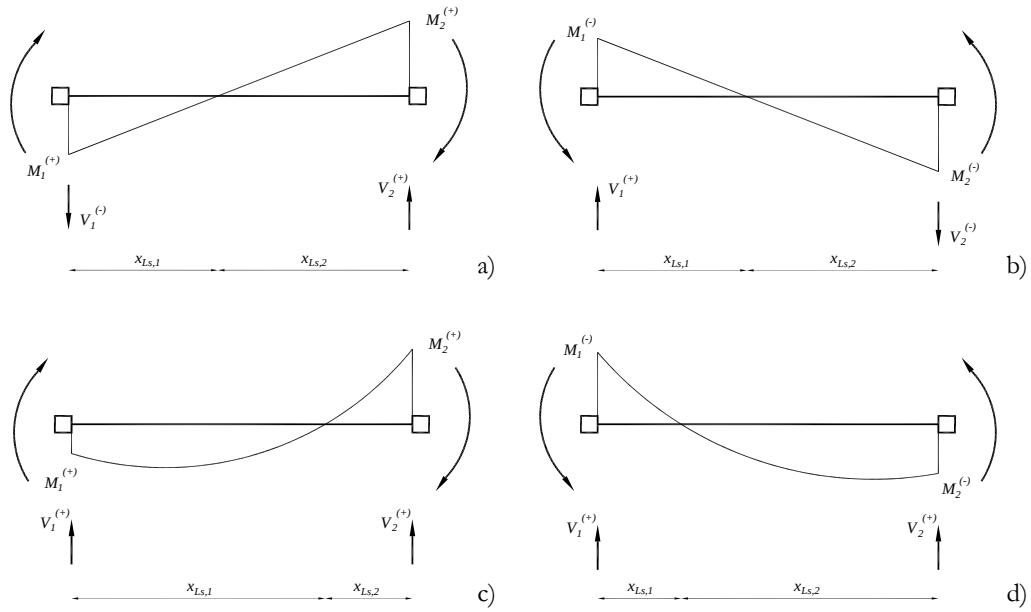

Figure 2.17. Moment diagrams with corresponding moments, shear forces and contraflexure points in columns a), b) and beams c) and d).

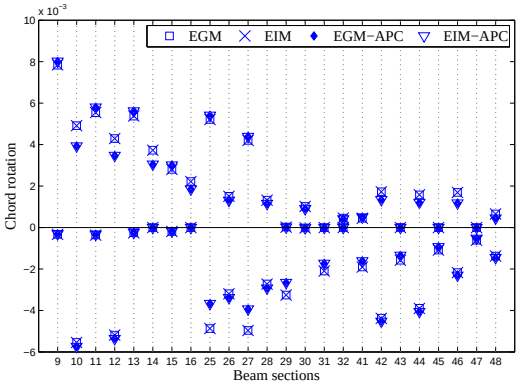

Figure 2.18. Performance of the EGM, the EIM, the EGM-APC and the EIM-APC for the limit state of DL considering one of the ReLUIS records for beam sections.

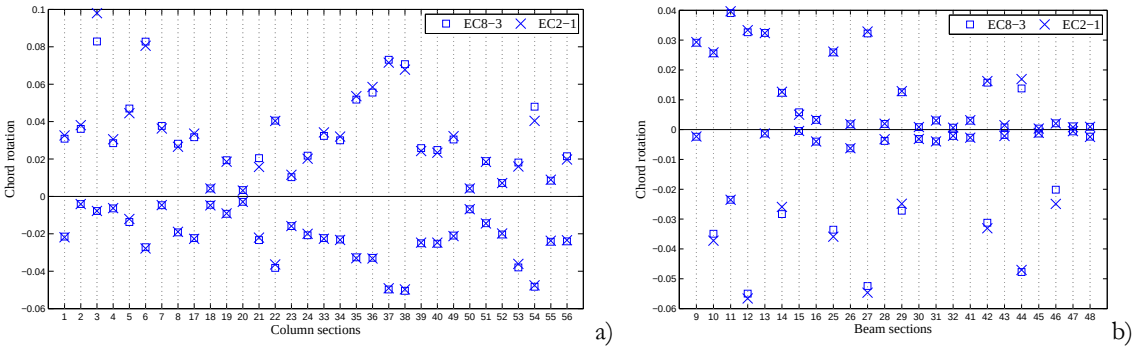

Figure 2.19. Comparison of the demand from the EGM considering the EC8-3 and the EC2-1 confinement models, the limit state of NC and one of the artificial records for column (a) and beam (b) sections.

The comparison of the performance of the different CRQMs based on the results of pushover and nonlinear dynamic analyses carried out for the several limit states, based on a section-by-section analysis and on the MSE values, leads to the following conclusions:

- With respect to the use of the theoretical approaches with the alternative proposals of Section 2.4.1, the EGM is preferred since it leads to results that are more regular and less sensitive to numerical issues than those of the EIM;
- With respect to the use of the approximate CRQMs defined in Section 2.4.2, the AGM-DR is recommended since it exhibited the best overall performance in columns and in beams. The AGM-DR is straightforward to compute after running the pushover or the dynamic analyses (i.e. in a post-processing stage) as long as the nodal displacements are stored at each step during the analyses;
- With respect to the use of the theoretical methods with x_{L_s} defined by M/V, this approach was seen to lead to adequate results in columns. In beams, adequate results were obtained by considering an alternative formulation when the relation between the bending moment and the shear force is not that which is expected in a seismic loading situation. In any case, the application of this approach is not straightforward and requires the consideration of a specific algorithm to handle cases where x_{L_s} is negative or larger than L.

2.7 Analysis of the EC8-3 capacity models of RC structures

Given the importance of the shear-span in the previously analysed situations, a sensitivity analysis of the EC8-3 limit state capacity models with respect to this parameter is carried out and discussed in the following. Furthermore, this analysis also aims to assess the validity of the simplifications proposed by a previous research study (Mpampatsikos *et al.*, 2008a) for the quantification of the EC8-3 limit state capacity values.

2.7.1 Review of the EC8-3 capacity models

Ductile capacities are defined in terms of the admissible DL, SD and NC member chord rotations while brittle capacities are characterized by the admissible NC shear force. For the quantification of the DL chord rotation capacity θ_{DL}, and assuming that no shear cracking is expected to precede flexural yielding, EC8-3 proposes the expression defined by Eq. (2.13). For the quantification of the NC chord rotation capacity θ_{NC}, EC8-3 proposes empirical and semi-empirical expressions. The former is defined by:

$$\theta_{NC} = \frac{1}{\gamma_{el}} \cdot 0.016 \cdot 0.3^{\upsilon} \cdot \left(\frac{\max(0.01, \omega')}{\max(0.01, \omega)} f_c \right)^{0.2} \cdot \left(\frac{L_s}{h} \right)^{0.35} \cdot 25^{\alpha \cdot \rho_{sx} \cdot \frac{f_{yw}}{f_c}} \cdot 1.25^{100\rho_d} \quad (2.16)$$

where γ_{el} is 1.5 for primary members, υ is the normalized axial force, ω and ω' are the mechanical reinforcement ratios of the tension and compression, respectively, longitudinal reinforcement, f_{yw} is the stirrup yield strength, ρ_{sx} is the ratio of transverse steel area A_{sx} parallel to the direction of loading, ρ_d is the steel ratio of diagonal reinforcement (if any) in each diagonal direction and α is the confinement effectiveness factor (EC8-3, 2005). The semi-empirical approach defines θ_{NC} by:

$$\theta_{NC} = \frac{1}{\gamma_{el}} \left[\theta_{DL} + \left(\phi_u - \phi_y \right) \cdot L_{pl} \cdot \left(1 - \frac{L_{pl}}{2L_s} \right) \right] \quad (2.17)$$

where ϕ_u is the ultimate curvature of the member end section. The definition of ϕ_u and of L_{pl} depends on the selected confined concrete model. For the case of the SD limit state, EC8-3 states that the corresponding chord rotation capacity θ_{SD} is defined as 75% of θ_{NC},.

With respect to the shear force capacity V_{NC} for the limit state of NC, EC8-3 proposes the formulation defined by:

$$V_{NC} = \frac{1}{\gamma_{el}} \left[\frac{h - x}{2 \cdot L_s} \cdot \min\left(N; 0.55 \cdot A_c \cdot f_c \right) + \left(1 + 0.05 \cdot \min\left(5; \mu_{\Delta}^{pl} \right) \right) \cdot \right.$$
$$\left. \cdot \left[0.16 \cdot \max\left(0.5; 100 \cdot \rho_{tot} \right) \cdot \left(1 - 0.16 \cdot \min\left(5; \frac{L_s}{h} \right) \right) \cdot \sqrt{f_c} \cdot A_c + V_w \right] \right] \quad (2.18)$$

where A_c is the cross section area taken as $b_w d$ (d is the structural depth), N is the axial load (equal to zero for tension), μ_{Δ}^{pl} is the ratio between the plastic part of the chord rotation demand and the yield chord rotation given by Eq. (2.13), ρ_{tot} is the total reinforcement ratio and V_w is the contribution of transverse reinforcement to shear resistance (EC8-3, 2005). The term $h - x$ represents the distance between the member compression centres and is assumed to be equal to *2h/3*.

2.7.2 Significance of the sensitivity analysis

The presented capacity models are seen to depend on geometrical and mechanical properties of the structural members as well as on parameters that depend on the seismic demand *D*. Since the capacity values may change from one analysis to the other, they should not be considered as member properties. Furthermore, if a single demand value is used for each control section when using nonlinear dynamic analysis, e.g. the mean value, the quantification of the capacity *C* of a given limit state may present some difficulties (Mpampatsikos *et al.*, 2008a). To overcome this, an approach similar to that presented by Mpampatsikos *et al.* (2008a) can be selected where, instead of the mean demand, the ratio D/C was computed for each ground motion based on their maximum demand. Then, the mean value of the ratios was chosen to characterize the safety measure of each section. Given that such approach can be computationally intensive, Mpampatsikos *et al.* (2008a) attempted to eliminate the demand-capacity coupling by testing several simplifications. Among other aspects, the study addressed the influence of considering a simplified value for:

- the axial load of the columns, by using the value obtained from gravity loads, instead of considering a more relevant value which varies during the analysis;
- ϕ_y, by using the value obtained from empirical expressions, instead of considering a more exact value obtained from a moment-curvature section analysis;
- L_s, by using the value of $L/2$, instead of considering the value of M/V which varies during the analysis.

Although the results of the referred study appear to favour the adoption of these simplified approaches, some aspects regarding the consideration of the proposal for L_s are unclear. The study does not report difficulties similar to those presented in Section 2.6 with respect to the use of M/V to define x_{L_s} (i.e. L_s). Since the study results are presented in the form of global percentages of unsafe/safe members, no indication of the influence of such simplification at the section level can be inferred, namely with respect to the closeness of $L/2$ and M/V. Furthermore, the study concludes that the use of $L/2$ with Eq. (2.17) is fundamental since it is very sensitive to small values of M/V. In view of these results, there is a definite need for a more detailed characterization of the relation between $L/2$ and M/V (or x_{L_s}) and for a discussion regarding the behaviour of the capacity model expressions to variations of parameter L_s. Moreover, the need for such characterization is also important for capacity assessment in situations where an approximate CRQM that does not require the computation of x_{L_s} is used.

Although the values of M/V and x_{L_s} are not always the same (e.g. in beams), their differences can be seen to have little practical influence, according to the previously presented methods and results for the EGM-APC and the EIM-APC. Hence, the following analysis of the capacity models and of the characterization of parameter L_s is based on the values of x_{L_s} obtained from the EGM. To observe the variation of x_{L_s} from one analysis to another, Figs. 2.20 and 2.21 present the x_{L_s} values associated to each section as a percentage of the member span obtained, respectively, from the ReLUIS records and the limit state of DL, and from the artificial records and the limit state of NC. Positive and negative values refer to x_{L_s} values associated with positive and negative chord rotation demand, respectively. In addition, the average value of each set of x_{L_s} values is also presented for each section. In general, the record-to-record variability of x_{L_s} is not significant, with the exception of few sections. However, the average values are far from $L/2$ in several cases, especially in beams. In light of these results, attention is brought to the conditions that are implicit in the development of the several EC8-3 capacity models, Eq. (2.13) and Eqs. (2.16) to (2.18). According to *fib* (2003a), the experimental results used to calibrate these models come either from simple- or double-cantilever specimens, or from simply-supported beams loaded at mid-span. In these tests, the geometrical and loading conditions correspond to a x_{L_s} value of $L/2$ and to a moment distribution that is linear. For columns, such conditions reflect situations which are, in many cases, in agreement with the demand. On the other hand, in beams, the assumptions behind the referred capacity models are inconsistent with the analysis of the demand.

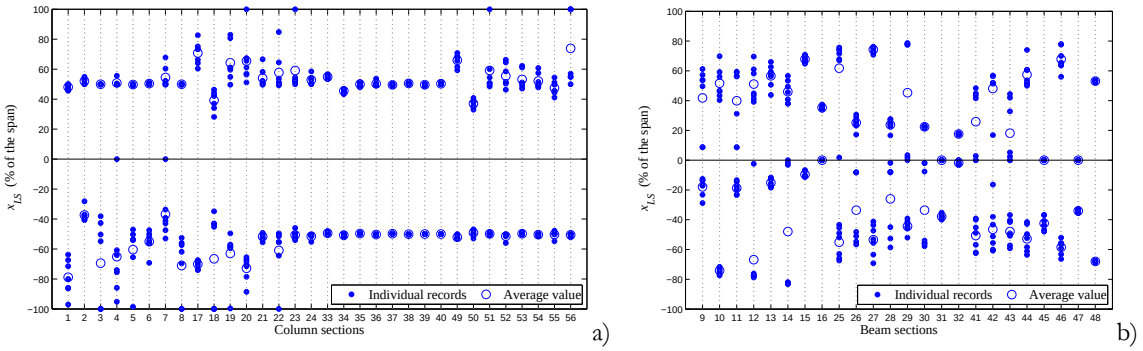

Figure 2.20. Comparison of the x_{L_s} values obtained from the ReLUIS records for the limit state of DL, for column (a) and beam (b) sections.

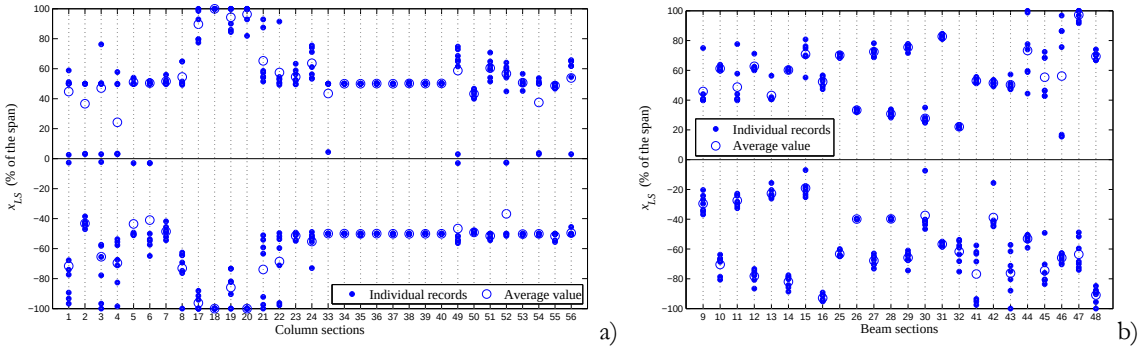

Figure 2.21. Comparison of the x_{L_s} values obtained from the artificial records for the limit state of NC, for column (a) and beam (b) sections.

2.7.3 Results of the sensitivity analysis

For a comprehensive understanding of the behaviour of the capacity models to variations of L_s, a sensitivity analysis of their expressions is presented in the following. For θ_{DL}, that is defined by Eq. (2.13), the sensitivity $\partial\theta_{DL}/\partial L_s$ is given by

$$\frac{\partial\theta_{DL}}{\partial L_s} = \frac{\phi_y}{3} - 0.00195\frac{h}{L_s^2} \tag{2.19}$$

which, by considering that $C_1 = L/h$, that ϕ_y can be approximated by $C_2 \cdot \varepsilon_{sy}/h$ and that $L_s = k \cdot L$ (with $0 \le k \le 1$), can be reorganized into:

$$\frac{\partial\theta_{DL}}{\partial L_s} = \frac{1}{L}\left(C_1 \cdot C_2 \frac{\varepsilon_{sy}}{3} - \frac{0.00195}{C_1 \cdot k^2}\right) \tag{2.20}$$

In order to observe the variation of θ_{DL}, the evolution of the term of Eq. (2.20) between parentheses is presented in Fig. 2.22a). Without loss of generality, C_1 values of 8, 10 and 12, C_2 values of 1.75 and 2.1 (Priestley, 2003; Biskinis, 2007) and $\varepsilon_{sy} = 0.002$ are considered. It can be seen that larger variations of θ_{DL} occur for $L_s < 0.2L$, below which θ_{DL} decreases considerably, and that for $L_s > 0.4L$, the rate of increase of θ_{DL} is almost constant. For larger or smaller values of ε_{sy}, the difference is that θ_{DL} starts to increase, respectively, at a smaller or larger, value of L_s, usually between $0.1L$ and $0.2L$.

For θ_{NC} defined by Eq. (2.16), the sensitivity $\partial\theta_{NC}/\partial L_s$ is given by

$$\frac{\partial\theta_{NC}}{\partial L_s} = \frac{0.0056}{\gamma_{el}} \cdot 0.3^{\upsilon} \cdot \left(\frac{\max(0.01,\omega')}{\max(0.01,\omega)} f_c\right)^{0.2} \cdot \left(\frac{1}{h}\right)^{0.35} \cdot 25^{\alpha\cdot\rho_{sx}\cdot\frac{f_{yw}}{f_c}} \cdot 1.25^{100\rho_d} \cdot L_s^{-0.65} \tag{2.21}$$

in which only the term $L_s^{-0.65}$ is seen to be relevant. Based on the evolution of this term presented in Fig. 2.22b), it can be seen that θ_{NC} increases throughout the whole range of

L_s, although larger variations occur for $L_s < 0.2L$. For the case where θ_{NC} is defined by Eq. (2.17), the sensitivity $\partial\theta_{NC}/\partial L_s$ is given by

$$\frac{\partial\theta_{NC}}{\partial L_s} = \frac{1}{\gamma_{el}}\left[\frac{\partial\theta_{DL}}{\partial L_s} + \left(\phi_u - \phi_y\right)\cdot\frac{L_{pl}^2}{2L_s^2}\right] \tag{2.22}$$

which, by setting $L_{pl} = C_3 \cdot L_s$ and $\mu_{pl} = \left(\phi_u - \phi_y\right)/\phi_y$, leads, without loss of generality, to

$$\frac{\partial\theta_{NC}}{\partial L_s} = \frac{1}{\gamma_{el}\cdot L}\left(C_1\cdot C_2\frac{\varepsilon_{sy}}{3} - \frac{0.00195}{C_1\cdot k^2} + C_1\cdot C_3^2\frac{\mu_{pl}\cdot\varepsilon_{sy}}{2}\right) \tag{2.23}$$

where C_1, C_2 and k are as previously defined. In order to observe the variation of θ_{NC}, the evolution of the term of Eq. (2.23) between parentheses is presented in Fig. 2.22c), for C_1 values of 8, 10 and 12, for C_3 values of 0.05, 0.3 and 0.6, for $C_2 = 1.75$ and for $\varepsilon_{sy} = 0.002$. It can be seen that larger variations, as well as a significant decrease of θ_{NC}, occur for $L_s < 0.2L$, above which the rate of increase of θ_{NC} is almost constant. The amount of decrease, which is governed by the term of Eq. (2.23) that includes parameter k^2, can be such as to lead to θ_{NC} values that are lower than θ_{DL} or even negative, as also reported by Mpampatsikos *et al.* (2008a). The comparison of Figs. 2.22a) and c) indicates that, for small values of L_{pl}, θ_{NC} will be mostly controlled by the contribution of θ_{DL}. Furthermore, the comparison of Figs. 2.22b) and c) shows that small values of L_s have opposite implications on the results of Eqs. (2.16) and (2.17).

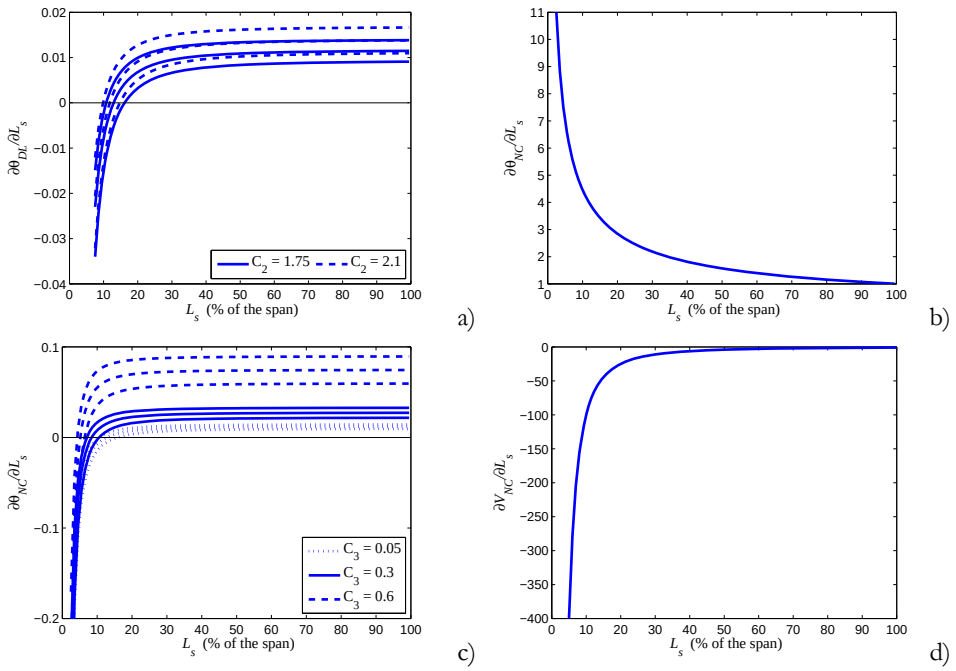

Figure 2.22. Sensitivity analysis of Eq. (2.13) (a), Eq. (2.16) (b), Eq. (2.17) (c) and Eq. (2.18) (d) to variations of parameter L_s.

For the case of V_{NC} defined by Eq. (2.18), the sensitivity $\partial V_{NC}/\partial L_s$ is given by

$$\frac{\partial V_{NC}}{\partial L_s} = -\frac{K_1}{L_s^2} - \begin{cases} 0.16 \cdot K_2 \cdot K_3 / h & for\ L_s < 5h \\ 0 & for\ L_s \geq 5h \end{cases} \tag{2.24}$$

in which constants K_1, K_2 and K_3 are defined as follows

$$\begin{cases} K_1 = (h - x) \cdot \min\left(N; 0.55 \cdot A_c \cdot f_c\right) / \left(2 \cdot \gamma_{el}\right) \\ K_2 = \left[1 + 0.05 \cdot \min\left(5; \mu_\Delta^{pl}\right)\right] / \gamma_{el} \\ K_3 = 0.16 \cdot \max\left(0.5; 100 \cdot \rho_{tot}\right) \cdot \sqrt{f_c} \cdot A_c \end{cases} \tag{2.25}$$

Although parameter K_2 is not truly constant, as μ_Δ^{pl} depends on the value of θ_{DL}, it was considered as so since, for $L_s < 0.2L$, μ_Δ^{pl} is most likely to be governed by the minimum admissible value and, for $L_s > 0.2L$, the variations of θ_{DL} are much smaller and can be neglected in this analysis. Since both terms of Eq. (2.24) are negative, only the term $-L_s^{-2}$ is seen to be relevant. Based on the evolution of this term presented in Fig. 2.22d), it can be seen that V_{NC} decreases throughout the whole range of L_s, though larger variations occur for $L_s < 0.2L$.

Based on the results of the sensitivity analysis, it is concluded that, for $L_s > 0.2L$, the approximation $L_s = L/2$ yields capacity results with an acceptable accuracy. Moreover, for the case of V_{NC}, since the consideration of $L_s = L/2$ for $L_s < 0.2L$ will lead to conservative safety assessment results, the use of this approximation is recommended throughout the whole range of L_s values. On the other hand, this recommendation is not applicable to the deformation capacity models. Although chord rotation demand in columns leads to x_{L_s} values that are, on average, close to $L/2$, in beams, x_{L_s} values lower than $0.2L$ are more frequent and their average evolution is not as clear. Results, thus, indicate that x_{L_s} should be computed for an adequate application of the deformation capacity models. Therefore, the results of this analysis do not validate the general use of $L_s = L/2$ as proposed by Mpampatsikos *et al.* (2008a). It is emphasized that the evaluation of x_{L_s} in a post-processing stage is straightforward, as long as *M* and *V* distributions are stored during the analysis. Furthermore, in light of the previously referred conditions that are implicit in the EC8-3 capacity models, and since the evolution of θ_{NC} according to Eqs. (2.16) and (2.17) may lead to inconsistent results for small values of L_s, the validity of these expressions, and of that of Eq. (2.13) due to its influence, should be re-examined based on additional experimental results, namely using results that reproduce demand conditions closer to those of beams.

2.8 Conclusions

The present chapter addressed the EC8-3 safety and demand assessment procedures based on an application for RC structures. The practical quantification of the member chord rotation according to EC8-3 was examined in detail along with several simplified alternative formulations. The performance of the several CRQMs was analyzed for a RC example structure, considering static and dynamic nonlinear analysis methods, and for earthquake intensity levels associated to the EC8-3 limit states. The comparison of the different CRQMs led to the following recommendations:

- The use of the EGM with the alternative proposals of Section 2.4.1 is preferred over the EIM, since it leads to results that are more regular and less sensitive to numerical issues;
- The AGM-DR is the recommended approximate method to use in columns and in beams;
- The use of the theoretical methods with x_{L_s} defined by M/V is recommended for columns and for beams. However, an alternative formulation needs to be considered to obtain adequate results in beams.

In addition, a sensitivity analysis of the EC8-3 limit state capacity models was carried out with respect to the shear-span in order to validate the results of previous research. Based on the results of the sensitivity analysis, it is concluded that, for $L_s > 0.2L$, the approximation $L_s = L/2$ will yield capacity results with an acceptable accuracy. Moreover, this approximation is recommended throughout the whole range of L_s values for the case of V_{NC}. On the other hand, such recommendation is not applicable to the deformation capacity models since results indicate that x_{L_s} values lower than $0.2L$ are more frequent, especially in beams. Hence, these results do not validate the general use of $L_s = L/2$ as proposed by Mpampatsikos *et al.* (2008a). Finally, given the different evolution of the two θ_{NC} expressions for small values of L_s, their validity should be re-examined based on additional experimental results.

Chapter 3
A comparative application of the EC8-3 seismic safety assessment procedures

3.1 Introduction

Following the previous chapter where the procedures for seismic safety assessment of existing structures proposed in Part 3 of the Eurocode 8 (EC8-3) (EC8-3, 2005) were introduced, the current chapter presents an application study of this methodology. Besides testing the applicability of some of the code procedures, the proposed study also aims to assess the possibility of establishing conclusions regarding the consistency and reliability of the safety levels that are obtained when using the EC8-3 proposed methodology. Based on the application of the deterministic procedure, the study aims to determine if the considered methods of analysis lead to similar safety results and to identify the factors that may affect these results. To reach these objectives, the application of the EC8-3 procedure is complemented with a probabilistic approach to obtain the fragility values corresponding to the deterministically assessed safety levels. By comparing the results obtained by the two approaches, the study aims to assess if similar deterministic results, defined in terms of demand-to-capacity (D/C) ratios, lead to similar probabilistic results (fragility values). Furthermore, the study tries to determine if a correlation can be established between deterministic D/C ratios and the expected fragility values.

The proposed application of the EC8-3 procedures is performed for two reinforced concrete (RC) structures. The structures were defined in order to be representative of this type of construction without being excessively complex, thus facilitating the presentation of the results and the drawing of conclusions.

In the following application, the terms *deterministic* and *fragility* are used with specific meanings. The term deterministic is used when referring to the EC8-3 safety assessment procedure. Although such procedure is semi-probabilistic, since partial safety factors and confidence factors are involved, the term deterministic is used in order to emphasize the

differences between this procedure and the probabilistic approach that is also considered. With respect to the fragility term, it is first reminded that a fragility curve represents the evolution of the probability of exceeding a given state of performance conditional to a parameter describing the intensity of the ground motions (Pinto *et al.*, 2004). A fragility value then refers to one ordinate of the fragility curve associated to a certain limit state describing structural performance. More specifically, in the context of the proposed application, this term is used when referring to the fragility value for the ground motion intensity in agreement with the return period associated to the considered limit state. Alternatively, this fragility value can also be defined as the probability of failure associated to a certain limit state, conditional to a demand distribution that was obtained from ground motions that are compatible with the return period of the considered limit state.

3.2 General conditions, structures and methods of analysis considered for the deterministic assessment

The EC8-3 deterministic procedure was applied for the safety assessment of two RC one-bay-four-storeys planar frame structures of similar geometry that can be considered to be part of larger structures. The seismic safety of the selected structures was assessed for both deformation- (ductile) and strength- (brittle) based limit states. In the former, the selected demand parameter was the member chord rotation, while in the latter, demand was assessed in terms of shear force. In terms of deformation demand, the three previously referred limit states (Near-Collapse (NC), Significant Damage (SD) and Damage Limitation (DL)) were considered while in terms of force demand only the NC limit state was selected, as defined in EC8-3. For all the considered limit states, capacities were defined according to the EC8-3 proposed expressions defined in Chapter 2 and that will be repeated in the current chapter for completeness.

For each limit state, the three previously referred Knowledge Level (KL) conditions were also considered for safety assessment. With respect to material properties, the Full Knowledge conditions, that correspond to KL3 and are associated to a Confidence Factor of 1.0, were assumed to be defined by assigning mean material property values to the selected material classes. The knowledge conditions corresponding to KL1 and KL2 were then assumed to be the KL3 conditions divided by the corresponding Confidence Factor: 1.35 for KL3 and 1.2 for KL2. These considerations indicate it was assumed that, for each KL, the same mean values of the needed material characteristics were obtained, irrespective of the fact that, for each KL, they would be based on different amounts of information and number of tests (EC8-3, 2005). This situation, although unlikely to occur, serves the purpose of assessing the influence of the Confidence Factor of each KL on the safety assessment results. In this application, the Confidence Factors values proposed by EC8-3

are not questioned. A more detailed study regarding the adequacy of such values is addressed in Chapter 4.

The safety assessment for each limit state and KL combination was performed using linear and nonlinear methods of analysis. In the latter case, both pushover and dynamic analyses were used, while in the former only static analysis was considered. Although EC8-3 states that only linear analyses can be used when KL1 conditions are available, as referred in Chapter 2, nonlinear analyses were also considered with this KL in this study to obtain a more comprehensive view of the influence of the Confidence Factor of each KL on the safety assessment results.

3.2.1 Structural configuration and detailing of the selected structures

The structural characteristics and detailing of these structures aim to simulate situations where seismic design was not considered. The two selected frames, hereon termed *TF1* and *TF2*, differ only on the orientation of the column cross sections. As previously referred, these structures were defined in order to represent simple examples facilitating the presentation of the results and the inference of conclusions. By considering the referred orientations of the column cross sections, two considerably different assessment cases were able to be defined, namely in terms of the global lateral stiffness and of the available beam-to-column stiffness ratios. Columns of the first structure, from which the frame *TF1* is selected, have a gross section of 0.25×0.50 m^2, while those from the second structure, from which the frame *TF2* is selected, have a gross section of 0.50×0.25 m^2. These characteristics and the remaining geometrical and detailing data are presented in Fig. 3.1. According to the selected material classes, which are C20/25 for concrete and S400 for steel, the following mean material property values were considered to characterize the nonlinear behaviour of the structural members:

- Concrete compressive strength f_c: mean $\mu_{f_c} = 28$ *MPa*
- Ultimate concrete strain ε_{cu}: mean $\mu_{\varepsilon_{cu}} = -0.006$
- Yield steel strength f_y: $\mu_{f_y} = 440$ *MPa*
- Ultimate steel strength f_{su}: $\mu_{f_{su}} = 506$ *MPa*
- Ultimate steel strain ε_{su}: mean $\mu_{\varepsilon_{su}} = 0.09$

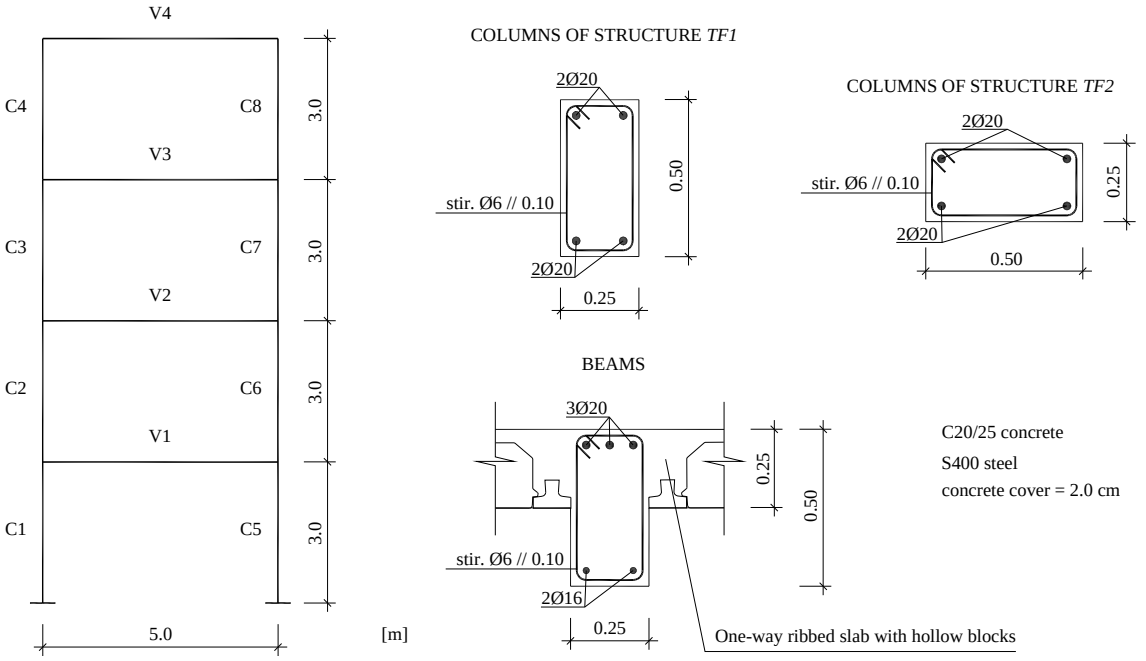

Figure 3.1. Geometrical and detailing characteristics of frames *TF1* and *TF2*.

3.2.2 Numerical modelling and definition of seismic demand

For the development of a numerical model of the frames for linear analysis, the previously presented data is sufficient. Nonetheless, two additional aspects should be mentioned. First, for the sake of simplicity, the effect of the lightweight slab-width on the beam stiffness and strength was not considered in the numerical modelling. Second, according to EC8-3, when carrying out the safety assessment for the limit state of DL in terms of deformations, the structural demand (i.e. the chord rotations) must be obtained from the analysis of a numerical model where the stiffness of the members is taken equal to the mean value of $M_y L_s \big/ \left(3\theta_y\right)$ at the two ends of the member, where M_y is the yield moment of the member, L_s is the shear-span (that, according to Mpampatsikos *et al.* (2008a), may be taken as half of the member length without loss of accuracy) and θ_y is the yield chord rotation. The latter can be defined by the yield capacity expression defined in EC8-3 presented in Chapter 2 and that will be presented again in a later Section of the present chapter.

The necessary data for the development of the numerical model of the frames for nonlinear analysis, static or dynamic, depends on the analysis programme that is used. For the present study, the response analysis of the frames was carried out using the computer programme referred in Chapter 2 that was developed during previous research studies (Varum, 1997; Romão, 2002; Rodrigues, 2005). This programme is a two-dimensional analysis platform for the study of the linear and nonlinear response of multi-storey RC

buildings. Column and beam elements are modelled as member-type nonlinear macro-models with three zones: one internal zone with linear elastic behaviour and two plastic hinges, located at the member ends, where inelastic flexural behaviour is considered. The nonlinear hysteretic flexural behaviour of the members was modelled by the piecewise linear hysteretic Costa-Costa model (Costa and Costa, 1987; CEB, 1996) which is a generalized Takeda-type model. Stiffness degradation and pinching effects were considered in the hysteretic behaviour of the structural members. Damping was only considered for the analyses involving the low intensity seismic actions of the DL limit state. In such cases, damping was assumed to be of the Rayleigh type with parameters computed for the first and second mode periods of the frames and a fraction of critical damping equal to 3% for both periods. The periods were obtained assuming a lumped mass distribution. Given that the considered program deals with moment-curvature member models, the chord rotation demand was computed according to the Exact Geometrical Method referred in Chapter 2

Since nonlinear structural behaviour is expected to develop at the structural member ends, the beam reinforcement defined in Fig. 3.1 is that of the end zones. Each structural member, defined according to the numbering also presented in Fig. 3.1, has, therefore, two demand control sections located at each end which are termed *bot* and *top*, in columns, and *left* and *right*, in beams. It should be noted that both aspects additionally brought to attention for the linear analysis model (the effect of the lightweight slab-width on the beams and the member stiffness modification for the safety assessment of the limit state of DL in terms of deformations) also apply for the modelling assumptions associated to nonlinear analysis.

The vertical loading considered in the analyses, either linear or nonlinear, consists in uniform loads of 30.2 kN/m on the first, second and third storeys, and of 26.6 kN/m in the fourth storey. These represent the self-weight of the beams and of the slabs, the finishings and the quasi-permanent value of the live load. In addition, a set of concentrated loads was considered to represent the self-weight of the columns.

Seismic demand was set for Zone 1 of the Italian territory and considering a soil of type B. According to OPCM 3274 (2003), the peak ground acceleration (PGA) values considered for the different limit states are 0.14*g*, 0.35*g* and 0.525*g* for the limit states of DL, SD and NC, respectively. It is noted that the PGA for the limit state of DL corresponds to a 72 years return period. To illustrate the seismic action definition for such conditions, Fig. 3.2 presents the corresponding elastic response spectra.

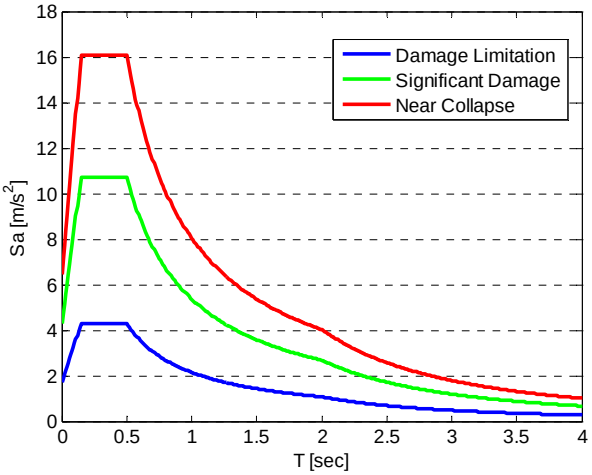

Figure 3.2. Elastic response spectra for the limit states of DL, SD and NC.

Based on these response spectra and depending on the selected analysis method, the effective seismic demand for the analysis was defined in different ways. When linear static analysis was used, the effective seismic demand was characterized by a set of horizontal forces obtained by the same methodology used for the design of new structures, as defined in Part 1 of Eurocode 8 (EC8-1) (EC8-1, 2004), and using the previously referred elastic response spectra instead of the design one. When pushover analysis was used, the effective seismic demand was characterized by a set of target displacements defined for each PGA value and for each force pattern. In this study, the safety assessment of the frames was performed using the following force patterns:

- A uniform pattern given by $F_i = \lambda$ where F_i is the force at the frame level i and λ is the factor that increases the force values;
- The standard EC8-1 proposed configuration given by $F_i = \lambda \cdot m_i \cdot \Phi_i$, where m_i and Φ_i are the mass and the modal coordinate at level i;

With respect to the computation of the target displacements, the following Section presents some comments about the procedure proposed by EC8-3 and a few application examples. In the cases where nonlinear dynamic analysis was used, five different sets of accelerograms were defined to set the effective seismic demand. Details and comments regarding the definition of these sets of ground motion records are presented in Section 3.2.2.2.

3.2.2.1 Definition of the target displacements for pushover analysis

According to EC8-3, by referring to what is defined in EC8-1, the computation of the target displacement for a multi-degree-of-freedom system requires the transformation of its capacity curve into an idealized bi-linearized curve, that represents the capacity curve

of an equivalent single-degree-of-freedom oscillator (Fig. 3.3), based on the equal energy assumption between both curves. A key feature for this transformation is the plastic mechanism point (Fig. 3.3) that EC8-3 defines as the point of the capacity curve that corresponds to the formation of the plastic mechanism of the structure. EC8-3 does not elaborate on the definition of plastic mechanism or on the criteria driving its definition (e.g. a global demand parameter, such as the maximum inter-storey drift, a local demand parameter, such as a maximum ductility demand in a member, or a combination of local demand parameters, such as the formation of a given number of plastic hinges). Depending on the assumptions considered regarding the numerical modelling of the structure for the nonlinear analysis, it is possible, in some cases, to define visually that the plastic mechanism occurs when the evolution of the capacity curve tends to be horizontal. Nonetheless, situations may occur when this approximation may not be possible or adequate (e.g. if the structure is sensitive to 2nd order effects). Some engineering judgement is thus required to define this point which plays an important role in the characterization of the target displacement.

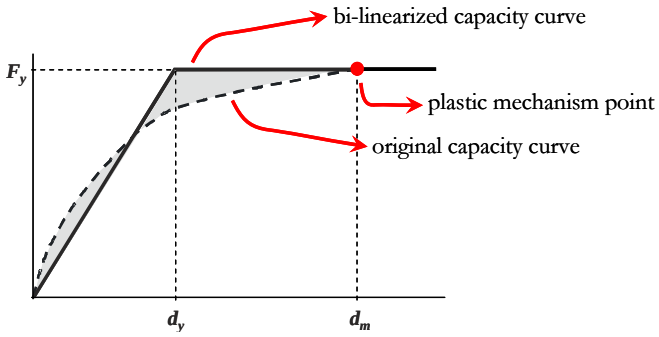

Figure 3.3. Original and bi-linearized capacity curves.

EC8-3 presents two procedures to determine the target displacement: a direct method and an (optional) iterative procedure. As expected, the direct method yields target displacements that are sensitive to the definition of the plastic mechanism point. On the other hand, the iterative procedure is able to compute the same target displacements, irrespective of the plastic mechanism point initially defined, hence dealing with the difficulty in objectively defining it directly by a single estimate. By using this iterative procedure, the initial guess of the plastic mechanism point becomes irrelevant, even when points corresponding to elastic behaviour of the structure are selected. To illustrate the application of the iterative procedure, Fig. 3.4 presents the target displacement of frame *TF1* under the standard EC8-1 proposed force pattern and for the limit state of SD, considering different values for the initial guess of the plastic mechanism point. As can be seen, the target displacement that is obtained is the same for all cases (within a *1.0 mm* tolerance). Besides showing the target displacement and the initial guess for the plastic mechanism point, Fig. 3.4 also shows the iterative points obtained before reaching the final

target displacement (the initial guess displacement corresponds to the first iteration and the final target displacement corresponds to the last iteration). As shown, the importance of an objective definition of the plastic mechanism point is now seen to be less relevant for the computation of the target displacements. Nonetheless, a formal definition of the plastic mechanism point was considered in this study. The plastic mechanism point was considered to be the point for which a sufficient number of idealized perfectly plastic hinges, i.e. with zero post-yield stiffness, has been developed, thus leading to a situation where equilibrium of the structure is not possible.

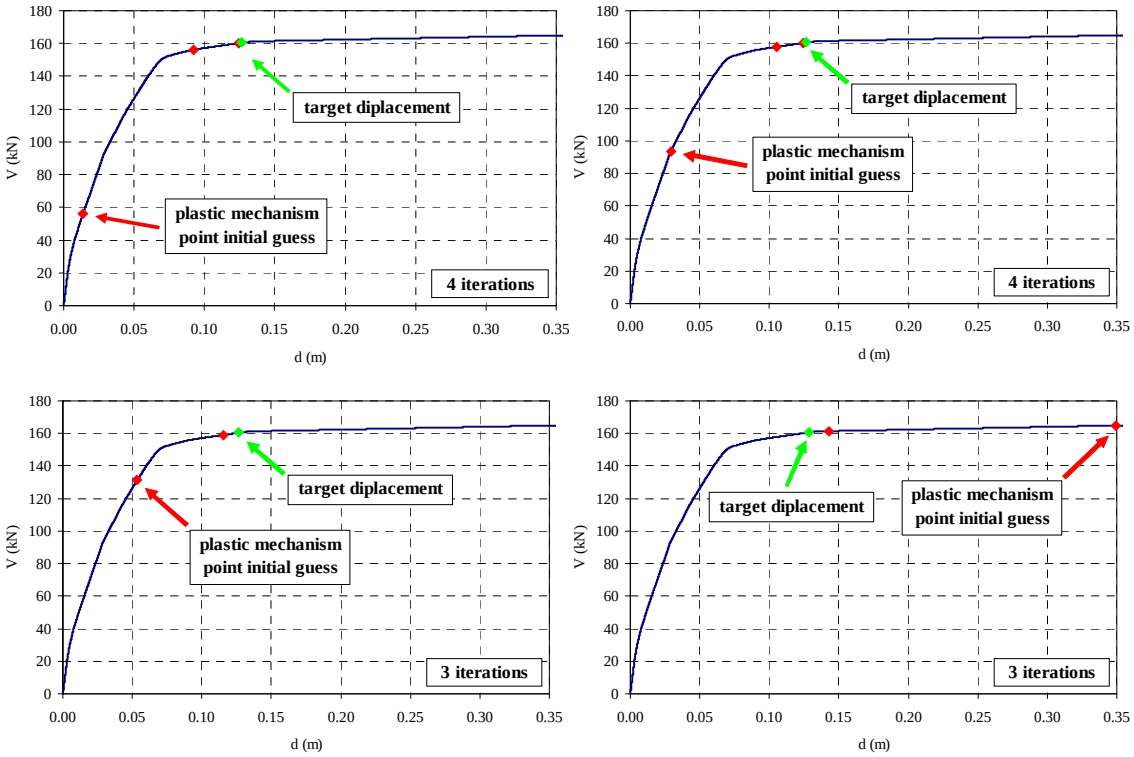

Figure 3.4. Target displacement of frame *TF1* under the standard EC8-1 proposed force pattern and for the limit state of SD for different initial guesses of the plastic mechanism point.

3.2.2.2 Definition of the accelerograms for nonlinear dynamic analysis

As previously stated, five different sets of accelerograms were defined to evaluate the effective seismic demand for the cases where safety assessment is performed using nonlinear dynamic analysis. The first set is made of seven artificial spectrum-compatible accelerograms with 15 seconds for each limit state and meeting the spectral-matching requirements defined by EC8-3. The second set corresponds to one of the unscaled real ground motion sets meeting the previously referred spectral matching criteria that are proposed by Iervolino *et al.* (2008). This set of records will be termed the ReLUIS set. The third to fifth sets are made out from seven real ground motion records that consider different scaling strategies. These recorded ground motions were considered in order to simulate a situation where spectral-matching ground motions are not available. In

alternative to more complex numerical techniques such as those proposed by Hancock *et al.* (2006), a possible way of addressing this situation is to consider a set of real records that are scaled in order to meet a certain code-compatible criterion. Although this type of approach is commonly used in performance-based probabilistic methods for seismic safety assessment (Aslani and Miranda, 2005; Luco and Cornell, 2007; Padgett *et al*, 2008), its suitability in the EC8-3 context is examined herein. These ground motions were chosen from an existing larger set of records that was established based on moment magnitudes and epicentral distances criteria (LessLoss, 2006) in order to have moment magnitudes between 5.3 and 5.7 and epicentral distances between 15 km and 30 km. The ground motions from the third set are scaled for the PGA of each limit state, those from the fourth set are scaled for the 5% damping spectral acceleration value at the fundamental period T_1, $S_a\left(T_1\right)$, for each limit state, while those of the fifth are scaled for the 5% damping spectral acceleration value at an alternative scaling period termed T_{inel}, $S_a\left(T_{inel}\right)$, and are only considered when assessing safety for the limit states of SD and NC. The period T_{inel} was considered to be representative of the first-mode inelastic period of the structure and was obtained from the effective period computed from the pushover analysis results. For frame *TF1*, the T_{inel}/T_1 ratio is $0.72/0.46=1.6$ while for frame *TF2* it is $1.2/0.65=1.8$. The proposed definition for T_{inel} shows that it ranges between $1.5T_1$ and $2T_1$, which is in close agreement with the "extended period" definition proposed by Haselton and Baker (2006). Although T_{inel} can be expected to change according to the selected bi-linearization procedure, if T_{inel} is evaluated by the following proposal (Chopra and Goel, 2001):

$$T_{inel}=T_1\cdot\sqrt{\mu/\left(1+\mu\cdot r-\mu\right)} \tag{3.1}$$

where r is the ratio of post-yield to elastic stiffness and μ is the displacement ductility, it can be seen that T_{inel} is relatively insensitive to the value of r and that μ is the governing parameter. For example, for μ values ranging from 2.0 to 5.0, one obtains T_{inel}/T_1 ratios ranging from 1.4 to 2.0. Hence, the T_{inel} values considered herein are seen to be acceptable and, given the expected low variability of the ground motion spectra for that period range, no significant variations in the analysis results are expected from considering different T_{inel} values across the previously referred T_{inel}/T_1 ratios.

In order to illustrate the differences between the several ground motion sets, their response spectra along with the code elastic response spectrum are presented in the following. To illustrate the characteristics of the artificial accelerograms that were generated, Fig. 3.5 shows the response spectra of the seven accelerograms generated for the limit state of SD, along with their average response spectrum, against the EC8-1 elastic response spectrum with ±10% bounding limits. For the ReLUIS set of records, Fig. 3.6 presents the corresponding response spectra for the limit state of NC. Since the original

ground motion set is defined for the PGA corresponding to the SD limit state, the records were scaled for the NC limit state using a scaling factor defined by $0.525g/0.35g$. Similar information is presented in Fig. 3.7 for the real ground motions when these are scaled using the PGA and for the limit state of DL. Similar information is also presented in Fig. 3.8 for real ground motions scaled using the $S_a(T_1)$ of frame *TF1* (T_1 = 0.46 sec) and for the limit state of NC. In Fig. 3.9, the same situation is represented using the $S_a(T_1)$ of frame *TF2* (T_1 = 0.65 sec). Analogous representations are also presented for the fifth set of accelerograms to allow for direct comparisons between the two scaling strategies. Hence, Fig. 3.10 presents the response spectra for the real ground motions scaled using the $S_a(T_{inel})$ of frame *TF1* (T_{inel} = 0.72 sec) for the limit state of NC, while Fig. 3.11 presents the corresponding response spectra for frame *TF2* (T_{inel} = 1.2 sec).

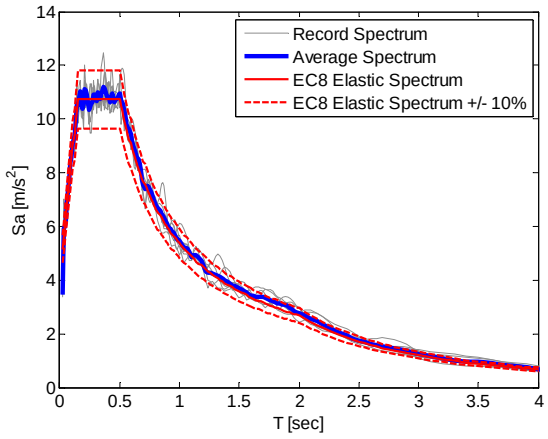

Figure 3.5. Response spectra of the artificial records for the limit state of SD, their average spectrum and the EC8-1 elastic response spectrum +/- 10%.

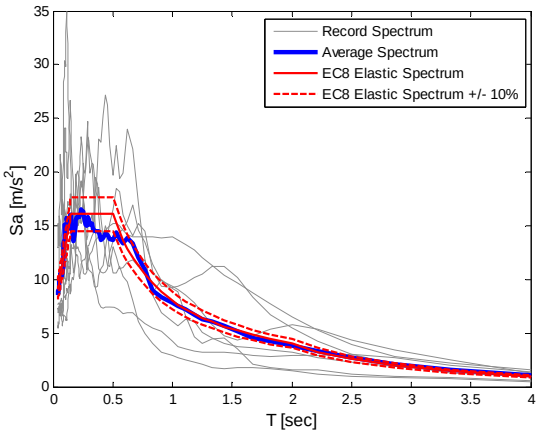

Figure 3.6. Response spectra of the unscaled ReLUIS ground motion set meeting the spectral matching criteria, for the limit state of NC, their average spectrum and the EC8-1 elastic response spectrum +/- 10%.

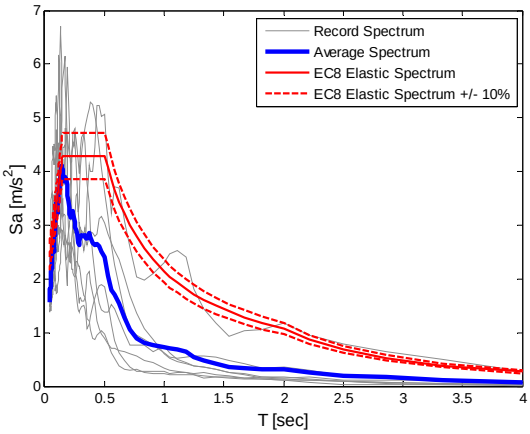

Figure 3.7. Response spectra of the PGA scaled records for the limit state of DL, their average spectrum and the EC8-1 elastic response spectrum +/- 10%.

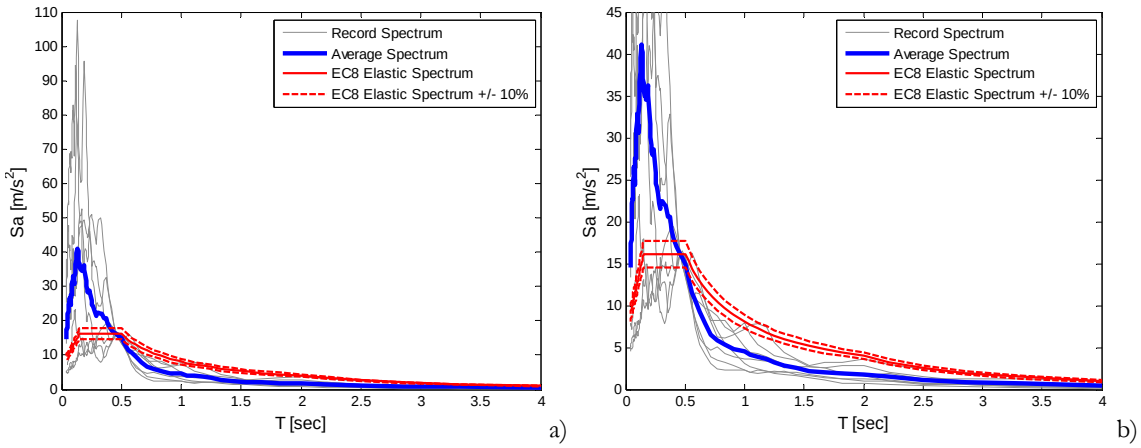

Figure 3.8. Response spectra of the $S_a(T_1)$ scaled records for the limit state of NC and frame *TF1*, their average spectrum and the EC8-1 elastic response spectrum +/- 10% (a); larger view (b).

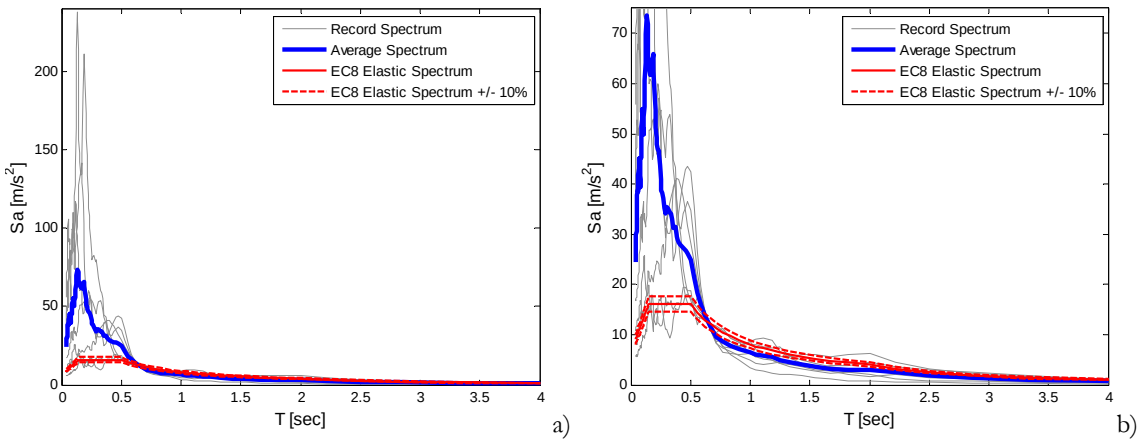

Figure 3.9. (a) Response spectra of the $S_a(T_1)$ scaled records for the limit state of NC and frame *TF2*, their average spectrum and the EC8-1 elastic response spectrum +/- 10% (a); larger view (b).

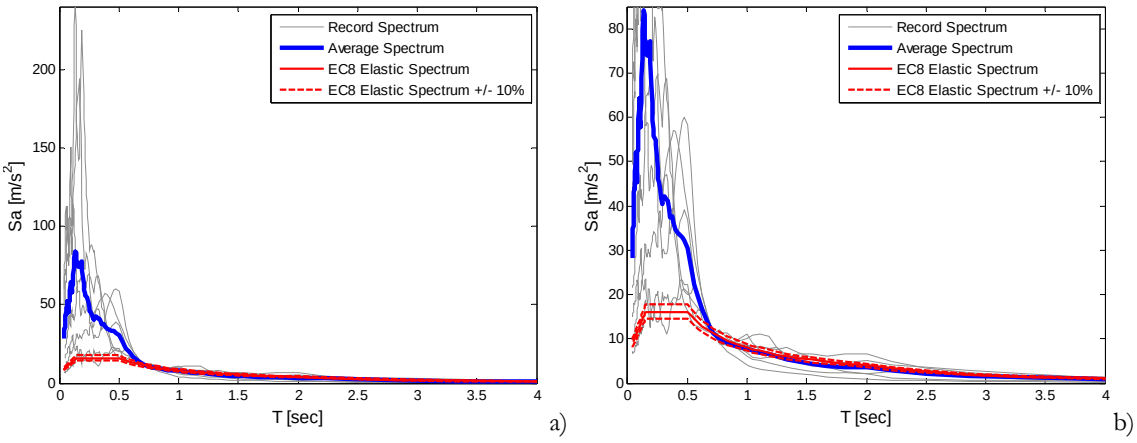

Figure 3.10. Response spectra of the $S_a(T_{inel})$ scaled records for the limit state of NC and frame *TF1*, their average spectrum and the EC8-1 elastic response spectrum +/- 10% (a); larger view (b).

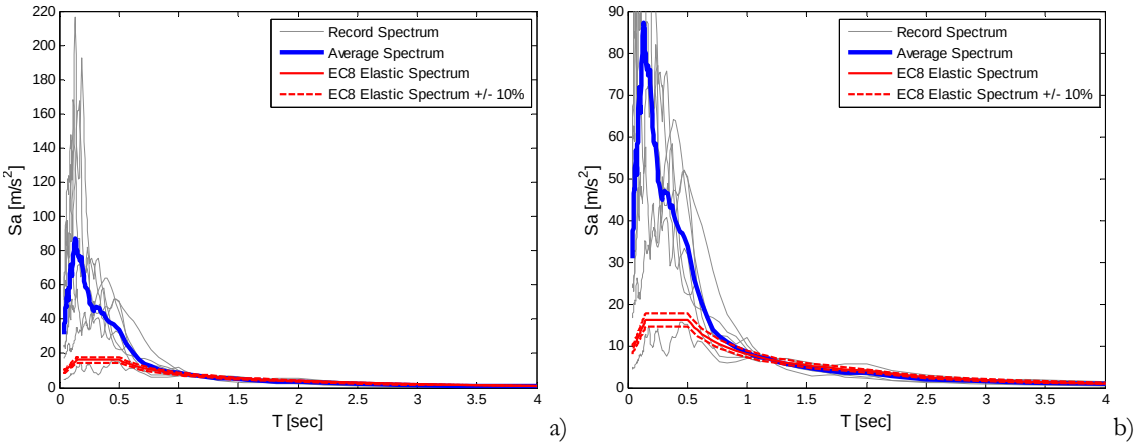

Figure 3.11. Response spectra of the $S_a(T_{inel})$ scaled records for the limit state of NC and frame *TF2*, their average spectrum and the EC8-1 elastic response spectrum +/- 10% (a); larger view (b).

Observation of these figures shows that the artificial accelerograms and the ReLUIS records meet the EC8-3 specifications in terms of spectrum matching, while the real ground motions scaled using the PGA do not. Nonetheless, when scaling is performed with the $S_a(T_1)$, the response spectra of the real ground motions is less distant from the code spectrum, especially for the case of frame *TF2*. For the cases where scaling is performed using the $S_a(T_{inel})$, the response spectra of the real ground motions can be seen to be less distant from the code spectrum in the region of the longer periods while increasing the referred distance in the region of T_1. By comparing the response spectra of the several record sets, it can be seen that records of the third to the fifth sets are not expected to lead to demand distributions that closely match those of the artificial and the ReLUIS accelerograms. Although the spectral differences are evident, it is considered that all the ground motion sets have a common seismic intensity. This consideration comes from the fact that all sets were defined, by using different scaling and spectral matching

approaches, to be compatible with the return period of a given limit state. Hence, a comparison between the demand of sets 1 and 2 with that of sets 3 to 5 is instructive in order to observe the significance of the demand differences and to determine if simpler ground motion selection criteria could be considered for seismic safety assessment in the context of EC8-3. From a global observation of Figs. 3.5 to 3.11, the following can be concluded:

- The ReLUIS set of ground motions is expected to produce demand distributions with a good agreement with those obtained when using the artificial accelerograms for the several limit states;
- The PGA based scaled records are expected to underestimate considerably the demand obtained by the artificial accelerograms;
- The $S_a\left(T_1\right)$ based scaled ground motions are expected to lead to a demand distribution that is closer to that of the artificial and of the ReLUIS accelerograms for the limit state of DL, while presenting larger differences for the limit states of SD and NC;
- The $S_a\left(T_{inel}\right)$ based scaled ground motions are expected to lead to a demand distribution that is closer to that of the artificial and of the ReLUIS accelerograms for the limit states of SD and NC.

3.2.3 Capacity models for the selected limit states

Although the capacity models proposed by EC8-3 for the selected limit states have been previously addressed in Chapter 2, they are nonetheless referred in the following for completeness. As stated in Chapter 2, EC8-3 defines member-level capacities for ductile and brittle mechanisms to be used in the safety assessment verifications for the several limit states. Ductile capacities are defined in terms of the admissible DL, SD and NC member chord-rotations while brittle capacities are characterized by the admissible NC shear force.

The NC chord-rotation capacity θ_{NC} was defined by the expression (EC8-3, 2005):

$$\theta_{NC}=\frac{1}{\gamma_{el}}\cdot 0.016\cdot 0.3^{\upsilon}\cdot\left(\frac{\max\left(0.01,\omega'\right)}{\max\left(0.01,\omega\right)}f_c\right)^{0.2}\cdot\left(\frac{L_s}{h}\right)^{0.35}\cdot 25^{\alpha\cdot\rho_{sx}\cdot\frac{f_{yw}}{f_c}}\cdot 1.25^{100\rho_d} \qquad (3.2)$$

where γ_{el} is 1.5 for primary members, υ is the normalized axial force, ω and ω' are the mechanical reinforcement ratios of the tension and compression, respectively, longitudinal reinforcement, f_c is the estimated value of the concrete compressive strength, f_{yw} is the estimated stirrup yield strength, L_s is the shear span taken constant and equal to half of

the member length, h is the section depth, ρ_{sx} is the ratio of transverse steel area A_{sx} parallel to the direction of loading, ρ_d is the steel ratio of diagonal reinforcement (if any) in each diagonal direction and α is the confinement effectiveness factor (EC8-3, 2005).

As stated in EC8-3, the SD chord-rotation capacity θ_{SD} is defined as 75% of θ_{NC}. In the case of the DL chord-rotation capacity θ_{DL}, and assuming that no shear cracking is expected to precede flexural yielding, the chosen expression is (EC8-3, 2005):

$$\theta_{DL} = \phi_y \cdot \frac{L_s}{3} + 0.0013 \cdot \left(1 + 1.5\frac{h}{L_s}\right) + 0.13 \cdot \phi_y \cdot \frac{d_b \cdot f_y}{\sqrt{f_c}} \tag{3.3}$$

in which ϕ_y is the yield curvature of the section, d_b is the mean diameter of the tension reinforcement and f_y is the estimated longitudinal reinforcement yield strength. Due to the asymmetry of longitudinal reinforcement of the beams, their chord rotation capacities are computed for both bending signs.

According to EC8-3, the NC shear force capacity V_{NC} is defined by (EC8-3, 2005):

$$V_{NC} = \frac{1}{\gamma_{el}}\left[\frac{h-x}{2 \cdot L_s} \cdot \min\left(N; 0.55 \cdot A_c \cdot f_c\right) + \left(1 + 0.05 \cdot \min\left(5; \mu_\Delta^{pl}\right)\right) \cdot \right.$$
$$\left. \cdot \left[0.16 \cdot \max\left(0.5; 100 \cdot \rho_{tot}\right) \cdot \left(1 - 0.16 \cdot \min\left(5; \frac{L_s}{h}\right)\right) \cdot \sqrt{f_c} \cdot A_c + V_w\right]\right] \tag{3.4}$$

where A_c is the cross section area taken as $b_w d$ (d is the structural depth), N is the axial load (equal to zero for tension), μ_Δ^{pl} is the ratio between the plastic part of the chord rotation demand and the yield chord rotation given by Eq. (3.3), ρ_{tot} is the total reinforcement ratio and V_w is the contribution of transverse reinforcement to shear resistance obtained by (EC8-3, 2005):

$$V_w = \rho_w \cdot b_w \cdot z \cdot f_{ywe} \tag{3.5}$$

in which ρ_w is the transverse reinforcement ratio and z is the length of the internal lever arm. With respect to Eq. (3.4), it should be noted that N is taken as the member axial force under gravity loads, as suggested by Mpampatsikos *et al.* (2008a), and the term $h - x$ represents the distance between the member compression centres and is assumed to be equal to *2h/3*.

3.3 Additional data for the probabilistic assessment

The probabilistic safety assessment of the selected structures was carried out to obtain the fragility values corresponding to the deterministically assessed safety levels, as previously referred. These fragility values were computed using nonlinear dynamic analysis

results only and seismic demand was considered to be defined by the same groups of accelerograms used in the deterministic assessment. Five groups of results were therefore obtained for each limit state and for each KL: results obtained using artificial spectrum-compatible accelerograms, using real ground motion records scaled for the PGA, using real ground motion records scaled for the 5% damping $S_a(T_1)$, using real ground motion records scaled for the 5% damping $S_a(T_{inel})$ and for the ReLUIS set. Based on these results, the probabilistic demand estimation due to record-to-record variability was assumed to be well represented by lognormal distribution functions fitted to the demand values of each limit state and KL using the maximum likelihood estimation method.

To illustrate the adequacy of the fitting process, Figs. 3.12a) and c) present, for the $C1_{bot}$ and $V1_{left}$ control sections of frame *TF2*, the empirical cumulative distribution functions (CDFs) of the chord rotation demand for the DL, SD and NC ground motion intensity levels when using real ground motion records scaled for the 5% damping $S_a(T_1)$ and the corresponding lognormal fitted CDFs. For the latter section, chord rotation demand for both bending signs is presented (the "+" and "-" represent chord rotation with tension in the bottom and top reinforcement, respectively), while for the former, chord rotation demand is the maximum of both bending signs. Additionally, Figs. 3.12b) and d) present the same data for the same control sections now for the case where demand is obtained from artificial spectrum-compatible accelerograms. For the same control sections and also for the case where demand is obtained from the real ground motion records scaled for the 5% damping $S_a(T_1)$, Fig. 3.13 presents the empirical CDFs of the maximum shear force demand for the NC ground motion intensity level and the corresponding lognormal fitted CDFs. From the results, and given the small size of the demand datasets, the lognormal CDFs can be seen to provide a reasonable fit to the demand data. As expected, the 5% damping $S_a(T_1)$ scaled real records were also seen to yield chord rotation demand distributions with larger variability than the artificial records. Moreover, this effect was also seen to be more important as the ground motion intensity increases, i.e. as the nonlinear behaviour of the structures becomes more pronounced. In terms of shear force demand, the influence of the type of record is seen to be less evident.

Randomness of the material properties was not considered in the probabilistic characterization of the demand. However, randomness of the concrete compressive strength and of the yield steel strength was considered for the definition of the probabilistic distributions of the limit state capacities. Assuming that these properties follow normal distributions with a given mean μ and coefficient of variation (*CoV*), the following values were set for both structures based on the proposals by Dymiotis *et al.* (1999):

- Concrete compressive strength f_c: mean $\mu_{f_c} = 28\ MPa$ and $CoV_{f_c} = 0.18$
- Yield steel strength f_y (assuming f_{yw} equal to f_y): $\mu_{f_y} = 440\ MPa$ and $CoV_{f_y} = 0.06$

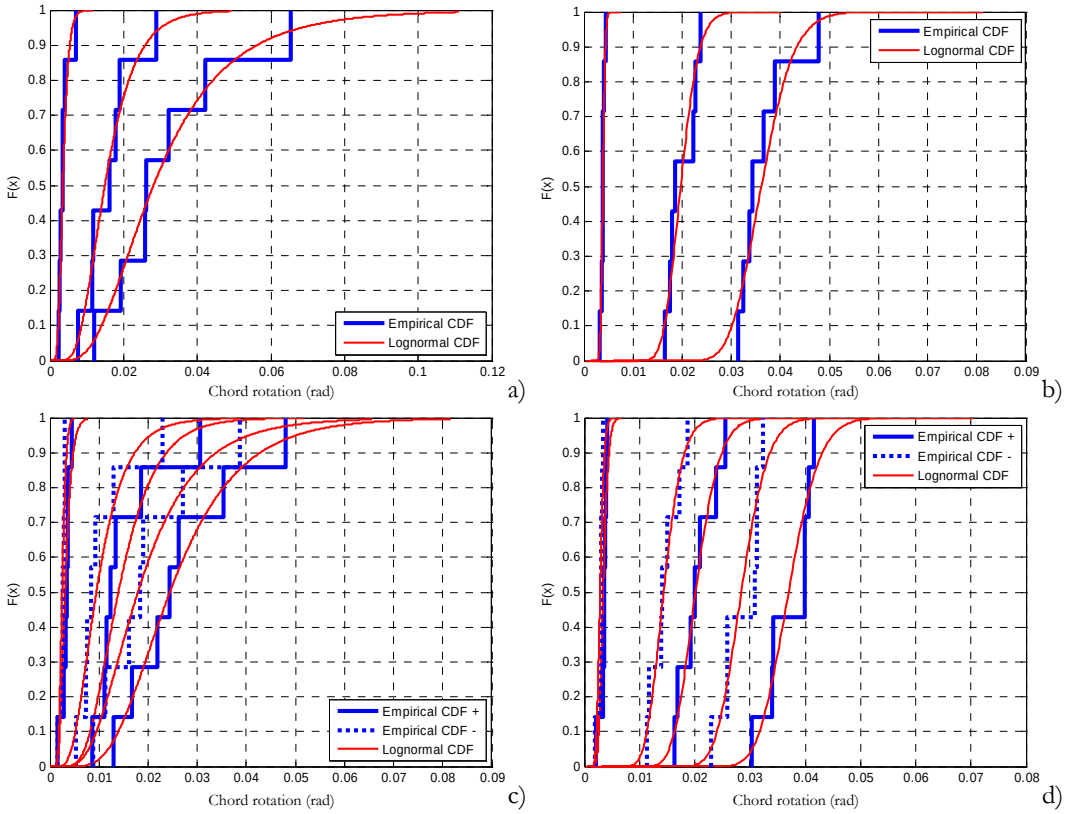

Figure 3.12. Empirical and fitted distribution functions of the chord rotation demand for the DL, SD and NC ground motion intensity levels of frame *TF2* at section $C1_{bot}$ when using real ground motion records scaled for the 5% damping $S_a(T_1)$ (a) and when using artificial records (b), and at $V1_{left}$ when using real ground motion records scaled for the 5% damping $S_a(T_1)$ (c) and when using artificial records (d).

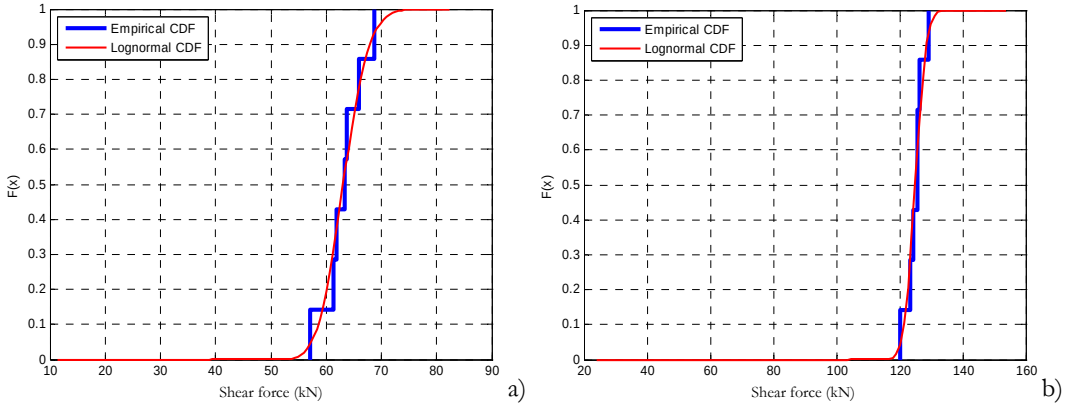

Figure 3.13. Empirical and fitted distribution functions of the shear force demand for the NC ground motion intensity level when using real ground motion records scaled for the 5% damping $S_a(T_1)$ at the $C1_{bot}$ (a) and $V1_{left}$ (b) control sections of frame *TF2*.

Considering the capacity models previously presented, limit state capacities were simulated for each KL using 200 values of the material properties f_c and f_y sampled from their probabilistic distributions and combined using the Latin Hypercube sampling scheme proposed by Iman and Conover (1982). Normal and lognormal distribution functions were

then fitted using the maximum likelihood estimation method. In order to illustrate the adequacy of the fitting process, Fig. 3.14 presents the empirical CDFs of capacities θ_{NC}, θ_{DL} and V_{NC} for the $C1_{bot}$ control section of frame *TF1* (assuming KL3), along with the corresponding normal and lognormal fitted CDFs. As can be observed, both distributions adequately fit the computed capacities of the several limit states. Globally, the DL, NC and shear force capacities were seen to exhibit maximum CoV values lower than 9%, 7% and 7%, respectively.

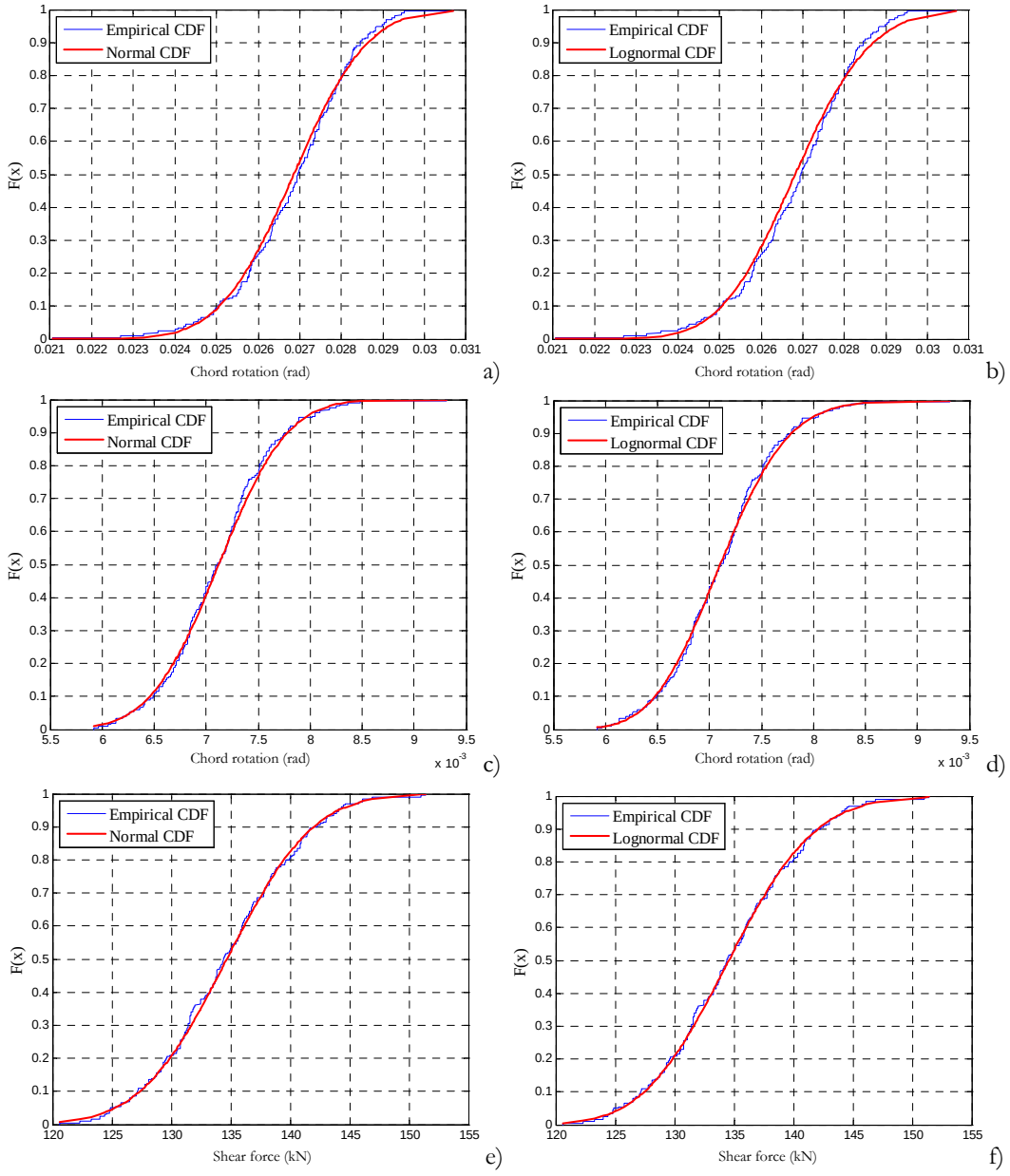

Figure 3.14. Empirical and fitted distribution functions for capacity θ_{NC} assuming a normal (a) and a lognormal distribution (b), for capacity θ_{DL} assuming a normal (c) and a lognormal distribution (d), for capacity V_{NC} assuming a normal (e) and a lognormal distribution (f) for the $C1_{bot}$ section of frame *TF1*.

3.4 Seismic safety assessment results from the deterministic approaches

The seismic safety assessment results obtained from the different deterministic approaches, which involve different methods of analysis (linear, pushover and nonlinear dynamic using different types of ground motions), different limit states and different KLs are presented in the following. For a given control section *i*, results are expressed in terms of D_i/C_i ratios where a value below or equal to 1.0 represents a safe situation, and an unsafe situation otherwise. The presentation of the results is initially divided according to the method of analysis and ends with a comparative assessment of the different approaches. For conciseness sake, only a few sample figures of the results are presented herein. In these figures, the chord rotation limit states of DL, SD and NC are simply termed DL, SD and NC while the shear force limit state of NC is simply termed V.

With respect to the beam results, it is noted that, for a given section, the presented value corresponds to the maximum D/C ratio obtained from the two bending signs. It is also referred that, given some of the choices made for the parameters entering the deformation capacity expressions previously presented (when needed, N is the member axial force under gravity loads and the shear span is taken equal to half of the member length) the member deformation capacities are independent of the demand. In the case of the shear force capacity, μ_Δ^{pl} is the only demand dependent parameter. However, its evaluation for each control section is only performed for the cases where demand comes from pushover analysis and nonlinear dynamic analysis using artificial accelerograms. For the remaining cases where demand is obtained from nonlinear dynamic analysis, μ_Δ^{pl} is the same as for the latter case to allow for a simpler comparison of the various D/C results.

3.4.1 Results from the linear analyses

As formerly referred, for linear analysis to be applicable, bending moment demand to capacity ratios ρ must be sufficiently uniform across the primary elements of the structure where plastic hinges are expected to form. According to EC8-3, this condition is met if the ratio ρ_{max}/ρ_{min} does not exceed a value in the range of 2 to 3 (considering only values $\rho \geq 1$), for which EC8-3 suggests the value of 2.5 that is also considered herein. As defined by EC8-3, the identification of the relevant ρ values, i.e. those referring to sections where plastic hinges are expected to develop, must be carried out by comparing the sum of the columns flexural capacities framing into a given joint with the corresponding beam flexural capacities. Depending on the structure, this task can be a complex one since it requires the analyst to evaluate the flexural equilibrium of each joint, in order to identify the critical

sections. Although leading to conservative results, a simplified approach can be defined to avoid the lengthy joint analysis that requires the evaluation of the ρ_{max}/ρ_{min} ratio across all primary elements of the structure where $\rho \geq 1$. In this situation, the ρ_{max} is still adequately evaluated while the ρ_{min} is assumed to be the lowest value of $\rho \geq 1$. In this approach, ρ_{min} can be considerably lower, hence yielding an overall larger value of ρ_{max}/ρ_{min}. Table 3.1 presents the ρ ratios of the control sections of the *TF1* and *TF2* frames for the three considered limit states and for a right-to-left lateral force pattern (the left-to-right pattern leads to similar ratios) and the ρ_{max}/ρ_{min} obtained for each limit state and for both approaches. The ρ_{max}/ρ_{min} ratio of the simplified approach is termed ρ_{max}/ρ_{min} *. The relevant ρ values according to the EC8-3 criterion are identified in bold.

Table 3.1. ρ ratios of the control sections of the *TF1* and *TF2* frames for the three considered limit states and corresponding ρ_{max}/ρ_{min} of each limit state, for both the EC8-3 and the simplified approaches.

	TF1			TF2		
	DL	SD	NC	DL	SD	NC
C1 bot	**2.0**	**4.3**	**6.4**	**2.2**	**6.2**	**9.4**
C1 top	0.7	1.8	2.7	**2.1**	**4.9**	**7.5**
C2 bot	1.4	3.1	4.4	**2.1**	**5.3**	**8.0**
C2 top	1.4	3.0	4.4	**2.2**	**5.5**	**8.2**
C3 bot	0.9	2.0	2.9	**1.7**	**4.1**	**5.9**
C3 top	1.4	2.9	4.1	**1.8**	**4.5**	**6.6**
C4 bot	0.5	0.9	1.2	**1.0**	**2.2**	**3.1**
C4 top	**1.1**	**2.0**	**2.8**	**1.1**	**2.8**	**4.0**
V1 left	**2.0**	**4.7**	**6.8**	1.9	4.2	6.1
V1 right	**3.1**	**8.8**	**13.1**	**3.6**	**8.1**	**12.0**
V2 left	**2.1**	**4.6**	**6.7**	1.6	3.7	5.3
V2 right	**3.2**	**8.6**	**12.8**	**2.9**	**6.8**	**10.2**
V3 left	**1.6**	**3.3**	**4.6**	1.1	2.4	3.5
V3 right	**2.0**	**5.6**	**8.5**	**1.7**	**4.1**	**6.2**
V4 left	0.9	1.7	2.3	0.4	1.0	1.3
V4 right	**0.8**	**2.5**	**3.9**	0.5	1.4	2.2
C5 bot	**1.8**	**4.2**	**6.2**	**2.1**	**5.9**	**9.2**
C5 top	0.4	1.6	2.4	1.8	4.5	7.0
C6 bot	1.0	2.7	4.1	1.7	4.7	7.3
C6 top	1.0	2.7	4.1	1.8	4.8	7.5
C7 bot	0.6	1.7	2.6	1.3	3.4	5.3
C7 top	1.0	2.5	3.8	1.4	3.9	6.0
C8 bot	0.0	0.5	0.8	0.6	1.4	2.3
C8 top	0.5	1.4	2.3	**0.7**	**1.9**	**3.1**
ρ_{max}/ρ_{min}	2.9	4.4	4.7	3.6	4.3	3.9
ρ_{max}/ρ_{min} *	3.2	6.3	10.9	3.6	8.1	9.2

As can be seen, results indicate that, for all the limit states, both frames fail to meet the ρ_{max}/ρ_{min} criterion, considering both approaches. Therefore, linear analysis is not considered to assess the safety of these structures. Even though the EC8-3 and the simplified approaches yield the same end result, i.e. linear analysis is not applicable, the comparison of the ρ_{max}/ρ_{min} ratios obtained by both methods leads to conclude that the simplified approach can yield results of increasing conservativeness as the limit state intensity increases. Nonetheless, for the limit state of DL, the simplified approach might be acceptable.

Considering that these two approaches represent two extreme situations in terms of application complexity, a more practical verification methodology that leads to the results of the EC8-3 approach and that allows for a reduction on the number of joints that need to be analysed can be defined according to the following steps:

- After establishing the admissible ratio ρ_{max}/ρ_{min} , termed η, determine the value of ρ_{max} among the sections of the primary elements;
- Compute the minimum admissible value of ρ_{min} that verifies η, $\rho_{min,adm}$, given by ρ_{max}/η;
- Among the primary elements, search for the section with the highest ρ value that is greater or equal to 1.0 and does not exceed $\rho_{min,adm}$, termed ρ^*_{min}, and determine if it is a section where a plastic hinge is expected to develop. If such section is expected to develop a plastic hinge, it can be concluded that linear analysis is not applicable;
- If a plastic hinge is not expected to develop at that section, the value of $\rho_{min,adm}$ is updated to ρ^*_{min} and the previous step is repeated. If there are no more sections to repeat the previous step, it can be concluded that linear analysis is applicable.

3.4.2 Results from the pushover analyses

As previously stated, pushover analysis of the frames was performed for two lateral force patterns, each one applied in two directions: left-to-right and right-to-left. For each pattern target displacements were determined for the several limit states according to the previously mentioned iterative procedure defined in EC8-1. The results presented in the following for a given limit state and KL, expressed in terms of D/C ratios, correspond to the most unfavourable results between the several patterns and loading directions.

Figure 3.15a) presents the D/C results for the control sections of frame *TF1* for the three chord rotation limit states and considering KL3 while Fig. 3.15b) presents the D/C results only for the NC chord rotation limit state but considering the three KLs. In addition, Fig. 3.16a) presents the D/C results for the control sections of frame *TF2* for the three chord rotation limit states and considering KL3 while Fig 3.16b) presents the D/C results only for the NC shear force limit states but considering the three KLs. Observation of the D/C results confirms that frame *TF2* is more vulnerable than frame *TF1* due to its higher flexibility, which was induced by changing the orientation of the columns. This increase in vulnerability has more practical implications for the limit state of DL since almost every element of *TF2* is now unsafe. Moreover, for the limit states of SD and NC, the increase of the D/C values from *TF1* to *TF2* can be seen to be in the range of 50% to 100%. It can also be seen that the influence of the KL is considerably different for chord rotation and shear force capacities, the latter being more sensitive to the different KLs. Finally, the results also indicate that DL seems to be the dominant deformation limit state for the two frames. A similar conclusion was also noted by Mpampatsikos *et al.* (2008b) which also refer that considering the previously defined equivalent secant-to-yield stiffness for the limit state of DL may lead to a significant underestimation of the global stiffness and, therefore, to a considerable overestimation of the D/C ratios.

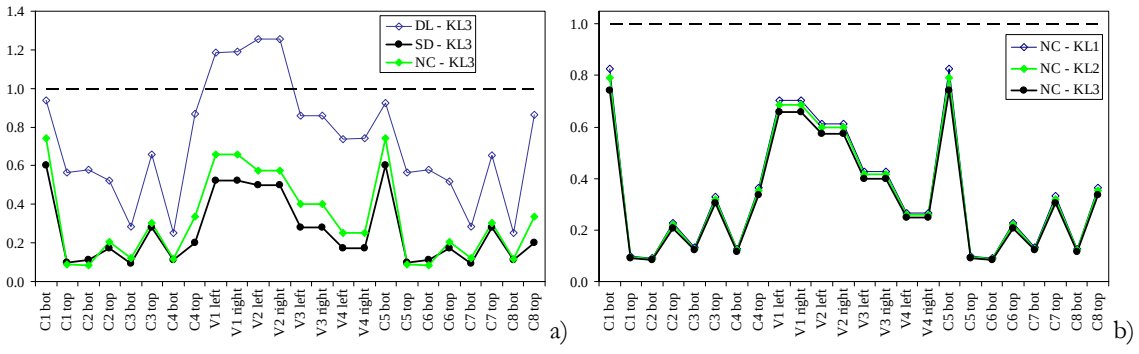

Figure 3.15. Safety assessment results of frame *TF1* considering pushover analysis, for the three chord rotation limit states and KL3 (a) and for the NC chord rotation limit state considering three KLs (b).

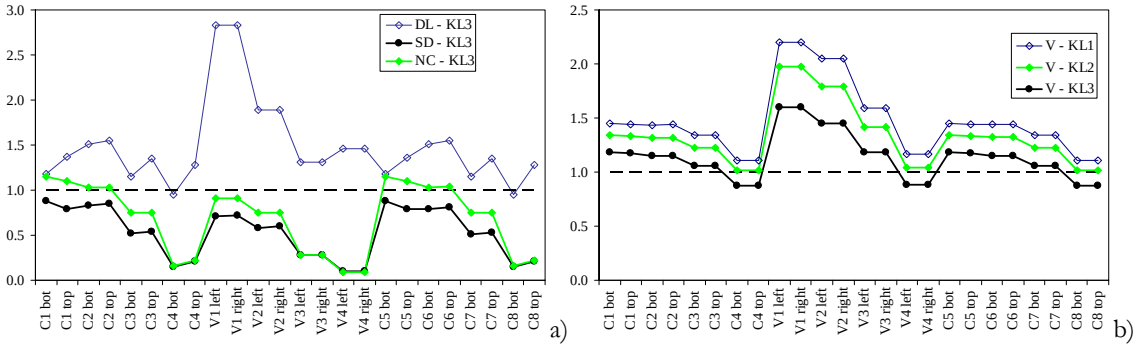

Figure 3.16. Safety assessment results of frame *TF2* considering pushover analysis, for the three chord rotation limit states and KL3 (a) and for the NC shear force limit state considering three KLs (b).

3.4.3 Results from the nonlinear dynamic analyses

Results presented in the following intend to provide a general overview of the effect of the type of accelerogram used for nonlinear dynamic analysis on the safety assessment results. Since seven ground motions were considered in all five sets of accelerograms, the demand values considered for the D/C ratios presented herein are mean values over the seven results obtained for each set of ground motions. When presenting results obtained from records scaled for $S_a(T_1)$, these are termed *Sa scaled*, while results obtained from records scaled for $S_a(T_{inel})$ are termed *Sa scaled - Tinel*. Moreover, it is recalled that results for the *Sa scaled - Tinel* set of records are only presented for the SD and NC limit states.

To illustrate the overall findings, Fig. 3.17 presents the D/C results for the control sections of frame *TF1* considering the different sets of accelerograms for the DL and SD chord rotation limit states and considering KL3. Figure 3.18 presents the same type of results for the control sections of frame *TF2*, now for the DL and NC chord rotation limit states. Figure 3.19 presents the results for the shear force NC limit state for frames *TF1* and *TF2* considering the different sets of accelerograms. Observation of these results confirms that the type of accelerogram has a significant influence on the safety assessment results. Still, such influence depends on the type of limit state, i.e. deformation- or strength-based, and on the structure. Namely, the influence of the different sets of accelerograms is larger for deformation-related D/C results, especially for frame *TF1*. As referred in Section 3.2.2.2, such differences are a direct result of the differences observed between the response spectra of the records and the code spectrum.

In general, it can be seen that the deformation demand based on the ReLUIS set has a very good agreement with the demand obtained from artificial accelerograms (which is considered as the reference seismic demand since the records match the code spectrum very closely). On the contrary, when using PGA scaled records, the corresponding demand is, in general, the one with less agreement with the reference demand. For the demand obtained from *Sa scaled* and *Sa scaled - Tinel* records, the agreement with the reference demand is seen to be variable. On average, the demand resulting from the *Sa scaled* set exhibits a better agreement with the reference demand for the lower intensity limit states. On the other hand, the demand resulting from the *Sa scaled - Tinel* set is likely to be closer to the reference demand of larger intensity limit states, with a tendency to overestimate it. For the shear force limit state, the assessment results are seen to be less sensitive to the record type as the D/C values are much closer. Still, the demand resulting from records scaled for PGA is also the one exhibiting less agreement with the reference demand.

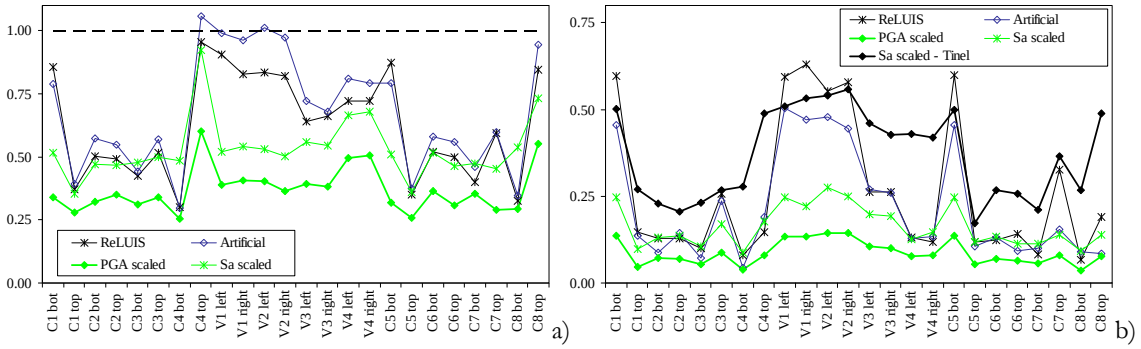

Figure 3.17. Safety assessment results of frame *TF1* considering different accelerogram sets, for the DL chord rotation limit state and KL3 (a) and for the SD chord rotation limit state and KL3 (b).

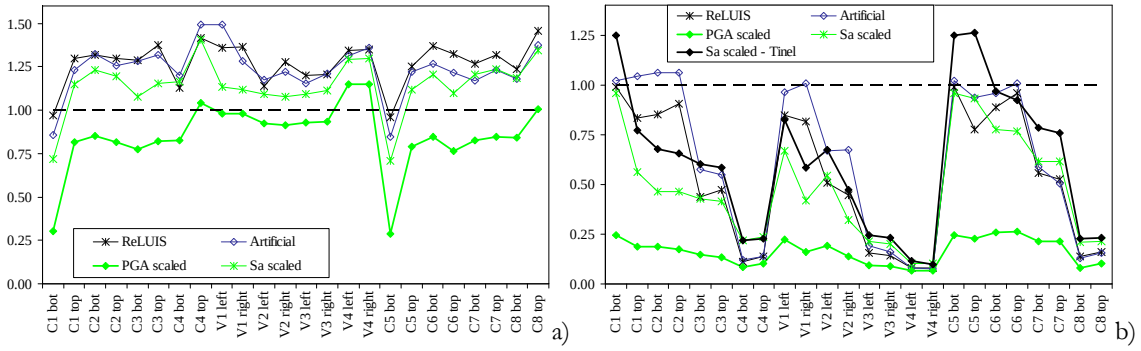

Figure 3.18. Safety assessment results of frame *TF2* considering different accelerogram sets, for the DL chord rotation limit state and KL3 (a) and for the NC chord rotation limit state and KL3 (b).

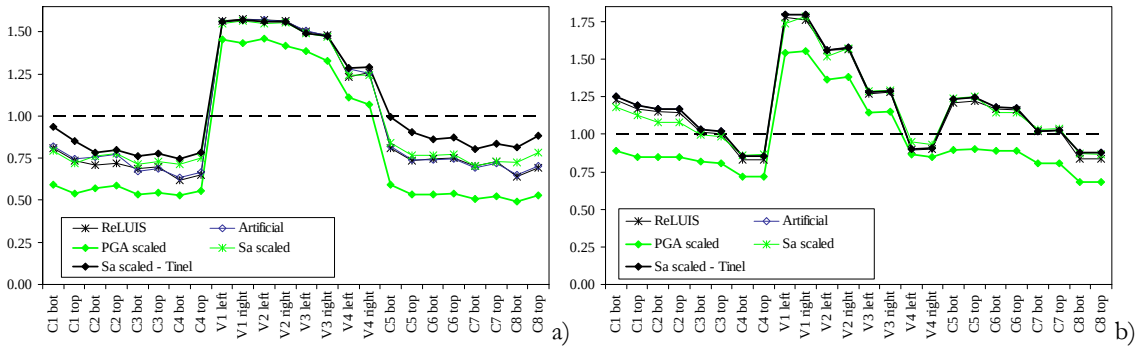

Figure 3.19. Safety assessment results of frame *TF1* (a) and frame *TF2* (b) considering different accelerogram sets, for the shear force NC limit state and KL3.

3.4.4 Comparative assessment of the different approaches

Since linear analysis assessment results are not available, comparison of results can only be performed for those obtained from nonlinear analysis. Given the added complexity of nonlinear dynamic analysis when compared to its static counterpart, this comparative evaluation aims fundamentally to verify if similar assessment results are obtained by both approaches, thus validating the use of pushover analysis.

Comparison between pushover analysis and nonlinear dynamic analysis results can be carried out by comparing results presented in Figs. 3.15 and 3.16 with those presented in Figs. 3.17 to 3.19 for the artificial and ReLUIS records. As expected, observation of these results leads to conclude that for deformation based limit states, correlation between pushover and nonlinear dynamic analysis results is best when considering artificial accelerograms. Nonetheless, there are some noticeable differences for the lower seismic intensity such as that of the DL limit state, namely for the beams of frame *TF2*. In terms of the shear force limit state, the agreement between dynamic and pushover results is much better. In the overall, it can be seen that, for the presented structures, pushover analysis leads to adequate safety assessment results.

With respect to the nonlinear dynamic analysis demand results, a further insight on the importance of its variability should be noted. When using real ground motion records, an inherent larger record-to-record variability of the results is usually expected, irrespective of the agreement between their average response spectrum and the code spectrum. The demand variability is known to be considerably affected by the seismic intensity level under consideration and it is generally agreed that such variability increases as the seismic intensity level also increases (Pinto *et al.*, 2004). However, for a seismic intensity that may result in demand values close to the yield limit of the members (e.g. the DL intensity), some ground motions might generate demand values much lower than the yield limit as others might produce values that are much larger (namely due to the changes in the element stiffness). When using the minimum number of records allowed by EC8-1, some care is required for the analysis of the demand as the variability of the demand might lead to an overestimation or an underestimation of the true average demand. Hence, the consideration of the mean value of the response in such cases may lead to unsafe demand estimations since the mean is a poor estimator of the central tendency of the demand, mainly due to its high sensitivity to demand distributions exhibiting larger variability (Hoaglin *et al.*, 1983).

To assess this effect for the present structures, a comparison is made between the D/C ratios obtained using the median as an estimator of the central tendency of the demand, which is known to be much less sensitive to the variability of the data (Hoaglin *et al.*, 1983) and those obtained by using mean demand. This comparison leads to conclude that when using artificial accelerograms, the demand distribution can be expected to have a lower variability than in any other situation for larger seismic intensity levels. On the other hand, when using real ground motion records or when analyzing the DL intensity level, there is no definite trend in the expected variability. It can be rather low, such as for the cases presented in Fig. 3.20, or much larger, as for those presented in Fig. 3.21. Moreover, from these results, it can also be seen that this variability can either lead to mean estimates that are larger or lower than the median estimates.

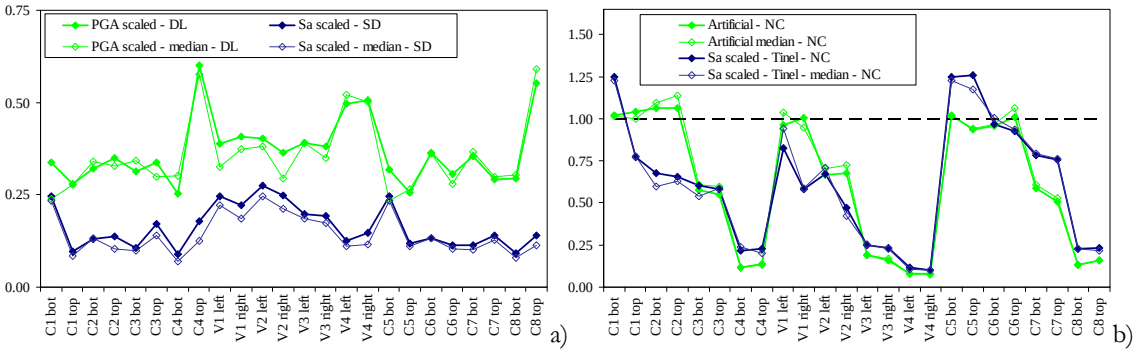

Figure 3.20. Examples of good agreement between safety assessment results considering mean and median demand obtained from different accelerogram sets, different limit states and KL3, for frame *TF1* (a) and for frame *TF2* (b).

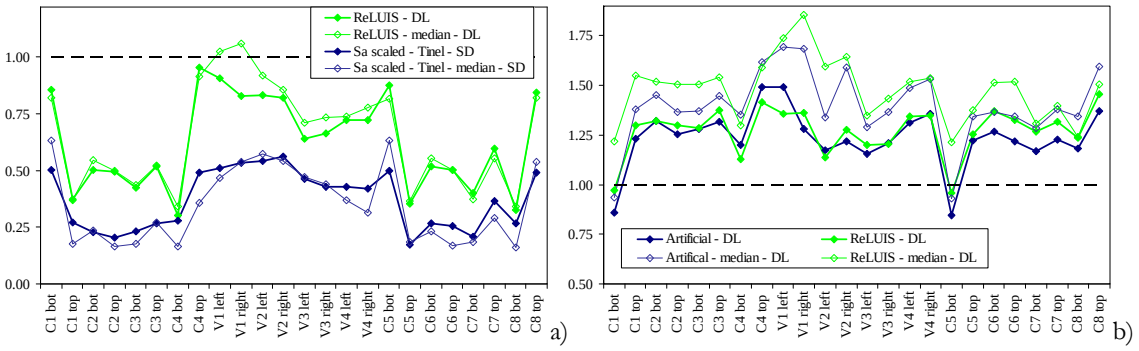

Figure 3.21. Examples of poor agreement between safety assessment results considering mean and median demand obtained from different accelerogram sets, different limit states and KL3, for frame *TF1* (a) and for frame *TF2* (b).

Finally, a brief comment is made with respect to the influence of the KL in the assessment results. Given the assumptions presented in Section 3.2 regarding the KL conditions (i.e. the sample mean value of the material properties is considered to be the same for the three KLs) and that demand is based on the analysis results for both nonlinear analysis methods, the effect of the KL is only felt on the capacity side. After evaluating the several limit state capacities for the different KLs and for all the members of both frames, and averaging the increase in capacity that is gained by moving from one KL to another, the values presented in Table 3.2 were obtained. These allow for a global view of the influence of the KL and reveal that, from a practical point of view, going from KL1 to KL2 or from KL2 to KL3 produces changes that vary according to the considered limit state. While for the case of the deformation-based SD and NC capacity values these changes are small, for the case of the DL and the shear force capacities the variations can be significant in some situations. Similar conclusions were drawn by Chrysostomou (2005) for the SD, NC and shear force limit state capacities. By analysing the ratios between the Confidence Factors of KL1 and KL2, of KL2 and KL3, and of KL1 and KL3, which are, respectively, 1.125, 1.20 and 1.35 and represent the direct increase of the material properties for the assumptions of this analysis, the increase of the DL and shear force

capacities presented in Table 3.2 can be seen to reflect a significant part of the referred ratios. More specifically, the DL capacity is seen to be considerably dependent on the value of f_y while the shear force capacity depends on both f_c and f_y. On the other hand, the SD and NC capacities are only marginally affected by the values of f_c and f_y. From this analysis it can be inferred that, depending on the selected limit state and from the material characterization point of view, the need for an increase in knowledge about their properties must be carefully thought out due to the increase in work, costs and on-site difficulties that may be implied.

Table 3.2. Average increase in the capacity of the several limit states by increasing the KL.

	DL	SD	NC	V
KL1 to KL2	8%	3%	3%	10%
KL2 to KL3	14%	5%	5%	17%
KL1 to KL3	24%	9%	9%	29%

3.5 Seismic safety assessment results from the probabilistic approach

Since a direct comparison between the previously presented deterministic results and the probabilistic ones is not possible, the purpose of this analysis is to assess if similar D/C ratios lead to similar fragility values. Based on these results, an attempt was also made to define a correlation between D/C ratios and the expected fragility values.

A numerical simulation method such as the multi-stripe analysis approach proposed by Jalayer and Cornell (2009) can be considered to obtain a fragility curve. Since the current analysis only requires the computation of a single fragility value for each limit state, the corresponding demand distribution is that of the stripe having a seismic intensity measure in agreement with the return period associated to the limit state. As referred in Section 3.3, the considered probabilistic demand distributions are those obtained from nonlinear dynamic analysis for the artificial and the ReLUIS records. The probabilistic distributions for the limit state capacities are those also referred in Section 3.3. The presented fragility values were computed using the fitted lognormal limit state capacity distributions referred in Section 3.3. Negligible differences were obtained when considering the normal capacity distributions. Fragility values for each control section, limit state and KL combination were obtained by standard demand-capacity convolution. With respect to the demand-capacity dependence, assumptions similar to those referred in Section 3.4 were considered for the probabilistic analysis. Hence, demand and capacity are assumed to be independent and results are not expected to be significantly affected by such considerations (Mpampatsikos *et al*, 2008a). It is noted that parameter μ_{Δ}^{pl} entering the shear force capacity is considered

with the same value obtained for the deterministic assessment based on nonlinear dynamic analysis using the artificial accelerograms.

For conciseness sake, Figs. 3.22 and 3.23 only present a sample of the results that were considered for comparison. Figure 3.22 shows the comparison between fragility values and deterministic D/C ratios for the DL chord rotation and the NC shear force limit states of frame *TF1*, considering the three KLs and the artificial accelerograms. On the other hand, Fig. 3.23 shows the comparison between fragility values and deterministic D/C ratios for the SD and NC chord rotation limit states of frame *TF2*, considering the three KLs and the artificial accelerograms. For an easier comparison, values of the D/C ratios above *1.0* were set to *1.0* in both figures. The examination of the results obtained shows that similar D/C ratios may lead to different fragility values. This variability of the fragility values was found to depend on the limit state and on the type of demand (chord rotation or shear force). Nonetheless, the overall results allowed for the definition of estimated average ranges for the expected fragility values, given a set of ranges of the D/C ratios. These expected fragility ranges are presented in Table 3.3. Observation of these ranges shows that upper bounds of the fragility values can be defined for D/C ratios lower than *1.0*. Nonetheless, for a given D/C range, there is the possibility of obtaining a fragility value much lower than its corresponding upper bound given the referred variability of the fragility values for similar D/C ratios. Hence, these ranges also indicate that, as the D/C ratio increases, there is also an increase in the expected variability of the fragility values. Moreover, it is noted that the referred upper bounds were seen to be approximately constant across the different limit states. This observation is consistent with the possible underlying assumption that, conditional to a certain earthquake intensity, the seismic safety assessment according to the EC8-3 procedure should lead to a limit state exceedance probability that is similar for all limit states.

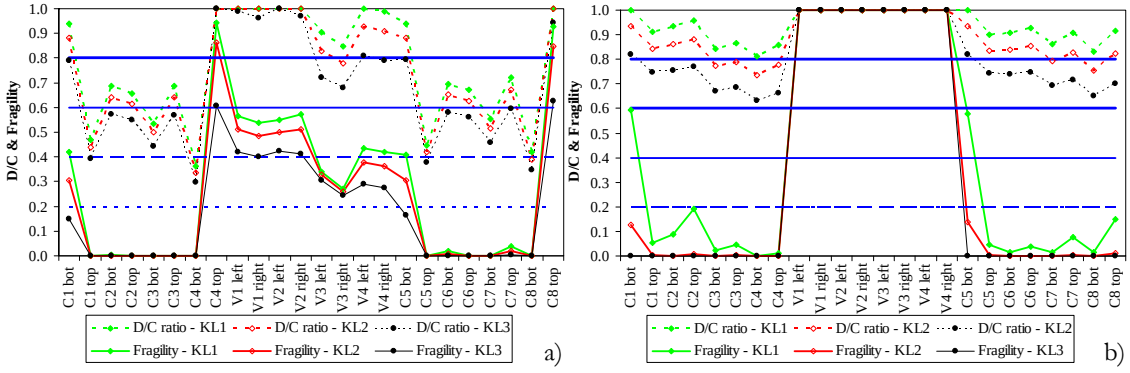

Figure 3.22. Fragility values *vs* deterministic D/C ratios for frame *TF1* considering the three KLs, artificial accelerograms, the DL chord rotation limit state (a) and the NC shear force limit state (b).

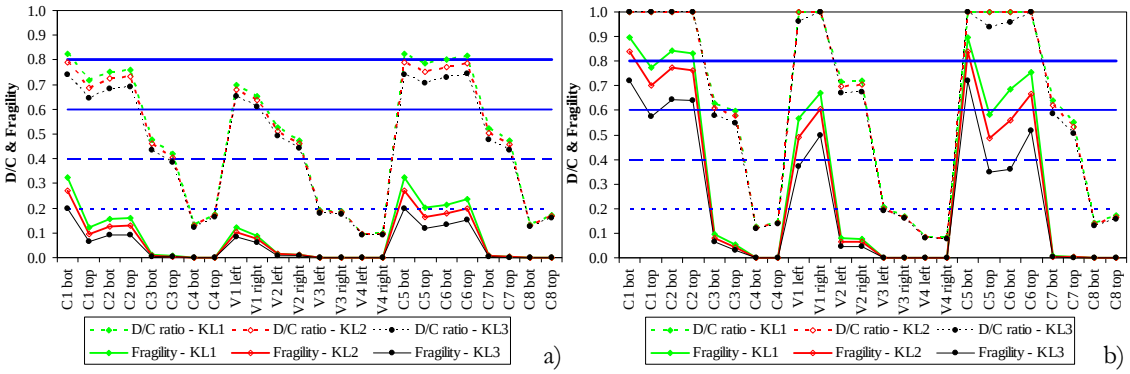

Figure 3.23. Fragility values *vs* deterministic D/C ratios for frame *TF2* considering the three KLs, artificial accelerograms, the SD chord rotation limit state (a) and the NC chord rotation limit state (b).

Table 3.3. Fragility estimated ranges based on deterministic D/C ranges.

D/C range	Fragility f range
$D/C < 0.2$	$f \approx 0$
$0.2 < D/C < 0.4$	$f < 5\%$
$0.4 < D/C < 0.6$	$f < 15\%$
$0.6 < D/C < 0.8$	$f < 30\%$
$0.8 < D/C < 1.0$	$f < 50\%$
D/C larger than 1.0	$f > 50\%$

Finally, it is emphasized that further application examples should be carried out in order to validate the presented probabilistic results, namely the expected fragility ranges of Table 3.3. Furthermore, a comprehensive discussion about the implications of such results will then be required to determine the potential implications in future revisions of the code procedures. As an example of matters to be examined, attention is brought to the upper bound of the fragility value corresponding to the D/C ratio of 1.0 which, for a certain limit state, indicates there is still a 50% safety margin against failure. The adequacy of this value should be examined within the scope of the general safety format of the EC8-3 procedure, namely in terms of its implications on the system-level safety.

3.6 Conclusions and final observations

An application of the EC8-3 seismic safety assessment procedure was presented and complemented by a probabilistic approach. The proposed application addressed the safety assessment of two RC one-bay-four-storeys planar frame structures of similar geometry. The seismic safety of the structures was assessed for both deformation and strength based limit states. For each limit state, the three EC8-3 KL conditions were also considered. The application of the EC8-3 procedures for each limit state and KL combination was performed using linear and nonlinear methods of analysis. In the latter case, both pushover

and dynamic analysis (using artificial and real records) were used, while in the former only the lateral force analysis was considered.

In terms of the admissibility of linear analysis, results of the selected structures showed that, for all the limit states, they failed to meet the ρ_{max}/ρ_{min} criterion. Therefore, linear analysis was not able to be considered for safety assessment of these structures. Similar difficulties were also referred by Pinto and Franchin (2008). The results of this analysis also indicated that, for structures where seismic design measures were not considered, the applicability of linear analysis might be restricted to the limit state of DL only. Nonetheless, by analysing the process that verifies if linear analysis is admissible, and accounting for the potential complexity of its application for larger structures, a more practical verification methodology was proposed.

From the results of the deterministic assessment based on nonlinear analyses it was possible to conclude that DL seems to be the dominant deformation limit state. A similar conclusion was also noted by Mpampatsikos *et al.* (2008b) which also refer that considering the equivalent secant-to-yield stiffness proposed by EC8-3 for the limit state of DL may lead to a significant overestimation of the D/C ratios. With respect to the results based on nonlinear dynamic analysis, these lead to conclude that the characteristics of the considered accelerograms have a considerable influence on the deformation assessment results. Such differences are a direct consequence of the differences observed between the response spectra of the records and the code spectrum. On the other hand, shear force assessment results can be seen to be much less sensitive to the record characteristics. By considering a set of real records having an average response spectrum that matches closely the code spectrum, the ReLUIS set, a good agreement is found between the mean demand obtained by such set and that obtained by using artificial accelerograms. To simulate a situation where a set of such real records is not available, different scaling procedures were tested for a set of real records chosen based on magnitude and distance criteria. Results indicated that demand obtained from PGA scaled records is, in general, the one with less agreement with that obtained by using artificial accelerograms, while demand obtained from *Sa scaled* records exhibits a better agreement with the reference demand for the lower intensity limit states. To improve the results for the SD and NC deformation limit states, an alternative scaling procedure based on a representative inelastic period was defined. This approach provided a better agreement with the results obtained when using the artificial and the ReLUIS accelerograms.

Demand variability and its importance on the estimation of the average demand were also addressed. It was observed that when using seven earthquake records as allowed by EC8-1, some care is required since the demand variability might lead to an underestimation (as well as to an overestimation) of the true average demand. Hence, the consideration of the mean value of the response in such cases may lead to unsafe demand estimations since the mean is a poor estimator of the central tendency of the data.

The comparative assessment between pushover and nonlinear dynamic analysis safety assessment results for the structures analysed leads to conclude that, with the exception of some control sections, pushover results can generally be seen to be on the safe side, when compared to the results of nonlinear dynamic analysis.

With respect to the influence of the KL in the assessment results, it was found that, from a practical point of view, going from KL1 to KL2 or from KL2 to KL3 produces changes that vary according to the considered limit state. While for the case of the deformation-based SD and NC capacity values these changes are small, for the case of the DL and the shear force capacities the variations can be significant in some situations. Hence, it can be inferred that, depending on the selected limit state and from the material characterization point of view, the need for an increase in knowledge about their properties must be carefully thought out due to the increase in work, costs and on-site difficulties that may be implied.

In terms of the probabilistic approach, the observation of the obtained fragility values for the several limit states and KLs leads to conclude that there is a considerable variability of the fragility values for similar deterministic D/C ratios. This variability was found to be dependent on the limit state and on the type of demand (chord rotation or shear force). Nonetheless, the overall results allowed for the definition of estimated ranges for the expected fragility values, given a set of ranges of the deterministic D/C ratios. The upper bounds of the fragility ranges were seen to be approximately constant across the several limit states. This observation is consistent with the possible underlying assumption that, conditional to a certain earthquake intensity, the seismic safety assessment according to the EC8-3 procedure should lead to a limit state exceedance probability that is similar for all limit states. Nonetheless, the adequacy of these values should be examined within the scope of the general safety format of the EC8-3 procedure, namely in terms of their implications on the system-level safety.

Although the results and conclusions presented herein are only based on the analysis of the selected structures, some aspects associated to the applicability of the EC8-3 procedures should be emphasized. For example, the application of linear analysis is expected to be difficult in many situations due to the EC8-3 severe conditions. With respect to the use of pushover analysis, results were seen to be generally on the safe side with respect to those of nonlinear dynamic analysis. Still, more applications should be carried out to determine if this conclusion can be extended to other structures. Furthermore, some aspects related to the limit state of DL should be the focus of additional research, namely aspects related to the influence of the modelling assumptions regarding the EC8-3 member stiffness and their implications on the safety of the members. Finally, although the importance of the material characterization in the seismic safety assessment context is clear, the adoption of higher KLs must be carefully thought out since, depending on the selected limit state, the practical consequences are limited.

Chapter 4
A probabilistic interpretation of the EC8-3 Confidence Factors for the characterization of material strength

4.1 Introduction

There are numerous differences between the design of a new structure according to structural design codes and the assessment of the same structure after many years in service (Melchers, 2001). Although the properties of an existing structure can be known to a certain extent, it should be noted that a number of uncertainties may arise from on-site inspection/testing and other procedures carried out to check the actual condition of the structure. For example, techniques for in-situ testing may be considered to be reasonably well developed but they involve measurement errors and the interpretation of the results may imply a considerable degree of uncertainty (Dimitri and Stewart, 2002). The consideration of several expert opinions on a specific matter is another possible source of uncertainty since opinions can vary considerably depending on the complexity of the problem at hand (Krinitzsky, 1993). In cases where important data have been lost, the need to estimate data values based on past experience or on the existence of similar structures also increases the uncertainty about the knowledge of the existing construction.

Whit respect to the assessment of the material properties of existing structures, these can be obtained with varying degrees of accuracy based on in-situ measurements. In order to deal with the uncertainty of those measurements, different degrees of knowledge are established by the codes, which reflect the type and quality of the gathered data, (EC8-3, 2005; OPCM 3431, 2005; ASCE, 2007; NTC, 2008). To reflect the referred levels of knowledge in a quantitative manner and to account for them in the assessment, penalty factors can be associated to those levels that will either reduce the "capacity" or increase the "demand". In this context, the present chapter addresses the evaluation of the referred penalty factors, which are termed Confidence Factors (CF), following the definition

proposed in EC8-3 (EC8-3, 2005). Although the values of the CFs to be used in a given country can be found in its National Annex, recommended values of the CFs are also proposed within the EC8-3 main document. Therefore, the present study assesses the reliability of those recommended values by establishing a probabilistic framework for their evaluation. Even though the general concept behind the consideration of CFs is independent of the type of structural material, their evaluation is presented herein for the case of reinforced concrete (RC) structures. Nonetheless, given the format of the proposed probabilistic approach, the validity of the CFs for other materials is also discussed based on the results obtained.

The proposed study contains two parts. The first one, presented in Section 4.3, addresses the major part of the probabilistic framework that is developed to analyse the reliability of the CFs proposed by EC8-3. This first part is developed in light of several conditions established in Section 4.2 that are based on the interpretation of the EC8-3 procedures for seismic safety assessment and on existing research on this topic. The second part of the study, which is presented in Section 4.4, addresses the situation of combining different sources of information for the purpose of assessing the material properties. The general outline of the necessary Bayesian framework is analysed and the combination of different sources of information are addressed within the scope of the EC8-3 procedures.

4.2 General framework for the definition of the CF

4.2.1 The CF in the EC8-3 procedures for seismic safety assessment

In EC8-3, the previously referred Knowledge Level (KL) is defined by combining the knowledge available in the following items: geometry, details and materials. In the context of RC structures, geometry refers to the geometrical identification of the structural elements, details refers to the amount and detailing of the reinforcement, and materials refers to the mechanical properties of the steel and concrete. Knowledge on the geometry is provided either by the original construction drawings or by survey. Details and materials are obtained through inspection and testing, respectively. As referred in Chapter 2, EC8-3 defines three levels of knowledge, denoted by KL1, KL2 and KL3 in increasing order of comprehensiveness, and also defines a CF associated with each level. The recommended values of these factors are 1.35, 1.2 and 1.0, for KL1, KL2 and KL3, respectively, and Table 4.1 summarises the combinations of information defining the KLs. The terms visual, full, limited, extended and comprehensive are defined in the code together with the recommended minimum amount of operations related to survey, inspection and testing. For the case of assessing material strengths, which is the context of the present study, the terms limited, extended and comprehensive are quantified in Table 4.2 and correspond to

the minimum number of material samples per floor and type of primary element (beam, column or wall) that are needed to assess the material strength according to a chosen KL.

Table 4.1. Knowledge levels and corresponding methods of analysis (LF: Lateral Force procedure; MRS: Modal Response Spectrum analysis)

Knowledge Level	Geometry	Details	Materials	Analysis	CF
KL1	From original architectural drawings with sample visual survey or from full survey	Simulated design in accordance with relevant practice and from limited in-situ inspection	Default values according to standards of the time of construction and from limited in-situ testing	LS-MRS	1.35
KL2		From incomplete original detailed construction drawings with limited in-situ inspection or from extended in-situ inspection	From original design specifications with limited in-situ testing or from extended in-situ testing	All	1.20
KL3		From original detailed construction drawings with limited in-situ inspection or from comprehensive in-situ inspection	From original test reports with limited in-situ testing or from comprehensive in-situ testing	All	1.00

Table 4.2. Recommended minimum percentage of elements to check for details and minimum number of tests of material samples, per floor and type of primary element for different KLs.

Knowledge Level	Level of testing	Percentage of elements to check for details	Number of material samples
KL1	Limited	20	1
KL2	Extended	50	2
KL3	Comprehensive	80	3

From the safety assessment stage point of view, depending on the type of analysis method that is selected (linear or nonlinear) and on the type of mechanism to be checked (ductile or brittle), the capacity is usually reduced by the CF. On the other hand, situations will occur where the demand needs to be increased by the CF, namely if certain conditions are met when examining brittle mechanisms based on linear analysis (EC8-3, 2005). The capacity reduction case is the focus of the present study for which two different situations are defined in EC8-3. With respect to the safety assessment of a certain ductile mechanism, its capacity is obtained from a given expression (e.g. see the previous chapters) where the material strength values are considered with mean values divided by the CF. In the case of a brittle mechanism of a primary element, EC8-3 sets a larger safety margin as the capacity is obtained from a given expression (e.g. see the previous chapters) where the material

strength values are considered with mean values divided by the CF and by the partial safety factor of the corresponding material. Of the two situations, the former is considered to be more critical.

Although the EC8-3 procedures acknowledge the importance of the existing KL about the geometry, the details and the materials, their interpretation leads to conclude that the definition of the CFs does not depend on all of these items. Namely, it can be seen, by analysing Table 4.1, that knowledge requirements related to the geometry are the same for all KLs. This implies that the existing information about the geometry is expected to be reliable enough to allow the definition of an adequate numerical model of the structure, irrespective of the selected KL. Therefore, it is concluded that, according to the EC8-3 procedures, the CF values do not depend on the uncertainty that may exist about the geometry. With respect to the details, Tables 4.1 and 4.2 indicate that selecting a KL requires that a certain amount of knowledge must be obtained about parameters such as longitudinal and transversal reinforcement ratios, and stirrup spacing (for the particular case of reinforced concrete structures). Bearing in mind that, in many cases, an adequate knowledge is only obtained if extensive and intrusive methods are considered, the use of such methods must be weighted against the implications on the continuous use of the building during these surveys. Considering that situations for which knowledge about the details of certain members is not available will occur, the analyst will have to decide whether to characterize them by using information on similar members or by using conservative estimates. In any case, the EC8-3 procedures are unclear regarding the practical effects of the existing uncertainty about the details since the CF only affects the material properties. To illustrate this situation, Eq. (4.1) presents the EC8-3 proposed expression for the Near Collapse chord rotation capacity θ_{NC}, where γ_{el} is 1.5 for primary members and 1.0 for secondary ones, υ is the normalized axial force, ω and ω' are the mechanical reinforcement ratios of the tension and compression, respectively, longitudinal reinforcement, f_{yw} is the stirrup yield strength, ρ_{sx} is the ratio of transverse steel area A_{sx} parallel to the direction of loading, ρ_d is the steel ratio of diagonal reinforcement (if any) in each diagonal direction and α is the confinement effectiveness factor (EC8-3, 2005):

$$\theta_{NC} = \frac{1}{\gamma_{el}} \cdot 0.016 \cdot 0.3^{\upsilon} \cdot \left(\frac{\max\left(0.01, \omega'\right)}{\max\left(0.01, \omega\right)} \frac{f_c}{\mathrm{CF}} \right)^{0.2} \cdot \left(\frac{L_s}{h} \right)^{0.35} \cdot 25^{\alpha \cdot \rho_{sx} \frac{f_{yw}/\mathrm{CF}}{f_c/\mathrm{CF}}} \cdot 1.25^{100\rho_d} \quad (4.1)$$

As can be seen, only the terms f_{yw} and f_c are divided by the CF while the terms ω, ω', ρ_{sx} and ρ_d related to the details remain unaffected, meaning that uncertainty is only explicitly reflected on the values of the material properties. Since knowledge about the details does not imply an increase of the knowledge about the material properties (and vice-versa), the two aspects are seen to be independent and it can be argued that the format of Eq. (4.1) reflects an indirect influence of the uncertainty related to the details that is inadequate in

some cases. For example, in a situation where the knowledge about the material properties is obtained according to KL3 but the knowledge about the details can only be obtained according to KL1, the considered CF should be that of KL1. Since this CF value is over-conservative for the material properties, as demonstrated in the following sections, and since, as stated before, it does not affect the detail-related properties, its consideration in the present EC8-3 format does not reflect adequately the true uncertainty.

Given the previous interpretation of the EC8-3 procedures, as well as arguments resulting from previous research addressing the adequacy of the CF concept to account for several types of uncertainties entering the seismic safety assessment process (Franchin *et al.*, 2008; Elefante, 2009; Franchin *et al.*, 2009; Monti and Alessandri, 2009; Franchin *et al.*, 2010; Jalayer *et al.*, 2011), the proposed study only focuses the evaluation of the CF values in the context of the characterization of the material properties. This is equivalent to say that CF values are evaluated assuming that KL3 conditions are available for the characterization of the details. In the opinion of the author, the adequate consideration of the uncertainty about the details requires a modification of the current EC8-3 format for the capacity expressions by introducing, for example, corrective factors affecting the detail-related parameters. Furthermore, as noted by Franchin *et al.* (2010), the influence of the detail-related uncertainty should also be reflected on the demand side of the assessment due to its potential influence on the global behaviour of the structure. However, such in-depth assessment of these aspects falls outside the scope of the present study.

Finally, it should be emphasized that the degree of impact of the EC8-3 proposed CF values on the member capacity properties clearly depends on the sensitivity of the type of property under consideration, i.e. deformation- or strength-based. For example, the study by Chrysostomou (2005) and the results presented in the previous chapter indicate that, from a practical point of view, going from KL1 to KL2 or from KL2 to KL3 produces changes in the capacity values of RC members that vary according to the considered limit state (between 8% to 14% for Damage Limitation rotational capacities, up to 5% for Significant Damage and Near Collapse rotational capacities and between 10% to 17% for Near Collapse shear force capacities). Based on these results, the degree of influence of the CF value can be seen to be relevant in some cases.

4.2.2 Quantification of the CFs

According to EC8-3, when there is no prior knowledge about the materials under assessment, the CF values depend mainly on the number of tests that are performed to assess the material properties of interest, hereafter simply referred as strength values. When there is prior knowledge (e.g. based on available design data or previous testing data), EC8-3 reflects the consideration of this information by reducing the required number of tests of a given KL. For the purpose of the following analysis regarding the minimum

number of required material tests and of the subsequent probabilistic quantification of the CFs presented in Section 4.3, it is assumed there is no prior knowledge about the materials under assessment. The situation of existing prior knowledge is addressed in Section 4.4.

Considering the situation with no prior knowledge, the following two scenarios are analysed to establish the worst case scenario, i.e. that corresponding to larger uncertainty, which will serve as the basis of the probabilistic framework:

- Scenario 1 – Only destructive tests are used to characterize the material properties;
- Scenario 2 – Different types of tests are combined to characterize the material properties, i.e. destructive tests and non-destructive tests (NDTs) (Neville, 1996; Bungey and Millard, 1996; Bartlett and MacGregor, 1994).

Scenario 2 is more likely to occur in real situations since the cost of NDTs is usually much lower than that of destructive tests. Nonetheless, NDTs have several disadvantages. For example, a reliable functional relation must be established between the property measured by the NDT and the material characteristic under assessment in order to be able to rely on their results. Such relation is usually obtained by performing a regression analysis using NDT results and results of destructive tests from the structure under assessment, e.g. see ACI 228.1R-03 (2003). Hence, NDTs must always be associated to more reliable destructive tests – a fact also acknowledged by EC8-3. Moreover, results obtained from NDTs have a larger variability than results of destructive tests. Besides the inherent variability of the material property under assessment, additional sources of variability, such as that resulting from the repeatability error associated to a certain NDT and that coming from the error associated to the regression relation, must be considered also, e.g. see Monti and Alessandri (2009), ACI 228.1R-03 (2003). Nonetheless, the negative effect of this larger variability can be overcome since a larger number of tests can be performed, a fact which can increase considerably the confidence in the results. Therefore, it is concluded that Scenario 2 leads to a characterization of the material properties with less uncertainty. Furthermore, since destructive tests must be carried out in both scenarios, Scenario 2 is seen as an extension of Scenario 1. Therefore, from the point of view of the uncertainty of the results, though using a testing procedure generally agreed to be more reliable, e.g. see EN 13791 (2007), Scenario 1 is considered to be more critical, since it will usually involve a lower number of tests. Hence, Scenario 1 will be considered as the basis of the development of the probabilistic framework presented in Section 4.3. Still, the combination of results coming from different types of tests (Scenario 2) will be addressed in Section 4.4 since it can be considered as a particular case of the situation where prior knowledge exists.

In the absence of prior knowledge and after selecting a given KL, the EC8-3 defines the minimum number of tests by multiplying the constants given in Table 4.2 by the number of storeys and by the number of primary element types. For example, considering the simple case of assessing the concrete compressive strength of a one-storey RC frame

structure with only beams and columns as primary elements and considering that KL1 is the selected KL, the minimum number of tests is two (one in a beam and one in a column). Although not clearly stated in EC8-3, if two different concrete grades are used in this structure, for example one for beams and one for columns, the minimum number of tests can be interpreted as being one for each concrete grade. Following the same reasoning, if the selected KL is KL3, the previously obtained minimum number of tests is now six, for the case of one concrete grade, and three for each concrete grade, for the case of two concrete grades. Although for taller structures the minimum number of tests will be proportionally larger, the fact remains that for shorter structures EC8-3 allows the determination of mean strength estimates based on a single test result, irrespective of the type of material.

For comparison purposes it is referred that, similar to the EC8-3, the Italian code (NTC, 2008) sets equivalent restrictions to define the CFs and recommends the same minimum number of tests. However, NTC (2008) sets an additional restriction related to the storey area. If this area exceeds 300 m^2, the minimum number of tests must be increased. In the context of assessing characteristic values of concrete compressive strength, it is further noted that EN 13791 (2007) refers that a minimum number of three core tests must be considered for the assessment of a certain concrete class, irrespective of the size of the structure. As another example, for existing steel structures, Kuhn *et al.* (2008) establishes values for the minimum number of tests to assess the steel yield strength that are dependent on the existence of prior knowledge. For the case where prior knowledge does not exist, at least three samples of each type of member must be obtained and at least two tests must be carried out to assess the steel yield strength. Furthermore, even though only two KLs are defined in ASCE (2007), the procedures proposed to obtain mean strength values are set depending on the material type and on various constraints established for the definition of the minimum number of material tests. The procedure defined in ASCE (2007) allows the consideration of existing prior knowledge about the material strength under assessment and of the variability of the test results as factors that will influence both the definition of the CF and of the required number of tests. For the case of concrete compressive strength, when neglecting other constraints based on the number of floors and on the number of element types, and assuming the existence of only one concrete grade for which there is no prior knowledge, the minimum number of tests set by ASCE (2007) for both KLs is six. Similar to NTC (2008), ASCE (2007) also sets a restriction related to the maximum storey area. If this area exceeds 930 m^2, the minimum number of tests must be increased. On the other hand, to assess the steel yield strength of existing mild steel structures, one test for each component type is required for the lower KL, while for the higher KL three tests for each component type are required (ASCE, 2007).

4.3 Probabilistic definition of the CFs

4.3.1 Basic hypotheses and definitions of the probabilistic analysis

In the context of EC8-3, an estimate $\overline{X}$ of the mean value μ of a given material property must be divided by a CF in order to provide a value of the property with an adequate safety level. Moreover, the CF value is seen to be larger if there is less knowledge about the material. From a safety perspective, the need for the CF reflects the underlying critical situation in terms of safety that occurs when $\overline{X}$ overestimates μ. Hence, the present study addresses the probabilistic quantification of the CFs that adjust the mean estimate of a material strength in order to provide a reliable value reflecting the KL that is attained in the assessment.

The number of material tests and the existence of prior knowledge about the strength under assessment are seen to be essential aspects for the quantification of the CFs. The number of material tests is the key factor used to set the probabilistic framework of the present Section, while the influence of the existence of prior knowledge is addressed in Section 4.4. Within the scope of the study, it is also assumed that the CFs proposed by EC8-3 guarantee a certain level of reliability of the material strength value (after its adjustment by the CF) that is associated to the minimum number of tests. Although the referred level of reliability is not easy to quantify, it is also addressed by the study by associating certain confidence levels to the quantification of the CFs. Furthermore, since the framework for the CF definition proposed by EC8-3 is material independent, the evaluation of the EC8-3 proposed CF values is illustrated herein for the case of RC structures. Nonetheless, part of the study is presented in a form independent of the material. Hence, it can be readily applied to any material and property.

For the safety assessment of RC structures, both the steel yield strength and the concrete compressive strength values are of interest. According to the probabilistic framework presented here for the CF definition, it is considered that performing the study for the material strength that exhibits larger variability represents the critical situation. Since it is generally accepted that the inherent variability of the steel yield strength is lower than that of the concrete compressive strength (e.g. see Kappos *et al.*, 1999; JCSS, 2001a), some of the basic hypotheses of the study are set for this material property. As stated in the previous Section, when concrete compressive strength test results are referred hereon, they are assumed to be obtained from destructive tests (i.e. core compression tests). It is also assumed that such test results have been converted to the corresponding in-place concrete strength. As an extensive discussion on such procedures is beyond the scope of this work, the reader is referred, for example, to Bartlett and MacGregor (1994), Bartlett and MacGregor (1995), Bartlett (1997), Kappos *et al.* (1999), JCSS (2001a), ACI 228.1R-03 (2003), Kuhn *et al.* (2008) for further details. In terms of the number of tests, and based on Section 4.2.2, the critical situation occurs for a one-storey structure with beams and

columns of different concrete grades as primary elements. To assess the strength of each concrete grade, the minimum number of tests can be interpreted as being one, two and three for each concrete grade for levels KL1, KL2 and KL3, respectively.

Two important assumptions are additionally considered for the case of concrete compressive strength. The statistical distribution of this material property is assumed to follow either a normal, lognormal or Weibull distribution (Stewart, 1995; Neville, 1996; Day, 1999; Tumidajski *et al.*, 2006). Secondly, it is also assumed that strength variability, characterized herein by its coefficient of variation (CoV), is within the range of 6% to 20% (Drysdale, 1973; Stewart, 1995; Bartlett, 1997; Bartlett and MacGregor, 1999; Tumidajski *et al.*, 2006; Wísniewski, 2007). Although larger CoV values can be found in the literature (Drysdale, 1973; Stewart, 1995; Aguiar *et al.*, 2003), a maximum of 20% is already considered to be very high for normal strength concrete, either site-mixed or ready-mixed. Further discussion on this topic can be found elsewhere (Bungey and Millard, 1996; Bartlett and MacGregor, 1999).

The proposed framework for the probabilistic definition of the CFs is based on the concept of confidence interval (an interval of real numbers expected to contain the true value of a population parameter, with a specified confidence). Considering that θ is a population parameter to be estimated, T as the statistic used as a point estimate for θ and denoting $\hat{\theta}$ as the observed value of the statistic, an interval estimate for θ has the form

$$\hat{\theta}_L \leq \theta \leq \hat{\theta}_U \tag{4.2}$$

where $\hat{\theta}_L$ and $\hat{\theta}_U$ are lower and upper bounds, respectively, of the confidence interval, computed from the sample data. Since different samples will produce different values of $\hat{\theta}_L$ and $\hat{\theta}_U$, these end-points are values of the random variables θ_L and θ_U, respectively. By knowing the sampling distribution of T, it is possible to determine values of θ_L and θ_U, $\hat{\theta}_L$ and $\hat{\theta}_U$ respectively, such that

$$P\left(\hat{\theta}_L \leq \theta \leq \hat{\theta}_U\right) = 1 - \alpha \tag{4.3}$$

where $0 \leq \alpha \leq 1$. This expression indicates there is a $(1-\alpha)$ probability of selecting a random sample producing an interval that contains θ and provides both lower and upper confidence bounds for θ. One-sided confidence bounds are obtained by setting either $\hat{\theta}_L = -\infty$ or $\hat{\theta}_U = \infty$.

4.3.2 Definition of the CFs for the case of a normal distributed strength

The proposed approach defines the CFs based on the confidence interval for the mean of the normal distribution with known variance (Montgomery and Runger, 2003). As

the present study focuses on assessing the adequacy of the EC8-3 proposed CF values, it is assumed that such values only account for the uncertainty in the estimation of the mean value and not for that of the variance. Hence the known variance hypothesis is favoured instead of the unknown variance one. Still, as shown in the following, the proposed approach does not require knowledge about the specific value of the variance, but instead demands for a measure of the relative variability which is defined by the CoV. As stated in the previous Section, the characterization of the variability of the material property in terms of the CoV is defined using a range of realistic values given in the literature.

The consideration of the unknown variance hypothesis presents some difficulties for the present study. For example, it does not allow the definition of the CF value for samples of size equal to one. Additionally, for samples of smaller size, the sample variance (or sample CoV) is known to be a poor estimator of the true variance and has a high sensitivity to potentially anomalous observations (Maronna *et al.*, 2006). Therefore, the definition of an adequate range for the expected values of the sample CoV is not as straightforward as for the known variance case. To clarify these issues and to observe the practical implications of considering this hypothesis in the context of the definition of CF values, the unknown variance case is also addressed herein.

4.3.2.1 The case of a normal distributed strength with known variance

Considering that $X_1, X_2, ...X_n$ is a random sample drawn from a normal distribution with unknown mean μ and known standard deviation σ, the sample mean $\overline{X}$ is known to be normally distributed with mean μ and standard deviation $\sigma/\sqrt{n}$ (Montgomery and Runger, 2003). By standardizing $\overline{X}$ one obtains variable *Z*:

$$Z = \frac{\overline{X} - \mu}{\sigma/\sqrt{n}} \tag{4.4}$$

which follows a standard normal distribution (Montgomery and Runger, 2003) and leads to:

$$P\left(-z_{1-\alpha/2} \le \frac{\overline{X} - \mu}{\sigma/\sqrt{n}} \le z_{1-\alpha/2} \right) = 1 - \alpha \tag{4.5}$$

where $z_{1-\alpha/2}$ is the $(1-\alpha/2)$ percentage point of the standard normal distribution. The one-sided lower bound expression equivalent to Eq. (4.5) is given by

$$P\left(\frac{\overline{X} - \mu}{\sigma/\sqrt{n}} \le z_{1-\alpha} \right) = 1 - \alpha \tag{4.6}$$

where $z_{1-\alpha}$ is the $(1-\alpha)$ percentage point of the standard normal distribution.

Based on the previously established critical safety situation, the definition of an adequate CF value must verify the following condition:

$$\frac{\overline{X}}{\mathrm{CF}} \leq \mu \;\Leftrightarrow\; \mathrm{CF} \geq \frac{\overline{X}}{\mu} \tag{4.7}$$

The minimum CF value that verifies Eq. (4.7) is:

$$\mathrm{CF} = \frac{\overline{X}}{\mu} \tag{4.8}$$

Combining Eq. (4.6) with Eq. (4.8) yields

$$P\left(\mathrm{CF} \leq 1 + z_{1-\alpha} \cdot CoV / \sqrt{n}\right) = 1 - \alpha \tag{4.9}$$

where the CoV is σ/μ and states that, for a known (expected) value of the CoV, there is a $(1-\alpha)$ probability that $\mathrm{CF} \leq 1 + z_{1-\alpha} \cdot CoV/\sqrt{n}$ if $\mu = \overline{X}/\mathrm{CF}$. Therefore, the $(1-\alpha)\cdot 100\%$ upper confidence bound on the value of CF is:

$$\mathrm{CF} \leq 1 + z_{1-\alpha} \cdot CoV / \sqrt{n} \tag{4.10}$$

In order to set the CF values, one is interested in the limiting values given by Eq. (4.10), hereafter termed CF_{LIM}, for increasing values of the number of tests *n*, for a prescribed $(1-\alpha)$ confidence level and a given CoV. In the situation of assessing the adequacy of the CFs recommended by EC8-3, the definition of a single CF value for each KL must account for the most unfavourable conditions, namely in terms of number of tests and CoV. Although critical situations can be identified for these two parameters based on the previously exposed arguments, there is little guidance for which $(1-\alpha)$ confidence level should be chosen. Even though there is no apparent justification, a minimum confidence level of 75% is commonly considered in the assessment of existing structures context, e.g. ISO 12491 (1997), ACI 228.1R-03 (2003), H2 (2005). Other authors propose to select the confidence level according to the importance of the structure defining levels of 75%, 85%-90% and 95% for ordinary, important and very important structures, respectively, (Hindo and Bergstrom, 1985; Wong *et al.*, 1993). For the study presented herein, the confidence levels must be defined as a function of the KLs set by EC8-3, thus reflecting the minimum number of material tests required. Assuming a minimum confidence level of 75% and considering that a confidence level of 95% is sufficiently large for practical purposes, confidence levels of 95%, 85% and 75% are proposed for KL1, KL2 and KL3, respectively. These values are set considering that when KL increases, the uncertainty about the materials decreases, thus the amplitude of the confidence interval, which is defined by the confidence level and reflects the uncertainty, can be smaller.

In order to observe the evolution of the CF_{LIM} values for levels KL1, KL2 and KL3, Figs. 4.1a), b) and c) present the upper limits of the confidence interval of the CF defined by Eq. (4.10), given the condition $\mu = \overline{X}/\mathrm{CF}$. These are defined for increasing values of n (from 1 to 30), for the previously defined range of the CoV (6% to 20% in 2% steps) and for the corresponding confidence levels (75%, 85% and 95%). Each graph presents also the computed CF_{LIM} corresponding to the larger CoV and to the minimum number of tests of the corresponding KL (underlined value). As expected, the analysis of the computed CFs indicates that, irrespective of the selected confidence level, CF_{LIM} tends asymptotically to 1.0 as n tends to infinity. Moreover, the analysis of the underlined values shows that, for the previously set of hypotheses, the CF values proposed by EC8-3 for KL1 and KL2 seem adequate, while for KL3 there is a significant difference between the proposed value and CF_{LIM}. Although approaching 1.0 for a very large n, such value of CF_{LIM} can only be attained for all values of n by setting the confidence level to 50%, for which the term $z_{1-\alpha}$ of Eq. (4.10) is zero. With respect to KL2, given the difference between CF_{LIM} (i.e. 1.15) and the EC8-3 proposed value (i.e. 1.2), CF_{LIM} value was also computed for a confidence level of 90%. Figure 4.1d) shows that, for the aforementioned conditions and for a confidence level of 90%, the CF_{LIM} value obtained is closer to the EC8-3 proposal. On the basis of this result, subsequent analyses will consider a confidence level of 90% for KL2.

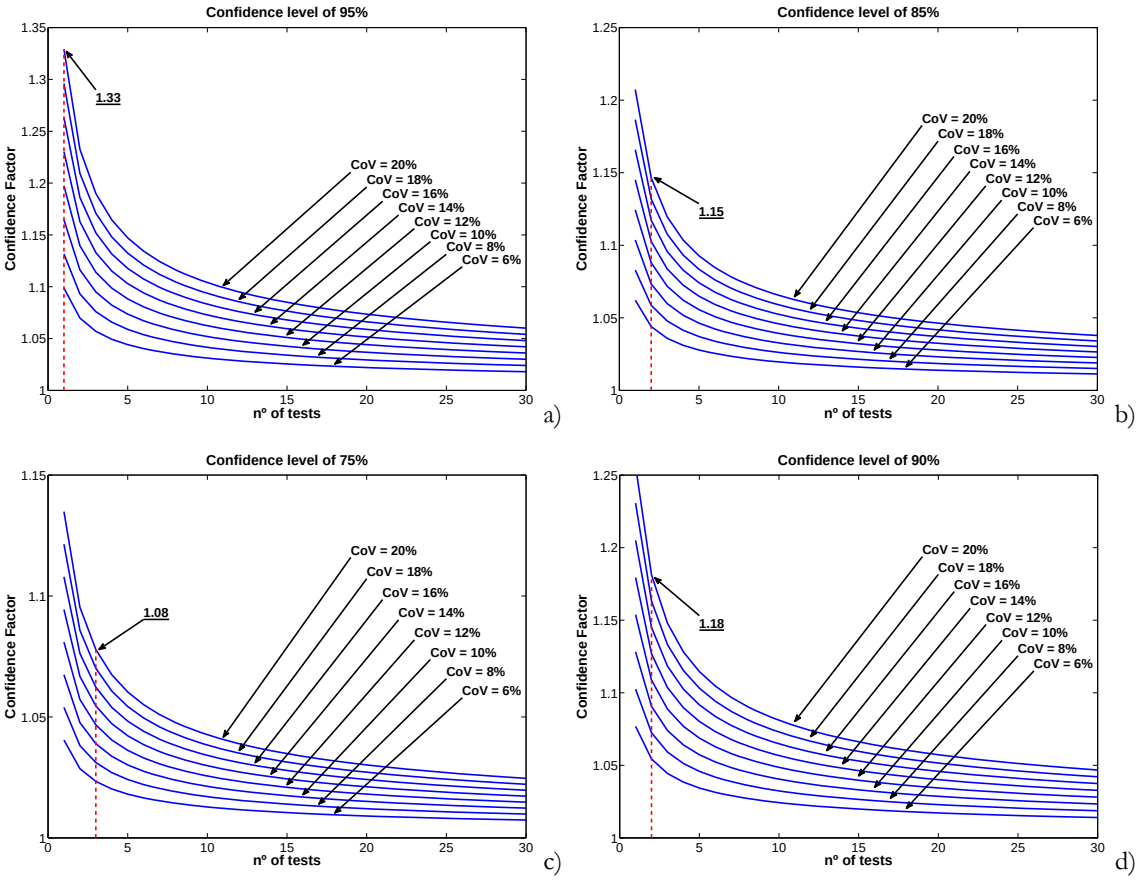

Figure 4.1. Values of CF_{LIM} considering a normal distributed strength, for increasing values of n, for the selected range of CoVs and for (1-α) confidence levels of 95% (a), 85% (b), 75% (c) and 90% (d).

4.3.2.2 The case of a normal distributed strength with unknown variance

For comparison purposes, the case of the normal distributed strength with unknown variance is considered herein and the corresponding expression for the upper confidence bound on the value of CF is also established. For a normal distribution with unknown mean and unknown standard deviation, the random variable T defined by

$$T = \frac{\overline{X} - \mu}{s/\sqrt{n}} \tag{4.11}$$

where s is the sample standard deviation, is known to follow a t distribution with $n-1$ degrees of freedom, (Montgomery and Runger, 2003). The one-sided lower bound expression equivalent to Eq. (4.5) is now given by

$$P\left(\frac{\overline{X} - \mu}{s/\sqrt{n}} \le t_{1-\alpha,n-1}\right) = 1-\alpha \tag{4.12}$$

where $t_{1-\alpha,n-1}$ is the $(1-\alpha)$ percentage point of the t distribution with $n-1$ degrees of freedom. Following the same reasoning as for the previous case and considering that $\overline{CoV}$ is the sample CoV defined by $s/\overline{X}$, the $(1-\alpha)\cdot 100\%$ upper confidence bound for the value of CF is now obtained by:

$$CF \le \left(1 - t_{1-\alpha,n-1}\cdot \overline{CoV}/\sqrt{n}\right)^{-1} \tag{4.13}$$

In order to observe the evolution of the CF_{LIM} values using Eq. (4.13), adequate values of the $\overline{CoV}$ must first be defined. Since for samples of small size, as those considered herein, the values of the CoV and of the $\overline{CoV}$ can be significantly different, the range of the $\overline{CoV}$ is considered to be wider than that of the CoV. To determine a possible upper limit for the referred $\overline{CoV}$ range, a simulation study was performed. The simulation started with the selection of a concrete class characterized by having a compressive strength following a normal distribution with a CoV of 20% and a μ selected from the range of 12 MPa to 50 MPa, in 1 MPa steps. Afterwards, 50000 samples of size two were randomly drawn from the normal distribution and the $\overline{CoV}$ was determined for each one. After computing the $\overline{CoV}$ for all samples, considering all possible values of μ from the previously set range, the 95th quantile of the corresponding empirical cumulative distribution function (CDF), which is around 40%, was selected as the upper limit for the $\overline{CoV}$. Therefore, the selected range of the $\overline{CoV}$ was 6% to 40%, in 2% steps. Considering this range, Figs. 4.2a), b) and c) present the CF_{LIM} values obtained from Eq. (4.13), given the condition $\mu = \overline{X}/CF$ and for levels KL1, KL2 and KL3. As previously referred, results for $n=1$ are not available and, for the case of KL1, Fig. 4.2a), results for $n=2$ are

also not presented because the term $t_{1-\alpha,n-1} \cdot \overline{CoV}/\sqrt{n}$ is larger than 1.0 for $\overline{CoV}$ values above 22%. This situation reflects the possibility of a negative value of μ, which is not admissible. Observation of Fig. 4.2 confirms the expected increase of the CF_{LIM} values for small values of *n*. According to Figs. 4.2a) and b), for KL1 and KL2, and for the upper value of the $\overline{CoV}$ range, the minimum number of tests that validate the CF values proposed by EC8-3 now need to be nine and eleven, respectively. For KL3, Fig. 4.2c), it can be seen that the CF_{LIM} corresponding to the larger $\overline{CoV}$ and to the minimum number of tests ($n = 3$) is now 1.23, when for the known variance case such value is 1.08. As can be seen from the results, the unknown variance case does not lead to values of the minimum number of tests (or of the CFs) that are in agreement with the EC8-3 proposals. Hence, it is believed that the known variance hypothesis may be underlining the CF definition in the context of the EC8-3 safety assessment procedures.

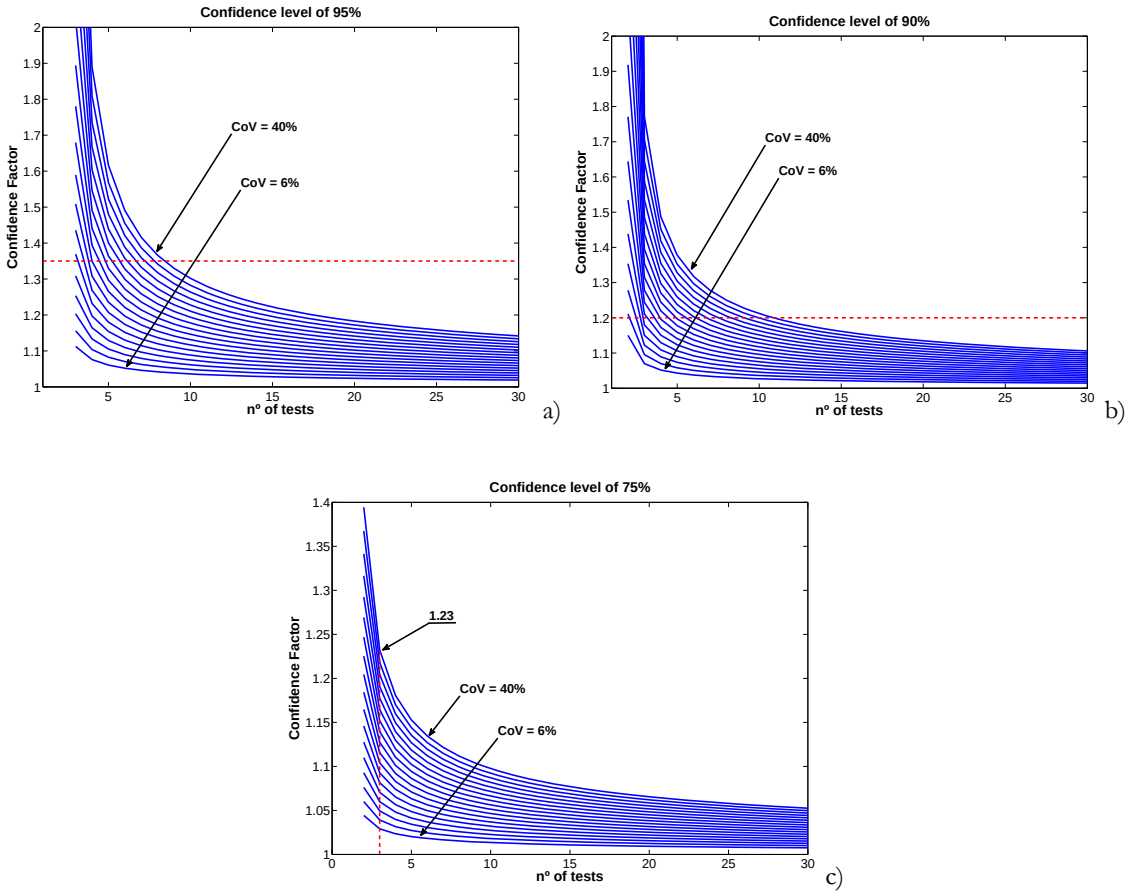

Figure 4.2. Values of CF_{LIM} considering a normal distributed strength with unknown variance, for increasing values of n, for the selected range of $\overline{CoV}s$ and for (1-α) confidence levels of 95% (a), 90% (b) and 75% (c).

4.3.3 Definition of the CFs for the case of a log normal distributed strength

As for the normal distribution case, the definition of the CFs is performed for the known and the unknown variance assumptions. Although the former hypothesis is considered to be more relevant for the EC8-3 context, the latter is considered for comparison purposes, in order to observe the variation of the CF values due to the uncertainty of the variance.

4.3.3.1 The case of a lognormal distributed strength with known variance

For this case, the CFs can be characterized following the approach of the normal distribution with known variance. Considering that $Y_1, Y_2, ...Y_n$ is a random sample from a lognormal distribution with unknown mean θ and known standard deviation δ, the variable $X = \ln(Y)$ follows a normal distribution with mean μ and standard deviation σ. As for the case of the normal distribution, the proposed approach does not require knowledge about the specific value of δ, but instead demands for a measure of the relative variability which is defined by the CoV. Upon this, it follows that Eq. (4.6) is applicable and can be rearranged to give the $(1-\alpha)$ probability that

$$\overline{X} - z_{1-\alpha} \cdot \frac{\sigma}{\sqrt{n}} \leq \mu \tag{4.14}$$

which, by adding $\sigma^2/2$ on both sides and taking exponentials of both sides, leads to

$$e^{\left(\overline{X}+\frac{\sigma^2}{2}\right)} \cdot e^{-z_{1-\alpha}\cdot\frac{\sigma}{\sqrt{n}}} \leq e^{\left(\mu+\frac{\sigma^2}{2}\right)} \tag{4.15}$$

Knowing that θ is given by

$$\theta = e^{\left(\mu+\frac{\sigma^2}{2}\right)} \tag{4.16}$$

and considering $\overline{Y}$ to be its sample estimate, yields

$$\overline{Y} \cdot e^{-z_{1-\alpha}\cdot\frac{\sigma}{\sqrt{n}}} \leq \theta \tag{4.17}$$

Considering a reasoning similar to that of Eq. (4.7):

$$\frac{\overline{Y}}{\mathrm{CF}} \leq \theta \Leftrightarrow \mathrm{CF} \geq \frac{\overline{Y}}{\theta} \tag{4.18}$$

Similar to Eq. (4.8), the minimum CF value that verifies Eq. (4.18) is:

$$\mathrm{CF} = \frac{\overline{Y}}{\theta} \tag{4.19}$$

Combining Eq. (4.17) with Eq. (4.19) and rearranging leads to

$$\mathrm{CF} \le e^{z_{1-\alpha}\cdot\sqrt{\frac{\ln\left(CoV^2+1\right)}{n}}} \tag{4.20}$$

where $\sqrt{\ln\left(CoV^2+1\right)}$ is σ. As in Eq. (4.10), Eq. (4.20) gives the upper confidence bound CF_{LIM} for which there is a $(1-\alpha)$ probability that $\mathrm{CF} \le e^{z_{1-\alpha}\cdot\sqrt{\frac{\ln\left(CoV^2+1\right)}{n}}}$ if $\theta = \overline{Y}/CF$.

As for the case of the normal distribution, evolutions of CF_{LIM} can be obtained simulating Eq. (4.20) for increasing values of *n*, for the previously defined range of the CoV and for the confidence levels of each KL. For the sake of brevity, graphical representations of the referred evolutions are not presented herein. Nonetheless, it should be noted that Eq. (4.20) gives larger CF_{LIM} values than Eq. (4.10). For the larger CoV (20%) and for the minimum number of tests of each KL, the CF_{LIM} values are 1.39, 1.20 and 1.08 for KL1, KL2 and KL3, respectively. When comparing these results with the CF values proposed by EC8-3, it is seen that only the value of KL2 agrees with the EC8-3 proposal. In order for the CF_{LIM} of KL1 to meet the EC8-3 proposed value (i.e. 1.35), there is the need to either reduce the prescribed confidence level or to reduce the maximum admissible CoV. Therefore, one of the following two situations can be observed:

- When fixing the CoV to 20% and when *n* is one, the $(1-\alpha)$ confidence level that yields a CF_{LIM} of 1.35 is 93.5%;
- When fixing the $(1-\alpha)$ confidence level to 95% and when *n* is one, the CoV that yields a CF_{LIM} of 1.35 is 18.5%.

Considering that the observed reduction can be seen to be relatively small, one is inclined to validate the adequacy of the EC8-3 proposal for KL1. Moreover, considering that the number of tests is fixed to one in both cases, a number that will most surely be exceeded in real situations, it is worth doing the analysis of the CF_{LIM} value when the number of tests is set to two. In this case, the CF_{LIM} value for a CoV of 20% and a confidence level of 95% is now 1.26, well below the EC8-3 proposal for this KL.

4.3.3.2 The case of a lognormal distributed strength with unknown variance

Statistical methods for inference involving the lognormal mean, namely addressing the estimation of confidence intervals when both mean and variance are unknown, have

received widespread attention in the literature over the years. Available methods for the development of such confidence intervals range from analytical, or semi-analytical, procedures to computationally intensive simulation approaches (Singh *et al.*, 1997; Zhou and Gao, 1997; Aoshima and Govindarajulu, 2002; Krishnamoorthy and Mathew, 2003; Shen, 2003; El-Shaarawi and Lin, 2007; Zou *et al.*, 2009). From observation of the available procedures, their complexity can be seen to be larger than that of the previously presented approaches. Although research on this topic appears to be far from over, the analytical method proposed by Zou *et al.* (2009) is seen to yield adequate results for small samples and presents a suitable form for the purpose of the present study.

According to Zou *et al.* (2009), the one-sided lower bound *LB* of the $(1-\alpha)$ confidence interval for the lognormal mean θ is defined by

$$LB = \overline{M} \cdot e^{-\left(\frac{z_{1-\alpha}^2 s^2}{n} + \left(\frac{s^2}{2} - \frac{(n-1)s^2}{2\chi_{1-\alpha,n-1}^2}\right)^2\right)^{0.5}} \tag{4.21}$$

where s^2 is the sample variance of the log-transformed data, $\chi_{1-\alpha,n-1}^2$ is the $(1-\alpha)$ percentage point of the χ^2 distribution with $n-1$ degrees of freedom and $\overline{M}$ is the sample mean given by

$$\overline{M} = e^{\left(\overline{X} + \frac{s^2}{2}\right)} \tag{4.22}$$

Following the same reasoning as for the previous cases and considering that $\overline{CoV}$ is the sample CoV now defined by $\sqrt{e^{s^2}-1}$, the $(1-\alpha)\cdot 100\%$ upper confidence bound on the value of CF is now obtained by:

$$\mathrm{CF} \le e^{\left[\frac{z_{1-\alpha}^2 \ln\left(\overline{CoV}^2+1\right)}{n} + \left(\frac{\ln\left(\overline{CoV}^2+1\right)}{2}\left(1-\frac{(n-1)}{\chi_{1-\alpha,n-1}^2}\right)\right)^2\right]^{0.5}} \tag{4.23}$$

As for the normal distribution with unknown variance case, to observe the evolution of the CF_{LIM} values using Eq. (4.23), adequate values of the $\overline{CoV}$ must also be defined. A simulation study similar to that of the normal distribution case was performed and the resulting 95th quantile of the $\overline{CoV}$ CDF was also seen to be near 40%. Hence, the selected range for the $\overline{CoV}$ was also considered to be 6% to 40%, in 2% steps, for this case.

Considering this range, Figs. 4.3a), b) and c) present the CF_{LIM} values obtained from Eq. (4.23), given the condition $\theta = \overline{M}/CF$ and for levels KL1, KL2 and KL3. As for the normal distribution case, results for $n=1$ are not available. Observation of Fig. 4.3 also confirms the expected increase of the CF_{LIM} values for small values of *n* when compared to those of the known variance case. According to Figs. 4.3a) and b), for KL1 and KL2, and

for the upper value of the $\overline{CoV}$ range, the minimum number of tests that validate the CF values proposed by EC8-3 now need to be five and eight, respectively. For KL3, Fig. 4.3c), it can be seen that the CF_{LIM} corresponding to the larger $\overline{CoV}$ and to the minimum number of tests $(n=3)$ is now 1.16, when for the known variance case such value is 1.08. By comparing these results with those of Section 4.3.2.2, it can be seen that considering the normal distribution with unknown variance yields more conservative results. On the other hand, when the variance uncertainty is not taken into account, it is the lognormal distribution that yields more conservative CF values. This change of status between the normal and the lognormal distributions results from the fact that Eq. (4.21) includes the contribution of the sampling distribution of s^2 which is a right-skewed chi-square distribution. Hence, the lognormal distribution hypothesis leads to unsymmetrical right-skewed two-sided confidence intervals while symmetric ones are obtained with the normal distribution assumption (Zou *et al.*, 2009).

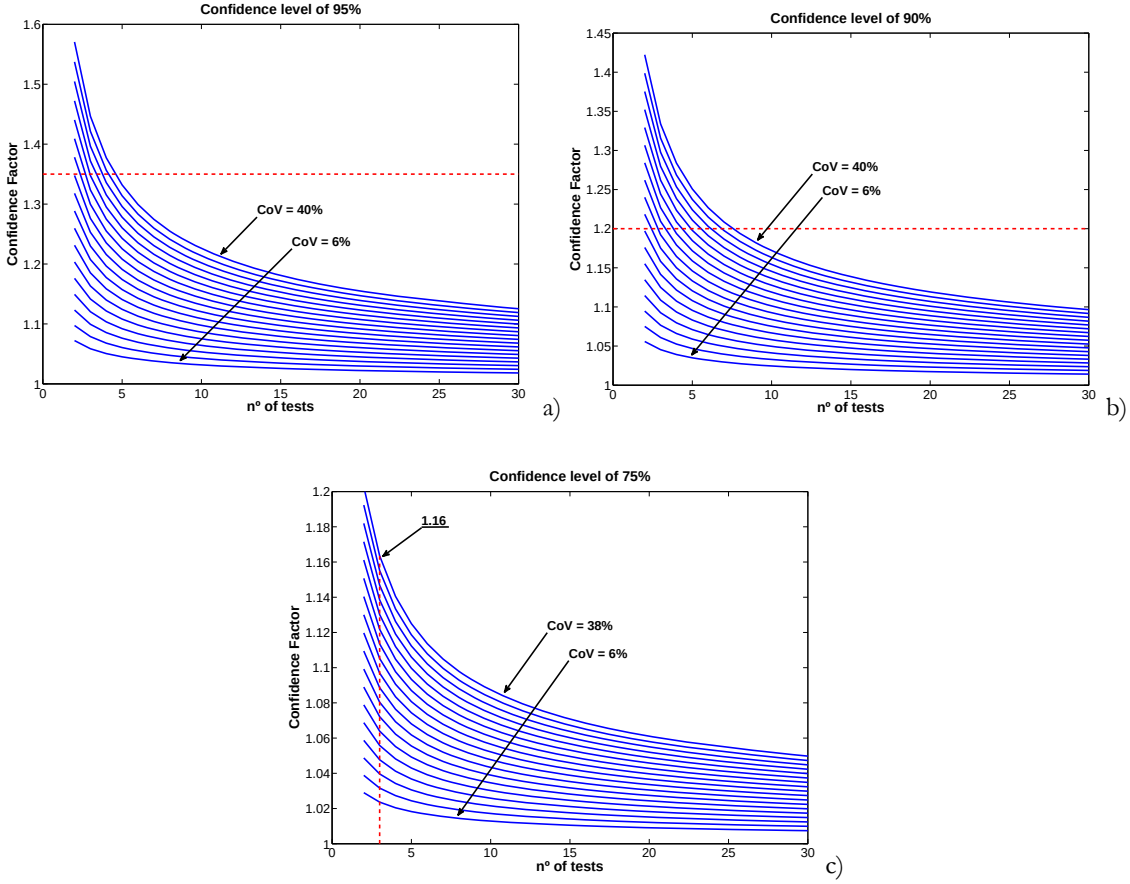

Figure 4.3. Values of CF_{LIM} considering a lognormal distributed strength with unknown variance, for increasing values of *n*, for the selected range of $\overline{CoV_S}$ and for (1-α) confidence levels of 95% (a), 90% (b) and 75% (c).

4.3.4 Definition of the CFs for the case of a Weibull distributed strength

The two-parameter Weibull distribution (Castillo, 1988) defined by the CDF of the form

$$F(x) = 1 - e^{-(x/\beta)^{\gamma}} \tag{4.24}$$

where γ and β are, respectively, the shape and the scale parameters, was chosen to characterize the CFs in the case of a Weibull distributed strength (Tumidajski *et al.*, 2006). Unlike for the case of the normal and the lognormal distributions, mathematically tractable confidence intervals are not available for the mean μ of the Weibull distribution. For the case of large samples, it is possible to assume that the distribution of the mean estimate $\overline{X}$ is asymptotically normal (Montgomery and Runger, 2003). However, this assumption is not applicable for the present case. Several alternatives providing confidence intervals for μ have been proposed considering the Weibull-to-exponential transform or considering Type II censored data (Lawless, 1982; Xie *et al.*, 2000; Yang *et al.*, 2007). Still, none of these approaches were found to be attractive due to the difficulty of their application to the present case. Given the simplicity of using a simulation approach, this method was selected to assess the CF_{LIM} values for the Weibull distribution case.

The simulation method started with the selection of a concrete class characterized by a compressive strength with chosen μ and CoV, the former being selected from the range of 12 MPa to 50 MPa, in 1 MPa steps, and the latter being selected from the previously set range, considering 2% steps. Knowing μ and CoV, the Weibull parameters γ and β are determined based on the following relations:

$$\mu = \beta \cdot \Gamma\left(1 + \frac{1}{\gamma}\right) \tag{4.25}$$

$$CoV = \frac{\left[\Gamma\left(1 + \frac{2}{\gamma}\right) - \Gamma^2\left(1 + \frac{1}{\gamma}\right)\right]^{1/2}}{\Gamma\left(1 + \frac{1}{\gamma}\right)} \tag{4.26}$$

where $\Gamma(.)$ is the Gamma function. Based on Eq. (4.26), parameter γ can be determined for the known CoV using a standard Newton-Raphson method after which parameter β can be obtained using Eq. (4.25). Afterwards, 50000 samples of a chosen size n were randomly drawn from the Weibull distribution. Next, the mean value of each sample i was computed and divided by μ to yield the CF_i, i.e. the CF value of sample i. After computing CF_i values for all samples, considering all possible values of μ from the previously set range and for a given CoV, an empirical CDF was defined, for which CF_{LIM} corresponds to

the $(1-\alpha)$ percentile. The simulation process was then repeated for different values of size *n*, from 1 to 30, and for the several CoV values from their previously set range. Since the CoV range was considered, instead of the $\overline{CoV}$ one, the simulation is assumed to represent a known variance situation. The unknown variance hypothesis was not considered for the Weibull distribution case.

In order to observe the evolution of the CF_{LIM} values for levels KL1, KL2 and KL3, Figs. 4.4a), b) and c) present the results obtained from the referred simulation study for increasing values of *n* (from 1 to 30), for the previously defined range of the CoV (6% to 20% in 2% steps) and for the corresponding confidence levels (75%, 90% and 95%). As for the case of the normal distributed strength with known variance, the computed CF_{LIM} corresponding to the larger CoV and to the minimum number of tests of the corresponding KL is also represented in each graph (underlined value). The analysis of the underlined values shows that, for the previous set of hypotheses, the CF values proposed by EC8-3 for KL1 and KL2 appear to be adequate while the proposed value for KL3 is significantly different from the obtained CF_{LIM}, as reported for the case of normal and lognormal distributed strengths.

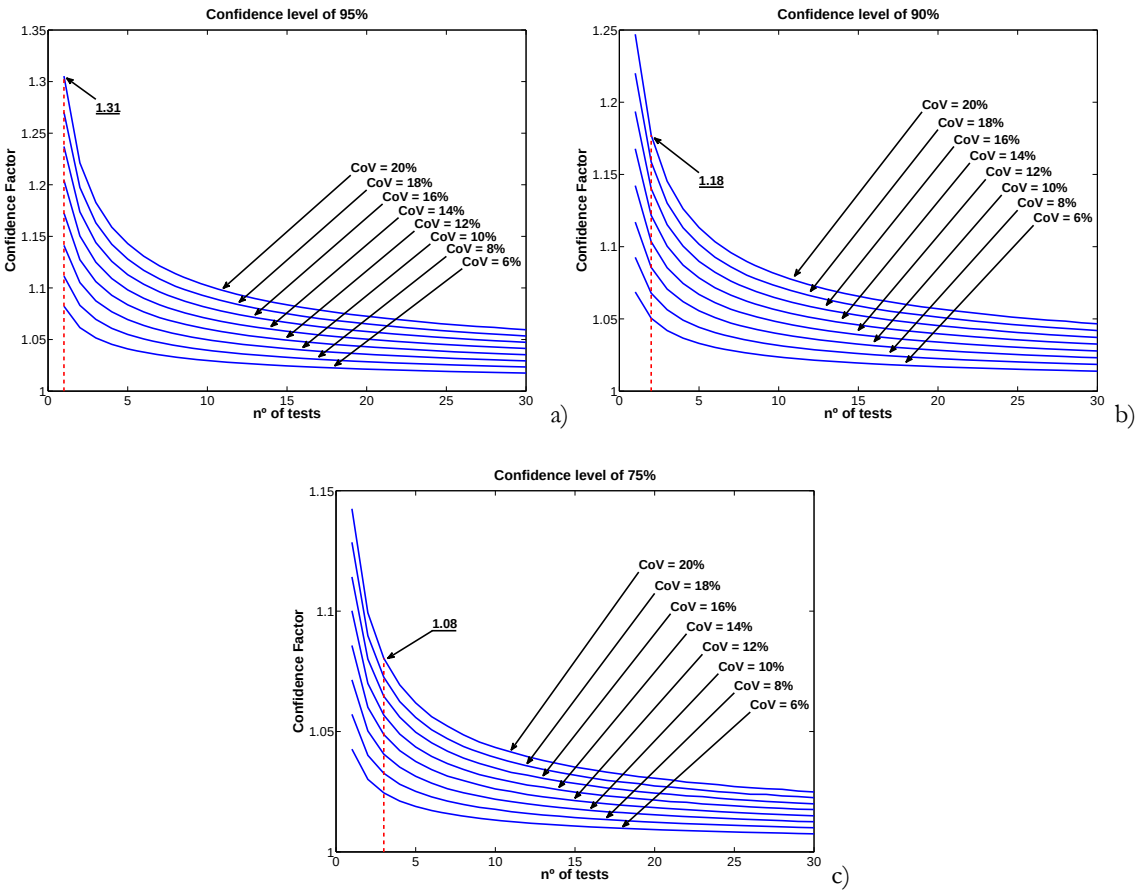

Figure 4.4. Values of CF_{LIM} considering a Weibull distributed strength, for increasing values of *n*, for the selected range of CoVs and for (1-α) confidence levels of (a) 95%, (b) 90% and (c) 75%.

4.3.5 Discussion of the results

Based on the results obtained for the different distributions and assumptions considered in the presented study, the EC8-3 proposed CFs for KL1 and KL2 are believed to be adequate for the purpose of establishing a conservative value of the material strength, assuming that the selected confidence levels are satisfactory. Moreover, the comparison of the results obtained with the CF values proposed by EC8-3 are seen to be more consistent with the known variance assumption. With respect to KL3, the EC8-3 proposed CF is not met by any of the cases studied. Nonetheless, the known variance assumption is also selected since it leads to lower values of the CF. For this case, a CF value of 1.08 is seen to be more adequate to the assumptions made in the study. Still, it is recalled that, for KL3, a CF value of 1.0 can only be obtained if the confidence level is assumed to be 50%.

The aforementioned conclusions are based on a limit CoV of 20% and for a number of tests corresponding to the minimum values established according to the conditions referred in Section 4.2.2. Nonetheless, it is useful to analyse such results in terms of the necessary CF associated to building structures of more common sizes. For example, let us consider three- and five-storey framed structures having a single concrete grade and only with beams and columns as primary elements. According to Table 4.1, the minimum number of tests for KL1, KL2 and KL3 are now 6, 12 and 18, respectively, for the three-storey building, and 10, 20 and 30, respectively, for the five-storey building. By determining the CF values for such number of tests, for the normal and the lognormal distributions (the Weibull distribution results are similar to those of the normal distribution), considering the known variance hypothesis and the limit CoV of 20%, the results presented in Table 4.3 are obtained (results for a one-storey structure are also presented for comparison). As can be seen, in comparison with the CF values of the one-storey building, CFs could be significantly reduced for the three-storey structure. On the other hand, going from the three- to the five-storey buildings implies a negligible reduction of the CF values. Hence, for buildings higher than three-storeys, significantly reduced CF values could be considered instead. A similar analysis considering the unknown variance hypothesis and for the $\overline{CoV}$ of 40% leads to the second set of CF values of Table 4.3. In this case, the EC8-3 proposed CF for KL2 can be seen to also include the unknown variance hypothesis for buildings higher than three-storeys. Moreover, it can also be seen that, for KL3, the proposed value of 1.08 is also able to include such hypothesis under the same conditions. On the other hand, for the case of KL1, this situation can only be attained if the maximum $\overline{CoV}$ is reduced to 32%.

Table 4.3. Analysis of the CF values for different building sizes, considering different distributions, KLs and variance knowledge hypotheses (KV: known variance; UV: unknown variance)

		1 storey		3 storeys		5 storeys	
Knowledge Level	Distribution	KV	UV	KV	UV	KV	UV
KL1	Normal	1.35	-	1.13	1.49	1.10	1.30
	Lognormal	1.35	-	1.14	1.30	1.11	1.23
KL2	Normal	1.20	-	1.07	1.19	1.06	1.13
	Lognormal	1.20	-	1.08	1.16	1.06	1.12
KL3	Normal	1.08	-	1.03	1.07	1.02	1.05
	Lognormal	1.08	-	1.03	1.06	1.02	1.05

4.3.6 Additional comments regarding the application of the results obtained to other materials

As can be seen from the cases where the normal and the lognormal distribution assumptions are considered, the probabilistic framework of the considered approach for the validation of the EC8-3 CF values depends on the CoV (or $\overline{CoV}$) of the material property under study. Hence, the proposed expressions can be applied to the properties of other materials of interest for which similar assumptions are valid. For these cases, the validity of the EC8-3 proposed CFs for these properties can be inferred from the results obtained for the concrete compressive strength.

The current seismic safety assessment procedures of EC8-3 for existing structures only address RC, steel and composite, and masonry structures. According to the capacity models proposed by EC8-3 for the case of RC structures, the concrete compressive strength and the steel yield strength are the material properties for which estimates of their mean value are meant to be adjusted by the CF. With respect to the steel yield strength, both the normal and the lognormal distribution assumptions can be seen to be acceptable and the CoV values available from the literature are found to be within the previously considered range of values, e.g. see JCSS (2001a), Stewart (1995) and references cited therein. Hence, the general conclusions obtained for the concrete compressive strength for each KL can be extended to the steel yield strength.

For the case of steel and composite structures, the main properties of interest, according to the EC8-3 capacity models, are also the steel yield strength and the concrete compressive strength. For the case of the steel yield strength, the lognormal distribution assumption can be seen to be acceptable (Melchers, 1999; JCSS, 2001a) and adequate CoV values are always within the previously referred range. Consequently, the general conclusions obtained for the concrete compressive strength can also be extended to this case.

For the case of masonry structures, the main properties of interest, according to the EC8-3 capacity models, are the masonry compressive strength and the masonry shear

strength in the absence of vertical load. The statistical characterization of these properties in existing structures is more complex than for the previous materials. The existence of different types of masonry units in terms of materials (e.g. clay or concrete) and of shape (e.g. hollow or solid), may imply the need to define statistical models for each type of masonry. Furthermore, masonry properties are known to exhibit larger variability than that of other materials. When dealing with existing structures, the variability of the workmanship and the uncertainty of the testing methods are important factors that contribute to such variability (Schueremans, 2001; Dymiotis and Gutlederer, 2002). Nevertheless, some of the existing proposals for the probabilistic modelling of the masonry properties refer the lognormal distribution as an acceptable model to characterize the masonry compressive strength (Schueremans, 2001; Dymiotis and Gutlederer, 2002; Mojsilovic and Faber, 2008). Furthermore, the generalized Pareto distribution has also been found to be applicable (Dymiotis and Gutlederer, 2002). In terms of variability, as expected, the proposed CoV values may vary considerably and values larger than the maximum value of the previously referred range have been observed (Schueremans, 2001; Dymiotis and Gutlederer, 2002). With respect to the masonry shear strength, no specific proposal has been found in terms of probabilistic model. Nonetheless, CoV values have been obtained (Dymiotis and Gutlederer, 2002) and are found to be within the previously considered range.

Hence it is concluded that, for the case of RC, steel and composite structures, the considered probabilistic approach and the results obtained can be used for the validation of the EC8-3 proposed CF values. On the other hand, for the case of masonry structures, the results obtained can only be partially taken into account. Namely, when the conditions considered in the probabilistic approach in terms of the selected statistical distributions and the variability range are valid assumptions. Nonetheless, further experimental research appears to be necessary for a better characterization of probabilistic models for masonry.

4.4 Quantification of the CFs when prior knowledge exists

The situation of existing prior knowledge about the materials covers cases where design data or previous testing data is available. It is also referred that, for practical purposes, this latter case is the same as that of combining testing data coming from different types of tests (i.e. the case previously defined as Scenario 2). When there is prior knowledge about the materials based on available design data or previous testing data, EC8-3 accounts for this information to produce a more accurate estimate of the material strength and allows the required number of tests of a given KL to be reduced. By considering only the situation of material characterization and by observing the information provided in Table 4.1 with respect to the materials, the existence of original design specifications can be seen to imply that KL2 can be selected and there is only the

need to carry out a minimum number of tests which corresponds to that of KL1. This value of the minimum number of tests implies a 50% reduction of the required number of tests, when compared to the situation of no prior knowledge (see Table 4.2). Furthermore, the existence of original test reports can be seen to imply that KL3 can be selected and there is only the need to carry out a minimum number of tests which corresponds also to that of KL1. In this case, a 67% reduction in the number of tests can be achieved when compared to the situation where there is no prior knowledge (see Table 4.2).

For a more clarified interpretation of the effects of existing prior knowledge in the context of the EC8-3 and its influence on the value of the CFs, an example analysis is presented in the following, considering the case of a normal distributed strength, the levels KL2 and KL3, and using a Bayesian formulation (Ang and Tang, 1984; JCSS, 2001b). Moreover, an additional example is presented for the case where testing data coming from different types of tests is combined, considering also a normal distributed strength and the previously referred Bayesian formulation. The reader is also referred to Ang and Tang (1984) and JCSS (2001b) for information regarding the consideration of alternative distributions. The examples presented in the following represent a possible interpretation of the code procedures but are not an extensive study of the case of existing prior knowledge. Nonetheless, a qualitative evolution trend of the CF values can be observed from the following results.

4.4.1 Considering prior knowledge and KL2

When KL2 is chosen in the context of a situation where prior knowledge exists, it is assumed that original design specifications can lead to the definition of a prior estimate of the mean of the material strength, X_0. In this case, the updated estimate of the mean value of the material strength X_U can be obtained using a Bayesian approach given by (Ang and Tang, 1984; JCSS, 2001b):

$$X_U = \frac{n_0 \cdot X_0 + n_1 \cdot X_1}{n_0 + n_1} \tag{4.27}$$

where n_0 is the number of tests considered for the estimate X_0, X_1 is the material strength estimate obtained from new data and n_1 is the number of tests that led to X_1. Since X_0 is based on design specifications and not on actual tests, n_0 must represent an equivalent number of tests. Although the adoption of other values could be foreseen, n_0 can be set to be the same as n_1 in order to guarantee the same level of reliability as when KL2 is considered with no prior knowledge (i.e $n_0 + n_1$ reflects the number of tests that would be considered for that situation with no prior knowledge). Upon this consideration, the value of X_U can therefore be seen to correspond to the average of X_0 and X_1. Given the

weight of the prior estimate X_0 on the value X_U (i.e. 50%, given that n_0 is equal to n_1), it should be emphasized that, in case the information between prior and new data (X_1) is contradictory, the analyst has to decide whether the prior data should or should not be taken into account.

In order to observe the effects of existing prior knowledge on the quantification of the CF for KL2, CF_{LIM} values were assessed using a simulation similar to the one considered in Section 4.3.4, considering the same ranges for the concrete compressive strength and for the CoV, but for the case of a normal distribution. To account for the existence of prior knowledge, an extra step was included in the method after the computation of the mean value of each sample *i*. This step consists of the calculation of the updated mean X_U according to Eq. (4.27), which is then divided by μ to yield the CF_i as referred in Section 4.3.4. The outcome of the process is the empirical CDF of the CF_is, for which CF_{LIM} is the $(1-\alpha)$ percentile. Figure 4.5a) presents the evolution of the CF_{LIM} values obtained from the referred simulation study for increasing values of n_1 (from 1 to 30), for the previously defined range of the CoV (6% to 20% in 2% steps), for the previously defined range of the concrete compressive strength (12 MPa to 50 MPa in 1 MPa steps) and for the 90% confidence level associated to KL2. Observation of these results allows concluding that, for the case of a normal distributed strength, when the prior knowledge and the new tests data are in agreement, the required CF_{LIM} decreases. Considering the case where the CoV is 20% and the new minimum number of tests set for KL2 (i.e. $n_1 = 1$), the results obtained yielded a CF_{LIM} value of 1.13, which is lower than the one previously obtained in the absence of prior knowledge.

Given that the obtained CF_{LIM} value is lower than the EC8-3 proposed value (i.e. 1.2), a second simulation study was performed to produce a situation where the prior knowledge and the new test data are contradictory. The simulation study was carried out as for the previous case, but considering the prior knowledge data representing a higher concrete strength to represent a critical situation of non-conformity. It was found that, for a CoV of 20% and for $n_1 = 1$, the value of X_0 could not exceed the mean of the distribution of the test data by more than 15% in order to yield a CF_{LIM} value up to 1.20. Figure 4.5b) presents the evolution of the CF_{LIM} values for the conditions set for the previous simulation study, but considering that X_0 exceeds the mean of the distribution of the test data by 15%.

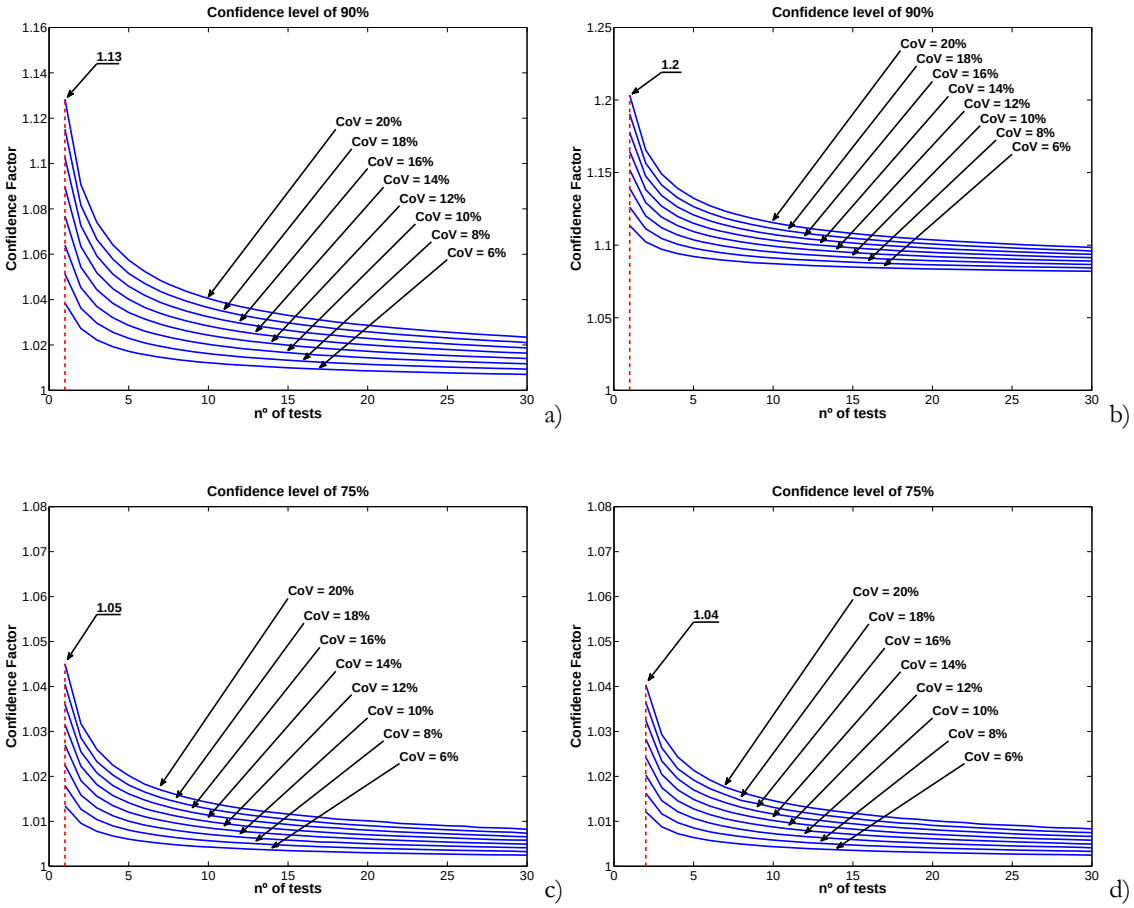

Figure 4.5. Values of CF_{LIM} obtained by simulation considering a normal distributed strength, the existence of prior knowledge, for increasing values of n, for the selected range of CoVs, for KL2 (confidence level of 90%) when the prior information and the new test data are in agreement (a), when the prior information exceeds the mean of the new test data by 15% (b); for KL3 (confidence level of 75%) when the prior information and the new test data are in agreement (c) and when the prior information and the new test data are in agreement and s_0 is known (d).

4.4.2 Considering prior knowledge and KL3

When KL3 is chosen in the context of a situation where prior knowledge exists, it is assumed that original test reports can lead to the definition of either a value of X_0, or a value of X_0 and a prior estimate of the standard deviation s_0 of the data. For the former situation (only X_0 is known), the updated estimate of the mean value X_U can also be obtained by Eq. (4.27). In this case, the value of n_0 reflecting the actual number of tests that were performed might be available from test reports and can be either smaller or larger than n_1. In the absence of such knowledge, an interpretation similar to the one considered for KL2 can also be applied, leading to the definition of n_0 with twice the value of n_1, in order to guarantee the level of reliability of KL3 in the absence of prior knowledge. This latter situation is considered herein to illustrate the effect of existing prior knowledge. Conclusions based on the presented results will be restricted to cases with similar conditions in terms of the n_0/n_1 ratio. As previously noted for the case of KL2, given the

weight of the prior estimate X_0 on the value X_U (i.e. 67%, given that n_0 has twice the value of n_1), if the information between prior and new data is contradictory, the analyst has to decide whether the prior data should or should not be taken into account.

In order to observe the effects of existing prior knowledge on the quantification of the CF for KL3, CF_{LIM} values were assessed using the simulation approach considered in Section 4.4.1. In order to observe the evolution of the CF_{LIM} values, Fig. 4.5c) presents the results obtained from this simulation study for increasing values of n (from 1 to 30), for the previously defined range of the CoV (6% to 20% in 2% steps), for the previously defined range of the concrete compressive strength (12 MPa to 50 MPa in 1 MPa steps) and for the 75% confidence level associated to KL3. Observation of the results confirms that when the prior knowledge and the new tests data are in agreement, the necessary CF_{LIM} decreases. As can be seen in the figure, the CF_{LIM} value corresponding to a CoV of 20%, and to the new minimum number of tests set for KL3 (i.e. $n_1 = 1$) is 1.05, which is lower than the value previously obtained in the absence of prior knowledge. It should also be noted that, since the obtained CF_{LIM} value is larger than the EC8-3 proposed value (i.e. 1.0), there seems to be no room for a situation where the prior information and the new test data are contradictory.

For the case where both X_0 and s_0 are known, the updated estimate of the mean value X_U can now be obtained by (Ang and Tang, 1984; JCSS, 2001b):

$$X_U = \frac{X_0 \cdot s_1^2/n_1 + X_1 \cdot s_0^2/n_0}{s_0^2/n_0 + s_1^2/n_1} \tag{4.28}$$

where s_1 is the standard deviation obtained from the new data. By considering the previously referred relation between n_0 and n_1, and by defining the variance ratio $\zeta = \left(s_1/s_0\right)^2$, Eq. (4.28) can be rearranged to yield:

$$X_U = \frac{2 \cdot X_0 \cdot \zeta + X_1}{2 \cdot \zeta + 1} \tag{4.29}$$

By analysing Eq. (4.29), the following can be observed:

- When ζ takes the value of 0.5, X_0 and X_1 have the same weight over the value of X_U, and when ζ takes the value of 1.0, Eq. (4.29) yields the results of Eq. (4.27);
- When ζ is lower than 0.5, X_1 dominates the value of X_U and when ζ is larger than 0.5, it is X_0 that dominates X_U;
- As ζ increases, the value of X_U asymptotically tends to X_0.

In order to exemplify these findings and for a better interpretation of the behaviour of Eq. (4.29), a simulation study is presented next. It is assumed that X_0 is 35 MPa, s_0 = 4.2 MPa (CoV = 12%) and that the new test data yields values of X_1 ranging from 25 MPa to 45 MPa (in steps of 1 MPa) and values of s_1 corresponding to CoVs ranging from 6% to 20% (in 1% steps). For each value of X_1, a range of values of s_1 is defined, in correspondence to the assumed CoVs, which then yields the corresponding values of ζ. For the conditions set, the evolution of Eq. (4.29) is represented in Fig. 4.6.

In order to observe the effects of the consideration of Eq. (4.29) on the quantification of the CF for KL3, CF_{LIM} values were assessed using the previously referred simulation approach. In this case, the updated mean X_U was computed according to Eq. (4.29). Since Eq. (4.29) is based on s_1, the new minimum number of tests set for KL3 (i.e. $n_1 = 1$) was not able to be considered; a value of $n_1 = 2$ was used instead. In order to observe the evolution of the CF_{LIM} values obtained in this case, Fig. 4.5d) presents the global results determined from the referred simulation study for increasing values of n_1 (from 2 to 30), for the previously defined range of the CoV (6% to 20% in 2% steps), for the previously defined range of the concrete compressive strength (12 MPa to 50 MPa in 1 MPa steps) and for the 75% confidence level associated to KL3. Considering the case where the CoV is 20% and $n_1 = 2$, the results obtained yielded a CF_{LIM} value of 1.04. To compare the performance of Eq. (4.27) with that of Eq. (4.29), the CF_{LIM} value obtained with Eq. (4.29) for $n_1 = 2$ must be determined. Observation of Fig. 4.5c) leads to a CF_{LIM} value of 1.03 for this case. Hence, it appears that Eq. (4.29) leads to slightly more conservative results than Eq. (4.27).

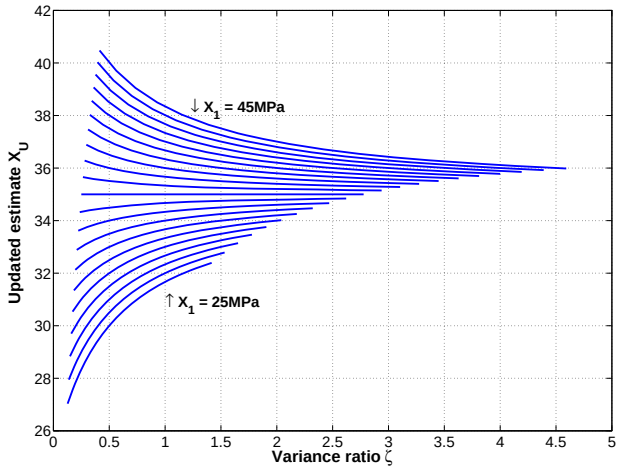

Figure 4.6. Values of X_U considering the existence of prior knowledge, for the case when both X_0 and s_0 are known.

4.4.3 Combining data from different types of tests

The combination of data coming from different types of tests is similar in formulation to the case of Section 4.4.2 where both X_0 and s_0 are known, Eq. (4.28), but without enforcing a specific relation between n_0 and n_1. Considering that X_0 and s_0 are known from core compression tests, that X_1 and s_1 are obtained from a chosen NDT and that the relation between n_0 (number of core tests) and n_1 (number of NDTs) is defined by $n_1 = k \cdot n_0$, Eq. (4.28) can be rearranged to yield X_U given by:

$$X_U = \frac{X_0 \cdot \zeta + k \cdot X_1}{\zeta + k} \tag{4.30}$$

where ζ is as previously defined. In order to observe the effects of the consideration of Eq. (4.30) on the quantification of the *CF* for the several KLs, CF_{LIM} values were assessed using a simulation approach similar to that of the previous Section and with the updated mean X_U computed according to Eq. (4.30). This simulation study considered increasing values of n_0 (from 2 to 30), three values for k (2, 5 and 10), X_0 values ranging from 12 MPa to 50 MPa, in 1 MPa steps, s_0 values corresponding to CoV values ranging from 6% to 20%, in 2% steps, X_1 values defined by the mean of random samples of size n_1 drawn from a normal distribution defined by X_0 and s_0, and s_1 values defined by:

$$s_1 = \sqrt{s_{1,s}^2 + s_{1,v}^2} \tag{4.31}$$

where $s_{1,s}$ is the standard deviation of the sample used to obtain X_1 and $s_{1,v}$ is an additional standard deviation aiming to represent the increased variability of the NDT results. In the proposed simulation study, $s_{1,v}$ was set as 15% of X_0. According to this simulation study, parameter ζ ranges between 1.0 and 10.0. Although conclusions based on the presented results will be restricted to cases with similar conditions in terms of the n_0/n_1 ratio and of the considered range of ζ, they allow for a qualitative interpretation of the influence of combining testing data from different test types. In order to observe the evolution of the CF_{LIM} values obtained in this case, Figs. 4.7a), c) and e) present the results obtained from the referred simulation study for $k = 2$ and for the 95%, 90% and 75% confidence levels associated to KL1, KL2 and KL3, respectively, while Figs. 4.7b), d) and f) present similar results for $k = 5$. As can be observed, results indicate that parameter k has a relatively reduced influence on the CF_{LIM} values. For the case of $k = 10$, CF_{LIM} values are slightly lower than those of $k = 5$. Furthermore, it can also be seen that combining different types of tests following the considered approach leads to CF_{LIM} values that are lower than those obtained in the first part of the proposed study for all KLs, thus validating the previously considered hypothesis that Scenario 1 is more critical.

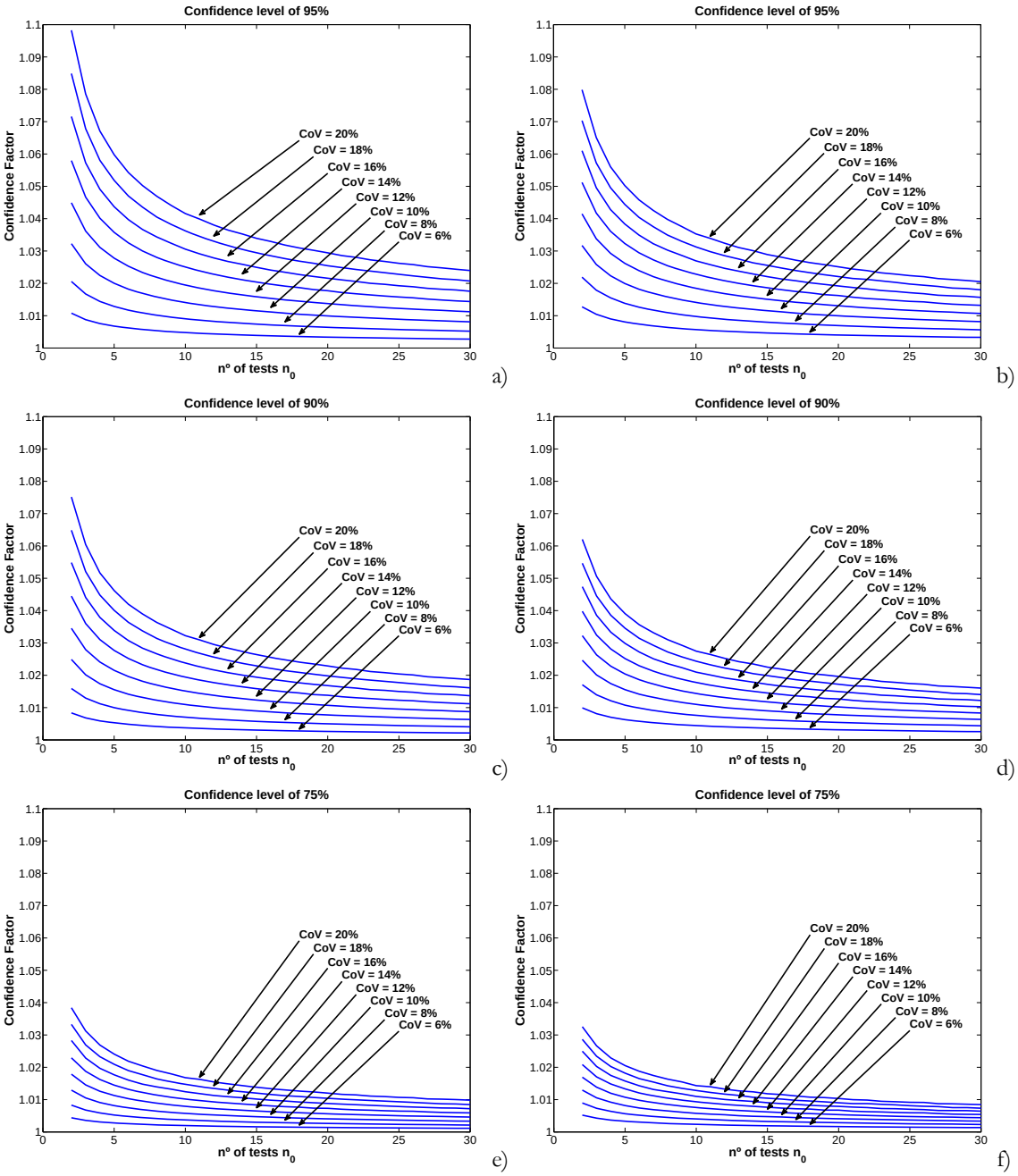

Figure 4.7. Values of CF_{LIM} obtained by simulation considering a normal distributed strength, two sources of testing data, for increasing values of n_0, for the selected range of CoVs, for KL1 (confidence level of 95%) and k = 2 (a) and k = 5 (b); for KL2 (confidence level of 90%) and k = 2 (c) and k = 5 (d); for KL3 (confidence level of 75%) and k =2 (e) and k = 5 (f).

4.5 Conclusions

The present study addresses the evaluation of the recommended values of the CFs proposed in the main document of the EC8-3 for the characterization of material properties of existing structures. In this context, the CF adjusts the mean estimate of a material property in order to reflect the KL that is attained in the assessment, in order to provide a design value of the property that is on the safe side. Prior to the evaluation of the

CFs, the influence of the level of knowledge and of the uncertainty about the parameters entering the EC8-3 safety assessment procedure is examined. From this analysis, it is concluded that only the uncertainty related to the materials is reflected in the quantification of the EC8-3 safety measures, thus justifying the focus of the proposed study.

The reliability of the EC8-3 proposed CF values is assessed using a probabilistic framework, in which the number of material tests and the existence of prior knowledge are seen to be essential aspects for the quantification of the CFs. Although the general concept behind the CFs is independent of the type of material, the evaluation is presented for the case of RC structures, more specifically for the concrete compressive strength. Nonetheless, conclusions regarding the validity of the CFs for other materials considered by EC8-3 are also inferred from the results.

In the first part of the study, where the existence of prior knowledge is not considered, different underlying statistical distributions are assumed for the concrete compressive strength (normal, lognormal and Weibull distributions) and different confidence levels are associated to the quantification of the CF of each KL (95%, 90% and 75% for KL1, KL2 and KL3, respectively). Moreover, the definition of the CFs reflects the critical situation that occurs when the estimate of the mean strength overestimates the real mean value. Based on the results obtained for the different distributions and assumptions of the presented study, the EC8-3 proposed CFs are seen to be more consistent with the known variance assumption. Moreover, the KL1 and KL2 CFs are believed to be adequate, assuming that the selected confidence levels are satisfactory. With respect to KL3, the EC8-3 proposed CF is not met by any of the cases studied. Nonetheless, the known variance assumption is also selected since it leads to lower values of the CF. For this case, a CF value of 1.08 is seen to be more adequate to the assumptions made in the study. Furthermore, considering the known variance hypothesis and for a CoV of 20%, it was observed that if the EC8-3 minimum number of tests are met, the CF values could be significantly reduced for buildings higher than three-storeys (e.g. from 1.35 to 1.14, for KL1, and from 1.20 to 1.08, for KL2). On the other hand, considering the unknown variance hypothesis and for a $\overline{CoV}$ of 40%, the EC8-3 proposed CF for KL2 and the proposed value of 1.08 for KL3 can be seen to also include such hypothesis for buildings higher than three-storeys. For the case of KL1, this situation can only be attained if the maximum $\overline{CoV}$ is reduced to 32%.

It was also found that, for the cases where the normal and the lognormal distribution assumptions are considered, the probabilistic framework that was defined to obtain the CF values depends only on the CoV of the material property under study. Hence, the proposed expressions can be applied to the properties of other materials of interest for which the referred statistical distribution assumptions are acceptable. Moreover, if the selected range of the CoV is acceptable for such material properties, the adequacy of the EC8-3 proposed CFs for these properties can be inferred from the results obtained for the concrete

compressive strength. The proposed study found that the obtained results can be used for the validation of the EC8-3 proposed CF values for the relevant material properties of RC, steel and composite structures. For the case of masonry structures, although some of the considered assumptions were found to be valid, further experimental research appears to be necessary.

In the second part of the study, the effects of prior knowledge on the quantification of the CFs are assessed. EC8-3 accounts for prior knowledge to produce a more accurate estimate of the material strength and allows the required number of tests of a given KL to be reduced. It should be noted that, in case the information between prior and new data is contradictory, the analyst has to decide whether the prior data should or should not be taken into account. By using a Bayesian framework and considering the case of a normal distributed strength, the results obtained lead to the conclusion that when the prior knowledge and the new test data are in agreement, the necessary CF decreases, when compared to the value obtained in the absence of prior knowledge. Nonetheless, the CF value obtained for KL3 is still larger than the value proposed by EC8-3. In addition, the case of combining different sources of testing data was also addressed considering the same Bayesian framework and the case of a normal distributed strength, as it is a special case of the situation where prior knowledge exists. Results of this analysis indicate that combining different types of tests leads to CF values that are lower than those obtained in the first part of the proposed study for all KLs. The presented analysis represents a possible interpretation of the code procedures but was not an extensive study of the case of existing prior knowledge. Although a qualitative evolution trend of the CF values was able to be observed, further research on this topic is required to be able to develop specific CF values accounting for prior knowledge.

Chapter 5
Assessment of the statistical distributions of structural demand under earthquake loading

5.1 Introduction

In the framework of Performance Based Earthquake Engineering and of the development of methodologies for seismic risk reduction, probabilistic methods are seen as superior means of assessing the performance of structures under earthquake loading. Among the possible features, probabilistic analyses are able to account for the propagation of various sources of uncertainty which affect the outcome of a given performance metric under assessment (Cornell and Krawinkler, 2000; Porter, 2003; Deierlein, 2004; Baker and Cornell, 2008). Nonetheless, the evaluation of performance parameters, such as the annual rate of exceeding a given structural demand level or the annual rate of exceeding some level of loss, is commonly seen to involve statistical assumptions regarding certain aspects of the probabilistic analysis (Aslani and Miranda, 2005; Goulet *et al.*, 2007; Baker and Cornell, 2008; Bradley and Lee, 2010).

In this context, one of the most common assumptions is that, for a given level of the considered earthquake intensity measure (IM), the probability distribution of a certain structural engineering demand parameter (EDP) can be modelled using a lognormal distribution. This hypothesis is considered in numerous research studies, namely for EDPs such as the maximum inter-storey drift over the height of a structure (Shome and Cornell, 1999; Song and Ellingwood, 1999; Shinozuka *et al.*, 2000; Sasani and Der Kiureghian, 2001; Cornell and Jalayer, 2002; Ibarra and Krawinkler, 2005; Kwon and Elnashai, 2006), the peak floor acceleration (Miranda and Aslani, 2003; Taghavi-Ardakan, 2006; Mitrani-Reiser, 2007), the maximum displacement (Decanini *et al.*, 2003; Ruiz-Garcia and Miranda, 2010) and the maximum displacement ductility (Goda *et al.*, 2009). However, a consistent assessment of this hypothesis using adequate statistical methods has yet to be carried out.

Until now, the consideration of this hypothesis has been essentially based on results derived from graphical methods (e.g. quantile-quantile (*Q-Q*) plots or cumulative distribution function plots) or based on the results obtained from the Kolmogorov-Smirnov/Lilliefors (K-S/L) statistical test (Lilliefors, 1967), usually applied to the logarithm of the data (Shome and Cornell, 1999; Decanini *et al.*, 2003; Ibarra and Krawinkler, 2005; Miranda and Aslani, 2003; Taghavi-Ardakan, 2006; Ruiz-Garcia and Miranda, 2010). However, it is widely accepted (e.g. see D'Agostino and Stephens (1986), Gan and Koehler (1990), Thode (2002) and references therein) that such approaches lack efficiency, robustness and objectivity in the assessment of the lognormality hypothesis, i.e. in assessing the normality hypothesis of the logarithm of the data. Therefore, a study addressing the probabilistic distribution of several EDPs using appropriate statistical methods is proposed herein to evaluate the hypothesis that the referred probabilistic demand could be adequately modelled by a lognormal distribution. In addition, the suitability of the normal distribution for that same purpose is also assessed.

5.2 Description of the proposed study

The presented study focuses both deformation- and strength-related EDPs and is based on local (section level) and global (system level) demand distributions obtained from the analysis of five reinforced concrete (RC) structures subjected to earthquake records of increasing intensities. At the section level, the selected EDPs are the maxima of the curvature, of the chord rotation and of the shear force, while at the system level, the chosen parameter is the maximum inter-storey drift over the height of the structure.

The selected structures were analysed for suites of fifty ground motions to obtain data samples with a size significant enough. The chosen records were scaled for several intensities in order to evaluate the referred hypotheses for different hazard levels. Furthermore, two different IMs were also considered to evaluate the influence of this parameter on the conclusions of the study.

A series of statistical tests was then applied to the demand samples to evaluate the adequacy of the demand distribution hypothesis. It is emphasized that the tests only aim to determine the validity of the hypothesis regarding the type of probabilistic distribution and do not make any kind of inference about the parameters of such distribution.

5.3 Statistical tests for demand distribution evaluation

The proposed study assesses both the normality and the lognormality hypotheses of structural demand distributions using statistical tests with adequate characteristics. As stated before, the lognormality assumption is tested by assessing the normality hypothesis

of the logarithm of the data. The considered tests were selected according to the results of a benchmark efficiency test previously carried out that is presented in Appendix A. This benchmark study considered a total of thirty-three goodness-of-fit tests, including the previously referred K-S/L test, and measured their efficiency in identifying non-normality situations in the presence of data coming from several alternative distributions. The tests considered herein are briefly presented in the following and represent the more efficient ones for the present study, based on the results of Appendix A. Since the random nature of the datasets under analysis does not allow the prediction of the characteristics of the data, it is not possible to propose the use of a single test that would lead to the best result in every situation. Therefore, the tests were selected in order to have different characteristics and test different aspects of the data.

The chosen tests were divided into two groups. The first group comprises tests which are best suited to identify non-normal distributions when the data is symmetric. The second group contains tests which are best suited to deal with potentially contaminated normally distributed data. In this latter case, it is assumed that the demand distribution may contain outliers. In several situations of statistical analysis of real data, outliers are considered to be errors (Hoaglin *et al.* 1983). Since such reasoning is not directly applicable to the present study, outliers are assumed to be observations which are numerically distant from the rest of the sample, thus masking the probability distribution of the majority of the data. For each test, the rejection of the normality hypothesis is based on the comparison of the test statistic with a pre-determined critical value of the statistic. The critical values of the several tests were derived empirically for the selected confidence level, i.e. 95%, and for a given sample size, following the methodology referred in Appendix A. In the following description of the tests, it is considered that $x_1, x_2, ...x_n$ represent a collection of data, hereon termed as a dataset, of size n and that $x_{(1)}, x_{(2)}, ...x_{(n)}$ represent the order statistics of that dataset.

5.3.1 Tests for symmetric data

5.3.1.1 The β_3^2 test

A normality test based on a polynomial regression focused on detecting symmetric non-normal distributions has been proposed in (Coin, 2008). Based on the analysis of standard normal *Q-Q* plots for different symmetric non-normal distributions, it is suggested that fitting a model of the type:

$$z_{(i)} = \beta_1 \cdot \alpha_i + \beta_3 \cdot \alpha_i^3 \tag{5.1}$$

where β_1 and β_3 are fitting parameters and α_i represent the expected values of standard normal order statistics (Royston, 1982), leads to β_3 values different from zero when in presence of symmetric non-normal distributions. Therefore, β_3^2 is suggested as a statistic for testing normality, thus rejecting the normality hypothesis of the data for values of β_3^2 larger than the critical value.

5.3.1.2 The R_{sJ} test

A normality test focussing on detecting heavier tails has been proposed in (Gel *et al.*, 2007). The test is based on the ratio of the standard deviation *s* and the robust measure of dispersion defined by:

$$J_n = \frac{\sqrt{\pi/2}}{n}\sum_{i=1}^{n}|x_i - M| \tag{5.2}$$

in which *M* is the sample median. The normality test statistic R_{sJ} is given by $R_{sJ} = s/J_n$ and should tend to one under a normal distribution. Since departure from normality can lead to either high or low values of R_{sJ}, the normality hypothesis of the data is rejected for values of R_{sJ} either smaller or larger than the critical values using a two-sided test.

5.3.1.3 The T_w *test*

A modified measure of kurtosis has been suggested in (Bonett and Seier, 2002) for testing normality. The test statistic of this new measure T_w is given by:

$$T_w = \frac{\sqrt{n+2}}{3.54}\left(13.29\left[\ln\sqrt{m_2} - \ln\left(n^{-1}\sum_{i=1}^{n}|x_i - \bar{x}|\right)\right] - 3\right) \tag{5.3}$$

in which $\bar{x}$ is the sample mean and m_2 is defined by $m_2 = n^{-1}\sum_{i=1}^{n}(x_i - \bar{x})^2$. The normality hypothesis of the data is rejected for values of T_w either smaller or larger than the critical values using a two-sided test.

5.3.1.4 *The CS* test

A test statistic *CS* based on normalized spacings has been defined in (Chen and Shapiro, 1995) by

$$CS = \frac{1}{s \cdot (n-1)} \sum_{i=1}^{n-1} \frac{x_{(i+1)} - x_{(i)}}{M_{i+1} - M_i} \tag{5.4}$$

in which M_i is the *ith* quantile of a standard normal distribution obtained by $\Phi^{-1}\left[(i-0.375)/(n+0.25)\right]$. The normality hypothesis of the data is rejected for values of *CS* smaller than the critical value.

5.3.2 Tests for data with potential outliers

5.3.2.1 *The* $T_{TLmom}^{(t)}$ test

This test has been proposed in Appendix A based on the robust generalization of the sample L-moments defined as the trimmed L-moments (Elamir and Seheult, 2003). The formulation of the trimmed L-moments allows for symmetric and asymmetric trimming of the smallest and largest sample observations, thus increasing their robustness towards outliers in the data when compared to that of the sample L-moments. However, only symmetric trimming is considered herein since there is no initial information regarding the nature of the potential outliers.

Considering an integer symmetric trimming level *t*, the *rth* order sample trimmed L-moment $l_r^{(t)}$ can be estimated by:

$$l_r^{(t)} = \frac{1}{r} \sum_{i=t+1}^{n-t} \left\{ \frac{\sum_{k=0}^{r-1} \left[(-1)^k \binom{r-1}{k} \binom{i-1}{r+t-1-k} \binom{n-i}{t+k} \right]}{\binom{n}{r+2t}} \right\} x_{(i)} \tag{5.5}$$

Based on the second, third and fourth sample trimmed L-moments, new measures of skewness and kurtosis, termed TL-skewness $\tau_3^{(t)}$ and TL-kurtosis $\tau_4^{(t)}$, are given by

$$\tau_3^{(t)} = l_3^{(t)} / l_2^{(t)}, \ \tau_4^{(t)} = l_4^{(t)} / l_2^{(t)} \tag{5.6}$$

Based on these measures, the following test can be defined:

$$T_{TL\_mom}{}^{(t)} = \frac{\tau_3^{(t)} - \mu_{\tau_3}^{(t)}}{\mathrm{var}\left(\tau_3^{(t)}\right)} + \frac{\tau_4^{(t)} - \mu_{\tau_4}^{(t)}}{\mathrm{var}\left(\tau_4^{(t)}\right)} \tag{5.7}$$

where, for a selected trimming level *t*, $\mu_{\tau_3}^{(t)}$ and $\mu_{\tau_4}^{(t)}$ are the mean of $\tau_3^{(t)}$ and $\tau_4^{(t)}$, and $\mathrm{var}\left(\tau_3^{(t)}\right)$ and $\mathrm{var}\left(\tau_4^{(t)}\right)$ are their corresponding variances. The values of $\mu_{\tau_3}^{(t)}$, $\mu_{\tau_4}^{(t)}$, $\mathrm{var}\left(\tau_3^{(t)}\right)$ and $\mathrm{var}\left(\tau_4^{(t)}\right)$ are obtained by simulation (see Appendix A). Three versions of this test are considered herein which correspond to symmetric trimming levels *t* of 1, 2 and

3. For each test, the normality hypothesis of the data is rejected for values of the statistic $T_{TL\_mom}^{(t)}$ larger than the critical value.

5.3.2.2 The $T_{MC\text{-}LR}$ test

A goodness-of-fit test based on robust measures of skewness and tailweight has been proposed in (Brys *et al.*, 2008). The considered robust measure of skewness is the medcouple MC (Brys *et al.*, 2004) defined as

$$MC = \underset{x_{(i)} \le m_F \le x_{(j)}}{med} h\left(x_{(i)}, x_{(j)}\right) \tag{5.8}$$

where *med* stands for the median operator, m_F is the sample median and the kernel function h is given by

$$h\left(x_{(i)}, x_{(j)}\right) = \frac{\left(x_{(j)} - m_F\right) - \left(m_F - x_{(i)}\right)}{x_{(i)} - x_{(j)}} \tag{5.9}$$

In a case where $x_{(i)} = x_{(j)} = m_F$, h is then set by

$$h\left(x_{(i)}, x_{(j)}\right) = \begin{cases} 1 & i > j \\ 0 & i = j \\ -1 & i < j \end{cases} \tag{5.10}$$

From Eq. (5.8), MC is seen to be the median of the results of function h applied to all couples of data points. Based on this, the left medcouple (LMC) and the right medcouple (RMC) were defined as robust measures of left and right tail weight (Brys *et al.*, 2006), respectively, by applying the MC function to the left and the right half of the dataset:

$$LMC = -MC\left(x < m_F\right);\ RMC = MC\left(x > m_F\right) \tag{5.11}$$

The test statistic $T_{MC\text{-}LR}$ is then defined by

$$T_{MC-LR} = n\left(w - \omega\right)^t \cdot V^1 \cdot \left(w - \omega\right) \tag{5.12}$$

in which w is set as $\left[MC, LMC, RMC\right]^t$, and ω and V are obtained based on the influence function of the estimators in w which, for the case of a normal distribution, are defined in (Brys *et al.*, 2008). The normality hypothesis of the data is rejected for values of $T_{MC\text{-}LR}$ larger than the critical value.

5.4 Selected case study structures

5.4.1 General description

The five RC structures chosen for the proposed study are briefly described in the following. The selection was such as to include both regular and irregular structures, as well as to consider non-seismically designed structures and structures designed according to modern seismic design procedures.

The first structure is the ICONS frame previously considered in Chapter 2. As previously referred, the ICONS frame is a four-storey, three-bay RC frame designed and built at the Joint Research Center in Ispra, Italy, for pseudo-dynamic testing (Carvalho *et al.*, 1999). The structure is representative of the design and construction common practice until the late 1970's in southern European countries and was designed for vertical loads only. The reinforcement details were specified in accordance to the normative available and to the construction practice at that time. The elevation view of the structure is presented in Fig. 5.1 along with the column cross section dimensions. All the beams are 0.25×0.50 m^2. In terms of the material properties, a concrete of class C16/20 and a hot-rolled steel of class S235 were selected, considering the mean values of the relevant properties. For additional information concerning the frame characteristics, the reader is referred to Carvalho *et al.* (1999).

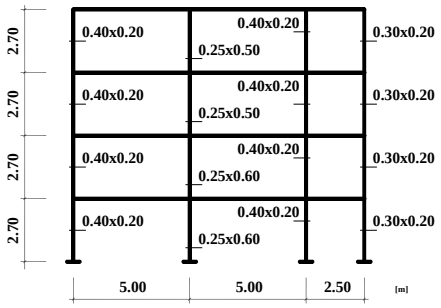

Figure 5.1. Elevation view of the ICONS frame and column cross section dimensions.

The second and third structures are the six-storey RC frames presented in (Ferracuti *et al.*, 2009). One of the frames, referred herein as REG6, is regular in elevation while the other, referred herein as IRREG6, has a setback. The elevation views of the frames are presented in Figs. 5.2a) and b) along with the column cross section dimensions. All the beams are 0.30×0.50 m^2. A steel with a yield strength of 414MPa and a concrete with a compressive strength of 33MPa were considered, following the values proposed in (Ferracuti *et al.*, 2009) for the material properties. Additional information concerning the frame characteristics can be found in (Ferracuti *et al.*, 2009). With respect to earthquake resistance, no available information indicates that seismic design provisions were considered for these structures.

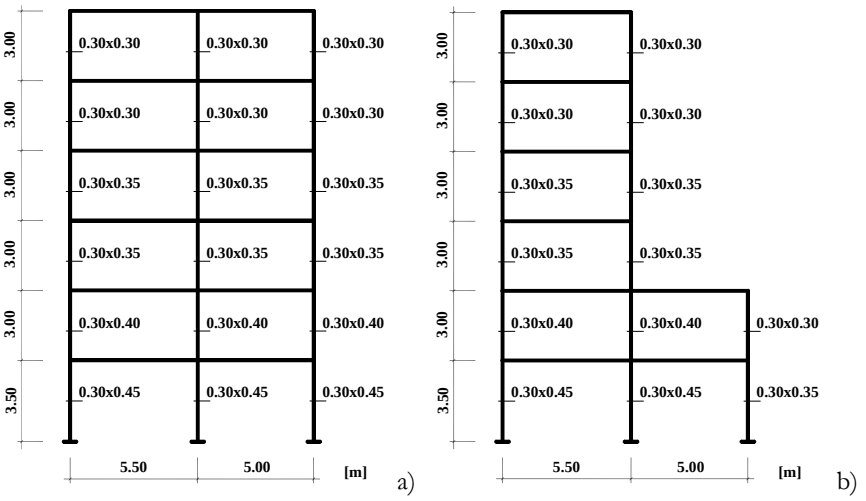

Figure 5.2. Elevation views of the REG6 and of the IRREG6 frames and of their column cross section dimensions.

The next structures are two ten-storey RC frames designed according to the requirements of Eurocode 8 (EC8-1, 2004) and presented in (Athanassiadou, 2008). The selected structures are the regular frame, referred herein as REG10, and one of the frames presenting irregularities over the height, referred herein as IRREG10, both designed for the high ductility class. These structures were designed considering a C20/25 concrete, a S400 steel and a peak ground acceleration (PGA) of 0.25*g*. The elevation views of the frames are presented in Figs. 5.3a) and b) along with the column cross section dimensions. The beams of structure REG10 are 0.25×0.75 m^2, in the first to the sixth storeys, 0.25×0.70 m^2, in the seventh and eighth storeys, and 0.20×0.60 m^2, in the ninth and tenth storeys. The beams of structure IRREG10 are 0.25×0.75 m^2, in the first to the fourth storeys, 0.25×0.70 m^2, in the fifth and sixth storeys, and 0.20×0.60 m^2, in the seventh to the tenth storeys. For additional information concerning the frame characteristics, the reader is referred to (Athanassiadou, 2008).

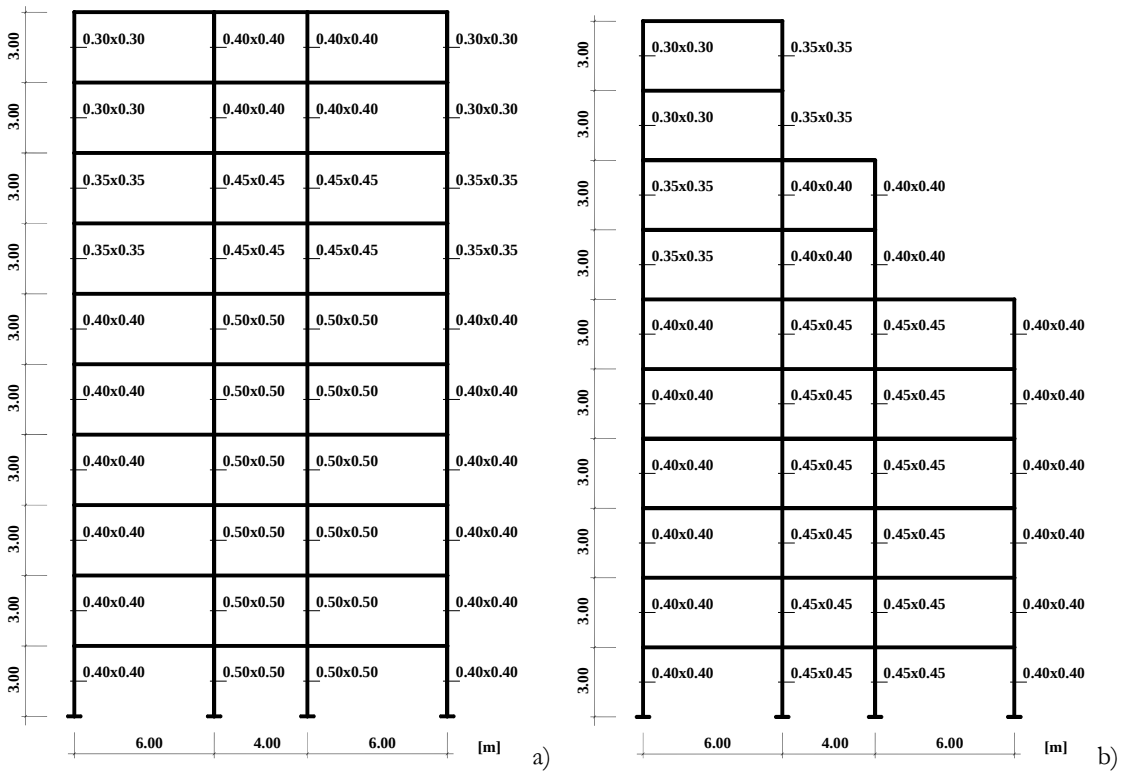

Figure 5.3. Elevation views of the REG10 and of the IRREG10 frames and of their column cross section dimensions.

5.4.2 Numerical modelling

The nonlinear response analysis of the frames under earthquake loading was carried out using a computer programme developed during previous research studies (Varum, 1997; Romão, 2002; Rodrigues, 2005). This computer programme is a two-dimensional analysis platform for the study of the nonlinear response of multi-storey RC buildings. The analysis of the structures is able to model the behaviour nonlinearities of beams and columns, as well as the large lateral deformations which are simulated by a leaning column that reproduces the destabilizing P-Δ effects of the gravity loading. Column and beam elements are modelled as member-type nonlinear macro-models with three zones: one internal zone with linear elastic behaviour and two plastic hinges, located at the member ends, where inelastic flexural behaviour is considered. Nonlinear analyses are carried out considering an event-to-event strategy with modification of the structure's stiffness matrix at each event and using the standard Newmark integration method for the dynamic analyses. Prior to a dynamic or pushover analysis, a nonlinear static analysis is carried out for the gravity loads acting on the structure, the results of which become the initial conditions for the subsequent analysis.

The inelastic behaviour of the plastic hinges is represented by moment-curvature relations. Trilinear skeleton curves associated with monotonic loading and with an initial slope reflecting the secant-to-yield stiffness were obtained following the work presented in

(Arêde and Pinto, 1996). Both asymmetric bending for beams and axial load effects for columns were considered. In beams, the elastic behaviour of the internal macro-model region was defined in order to reflect the cracked stiffness of the central part of the members when their bottom reinforcement is under tension. Slab participation to the beam tension flange was not considered.

Hysteretic flexural behaviour of the members was modelled by the piecewise linear hysteretic Costa-Costa model (Costa and Costa, 1987; CEB, 1996) which is a generalized Takeda-type model. Stiffness degradation and pinching effects were considered in the hysteretic behaviour of the structural members. With respect to the plastic hinge lengths, their values were considered equal to the depth of the member cross section for beams and equal to half of the depth of the member cross section for columns. Viscous damping was assumed to be proportional to the initial stiffness since, according to Faria *et al.* (2002) and references cited therein, the mass proportional term may induce a physically inadmissible dissipation under a rigid body motion, an aspect of particular importance when a soft-storey mechanism develops in the structure. The damping parameter was calculated for the first period of the structure considering a fraction of the critical damping equal to 2%. Periods were obtained assuming the mass of the structure to be distributed on the beams and the stiffness of the members to be defined by their secant-to-yield stiffness. Gravity loading was defined for each structure according to the values set in Carvalho *et al.* (1999), Ferracuti *et al.* (2009) and Athanassiadou (2008). Table 5.1 presents the periods of the first and second modes of the five structures along with their participating mass ratios. As can be seen, most structures are governed by the first mode since only structure IRREG6 has a stronger influence of the second mode.

Table 5.1. Periods and participating mass ratios (PMRs) of the selected structures.

Structure	Mode number	T (s)	PMR (%)
ICONS	1	1.10	79.4
	2	0.34	12.1
IRREG6	1	1.24	67.5
	2	0.46	21.9
REG6	1	1.40	79.9
	2	0.46	11.2
REG10	1	2.03	77.6
	2	0.72	10.8
IRREG10	1	1.82	75.2
	2	0.79	10.5

5.4.3 Seismic demand

The seismic demand considered for each structure consisted of a suite of fifty real ground motions extracted from the Pacific Earthquake Engineering Research Center NGA database (PEER-NGA, 2009). Each structure was analysed using a multi-stripe analysis (Jalayer and Cornell, 2009) where the selected ground motions are scaled for nine intensities in order to reflect different return periods. The selected return periods were 37, 73, 95, 225, 475, 976, 1980, 2480 and 4950 years which correspond to PGA values of 0.06*g*, 0.08*g*, 0.09*g*, 0.13*g*, 0.17*g*, 0.22*g*, 0.29*g*, 0.31*g* and 0.39*g*, respectively. The reference seismic scenario selected to define the scaling factors for each return period corresponds to that of Zone 3 of the Portuguese territory considering the intraplate seismic action and a soil of type B according to the Portuguese National Annex of Eurocode 8 (EC8-1, 2010). The PGA considered for this scenario was 0.17*g*, corresponding to a return period of 475 years. The values of the remaining parameters defining the response spectrum of the selected scenario are S = 1.35, T_B = 0.1s, T_C = 0.25s, T_D = 2.0s (EC8-1 2009). The PGA values associated to the other return periods were obtained based on the results of the hazard studies presented in Campos Costa *et al.* (2008).

For each structure, a specific suite of fifty ground motions was selected from the global NGA database according to the following criteria:

- Criterion 1: ground motions with moment magnitudes between 6.0 and 7.5, and epicentral distances between 25 km and 75 km.
- Criterion 2: ground motions, from those filtered by Criterion 1, that lead to a spectral matching scaling factor (*SF*) between 0.75 and 1.33, where *SF* is defined by

$$SF = S_a\left(T_1\right) \Big/ S_{a,ref}\left(T_1\right) \tag{5.13}$$

  in which $S_a\left(T_1\right)$ is the 5% damping spectral acceleration ordinate of the ground motion for the fundamental period of the structure T_1 and $S_{a,ref}\left(T_1\right)$ is the 5% damping spectral acceleration ordinate of the reference response spectrum for that same period and a return period of 475 years.
- Criterion 3: ground motions, from those filtered by Criterion 2, leading to a D_{rms} factor not higher than 0.20. The D_{rms} factor is the root-mean-square difference between the log of the response spectrum of the real record scaled by *SF* and the log of the reference response spectrum, over a given period range, defined by Eq. (5.14) (Buratti *et al.*, 2011). The selected period range was defined as being between T_2 and $1.5T_1$, where T_2 is the period of the second mode of the structure under consideration.

$$D_{rms} = \sqrt{\frac{\sum_{i=1}^{n}\left[\log\left(SF \cdot S_a\left(T_i\right)\right) - \log\left(S_{a,ref}\left(T_i\right)\right)\right]^2}{n}} \tag{5.14}$$

- Criterion 4: the fifty ground motions, from those filtered by Criterion 3, that present the lowest positive and negative (absolute values) mismatches between the response spectrum of the real record scaled by *SF* and the reference response spectrum, over the selected period range.

After selecting the fifty ground motions for a given structure, these were then scaled for the values of a selected intensity measure (IM) matching the return periods previously referred. Two IMs were considered therefore leading to two different sets of records that were used in the analysis of each structure. One of the considered IMs is the PGA and the other is the $S_a\left(T_1\right)$, simply referred to as S_a hereon. It is noted that a comprehensive discussion on the effects of ground motion scaling is beyond the scope of the proposed work. The reader is referred, for example, to Shome *et al.* (1998), Stewart et *al.* (2001), Kurama and Farrow (2003) and Luco and Bazzurro (2004) for discussions on this matter.

5.5 Results of the goodness-of-fit assessment

5.5.1 Initial considerations

General conclusions regarding the assessment of the selected statistical distribution hypotheses are presented in the following. For the sake of brevity, only a sample of the results is shown, along with representative figures illustrating the more important findings. The goodness-of-fit tests were applied to the structural demand data recorded at the control sections of the previously referred structures which were analysed under increasing levels of earthquake loading. As previously referred, each structure was analysed under a suite of fifty ground motions scaled up to nine intensities. However, in some of the structures, and for a given intensity level, convergence of the structural analyses was not achieved for all the ground motions due to global dynamic instability of some of the numerical analyses. To maintain the size representativeness of the considered demand datasets, a specific intensity level of a given structure was disregarded in the goodness-of-fit analysis when convergence was not achieved for more than five ground motions. Therefore, the size of the analysed datasets is always between forty-five and fifty. For these sample sizes *n*, Table 5.2 shows the critical values of the considered goodness-of-fit tests. Some of the critical values can be seen to be nearly constant across the different sizes while others exhibit more variability. Furthermore, it can also be observed that some of the critical values have a decreasing or increasing trend as the sample size decreases, while

others show a more erratic evolution. This latter aspect is a consequence of the empirical method used to obtain such critical values.

Table 5.2. Critical values of the selected tests for different sample sizes (LCV and UCV are the lower and upper critical values, respectively).

n	β_3^2	R_{sf}		T_w		CS	$T_{Π\_mom}^{(1)}$	$T_{Π\_mom}^{(2)}$	$T_{Π\_mom}^{(3)}$	$T_{MC\text{-}LR}$
		LCV	UCV	LCV	UCV					
50	5.98E-03	0.936	1.147	-1.912	2.005	1.015	5.962	5.952	5.950	7.321
49	6.15E-03	0.946	1.096	-1.912	2.003	1.015	5.952	5.957	5.959	7.384
48	6.33E-03	0.945	1.097	-1.913	2.007	1.015	5.965	5.954	5.950	6.614
47	6.50E-03	0.945	1.099	-1.911	2.007	1.016	5.952	5.951	5.951	6.735
46	6.74E-03	0.944	1.100	-1.910	2.006	1.016	5.958	5.955	5.954	7.253
45	6.95E-03	0.944	1.101	-1.914	2.005	1.016	5.954	5.950	5.943	7.357

The goodness-of-fit results are presented separately for the distributions of beam and column demand data, obtained from control sections located at the member ends, and for the maximum inter-storey drift demand over the height of the structure, ⊿. For beams and columns, test results are presented for the maxima of the curvature φ, of the chord rotation θ and of the shear force demand V. The chord rotation was computed according to the Exact Geometrical Method referred in Chapter 2. For curvature and chord rotation demand, tests were applied separately for positive and negative data. However, the combination of the random nature of the ground motions with the characteristics of a given structure imply that positive and negative demand values may not be obtained at some control sections for some of the records considered (e.g. in some sections, only negative curvatures reached the minimum size of forty-five while positive curvatures did not). Therefore, to maintain the size representativeness of the demand datasets, any curvature or chord rotation dataset for which such situation was observed for more than five ground motions is disregarded in the goodness-of-fit analysis. For these EDPs, the presented results are the average of the results obtained for both signs. To illustrate the size of the presented statistical study, Table 5.3 presents the number of considered datasets for φ, θ and V, for each structure, by type of structural element, and for both IMs, after removing the datasets that do not meet the minimum size of forty-five. Globally, the number of datasets is over 33000 (more than 16000 for each IM). With respect to ⊿, a total of 85 datasets were analysed.

Table 5.3. Number of analysed datasets by structure, by type of structural element, for EDPs of each section and for both IMs

		Beams						Columns					
Structure	IM →	PGA			S_a			PGA			S_a		
ICONS	EDP	φ	θ	V	φ	θ	V	φ	θ	V	φ	θ	V
	nº of datasets	223	219	120	362	357	192	319	319	160	511	512	256
REG6	EDP	φ	θ	V	φ	θ	V	φ	θ	V	φ	θ	V
	nº of datasets	381	372	216	372	364	216	591	598	324	579	584	324
IRREG6	EDP	φ	θ	V	φ	θ	V	φ	θ	V	φ	θ	V
	nº of datasets	270	261	144	259	251	144	446	449	252	431	435	252
REG10	EDP	φ	θ	V	φ	θ	V	φ	θ	V	φ	θ	V
	nº of datasets	957	924	540	940	906	540	1298	1299	720	1266	1266	720
IRREG10	EDP	φ	θ	V	φ	θ	V	φ	θ	V	φ	θ	V
	nº of datasets	781	768	432	769	753	432	1107	1115	612	1088	1092	612

Results are presented in terms of average percentage of acceptance (APA) data for the considered levels of seismic intensity, for the two selected IMs, and for both the normal and the lognormal statistical distribution hypotheses. The APA represents the number of times a certain group of tests does not reject a given distribution hypothesis, considering a confidence level of 95%. In quantitative terms, it is necessary to define a threshold APA value above which a given distribution hypothesis is accepted to be appropriate to model the probabilistic distribution of an EDP. Since demand distributions are not expected to follow a theoretical and idealized statistical model perfectly, a limit APA value of 75% was considered to be adequate to represent the average contribution of the control sections of all the structures, as well as the result of the different tests being considered. APA results below this 75% threshold are further analysed to examine the reasons for such score. With respect to the selected groups of tests, the following three groups are defined:

- Group 1 - Tests for symmetric data
- Group 2 - Tests for data with potential outliers
- Group 3 - All the tests from Group 1 and from Group 2

The subsequent discussion begins by presenting global results, i.e. average goodness-of-fit results considering the demand datasets of all the structures simultaneously, followed then by a more detailed structure-by-structure analysis. Based on this more detailed assessment, some aspects related to the individual demand datasets are also

discussed, namely in terms of the existence of potential outliers and of their influence on the goodness-of-fit results.

5.5.2 Presentation and discussion of the results

5.5.2.1 Global goodness-of-fit results

The goodness-of-fit results obtained from the application of the tests from Group 3 to the column and beam demand datasets of all the structures are presented in Figs. 5.4a) and b), respectively, for the case where PGA is the selected IM. Observation of these results shows that the lognormal distribution hypothesis yields better results for the probabilistic modelling of the φ and θ demand distributions. For the probabilistic representation of the shear force demand, both distribution hypotheses yield similar results. However, the APA results of the several EDPs do not meet the 75% threshold for several seismic intensities, particularly for the V demand in beams.

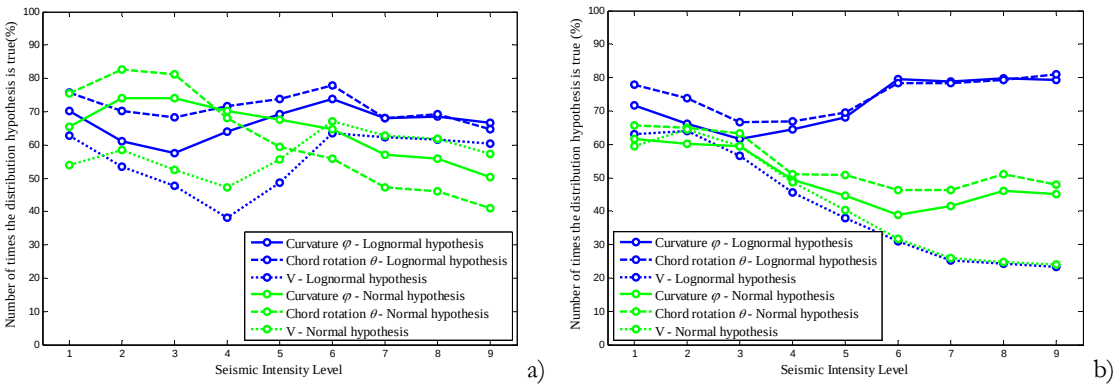

Figure 5.4. APA results from the tests of Group 3 for the column (a) and beam (b) datasets of all the structures, when PGA is the IM.

Figures 5.5a) and b) present results similar to those of Figs. 5.4a) and b) now for the case where S_a is the selected IM. As for the previous case, the lognormal distribution is seen to be more adequate to model the probabilistic distribution of the φ and θ demand. With respect to the shear force demand, again both distribution hypotheses yield similar results. More importantly, the observation of these results allows concluding that selecting S_a as the IM generally leads to higher APA results. Moreover, for the φ and θ demands, such APA results meet the 75% threshold for most seismic intensities. However, for the case of shear force demand, there are APA values below the referred threshold for several seismic intensities, particularly in beams.

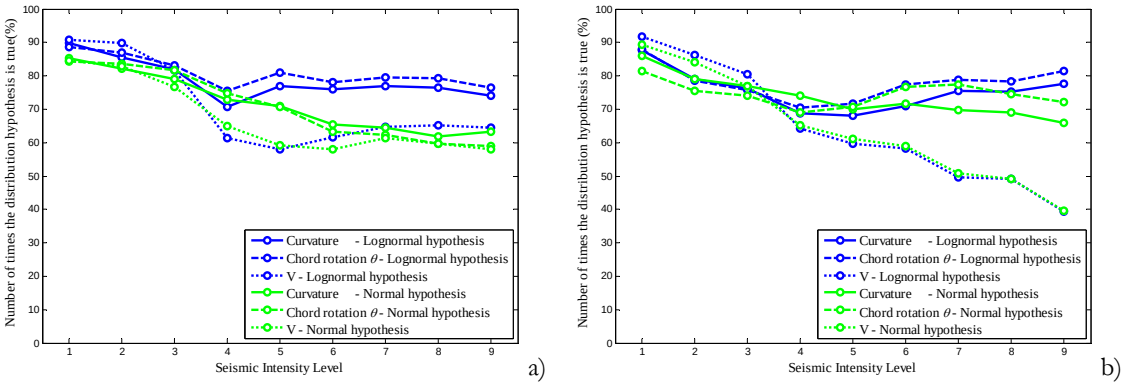

Figure 5.5. APA results from the tests of Group 3 for the column (a) and beam (b) datasets of all the structures, when S_a is the IM.

With respect to the ∠ demand, Figs. 5.6a) and b) present the goodness-of-fit results obtained from the application of the tests from Group 3 to the datasets of all the structures for the cases where PGA and S_a are the IM, respectively. The presented results indicate that the lognormal distribution is generally more adequate than the normal distribution to represent the probabilistic distribution of ∠. Furthermore, the advantage of one IM over the other is not as clear as for the previous EDPs. Still, S_a is favoured since it leads to higher APA results for the higher IM levels. Nonetheless, there are some APA values below the 75% threshold.

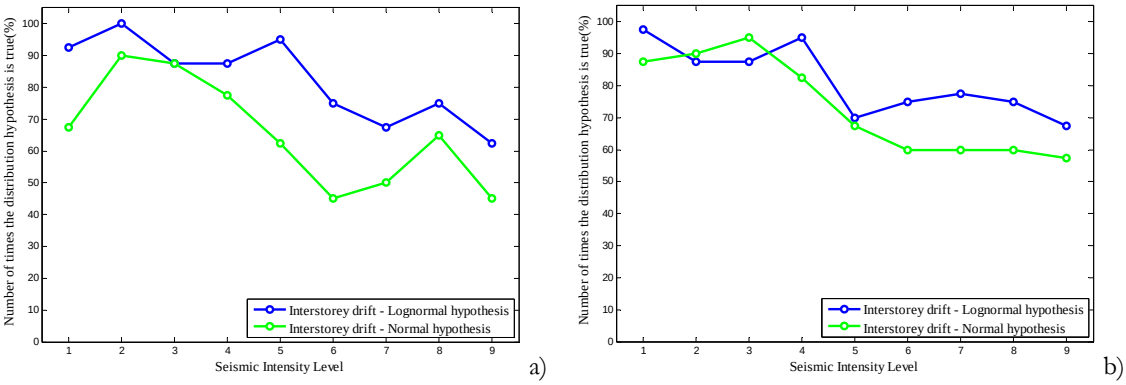

Figure 5.6. APA results from the tests of Group 3 for the inter-storey drift datasets of all the structures when PGA is the IM (a) and when S_a is the IM (b).

Globally, the presented results indicate that the lognormal distribution could be suitable for the probabilistic modelling of the φ and θ demand of beams and columns, as well as for the probabilistic modelling of the ∠ demand. With respect to the shear force demand, the results indicate that both the normal and the lognormal distributions may have the same potential to model the probabilistic distribution of this parameter. Furthermore, it is seen that S_a is a more adequate IM than PGA for the purpose of obtaining demand

distributions that are more compatible with the referred distribution hypotheses. However, the goodness-of-fit results are not totally satisfactory since there are APA values lower than the defined acceptance threshold for some of the IM levels. The reasons for such results are addressed in the more detailed structure-by-structure analysis presented in the following section where a more refined analysis of the demand datasets is proposed, along with some data processing measures that will improve the APA results.

5.5.2.2 Structure-by-structure goodness-of-fit results

In order to examine the reasons behind some of the lower APA results previously referred, some example situations exhibiting less satisfactory goodness-of-fit results are discussed next. It is noted that an extensive structure-by-structure presentation of the analysis of all the EDPs represents a prohibitive amount of information to be shown herein. Hence, for the sake of brevity, only a few selected cases are referred.

To illustrate a situation where goodness-of-fit results for φ are less satisfactory, Fig. 5.7a) presents the APA results obtained from the application of the tests from Groups 1, 2 and 3 for the columns of the REG10 structure when PGA is the selected IM. As can be observed, the goodness-of-fit results of the Group 3 tests for the lognormal distribution hypothesis do not meet the 75% APA threshold for some of the intensities and, for the lower intensities, the normal distribution hypothesis yields better APA results. Moreover, it can also be observed that, particularly for intensities 4 and 5, the results from the tests of Group 1 (tests for symmetric data) and 2 (tests for data with potential outliers) are considerably different. Since the APA results from the Group 2 tests are higher, such differences indicate that the demand datasets are asymmetric due to the existence of outliers in a number close to three (at each end of the datasets or at one end only). To illustrate this finding, Figs. 5.8a) and b) present, for intensity 4, the positive and negative, respectively, φ datasets (in log units) of all the columns of the REG10 structure. The vertical lines separate the φ datasets for the columns of the outer left, the inner left, the inner right and the outer right alignments, and each tick mark of the horizontal axis represents one control section. The presented demand distributions exhibit some asymmetry associated, in many sections, to a negative skew (the distribution tail is longer for the lower demand values) which indicates the presence of low demand values that are more distant from the core of the remaining values and that can be considered to be outliers.

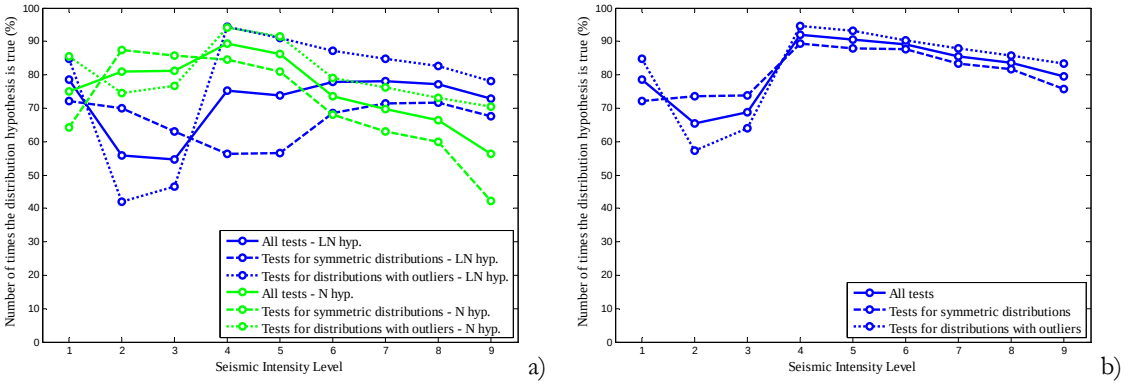

Figure 5.7. APA results for the REG10 column curvatures for the different test types when PGA is the IM (LN hyp. is the lognormal hypothesis and N hyp. is the normal hypothesis) (a) and enhanced APA results after the application of the DPMs for the lognormal hypothesis only (b).

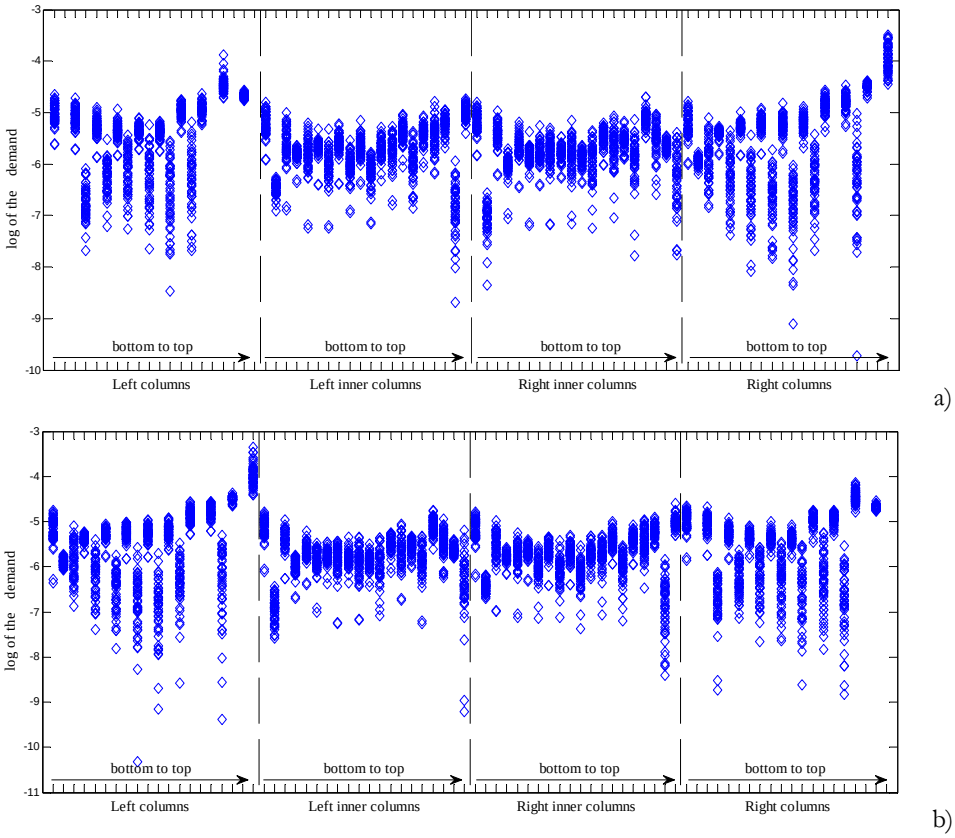

Figure 5.8. Individual positive (a) and negative (b) curvature datasets of the column sections of the REG10 when PGA is the IM.

To reduce the influence of the referred outlying observations and improve the APA results, several data processing measures were defined. Based on the observation of individual demand datasets of several intensity levels, the following three global data processing measures were considered:

- Data Processing Measure 1 (DPM 1) - Exclusion of the three lowest values from a given dataset (in absolute values, if the EDP is negative)
- Data Processing Measure 2 (DPM 2) - Exclusion of the three largest values from a given dataset (in absolute values, if the EDP is negative)

- Data Processing Measure 3 (DPM 3) - Exclusion of the three largest and of the three lowest values from a given dataset

In order to apply DPM 3, additional critical values of the tests were obtained for datasets of size forty-four. Due to the dataset size related aspects referred in Section 5.5.1, DPM 3 was applied to a smaller number of datasets than DPM 1 and DPM 2. On average, DMP 3 was applied to 90% of the datasets used for DPM 1 and DPM 2.

Since the thorough analysis of each individual dataset is beyond the scope of the present study, the selected measures are seen as global data processing approaches to be applied to all the datasets of a given EDP and for a certain intensity level.

For the referred case of structure REG10, the several DPMs were applied to the column φ datasets of all the intensity levels to obtain the highest possible APA results associated to the lognormal distribution hypothesis since, according to the preliminary conclusions previously referred, this distribution is favoured for the probabilistic modelling of φ. For intensity 1, the original APA values from Fig. 5.7a) are the highest, for intensities 2 to 5, which includes the case of the φ datasets of Figs. 5.8a) and b), the highest APA results were obtained by applying the DPM 1, for intensity 6, the highest values were obtained by applying the DPM 3, for intensities 7 and 8, the highest values were obtained by applying the DPM 2, and for intensity 9, the highest values were obtained by applying the DPM 2 to the positive φ datasets and the DPM 3 to the negative φ datasets. To illustrate these findings, Fig. 5.7b) presents the enhanced APA results of Fig. 5.7a) only for the lognormal distribution hypothesis. As can be observed, the APA results are now generally higher. Nonetheless, the results of intensities 2 and 3 are still below the 75% threshold. For these intensities, a number of datasets has been found to be mostly symmetric, since the results of the Group 1 tests are higher than those of Group 2, while other datasets are negatively skewed and exhibit more than 3 outliers (at each end of the datasets or at one end only), meaning that the application of the DPM 1 may be insufficient to lead to APA results that meet the target threshold. For the remaining intensities, it is noted that the results from the tests of Group 1 and 2 are closer to each other, meaning that the censored datasets are more symmetric and less influenced by outliers.

To further illustrate this type of analysis, Fig. 5.9a) presents another example now for the φ of the beams of the IRREG6 structure when S_a is the selected IM. In this example, it can be observed, for the particular case of intensity 4, that all groups of tests yield similar low results. Furthermore, it can be also seen that the normal distribution hypothesis leads to considerably higher APA results. Based on these results, it can be concluded that, for intensity 4, the original data is more symmetric than its logarithmic transformation and that, if there are datasets for which outliers occur under this transformation, their number will exceed three (at each end of the datasets or at one end only). To illustrate this latter aspect, Figs. 5.10a) and b) present, for intensity 4, the positive and negative, respectively, φ

datasets (in log units) of all the beams of the IRREG6 structure. The vertical lines of Figs. 5.10a) and b) separate the φ datasets for the beams of the left and the right bays. As can be observed, the datasets are, in general, negatively skewed, exhibiting a considerable number of outlying observations, particularly for the case of Fig. 5.10a). The reason behind such type of demand distribution is due to the fact that, for such intensity, some of the ground motions still lead to elastic demand, while others lead to demand values already in the plastic range. This mixture of demand values resulting from different behaviours observed in some sections then leads to the lower APA values that are observed. Still, this aspect does not invalidate the possible adequacy of the lognormal distribution to model the core of the datasets. As for the previous example, the several DPMs were applied to the beam φ datasets of all the intensity levels to obtain the highest possible APA results associated to the lognormal distribution hypothesis. The enhanced APA results presented in Fig. 5.9b) for this distribution can be seen to be globally higher, particularly those of intensity 4 which were obtained by applying the DPM 3 to the positive φ datasets and the DPM 1 to the negative φ datasets.

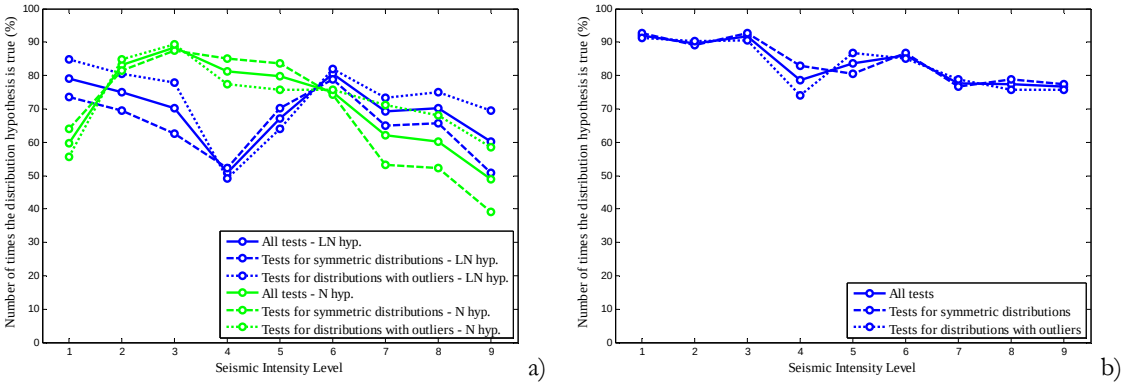

Figure 5.9. APA results for the IRREG6 beam curvatures for the different test types when S_a is the IM (LN hyp. is the lognormal hypothesis and N hyp. is the normal hypothesis) (a) and enhanced APA results after the application of the DPMs for the lognormal hypothesis only (b).

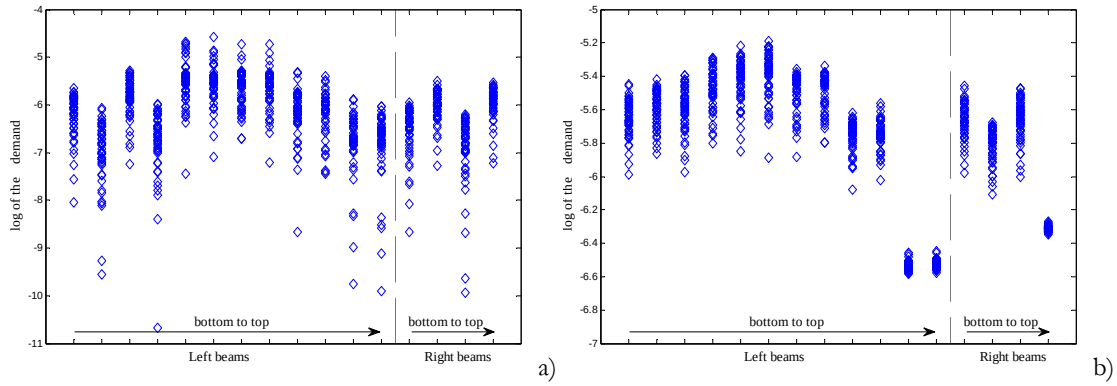

Figure 5.10. Individual positive (a) and negative (b) curvature datasets of the beam sections of the IRREG6 when S_a is the IM.

Similar analyses and conclusions were obtained for the other EDPs. For the case of θ, Figs. 5.11a) and b) present two examples for the case of the IRREG10 columns, when PGA is the IM, and of the REG6 beams, when S_a is the IM, respectively. As can be seen, the REG6 structure presents, for intensity 5, a case similar to that of the IRREG6 structure, while the IRREG10 presents, for intensities 7 to 9, a situation similar to the one analysed for the REG10 structure. After applying the DPMs to obtain the highest APA values, the results presented in Figs. 5.12a) and b) were obtained.

For the case of ⊿, Figs. 5.13a) and b) present two examples for the case of the REG10 structure, when PGA is the IM, and of the REG6 structure, when S_a is the IM, respectively. The observation of these results shows that the presented APA values are considerably low. However, it should be noted that, for each structure and for each intensity level, there is only one ⊿ dataset under analysis. Therefore, the presented results of the tests of Groups 1, 2 and 3 are, respectively, the average of 4, 4 and 8 test results only. These results also indicate that considering PGA as the IM leads to higher APA results for the lognormal distribution hypothesis. Furthermore, the results also show that, for intensities 5 to 9, the APA results of the REG6 structure are considerably influenced by the existence of outlying observations in a number up to three (at each end of the datasets or at one end only), since the results of the tests of Group 2 are all 100%. To illustrate this situation, Fig. 5.14 shows the inter-storey drift datasets (in log units) of the REG6 structure for all intensities. After applying the DPMs to obtain the highest APA values, the results for these structures and the lognormal distribution hypothesis are 100% for all intensities.

Based on the more detailed analysis of the results presented so far, it is possible to observe that the probability of acceptance of the lognormality or normality hypotheses may reach high values, e.g. close to 100%, but also very low values, e.g. close to zero, due to the individual characteristics of each dataset. Still, there is no single test that gives systematically lower acceptance results than the others, but it is possible to observe that when outliers are present, the results of tests from Group 1 are lower.

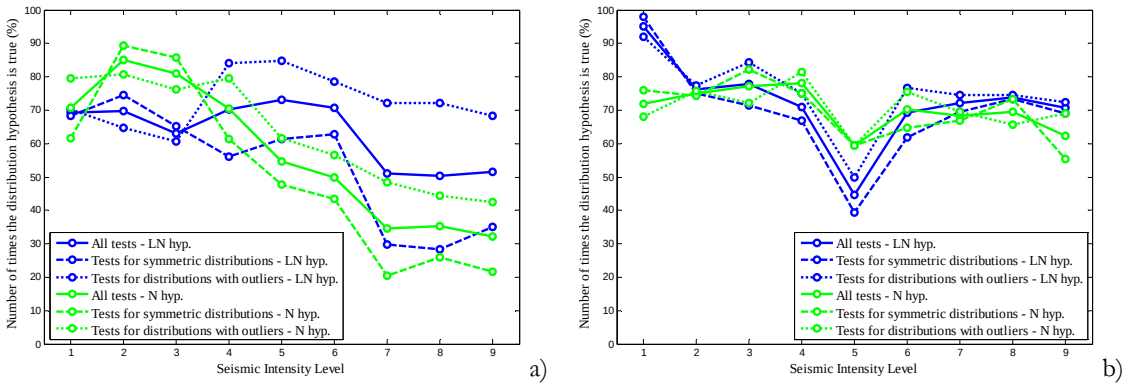

Figure 5.11. APA results for the IRREG10 column chord rotations for the different test types when PGA is the IM (a) and for the REG6 beam chord rotations for the different test types when S_a is the IM (b) (LN hyp. is the lognormal hypothesis and N hyp. is the normal hypothesis)

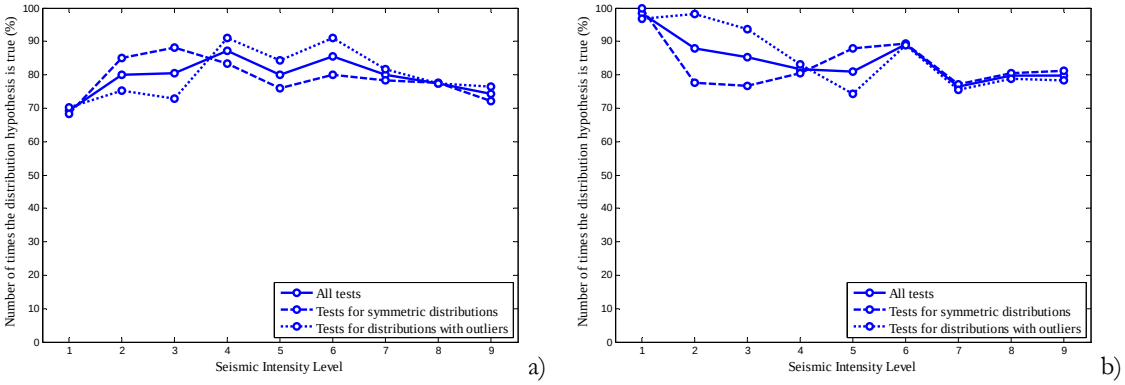

Figure 5.12. Enhanced APA results for the IRREG10 column chord rotations for the different test types when PGA is the IM (a) and for the REG6 beam chord rotations for the different test types when S_a is the IM (b), after the application of the DPMs for the lognormal hypothesis only

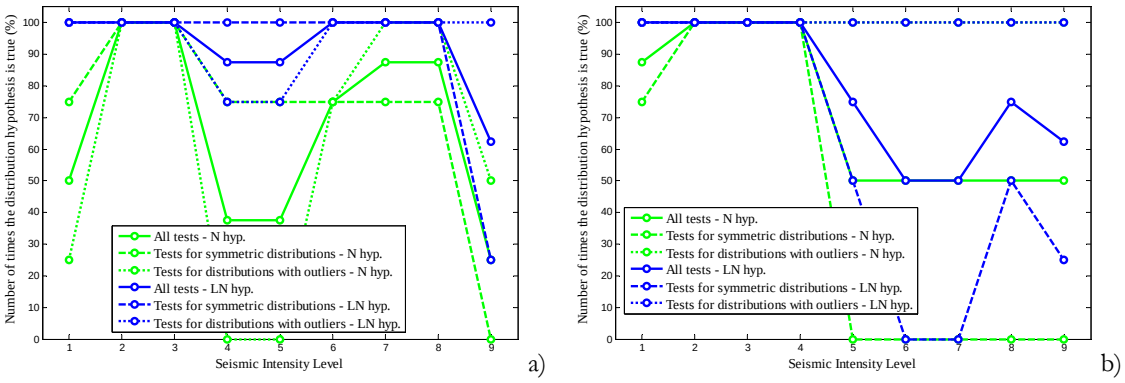

Figure 5.13. APA results for the inter-storey drift of REG10 for the different test types when PGA is the IM (a) and of REG6 for the different test types when S_a is the IM (b) (LN hyp. is the lognormal hypothesis and N hyp. is the normal hypothesis)

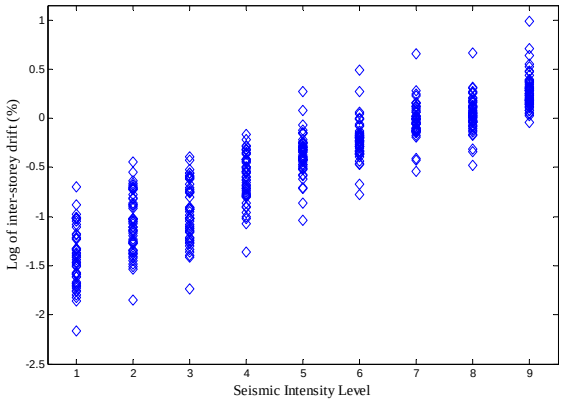

Figure 5.14. Inter-storey drift datasets of REG6 for all intensity levels when S_a is the IM.

With respect to V, Figs. 5.15a) and b) present examples, respectively, for the ICONS columns, when S_a is the IM, and for the IRREG10 columns, when PGA is the IM (the legend of Fig. 5.15b) is the same as that of Fig. 5.15a)). Generally, the APA values are lower for V than for the other EDPs and, as previously observed, both distribution hypotheses yield similar results. For intensities 2, 3 and 8, the ICONS structure presents a situation similar to that of the φ values referred in Fig. 5.9a). On the other hand, the IRREG10 case

is, for several intensities, similar to the situation analysed for the φ values of Fig. 5.7a). After applying the DPMs to obtain the highest APA values, the results presented in Fig. 5.16b) show there is a considerable increase in the APA results of the IRREG10 structure for intensities 4 to 9 and for both distribution hypotheses. On the other hand, for most intensity levels, the new APA results of the ICONS structure, Fig. 5.16a), have not increased sufficiently to meet the APA threshold. The reason behind the lower APA values obtained in this case is directly connected to the expected evolution of the V values. Since the post-yield stiffness of a structural member is usually low, the spread of the shear force demand distribution tends to be very small when a given structural member has yielded at both ends. In such cases, two caveat conditions were found to occur. In the first condition, some sections exhibited a shear force distribution which was found to be very irregular and, in some cases, almost uniform. In the second condition, some sections exhibited a shear force demand distribution with a set of values following the proposed distribution hypotheses mixed with a considerable number of outliers. This second condition was observed, for example, in sections where, for a particular IM level, some of the considered ground motions led to yielding while others did not.

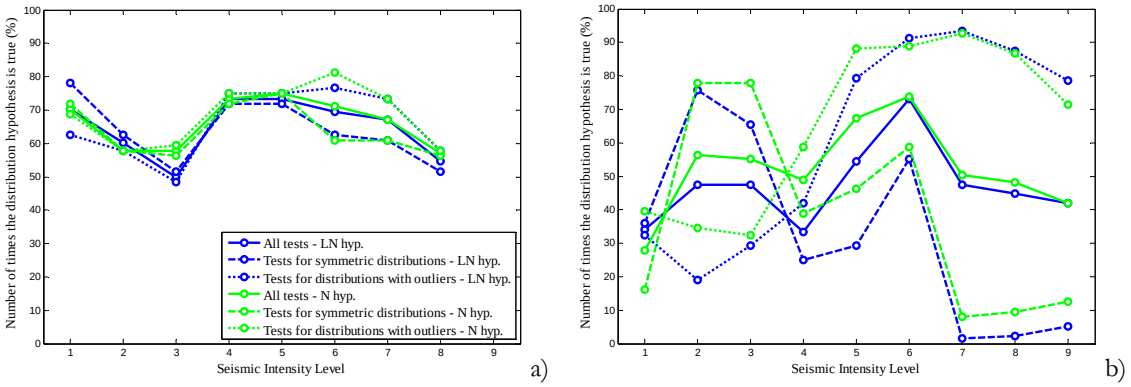

Figure 5.15. APA results for the ICONS column shear forces for the different test types when S_a is the IM (a) and for the IRREG10 column shear forces for the different test types when PGA is the IM (b) (LN hyp. is the lognormal hypothesis and N hyp. is the normal hypothesis)

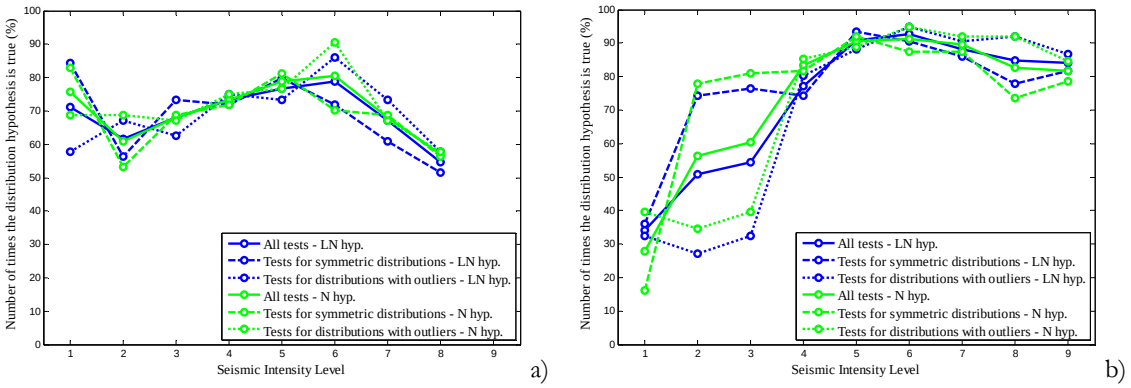

Figure 5.16. Enhanced APA results for the ICONS column shear forces for the different test types when S_a is the IM (a) and for the IRREG10 column shear forces for the different test types when PGA is the IM (b) (LN hyp. is the lognormal hypothesis and N hyp. is the normal hypothesis)

To illustrate the first condition, Fig. 5.17a) presents the shear force demand datasets of intensity 8 (in log units) for the column sections of the ICONS structure. As referred, the dispersion of the demand values is very low and such uniformity leads to more difficulties in fitting a normal or a lognormal distribution to the demand. To illustrate the second condition, Fig 5.17b) presents the *Q-Q* plot of the shear force demand for one of the central beam sections of the REG10 structure for intensity 9, when S_a is the IM, where it is clear that ten demand values fall outside the range of the remaining ones. The totality of the datasets for that case is presented in Fig. 5.17c) where both conditions can be observed. For this intensity, most of the left and right beams of the lower storeys have yielded, thus leading to the low dispersion of the demand, while the second caveat condition occurs in several central beams, namely in the top storeys. To further observe the influence of these two conditions, the APA results for that case are presented in Fig. 5.18a) where a clear decrease of the APA values can be observed as the IM level increases, i.e. as the nonlinearity extends to more beams. Moreover, the application of the DPMs does not lead to enhanced APA results that are much higher, as can be seen from the results presented in Fig. 5.18b).

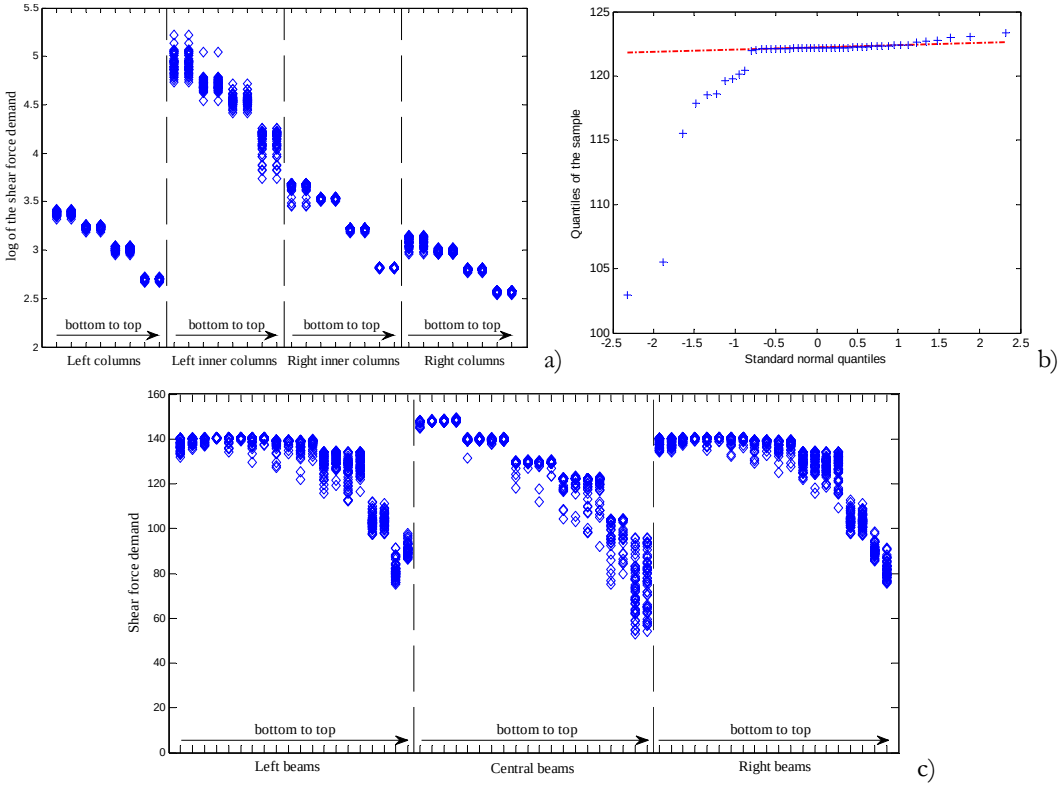

Figure 5.17. Individual shear force datasets for the columns of the ICONS structure and intensity 8 (in log units) (a), *Q-Q* plot of the shear force demand for one of the central beam sections of the REG10 structure for intensity 9, when S_a is the IM (b), and corresponding individual shear force datasets (c).

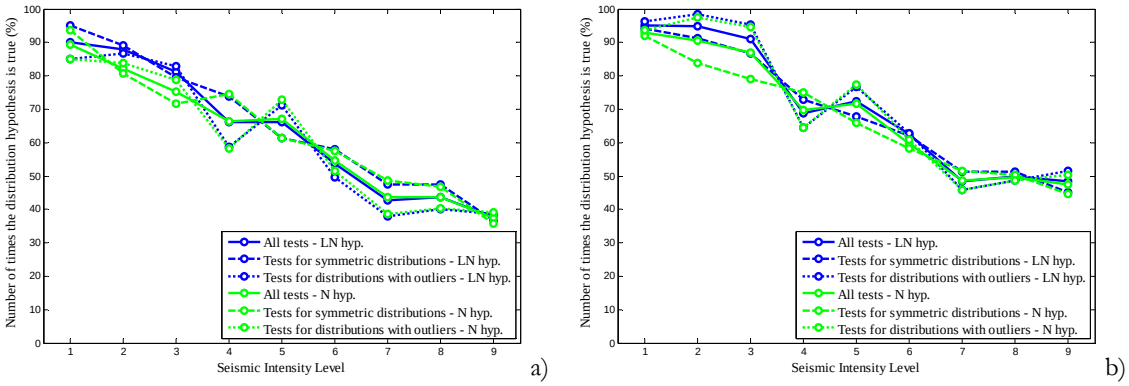

Figure 5.18. Shear force APA results (a) and enhanced APA results (b) for the beams of REG10 when S_a is the IM (LN hyp. is the lognormal hypothesis and N hyp. is the normal hypothesis)

Based on these results, it appears that the normal and the lognormal distribution may not be adequate to model the shear force demand distribution in some cases. Nonetheless, since such distributions are still appropriate in a number of situations, the effect of considering them in cases for which they are less adequate is addressed in the following to determine if their use can be foreseen. This analysis is based on the comparison of the shear force fragility values of selected sections calculated using the empirical and a fitted cumulative distribution function (CDF) of the demand, $F_{DP}(.)$. These fragility values p_f were calculated according to Eq. (5.15), where $f_C(.)$ is the probability density function (PDF) of the capacity, for the higher IM levels where the APA results are lower.

$$p_f = \int_0^\infty \left(1 - F_{DP}(\alpha)\right) f_C(\alpha) d\alpha \tag{5.15}$$

To illustrate this analysis and the results found, only a few selected examples are presented herein for the case of the normal distribution. It is nonetheless noted that similar results were obtained for the lognormal distribution. Figures 5.19a) to d) present the comparison of the empirical and fitted CDFs of the shear force demand of four sections: one column section of the ICONS structure for intensity 8, one beam section of the IRREG10 structure for intensity 9, one column section of the IRREG6 structure for intensity 9, when S_a is the IM, and the section of Fig. 5.17b). It can be observed that the normal distributions, which are based on the sample mean and standard deviation, produce a rather poor fit, particularly in the last two cases.

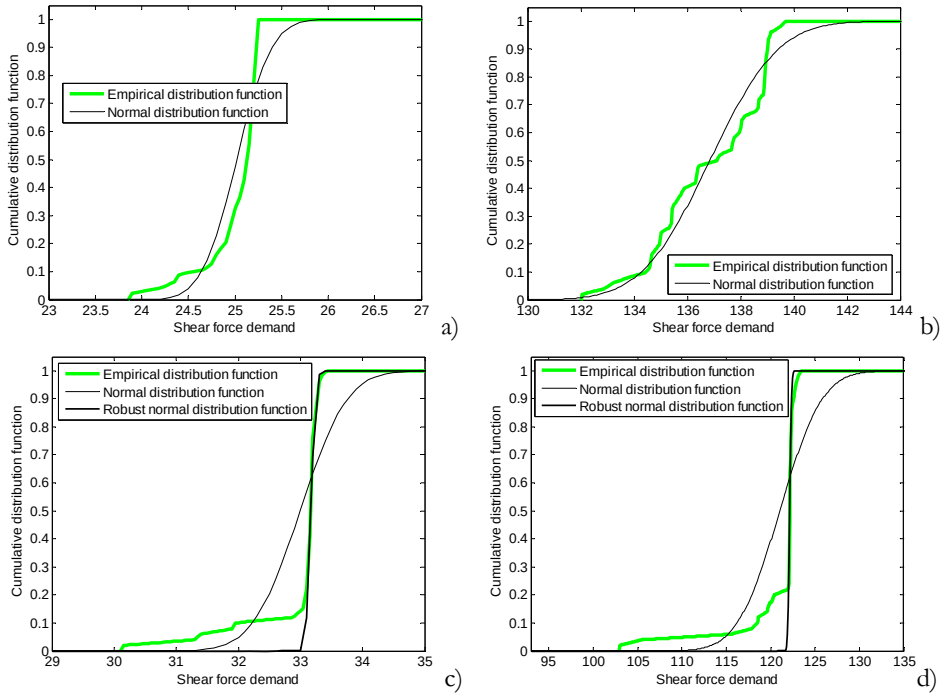

Figure 5.19. Comparison of the empirical and fitted demand CDFs for one column section of the ICONS structure for intensity 8 (a), one beam section of the IRREG10 structure for intensity 9 (b), one column section of the IRREG6 structure for intensity 9 (c), when S_a is the IM, and for the case of Fig. 5.17b) (d).

To be able to compare p_f values of different ranges, four capacity PDFs were considered for each section. The PDFs were defined by a normal distribution with a mean value C_μ and a standard deviation compatible with a selected coefficient of variation (CoV). Two values of the CoV were considered for each section in order to define situations of lower variability (CoV = 5%) and of larger variability (CoV = 30%). Although more sophisticated probabilistic models of the shear capacity could imply the consideration of a value larger than 30% (Song *et al.*, 2010), such limit serves the purpose of this analysis. On the other hand, the consideration of a CoV value of 5%, which can be seen to be rather low, enables highlighting a particular type of results of this analysis. For the selected sections, Table 5.4 presents the p_f values obtained for the empirical ($p_{f,emp}$) and the fitted normal ($p_{f,fit}$) demand CDFs, considering the referred capacity PDFs. As can be observed, the $p_{f,fit}$ values are always larger, i.e. on the safe side. The relative errors ε between the $p_{f,emp}$ and the $p_{f,fit}$ values are also presented in Table 5.4. As can be seen, the ε values obtained for all the sections are very low when the capacity distribution exhibits larger variability (CoV = 30%). Contrariwise, ε values are larger when the CoV is 5%. Furthermore, in this case, the ε values of the ICONS and IRREG10 sections are similar for both capacity PDFs while those of the IRREG6 and REG10 sections are considerably larger for the lower $p_{f,fit}$ values. This aspect is related to the inadequate normal distribution fits obtained for these two sections and to the lower degree of

overlapping between the demand and the capacity distributions in this case. When the CoV is larger, the numerically significant contribution of the PDF to the value of Eq. (5.15) is defined over a larger domain. This aspect appears to mask the differences between the empirical and the inadequate normal distribution fits that would lead to larger ε values, as for the case of a lower CoV.

To overcome the larger ε values, alternative normal distributions fits were considered for these two sections and for the CoV of 5%. These alternative fits were defined by computing the distribution parameters using robust estimators, namely the median, instead of the mean, and the dispersion measure s_{iqr}, instead of the standard deviation. Parameter s_{iqr} is based on the inter-quartile range of the data (Hoaglin *et al.*, 1983) and is defined by

$$s_{iqr} = \frac{P_{75\%} - P_{25\%}}{1.349} \tag{5.16}$$

where $P_{75\%}$ and $P_{25\%}$ are the 75th and 25th percentiles of the data, respectively. To observe how close these robust fitted CDFs are to the empirical CDFs, Figs. 5.19c) and d) present also the plots of the robust CDFs. As can be seen, the empirical and the fitted CDFs are much closer now for nearly 80% of the relevant domain. Furthermore, the new $p_{f,fit}$ values obtained for the robust fits, which are also presented in Table 5.4, are seen to be closer to the $p_{f,emp}$ values and to have ε values similar for both capacity PDFs.

From this analysis, the normal (and the lognormal) distribution may be seen to lead to inadequate fits of the demand or to inadequate APA results. However, the presented p_f results and those obtained for other sections indicate that the errors of considering this distribution tend to be low when the variability of the capacity is larger, and can be accepted when the variability of the capacity is lower. Furthermore, larger errors can be considerably reduced if adequate robust methods are used to determine the distribution parameters.

Table 5.4. Shear force fragility values p_f of the selected sections with the mean values C_μ and the CoVs of the considered shear force capacities, and the relative errors ε.

	CoV	ICONS column section	IRREG10 beam section	IRREG6 column section	REG10 beam section
Empirical CDF	0.05	3.34E-3 (C_μ = 29kN)	2.37E-3 (C_μ = 160kN)	1.26E-3 (C_μ = 39kN)	4.77E-3 (C_μ = 140kN)
		1.78E-2 (C_μ = 28kN)	1.13E-2 (C_μ = 155kN)	1.73E-2 (C_μ = 37kN)	2.52E-2 (C_μ = 135kN)
	0.30	8.89E-3 (C_μ = 85kN)	7.30E-3 (C_μ = 500kN)	7.38E-3 (C_μ = 120kN)	6.97E-3 (C_μ = 450kN)
		4.74E-2 (C_μ = 50kN)	2.07E-2 (C_μ = 350kN)	2.46E-2 (C_μ = 80kN)	2.29E-2 (C_μ = 300kN)
Normal fitted CDF	0.05	3.56E-3; ε = *6.73%* (C_μ = 29kN)	2.50E-3; ε = *5.58%* (C_μ = 160kN)	1.62E-3; ε = *28.5%* (C_μ = 39kN)	8.49E-3; ε = *77.9%* (C_μ = 140kN)
		1.86E-2; ε = *4.31%* (C_μ = 28kN)	1.17E-2; ε = *3.87%* (C_μ = 155kN)	1.97E-2; ε = *13.6%* (C_μ = 37kN)	3.53E-2; ε = *40.2%* (C_μ = 135kN)
	0.30	8.90E-3; ε = *0.18%* (C_μ = 85kN)	7.31E-3; ε = *0.15%* (C_μ = 500kN)	7.40E-3; ε = *0.28%* (C_μ = 120kN)	7.00E-3; ε = *0.43%* (C_μ = 450kN)
		4.75E-2; ε = *0.22%* (C_μ = 50kN)	2.08E-2; ε = *0.18%* (C_μ = 350kN)	2.47E-2; ε = *0.35%* (C_μ = 80kN)	2.30E-2; ε = *0.52%* (C_μ = 300kN)
Robust normal fitted CDF	0.05	-	-	1.40E-3; ε = *11.5%* (C_μ = 39kN)	5.44E-3; ε = *14.1%* (C_μ = 140kN)
				1.93E-2; ε = *11.2%* (C_μ = 37kN)	2.87E-2; ε = *14.0%* (C_μ = 135kN)

5.5.2.3 Enhanced global goodness-of-fit results

To emphasize the influence of the DPMs on the final APA values, goodness-of-fit results representing the enhanced APA results of Figs. 5.4a) and b), Figs. 5.5a) and b) and Figs. 5.6a) and b) are shown in Figs. 5.20a) and b), Figs. 5.21a) and b) and Fig. 5.22, respectively. Based on the previous analysis of the results, only the lognormal hypothesis is considered for φ, θ and ⊿. The analysis of the enhanced APA results indicates that for the φ, θ, and V demands, the best APA results are obtained when S_a is the IM. For ⊿ such trend is not as clear, though S_a is better for more intensities. It is also observed that only the APA results for the shear force do not meet the 75% threshold value, namely for

most intensities of the beam datasets and for intensity 4 of the column datasets. Still, the lognormal and normal distribution hypotheses are accepted in light of the fragility analysis previously presented. From the analysis of the enhanced APA results, the influence of outlying observations becomes clear and implies that adequate robust methods should be used to determine the distribution parameters.

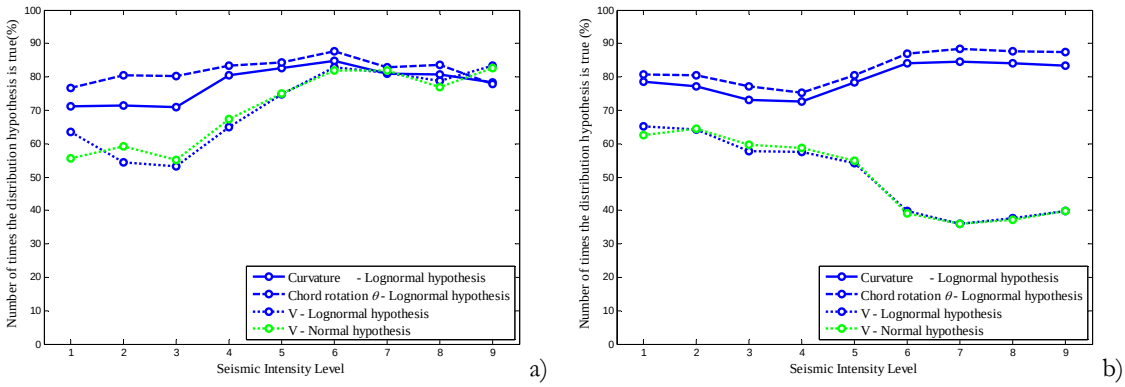

Figure 5.20. Enhanced APA results from the tests of Group 3 for the column (a) and beam (b) datasets of all the structures, when PGA is the IM.

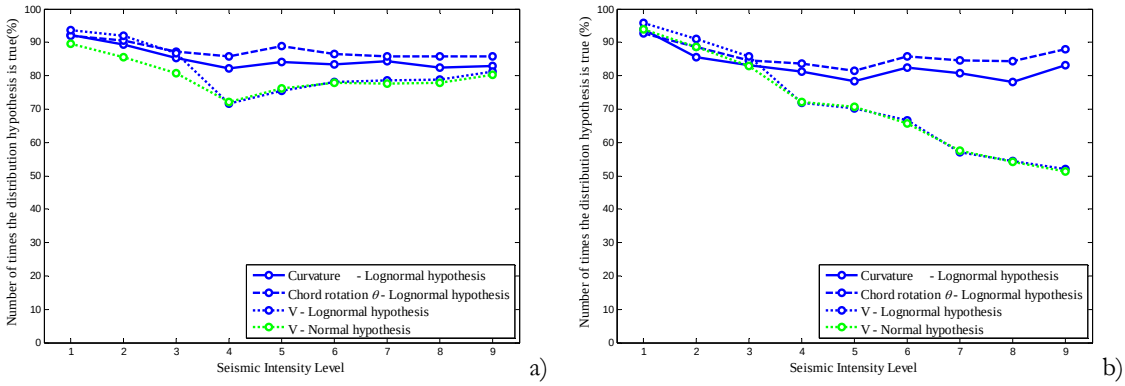

Figure 5.21. Enhanced APA results from the tests of Group 3 for the column (a) and beam (b) datasets of all the structures, when S_a is the IM.

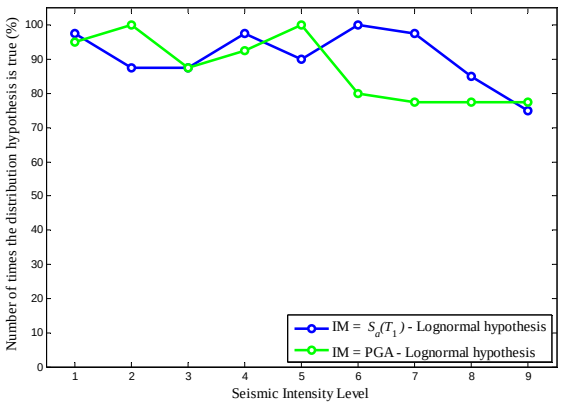

Figure 5.22. Enhanced APA results from the tests of Group 3 for the inter-storey drift datasets of all the structures for both IMs

5.5.3 Complimentary discussion of the results obtained by the Kolmogorov-Smirnov/Lilliefors test

Although the inadequacy of the K-S/L test to assess the normality (or lognormality) hypothesis of the data has been widely addressed in the previously referred statistics literature, its widespread use and large availability in commercial software make it interesting to briefly present and discuss some of the results that it can lead to.

The K-S/L test is a modification of the Kolmogorov-Smirnov test for normality proposed by Lilliefors (Lilliefors, 1967) for the case where the mean and the variance of the distribution are unknown and must be estimated from the data. The test statistic K-S/L is defined as

$$\text{K-S/L} = \max_{1 \le i \le n} \left[\Phi\left(x_i; \overline{x}; s^2\right) - (i-1)/n;\ i/n - \Phi\left(x_i; \overline{x}; s^2\right) \right] \tag{5.17}$$

where $\Phi\left(x_i; \overline{x}; s^2\right)$ is the cumulative distribution function of the normal distribution with parameters estimated from the data. The normality hypothesis of the data is then rejected for values of the statistic K-S/L larger than the critical value.

In order to illustrate the type of results that can be obtained when applying the K-S/L test to the EDP data of the structures considered herein, Fig. 5.23 presents APA results of this test along with those of the Group 3 tests before applying the DPMs. The results presented in Fig. 5.23a) are for the IRREG10 column shear forces, while those of Fig. 5.23b) are for the θ of the REG10 beams, both when S_a is the selected IM. As can be observed, the results of Fig. 5.23a) indicate that the K-S/L test is much more permissive than the Group 3 tests, leading, for the case of the lognormal distribution hypothesis, to APA values of 100% for all the intensities. On the contrary, Fig. 5.23b) shows an opposite trend of the K-S/L test APA results. In this case, the K-S/L test yields considerably lower results than those obtained by the Group 3 tests for all the intensities. Results obtained by the K-S/L test such as those of Fig. 5.23a) are common and are the reason for the widespread conclusion found in the statistics literature which refers that the K-S/L test is not adequate to test the normality (or the lognormality) hypothesis of the data. On the other hand, results such as those of Fig. 5.23b) are seldom mentioned. Still, this type of result has been recently addressed in (Drezner *et al.*, 2010) where it is referred that situations such as these may occur when the sample mean and standard deviation may not be the best choice of parameters to characterize the distribution required for the K-S/L test. According to the referred study, in some cases, the rejection/acceptance of the normality hypothesis by the K-S/L test depends on the distribution parameters considered. Hence, it is sometimes possible to define an optimized set of parameters leading to a fitted distribution that is closer to the empirical one (Drezner *et al.*, 2010). However, this optimization procedure does not correspond to the standard application of the K-S/L test. As an example of this situation, Fig. 5.24 presents the empirical CDF of the log of the

curvatures of one column of the REG6 structure, for intensity 5 and when S_a is the IM, with the CDF of two different fitted normal distributions. The difference between the two fitted distributions is in the way the central value is determined: in the first case the sample mean is used, while in the second case the median is considered instead. Goodness-of-fit results for this dataset indicate that all the Group 3 tests accept the normality hypothesis of the log of the data. However, the K-S/L test results vary: the hypothesis is rejected when the sample mean is used but it is accepted when using the median instead. It can be seen from Fig. 5.24 that the fitted distribution that uses the median is closer to the empirical CDF, a fact that leads to a value of the K-S/L statistic given by Eq. (5.17) of 0.12, instead of the value of 0.15 obtained when using the mean.

Based on the two examples of Fig. 5.23, the lack of objectivity of the K-S/L goodness-of-fit results becomes clear since this test can be either very permissive, or very severe. Hence, the acceptance of the normality or of the lognormality hypothesis of the data based on this test is not recommended.

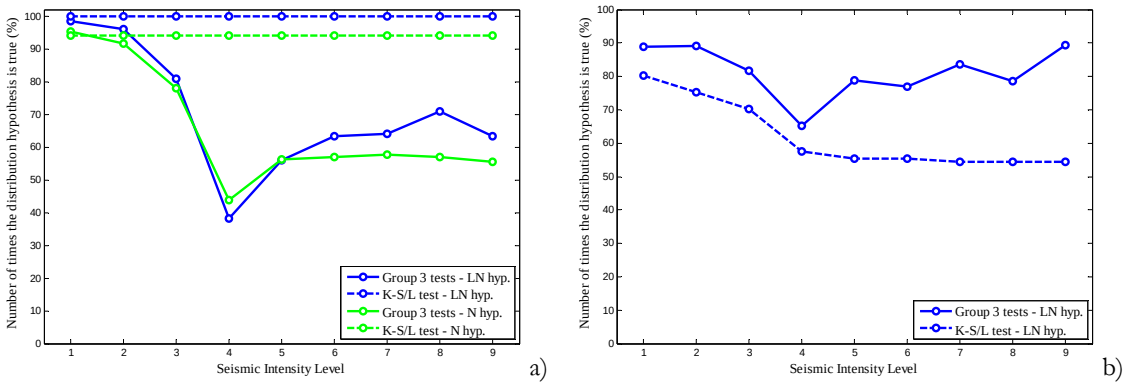

Figure 5.23. APA results from the tests of Group 3 (before applying the DPMs) and from K-S/L for the (a) IRREG10 column shear forces and for the (b) REG10 beam chord rotations, when S_a is the IM.

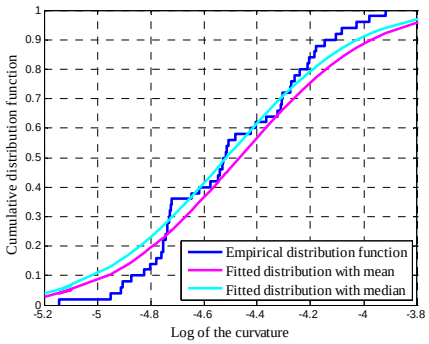

Figure 5.24. Empirical CDF of the log of the curvatures of one column of the REG6 structure, for intensity 5 and when S_a is the IM, with the CDF of two different fitted normal distributions.

5.6 Conclusions

A study was proposed to evaluate the hypothesis that a lognormal or a normal distribution could adequately model the probabilistic distribution of several EDPs. The selected EDPs were the curvature, the chord rotation, the shear force and the inter-storey drift over the height of the structure. Five structures were analysed for suites of fifty ground motions to obtain data samples with a size significant enough. The chosen records were scaled for several intensities to evaluate the referred hypotheses for different hazard levels, and two different IMs were also considered to evaluate the influence of this parameter.

The goodness-of-fit results were obtained using appropriate statistical methods and were presented in terms of APA (average percentage of acceptance) values data for the considered levels of seismic intensity, for the selected IMs, and for both distribution hypotheses. The APA results indicated that the lognormal distribution is suitable for the probabilistic modelling of the curvature, of the chord rotation and of the inter-storey drift demands. With respect to the shear force demand, the results indicated these distributions have the same potential to model its probabilistic distribution. In this case, the shear force APA results found were not totally satisfactory, either due to a distribution of the demand with very low levels of dispersion in yielding elements or due to the occurrence of a larger number of outlying observations. A fragility analysis was, nonetheless, performed to determine if the consideration of these distributions would lead to unacceptable errors. The results obtained from this analysis indicate that, for the structures considered herein, the selected distributions hypotheses lead to fragility values that are on the safe side with acceptable errors. Still, further structures should be analysed to confirm this conclusion. Although both distributions are acceptable to model the shear force demand, robust methods should be used to determine the distribution parameters in order to obtain more adequate fittings. With respect to the type of IM, S_a was seen to be typically more adequate than PGA for the purpose of obtaining demand distributions compatible with the selected distribution hypotheses.

Finally, the analysis of the individual datasets indicated that outlying observations were seen to occur in many situations. Enhanced APA results were obtained after defining and applying several DPMs (data processing measures) to the datasets. The differences between the original and the enhanced APA results emphasized the influence of the outliers, thus implying that adequate robust methods should be used to determine the distribution parameters in order to minimize their effects.

Chapter 6
Statistical characterization of structural demand under earthquake loading - Robust estimation of the central value of the data

6.1 Introduction

Performance-based earthquake engineering (PBEE) methodologies often require the adequate characterization of a "best estimate" of the structural demand, either in the context of deterministic or probabilistic analyses. In the former, a small number of nonlinear dynamic analyses is usually involved and the demand characterization can only be focussed on the "average" (central value) response of the system (Watson-Lamprey and Abrahamson, 2006; EC8-1, 2004). In the latter case, the evaluation of probabilistic performance parameters, such as the annual rate of exceeding a given structural demand level or the annual rate of exceeding some level of loss, requires the adequate characterization of the probabilistic demand. Considering that the referred probabilistic modelling of the demand can be achieved by fitting a lognormal or a normal distribution (see Chapter 5), its characterization requires estimates of the central value and of the dispersion of the data.

When analysing the statistics of real data, anomalous observations or outliers are often found. Although such outlying observations are considered to be errors in several situations (Hoaglin *et al.*, 1983), such reasoning is not directly applicable when seismic structural demand data is analysed. In this case, outliers can be, for example, inadequate demand parameters resulting from a structural analysis for which convergence was not achieved. Alternatively, outliers can also be demand values which are numerically distant from the rest of the sample due to an unforeseen reason. In this context, an outlier can be the result of a ground motion that led to an excessively low or high demand value when compared to that of other ground motions associated to the same intensity measure (IM).

In any case, outliers are observations masking the probability distribution of the majority of the data, thus requiring an adequate consideration of their significance.

Given that outliers can occur in the deterministic and the probabilistic analysis contexts, efficient statistical methods, such as robust estimation methods (Hoaglin *et al.*, 1983), should be used to obtain adequate estimates of the required demand statistics. In the presence of small departures from an assumed model, e.g. due to the existence of outliers, robust estimation methods are more suitable to characterize such statistical parameters since they are not overly affected by these departures. In this context, the current chapter and Chapter 7 present a wide scope study that focuses the statistical characterization of seismic demand using robust statistical methods. The current chapter presents a study addressing the characterization of the central value of structural demand distributions obtained under earthquake loading using different robust estimators. The study aims to test the performance of several estimators in order to identify those best suited for different types of data and sample sizes using adequate measures of statistical efficiency. In association to this study, Chapter 7 addresses the characterization of the dispersion of the structural demand distributions considered herein also using robust statistical methods.

6.2 Description of the proposed study

The presented study focuses both deformation- and strength-related engineering demand parameters (EDPs) and is based on local (section level) and global (system level) demand distributions obtained from the analysis of five reinforced concrete (RC) structures subjected to earthquake records of increasing intensities. At the section level, the selected EDPs are the maxima of the curvature, of the chord rotation and of the shear force, while at the system level, the chosen parameter is the maximum inter-storey drift over the height of the structure. It should be noted that the focus of the study does not address the magnitude of the central value in itself, but only deals with methods to assess this parameter with appropriate reliability.

The selected structures were analysed for suites of fifty ground motions to obtain data samples with a size significant enough. The chosen records were scaled for several intensities in order to evaluate the referred hypotheses for different hazard levels. In addition it is referred that two different IMs were also considered to evaluate the influence of this parameter on the conclusions of the study.

A series of estimators was then applied to the demand samples to identify those more adequate to characterize their central value. In order to assess the performance of the estimators for a wide range of conditions, they were applied to the samples of size fifty as well as to subsamples of size forty, thirty, fifteen and seven drawn from the samples of size fifty.

Since the proposed study is based on the structural demand results obtained for the five structures presented in Chapter 5, details about the modelling and analyses procedures, the quantification of the demand parameters, and the suites of fifty ground motions that were considered to represent the seismic demand are omitted herein.

6.3 Main concepts in robust estimation

The fundamentals of robust statistics, as well as of the robustness properties of estimators, are comprehensively addressed in a number of reference books, e.g. see Hoaglin *et al.* (1983), Hampel *et al.* (1986), Staudte and Sheather (1990), Wilcox (2005) Maronna *et al.* (2006). Still, some of the more important concepts are briefly reviewed in the following to provide some background context for the study presented herein.

In the presence of a "well behaved" data sample $x_1, x_2, ... x_n$ of size n, i.e. a sample without outliers, the best estimate of the central value is expected to be the mean $\bar{x}$

$$\bar{x} = \frac{1}{n}\sum_{i=1}^{n} x_i \tag{6.1}$$

which can be written also as

$$\bar{x} = \frac{1}{W}\sum_{i=1}^{n} w_i \cdot x_{(i)} \tag{6.2}$$

where w is a weight function with a value of one for each data value of the sample in this case, $x_{(i)}$ represents the *ith* order statistic of the sample and $W = \sum_{i=1}^{n} w_i = n$. The alternative form of representing $\bar{x}$ defined by Eq. (6.2) enables other estimators to be represented using this unified format. In a probabilistic context, under the hypothesis that the available data has been drawn from a normal distribution, $\bar{x}$ is also the most *efficient* estimate of the central value. In a similar situation, if the data follows a lognormal distribution instead, $\bar{x}$ is now the most efficient estimate of the central value of the log of the data. In this situation, the *efficiency* of an estimator is judged by its variance which can be obtained after applying the estimator to several samples of a given size drawn from the reference population. The most efficient estimator is that which exhibits the smallest variance. However, outlying observations are likely to occur in most practical situations, since a real data sample seldom follows an exact theoretical distribution model. In this case, it is well established that $\bar{x}$ is no longer a reliable estimate of the central value due to the potential bias introduced by the outliers. Therefore, the adequate characterization of the central value of the underlying normal or lognormal distribution must be carried out with methods having adequate *resistance* properties. The *resistance* of an estimator refers to its sensitivity to misbehaviour of the data (Hoaglin *et al.*, 1983). The *breakdown point* (Hampel, 1971) and the *influence function* (Hampel *et al.*, 1986; Staudte and Sheather, 1990) are two

widely used measures of the resistance of an estimator. The *breakdown point* is the smallest percentage of the sample observations that can be substituted by arbitrarily small or large values before the estimator no longer provides reliable information. For the case of $\overline{x}$, the breakdown point is known to be 0, while for the median it is 50%, which is actually the largest possible value for central value estimators (CVEs) that treat observations on both sides of the estimate symmetrically (Hoaglin *et al.*, 1983). The *influence function* measures the sensitivity of an estimator to different values of the observations and it may be used to describe the effect of outliers on the estimator. To illustrate this concept, Fig. 6.1 presents the influence functions of several estimators. From Fig. 6.1, it can be observed that, for the mean, the absolute value of the influence function increases as the distance between a certain observation and the central value of the data (zero in this case) increases, meaning that very large (or very small) observations will have a significant contribution to the estimate. On the other hand, for other estimators that will be reviewed with more detail in Section 6.4, the influence function can be seen to have a bounding value, beyond which the influence of the observations remains constant or decreases. For such estimators, the influence of very large (or very small) values is clearly reduced.

The *resistance* properties of robust estimators can also be seen as indirect indicators of their *sufficiency*. A sufficient estimator for a certain parameter θ of the data is one that captures all the information about θ contained in the sample. Assuming that all the data in the sample is important to estimate θ, a given estimator can be seen to be sufficient if it makes use of the whole sample to estimate θ. Since robust estimators reduce the importance of certain parts of the sample (either by trimming or by giving less weight to extreme values of the data), a loss in *sufficiency* is a characteristic of their definition. However, as referred by Hampel (1973), robust estimators are "nearly as" sufficient for the parametric model as the classical ones. Still, when using robust estimators to deal with samples with potential outlying values, i.e. when not all the data in the sample can be considered to be important to estimate θ, the gains in the accuracy of the inference and in the efficiency outweighs the loss in sufficiency.

Although the *efficiency* and *resistance* properties of an estimator are equally important, they are competing parameters; resistant procedures are less efficient when the underlying distribution is a true theoretical model, e.g. the normal distribution, but provide better results when the sample contains outliers. Therefore, the identification of the more suitable estimator for a given data sample is not evident, especially in situations where the level of departure from a considered underlying distribution is not known and may vary from sample to sample, as for the case of structural demand samples obtained under earthquake loading (e.g. see Chapter 5). Hence, to select estimators best suited to characterize the central value of this type of data, the performance evaluation of the estimators presented in the following is proposed.

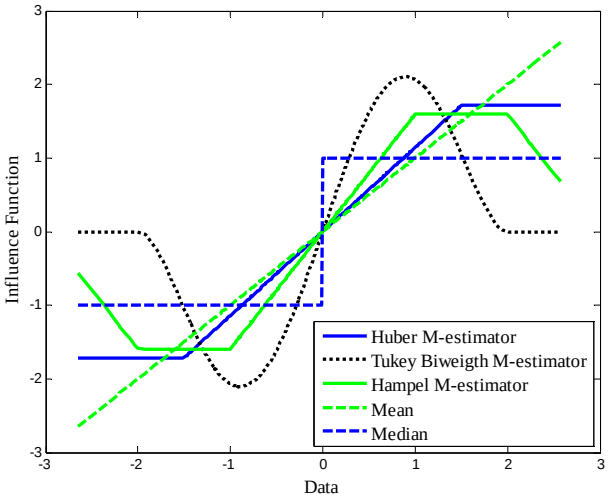

Figure 6.1. Influence functions of different estimators.

6.4 Selected central value estimators

The CVEs considered in the proposed study, other than $\bar{x}$, are addressed in the following. Fifty robust estimators are selected and grouped into three general categories. A brief review of each robust estimator is presented and additional information can be found in the references cited herein.

6.4.1 Estimators based on trimming

Estimators in this group reduce the influence of outlying observations by using subsamples of the original data.

6.4.1.1 The α-trimmed mean

The α-trimmed mean ($\bar{x}_{\alpha-tr}$) is the mean value of the data sample when the $p/2$ highest and lowest values are removed, where $p = \alpha \cdot n$. The value of $\bar{x}_{\alpha-tr}$ can be obtained using the unified format of Eq. (6.2) with $W = 1$ and w replaced by:

$$w_i = \begin{cases} \dfrac{1}{n-2p} & p+1 \le i \le n-p \\ 0 & otherwise \end{cases} \tag{6.3}$$

Several trimmed means are considered in the proposed study with different α values, namely with α set as 0.08, 0.12, 0.16, 0.20 and 0.24 which define the estimators $\bar{x}_{0.08-tr}$, $\bar{x}_{0.12-tr}$, $\bar{x}_{0.16-tr}$, $\bar{x}_{0.20-tr}$ and $\bar{x}_{0.24-tr}$, respectively.

6.4.1.2 The adaptive trimming estimators

While $\bar{x}_{\alpha-tr}$ only allows symmetric trimming of the samples, estimators based on adaptive trimming methods enable the possibility of asymmetric trimming based on measures of tail length and skewness of the data. Several CVEs using adaptive trimming methods have been tested by Keselman *et al.* (2007), following the proposals found in (Hogg, 1974; Hogg, 1982; Reed and Stark, 1996), and their results suggest the use of the estimators termed HQ1, HSK2 and HSK5.

After setting the desired level of trimming α, the proportion to be trimmed from the lower end of the sample $\alpha_{L,HSK2}$, $\alpha_{L,HSK5}$ and $\alpha_{L,HQ1}$ for estimators HSK2, HSK5 and HQ1, respectively, is:

$$\alpha_{L,HSK2} = \alpha \frac{x_{(1)} - M}{x_{(1)} - x_{(n)}} \tag{6.4}$$

$$\alpha_{L,HSK5} = \alpha \frac{x_{(1)} - \bar{x}}{x_{(1)} - x_{(n)}} \tag{6.5}$$

$$\alpha_{L,HQ1} = \alpha \frac{U_{(0.20)} - L_{(0.20)}}{U_{(0.20)} - L_{(0.20)} + U_{(0.50)} - L_{(0.50)}} \tag{6.6}$$

where $U_{(i)}$ and $L_{(i)}$ are the mean of the smallest and of the largest, respectively, $\lceil \alpha n \rceil$ observations of the sample, in which $\lceil k \rceil$ means that k is rounded to the nearest integer, and M is the median defined by:

$$M = med(x) = \begin{cases} x_{((n+1)/2)} & \text{if } n \text{ is odd} \\ \frac{1}{2}\left[x_{(n/2)} + x_{(n/2+1)} \right] & \text{if } n \text{ is even} \end{cases} \tag{6.7}$$

The proportions to be trimmed from the upper end of the sample $\alpha_{U,HSK2}$, $\alpha_{U,HSK5}$ and $\alpha_{U,HQ1}$ are then:

$$\alpha_{U,HSK2} = \alpha - \alpha_{L,HSK2}; \quad \alpha_{U,HSK5} = \alpha - \alpha_{L,HSK5}; \quad \alpha_{U,HQ1} = \alpha - \alpha_{L,HQ1} \tag{6.8}$$

The corresponding adaptive trimmed means $\bar{x}_{\alpha-HSK2}$, $\bar{x}_{\alpha-HSK5}$ and $\bar{x}_{\alpha-HQ1}$ can then be obtained by the following unified operator $\bar{x}_{\alpha-ad\_tr}$:

$$\bar{x}_{\alpha-ad\_tr} = \frac{1}{h} \sum_{i=t_L+1}^{n-t_U} x_{(i)} \tag{6.9}$$

where $h = n - t_U - t_L$, $t_U = \lfloor \alpha_U n \rfloor$ and $t_L = \lfloor \alpha_L n \rfloor$, and where α_U and α_L are replaced by the values obtained from Eqs. (6.4) to (6.8) for the different estimators. As for $\bar{x}_{\alpha-tr}$, the considered α levels of trimming were set as 0.08, 0.12, 0.16, 0.20 and 0.24.

6.4.1.3 The trimmed L-mean

A robust generalization of the sample L-moments (Hosking, 1990) has been formulated by Elamir and Seheult (2003) leading to the development of trimmed L-moments. The trimmed L-mean $\bar{x}_{\alpha-TL}$ can be obtained using the unified format of Eq. (6.2) with $W = 1$ and w_i replaced by:

$$w_i = \begin{cases} \dfrac{\binom{i-1}{p}\binom{n-i}{p}}{\binom{n}{2p+1}} & p+1 \le i \le n-p \\ 0 & otherwise \end{cases} \qquad (6.10)$$

where $\binom{i}{p}$ is $\dfrac{i!}{p!(i-p)!}$. As for $\bar{x}_{\alpha-tr}$, $p = \alpha \cdot n$ means that, for a trimming level α, the $p/2$ highest and lowest values are removed. Several $\bar{x}_{\alpha-TL}$ are considered in the proposed study with different α values, namely with α set as 0.08, 0.12, 0.16, 0.20 and 0.24 which define the estimators $\bar{x}_{0.08-TL}$, $\bar{x}_{0.12-TL}$, $\bar{x}_{0.16-TL}$, $\bar{x}_{0.20-TL}$ and $\bar{x}_{0.24-TL}$, respectively.

6.4.1.4 The Minimum Covariance Determinant estimator

The Minimum Covariance Determinant (MCD_a) estimator belongs to the class of high breakdown point estimators based on subranges (Rousseeuw, 1984). This estimator was originally targeted for multivariate data but it can also be applied to univariate samples. In this case, all the subsamples of size h of the original data must be defined, where $h = n(1-\alpha)$, and the MCD_a is set to be the mean of the subsample having the smallest standard deviation. To obtain MCD_a, the algorithmic procedure proposed by Rousseeuw *et al.* (1999) was considered. Several MCD_a are considered in the proposed study with different α values, namely with α set as 0.08, 0.12, 0.16, 0.20 and 0.24 which define the estimators $MCD_{0.08}$, $MCD_{0.12}$, $MCD_{0.16}$, $MCD_{0.20}$ and $MCD_{0.24}$, respectively.

6.4.2 M-estimators

M-estimators reduce the influence of outlying observations without removing them from the data. An M-estimator T_n is an estimator that is the solution of the equation:

$$\frac{1}{n}\sum_{i=1}^{n}\psi\left(\frac{x_{(i)}-T_n}{S_n}\right)=0 \tag{6.11}$$

where S_n is an auxiliary estimator of the spread of the data and ψ is a special weight function that reflects the influence function of the estimator. Since an iterative root-finding algorithm is required to compute T_n, the following procedure, based on the Newton-Raphson method and proposed by Rousseeuw and Verboven (2002), was used herein:

$$T_n^{(k)}=T_n^{(k-1)}+\frac{S_n}{n}\frac{\sum_{i=1}^{n}\psi\left(\frac{x_{(i)}-T_n^{(k-1)}}{S_n}\right)}{\int\psi'(u)d\Phi(u)} \tag{6.12}$$

where $T_n^{(k)}$ is the *kth* iteration estimate of T_n and $\Phi(.)$ is the standard normal distribution function.

6.4.2.1 The Huber M-estimator

For the case of the Huber M-estimator, the ψ-function is (Huber, 1981):

$$\psi(x)=\begin{cases}x & if\ |x|\le c\\ c\cdot sign(x) & if\ |x|>c\end{cases} \tag{6.13}$$

where $sign(x)$ is the sign function and c is a tuning constant. An example of the Huber ψ-function is presented in Fig. 6.1. The proposed study considers three versions of this estimator with c values of 1.0, 1.5 and 2.0 (Hoaglin *et al.*, 1983) termed $T_{Hub,1}$, $T_{Hub,2}$ and $T_{Hub,3}$, respectively. For all three cases, as well as for all the M-estimators defined hereon, the initial estimate $T_n^{(0)}$ was considered to be the *M*, and S_n was considered to be the median absolute deviation (*MAD*) given by:

$$MAD=1.4826\cdot med\left(|x_i-M|\right) \tag{6.14}$$

6.4.2.2 The modified Huber M-estimator

Due to the possibility of numerical instability issues associated to the original estimator, a modified version of the Huber M-estimator is presented by Pennacchi (2008) where the ψ-function is replaced by:

$$\psi(x) = \begin{cases} c \cdot sign(x) \cdot \sin(|x|/c) & if\ |x|/c \le \pi/2 \\ c \cdot sign(x) & if\ |x|/c > \pi/2 \end{cases} \tag{6.15}$$

In this case, a value of 1.2107 is suggested for c (Pennacchi, 2008) which defines the estimator T_{Hub_m}.

6.4.2.3 The Hampel M-estimator

In the case of the Hampel M-estimator, the ψ-function belongs to the class of redescending ψ-functions, i.e. functions which decrease towards zero for large values of the abscissa. For this estimator the ψ-function is defined as (Hoaglin *et al.*, 1983):

$$\psi(x) = \begin{cases} x & if\ |x| \le a \\ a \cdot sign(x) & if\ a < |x| \le b \\ \dfrac{a \cdot x - c \cdot sign(x)}{b - c} & if\ b < |x| \le c \\ 0 & if\ |x| > c \end{cases} \tag{6.16}$$

where a, b and c are tuning constants. An example of the Hampel ψ-function is presented in Fig. 6.1. The proposed study considers three versions of this estimator with (a, b, c) values of (1.7, 3.4, 8.5), (2.1, 4.0, 8.2) and (2.5, 4.5, 9.5) (Hoaglin *et al.*, 1983) termed $T_{Ham,1}$, $T_{Ham,2}$ and $T_{Ham,3}$, respectively.

6.4.2.4 The Andrew´s sine wave M-estimator

Andrew´s sine wave M-estimator T_{And} also uses a redescending ψ-function that is defined by (Hoaglin *et al.*, 1983):

$$\psi(x) = \begin{cases} \sin(x/c) & if\ |x| \le c \cdot \pi \\ 0 & if\ |x| > c \cdot \pi \end{cases} \tag{6.17}$$

where c is a tuning constant considered with a value of 2.1 (Hoaglin *et al.*, 1983).

6.4.2.5 The Tukey biweight M-estimator

The Tukey biweight M-estimator uses the redescending ψ-function presented in Fig. 6.1 and that is defined by (Hoaglin *et al.*, 1983):

$$\psi(x) = \begin{cases} x\left(1 - \dfrac{x^2}{c^2}\right)^2 & if\ |x| \le c \\ 0 & if\ |x| > c \end{cases} \tag{6.18}$$

where c is a tuning constant. The proposed study considers three versions of this estimator with c values of 4.0, 6.0 and 8.0 (Hoaglin *et al.*, 1983) termed $T_{Tuk,1}$, $T_{Tuk,2}$ and $T_{Tuk,3}$, respectively.

6.4.2.6 The logistic M-estimator

In this case, the ψ-function is characterized by the smoothed function proposed by Rousseeuw and Verboven (2002):

$$\psi(x) = \frac{e^x - 1}{e^x + 1} \tag{6.19}$$

which defines the estimator termed T_{log}.

6.4.2.7 The Welsch M-estimator

The Welsch M-estimator T_{Wel} was proposed by Dennis and Welsch (1978) and uses a soft redescending ψ-function defined by:

$$\psi(x) = x \cdot e^{-(x/c)^2} \tag{6.20}$$

where c is a tuning constant considered with a value of 2.9846.

6.4.3 Other estimators

Estimators in this group fall outside the previous categories and reduce the influence of outlying observations without removing them from the data.

6.4.3.1 The median

The median *M* is a commonly used CVE in the context of PBEE methodologies (e.g. see Aslani and Miranda (2005), Tothong and Luco (2007) among others) which is defined by Eq. (6.7).

6.4.3.2 The Hodges-Lehman estimator

The Hodges-Lehman estimator (*HL*) is well known in the robustness literature (Hampel *et al.*, 1986) and it is based on the $n(n+1)/2$ pairs of elements of the sample that can be defined (allowing each element to pair with itself). After computing the average value of each pair, *HL* is the median of the $n(n+1)/2$ averages, i.e.:

$$HL = med\left(\left(\frac{x_i + x_j}{2}\right); 1 \le i < j \le n\right) \tag{6.21}$$

6.4.3.3 The least power estimator

According to Sposito (1990), the least power (L_p) estimator of a central value can be generally defined as:

$$L_p = \arg_a \min\left\{\left(\sum_{i=1}^{n}\left|x_i - a\right|^p\right)\right\} \tag{6.22}$$

where $\arg_a \min$ stands for the value of argument *a* which minimizes the expression and *p* is a tuning constant. It can be seen (Pennecchi and Callegaro, 2006) that such value of *a* is the solution of:

$$\sum_{i=1}^{n}\left|x_i - a\right|^p \cdot sign\left(x_i - a\right) = 0 \tag{6.23}$$

Following the recommendation of Sposito (1990), the value of *p* was considered to be 1.5 in order to balance the robustness and the efficiency properties of this estimator.

6.4.3.4 The modified maximum likelihood estimator

The modified maximum likelihood estimator (*MMLE*) proposed by Tiku and Sürücü (2009), which has shown adequate robustness properties, can be obtained using the unified format of Eq. (6.2) with the weighting function defined by:

$$w_i = \left[1 + \frac{1}{k} \left(\frac{x_{(i)} - T_0}{S_0} \right)^2 \right]^{-2} \tag{6.24}$$

where k is a tuning constant considered to be 30 (Tiku and Sürücü, 2009) in order to balance the robustness and the efficiency properties of this estimator, and T_0 and S_0 are auxiliary initial estimates defined by the *M* and the *MAD*, respectively.

6.4.3.5 The T_{tanh} estimator

The robust and flexible T_{tanh} estimator is based on the hyperbolic tangent function and was proposed by Leonowicz *et al.* (2005). The T_{tanh} can be obtained using the unified format of Eq. (6.2) with the weighting function defined by:

$$w_i = \begin{cases} \tanh\left(k \cdot i - k\right) - s & i < n/2 \\ \tanh\left(k \cdot i - k \cdot n\right) - s & i \geq n/2 \end{cases} \tag{6.25}$$

where k and s are factors controlling the slope and the vertical shift of w_i. These factors were defined based on a preliminary sensitivity analysis of T_{tanh} for the standard normal distribution which led to the definition of two sets of parameters with different balances between robustness and efficiency. Therefore, $T_{tanh,1}$ considers k and s with values of 0.05 and 0 while $T_{tanh,2}$ considers both factors equal to 0.1.

6.4.3.6 The half-sample mode

The half-sample mode (*HSM*), which is a simple and fast estimator of the mode of a continuous distribution, was proposed by Bickel and Frühwirth (2006) as a CVE that is less sensitive to outliers. The process of determining *HSM* starts by finding the densest half-subset, i.e. the subset of the sample that is half the size and covers the shortest possible range. This process is then applied to this densest half-subset, and so on. Eventually, the set being considered has only two or three elements. In the former case, *HSM* is the mean of this set, while in the latter *HSM* is the mean of the two elements that are closer. To obtain *HSM*, the algorithmic procedure proposed by Bickel and Frühwirth (2006) was considered.

6.5 Selected methodology for the performance evaluation of the estimators

The question of determining which estimator is more adequate to characterize the central value of a given sample raises some issues on how to assess the efficiency of the estimator (the term efficiency is considered here with a wider scope than that of Section 6.3). Still, several approaches have been proposed to address this question. One possibility involves the quantification of an efficiency measure defined by a parameter associated to a given estimator which is then compared with that of a reference estimator. A common example of this approach is defined by the ratio between the variance of a given estimator and that of a reference estimator (Hoaglin *et al.*, 1983; Staudte and Sheather, 1990). This approach, however, has the drawback of requiring a sufficiently large number of estimates obtained from the reference data population to enable the reliable assessment of the variance of the estimator. When working with real data samples, this approach may not be possible to pursue since, as in the present study, only one sample is often available to estimate a given parameter. Therefore, this approach is best suited for performance assessment situations where theoretical probability distributions, either pure or contaminated by outliers, are simulated. A second possibility is the one proposed in Stigler (1977) which involves the quantification of several error metrics between a statistical estimate based on measured data and the true population value. This approach, however, is only applicable when the central value of the data under analysis is exactly known, a situation which is not that of the present study.

In the proposed study, the evaluation of the performance of the selected estimators is carried out over two different assessment stages. In Stage 1, all the selected estimators are compared against each other based on their performance for samples of size n_{ref} (the *reference size*). In this case, only one sample of the *reference size* is available for each parameter that needs to be estimated. The *reference size* considered in the present study is fifty. However, due to aspects which are related to the structural analyses and will be detailed in Section 6.6.1, some variability of this size is allowed. Therefore, without loss of generality of the results obtained in Stage 1, the *reference size* will be a value between forty-five and fifty, depending on the dataset under analysis.

Two measures of efficiency are considered in Stage 1 to assess the performance of the estimators: the Location Relative Efficiency (LRE) and the Relative Standard Error (RSE). The definition of the LRE follows the suggestion found in Hill and Padmanabhan (1991) of comparing the estimators on the basis of the estimated lengths of the confidence intervals (CIs), and involves a relative efficiency measure similar to those proposed by Sawilowsky (2002). The LRE of a certain estimator T, LRE_T, is defined by:

$$\mathrm{LRE}_T = \frac{T_{U95\%CI} - T_{L95\%CI}}{T_{ref,U95\%CI} - T_{ref,L95\%CI}} \tag{6.26}$$

where $T_{U95\%CI}$ and $T_{L95\%CI}$ are the upper and lower bounds of the 95% CI of estimator *T*, respectively, while $T_{ref,U95\%CI}$ and $T_{ref,L95\%CI}$ are the same parameters obtained for the *reference estimator* T_{ref}. The 95% CI of a given estimator is obtained by a bootstrap procedure with a bias corrected and accelerated percentile method (Wilcox, 2005), considering 1000 bootstrap samples, and T_{ref} is considered to be $\bar{x}$. Since an estimator *T* having a shorter CI means that the estimates it produces are less variable, values of LRE_T which are lower than one (the value of $\mathrm{LRE}_{T_{ref}}$) indicate that *T* is more efficient than T_{ref}.

With respect to the RSE, this efficiency measure is a modification of the previously referred ratio of variances from two estimators. The RSE of a certain estimator *T*, RSE_T, is defined by:

$$\mathrm{RSE}_T = \frac{s_T}{s_{T_{ref}}} \tag{6.27}$$

where s_T and $s_{T_{ref}}$ are the estimates of the standard deviation of *T* and T_{ref} obtained from the 1000 bootstrap samples, following the proposal from Wilcox (2005). As for LRE_T, values of RSE_T which are lower than one (the value of $\mathrm{RSE}_{T_{ref}}$) indicate that *T* is more efficient than T_{ref}.

As a result of Stage 1, the estimator exhibiting the best average performance over all the considered data samples is selected as the *reference estimator* for the Stage 2 evaluation. Furthermore, a subgroup of the initial estimators, corresponding to those with best performance, is also selected for Stage 2. It should be emphasized that, for the present study, a robust estimator will always be preferred with respect to a non-robust one such as $\bar{x}$. Therefore, the main goal of Stage 1 is to determine a subgroup of robust estimators that are more efficient than $\bar{x}$.

In Stage 2, for a given parameter that needs to be estimated, the performance of the subgroup of estimators is evaluated considering several samples of smaller size *n** which are drawn from the sample of the *reference size*. The considered sizes *n** are forty, thirty, fifteen and seven. The performance of a given estimator is then carried out with respect to the value of the new *reference estimator* T_{ref2} which is selected based on the LRE and RSE values obtained for all the estimators in Stage 1. Since *m* samples of size *n** are available to estimate each parameter in Stage 2, performance assessment measures different than those of Stage 1 are now considered. Such measures are the Relative Squared Error (RSE^*) and the Relative Absolute Error (RAE^*). The RSE^* of a given estimator *T*, RSE_T^*, is defined by:

$$\mathrm{RSE}_T^* = \frac{\sum_{i=1}^{m}\left(T_{i,n^*} - T_{ref\,2,n_{ref}}\right)^2}{\sum_{i=1}^{m}\left(T_{i,ref\,2\_n^*} - T_{ref\,2,n_{ref}}\right)^2} \tag{6.28}$$

where T_{i,n^*} is the value of estimator T for the *ith* sample of size n^*, $T_{i,ref\,2\_n^*}$ is the value of $T_{ref\,2}$ for the *ith* sample of size n^*, $T_{ref\,2,n_{ref}}$ is the value of $T_{ref\,2}$ for the original sample of size n_{ref} and m is selected to be 10000 for each sample size n^*. In a similar form, the RAE^* of a given estimator T, RAE_T^*, is defined by:

$$\mathrm{RAE}_T^* = \frac{\sum_{i=1}^{m}\left|T_{i,n^*} - T_{ref\,2,n_{ref}}\right|}{\sum_{i=1}^{m}\left|T_{i,ref\,2\_n^*} - T_{ref\,2,n_{ref}}\right|} \tag{6.29}$$

6.6 Results of the performance evaluation of the estimators

6.6.1 Initial considerations

General conclusions regarding the performance of the selected estimators are presented in the following. For the sake of brevity, only a sample of the results is shown, along with representative figures illustrating the more important findings. The estimators were applied to the structural demand data recorded at the control sections of the previously referred structures which were analysed under increasing levels of earthquake loading. As previously referred, each structure was analysed under a suite of fifty ground motions scaled up to nine intensities. However, in some of the structures, and for a given intensity level, convergence of the structural analyses was not achieved for all the ground motions due to global dynamic instability of some of the numerical analyses. To maintain the size representativeness of the considered demand datasets, a specific intensity level of a given structure was disregarded when convergence was not achieved for more than five ground motions. Therefore, in Stage 1 of the performance evaluation of the estimators, the *reference size* n_{ref} of the analysed datasets is always between forty-five and fifty, as referred in Section 6.5.

The performance assessment results are presented for the distributions of beam and column demand data, obtained from control sections located at the member ends, and for the maximum inter-storey drift demand over the height of the structure, ⊿. For beams and columns, results are presented for the maxima of the curvature φ, of the chord rotation θ and of the shear force demand V. The chord rotation was computed according to the Exact Geometrical Method referred in Chapter 2. For curvature and chord rotation

demand, the estimators were applied separately for positive and negative data. However, the combination of the random nature of the ground motions with the characteristics of a given structure imply that positive and negative demand values may not be obtained at some control sections for some of the records considered (e.g. in some sections, only negative curvatures reached the minimum sample size of forty-five while positive curvatures did not). Therefore, to maintain the size representativeness of the demand datasets and to keep n_{ref} between forty-five and fifty, any curvature or chord rotation dataset for which such situation was observed for more than five ground motions is also disregarded. Furthermore, it is noted that for estimators involving trimming of a dataset, when the trimming level is not an integer, the number of trimmed data values was rounded to the closest upper integer.

Results of Stage 1 are essentially presented in terms of the average percentage of larger efficiency (APLE) of an estimator T with respect to T_{ref} which was selected to be $\overline{x}$. APLE values represent the number of times that T is more efficient than T_{ref} and are obtained for the different EDPs considering the LRE and the RSE measures. Depending on the situation, APLE values are obtained by averaging across all the control sections of the structure or by averaging simultaneously across all the control sections of the structure and all the earthquake intensities. The approach of averaging across the earthquake intensities was selected since no specific range of ground motion intensities was seen to show that a given set of estimators was standing out from the others. Hence, the efficiency of the estimators was equally weighted across the whole range of intensities. Moreover, it was also observed that, for a given EDP obtained for a certain structure, the sequence of ground motion intensities for which a certain estimator is more efficient is roughly the same from estimator to estimator. In light of this, the performance results of all the intensities were able to be presented in a more concise form using the mean and the coefficient of variation (CoV) of the results for all the intensities.

Although Chapter 5 refers that the 5% damping spectral acceleration ordinate of the ground motion for the fundamental period of the structure T_1, $S_a(T_1)$, is a more adequate IM than the peak ground acceleration (PGA) for the purpose of obtaining EDP distributions more compatible with the lognormal or the normal distribution hypotheses, PGA is also considered herein in order to simulate a situation of larger variability of the demand and to assess the performance of the selected estimators under such conditions. In addition, it is noted that results are presented considering the curvature, the chord rotation and the inter-storey drift demands in log units, i.e. in order to be compatible with the assumption that demand follows a lognormal distribution (see Chapter 5). For the case of shear force demand, results are presented for the cases where V is in original and in log units, i.e. in order to be compatible with the assumption that demand can follow either a normal or a lognormal distribution (see Chapter 5). For a clear comprehension of the presented graphical results, the CVEs are numbered according to Table 6.1.

Based on the results of Stage 1, a subgroup of thirteen (i.e. ≈ 25% of the fifty-one) estimators and a new *reference estimator* $T_{ref\,2}$ are selected for the performance assessment carried out in Stage 2. The results of Stage 2 are similar to those of Stage 1, with the APLE value of an estimator T of the referred subgroup now being determined with respect to $T_{ref\,2}$, considering the RSE^* and the RAE^* measures, and considering samples sizes n^* of forty, thirty, fifteen and seven which are drawn from the sample of the *reference size*.

Table 6.1. Numbering of the selected CVEs

Number	CVE	Number	CVE	Number	CVE
1	$\overline{x}$	18	$\overline{x}_{0.12-HQ1}$	35	T_{Hub_m}
2	$\overline{x}_{0.08-tr}$	19	$\overline{x}_{0.16-HQ1}$	36	$T_{Ham,1}$
3	$\overline{x}_{0.12-tr}$	20	$\overline{x}_{0.20-HQ1}$	37	$T_{Ham,2}$
4	$\overline{x}_{0.16-tr}$	21	$\overline{x}_{0.24-HQ1}$	38	$T_{Ham,3}$
5	$\overline{x}_{0.20-tr}$	22	$\overline{x}_{0.08-TL}$	39	T_{And}
6	$\overline{x}_{0.24-tr}$	23	$\overline{x}_{0.12-TL}$	40	$T_{Tuk,1}$
7	$\overline{x}_{0.08-HSK2}$	24	$\overline{x}_{0.16-TL}$	41	$T_{Tuk,2}$
8	$\overline{x}_{0.12-HSK2}$	25	$\overline{x}_{0.20-TL}$	42	$T_{Tuk,3}$
9	$\overline{x}_{0.16-HSK2}$	26	$\overline{x}_{0.24-TL}$	43	T_{log}
10	$\overline{x}_{0.20-HSK2}$	27	$MCD_{0.08}$	44	T_{Wel}
11	$\overline{x}_{0.24-HSK2}$	28	$MCD_{0.12}$	45	M
12	$\overline{x}_{0.08-HSK5}$	29	$MCD_{0.16}$	46	HL
13	$\overline{x}_{0.12-HSK5}$	30	$MCD_{0.20}$	47	L_p
14	$\overline{x}_{0.16-HSK5}$	31	$MCD_{0.24}$	48	$MMLE$
15	$\overline{x}_{0.20-HSK5}$	32	$T_{Hub,1}$	49	$T_{tanh,1}$
16	$\overline{x}_{0.24-HSK5}$	33	$T_{Hub,2}$	50	$T_{tanh,2}$
17	$\overline{x}_{0.08-HQ1}$	34	$T_{Hub,3}$	51	HSM

6.6.2 Presentation and discussion of the results

6.6.2.1 Results of Stage 1

The APLE results for the LRE and the RSE of all the estimators obtained for the positive curvature φ demand of the REG6 sections, for all the intensities and when $S_a(T_1)$ is the IM, are presented in Figs. 6.2 and 6.3, respectively. Each point represents an APLE value that considers all the sections of the structure. From these results, the APLE values of the LRE and the RSE can be seen to exhibit a similar trend, thus indicating the same estimators as being the more efficient. Furthermore, the variability of the APLE values between estimators is seen to be large and to depend also on the selected earthquake intensity. For the presented case, it appears that mid-range intensities are those where the estimators have a better performance, with some estimators reaching APLE values close to 80%. This fact is related to the type of demand distribution that is obtained for these

intensities. As referred in Chapter 5, some of the ground motions lead to elastic demand, while others lead to demand values already in the plastic range. This mixture of demand values resulting from different behaviours, which is observed in some sections, enhances the higher efficiency of robust estimators in dealing with more irregular demand data when compared to that of $\overline{x}$.

Although there are considerable differences between the performance of the estimators, the central values they yield do not exhibit large variability. To illustrate this, Fig. 6.4 presents the CoV of the fifty-one central values obtained by the estimators, for each REG6 positive φ dataset, for all the intensities, and after transforming the data back to original units. As can be seen, most CoVs are below 10% (similar values are obtained for the negative φ demand) which indicates that, although the several estimators may yield central value estimates that are not far from each other, the efficiency measured by the LRE and the RSE enables the identification of the more adequate estimators. To obtain a more global view of the performance of the estimators, APLE values of the LRE and the RSE now also averaged across the earthquake intensities are presented in Figs. 6.5 and 6.6 for the positive and negative, respectively, φ demand of the REG6 sections. Due to the referred variability of the APLE values between earthquake intensities, it can be seen that, for the more efficient estimators, both LRE and RSE APLE values are not higher than 50% (left-hand side scale of the graphs). From these results, estimators 17, 18, 19, 20, 34, 37, 38, 42, 43, 47, 48 and 49 ($\overline{x}_{0.08-HQ1}$, $\overline{x}_{0.12-HQ1}$, $\overline{x}_{0.16-HQ1}$, $\overline{x}_{0.20-HQ1}$, $T_{Hub,3}$, $T_{Ham,2}$, $T_{Ham,3}$, $T_{Tuk,3}$, T_{log}, L_p, *MMLE* and $T_{tanh,1}$) are seen to be some of the more efficient in this case. To give a measure of the relative variability of the APLE values across the earthquake intensities, Figs. 6.5 and 6.6 also present the CoV of both the LRE and the RSE APLE values. As can be seen, most CoVs are below 50%.

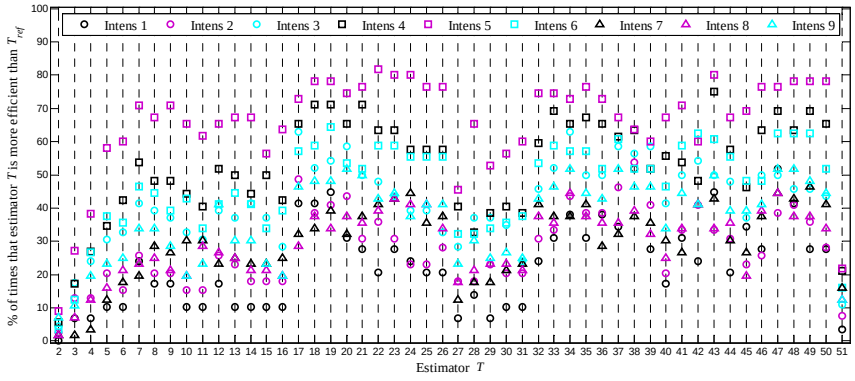

Figure 6.2. APLE values of the estimators, for the LRE, for the REG6 positive curvatures when $S_a(T_1)$ is the IM, for all the intensities.

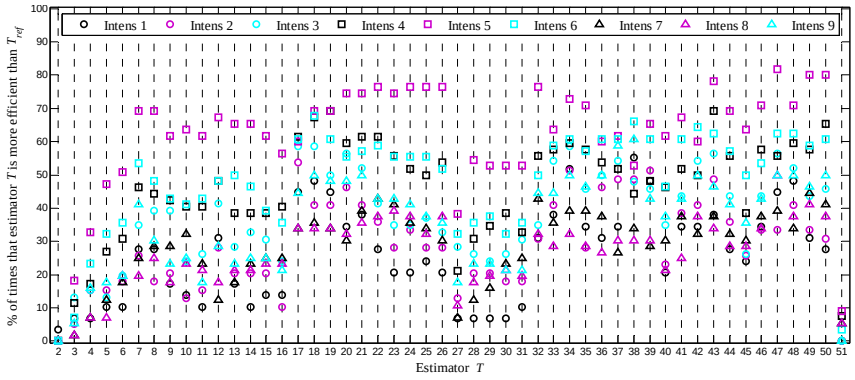

Figure 6.3. APLE values of the estimators, for the RSE, for the REG6 positive curvatures when $S_a(T_1)$ is the IM, for all the intensities.

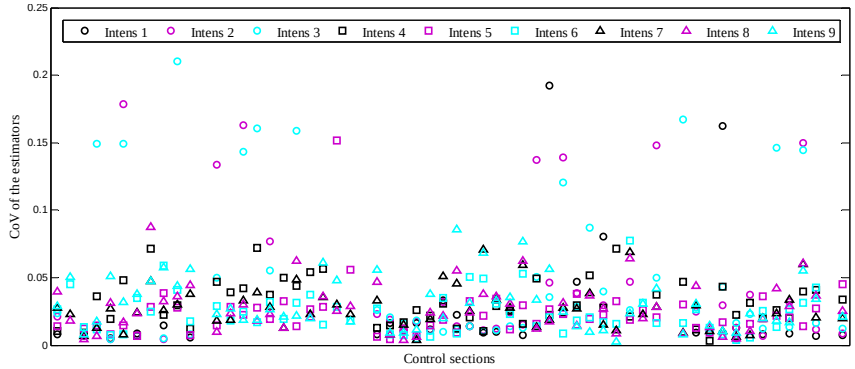

Figure 6.4. CoV of the central values obtained by all the estimators for the REG6 positive curvatures when $S_a(T_1)$ is the IM, for all the intensities and control sections.

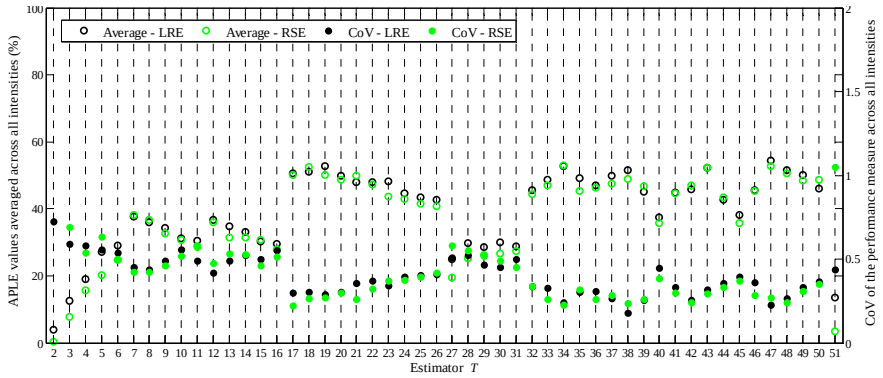

Figure 6.5. APLE values of the estimators, for the LRE and the RSE, for the REG6 positive curvatures when $S_a(T_1)$ is the IM, averaged across all the intensities, and CoVs representing the variability between intensities.

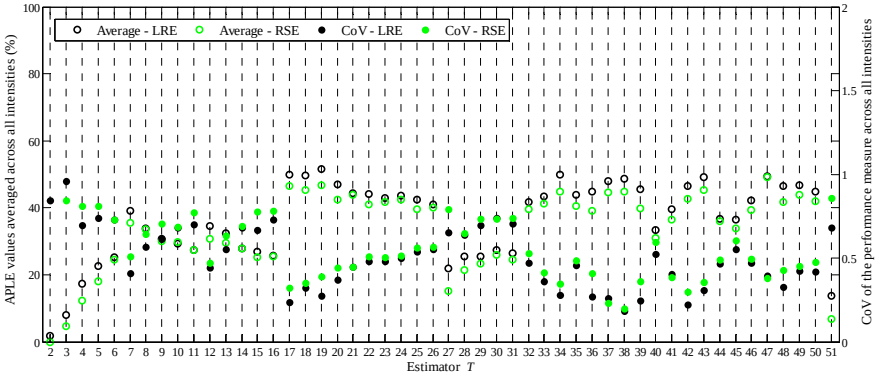

Figure 6.6. APLE values of the estimators, for the LRE and the RSE, for the REG6 negative curvatures when $S_a(T_1)$ is the IM, averaged across all the intensities, and CoVs representing the variability between intensities.

In terms of chord rotation demand, Fig. 6.7 presents, for the case of the IRREG10 negative θ demand, the APLE results for the LRE of all the estimators, for all the intensities and when PGA is the IM. APLE results obtained for the RSE and for the positive θ demand are similar. As for the results of REG6, the variability of the APLE values between estimators and between the selected earthquake intensities is seen to be large. For this structure, the higher ground motion intensities are those where the estimators have a better performance, with some estimators reaching APLE values close to 90%. Furthermore, as for the previous case, the CoV of the fifty-one central values obtained by the estimators for each IRREG10 negative θ dataset, for all the intensities, and after transforming the data back to original units, is also mostly below 10% (Fig. 6.8). Similar to Fig. 6.5, Fig. 6.9 presents, for the negative θ demand of the IRREG10 sections, APLE values of the LRE and the RSE now also averaged across the earthquake intensities. These results also include the CoVs of these APLE values reflecting their variability across the earthquake intensities. Again, the LRE and RSE APLE values are very similar and, due to the referred variability between earthquake intensities, not higher than 60%, while CoVs are generally below 50%. With respect to the more efficient estimators for θ, these are seen to be similar to those identified for φ.

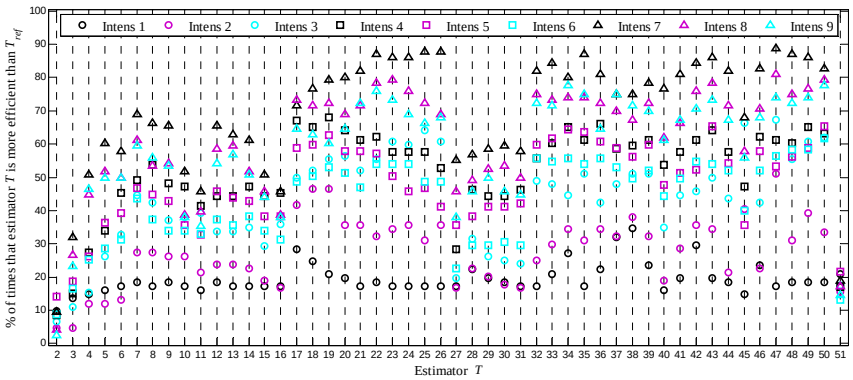

Figure 6.7. APLE values of the estimators, for the LRE, for the IRREG10 negative chord rotation when PGA is the IM, for all the intensities.

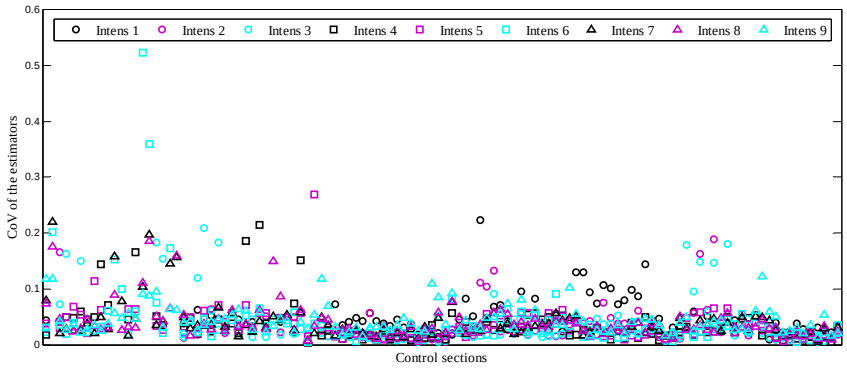

Figure 6.8. CoV of the central values obtained by all the estimators for the IRREG10 negative chord rotation when PGA is the IM, for all the intensities and control sections.

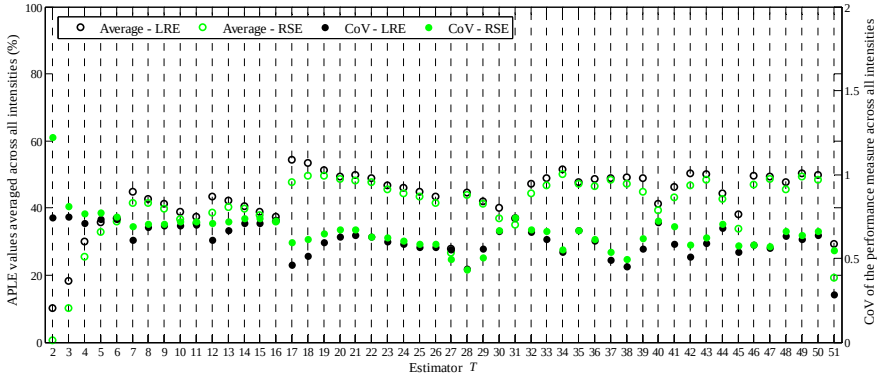

Figure 6.9. APLE values of the estimators, for the LRE and the RSE, for the IRREG10 negative chord rotation when PGA is the IM, averaged across all the intensities, and CoVs representing the variability between intensities.

With respect to the shear force demand V, Figs. 6.10 and 6.11 present the LRE and RSE APLE values averaged across the sections and the earthquake intensities for the REG10 shear force demand in original and log units, respectively, when PGA is the IM, along with the CoVs reflecting their variability across the earthquake intensities. As for the previous cases, the LRE and RSE APLE values are also close, with maximum values near 50%, and exhibit CoVs around 50%. Furthermore, it can also be seen that APLE results in original and log units are similar. Additionally, Fig. 6.12 presents the CoV of the fifty-one central values obtained by the estimators, for each REG10 shear force dataset in original units and for all the intensities, which can be seen to be generally lower than 5% (similar values are obtained for the shear force demand in log units). In terms of the more efficient estimators for V, these are similar to those of the previous EDPs.

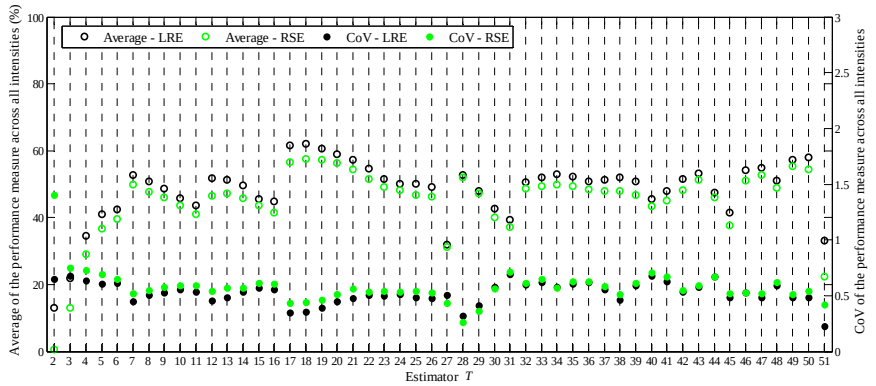

Figure 6.10. APLE values of the estimators, for the LRE and the RSE, for the REG10 shear force in original units when PGA is the IM, averaged across all the intensities, and CoVs representing the variability between intensities.

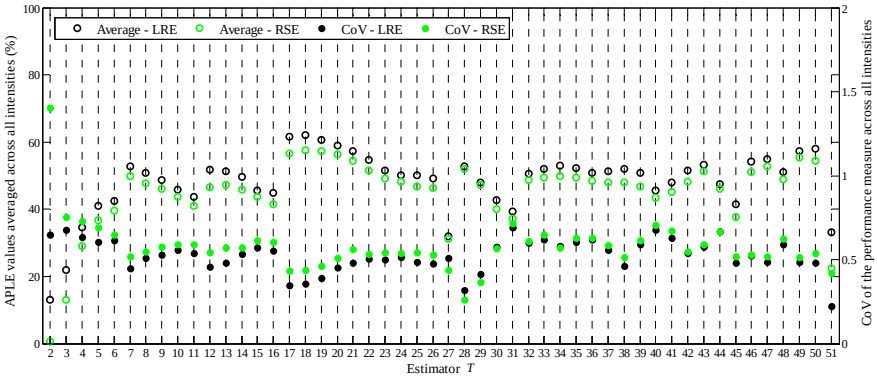

Figure 6.11. APLE values of the estimators, for the LRE and the RSE, for the REG10 shear force in log units when PGA is the IM, averaged across all the intensities, and CoVs representing the variability between intensities.

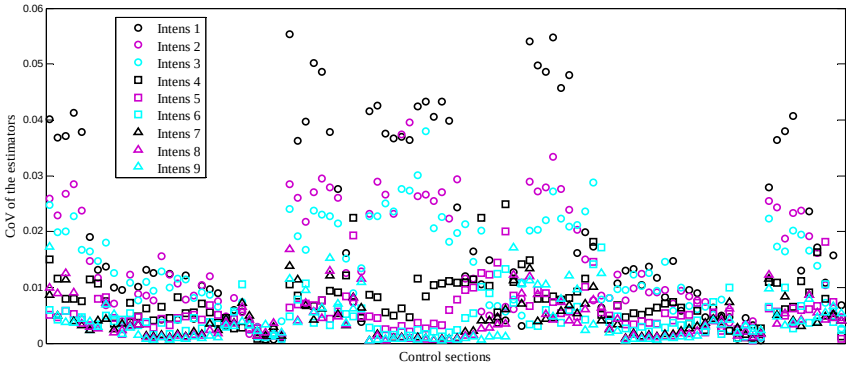

Figure 6.12. CoV of the central values obtained by all the estimators for the REG10 shear force in original units when PGA is the IM, for all the intensities and control sections.

For the case of the inter-storey drift ⊿, and since for a given structure there is only one dataset for each earthquake intensity, Fig. 6.13 presents APLE values of the LRE and the RSE averaged across all the structures and earthquake intensities when $S_a(T_1)$ is the

IM, and the CoVs representing their variability across these intensities. Keeping in mind that only forty-four datasets are considered (the intensity nine dataset of the ICONS structure was disregarded by the reasons highlighted in Section 6.6.1), it can be observed that the APLE values are lower than for the previous EDPs (only a few APLE values are above 40%) while CoV values are similar to those of the earlier cases. Although it appears that, on average, the estimators are less efficient for ⊿, the effect of the lower number of datasets should not be ignored. With respect to the more efficient estimators, these are also seen to be those of the previous EDPs. Additionally, Fig. 6.14 presents the CoV of the fifty-one central values obtained by the estimators for each structure and ⊿ dataset (after transforming the data back to original units) which can be seen to be globally lower than 5%. Again, although the estimators yield central values close to each other, the LRE and the RSE values indicate which are more efficient.

Based on the analysis of the results of Stage 1, the most efficient estimators to be considered in Stage 2 were identified. For the case of φ, θ and V, Table 6.2 presents the thirteen best estimators for each structure and for both IMs. For each structure and IM, the LRE and RSE APLE values of the six EDPs (i.e. the positive and negative φ and θ, and V in original and in log units) were sorted in ascending order, and the corresponding thirteen estimators appearing more times over all twelve situations were selected. A similar analysis was also carried out for ⊿ considering all the structures simultaneously and the resulting estimators were also those presented in Table 6.2. As can be observed, Table 6.2 refers to twenty-four different estimators. Moreover, for a given structure, estimators that are more efficient when PGA is the IM are not always those that are more efficient when $S_a(T_1)$ is the IM. Since the purpose of the study is to identify CVEs providing efficient performances for both cases, a second filtering of this preliminary selection was carried out. Therefore, among the estimators of Table 6.2, the following fifteen CVEs were found to be those with better efficiency (i.e. those with higher scores when summing up the number of times *NT* they appear in Table 6.2) considering the results obtained for all the structures and for both IMs simultaneously: estimators 43, 47, 17, 49, 20, 34, 19, 38, 18, 50, 37, 21, 22, 42 and 33 (T_{log}, L_p, $\overline{x}_{0.08-HQ1}$, $T_{tanh,1}$, $\overline{x}_{0.20-HQ1}$, $T_{Hub,3}$, $\overline{x}_{0.16-HQ1}$, $T_{Ham,3}$, $\overline{x}_{0.12-HQ1}$, $T_{tanh,2}$, $T_{Ham,2}$, $\overline{x}_{0.24-HQ1}$, $\overline{x}_{0.08-TL}$, $T_{Tuk,3}$ and $T_{Hub,2}$). Given the smaller size of the datasets chosen for Stage 2, $\overline{x}_{0.16-HQ1}$, $\overline{x}_{0.20-HQ1}$ and $\overline{x}_{0.24-HQ1}$ were not considered since they involve data trimming levels that would not be able to be contemplated. Furthermore, for $\overline{x}_{0.08-HQ1}$, $\overline{x}_{0.12-HQ1}$ and $\overline{x}_{0.08-TL}$, when the trimming level is not an integer, the number of trimmed data values was rounded to the closest upper integer. Although *M* is not one of the most efficient estimators, due to its wide use in PBEE methodologies, it was also selected for Stage 2 to compare its performance to that of more efficient estimators when samples of smaller size are considered. Finally, T_{log} was seen to be the estimator with best performance and was selected as the new *reference estimator*.

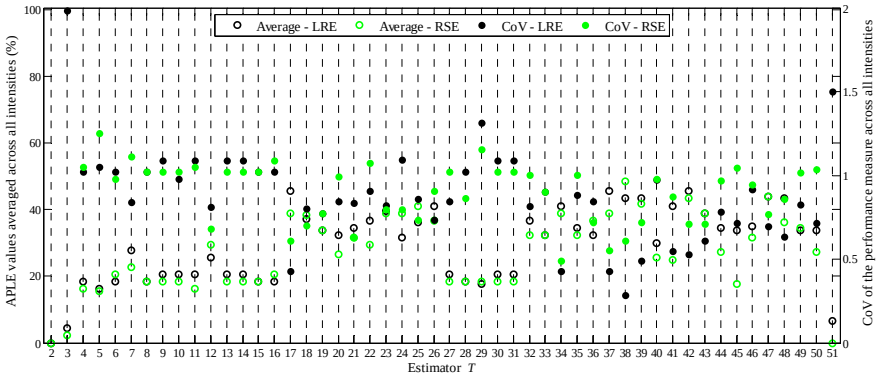

Figure 6.13. APLE values of the estimators, for the LRE and the RSE, for the inter-storey drift of all the structures when $S_a(T_1)$ is the IM, averaged across all the intensities, and CoVs representing the variability between intensities.

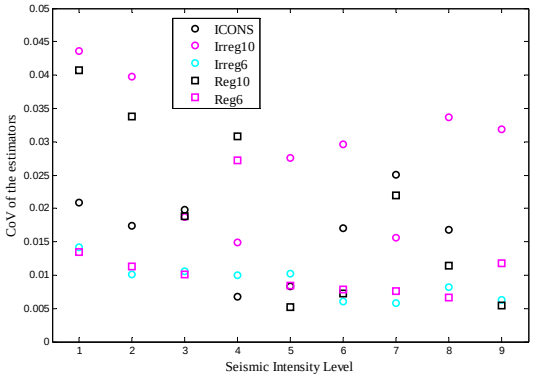

Figure 6.14. CoV of the central values obtained by all the estimators, for the inter-storey drift of all structures and for all the intensities, when $S_a(T_1)$ is the IM.

Table 6.2. The thirteen most efficient CVEs, for each structure and IM, and the number of times NT they appear

ICONS				IRREG10				IRREG6				REG10				REG6			
PGA		$S_a(T_1)$		PGA		$S_a(T_1)$		PGA		$S_a(T_1)$		PGA		$S_a(T_1)$		PGA		$S_a(T_1)$	
CVE	*NT*	CVE	*NT*	CVE	*NT*	CVE	*NT*	CVE	*NT*	CVE	*NT*	CVE	*NT*	CVE	*NT*	CVE	*NT*	CVE	*NT*
17	*12*	17	*12*	19	*12*	17	*12*	34	*12*	43	*12*	19	*12*	33	*12*	47	*12*	17	*12*
18	*12*	18	*12*	47	*12*	18	*12*	38	*12*	47	*12*	34	*12*	34	*12*	22	*12*	19	*12*
19	*12*	19	*12*	22	*12*	19	*12*	47	*12*	48	*12*	43	*12*	37	*12*	23	*12*	47	*12*
20	*12*	20	*12*	49	*12*	20	*12*	37	*11*	24	*12*	47	*12*	38	*12*	49	*12*	18	*11*
47	*12*	34	*12*	50	*12*	34	*12*	43	*11*	49	*12*	17	*11*	43	*12*	50	*12*	20	*11*
49	*12*	37	*12*	18	*11*	37	*12*	49	*11*	22	*11*	18	*11*	47	*12*	43	*9*	49	*11*
21	*10*	38	*12*	20	*11*	38	*12*	50	*10*	23	*11*	49	*11*	39	*11*	21	*8*	34	*10*
22	*10*	42	*12*	17	*9*	43	*12*	42	*8*	50	*10*	20	*10*	42	*11*	35	*8*	43	*10*
38	*7*	43	*12*	43	*9*	42	*11*	22	*8*	25	*9*	46	*8*	17	*10*	24	*8*	38	*8*
43	*7*	21	*8*	34	*8*	33	*10*	20	*7*	35	*8*	50	*8*	36	*10*	19	*7*	21	*7*
50	*7*	33	*8*	35	*7*	39	*8*	17	*6*	26	*7*	21	*7*	49	*10*	25	*7*	37	*6*
23	*5*	39	*8*	23	*7*	47	*7*	21	*6*	42	*6*	37	*7*	48	*7*	20	*6*	48	*6*
24	*5*	50	*7*	21	*6*	21	*6*	33	*6*	20	*5*	38	*7*	46	*5*	17	*5*	22	*6*

6.6.2.2 Results of Stage 2

In general terms, the results of Stage 2 exhibit a trend found to be generally the same across all structures, for all EDPs, for both IMs and for both the RSE^* and the RAE^* measures. Therefore, only a few illustrative results are presented herein. When comparing the efficiency of the several estimators based on the presented results, it should be kept in mind that the APLE value is a relative measure of the performance. Hence, when the APLE value of a certain estimator is close to 50%, its efficiency is similar to that of the new *reference estimator* (T_{log}, estimator 43 in Table 6.1). On the other hand, when the APLE value of the estimator falls below 50%, the efficiency of T_{log} is then larger than 50%.

The APLE results for the RSE^* of the estimators selected for Stage 2, obtained for the positive θ demand of the IRREG6 sections, for all the intensities, for a sample size n^* of forty and when PGA is the IM, are presented in Fig. 6.15 a). It can be observed that estimators 34, 37, 38 and 42 ($T_{Hub,3}$, $T_{Ham,2}$, $T_{Ham,3}$ and $T_{Tuk,3}$) are generally more efficient than the other estimators. Still, when comparing the performance of these four estimators with that of T_{log}, they are found to be similar. Figures 6.15b), c) and d) present, for the same structure and EDP, the RSE^* and RAE^* APLE values averaged across the ground motion intensities for n^* values of thirty, fifteen and seven, respectively, and the CoVs reflecting the variability between earthquake intensities. As can be seen, the results obtained when n^* is thirty are similar to those obtained when n^* is forty. On the other hand, when n^* is fifteen, the efficiency of some of these estimators is seen to decrease while that of others increases (e.g. estimator 17). The situation changes when n^* is seven, where the more efficient estimators can now be seen to be estimators 17 and 18 ($\overline{x}_{0.08-HQ1}$ and $\overline{x}_{0.12-HQ1}$) which exhibit RSE^* and RAE^* APLE values much larger than those of the remaining estimators. In terms of the variability between earthquake intensities, it can be observed that the CoVs of the more efficient estimators are generally in the range of 20%-40%, irrespective of n^*.

In order to highlight the influence of the sample size on the results obtained by the CVEs, Fig. 6.16 presents maximum Range and CoV values obtained from the simulations with different n^* values, considering only estimators 34, 37, 38, 42 and 43. For a given sample size n^*, a given earthquake intensity and for each section, the average and the CoV of the 10000 estimates obtained using each CVE were computed. The Range was then determined by the difference between the maximum and the minimum of those averages, previously normalized by $T_{ref2,n_{ref}}$ to obtain a measure relative to a reference value of the demand. The results presented in Fig. 6.16 are then, for each section and for each n^* value, the maximum of the Ranges obtained for all the earthquake intensities and the maximum CoV value considering all the earthquake intensities and the referred estimators (with the data transformed back to original units). Based on the presented results, it can be observed

that CoV values increase as n^* decreases, which, as expected, indicates that the variability of the 10000 estimates increases when the sample size is smaller. On the other hand, it can be seen that, in many sections, the Range values are higher for larger sample sizes, indicating that the differences between the average of the 10000 estimates obtained by each method is larger in such cases. This situation can be explained by observing Figs. 6.17a) and b) that show the influence function (as defined in Section 6.3) of the estimators for the positive θ demand of a beam section for one sample of size forty and for one sample of size seven. As can be seen, the differences between the influence function of each estimator are more significant when the sample is larger. When n^* is equal to forty, ten data values (the first two at the beginning of the curve, which are almost coincident, and the last eight values on the right side of the curve) can be considered to be affected by the differences in the influence functions, while for n^* equal to seven, only one data value is significantly affected. Although this situation does not occur for every control section and for every simulated sample, the estimators have the potential to yield CVEs with more significant differences in larger samples, thus making the Range wider than for samples of smaller size.

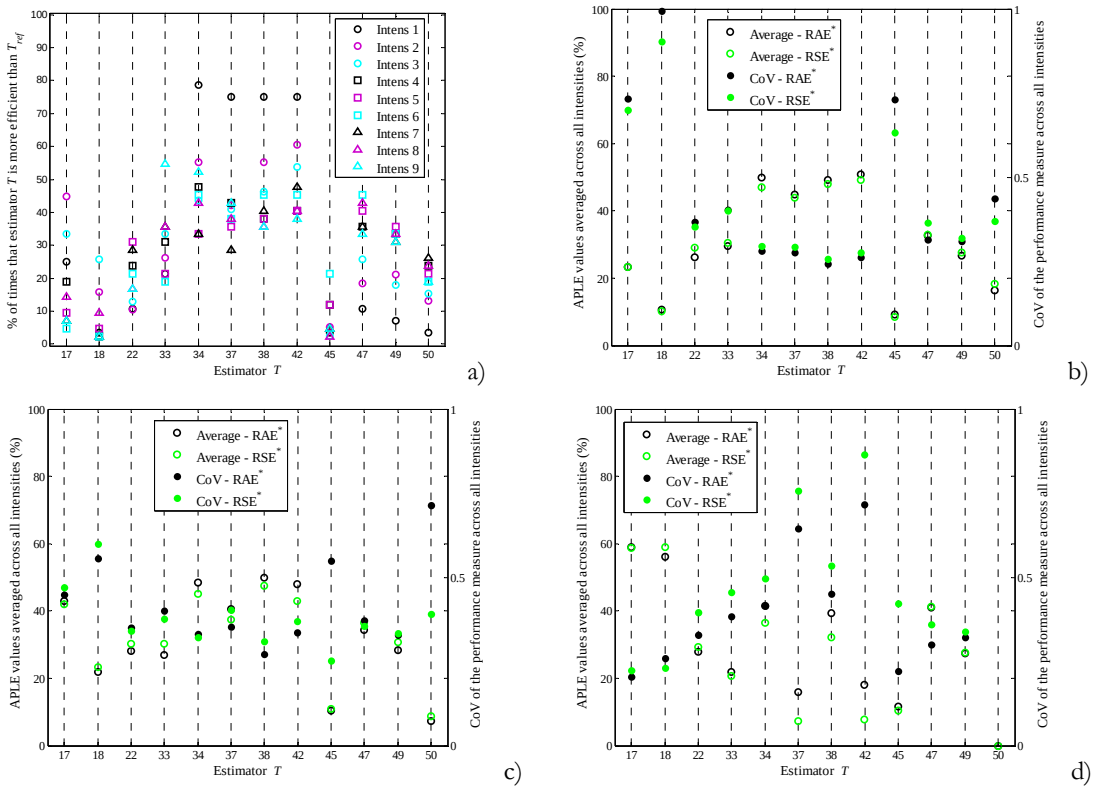

Figure 6.15. APLE values of the estimators for the IRREG6 positive chord rotation when PGA is the IM, for the RSE^* and all the intensities (a); for the RSE^* and RAE^* averaged across all the intensities along with the CoVs representing the variability between intensities when n^* is thirty (b); fifteen (c); and seven (d).

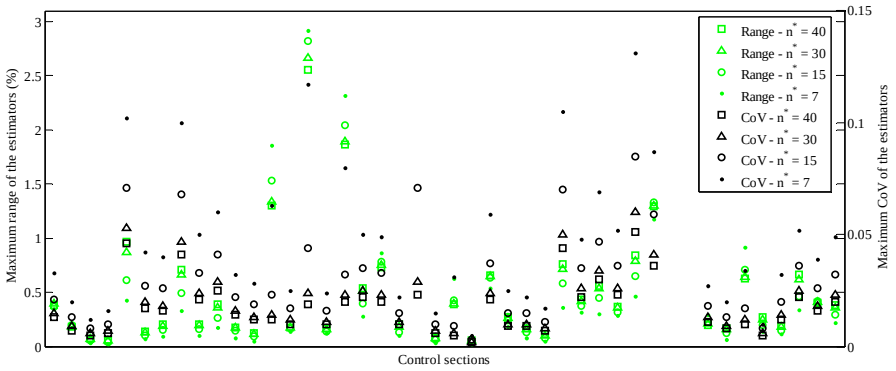

Figure 6.16. Range and CoV values of estimators 34, 37, 38, 42 and 43 for the IRREG6 positive chord rotation when PGA is the IM and for the different n^* sample sizes.

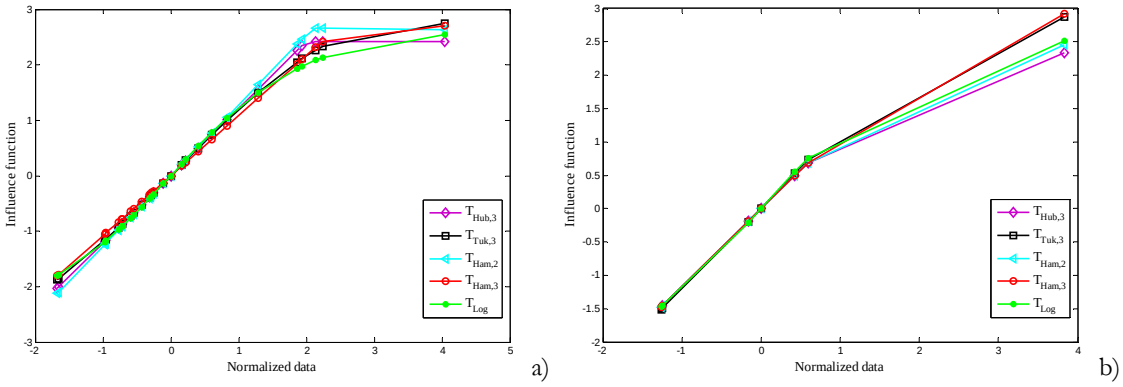

Figure 6.17. Influence function of the estimators for the positive chord rotation demand of a beam section from IRREG6 when PGA is the IM for one sample of size forty (a) and for one sample of size seven (b).

To further illustrate the results of Stage 2, Fig. 6.18 presents APLE values of the estimators averaged across all the intensities along with the CoVs reflecting the variability between these intensities, for the RSE^* and the RAE^* of the ICONS shear force in original units, when $S_a(T_1)$ is the IM, and for the cases where n^* is equal to forty and to seven. As for the previously shown results, estimators 34, 37, 38, 42 and 43 are seen to be the more efficient ones for the larger sample size, although the efficiency of estimator 43 is slightly larger than that of the other four estimators. With respect to the samples of smaller size, estimators 17 and 18 are seen to be more efficient. Furthermore, it is referred that the APLE values for the remaining sample sizes follow the trend of the results presented in Figs. 6.15b) and c). To complement these results, Fig. 6.19 presents, for estimators 34, 37, 38, 42 and 43, the maximum Range and CoV values obtained from the simulations with different n^* values. From these results, a trend similar to that of the results presented in Fig. 6.16 can also be identified. Finally, Fig. 6.20 presents APLE values of the estimators averaged across all the earthquake intensities along with the CoVs reflecting the variability between the intensities, for the RSE^* and the RAE^* of the inter-storey drift of all the structures, when $S_a(T_1)$ is the IM, and for the cases where n^* is equal to fifteen and to

seven. As can be observed, the trend of the obtained APLE values is similar to those of the other EDPs, but the CoV values of the more efficient estimators increase slightly for this EDP due to the lower number of samples.

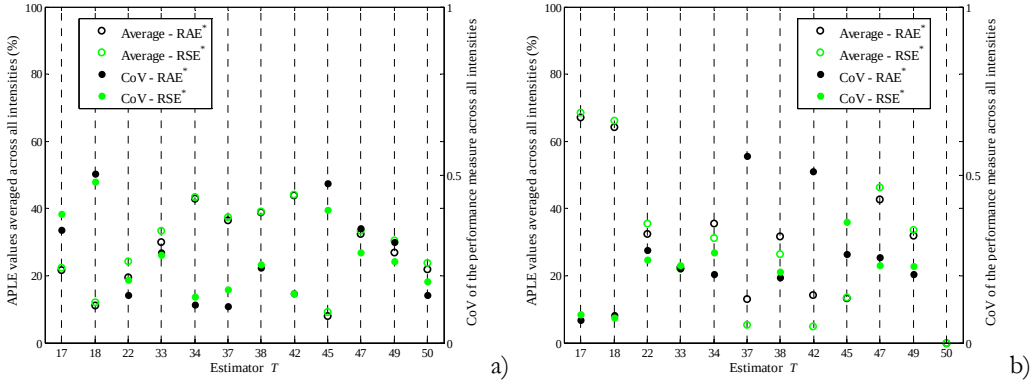

Figure 6.18. APLE values of the estimators averaged across all the intensities along with the CoVs representing the variability between intensities, for the RSE^* and RAE^*, for the ICONS shear force in original units, when $S_a(T_1)$ is the IM when n^* is forty (a) and seven (b).

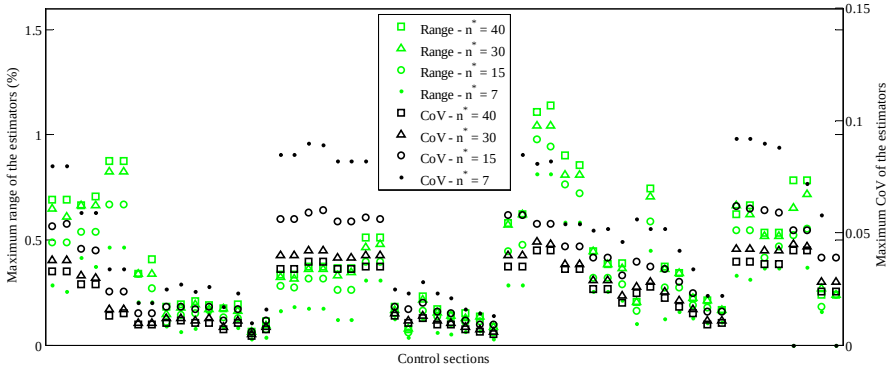

Figure 6.19. Range and CoV values of estimators 34, 37, 38, 42 and 43 for the ICONS shear force in original units when $S_a(T_1)$ is the IM and for the different n^* sample sizes.

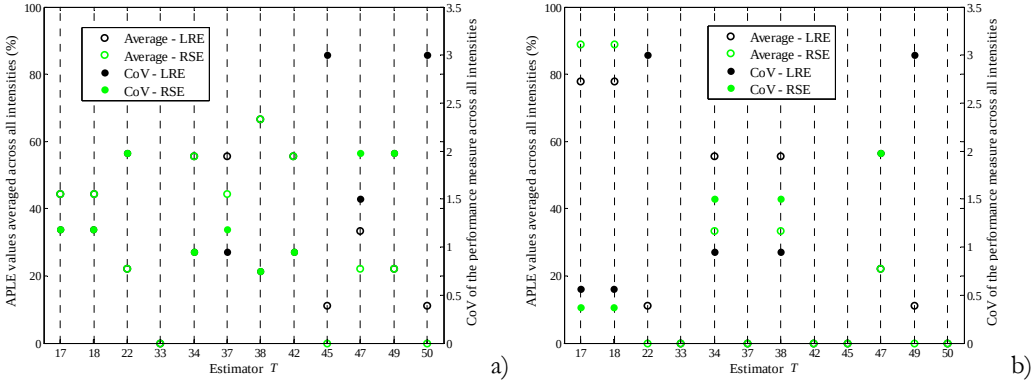

Figure 6.20. APLE values of the estimators averaged across all the intensities along with the CoVs representing the variability between intensities, for the RSE^* and RAE^*, for the inter-storey drift of all the structures, when $S_a(T_1)$ is the IM when n^* is fifteen (a) and seven (b).

After a general analysis of the results of Stage 2, the effect of the sample size on the efficiency of the estimators was seen to be mostly felt when n^* is equal to seven, for which the more efficient estimators are different from those identified for the larger sample sizes. With respect to the effect of the IM on the efficiency of the estimators, no definite trend was observed as their efficiencies are similar irrespective of the IM. This observation indicates that these estimators are fit to be considered under various conditions of the dispersion obtained for the demand. When considering all the structures, EDPs and IMs, the efficiency of estimators 34, 37, 38 and 42, for sizes n^* of forty and thirty, is found to be in the range of 23% to 70%, with an average value around 45%, and with small differences between the performances of each estimator. For a size n^* of fifteen, estimator 17 can be seen to have an efficiency similar to that of estimators 34, 37, 38 and 42. For this sample size, the efficiency of these five estimators ranges from 18% to 70% with an average value around 43%. From this results it can be seen that, for these three sample sizes, there is a significant number of cases where the APLE values of these estimators are below 50%, which correspond to situations where estimator 43 (the new *reference estimator* selected for Stage 2) is more efficient. When n^* is seven, the efficiency of estimators 17 and 18 ranges from 44% to 85% with an average value above 61%. In addition to this analysis, it is also referred that M (estimator 45) was seen to exhibit inadequate performance in all cases considered, when compared to that of the recommended estimators.

Finally, an additional aspect must be noted about the results of Stage 2. The RSE^* and the RAE^* efficiency measures were obtained using the result of estimator 43 (T_{log}) for size n_{ref} ($T_{ref\,2,n_{ref}}$) as a reference for the "true value" of the central value of the datasets. In order to strengthen the validity of the results obtained for Stage 2, it becomes important to determine how different would these results be if $T_{ref\,2,n_{ref}}$ was defined by another estimator. Therefore, the Stage 2 analyses were repeated using estimator 38 ($T_{Ham,3}$) to define $T_{ref\,2,n_{ref}}$. To illustrate the findings of this new analysis, Fig. 6.21 presents APLE results obtained by using $T_{Ham,3}$ to quantify $T_{ref\,2,n_{ref}}$. These results correspond to those of Figs. 6.15b), 6.15c), 6.18a) and 6.18b) that were obtained using estimator 43 to quantify $T_{ref\,2,n_{ref}}$. An overall analysis of these new results indicates that the more efficient estimators are still those identified from the first set of Stage 2 results (i.e. when $T_{ref\,2,n_{ref}}$ is defined by T_{log}). Still, these new results show that, for sample sizes n^* of forty and thirty, the APLE values obtained for estimators 34, 37, 38 and 42 are, on average, between 50% and 60%. Since these are larger than those of the first set of Stage 2 results, it indicates that the efficiency of these estimators is better than that of T_{log} when the reference used for the "true value" of the central value of the data is changed. With respect to the sample size n^* of fifteen, an increase of the APLE values for these estimators is also observed in some cases, but its global effect is less significant. For the sample size n^* of seven, the results are similar to

those of the first Stage 2 analysis. Finally, it is noted that the relatively small variability of the results observed when $T_{ref\,2,n_{ref}}$ is changed reflects the previously referred closeness of the central value estimates obtained by each method (e.g. see Section 6.6.2.1, based on the low CoV values of Fig. 6.4) which then leads to the stability of the Stage 2 results.

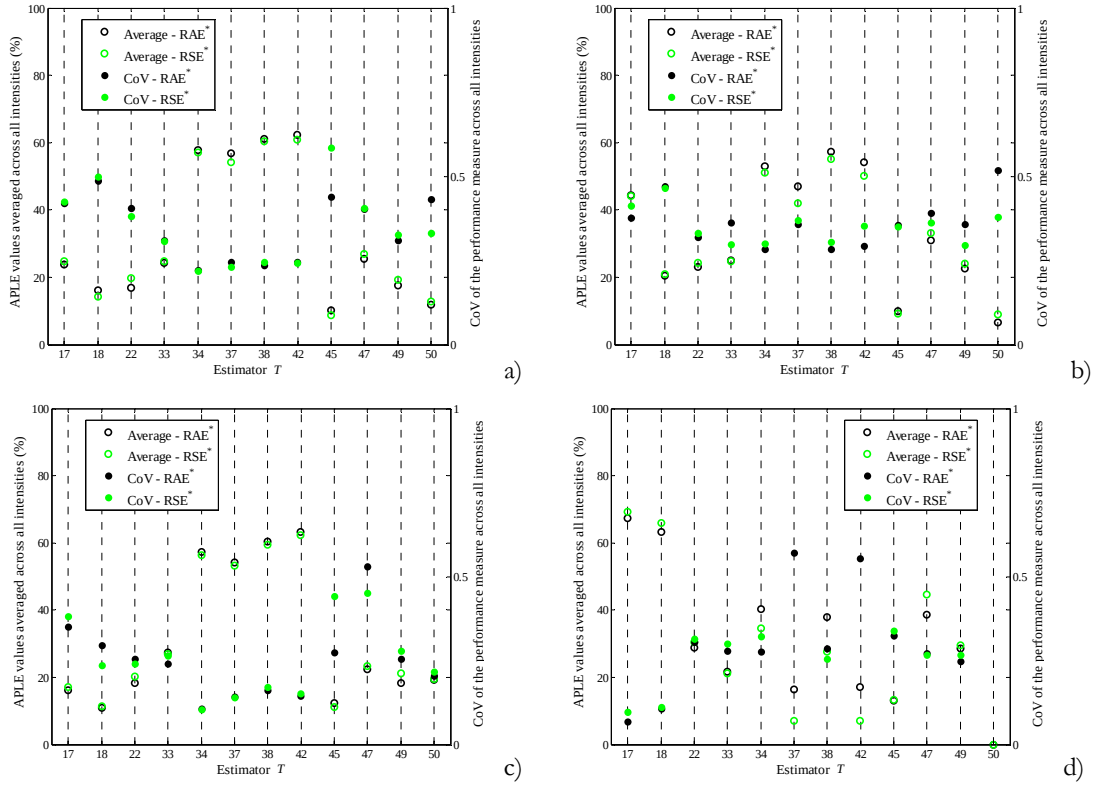

Figure 6.21. APLE values of the estimators, for the RSE^* and RAE^* averaged across all the intensities, along with the CoVs representing the variability between intensities, and obtained using $T_{Ham,3}$ as the *reference estimator*, for the IRREG6 positive chord rotation when PGA is the IM, when n^* is thirty (a) and fifteen (b); for the ICONS shear force in original units, when $S_a\left(T_1\right)$ is the IM when n^* is forty (c) and seven (d).

6.7 Conclusions

A study addressing the characterization of the central value of structural demand distributions of several EDPs obtained under earthquake loading using different robust estimators was presented. The selected EDPs were the curvature, the chord rotation, the shear force and the inter-storey drift over the height of the structure. Five structures were analysed for suites of fifty ground motions to obtain data samples with a size significant enough. The chosen records were scaled for several intensities and two different IMs were also considered to evaluate the influence of this parameter. The fundamental objective of the study was to test the use of fifty robust estimators using adequate measures of statistical efficiency, in order to identify those best suited for different types of data and sample sizes.

The performance of the estimators was tested using a two-stage approach. In Stage 1, the performance of the fifty robust estimators is compared with that of the reference estimator $\overline{x}$ considering datasets of larger size (between forty-five and fifty). In Stage 2, a subgroup of thirteen estimators with better efficiency was considered to assess their performance for datasets of smaller size (forty, thirty, fifteen and seven).

The results of Stage 2 indicate that estimators 34, 37, 38, 42 and 43 ($T_{Hub,3}$, $T_{Ham,2}$, $T_{Ham,3}$, $T_{Tuk,3}$ and T_{log}) are recommended to compute central value estimates of the demand for samples of size larger than fifteen. On the other hand, for samples of smaller size, estimators 17 and 18 ($\overline{x}_{0.08-HQ1}$ and $\overline{x}_{0.12-HQ1}$) are recommended instead. The results of Stage 2 also show that the performance of these estimators is similar across the structures, the EDPs and the earthquake intensities considered in the study. The effect of sample size on the efficiency of the estimators was seen to be mostly felt for samples of size seven, for which the more efficient estimators are different from those identified for the larger sample sizes. With respect to the selected IMs and their effect on the efficiency of these estimators, no definite trend was observed as their efficiencies are similar irrespective of the IM. Although such results indicate that these estimators are fit to be considered under various conditions of the variability of the demand, further IMs should be analysed to confirm this conclusion.

Finally, it is noted that the median *M*, which is widely used in the context of PBEE methodologies, was seen to exhibit inadequate performance in all cases analysed, when compared to that of the recommended estimators. Therefore, it is suggested that in future PBEE applications, central values estimates of seismic demand should be obtained by one of these estimators instead.

Chapter 7
Statistical characterization of structural demand under earthquake loading - Robust estimation of the dispersion of the data

7.1 Introduction

The present chapter corresponds to the second part of the study that addresses the statistical characterization of seismic demand data using robust estimation methods. The first part of the study presented in Chapter 6 analysed the applicability of several robust estimators to define the central value of demand distributions obtained for different engineering demand parameters (EDPs), considering data samples of various sizes. Based on statistical measures of their performance, seven robust estimators were considered to be adequate for different sample sizes.

When analyzing probabilistic performance parameters which are often considered in performance-based earthquake engineering (PBEE) methodologies, a probabilistic model of the demand is usually required. Considering that such model can be defined by a lognormal or a normal distribution, as observed in Chapter 5, the complete characterization of the distribution requires estimates of the central value and of the dispersion of the data. Since Chapter 6 addressed the characterization of the central value of the data, the current chapter deals with the estimation of the dispersion of the data using adequate statistical methods. Given the aspects referred in Chapters 5 and 6 regarding the occurrence of outliers, and the advantages of using robust statistical estimation methods, the study proposed herein tests the use of robust estimators to characterize the dispersion of structural demand distributions obtained under earthquake loading. As for the study presented in the previous chapter, the performance of several robust estimators are tested using appropriate measures of statistical efficiency, in order to identify those best suited for different types of data and sample sizes.

7.2 Description of the proposed study

The presented study focuses both deformation- and strength-related EDPs and is based on local (section level) and global (system level) demand distributions obtained from the analysis of five reinforced concrete (RC) structures subjected to earthquake records of increasing intensities. At the section level, the selected EDPs are the maxima of the curvature, of the chord rotation and of the shear force, while at the system level, the chosen parameter is the maximum inter-storey drift over the height of the structure. It should be noted that the focus of the study does not address the magnitude of the dispersion in itself, but only deals with methods to assess this parameter with appropriate reliability.

The selected structures were analysed for suites of fifty ground motions to obtain data samples with a size significant enough. The chosen records were scaled for several intensities in order to evaluate the referred hypotheses for different hazard levels. Furthermore, two different IMs were also considered to evaluate the influence of this parameter on the conclusions of the study.

A series of estimators was then applied to the demand samples to identify those more adequate to characterize their dispersion. In order to assess the performance of the estimators for a wide range of conditions, they were applied to the samples of size fifty as well as to subsamples of size forty, thirty, fifteen and seven drawn from the samples of size fifty.

Since the proposed study is based on the structural demand results obtained for the five structures presented in Chapter 5, details about the modelling and analyses procedures, the quantification of the demand parameters, and the suites of fifty ground motions that were considered to represent the seismic demand are omitted herein.

7.3 Selected dispersion estimators

The dispersion estimators (DEs) considered in the proposed study are presented in the following. Thirty-three robust estimators are selected and grouped into three general categories. A brief review of each estimator is presented and additional information can be found in the references cited herein. Besides these estimators, the classical (non-robust) sample standard deviation s is also considered. For a data sample $x_1, x_2, ... x_n$ of size n, s is defined by:

$$s = \sqrt{\frac{1}{n-1}\sum_{i=1}^{n}\left(x_i - \bar{x}\right)^2} \tag{7.1}$$

which can be written also as

$$s = \sqrt{\frac{1}{W_s}\sum_{i=1}^{n} w_i \cdot \left(x_{(i)} - \bar{x}\right)^2} \tag{7.2}$$

where $x_{(i)}$ represents the *ith* order statistic of the sample, w is a weight function with a value of one for each data value of the sample in this case, $W_s = \sum_{i=1}^{n-1} w_i = n-1$ and $\bar{x}$ is the sample mean defined as

$$\bar{x} = \frac{1}{n}\sum_{i=1}^{n} x_i \tag{7.3}$$

which can also be written as

$$\bar{x} = \frac{1}{W}\sum_{i=1}^{n} w_i \cdot x_{(i)} \tag{7.4}$$

where $W = \sum_{i=1}^{n} w_i = n$. The alternative forms of representing s and $\bar{x}$ which are defined by Eqs. (7.2) and (7.4) enable other estimators to be represented using this unified format.

7.3.1 Location-free and scale-free estimators

Estimators in this group do not require auxiliary measures of the central value (i.e. the location parameter) and of the dispersion (i.e. the scale parameter) to obtain a robust estimate of the dispersion of the data.

7.3.1.1 The interquartile range

The interquartile range *IQR* is a robust DE well known for its simplicity (Hoaglin *et al.*, 1983) that is defined by:

$$IQR = c \cdot \left(x_{(n-m+1)} - x_{(m)}\right) \tag{7.5}$$

where c is a tuning constant which takes the value of 0.7413 so that *IQR* is consistent with the normal distribution and $m = \lfloor n/4 \rfloor$ in which $\lfloor . \rfloor$ stands for the integer part. In the context of PBEE methodologies, it is noted that the *IQR* has been previously used by Miranda and Aslani (2003).

7.3.1.2 The median absolute deviation

The median absolute deviation (*MAD*) is another well known estimator in the robust statistics context (Hoaglin *et al.*, 1983). Considering that the sample median M is defined by:

$$M = med(x) = \begin{cases} x_{((n+1)/2)} & \text{if } n \text{ is odd} \\ \frac{1}{2}\left[x_{(n/2)} + x_{(n/2+1)}\right] & \text{if } n \text{ is even} \end{cases} \tag{7.6}$$

the *MAD* is then given by:

$$MAD = b_n \cdot c \cdot med\left(\left|x_i - M\right|\right) \tag{7.7}$$

where c is a tuning constant with a value of 1.4826 so that *MAD* is consistent with the normal distribution and b_n is the small-sample correction factor referred by Rousseeuw and Verboven (2002).

7.3.1.3 The Q_n estimator

The estimator Q_n proposed by Rousseeuw and Croux (1993) is based on an order statistic of all pairwise differences between the data values and is defined by:

$$Q_n = b_n \cdot c \cdot \left\{\left|x_i - x_j\right|; i < j\right\}_{(l)} \tag{7.8}$$

where (l) is the *lth* ordered statistic among the set of $\binom{n}{2}$ distances between the data values, in which $l = \binom{h}{2} \approx 0.25\binom{n}{2}$ with $h = \lfloor n/2 \rfloor + 1$ and where $\binom{n}{2}$ is $0.5\left(n^2 - n\right)$. The value of the tuning constant c is 2.2219 (to be consistent with the normal distribution) and b_n is the small-sample correction factor referred by Rousseeuw and Verboven (2002).

7.3.1.4 The S_n estimator

The estimator S_n, also proposed by Rousseeuw and Croux (1993), is based on the median of all pairwise differences between the data values and is defined by:

$$S_n = b_n \cdot c \cdot med_i\left(med_j\left|x_i - x_j\right|\right) \tag{7.9}$$

where c is a tuning constant with a value of 1.1926 so that S_n is consistent with the normal distribution and b_n is a small-sample correction factor.

7.3.1.5 The length of the shorth S_{sh}

The length of the shorth S_{sh} (Rousseeuw and Leroy, 1988) is a DE based on the shortest half of the sample defined by:

$$S_{sh} = c \cdot \min_{i \in \{1,\ldots,\, n-v+1\}} \left(x_{(i+v-1)} - x_{(i)} \right) \tag{7.10}$$

where $v = \lfloor n/2 \rfloor + 1$ and c is a tuning constant which takes the value of 0.7413 so that S_{sh} is consistent with the normal distribution.

7.3.1.6 The trimmed L- standard deviation

A robust generalization of the sample L-moments (Hosking, 1990) has been formulated by Elamir and Seheult (2003) leading to the development of trimmed L-moments. The trimmed L-standard deviation $s_{\alpha-TL}$ reduces the influence of outlying observations by using a subsample of the original data and can be obtained using the unified format of Eq. (7.4) with $W = 1/2$ and w_i replaced by:

$$w_i = \begin{cases} \dfrac{\binom{i-1}{1+p}\binom{n-i}{p} - \binom{i-1}{p}\binom{n-i}{p+1}}{\binom{n}{2p+1}} & p+1 \le i \le n-p \\ 0 & \textit{otherwise} \end{cases} \tag{7.11}$$

where $\binom{i}{p}$ is $\dfrac{i!}{p!(i-p)!}$ and $p = \alpha \cdot n$ means that, for a trimming level α, the $p/2$ highest and lowest values are removed. Several $s_{\alpha-TL}$ are considered in the proposed study with different α values, namely with α set as 0.08, 0.12, 0.16, 0.20 and 0.24 which define the estimators $s_{0.08-TL}$, $s_{0.12-TL}$, $s_{0.16-TL}$, $s_{0.20-TL}$ and $s_{0.24-TL}$, respectively.

7.3.1.7 The dispersion estimator based on the empirical characteristic function

The dispersion estimator S_{ecf}, that is based on the empirical characteristic function and was proposed by Markatou *et al.* (1995), is defined by:

$$S_{ecf} = \frac{\sqrt{-2\log(c)}}{t_{ecf}} \tag{7.12}$$

where c is a tuning constant and t_{ecf} is the solution of

$$\sum_{i=1}^{n} \left[\cos\left(t_{ecf} \cdot x_i \right) \right]^2 + \sum_{i=1}^{n} \left[\sin\left(t_{ecf} \cdot x_i \right) \right]^2 = n^2 \cdot c^2 \tag{7.13}$$

According to the results presented by Markatou *et al.* (1995), c was considered to be 0.7 in order to balance robustness and efficiency.

7.3.2 Location-based and scale-free estimators

Estimators in this group require the definition of an auxiliary measure of the central value to obtain a robust estimate of the dispersion of the data.

7.3.2.1 The α-trimmed standard deviation

As for $s_{\alpha-TL}$, the α-trimmed standard deviation ($s_{\alpha-tr}$) also reduces the influence of outlying observations by using a subsample of the original data. This estimator is the standard deviation of the data sample when the $p/2$ highest and lowest values are removed, where $p = \alpha \cdot n$. The value of $s_{\alpha-tr}$ can be obtained using the unified format of Eq. (7.2) with $W_s = 1$, w_i replaced by

$$w_i = \begin{cases} \dfrac{1}{n-2p} & p+1 \le i \le n-p \\ 0 & otherwise \end{cases} \tag{7.14}$$

and $\bar{x}$ replaced by the α-trimmed mean obtained using the unified format of Eq. (7.4) with $W = 1$ and w_i defined by Eq. (7.14). Several $s_{\alpha-tr}$ are considered in the proposed study with different α values, namely with α set as 0.08, 0.12, 0.16, 0.20 and 0.24 which define the estimators $s_{0.08-tr}$, $s_{0.12-tr}$, $s_{0.16-tr}$, $s_{0.20-tr}$ and $s_{0.24-tr}$, respectively.

7.3.3 Location-based and scale-based estimators

Estimators in this group require the definition of auxiliary measures of the central value and of the dispersion to obtain a robust estimate of the dispersion of the data.

7.3.3.1 The τ-scale estimator

The τ-scale DE τ_s, proposed by Yohai and Zamar (1988), is a truncated standard deviation defined by

$$\tau_s = s_0 \sqrt{\frac{1}{n}\sum_{i=1}^{n} \rho_{c_2}\left(\frac{x_i - m}{s_0}\right)} \tag{7.15}$$

where s_0 is a preliminary dispersion estimate defined by the *MAD*, the function $\rho_{c_2}(.)$ is defined by

$$\rho_{c_2}(u) = \min\left(c_2^2, u^2\right) \tag{7.16}$$

and m is an auxiliary weighted mean obtained using the unified format of Eq. (7.4) with $w_i = w_{c_1}\left(\left(x_i - M\right)/s_0\right)$, in which the function $w_{c_1}(.)$ is defined by

$$w_{c_1}(u) = \max\left(0, \left(1 - u^2/c_1^2\right)^2\right) \tag{7.17}$$

The constants c_1 and c_2 are taken with values of 4.5 and 3.0, respectively, in order to balance robustness and efficiency (Maronna and Zamar, 2002).

7.3.3.2 The M-estimator of scale with logistic function

M-estimators reduce the influence of outlying observations without removing them from the data. An M-estimator of scale s_n is an estimator that is the solution of:

$$\frac{1}{n}\sum_{i=1}^{n}\rho\left(\frac{x_i - T_n}{s_n}\right) = \beta \tag{7.18}$$

where T_n is an auxiliary estimator of the central value of the data and $\beta = \int \rho(u)\, d\Phi(u)$, in which $\Phi(.)$ is the standard normal distribution function. The function $\rho(x)$ is an even bounded weight function that is monotone for $x \geq 0$ and for which $\rho(0) = 0$. Since an iterative root-finding algorithm is required to compute s_n, the following procedure was used herein (Rousseeuw and Verboven, 2002):

$$s_n^{(k)} = s_n^{(k-1)} \cdot \sqrt{\frac{1}{\beta \cdot n}\sum_{i=1}^{n}\rho\left(\frac{x_i - m_n}{s_n^{(k-1)}}\right)} \tag{7.19}$$

where $s_n^{(k)}$ is the *kth* iteration estimate of s_n. For all considered M-estimators of scale, the initial estimate $s_n^{(0)}$ was set as the *MAD* and m_n was set as the *M*.

For the case of the M-estimator of scale with logistic function, s_{log}, the ρ-function is defined by Rousseeuw and Verboven (2002) as:

$$\rho(x) = \psi^2\left(x/0.3739\right) \tag{7.20}$$

where the ψ-function is characterized by the following smoothed function proposed by Rousseeuw and Verboven (2002):

$$\psi(x) = \frac{e^x - 1}{e^x + 1} \tag{7.21}$$

7.3.3.3 The Huber M-estimator of scale

For the case of the Huber M-estimator, the ρ-function is defined by Huber (1981):

$$\rho(x) = \begin{cases} x^2 & if\ |x| \le c \\ c^2 & if\ |x| > c \end{cases} \tag{7.22}$$

where c is a tuning constant. The proposed study considers three versions of this estimator with c values of 1.4, 1.7 and 2.0 (Hoaglin *et al.*, 1983) termed $s_{Hub,1}$, $s_{Hub,2}$ and $s_{Hub,3}$, respectively.

7.3.3.4 The biweight A-estimator of scale

The biweight A-estimator s_{Abw} was proposed as an efficient dispersion estimator in several studies, e.g. see (Lax, 1985; Randal, 2008), and is defined by the following iterative procedure:

$$s_{Abw}^{(k)} = \frac{n}{\sqrt{n-1}} \frac{\sqrt{\sum_{|u_i^k|<1} (x_i - m_n)^2 \left(1-\left(u_i^k\right)^2\right)^4}}{\left|\sum_{|u_i^k|<1} \left(1-\left(u_i^k\right)^2\right)\left(1-5\cdot\left(u_i^k\right)^2\right)\right|} \tag{7.23}$$

where m_n is considered to be the *M* and u_i^k is defined by:

$$u_i^k = \frac{x_i - m_n}{c \cdot s_{Abw}^{(k-1)}} \tag{7.24}$$

where c is a tuning constant. The proposed study considers six versions of this estimator with different values for c and different methods to obtain the initial estimate $s_{Abw}^{(0)}$. According to results obtained by Randal (2008), the following estimators were considered:

- Estimators termed $s_{Abw,1}$ and $s_{Abw,2}$ that involve c values of 10.0 and 11.0, respectively, and $s_{Abw}^{(0)}$ given by the *MAD*;
- Estimators termed $s_{Abw,3}$ and $s_{Abw,4}$ that involve c values of 11.0 and 11.5, respectively, and $s_{Abw}^{(0)}$ given by the Q_n estimator;
- Estimators termed $s_{Abw,5}$ and $s_{Abw,6}$ involving c values of 7.0 and 7.5, respectively, and $s_{Abw}^{(0)}$ given by the S_n estimator.

7.3.3.5 The Andrew´s sine wave A-estimator of scale

The Andrew´s sine wave A-estimator s_{And} has also been proposed in several studies, e.g. see (Lax, 1985; Randal, 2008), and is defined by the following iterative procedure:

$$s_{And}^{(k)} = \frac{c \cdot n \cdot s_{And}^{(0)}}{\sqrt{n-1}} \frac{\sqrt{\sum_{\left|u_i^k\right| \le \pi} \sin^2\left(u_i^k\right)}}{\left|\sum_{\left|u_i^k\right| \le \pi} \cos\left(u_i^k\right)\right|} \tag{7.25}$$

in which c is a tuning constant considered with a value of 2.1 (Lax, 1985) and u_i^k is obtained by Eq. (7.24) where $s_{Abw}^{(0)}$ is replaced by $s_{And}^{(0)}$. The initial estimate $s_{And}^{(0)}$ was set as the *MAD* and m_n was set as the *M*.

7.3.3.6 The Andrew´s modified sine wave A-estimator of scale

The modified version of s_{And}, termed $s_{And,m}$, proposed by Lax (1985) has shown, in some cases, to be more efficient than s_{And} (Randal, 2008). This modified estimator is defined by the following iterative procedure:

$$s_{And,m}^{(k)} = \frac{c \cdot n \cdot s_{And,m}^{(0)}}{\sqrt{n-1}} arctg\left(\frac{\sqrt{\sum_{\left|u_i^k\right| \le \pi} \sin^2\left(u_i^k\right)}}{\left|\sum_{\left|u_i^k\right| \le \pi} \cos\left(u_i^k\right)\right|} \right) \tag{7.26}$$

in which c is a tuning constant considered with a value of 2.1 (Lax, 1985) and u_i^k is obtained by Eq. (7.24) where $s_{Abw}^{(0)}$ is replaced by $s_{And,m}^{(0)}$. As for s_{And}, the initial estimate $s_{And,m}^{(0)}$ was set as the *MAD* and m_n was set as the *M*.

7.3.3.7 The t-estimator of scale

The t-estimator of scale, s_t, is based on the *t*-distribution and was proposed in the study presented by Randal (2008) which demonstrated that s_t is also a very efficient dispersion estimator. This estimator is defined by the following iterative procedure:

$$s_t^{(k)} = \sqrt{\frac{1}{n}\sum_{i=1}^{n}\left(x_i - m_n\right)^2\left[1+\left(u_i^k\right)^2\right]^{-1}} \tag{7.27}$$

in which u_i^k is obtained by Eq. (7.24) where $s_{Abw}^{(0)}$ is replaced by $s_t^{(0)}$ and c is a tuning constant. Based on the results obtained by Randal (2008), the proposed study considers three versions of this estimator with c values of 4.0, 4.25 and 4.5, termed $s_{t,1}$, $s_{t,2}$ and $s_{t,3}$, respectively, with the initial estimate $s_t^{(0)}$ defined by Q_n and m_n defined by the *M*.

7.3.3.8 The modified maximum likelihood dispersion estimator

The modified maximum likelihood dispersion estimator ($MMLE_s$) proposed by Tiku and Sürücü (2009), which has shown adequate robustness properties, can be obtained using the unified format of Eq. (7.2) with the weighting function defined by:

$$w_i = \left[1 + \frac{1}{k} \left(\frac{x_{(i)} - m_0}{S_0} \right)^2 \right]^{-2} \tag{7.28}$$

with $W_s = \sum_{i=1}^{n} w_i \Big/ 1.13$ and $\bar{x}$ replaced by the *MMLE* central value estimator (CVE) obtained using the unified format of Eq. (7.4) in which w_i is defined by Eq. (7.28). Parameter k is a tuning constant considered to be 30 (Tiku and Sürücü, 2009) in order to balance the robustness and the efficiency properties of this estimator, and m_0 and S_0 are defined by the *M* and the *MAD*, respectively.

7.4 Selected methodology for the performance evaluation of the estimators

In order to determine which estimator is more adequate to characterize the dispersion of a given sample, a methodology based on the one defined in Chapter 6 for the case of the CVEs was used. The methodology considered herein comprises two stages similar to those presented in Chapter 6 and a third stage which involves the simultaneous performance evaluation of a series of central value and dispersion estimators.

In Stage 1, all the selected estimators are compared against each other based on their performance for samples of size n_{ref} (the *reference size*). In this case, only one sample of the *reference size* is available for each parameter that needs to be estimated. The *reference size* considered in the present study is fifty. However, due to aspects related to the structural analyses that were detailed in Chapter 6, demand values may not be obtained at some control sections for some of the records considered, and some variability of this size is allowed. Therefore, without loss of generality of the results obtained in Stage 1, the *reference size* will be a value between forty-five and fifty, depending on the dataset under analysis.

Two measures of efficiency are considered in Stage 1: the Scale Relative Efficiency (SRE), based on the proposal of Sawilowsky (2002), and the Relative Standard Error (RSE). The SRE of a certain estimator T, SRE_T, is defined by:

$$\mathrm{SRE}_T = \frac{T_{U95\%CI} - T_{L95\%CI}}{T_{ref,U95\%CI} - T_{ref,L95\%CI}} \tag{7.29}$$

where $T_{U95\%CI}$ and $T_{L95\%CI}$ are the upper and lower bounds of the 95% confidence interval (CI) of estimator T, respectively, while $T_{ref,U95\%CI}$ and $T_{ref,L95\%CI}$ are the same parameters obtained for the *reference estimator* T_{ref}. The 95% CI of a certain estimator is obtained by a bootstrap procedure with a bias corrected and accelerated percentile method (Wilcox, 2005), considering 1000 bootstrap samples, and considering T_{ref} to be defined by the sample standard deviation s. Since an estimator T having a shorter CI means that the estimates it produces are less variable, values of SRE_T which are lower than one (the value of $\mathrm{SRE}_{T_{ref}}$) indicate that T is more efficient than T_{ref}.

With respect to the other measure, the RSE of a certain estimator T, RSE_T, is defined by:

$$\mathrm{RSE}_T = \frac{s_T}{s_{T_{ref}}} \tag{7.30}$$

where s_T and $s_{T_{ref}}$ are the estimates of the standard deviation of T and T_{ref} obtained from the 1000 bootstrap samples, following the proposal from (Wilcox, 2005). As for SRE_T, values of RSE_T which are lower than one (the value of $\mathrm{RSE}_{T_{ref}}$) indicate that T is more efficient than T_{ref}.

As a result of Stage 1, the estimator exhibiting the best average performance over all the considered data samples is selected as the *reference estimator*, T_{ref2}, for the Stage 2 evaluation. A subgroup of the initial estimators, corresponding to those with a good efficiency, is also selected for the performance analysis of Stage 2. It should be emphasized that, for the present study, a robust estimator will always be preferred with respect to a non-robust one such as s. Therefore, the main goal of Stage 1 is to determine a subgroup of robust estimators that are more efficient than s.

In Stage 2, for a given parameter that needs to be estimated, the performance of the subgroup of estimators is evaluated considering several samples of smaller size n^* which are drawn from the sample of the *reference size*. The considered sizes n^* are forty, thirty, fifteen and seven. The performance of a given estimator is evaluated with respect to the value of T_{ref2}. Since m samples of size n^* are available to estimate each parameter in Stage 2, performance assessment measures different than those of Stage 1 are now considered.

Such measures are the Relative Squared Error (RSE^*) and the Relative Absolute Error (RAE^*). The RSE^* of a given estimator *T*, RSE_T^*, is defined by:

$$\text{RSE}_T^* = \frac{\sum_{i=1}^{m}\left(T_{i,n^*} - T_{ref\,2,n_{ref}}\right)^2}{\sum_{i=1}^{m}\left(T_{i,ref\,2\_n^*} - T_{ref\,2,n_{ref}}\right)^2} \tag{7.31}$$

where T_{i,n^*} is the value of estimator *T* for the *ith* sample of size *n**, $T_{i,ref\,2\_n^*}$ is the value of $T_{ref\,2}$ for the *ith* sample of size *n**, $T_{ref\,2,n_{ref}}$ is the value of $T_{ref\,2}$ for the original sample of size n_{ref}, and *m* is selected to be 10000 for each sample size *n**. In a similar form, the RAE^* of a given estimator *T*, RAE_T^*, is defined by:

$$\text{RAE}_T^* = \frac{\sum_{i=1}^{m}\left|T_{i,n^*} - T_{ref\,2,n_{ref}}\right|}{\sum_{i=1}^{m}\left|T_{i,ref\,2\_n^*} - T_{ref\,2,n_{ref}}\right|} \tag{7.32}$$

As stated initially, one fundamental objective is to establish a suitable probabilistic model of the data. Therefore, an additional evaluation stage is then performed to assess the combined performance of efficient central value and dispersion estimators in defining adequate probabilistic distributions of the data. In Stage 3, some of the more efficient CVEs identified in Chapter 6 are associated with the more efficient DEs resulting from Stage 2 in order to define fitted statistical distributions that are compared to the empirical distributions of the data. In this stage, a given pair of central value and dispersion estimates is computed from a sample of size *n** drawn from the empirical distribution data of the *reference size*. This pair defines a theoretical distribution (a lognormal or a normal distribution, depending on the EDP under analysis (see Chapter 5), whose distance to the empirical distribution is assessed using measures of distribution closeness: the Average Kolmogorov Distance (AKD^*), based on the Kolmogorov distance (van der Vaart, 1998), and the Average Wasserstein Distance (AWD^*), based on the Wasserstein distance (Vallander, 1974). The AKD^* of a given combination *C* of central value and dispersion estimators, AKD_C^*, is defined by:

$$\text{AKD}_C^* = \frac{1}{m}\sum_{i=1}^{m} KD_{C,i} \tag{7.33}$$

where $KD_{C,i}$ is the Kolmogorov distance (*KD*) that considers a fitted distribution with parameters obtained from the *ith* sample of size *n** using the estimators of combination *C*. Sample sizes *n** of forty, thirty, fifteen and seven are considered and *m* samples are drawn for each sample size. The computation of the *KD* is based on the general form defined by:

$$KD = \max_{1 \le j \le n_{ref}} \left| F_{emp}\left(x_j\right) - F_{fit}\left(x_j\right) \right| \tag{7.34}$$

where F_{emp} is the cumulative distribution function (CDF) of the empirical data and F_{fit} is the fitted CDF. In a similar form, the AWD^* of a given combination *C* of central value and dispersion estimators, AWD_C^*, is defined by:

$$\mathrm{AWD}_C^* = \frac{1}{m}\sum_{i=1}^{m} WD_{C,i} \tag{7.35}$$

where $WD_{C,i}$ is the Wasserstein distance (*WD*) that considers a fitted distribution with parameters obtained from the *ith* sample of size *n** using the estimators of combination *C*. The computation of the *WD* is based on the general form defined by:

$$WD = \int_{-\infty}^{+\infty} \left| F_{emp}\left(x\right) - F_{fit}\left(x\right) \right| dx \tag{7.36}$$

7.5 Results of the performance evaluation of the estimators

7.5.1 Initial considerations

General conclusions regarding the performance of the selected estimators are presented in the following. For the sake of brevity, only a sample of the results is shown, along with representative figures illustrating the more important findings. The estimators were applied to the structural demand data recorded at the control sections of the previously referred structures which were analysed under increasing levels of earthquake loading. As previously referred, each structure was analysed under a suite of fifty ground motions scaled up to nine intensities. As referred in the previous chapters, in some of the structures, and for a given intensity level, convergence of the structural analyses was not achieved for all the ground motions due to global dynamic instability of some of the numerical analyses. To maintain the size representativeness of the considered demand datasets, a specific intensity level of a given structure was disregarded when convergence was not achieved for more than five ground motions. Therefore, in Stage 1 of the performance evaluation of the estimators, the *reference size* n_{ref} of the analysed datasets is always between forty-five and fifty.

The performance assessment results are presented for the distributions of beam and column demand data, obtained from control sections located at the member ends, and for the maximum inter-storey drift demand over the height of the structure, ⊿. For beams and columns, results are presented for the maxima of the curvature φ, of the chord rotation θ and of the shear force demand V. The chord rotation was computed according to the

Exact Geometrical Method referred in Chapter 2. For curvature and chord rotation demand, the estimators were applied separately for positive and negative data. However, the combination of the random nature of the ground motions with the characteristics of a given structure imply that positive and negative demand values may not be obtained at some control sections for some of the records considered (e.g. in some sections, only negative curvatures reached the minimum sample size of forty-five while positive curvatures did not). Therefore, to maintain the size representativeness of the demand datasets and to keep n_{ref} between forty-five and fifty, any curvature or chord rotation dataset for which such situation was observed for more than five ground motions is also disregarded. Furthermore, it is noted that for estimators involving trimming of a dataset, when the trimming level is not an integer, the number of trimmed data values was rounded to the closest upper integer.

Results of Stage 1 are essentially presented in terms of the average percentage of larger efficiency (APLE) of an estimator T with respect to T_{ref}, i.e. *s*. APLE values represent the number of times that T is more efficient than T_{ref} and are obtained for the different EDPs considering the SRE and the RSE measures. Depending on the situation, APLE values are obtained by averaging across all the control sections of the structure or by averaging simultaneously across all the control sections of the structure and all the earthquake intensities. The approach of averaging across the earthquake intensities was selected since no specific range of ground motion intensities was seen to show that a given set of estimators was standing out from the others. Hence, the efficiency of the estimators was equally weighted across the whole range of intensities. In light of this, the performance results of all the intensities were able to be presented in a more concise form using the mean and the coefficient of variation (CoV) of the results for all the intensities.

Although Chapter 5 refers that the 5% damping spectral acceleration ordinate of the ground motion for the fundamental period of the structure T_1, $S_a(T_1)$, is a more adequate IM than the peak ground acceleration (PGA) for the purpose of obtaining EDP distributions more compatible with the lognormal or the normal distribution hypotheses, PGA is also considered herein in order to simulate a situation of larger variability of the demand and to assess the performance of the selected estimators under such conditions. In addition, it is noted that results are presented considering the curvature, the chord rotation and the inter-storey drift demands in log units, i.e. in order to be compatible with the assumption that demand follows a lognormal distribution (see Chapter 5). For the case of shear force demand, results are presented for the cases where V is in original and in log units, i.e. in order to be compatible with the assumption that demand can follow either a normal or a lognormal distribution (see Chapter 5). For a clear comprehension of the presented graphical results, the DEs are numbered according to Table 7.1.

From the results of Stage 1, a subgroup of ten estimators and a new *reference estimator* $T_{ref\,2}$ are selected for the performance assessment carried out in Stage 2. The results of Stage 2 are similar to those of Stage 1, with the APLE value of an estimator T of the referred subgroup now being determined with respect to $T_{ref\,2}$, considering the RSE^* and the RAE^* measures, and considering samples of sizes n^* of forty, thirty, fifteen and seven which are drawn from the sample of the *reference size*.

Table 7.1. Numbering of the selected DEs

Number	DE	Number	DE
1	s	18	τ_s
2	IQR	19	s_{log}
3	MAD	20	$s_{Hub,1}$
4	Q_n	21	$s_{Hub,2}$
5	S_n	22	$s_{Hub,3}$
6	S_{sh}	23	$s_{Abw,1}$
7	$s_{0.08-TL}$	24	$s_{Abw,2}$
8	$s_{0.12-TL}$	25	$s_{Abw,3}$
9	$s_{0.16-TL}$	26	$s_{Abw,4}$
10	$s_{0.20-TL}$	27	$s_{Abw,5}$
11	$s_{0.24-TL}$	28	$s_{Abw,6}$
12	S_{ecf}	29	s_{And}
13	$s_{0.08-tr}$	30	$s_{And,m}$
14	$s_{0.12-TL}$	31	$s_{t,1}$
15	$s_{0.16-TL}$	32	$s_{t,2}$
16	$s_{0.20-TL}$	33	$s_{t,3}$
17	$s_{0.24-TL}$	34	$MMLE_s$

Based on the results of Stage 2, a group of DEs with best performance is selected and combined with CVEs identified in Chapter 6 as having an efficient performance. The results of Stage 3 are presented in terms of the AKD^* and AWD^* values obtained for the selected combinations of estimators, the different EDPs, both IMs, and samples of sizes n^* of forty, thirty, fifteen and seven which are drawn from the sample of the *reference size*. In order to reduce the amount of data to be displayed, the totality of the AKD^* and AWD^* values are simultaneously averaged across all the control sections of a given structure and all the earthquake intensities. In addition to these average results, their corresponding CoVs are also presented. According to the results of Chapter 5, the selected combination of estimators will define a lognormal distribution for the curvature, the chord rotation and the inter-storey drift demands. For the case of shear force demand, both lognormal and normal distributions will be defined (see Chapter 5).

7.5.2 Presentation and discussion of the results

7.5.2.1 Results of Stage 1

The APLE results for the SRE and the RSE of all the estimators obtained for the negative curvature φ demand of the REG10 sections, for all the intensities and when $S_a(T_1)$ is the IM, are presented in Figs. 7.1 and 7.2, respectively. Each point represents an APLE value that considers all the sections of the structure. From these results, the APLE values of the SRE and the RSE can be seen to exhibit a similar trend, thus indicating the same estimators as being the more efficient. The results also indicate that the variability of the APLE values between estimators is large and depends also on the selected earthquake intensity. Furthermore, it can also be seen that the earthquake intensity for which each estimator performs best is variable.

Although there are considerable differences between the performances of the estimators, the dispersion values they yield do not exhibit large variability. To illustrate this, Fig. 7.3 presents the CoV of the thirty-four dispersion values obtained by the estimators, for each REG10 negative φ dataset and for all the intensities, where it can be seen that, although there are a few sections and intensities exhibiting large CoVs, most of them are below 20% (similar values are obtained for the positive φ demand). This fact indicates that, although the several estimators may yield dispersion estimates that are not far from each other, the efficiency measured by the SRE and the RSE enables the identification of the more adequate estimators. Even though these CoV values are low, it should be noted that the CoVs obtained for the CVEs in similar analyses presented in Chapter 6 are lower. To obtain a more global view of the performance of the estimators, APLE values of the SRE and the RSE now also averaged across the earthquake intensities are presented in Figs. 7.4 and 7.5 for the positive and negative, respectively, φ demand of the REG10 sections. The results of Figs. 7.4 and 7.5 also include the CoVs of these APLE values reflecting their variability across the earthquake intensities. It can be observed that some of the estimators exhibit SRE and RSE APLE values higher than 60% (left-hand side scale of the graphs) along with low values of the CoV (right-hand side scale of the graphs), which indicates that, in these cases, the variability of the APLE values between earthquake intensities is low. According to the results, estimators 15, 16, 17, 18, 31, 32 and 33 ($s_{0.16-tr}$, $s_{0.20-tr}$, $s_{0.24-tr}$, τ_s, $s_{t,1}$, $s_{t,2}$ and $s_{t,3}$) are seen to be some of the more efficient in this case.

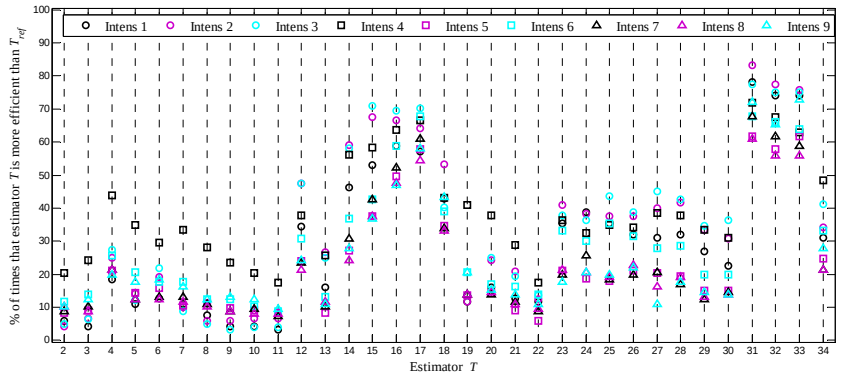

Figure 7.1. APLE values of the estimators, for the SRE, for the REG10 negative curvatures when $S_a(T_1)$ is the IM and for all the intensities.

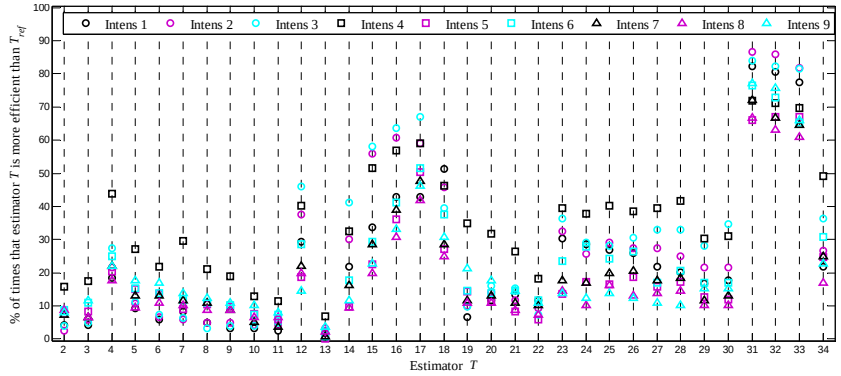

Figure 7.2. APLE values of the estimators, for the RSE, for the REG10 negative curvatures when $S_a(T_1)$ is the IM and for all the intensities.

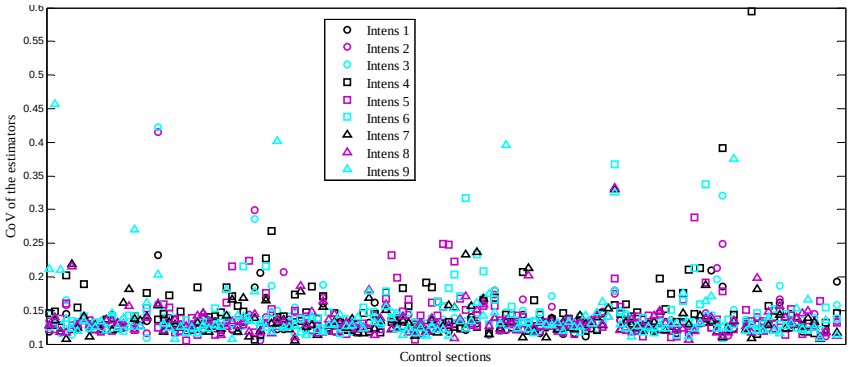

Figure 7.3. CoV of the dispersion values obtained by all the estimators for the REG10 negative curvatures, for all the intensities and control sections, when $S_a(T_1)$ is the IM.

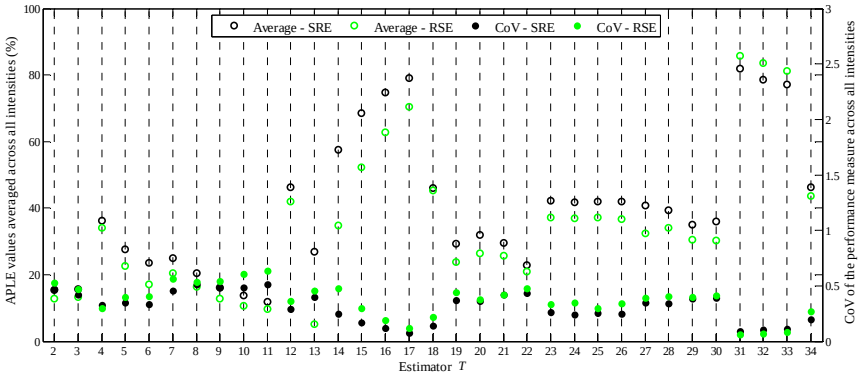

Figure 7.4. APLE values of the estimators, for the SRE and the RSE, for the REG10 positive curvatures when $S_a(T_1)$ is the IM, averaged across all the intensities, and CoVs representing the variability between intensities.

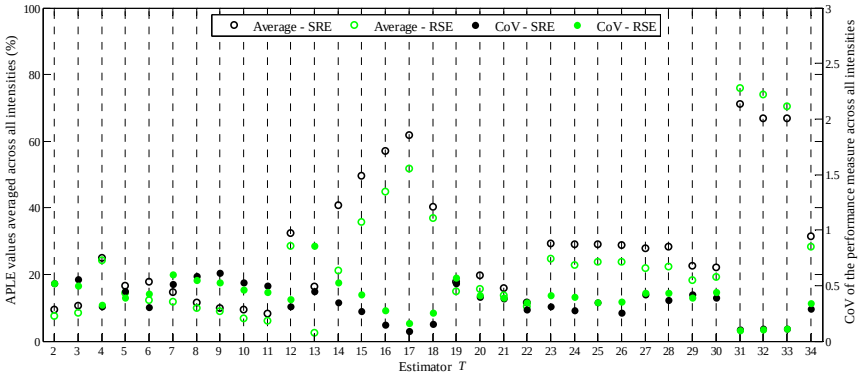

Figure 7.5. APLE values of the estimators, for the SRE and the RSE, for the REG10 negative curvatures when $S_a(T_1)$ is the IM, averaged across all the intensities, and CoVs representing the variability between intensities.

In terms of chord rotation demand, Fig. 7.6 presents, for the case of the IRREG6 negative θ demand, the APLE results for the SRE of all the estimators, for all the intensities and when PGA is the IM. APLE results obtained for the RSE and for the positive θ demand are similar. As for the results of REG10, the variability of the APLE values between estimators and between the selected earthquake intensities is seen to be large, and the earthquake intensity for which each estimator performs best is also variable. Furthermore, as for the previous case also, the CoV of the thirty-four dispersion values obtained by the estimators for each IRREG6 negative θ dataset and for all the intensities exhibit some large values for a few sections and intensities. Still, the majority of the CoV values is mostly below 20% (Fig. 7.7). Similar to Fig. 7.4, Fig. 7.8 presents, for the negative θ demand of the IRREG6 sections, APLE values of the SRE and the RSE now also averaged across the earthquake intensities, along with the CoVs reflecting their variability across the earthquake intensities. In this case, the average SRE and RSE APLE values of some of the more efficient estimators exhibit some noticeable differences. Although the SRE and RSE measures identify the same estimators as the more efficient, the performance

of some of the estimators correlates differently with each measure. Even though there are APLE values in the range of 80%-90% for some of the earthquake intensities, the referred variability between these intensities leads to average APLE values that are between 50% and 70% for the more efficient estimators, with the corresponding CoVs being generally below 50%. With respect to the more efficient estimators for θ, these are seen to be similar to those identified for φ.

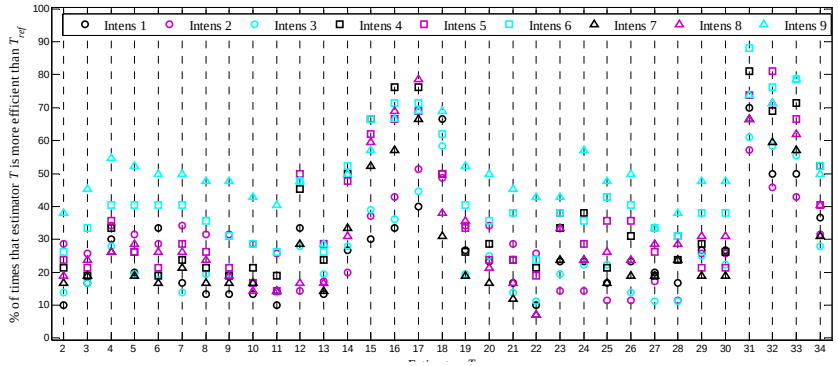

Figure 7.6. APLE values of the estimators, for the SRE, for the IRREG6 negative chord rotation when PGA is the IM and for all the intensities.

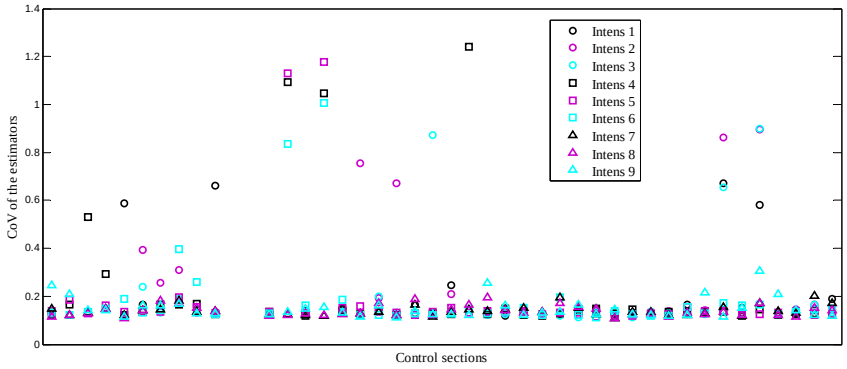

Figure 7.7. CoV of the dispersion values obtained by all the estimators for the IRREG6 negative chord rotation, for all the intensities and control sections, when PGA is the IM.

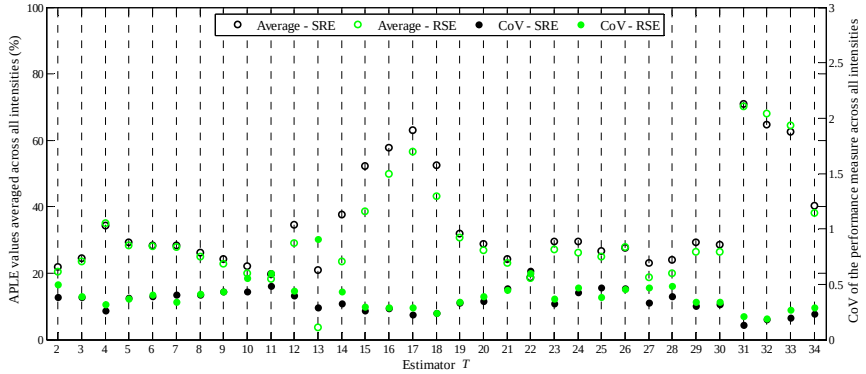

Figure 7.8. APLE values of the estimators, for the SRE and the RSE, for the IRREG6 negative chord rotation when PGA is the IM, averaged across all the intensities, and CoVs representing the variability between intensities.

In terms of shear force demand, Figs. 7.9 and 7.10 present the SRE and RSE APLE values averaged across the sections and the earthquake intensities for the REG6 shear force demand in original and log units, respectively, when $S_a(T_1)$ is the IM, along with the CoVs reflecting their variability across the earthquake intensities. As for the previous cases, the SRE and RSE APLE values are also close, with maximum values above 60% for the more efficient estimators, and their corresponding CoVs being below 50%. Furthermore, it can also be observed that APLE results in original and log units are similar. Additionally, Fig. 7.11 presents the CoV of the thirty-four dispersion values obtained by the estimators, for each REG6 shear force dataset in original units and for all the intensities. As for the previous cases, some large CoV values are observed for a few sections and intensities. Still, the majority of the values can be seen to be generally lower than 20% (almost identical values are obtained for the V demand in log units). With respect to the more efficient estimators for V, these are similar to those of the previous EDPs.

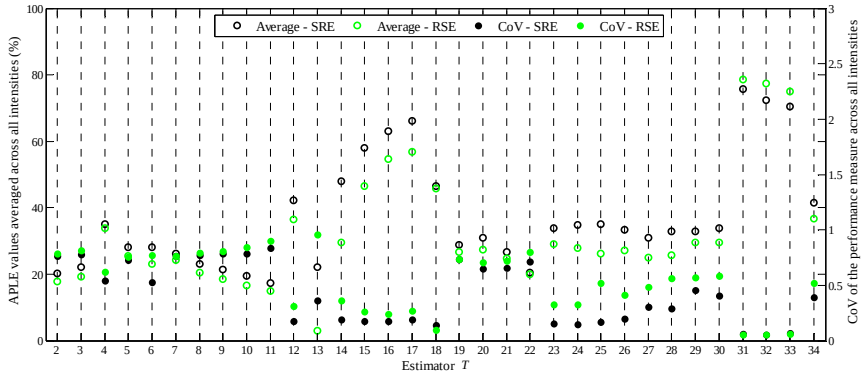

Figure 7.9. APLE values of the estimators, for the SRE and the RSE, for the REG6 shear force in original units when $S_a(T_1)$ is the IM, averaged across all the intensities, and CoVs representing the variability between intensities.

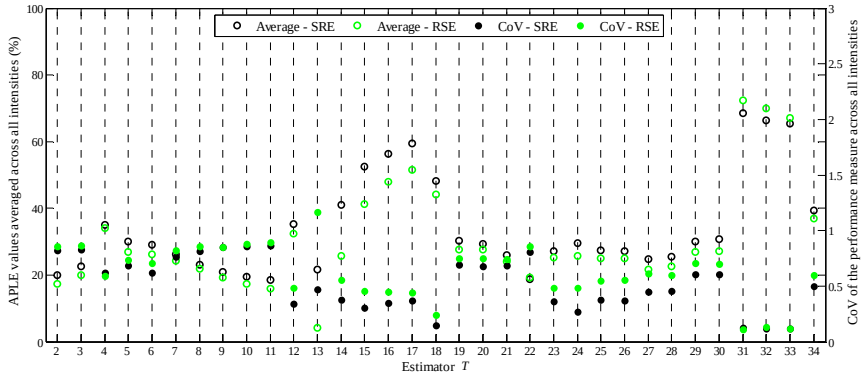

Figure 7.10. APLE values of the estimators, for the SRE and the RSE, for the REG6 shear force in log units when $S_a(T_1)$ is the IM, averaged across all the intensities, and CoVs representing the variability between intensities.

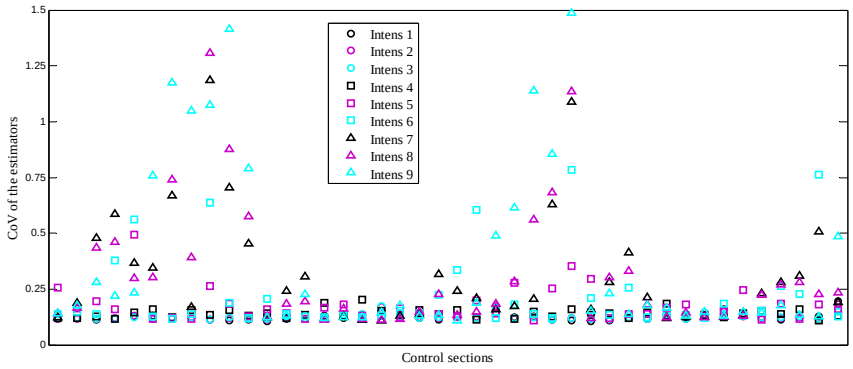

Figure 7.11. CoV of the dispersion values obtained by all the estimators for the REG6 shear force in original units, for all the intensities and control sections, when $S_a(T_1)$ is the IM.

For the case of the inter-storey drift ⊿, and since for a given structure there is only one dataset for each earthquake intensity, Fig. 7.12 presents APLE values of the SRE and the RSE averaged across all the structures and all the earthquake intensities, and the CoVs representing their variability across these intensities, when $S_a(T_1)$ is the IM. Although only forty-four datasets are considered (the intensity nine dataset of the ICONS structure was disregarded by the reasons highlighted in Section 7.5.1), it can be observed that both the APLE values and the CoVs are similar to those of the previous EDPs. With respect to the more efficient estimators, these are also seen to be those of the previous cases. In addition, Fig. 7.13 presents the CoV of the thirty-four dispersion values obtained by the estimators for each structure and ⊿ dataset which can be seen to be between 12% and 20%.

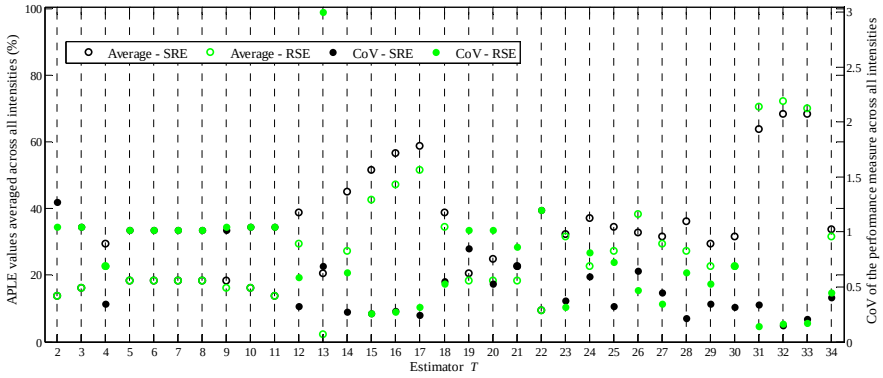

Figure 7.12. APLE values of the estimators, for the SRE and the RSE, for the inter-storey drift of all the structures when $S_a(T_1)$ is the IM, averaged across all the intensities, and CoVs representing the variability between intensities.

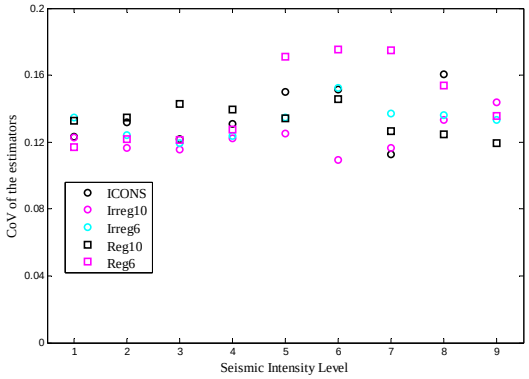

Figure 7.13. CoV of the dispersion values obtained by all the estimators, for the inter-storey drift of all structures and for all the intensities, when $S_a(T_1)$ is the IM.

Based on the analysis of the results of Stage 1, the most efficient estimators to be considered in Stage 2 were identified. For the case of φ, θ and V, Table 7.2 presents the ten best DEs for each structure and for both IMs. For each structure and IM, the SRE and RSE APLE values of the six EDPs (i.e. the positive and negative φ and θ, and V both in original and in log units) were sorted in ascending order, and the corresponding ten estimators appearing more times over all twelve situations were selected. A similar analysis was also carried out for $\measuredangle$ and the resulting estimators were also those found in Table 7.2. As can be observed, Table 7.2 refers to twelve different estimators. However, the following ten estimators can be seen to appear for almost every structure and IM: estimators 4, 12, 15, 16, 17, 18, 31, 32, 33 and 34 (Q_n, S_{ecf}, $s_{0.16-tr}$, $s_{0.20-tr}$, $s_{0.24-tr}$, τ_s, $s_{t,1}$, $s_{t,2}$, $s_{t,3}$, and $MMLE_y$). Given the smaller size of the datasets chosen for Stage 2, the consideration of the data trimming levels involved in estimators $s_{0.16-tr}$, $s_{0.20-tr}$ and $s_{0.24-tr}$ presents some problems. Therefore, in order to still be able to include this type of estimators in the analyses of Stage 2, the following modifications were considered for each sample size n^*:

- For the sample size n^* of forty, estimator $s_{0.20-tr}$ was considered and estimators $s_{0.16-tr}$ and $s_{0.24-tr}$ were replaced by estimators $s_{0.15-tr}$ and $s_{0.25-tr}$ instead, since each one of these allows to trim an integer number of data values from each side of the samples (three and five values, respectively);
- For the sample size n^* of thirty, estimator $s_{0.20-tr}$ was considered and estimators $s_{0.16-tr}$ and $s_{0.24-tr}$ were replaced by estimators $s_{0.133-tr}$ and $s_{0.267-tr}$ instead, since each one of these allows to trim an integer number of data values from each side of the samples (two and four values, respectively);
- For the sample size n^* of fifteen, estimator $s_{0.20-tr}$ was not considered and estimators $s_{0.16-tr}$ and $s_{0.24-tr}$ were replaced by estimators $s_{0.133-tr}$ and $s_{0.267-tr}$

instead, since each one of these allows to trim an integer number of data values from each side of the samples (one and two values, respectively);

- For the sample size n^* of seven, estimators $s_{0.16-tr}$ and $s_{0.20-tr}$ were not considered and estimator $s_{0.24-tr}$ was replaced by estimator $s_{0.285-tr}$ instead, since it allows to trim an integer number of data values from each side of the samples, i.e. one value.

Therefore, the estimators selected for the Stage 2 analyses are τ_s, $s_{t,1}$, $s_{t,2}$, $s_{t,3}$, $MMLE_s$, Q_n, S_{ecf}, along with these different cases of the $s_{\alpha-tr}$ estimator. The numbering of each new case of $s_{\alpha-tr}$ corresponds to that of the original estimator being replaced. Finally, estimator 31, $s_{t,1}$, was seen to be the estimator with best performance, i.e. it yields higher APLE values than the remaining estimators in a larger number of cases, and was selected as the new *reference estimator* $T_{ref\,2}$.

Table 7.2. The ten most efficient DEs, for each structure and IM, and the number of times *NT* they appear

ICONS				IRREG10				IRREG6				REG10				REG6			
PGA		$S_a(T_1)$		PGA		$S_a(T_1)$		PGA		$S_a(T_1)$		PGA		$S_a(T_1)$		PGA		$S_a(T_1)$	
DE	*NT*	DE	*NT*	DE	*NT*	DE	*NT*	DE	*NT*	DE	*NT*	DE	*NT*	DE	*NT*	DE	*NT*	DE	*NT*
15	*12*	15	*12*	3	*12*	15	*12*	3	*12*	3	*12*	3	*12*	12	*12*	3	*12*	15	*12*
16	*12*	16	*12*	15	*12*	16	*12*	12	*12*	12	*12*	12	*12*	15	*12*	15	*12*	16	*12*
17	*12*	17	*12*	16	*12*	17	*12*	15	*12*	15	*12*	15	*12*	16	*12*	16	*12*	17	*12*
18	*12*	18	*12*	17	*12*	18	*12*	16	*12*	16	*12*	16	*12*	17	*12*	17	*12*	18	*12*
31	*12*	31	*12*	18	*12*	31	*12*	17	*12*	17	*12*	17	*12*	18	*12*	18	*12*	31	*12*
32	*12*	32	*12*	31	*12*	32	*12*	18	*12*	18	*12*	18	*12*	31	*12*	31	*12*	32	*12*
33	*12*	33	*12*	32	*12*	33	*12*	31	*12*	31	*12*	31	*12*	32	*12*	32	*12*	33	*12*
34	*12*	34	*12*	33	*12*	34	*12*	32	*12*	32	*12*	32	*12*	33	*12*	33	*12*	34	*12*
3	*11*	3	*11*	34	*12*	3	*12*	33	*12*	33	*12*	33	*12*	34	*12*	34	*12*	12	*10*
12	*11*	12	*10*	19	*11*	12	*9*	34	*12*	34	*12*	34	*12*	8	*9*	19	*11*	3	*9*

7.5.2.2 Results of Stage 2

Only a sample of the results of Stage 2, in terms of the RSE^* and of the RAE^* measures, are presented herein since they were found to be generally the same across all structures, for all EDPs and for both IMs. The large majority of the Stage 2 results are similar to those presented in Figs. 7.14a) to d). Figure 7.14a) shows the APLE results for the RSE^* of the estimators selected for Stage 2, obtained for the positive φ demand of the ICONS sections, for all the intensities, for a sample size n^* of forty and when $S_a(T_1)$ is the IM. With the exception of estimator 32 ($s_{t,2}$), these results show that the considered estimators do not exhibit APLE values above 50%, which means that their performance is not superior to that of $T_{ref\,2}$ ($s_{t,1}$). To confirm that similar results were obtained for other

sample sizes, Figs. 7.14b), c) and d) present, for the same structure and EDP, the RSE^* and RAE^* APLE values averaged across the earthquake intensities for n^* values of thirty, fifteen and seven, respectively, and the CoVs reflecting the variability between earthquake intensities. These results indicate that estimator 32 has a performance close to that of $s_{t,1}$ (APLE values are close to 50%), and that, in some cases, estimator 33 ($s_{t,3}$) also exhibits APLE values which correspond to an average performance close to 40%. With respect to the remaining estimators, their performance is much lower. In terms of the variability between earthquake intensities, it can be observed that the CoVs of the more efficient estimators are generally in the range of 25%-40%, irrespective of n^*.

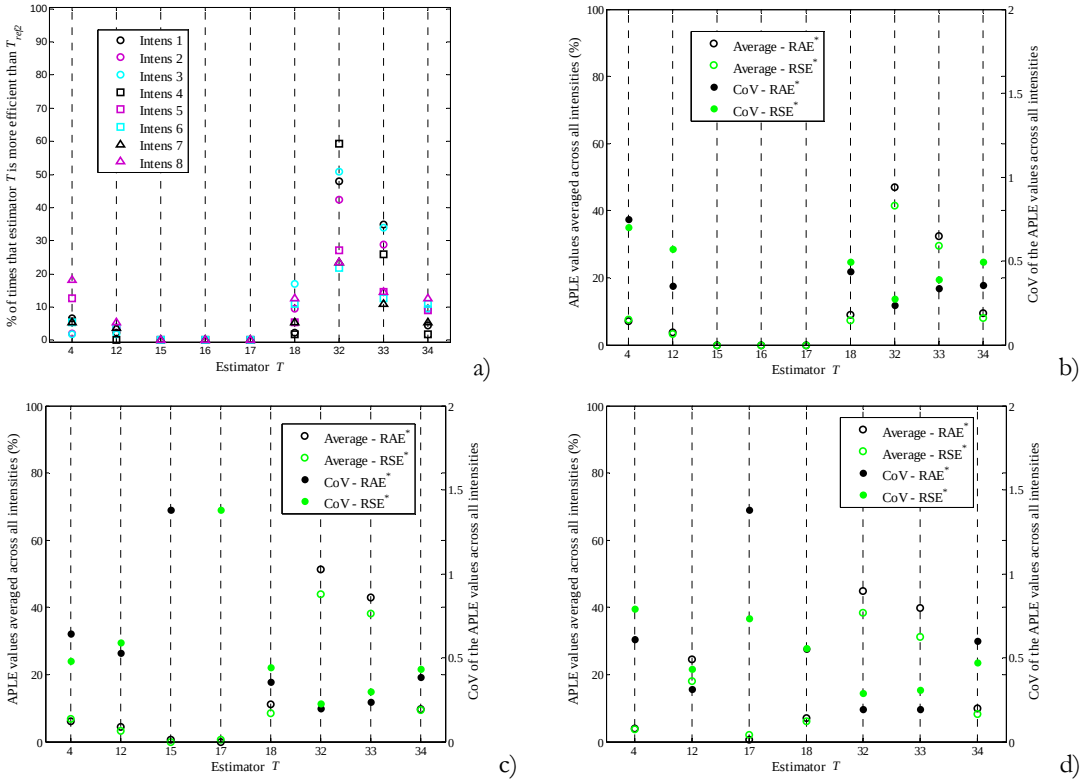

Figure 7.14. APLE values of the estimators for the ICONS positive curvature when $S_a(T_1)$ is the IM, for the RSE^* and all the intensities (a) for the RSE^* and RAE^* averaged across all the intensities along with the CoVs representing the variability between intensities when n^* is thirty (b), when n^* is fifteen (c), when n^* is seven (d).

As referred, these findings illustrate the large majority of the results obtained and indicate that estimators 31, 32 and 33 ($s_{t,1}$, $s_{t,2}$ and $s_{t,3}$) are those with best performance - estimator 33 to a lesser extent though. Although in a much less frequent number of cases, other situations also identified, especially for the shear force EDP, are briefly illustrated in the following. As an example, Fig. 7.15 presents APLE values of the estimators averaged across all the intensities and the CoVs reflecting their variability across these intensities, for the RSE^* and the RAE^* of the IRREG10 shear force, both in log and in original units,

when PGA is the IM, and for several cases of n^*. These results exhibit situations where estimators 4, 12, 18 and 34 (Q_n, S_{ecf}, τ_s and $MMLE_s$) exhibit a better performance than that of estimators 32 and 33. Nonetheless, even in these cases, the performance of $s_{t,1}$ is still higher.

Based on a global analysis of the Stage 2 results, no definite trend was observed with respect to the effect of the IM on the efficiency of the estimators. In general terms, the efficiency of the estimators was found to be similar irrespective of the IM. This situation indicates that these estimators are fit to be considered under various conditions of the dispersion obtained for the demand.

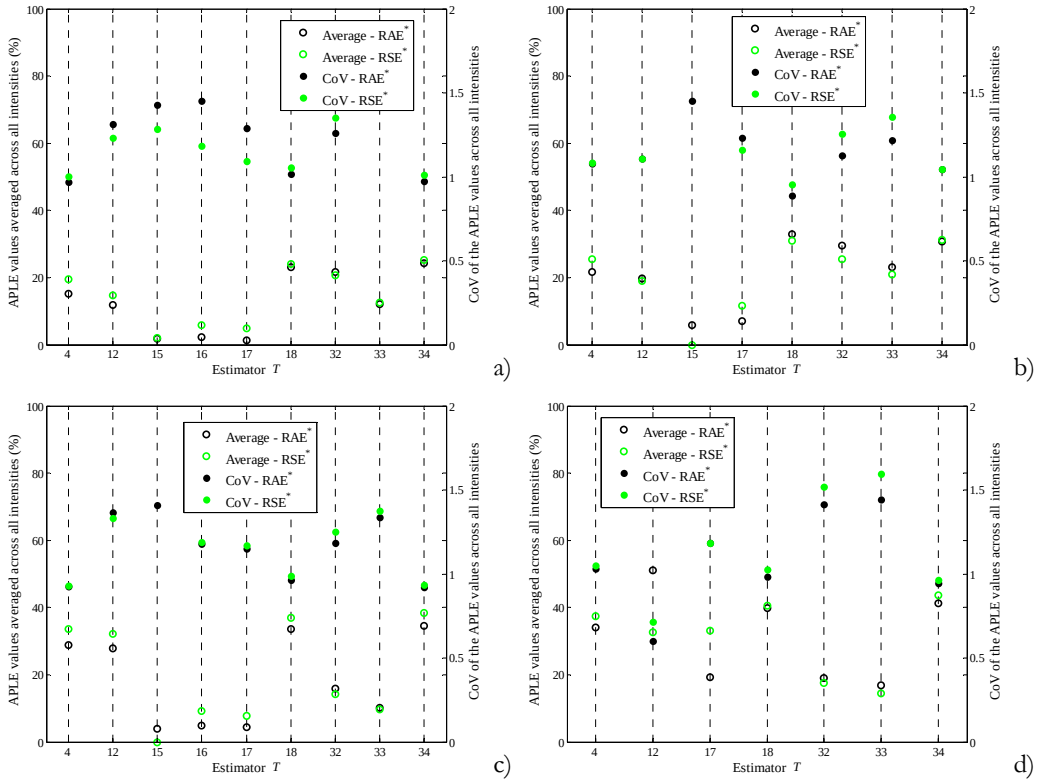

Figure 7.15. APLE values of the estimators averaged across all the intensities along with the CoVs representing the variability between intensities, for the IRREG10 RSE^* and RAE^* values, when PGA is the IM, for the shear force in log units when n^* equal to forty (a) and to fifteen (b), and for the shear force in original units when n^* equal to thirty (c) and to seven (d).

To further illustrate the results of Stage 2, and to highlight the differences between the different estimators, namely in terms of the influence of the sample size in the value of the dispersion estimates, a more detailed view of the results obtained by some of the estimators considered in Stage 2 is presented in the following. This analysis is focussed on estimators 31 and 18 ($s_{t,1}$ and τ_s) since the results of estimator $s_{t,1}$ are representative of those obtained with $s_{t,2}$ and $s_{t,3}$, while the results of τ_s are considered to be representative of those obtained with Q_n, S_{ecf} and $MMLE_s$. For the case of the positive φ demand of the

ICONS structure when $S_a(T_1)$ is the IM, Figs 7.16a) and b) present, for all the sections and all the intensities, the average value of the 10000 estimates, normalized by $T_{ref2,n_{ref}}$, obtained with $s_{t,1}$ for sample sizes *n** of forty and seven, respectively. Figures 7.16c) and d) present similar results obtained with τ_s. These results indicate that, for most sections and intensities, the average of the 10000 estimates is very close to the value of $T_{ref2,n_{ref}}$, irrespective of the considered estimator. Moreover, the average estimates produced by $s_{t,1}$ are seen to exhibit a small bias, while those obtained with τ_s exhibit a larger bias. This bias is seen to increase as *n** decreases and reveals that these estimators tend to (on average) underestimate the value of $T_{ref2,n_{ref}}$. To complement these results, Figs. 7.17a) to d) present the CoV of the 10000 estimates obtained with $s_{t,1}$ and τ_s for sample sizes *n** of forty and seven. As expected, the CoV increases as *n** decreases (the average CoV is seen to double its value from a size *n** of forty to a size *n** of seven). However, the CoV values are seen to be very similar from one estimator to another. Furthermore, it is noted that comparable results were also obtained for the remaining deformation-based EDPs and structures.

A similar analysis carried out for the results of the IRREG10 shear force in log units, when PGA is the IM, yields a different type of outcome. Figures 7.18a) to d) present, for all the sections and all the intensities, the average value of the 10000 estimates obtained with $s_{t,1}$ and τ_s, normalized by $T_{ref2,n_{ref}}$, and for sample sizes *n** of forty and seven. The results obtained for $s_{t,1}$, Figs. 7.18a) and b), indicate that the average dispersion estimate of several sections exhibits a considerable bias, which increases as *n** decreases, that tends to overestimate the dispersion of the data. This bias is seen to occur in the results of the beam sections, with larger values being observed for the higher earthquake intensities. The reason behind these results is connected to the expected evolution of the shear force values. Since the post-yield stiffness of a structural member is usually low, the dispersion of the shear force demand distribution tends to be very small when a given member as yielded at both ends. All structures with members having this type of behaviour exhibited a similar anomalous performance of $s_{t,1}$. However, considerably large bias values were only seen for the IRREG10 and REG10 structures. With respect to the results obtained with τ_s, these exhibit similar irregularities although the observed bias shows that this estimator has the tendency to underestimate the dispersion of the data. Globally, this analysis indicates that these estimators yield less accurate results when the ratio between the dispersion and the central value is small. To complement these results, Figs. 7.19a) to d) present the CoV of the 10000 estimates obtained with $s_{t,1}$ and τ_s for sample sizes *n** of forty and seven. As expected, the CoV increases as the sample size decreases and the larger values reflect the irregular behaviour of the estimators applied to the data of the beam sections. As for the previous EDPs, the CoV values are seen to be similar from one estimator to another.

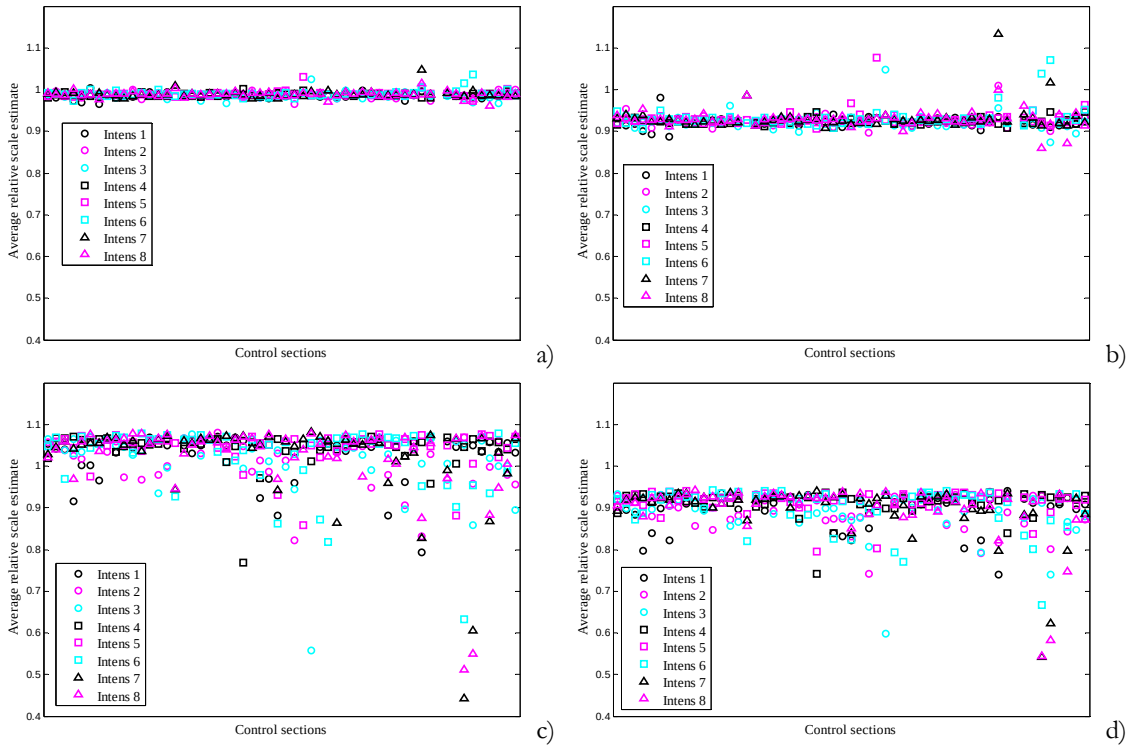

Figure 7.16. Average estimates of the dispersion of the positive curvature of all the sections of the ICONS structure, when $S_a(T_1)$ is the IM, with $s_{t,1}$ when n^* equal to forty (a) and to seven (b), and with τ_s when n^* equal to forty (c) and to seven (d).

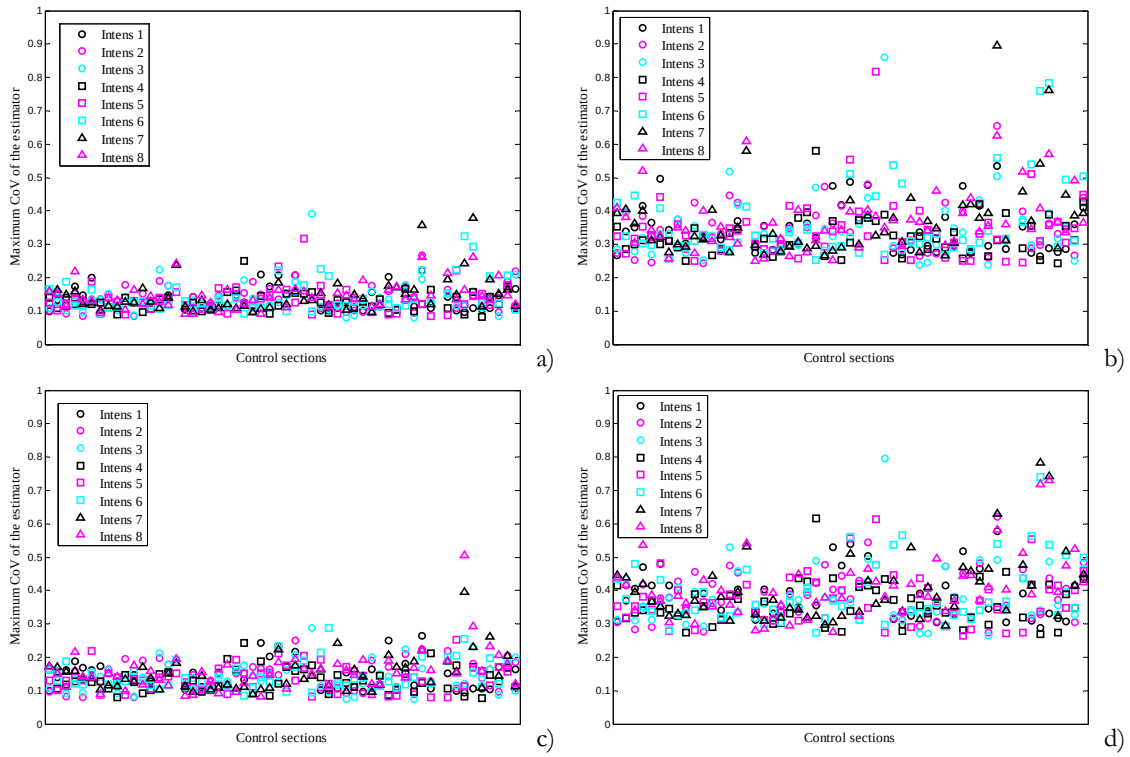

Figure 7.17. CoV of the estimates of the dispersion of the positive curvature of all the sections of the ICONS structure, when $S_a(T_1)$ is the IM, with $s_{t,1}$ when n^* equal to forty (a) and to seven (b), and with τ_s when n^* equal to forty (c) and to seven (d).

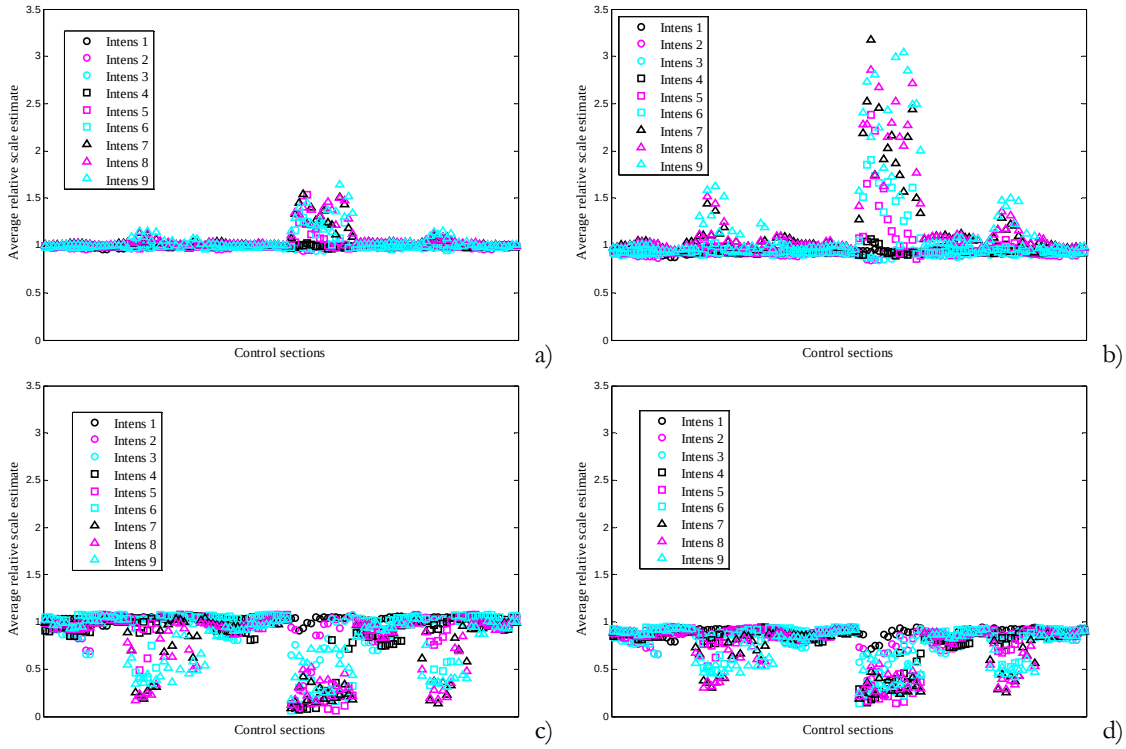

Figure 7.18. Average estimates of the dispersion of V, in log units, for all the sections of the IRREG10 structure, when PGA is the IM, with $s_{t,1}$ when n^* equal to forty (a) and to seven (b), and with τ_s when n^* equal to forty (c) and to seven (d).

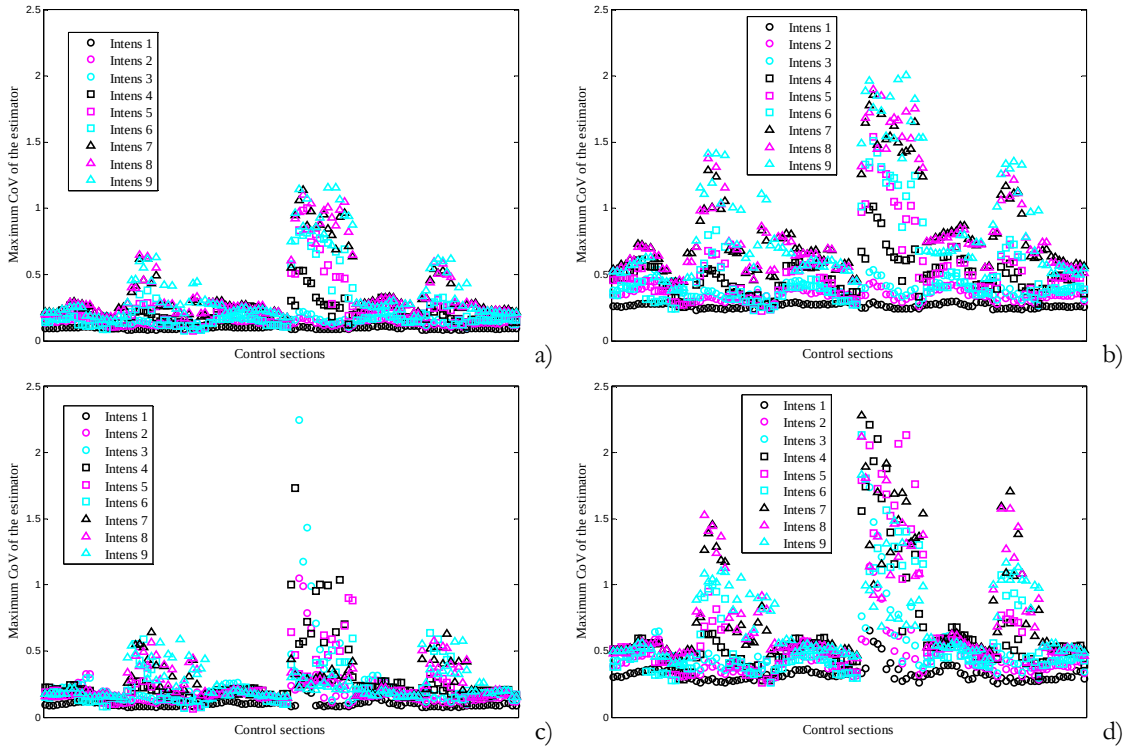

Figure 7.19. CoV of the estimates of the dispersion of V, in log units, for all the sections of the IRREG10 structure, when PGA is the IM, with $s_{t,1}$ when n^* equal to forty (a) and to seven (b), and with τ_s when n^* equal to forty (c) and to seven (d).

Based on this analysis, it is recalled that the RSE* and the RAE* efficiency measures are obtained using the result of estimator 31, $s_{t,1}$, for size n_{ref} ($T_{ref\,2,n_{ref}}$) as a reference for the "true value" of the dispersion of the datasets. Similar to what was performed for the central value estimators analyzed in Chapter 6, the Stage 2 analyses were repeated using a different estimator to quantify $T_{ref\,2,n_{ref}}$, in this case estimator 18 (τ_s), and to observe how different are the results. To illustrate the findings of this new analysis, Fig. 7.20 presents APLE results obtained using τ_s to quantify $T_{ref\,2,n_{ref}}$. These results correspond to those of Figs. 7.14a), 7.14d), 7.15a) and 7.15d) that were obtained by defining $T_{ref\,2,n_{ref}}$ using estimator 31. Although, in some cases, these new results show an increase in the performance of estimators 32 and 33 ($s_{t,2}$ and $s_{t,3}$) with respect to that of $s_{t,1}$, other results indicate the occurrence of a larger number of situations where estimators 12, 18 and 34 (S_{ecf}, τ_s, and $MMLE_s$) perform better than $s_{t,1}$. With respect to the case of estimators 15, 16 and 17, their performance still remains well below that of the other methods.

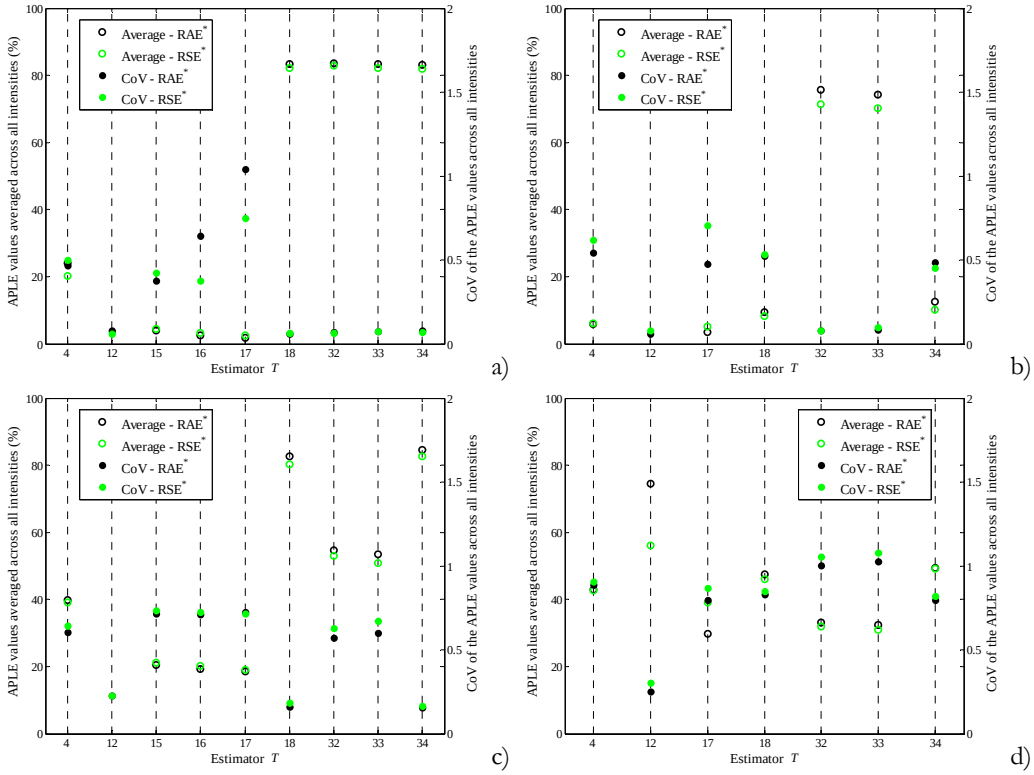

Figure 7.20. APLE values of the estimators averaged across all the intensities along with the CoVs representing the variability between intensities, for the RSE* and RAE* values, when $S_a(T_1)$ is the IM, for the ICONS positive curvature when n^* is forty (a) and when n^* is seven (b), and when PGA is the IM, for the IRREG10 shear force in log units when n^* equal to forty (c), and for the shear force in original units when n^* equal to seven (d).

In light of this latter analysis, it is observed that, in the overall, the results of Stage 2 are not totally conclusive. With the exception of estimators 15, 16 and 17 that were seen to perform poorly across all cases, the performance of the remaining estimators selected for Stage 2 is seen to oscillate, namely as a function of the selected sample size *n** and the value of $T_{ref\,2,n_{ref}}$. This fact indicates that, although the several estimators may lead to similar dispersion values for samples of the *reference size* (see Section 7.5.2.1, based on the low CoV values of Fig. 7.3), the differences are still significant enough to influence the results of Stage 2. Given this outcome, an additional analysis stage was carried out to be able to identify the most suitable dispersion estimators. In this stage, estimators of the central value and of the dispersion of the data are combined to establish a probabilistic model whose adequacy is assessed.

7.5.2.3 Results of Stage 3

In this stage, efficient CVEs identified in Chapter 6 are associated with DEs to define fitted statistical distributions that are compared to the empirical distributions of the data using the AKD^* and the AWD^* performance measures defined in Section 7.4. Based on the results of Chapter 6, the selected CVEs are $T_{Hub,3}$, $T_{Ham,3}$, $T_{Tuk,3}$, T_{log} and $\overline{x}_{0.08-HQ1}$. Details about their definition can be found in Chapter 6 and are, therefore, omitted herein. With respect to the DEs, given the results of Stage 2, estimators 4, 12, 18, 31, 32, 33 and 34 (Q_n, S_{eql}, τ_s, $s_{t,1}$, $s_{t,2}$, $s_{t,3}$ and $MMLE_s$) were considered. These estimators were paired according to the combinations defined in Table 7.3. After analysing the results of Stage 3 in terms of the AKD^* and the AWD^* performance measures, the best combinations of estimators will be selected according to the following criteria:

- Combinations leading to the lowest average values of the measures AKD^* and AWD^*;
- Combinations leading to the lowest average variability of AKD^* and AWD^* across the selected earthquake intensities;
- Combinations leading to regular results of AKD^* and AWD^* from structure to structure and for both IMs.

Table 7.3. Numbering of the Stage 3 combinations of central value and dispersion estimators.

Number	CVE	DE	Number	CVE	DE
1	$T_{Ham,3}$	$s_{t,1}$	22	T_{log}	$s_{t,1}$
2		$s_{t,2}$	23		$s_{t,2}$
3		$s_{t,3}$	24		$s_{t,3}$
4		Q_n	25		Q_n
5		τ_s	26		τ_s
6		S_{ecf}	27		S_{ecf}
7		$MMLE_s$	28		$MMLE_s$
8	$T_{Hub,3}$	$s_{t,1}$	29	$\overline{x}_{0.08-HQ1}$	$s_{t,1}$
9		$s_{t,2}$	30		$s_{t,2}$
10		$s_{t,3}$	31		$s_{t,3}$
11		Q_n	32		Q_n
12		τ_s	33		τ_s
13		S_{ecf}	34		S_{ecf}
14		$MMLE_s$	35		$MMLE_s$
15	$T_{Tuk,3}$	$s_{t,1}$			
16		$s_{t,2}$			
17		$s_{t,3}$			
18		Q_n			
19		τ_s			
20		S_{ecf}			
21		$MMLE_s$			

The general overview of the Stage 3 results presented in the following addresses their more relevant aspects and focuses on the main conclusions that can be extracted. In the overall, the results obtained for both the AKD^* and AWD^* measures exhibit a relatively regular pattern that is found for all the considered structures and EDPs. To illustrate such findings, Fig. 7.21 presents, for several EDPs and values of *n**, the AKD^* and AWD^* results of the selected combinations of estimators averaged across all the ground motion intensities, for the REG6 structure when PGA is the IM. Figures 7.21a) to d) present results for the negative chord rotation when *n** is forty, the negative curvature when *n** is thirty, the positive chord rotation when *n** is fifteen, and the shear force in original units when *n** is seven, respectively. In all the cases, the corresponding CoVs representing the variability of the AKD^* and AWD^* measures across the earthquake intensities is included also. These results indicate the existence of a pattern composed by a group of seven combinations that repeats itself five times across the selected combinations (although it exhibits some variability in the last repetition). This pattern indicates that, for a given DE, the several CVEs yield similar AKD^* and AWD^* results (except combinations involving estimator $\overline{x}_{0.08-HQ1}$ which was seen, in Chapter 6, to be best suited for smaller sample sizes and thus yields larger differences for *n** values of forty, thirty and fifteen). On the other

hand, when analysing the results of each individual group of seven combinations, a larger variability of the AKD^* and AWD^* measures is observed. Therefore, the influence of the considered CVEs on the AKD^* and AWD^* values is seen to be lower than that of the DEs.

When analysing with more detail the effects of the individual DEs, preliminary observations indicate that combinations involving estimators 12 and 34 (S_{ecf} and $MMLE_s$) exhibit, for most cases, lower values of the AKD^* measure. On the other hand, the results of such combinations in terms of AWD^* are, in many cases, some of the worst, e.g. see Figs. 7.21a) and b). With respect to the values of the CoVs, those of the AKD^* measure corresponding to combinations involving S_{ecf} and $MMLE_s$ are seen to be significantly larger than the remaining ones. To complement this analysis, Fig. 7.22 presents, for several EDPs and values of n^*, the AKD^* and AWD^* results of the selected combinations of estimators averaged across all the earthquake intensities, along with the corresponding CoVs reflecting the variability of the results between these intensities, for the REG10 structure when $S_a(T_1)$ is the IM. Figures 7.22a) to d) present results for the shear force in log units when n^* is forty, the negative chord rotation curvature when n^* is thirty, the positive chord rotation when n^* is fifteen, and the negative curvature when n^* is seven, respectively. These results indicate that combinations involving S_{ecf} and $MMLE_s$ have a distinctive worse performance in terms of the AWD^* measure. Since similar results were found for the remaining structures, combinations involving these DEs were disregarded hereon.

With respect to the remaining combinations, as can be observed from Figs. 7.21 and 7.22, their performance is more regular, both in terms of the average and of the CoV values, and for both the AKD^* and the AWD^* measures. Furthermore, the differences between values of the AKD^* and the AWD^* measures from one combination to another are, in many cases, very small. Given that such type of results was found across all the structures and for both IMs, the analysis of the best combinations of estimators to characterize the probabilistic distribution of the demand of the several EDPs was carried out globally. Such overall analysis indicated that, for all the structures and both IMs, some combinations were systematically found to be among the best four. Such analysis was then extended to obtain the best four combinations for each EDP and sample size, according to the AKD^* and the AWD^* measures separately. The analysis of these results was carried out separately for the deformation-based EDPs and for the shear force. Simultaneously, separate analyses were also performed for the group of results obtained for sample sizes n^* of forty, thirty and fifteen, and for the results obtained for the sample size n^* of seven. Table 7.4 summarizes the results of these analyses by presenting the number of times (in

percentage) that each combination is found on the list of the top four combinations. According to these results, the following aspects were found:

- The selection of the best combinations based on the results of AKD^* is simpler since, for each group of EDPs and sample sizes, there are combinations with significantly better performances than others. With respect to the AWD^* measure, the group of best performing combinations is larger thus making the selection of the best combinations less objective. Still, it should be noted that, for all the EDPs and sample sizes, the largest variation between the AKD^* and the AWD^* values obtained for the best combination and for the combination in the fourth place is always below 6%;

- The results of the AKD^* and the AWD^* measures obtained for the deformation-based EDPs (φ, θ and $\measuredangle$) and for the sample sizes n^* of forty, thirty and fifteen indicate that combinations 5, 12, 19 and 26 have a similar performance that is superior to that of the remaining combinations;

- The results obtained for the deformation-based EDPs (φ, θ and $\measuredangle$) and for the sample size n^* of seven indicate that combinations 10, 24 and 31 have a superior performance in terms of the AKD^* measure. On the other hand, no combination has a distinctive superior performance in terms of the AWD^* measure. In this case, several combinations are found among the top four with percentages between 33% and 48%;

- The results obtained for the shear force and for the sample sizes n^* of forty, thirty and fifteen indicate that combinations 5, 12, 19 and 26 have a superior performance in terms of the AKD^* measure. On the other hand, the results obtained for the AWD^* measure indicate combinations 10 and 24 as performing better. The third and fourth best performances are those of combinations 12 and 26 with values close to 45%;

- The results of the AKD^* and the AWD^* measures obtained for the shear force and for the sample size n^* of seven indicate that combinations 24 and 31 have a similar performance which is superior to that of the remaining combinations. Even though the performance of combinations 29 and 30 in terms of AKD^* also exhibits high values, the results obtained for the AWD^* measure indicate that combinations 24 and 31 are best.

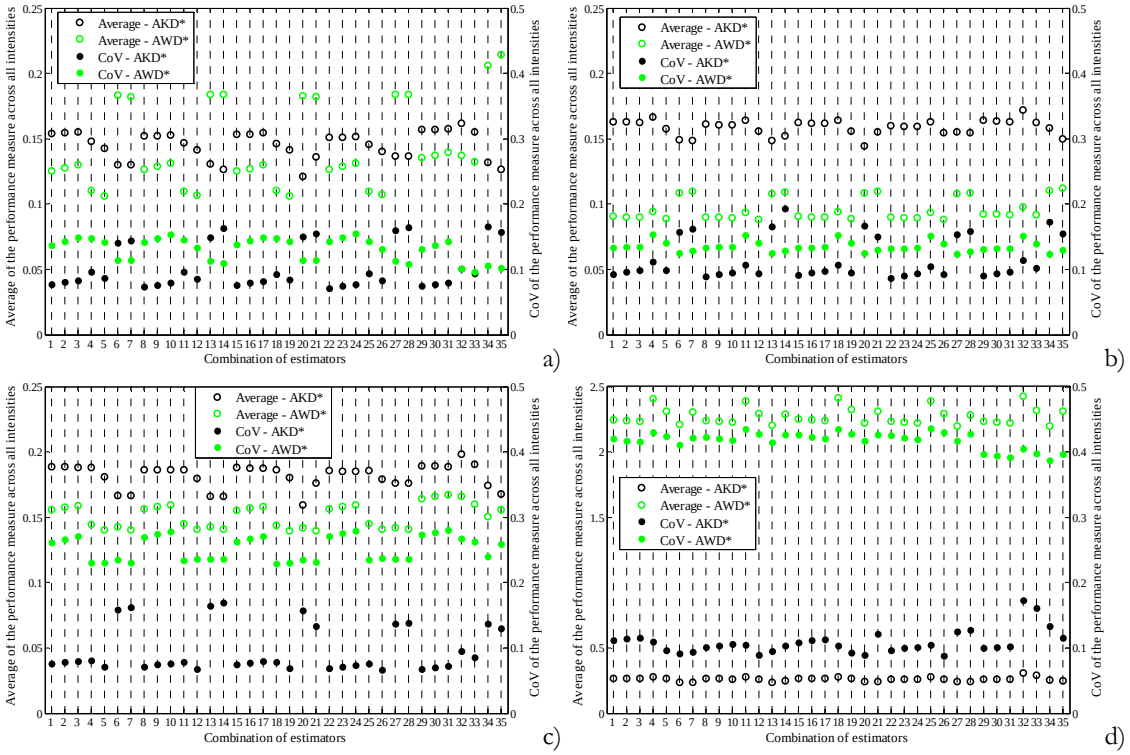

Figure 7.21. AKD* and AWD* results of the estimator combinations averaged across all the intensities along with the CoVs representing the variability between intensities, when PGA is the IM, for the REG6 negative chord rotation when *n** is forty (a), the negative curvature when *n** is thirty (b), the positive chord rotation when *n** is fifteen (c), and the shear force in original units when *n** is seven (d).

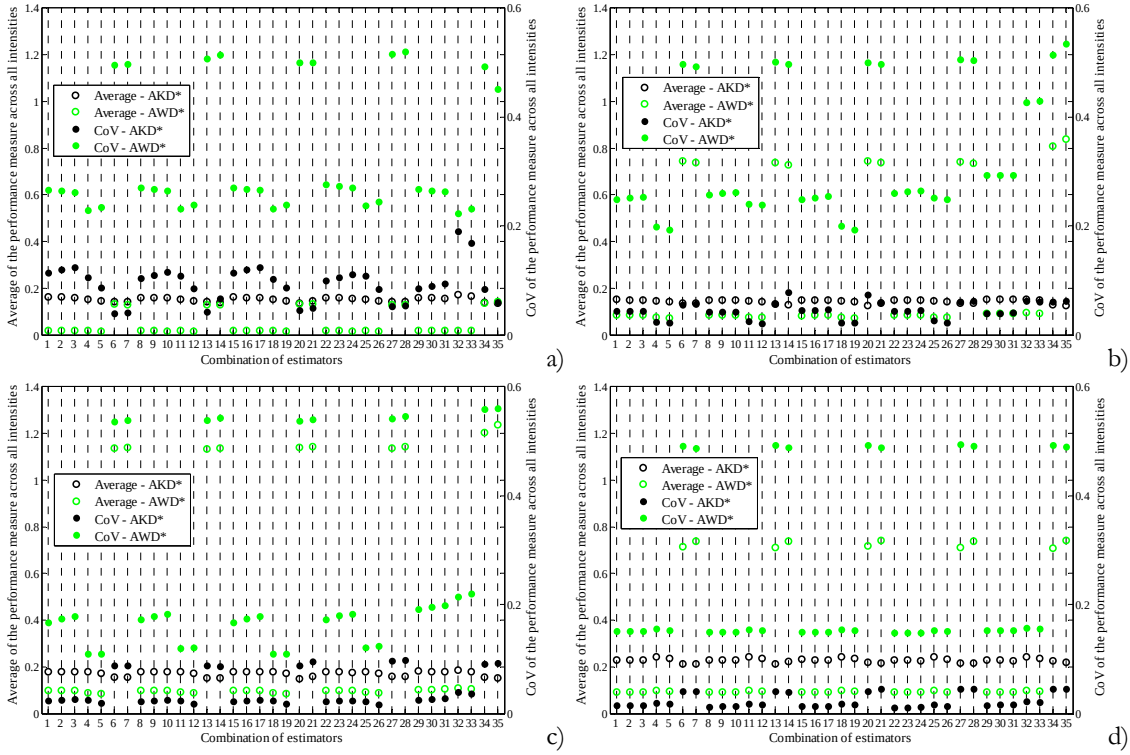

Figure 7.22. AKD* and AWD* results of the estimator combinations averaged across all the intensities along with the CoVs representing the variability between intensities, when $S_a\left(T_1\right)$ is the IM, for the REG10 shear force in log units when *n** is forty (a), the negative chord rotation when *n** is thirty (b), the positive chord rotation when *n** is fifteen (c), and the negative curvature when *n** is seven (d).

Table 7.4. Best four combinations of central value and dispersion estimators for each EDP and sample size.

	φ, θ, $\measuredangle$				V			
	n^* = 40, 30, 15		n^* = 7		n^* = 40, 30, 15		n^* = 7	
Combination	AKD*	AWD*	AKD*	AWD*	AKD*	AWD*	AKD*	AWD*
1	0.0	0.0	0.0	0.0	0.0	0.0	0.0	0.0
2	0.0	0.0	0.0	0.0	0.0	0.0	0.0	0.0
3	0.0	2.4	0.0	0.0	0.0	35.0	0.0	5.0
4	0.8	5.6	0.0	0.0	0.0	0.0	0.0	0.0
5	88.9	88.9	0.0	47.6	96.7	25.0	0.0	0.0
8	0.0	0.0	0.0	0.0	0.0	0.0	0.0	0.0
9	0.0	0.0	9.5	2.4	0.0	10.0	0.0	10.0
10	0.0	5.6	85.7	35.7	0.0	73.3	0.0	55.0
11	1.6	1.6	0.0	0.0	0.0	0.0	0.0	0.0
12	98.4	91.3	0.0	47.6	100.0	46.7	5.0	5.0
15	0.0	0.0	0.0	0.0	0.0	0.0	0.0	0.0
16	0.0	0.0	0.0	0.0	0.0	0.0	0.0	0.0
17	0.0	0.0	0.0	0.0	0.0	18.3	0.0	0.0
18	1.6	9.5	0.0	2.4	0.0	0.0	0.0	0.0
19	97.6	88.1	0.0	47.6	96.7	26.7	0.0	0.0
22	0.0	0.8	4.8	16.7	0.0	1.7	0.0	5.0
23	0.8	6.3	64.3	35.7	0.0	30.0	10.0	40.0
24	9.5	10.3	100.0	47.6	0.0	68.3	95.0	85.0
25	1.6	1.6	0.0	0.0	0.0	0.0	0.0	0.0
26	98.4	88.1	0.0	45.2	96.7	45.0	0.0	5.0
29	0.0	0.0	7.1	11.9	3.3	1.7	90.0	50.0
30	0.0	0.0	42.9	26.2	3.3	5.0	100.0	60.0
31	0.8	0.0	85.7	33.3	3.3	13.3	100.0	80.0
32	0.0	0.0	0.0	0.0	0.0	0.0	0.0	0.0
33	0.0	0.0	0.0	0.0	0.0	0.0	0.0	0.0

Based on the overall analysis of these findings, the use of combinations 12 and 26 is suggested when considering sample sizes n^* of forty, thirty and fifteen. When dealing with smaller sample sizes, the use of combinations 24 and 31 is proposed instead. Furthermore, in terms of the dispersion estimators involved in these combinations, it can be seen that, for sample sizes n^* of forty, thirty and fifteen, both suggested combinations involve the τ_s dispersion estimator, while those suggested for smaller sample sizes involve $s_{I,3}$.

7.6 Conclusions

A study addressing the characterization of the dispersion of structural demand distributions of several EDPs obtained under earthquake loading using different robust estimators was presented. The selected EDPs were the curvature, the chord rotation, the shear force and the inter-storey drift over the height of the structure. Five structures were analysed for suites of fifty ground motions to obtain data samples with a size significant

enough. The chosen records were scaled for several intensities and two different IMs were also considered to evaluate the influence of this parameter. The fundamental objective of the study was to test the use of thirty-three robust estimators using adequate measures of statistical efficiency, in order to identify those best suited for different types of data and sample sizes. Furthermore, this study complements the one presented in Chapter 6 which addresses the characterization of the central value of the same EDPs.

The performance of the estimators was assessed in three stages. In Stage 1, the performance of the thirty-three robust estimators is compared with that of the reference estimator s considering datasets of larger size (between forty-five and fifty). In Stage 2, a subgroup of ten estimators with higher efficiency is considered to assess their performance for datasets of smaller size (forty, thirty, fifteen and seven). Since the results of Stage 2 were not conclusive, a third stage was considered where some of the more efficient CVEs identified in Chapter 6 ($T_{Hub,3}$, $T_{Ham,3}$, $T_{Tuk,3}$, T_{log} and $\overline{x}_{0.08-HQ1}$) are associated with the seven more efficient DEs resulting from Stage 2. The combination of these estimators allows the definition of fitted statistical distributions of the demand that are compared to the empirical distributions using measures of distribution closeness.

The overall analysis of the results of Stage 3 suggests that, for larger sample sizes (e.g. larger than fifteen), combinations involving $T_{Hub,3}$ or T_{log} as the CVE and with τ_s as the DE should be used. For smaller sample sizes (e.g. lower than fifteen), combinations involving $\overline{x}_{0.08-HQ1}$ or T_{log} as the CVE and with $s_{t,3}$ as the DE are suggested instead.

Finally, the results obtained over the three stages indicate there is no significant difference between the efficiency of the estimators due to the influence of the selected IMs. Although this indicates these estimators are fit to be considered under various conditions of the variability of the demand, further IMs should be analysed to confirm this conclusion. Furthermore, it was also observed that, in some cases, when the ratio between the dispersion and the central value is small (a situation which was found to occur when the EDP is the shear force), the estimators may yield less accurate results.

Chapter 8
Analytical evaluation of structural component limit state probabilities

8.1 Introduction

In the field of seismic risk assessment of structures, existing work on evaluation of component (member/section) seismic limit state probabilities focuses essentially on the fragility curve approach. A fragility value yields the probability of occurrence the limit state conditional on a value of the intensity measure (IM) of the input ground motion. A fragility curve is therefore defined as a relationship between the ground motion intensity and the probability of reaching or exceeding a certain response level, irrespective of the probability of occurrence of the corresponding ground motion intensities. A number of methods have been proposed to obtain fragility curves, ranging from expert judgment (ATC, 1985), to the analysis of data on observed damages (Singhal and Kiremidjian, 1998; Shinozuka *et al.*, 2000), to fully numerical approaches, as, for example, those proposed in (Cornell *et al.*, 2002; Au and Beck, 2003; Lupoi *et al.,* 2003; Schotanus *et al.*, 2004). General reviews on this matter can be found, for example, in (Der Kiureghian, 1996; Pinto, 2001; Pinto *et al.*, 2004).

A feature common to most of the numerical approaches is the use of a number of simulations consisting of analyses of a given structural model under increasing earthquake loads. Within this context, a common methodology involves the use of the previously referred multi-stripe analysis approach (Jalayer and Cornell, 2009). In this approach, a number of earthquake records are scaled to several target earthquake intensities and response simulations are carried out for each level. For each level, structural damage/response maxima obtained from the simulations are then used to fit a statistical distribution, often lognormal (see Chapter 5). Convolution of the demand distribution with that of the limit state capacity, for each level, then yields the fragility curve values. The difference among the various numerical methods lies essentially in their balance between cost and accuracy, i.e. in their ability to account economically for all the aspects entering

the reliability problem. Therefore, the choice of a method should be made considering the trade-off between computational effort and precision.

Although the fragility curve approach yields important structure-specific results, it is known that the fragility curve alone is not sufficient for practical use on cost/effectiveness decision-making processes if information about the earthquake hazard, the complementary cumulative distribution function (CCDF) of the ground motion intensity, is not included. One may see that if a fragility value indicates a limit state exceedance probability of 50%, this result carries no information regarding both the probability of occurrence of the considered ground motions and the period of time under consideration. The inverse is also truth, as noted by Hadjian (2002): designing to a specific annual exceedance probability of the ground motion does not provide direct information about the fragility value. In the fragility analysis approach, computation of the unconditional probability that, at a given site and in a given period of time, the structure fails to perform satisfactorily or reaches a given limit state, needs the uncertainty in the seismic intensity to be reintroduced by means of the hazard function. By convolving the hazard derivative with the fragility curve, one obtains what is usually called seismic risk, (e.g. see Pinto, 2001; Hadjian, 2002; Pinto *et al*, 2004).

In order to obtain the component seismic limit state unconditional probability of occurrence or risk by alternative approaches, the current chapter presents several methods that do not require the fragility curve to be determined. The proposed procedures use a strategy similar to the one presented by Cornell *et al.* (2002) known as the SAC/FEMA method. However, the present work extends that approach by introducing different functional forms to represent the earthquake hazard and by addressing the issue of force-based engineering demand parameter (EDP) limit state probabilities. These procedures are established using two different strategies that involve different levels of analytical tractability and comprehensiveness, which are termed Methodology 1 and Methodology 2. Methodology 1 proposes six approaches considering different earthquake hazard functions and EDPs. On the other hand, Methodology 2 proposes two approaches and discusses several issues related to the development of a third one.

Over the past years, there have been several studies addressing the applicability of the SAC/FEMA method and/or reporting its weaknesses (e.g. see Lupoi *et al.*, 2002; Lupoi *et al.*, 2003; Pinto *et al.*, 2004, Aslani and Miranda, 2005; Mackie and Stojadinovic, 2007; Kwon and Elnashai, 2007; Zareian and Krawinkler, 2007; Bradley and Dhakal, 2008; Skokan and Hart, 2008). The linear form in the log-log space of the earthquake hazard that is assumed by the SAC/FEMA method is known to be one of its main sources of error (e.g. see Aslani and Miranda, 2005; Bradley and Dhakal, 2008). Another reported source of error of the method is the fact that it assumes the variability of the demand to be constant for increasing levels of the selected IM (Pinto *et al.*, 2004; Aslani and Miranda, 2005). Furthermore, the application of the SAC/FEMA method to force-based EDPs has also been reported to yield inadequate results (Pinto *et al.*, 2004). Hence, alternative procedures are proposed herein that address some of these issues.

8.2 Brief review of the SAC/FEMA method

Since the proposed methodologies are based on the SAC/FEMA method, a brief review of its analytical definition is presented in the following for completeness. The SAC/FEMA method provides the basis for the FEMA-350 (2000) guidelines for seismic design and assessment of steel moment-resisting frames. In this method, the IM considered to define the earthquake hazard is the spectral acceleration $S_a(T)$ for a period T close to the fundamental period of the structure T_1. The method also considers that a limit state is attained when the maximum demand D over the duration of the ground motion exceeds the corresponding capacity C, assuming also that D and C are lognormally distributed random variables. Originally, the EDP considered by the method to represent D and C was the maximum inter-storey drift over the height of the structure. However, D and C may refer to any other scalar deformation-based or force-based EDP. The main limitation of the method remains to be that it only addresses limit states defined by a single EDP.

In general terms, the SAC/FEMA method provides a closed form expression for the risk λ written according to the following classical reliability formulation (e.g. see Ditlevsen and Madsen, 1996):

$$\lambda = \int_{-\infty}^{+\infty} \left[1 - F_D(\alpha)\right] \cdot f_C(\alpha) d\alpha \tag{8.1}$$

where $F_D(\cdot)$ represents the cumulative distribution function (CDF) of the maxima of D, and $f_C(\cdot)$ is the probability density function (PDF) of C. The method begins by defining the best estimate of the earthquake hazard $H(.)$ for a selected reference period t_{ref} as

$$H(s) = \Pr\left(S_a \geq s \middle| t_{ref}\right) = k_0 s^{-k_1} \tag{8.2}$$

in which k_0 and k_1 are constants fitted to the ground motion hazard data, and $S_a(T)$ is simply termed S_a. In order to obtain adequate values of k_0 and k_1, it is recommended to perform the hazard fitting in the region of the S_a values whose probability of exceedance is close to the value of λ that will be estimated by the SAC/FEMA method (which might require a first "blind" application of the method only to obtain its order of magnitude). To obtain the demand hazard from the earthquake hazard defined by Eq. (8.2), it is assumed that the evolution of the median value $\hat{D}$ of D can be expressed as a function of S_a by:

$$\hat{D} = a \cdot s^b \tag{8.3}$$

where a and b are to be determined from demand distributions obtained from a number of nonlinear dynamic analyses of the structure. These distributions also provide an estimate of the dispersion β_D, i.e. the standard deviation of the natural logarithm of D, for the range of s values considered in the analyses. Therefore, D can be defined as:

$$D = \left(a \cdot s^{b}\right)\varepsilon \tag{8.4}$$

where ε is a lognormal random variable with unit median and dispersion equal to β_D. By inverting Eq. (8.4) to give

$$s = \left(\frac{D}{a\varepsilon}\right)^{\frac{1}{b}} \tag{8.5}$$

and combining it with Eq. (8.2), one obtains the demand hazard $\Pr\left(D > d\right) = 1 - F_D\left(d\right)$ by first conditioning it to the random variable ε as follows:

$$\Pr\left(D > d\right) = \int_0^\infty \Pr\left(D > d \middle| \varepsilon\right) f_\varepsilon\left(\varepsilon\right) d\varepsilon = \int_0^\infty \Pr\left[S_a > \left(\frac{d}{a\varepsilon}\right)^{\frac{1}{b}}\right] f_\varepsilon\left(\varepsilon\right) d\varepsilon \tag{8.6}$$

The solution of Eq. (8.6), which can be found analytically (e.g. see Jalayer and Cornell (2000) for details), is then

$$\Pr\left(D > d\right) = k_0 \left(\frac{d}{a}\right)^{-\frac{k_1}{b}} e^{\frac{1}{2}\frac{k_1^2}{b^2}\beta_D^2} \tag{8.7}$$

The final step of the method involves the probabilistic definition of the capacity C and then solving Eq. (8.1). The capacity C is assumed to be independent from D and to follow a lognormal distribution with median $\hat{C}$ and dispersion β_C. By considering Eq. (8.7), Eq. (8.1) becomes

$$\lambda = \int_0^\infty k_0 \left(\frac{\alpha}{a}\right)^{-\frac{k_1}{b}} e^{\frac{1}{2}\frac{k_1^2}{b^2}\beta_D^2} f_C\left(\alpha\right) d\alpha \tag{8.8}$$

where $f_C(\cdot)$ is the lognormal PDF of C. Integration of the previous expression gives

$$\lambda = k_0 \left(\frac{\hat{C}}{a}\right)^{-\frac{k_1}{b}} e^{\frac{1}{2}\frac{k_1^2}{b^2}\left(\beta_D^2 + \beta_C^2\right)} = H\left[S_a\left(\hat{C}\right)\right] e^{\frac{1}{2}\frac{k_1^2}{b^2}\left(\beta_D^2 + \beta_C^2\right)} \tag{8.9}$$

The solution found for λ can be read as saying that the limit state unconditional probability of occurrence, or risk, is given by the product of the probability that the spectral acceleration exceeds the value necessary to produce a demand D equal to the median capacity $\hat{C}$, as if the *s-d* relationship was deterministic, times a factor containing the dispersions β_D and β_C.

It is noted that the SAC/FEMA method includes some additional steps. Since the variability assigned to D and C by dispersions β_D and β_C reflect only a portion of their total uncertainty, their epistemic uncertainty remains to be accounted for. The incomplete

knowledge of D and C may arise from the simplifications of the selected mechanical models, and/or from the limited statistical basis used to evaluate D and C. Furthermore, it is also customary to account for the uncertainty in the earthquake hazard definition, which can then be translated into an additional random variable representing the variability of the best estimate defined by Eq. (8.2). Since the development of Eq. (8.9) establishes sufficient context for presenting the proposed risk assessment methodologies, the steps considering these additional sources of uncertainty are omitted herein for the sake of brevity. Nonetheless, details can be found in Jalayer and Cornell (2000) and Pinto *et al.* (2004).

Finally, as a side note, it is also referred that the earthquake hazard function defined by Eq. (8.2) has the form of the Pareto distribution (Johnson *et al.*, 1994) given by

$$\Pr\left(X \geq x\right) = \begin{cases} \left(x/x_{\min}\right)^{-\alpha} & x \geq x_{\min} \\ 1 & x < x_{\min} \end{cases} \tag{8.10}$$

As can be seen, Eq. (8.2) does not account for the lower limit $x_{\min}$ of the support since usual fitting results of k_0 and k_1 lead to values of $x_{\min} = k_0^{1/k_1}$ that are very close to zero. However, when establishing the demand hazard defined by Eq. (8.7), which also takes the form of a Pareto distribution, the value of $x_{\min}$ is now given by

$$x_{\min} = a\left(k_0 \cdot e^{\frac{1}{2}\frac{k_1^2}{b^2}\beta_D^2} \right)^{b/k_1} \tag{8.11}$$

Depending on the selected EDP, the parameters entering this new $x_{\min}$ expression can lead to a value of the lower limit of the support that is much higher than zero (e.g. see some of the examples presented in Pinto *et al.* (2004)). Therefore, if $x_{\min}$ is not accounted for, unrealistic values (i.e. much higher than one) of the demand hazard will be considered when solving Eq. (8.8). In this situation, Eq. (8.8) leads to unrealistic values of λ, which can also be higher than one in some cases.

8.3 Proposed procedures

The next Sections present two approaches to obtain the component seismic limit state unconditional probability of occurrence or risk. As previously referred, the procedures follow a strategy similar to that of the SAC/FEMA method, but extend that approach to overcome some of its limitations. The procedures are proposed for the risk analysis at the structural section level but they can also be applied to other cases where the occurrence of the limit state can be defined by a single EDP. Furthermore, the presentation of the procedures is made assuming that sufficient earthquake hazard data is available to establish the hazard function for the chosen IM and for the selected reference period.

8.3.1 Methodology 1

Methodology 1 begins by fitting a probabilistic CCDF to the available earthquake hazard data to obtain the earthquake hazard function $H(.)$. This adjustment is performed assuming the functional dependency between the ground motion IM and the hazard data follows an Extreme-type distribution, namely a Fréchet or a Weibull distribution (whichever fits best). These distributions have their cumulative distribution function and corresponding CCDF defined by Eqs. (8.12) and (8.13), respectively, (Castillo, 1988):

$$F_{Fréchet}(x) = e^{-\left(\frac{x}{\alpha}\right)^{-\gamma}} \rightarrow H_{Fréchet}(x) = 1 - e^{-\left(\frac{x}{\alpha}\right)^{-\gamma}} \tag{8.12}$$

$$F_{Weibull}(x) = 1 - e^{-\left(\frac{x}{\delta}\right)^{\beta}} \rightarrow H_{Weibull}(x) = e^{-\left(\frac{x}{\delta}\right)^{\beta}} \tag{8.13}$$

where α, γ, δ and β are the parameters of the distribution functions. Equations (8.12) and (8.13) are better suited for seismic hazard representation than the approximated power law, Eq. (8.2), proposed by Kennedy and Short (1994) and used by Cornell *et al.* (2002), since they actually represent probabilistic CCDFs, thus valid throughout the entire IM domain.

The following step corresponds to the numerical simulation part of the procedure. After selecting an appropriate accelerogram from an existing ground motion database or artificially generating one, nonlinear dynamic analyses are performed to determine the structure's peak response to increasing scaled intensities of that accelerogram. The EDPs for which the limit state probabilities are required must be recorded for each intensity.

The third step of the procedure is the fitting of a mathematical expression to the evolution of the chosen EDP for increasing values of the ground motion IM, the so-called Incremental Dynamic Analysis (IDA) curve (Vamvatsikos and Cornell, 2002). The form of the functional dependency between the ground motion IM and the chosen EDP fitting the IDA data must be carefully chosen and will depend on the EDP type (deformation-based or force-based). In addition, in order to maintain mathematical tractability, this expression must be an increasing, continuous and invertible function. In light of some of the results presented by Vamvatsikos and Cornell (2002), e.g. regarding the more extreme *weaving* and *resurrection* behaviour of the IDA curves, the monotonicity condition may seem difficult to comply with. However, such extreme phenomena were not found for the reinforced concrete (RC) structures and the class of EDPs studied herein. For deformation-based EDPs, the chosen functional form is the power function defined by Eq. (8.14), also considered in the SAC/FEMA method, Eq. (8.3), which was seen to perform adequately. In Eq. (8.14) *D* represents the EDP while *a* and *b* are the functions' parameters to be fitted from numerical data.

$$D(x) = a \cdot x^{b} \Rightarrow \text{power function} \tag{8.14}$$

In terms of force-based EDPs, namely for the shear force demand which is of main interest herein, its variation for increasing values of the chosen ground motion IM appears to be functionally different than that of deformation-based EDPs. After exhibiting larger variations for low values of the ground motion IM, the member shear force tends to a limiting top value due to the reduced post-yield stiffness of the member, as mentioned in previous chapters. Depending on the member flexural strength and stiffness, the limiting value may be attained for lower or higher ground motion IM values. These different types of shear force demand evolutions cannot be neglected when defining a suitable form of the functional dependency between the ground motion IM and shear force.

An extensive study was carried out to find the most adequate functional form for the shear force demand evolution with increasing values of the ground motion IM. Several fitting examples were performed considering the functional form defined by Eq. (8.14) and those defined by Eqs. (8.15), (8.16), (8.17) and (8.18). Equation (8.15) involves a logarithmic function, Eq. (8.16) involves an inverted exponential function, Eq. (8.17) involves a double exponential function and Eq. (8.18) is the functional form proposed by Aslani (2005) denoted herein as the "Aslani proposal". In Eqs. (8.15), (8.16), (8.17) and (8.18) D represents the EDP and a, b, c and d are parameters to be fitted from numerical data. With respect to the value of parameter k in Eq. (8.16), its value was found to be 1.0, 1.5 or 2.0, depending on the performance of the fit. The influence of this parameter on the form of Eq. (8.16) while the other parameters remain constant can be seen in Fig. 8.1.

$$D(x) = a \cdot \ln(x) + b \Rightarrow \text{ logarithmic function} \tag{8.15}$$

$$D(x) = a \cdot e^{(-k \cdot x)} + b \Rightarrow \text{ inverted exponential function} \tag{8.16}$$

$$D(x) = a \cdot e^{(b \cdot x)} + c \cdot e^{(d \cdot x)} \Rightarrow \text{ double exponential function} \tag{8.17}$$

$$D(x) = a \cdot b^{x} \cdot x^{c} \Rightarrow \text{ Aslani proposal} \tag{8.18}$$

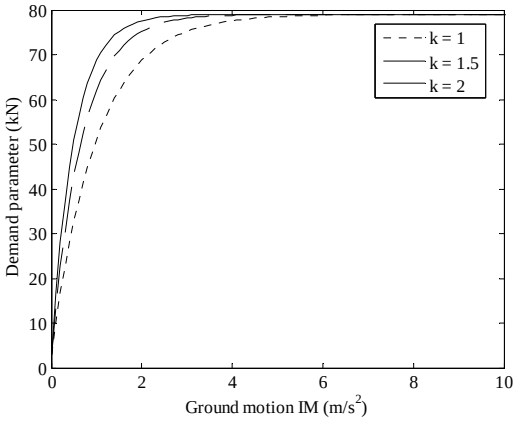

Figure 8.1. Influence of parameter k in Eq. (8.16).

To see how these functions perform, Fig. 8.2 presents two fitting examples of real data samples. Figures 8.2a), b) and c) present the results of the shear force demand of a column for a given ground motion of increasing intensity and corresponding fitting using Eqs. (8.14) to (8.18). The selected ground motion IM was the 5% damped spectral acceleration at the fundamental period of the structure, $S_a\left(T_1\right)$. Figure 8.2a) presents the fit over the full range of the available data while Fig. 8.2b) presents a partial view focussing on the fitting results over the lower range of the ground motion IM and Fig. 8.2c) presents the behaviour of the functions when extrapolating outside the fitting domain. Figures 8.2d), e) and f) present the results of shear force demand of a beam for the same conditions and corresponding fitting using Eqs. (8.14) to (8.18). Figure 8.2d) presents the fit over the full range of the available data while Fig. 8.2e) presents a partial view focussing on the fitting results over the lower range of the ground motion IM and Fig. 8.2f) presents the behaviour of the functions when extrapolating outside the fitting domain. In the case of Eq. (8.16), parameter k was considered with a value of 1.5. The fitting of these expressions was carried using either the Trust-Region or the Levenberg-Marquardt nonlinear curve fitting algorithms available in Matlab (Matlab, 2008) and considering a number of data points larger than strictly required to obtain the values of the parameters.

Global analysis of Fig. 8.2a) indicates the considered expressions yield an overall good fit. However, the closer view provided by Fig. 8.2b) indicates the Aslani proposal and the logarithmic function are closer to the data in the range of the lower ground motion IMs. When analysing the performance of the different functions outside the fitting range, Fig. 8.2c), three distinct behaviours can be observed: functions may continue to increase at different rates, Eqs. (8.14), (8.15) and (8.17); functions may start to decrease after a certain IM level, Eq. (8.18); functions may start to stabilize after a certain IM level, Eq. (8.17). With respect to the second fitting example, global analysis of Fig. 8.2d) shows it is more difficult to fit the proposed functional forms to the available data of this second example. In the overall, only the inverted exponential function appears to yield an adequate fit, namely by analysing the performance of the fits over the lower range of IMs, Fig. 8.2e), as well as outside the fitting range, Fig. 8.2f). Based on these examples, it can be seen that finding adequate expressions to suitably fit shear force demand data is not an easy task, especially in situations similar to those of the beam example. In addition, as previously stated, the chosen expression must be an increasing and invertible function, in order to maintain the mathematical tractability of the proposed procedure. To comply with these requirements, both the Aslani proposal and the double exponential function, Eqs. (8.17) and (8.18), respectively, must be rejected. As can be seen in Figs. 8.2e) and f), the Aslani proposal is not an increasing function throughout the IM domain. In the case of the double exponential function, although it may yield good fits in some situations, it cannot be considered within the proposed procedure since it is not an invertible function. Of the remaining functional forms, and considering the type of shear force demand evolutions

that were presented in Fig. 8.2, Eqs. (8.15) and (8.16) were selected as those being more adequate. Nonetheless, the choice between one or the other should be decided on a case-by-case situation upon observation of the shape of the IDA curve. Moreover, the presented demand evolution examples are considerably influenced by the nonlinear flexural behaviour of the sections under study. In a case where a more linear behaviour is observed, another functional form, e.g. Eq. (8.14), could provide a better fit.

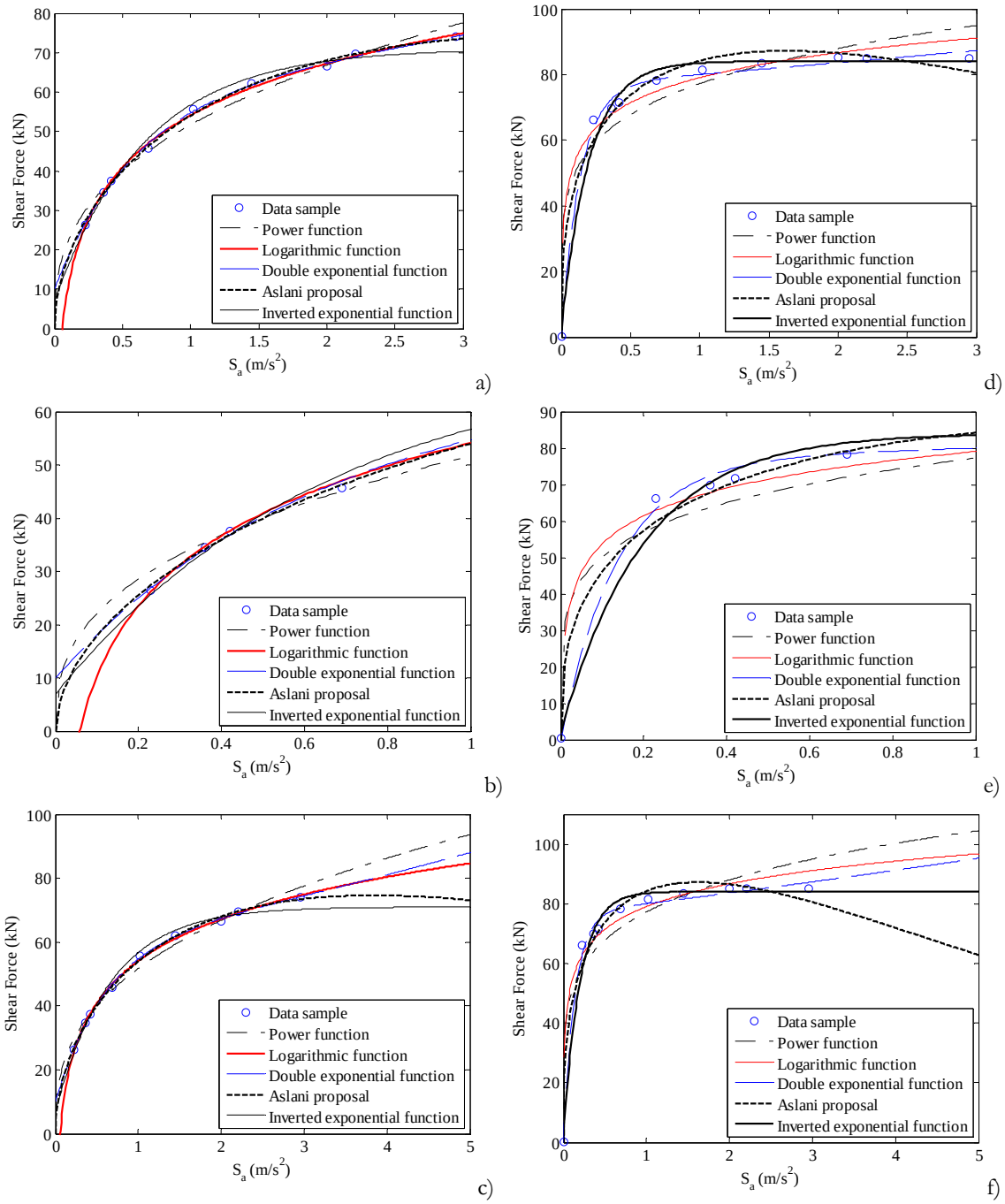

Figure 8.2. Fitting example for shear force demand of a column section (a), (b) and (c), and of a beam section (d), (e) and (f).

The next step of the proposed procedure addresses the definition of the unconditional probabilistic distribution of the demand *D*, namely in terms of its CCDF $H(D)$. For this purpose, it is necessary to introduce the analytical relations between *D* and $H(D)$. To derive such relations, it is necessary to invert Eqs. (8.14), (8.15) and (8.16) and substitute these new relations back into Eqs. (8.12) and (8.13). This way, the probabilistic distribution of the ground motion hazard is analytically transformed into the curve giving the probability of exceedance of the chosen EDP. Therefore, if the earthquake hazard function is fitted using Eq. (8.12), one obtains Eqs. (8.19), (8.20) and (8.21) if the demand *D* is defined by Eqs. (8.14), (8.15) and (8.16), respectively. It can be seen that for Eq. (8.19) *D* has the CCDF of a Fréchet distribution, for Eq. (8.20) *D* has the CCDF of a Gumbel distribution for maxima (Castillo, 1988) and for Eq. (8.21) the auxiliary variable χ has the CCDF of a Fréchet distribution.

$$H(D) = 1 - e^{-\left(\frac{D}{k_1}\right)^{-k_2}} \;;\; k_1 = a \cdot \alpha^b;\; k_2 = \gamma / b \tag{8.19}$$

$$H(D) = 1 - e^{-e^{-\left(\frac{D-k_1}{k_2}\right)}} \;;\; k_1 = b + a \cdot \ln(\alpha);\; k_2 = a/\gamma \tag{8.20}$$

$$H(\chi) = 1 - e^{-\left(\frac{\chi}{k_1}\right)^{-\gamma}} \;;\; \chi = \ln\left(\frac{a}{D-b}\right);\; k_1 = k \cdot \alpha \tag{8.21}$$

In case the earthquake hazard function is fitted using Eq. (8.13), one obtains Eqs. (8.22), (8.23) and (8.24) if the demand *D* is defined by Eqs. (8.14), (8.15) and (8.16), respectively. It can be seen that for Eq. (8.22) *D* has the CCDF of a Weibull distribution, for Eq. (8.23) *D* has the CCDF of a Gumbel distribution for minima (Castillo, 1988) and for Eq. (8.24) the auxiliary variable χ has the CCDF of a Weibull distribution.

$$H(D) = e^{-\left(\frac{D}{k_1}\right)^{k_2}} \;;\; k_1 = a \cdot \delta^b;\; k_2 = \beta / b \tag{8.22}$$

$$H(D) = e^{-e^{\left(\frac{D-k_1}{k_2}\right)}} \;;\; k_1 = b + a \cdot \ln(\delta);\; k_2 = a/\beta \tag{8.23}$$

$$H(\chi) = e^{-\left(\frac{\chi}{k_1}\right)^{\beta}} \;;\; \chi = \ln\left(\frac{a}{D-b}\right);\; k_1 = k \cdot \delta \tag{8.24}$$

Following this, it is necessary to define the capacity value *C* corresponding to the selected EDP for the chosen limit state in order to obtain the limit state exceedance probability by substituting *D* by *C* in the corresponding demand CCDF, Eqs. (8.19) to (8.24). Due to the particular form of Eq. (8.16), it should be noted that Eqs. (8.21) and (8.24) may yield limit state exceedance probabilities with a value of zero. Since the

evolution of Eq. (8.16) has an upper bound (e.g. see Fig. 8.1), if the selected value of C is higher than that upper limit, the corresponding limit state probability is zero.

In the overall, the proposed procedure can be briefly outlined as follows:

- Fitting of the hazard data for the site under consideration to one of the functions defined by Eqs. (8.12) and (8.13) to obtain $H(x)$;
- Running of nonlinear dynamic analyses using an appropriate ground motion to determine the maxima of the selected EDP for increasing intensities of that ground motion;
- Fitting of the recorded EDP evolution data using Eqs. (8.14), (8.15) or (8.16) for the EDP type under analysis to obtain $D(x)$;
- Depending on the considered function for the seismic hazard and on the type of functional curve considered for the EDP, substitute the fitted parameters into the corresponding limit state CCDF $H(D)$, Eqs. (8.19) to (8.24);
- Determine the EDP capacity C for the chosen limit state and substitute D by C in $H(D)$ to obtain the limit state exceedance probability.

By analysing the proposed procedure, using Eqs. (8.19) to (8.24) can be seen to only require knowledge regarding two parameters resulting from the ground motion hazard fit and two parameters resulting from the EDP evolution fit (or three considering that parameter k in Eq. (8.16) is not exactly known). Consequently, Eqs. (8.19) to (8.24) may be used to assess the probability of exceedance of any desired limit state, considering any EDP and ground motion IM, without the need to determine the fragility curve.

Since there are several important sources of uncertainty in the seismic risk assessment problem (Jalayer and Cornell, 2000; Pinto *et al.*, 2004), some strategies are presented in the following to address such issues within the proposed methodology. In order to account for the effect of record-to-record variability in the selected EDP and thus in the limit state probability, one must repeat the previously outlined steps for a set of several ground motions. In addition, non-deterministic values of material properties and/or of geometrical data of the structural elements may also be considered in these analyses using pre-defined statistical distributions of these variables. This means that, for each ground motion, one should repeat the proposed procedure for different material and/or geometrical properties sampled from their respective distributions. Representing the randomness of these mechanical parameters is, therefore, feasible at the cost of additional sets of analyses, each one performed for a given set of values of mechanical properties. However, alternative approaches can be pursued to account for randomness in the mechanical parameters by using the proposal suggested by Lupoi *et al.* (2003) or by using response-sensitivities, i.e. the first-order partial derivatives of the response with respect to

the random mechanical parameters. To obtain response-sensitivities, several methods can be followed, such as the direct differentiation method or the finite difference scheme, i.e. repeating the analysis for perturbed values of the parameters. Extensive presentation of these methods is beyond the scope of the present work. The reader is referred, for example, to Haukaas (2003) and Franchin (2004) for further details on the application of these procedures. Randomness of the limit state capacity C is another source of uncertainty that may also be considered. Assuming that capacity C and demand D are independent variables, a commonly considered assumption though sometimes approximate (Pinto *et al.*, 2004), non-deterministic values of the mechanical parameters can be sampled from their respective distributions to obtain random samples of the capacity C. Then, one can assess the limit state exceedance probability for each value of C without having to run additional structural analyses.

Whether all or only part of the sources of variability and uncertainty are considered, one issue still remains to be addressed since one ends up with several values of the selected limit state probability. Since the individual values of the limit state probability represent probabilities conditioned to a particular sample, the conditioning can be eliminated by integrating the product of the conditional probability by the probability of the conditioning sample. For discrete terms, as in the present case, if it can be assumed that all samples have the same probability of occurrence, the integral can be approximated by the average of the individual probabilities. On the other hand, if different samples have different probabilities of occurrence, a weighted average of the individual probabilities can represent the integral instead.

When comparing the proposed approach to the SAC/FEMA method, the following aspects should be highlighted:

- The proposed method uses seismic hazard expressions which are actual CCDFs, instead of approximated functions that are not valid throughout the full IM domain and require careful fitting within the IM range of interest (Pinto *et al.*, 2004);
- The proposed method addresses both deformation-based and force-based EDPs by using different demand evolution functions depending on the EDP type;
- Since the limit state exceedance probability equations are defined for each ground motion, the proposed method includes the full dispersion of the demand, namely the variation of the dispersion as a function of the IM level, instead of considering it constant as in the SAC/FEMA method. Still, it should be noted that the constant dispersion factor considered by this latter method also accounts for the fitting error of the chosen functional form between the ground motion IM and the EDP, e.g. see Giovenale *et al.*, (2004). This aspect is not considered in the proposed approach since the referred relation is treated as deterministic for each ground motion;

8.3.1.1 Discussion of the probabilistic consistency and computational efficiency of the procedure

The probabilistic consistency of the proposed approach for the calculation of the limit state exceedance probability for a structural component, for a given ground motion record and considering that the limit state capacity C is a constant, will be demonstrated by performing the integration of the fragility curve with the seismic hazard function to show that both approaches lead to the same result.

Consider that $p_f(x) = \Pr(D \geq C | IM = x)$ is the fragility curve of the component. Since only one ground motion is considered and the limit state capacity is a constant, the fragility curve is

$$p_f(x) = \begin{cases} 0 \ ; \ x < IM* \\ 1 \ ; \ x \geq IM* \end{cases} \tag{8.25}$$

where $IM*$ represents the IM level for which the demand D equals the capacity C. The component limit state exceedance probability λ is obtained by (e.g. see Pinto *et al.* (2004))

$$\lambda = \int_0^\infty p_f(x)\, h(x)\, dx \tag{8.26}$$

where $h(x)$ is

$$h(x) = -\frac{dH(x)}{dx} = \left|\frac{dH(x)}{dx}\right| \tag{8.27}$$

Considering Eq. (8.25), Eq. (8.26) can then be developed into

$$\lambda = \int_0^{IM*} p_f(x)\, h(x)\, dx + \int_{IM*}^\infty p_f(x)\, h(x)\, dx = \int_{IM*}^\infty h(x)\, dx \tag{8.28}$$

which, by using Eq. (8.27), yields

$$\lambda = -\left[H(x)\right]_{IM*}^\infty = H(x = IM*) \tag{8.29}$$

Assuming that the ground motion record IDA curve is $D = f(x)$, inverting this relation and considering that $x = IM*$ implies $D = C$ gives

$$IM* = f^{-1}(C) \tag{8.30}$$

that when substituted back into Eq. (8.29) yields expressions similar to Eqs. (8.19) to (8.24).

Regarding computational efficiency, and comparing the proposed approach with the general method that is based on the integration of the fragility curve with the hazard function, Eq. (8.26), the current methodology reduces the number of ground motion IM levels for which samples of the structural response are needed. As previously referred,

Eqs. (8.19) to (8.24) only require knowledge regarding two parameters that depend on samples of the structural response. For practical purposes, it is recommended that these parameters are estimated at three levels. Two of these levels should correspond to a lower limit and upper limit of the range of interest and the third one to approximately the average of the other two levels. Quantitative confirmation of this suggestion will be shown in the application example presented in the following.

8.3.1.2 Application example

To illustrate the applicability of the proposed approach, the probability of occurrence of several limit states is determined for two structural sections of the six-storey RC frame previously referred as IRREG6. The chosen sections, termed section 1 and section 2, are the beam and column sections represented in Fig. 8.3. The application example is based on the structural analysis results presented in the previous chapters for this structure. Therefore, details about the modelling and analyses procedures, the quantification of the demand parameters, and the suite of fifty ground motions representing the seismic demand are omitted herein.

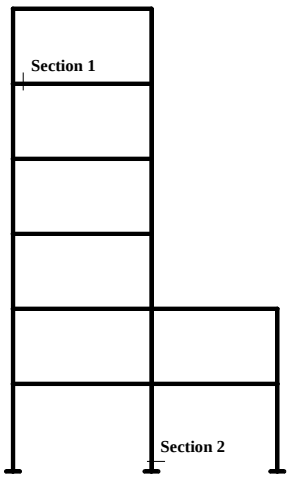

Figure 8.3. Selected sections of the IRREG6 structure for the application example.

8.3.1.2.1 Limit states, capacity models and probabilistic modelling

The considered limit states were defined using the proposals of Part 3 of the Eurocode 8 (EC8-3) (EC8-3, 2005). Therefore, the selected limit states are the Near Collapse (NC) limit state, the Significant Damage (SD) limit state and the limit state of Damage Limitation (DL). In terms of ductile mechanisms, the probabilistic assessment of these limit states was carried out for the deformation capacity of the structural members defined by the chord rotation θ. As referred in Chapter 2, the chord rotation capacity of the DL limit state is defined by the chord rotation at yielding θ_{DL} (EC8-3, 2005) given by:

$$\theta_{DL} = \phi_y \cdot \frac{L_s}{3} + 0.0013 \cdot \left(1 + 1.5\frac{h}{L_s}\right) + 0.13 \cdot \phi_y \cdot \frac{d_b \cdot f_y}{\sqrt{f_c}} \tag{8.31}$$

where ϕ_y is the yield curvature of the section, L_s is the shear span taken constant and equal to half of the member length, h is the section depth, d_b is the mean diameter of the tension reinforcement, f_y is the estimated steel yield strength and f_c is the estimated value of the concrete compressive strength. For the quantification of the NC chord rotation capacity θ_{NC}, the following semi-empirical expression (EC8-3, 2005) is considered herein:

$$\theta_{NC} = \frac{1}{\gamma_{el}}\left[\theta_{DL} + \left(\phi_u - \phi_y\right) \cdot L_{pl} \cdot \left(1 - \frac{L_{pl}}{2L_s}\right)\right] \tag{8.32}$$

where γ_{el} is 1.5 for primary members, ϕ_u is the ultimate curvature of the member end section and L_{pl} is the plastic hinge length. The definition of ϕ_u and of L_{pl} depends on the selected confined concrete model (EC8-3, 2005). For the limit state of SD, the chord rotation capacity θ_{SD} is defined as 3/4 of θ_{NC} (EC8-3, 2005). According to EC8-3, factor γ_{el} accounts for the variability of the capacity by transforming mean capacity values into mean-minus-one-standard-deviation ones. However, γ_{el} is considered equal to one in the present application since the variability of the capacity values will also be simulated.

With respect to brittle mechanisms, the probabilistic assessment was carried out in terms of shear force capacity. For this type of mechanism, EC8-3 (EC8-3, 2005) only defines the limit state of NC. The shear force capacity V_{NC} for this limit state is defined by:

$$V_{NC} = \frac{1}{\gamma_{el}}\left[\frac{h-x}{2 \cdot L_s} \cdot \min\left(N; 0.55 \cdot A_c \cdot f_c\right) + \left(1 + 0.05 \cdot \min\left(5; \mu_\Delta^{pl}\right)\right) \cdot \right.$$
$$\left. \cdot \left[0.16 \cdot \max\left(0.5; 100 \cdot \rho_{tot}\right) \cdot \left(1 - 0.16 \cdot \min\left(5; \frac{L_s}{h}\right)\right) \cdot \sqrt{f_c} \cdot A_c + \rho_w \cdot b_w \cdot z \cdot f_{yw}\right]\right] \tag{8.33}$$

where A_c is the cross section area taken as $b_w d$ (d is the structural depth), N is the axial load, here taken as the member demand under gravity loads (Mpampatsikos *et al.*, 2008a), μ_Δ^{pl} is the ratio between the plastic part of the chord rotation demand and the yield chord rotation given by Eq. (8.31), ρ_{tot} is the total reinforcement ratio, ρ_w is the transverse reinforcement ratio and z is the length of the internal lever arm. The term $h - x$ represents the distance between the member compression centres and is assumed to be equal to *2h/3*.

In order to evaluate the influence of the variability in the limit state capacity values, the probability of occurrence of the limit states was analysed for the following cases:

- Case 1 - The probability of occurrence of the limit state is analysed assuming that the capacity is deterministic. Therefore, the material properties entering Eqs. (8.31) to (8.33) are considered with their mean values.

- Case 2 - The probability of occurrence of the limit state is analysed considering the variability of the capacity due to the randomness of the material properties entering Eqs. (8.31) to (8.33). By assigning statistical distributions to these properties, the variability of the capacity can be simulated for a number of samples of the material properties. The probability of occurrence of the limit state is then evaluated for each simulated capacity value.

- Case 3 - The probability of occurrence of the limit state is analysed considering the variability of the capacity due to the modelling error associated to Eqs. (8.31) to (8.33). In this case, the limit state capacities C are modelled by the following:

$$C = \hat{C} \cdot \varepsilon_{UC} \tag{8.34}$$

  where $\hat{C}$ is the capacity estimate of Case 1, and ε_{UC} is a lognormal random variable with unit median and a dispersion β_{UC} accounting for the modelling error.

- Case 4 - The probability of occurrence of the limit state is analysed considering the variability of the capacity due to both the randomness of the material properties and the modelling error referred in Case 2 and Case 3, respectively.

To simulate the limit state capacity values according to Case 2, the relevant material properties were assumed to be represented by normal random variables with a mean μ and coefficient of variation (CoV) based on Ferracuti *et al.* (2009) and Dymiotis *et al.* (1999):

- Concrete compressive strength f_c: mean $\mu_{f_c} = 33\ MPa$ and $CoV_{f_c} = 0.18$
- Ultimate concrete strain ε_{cu}: mean $\mu_{\varepsilon_{cu}} = -0.006$ and $CoV_{\varepsilon_{cu}} = 0.35$
- Yield steel strength f_y (assuming f_{yw} equal to f_y): $\mu_{f_y} = 414\ MPa$ and $CoV_{f_y} = 0.06$
- Ultimate steel strain ε_{su}: mean $\mu_{\varepsilon_{su}} = 0.09$ and $CoV_{\varepsilon_{su}} = 0.09$

In addition, it is referred that the ultimate steel strength f_{su} was assumed to be $1.15 f_y$ (Dymiotis *et al.*, 1999). Limit state capacities were then simulated for 2000 values of the material properties sampled from their corresponding distributions according to the Latin Hypercube sampling scheme proposed by Iman and Conover (1982). Yield and ultimate curvatures ϕ_y and ϕ_u were obtained following the procedure of Arêde and Pinto (1996). In order to simulate the limit state capacity values according to Case 3, the dispersion β_{UC} was considered to be 0.36 for θ_{DL} (*fib*, 2003b), 0.90 for θ_{NC} and θ_{SD} (*fib*, 2003b), and 0.14 for V_{NC} (*fib*, 2003a). As for Case 2, limit state capacities were then obtained by simulating Eq. (8.34) for 2000 values of ε_{UC} sampled from its corresponding distribution. To simulate limit state capacities for Case 4, the 2000 capacity values simulated in Case 2 for a given

mechanism were randomly combined with the corresponding 2000 ε_{UC} values simulated in Case 3. The combination of these empirical distributions was carried out according to the referred Latin Hypercube sampling scheme, assuming the two sets of data are uncorrelated, to produce a new set of 2000 limit state capacities. Finally, it is noted that the confidence factor, accounting for the available level of knowledge, was taken equal to one in all cases.

8.3.1.2.2 Hazard curves for the considered seismic scenario

To apply the proposed procedure, the hazard curves defined by Eqs. (8.12) and (8.13) were fitted to the hazard data of the considered seismic scenario. Seismic hazard data was obtained for the spectral acceleration at the fundamental period of the IRREG6 structure, $S_a(T_1)$, and for reference periods of one year and fifty years. The selected methodology and hazard data were those considered to carry out the hazard studies supporting the seismic zonation and the seismic action levels of the Portuguese National Annex of Eurocode 8 (EC8-1, 2010), e.g. see the probabilistic seismic hazard analysis presented by Campos Costa *et al.* (2008). The considered seismic hazard was defined for the intraplate seismic action and a soil of type B (EC8-1, 2010), referring to events with their epicentres mainly inland, in which the model of mainland gross-source zones and the parameters defining the seismic occurrence process in each source zone, such as the Poissonian process and the exponential distribution of magnitudes, were adapted from the proposals presented by Sousa and Oliveira (1996). The attenuation of intensity with distance was described by the relationships defined in Ambraseys *et al.* (1996).

The considered hazard data for the reference periods of one year and fifty years are presented in Figs. 8.4a) and b), respectively, in log-log scale along with the fitted hazard curves. The hazard curve for the reference period of one year was fitted using Eq. (8.13) for hazard values below 0.1, since the expected limit state annual exceedance probabilities are low. The hazard curve for the reference period of fifty years was fitted using Eq. (8.12) for hazard values up to 0.995.

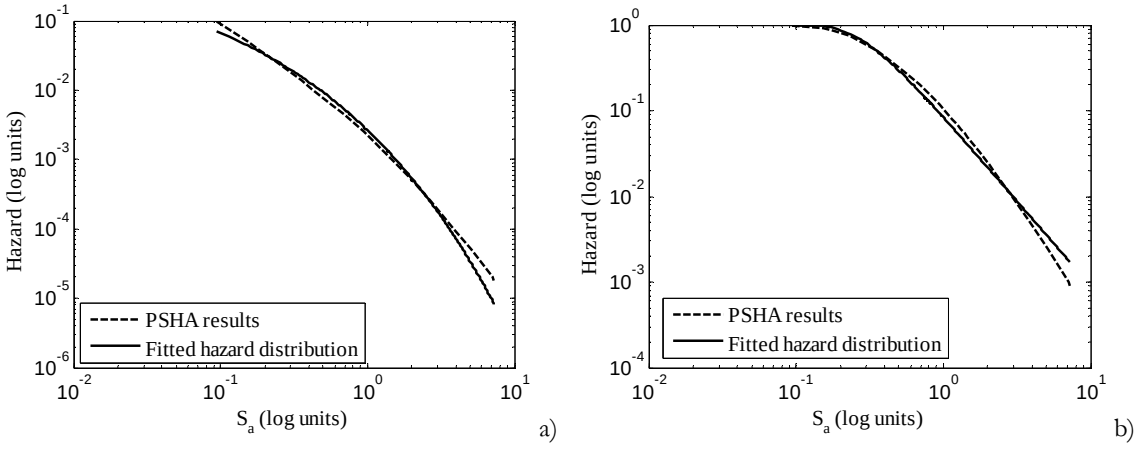

Figure 8.4. Probabilistic seismic hazard analysis (PSHA) results and fitted distribution for a reference period of one year (a) and a reference period of fifty years (b).

8.3.1.2.3 Analysis of the structural demand of sections 1 and 2

The structural demand results of sections 1 and 2 (Fig. 8.3) for the two EDPs associated to the previously referred limit states are presented in the following. With respect to the chord rotation demand results of section 1 (beam), distinction is made between chord rotation causing maximum positive and negative bending, since the beam reinforcement is asymmetric (it is considered herein that negative bending causes tension stresses in the top reinforcement). For results concerning this section, distinction will be made by terming the former as *chord rotation+* and the latter as *chord rotation-*. On the other hand, the results of section 2 (column) are presented for the maximum chord rotation from both bending signs.

As referred in Chapter 5, the structure was analysed using a multi-stripe analysis (Jalayer and Cornell, 2009) where the selected ground motions were scaled for nine intensities in order to reflect different return periods. The selected return periods were 37, 73, 95, 225, 475, 976, 1980, 2480 and 4950 years which correspond to $S_a(T_1)$ values ranging from 0.03g to 0.30g. The dispersion of the response due to record-to-record variability is accounted for by considering the suite of fifty ground motions previously referred. The demand evolutions were then fitted to Eqs. (8.14), (8.15) and (8.16) considering all the referred IM levels. To fully assess the suitability of Eqs. (8.15) and (8.16) to fit the IDA curves of shear force, Figs. 8.5 and 8.6 present the fitting of the shear force evolution produced by each ground motion for sections 1 (beam) and 2 (column), respectively. Vertical axes of the graphs represent shear force in *kN* while horizontal axes represent $S_a(T_1)$ in m/s^2. Equation (8.16) was used for all the fittings represented in Fig. 8.5 while Eq. (8.15) was used for all the fittings represented in Fig. 8.6. With respect to the former, it is noted that parameter k was considered with a value of 2.0.

As can be seen from Figs. 8.5 and 8.6, each set of IDA curves exhibits a low variability, a fact denoting the small influence of the record-to-record variability for shear demand, especially in section 1 (beam). To illustrate the fittings obtained with Eq. (8.14), Fig. 8.7 presents the fitting of the chord rotation+ of section 1 for each ground motion. Vertical axes of the graphs represent *rads* while horizontal axes represent $S_a(T_1)$ in m/s^2.

To evaluate the effectiveness of the suggestion made in Section 8.3.1.1 regarding the use of less IM levels for the fitting of the IDA curves, an additional fitting case was also performed for each ground motion. For such case, Eqs. (8.14), (8.15) and (8.16) were fitted using demand data of only three IM levels (0.03g, 0.15g and 0.30g).

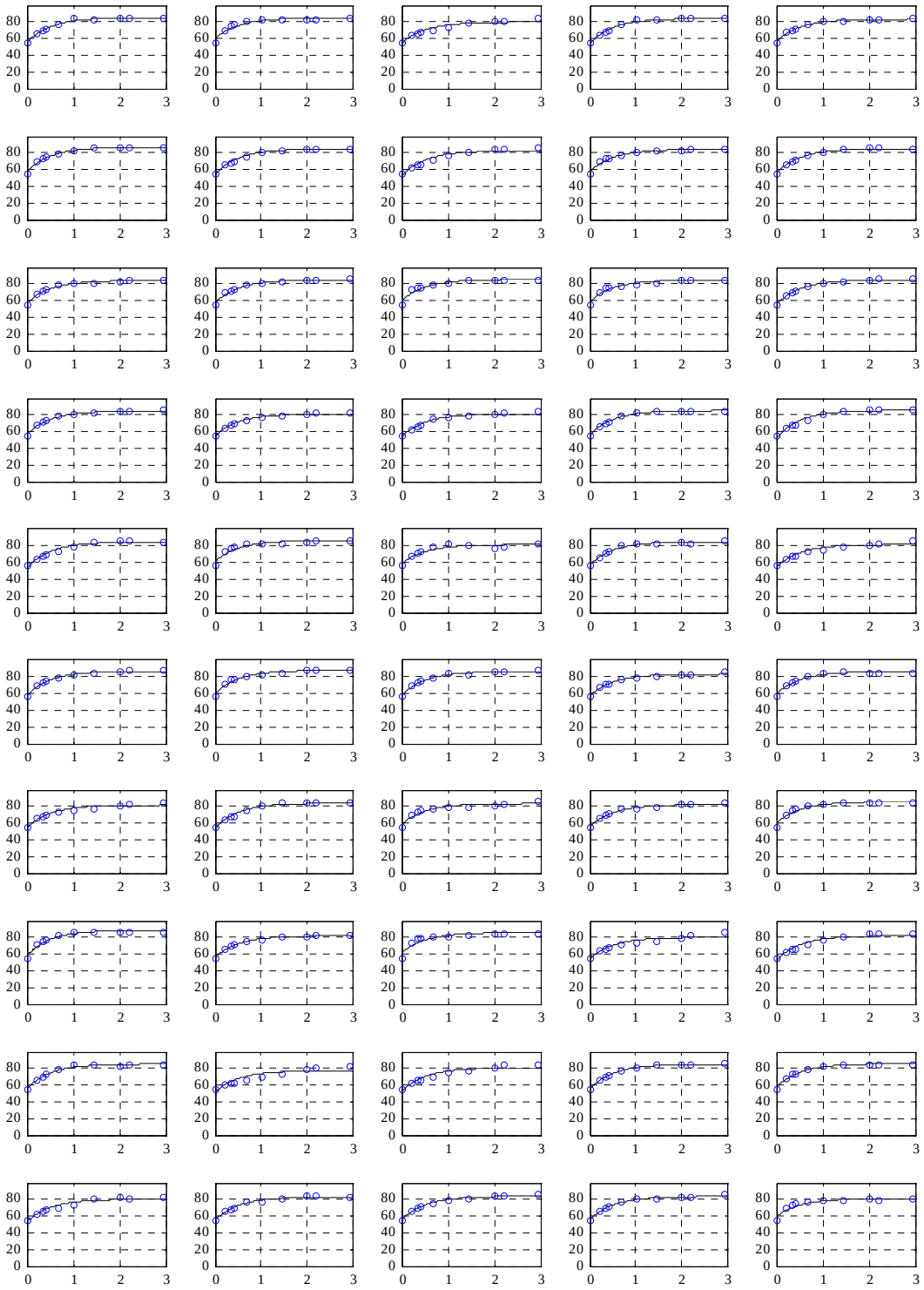

Figure 8.5. Shear force demand IDA curves for section 1 and corresponding fittings for the fifty ground motions (vertical axes are shear force in kN and horizontal axes are $S_a\left(T_1\right)$ in m/s^2).

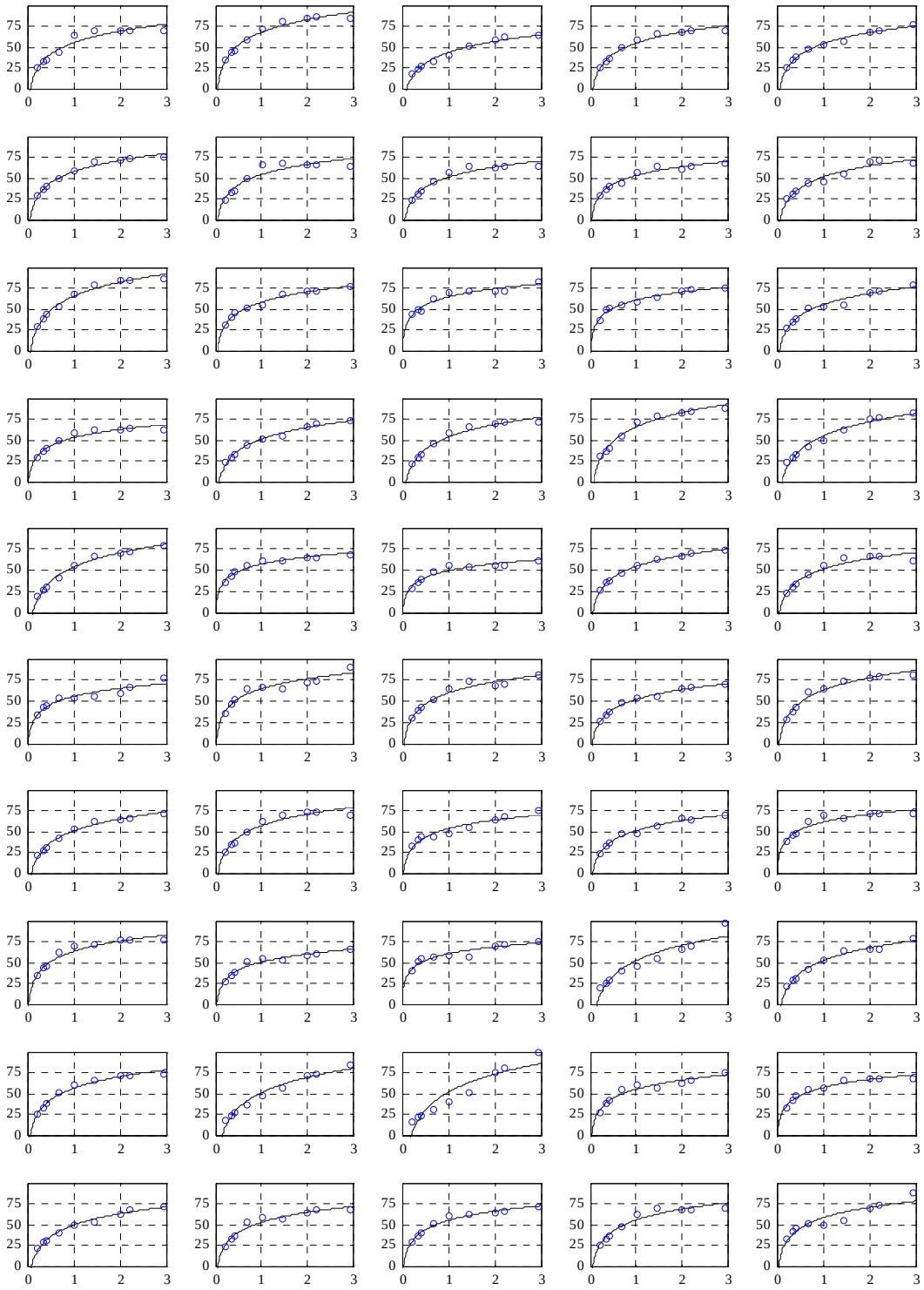

Figure 8.6. Shear force demand IDA curves for section 2 and corresponding fittings for the fifty ground motions (vertical axes are shear force in *kN* and horizontal axes are $S_a(T_1)$ in m/s^2).

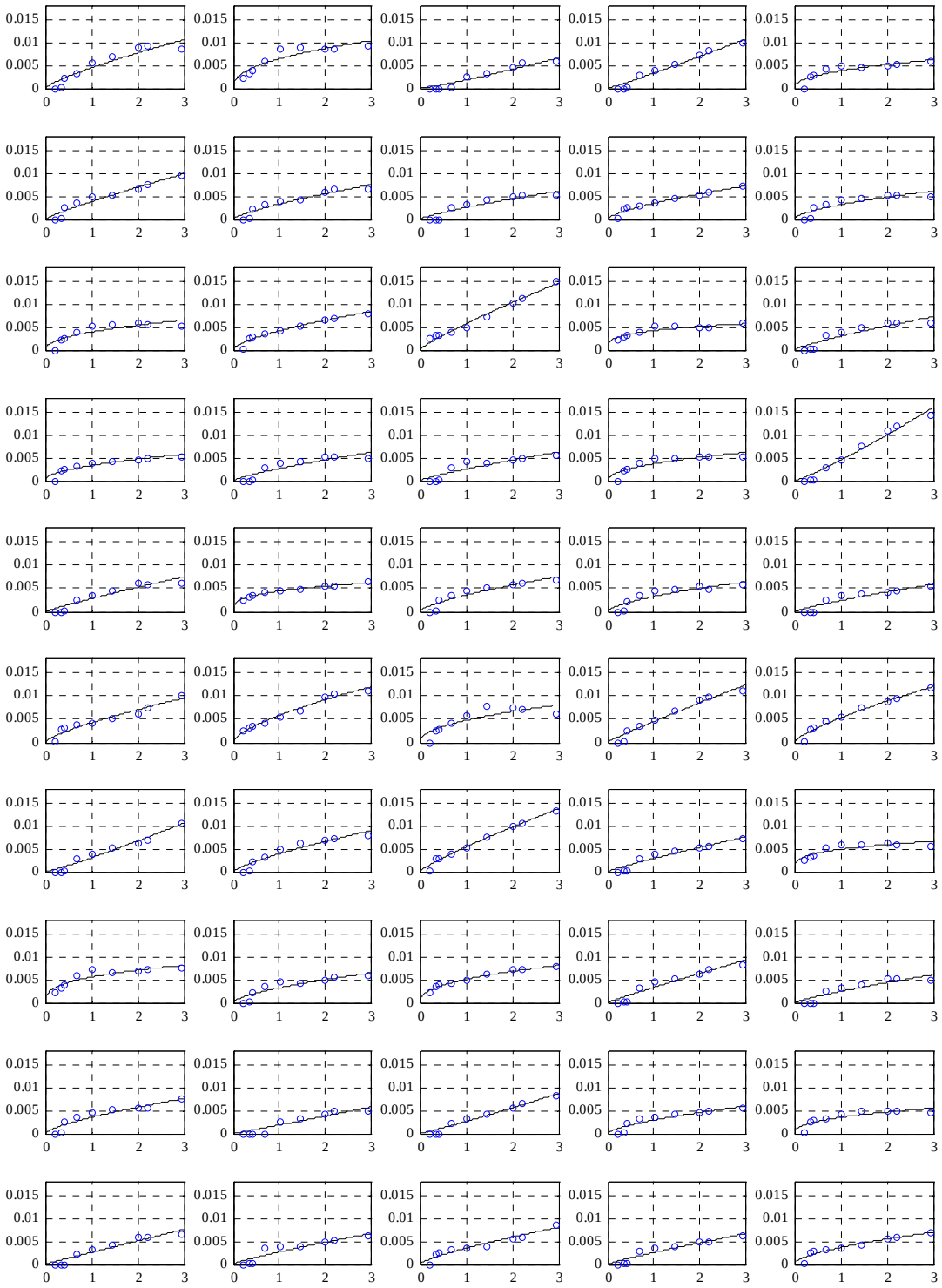

Figure 8.7. Chord rotation+ IDA curves for section 1 and corresponding fittings for the fifty ground motions (vertical axes are chord rotation in *rads* and horizontal axes are $S_a\left(T_1\right)$ in m/s^2).

8.3.1.2.4 Results of the component limit state probabilities by the proposed method

8.3.1.2.4.1 Limit state probabilities considering deterministic capacities and demand from all IM levels

The results presented in the following are those referring to Case 1, as defined in Section 8.3.1.2.1. To obtain the limit state exceedance probabilities, capacities for each limit state were computed according to Eqs. (8.31) to (8.33). The limit state exceedance probabilities were then computed for each ground motion using Eqs. (8.19) to (8.24), depending on the demand type, the section and the selected reference period. For each limit state, a total of fifty exceedance probabilities was therefore obtained. As described in Section 8.3.1, since all the records are assumed to have the same probability of occurrence, the mean of each set of limit state exceedance probabilities was determined in order to obtain a single descriptive value representing the expected limit state probabilities. Besides the mean of the probabilities for each limit state, the estimated standard error of the mean was also computed to obtain a measure of the precision of the mean estimate. For the chord rotation+, chord rotation- and shear force demand of section 1, and for the chord rotation and shear force demand of section 2, Table 8.1 presents the expected limit state exceedance probability estimates (the mean of the individual values), μ_{LS}, and the corresponding estimates of the standard errors of μ_{LS}, SE_{μ}, expressed as percentages of μ_{LS}, for the considered reference periods. One should note that some of the large values of the SE_{μ}'s (above 30%) are associated to very low limit state exceedance probabilities. In such cases, this variability results mainly from dealing with very small numbers (i.e. small changes in very small members will most times lead to a large variability). However, for situations where the limit state exceedance probabilities have higher values, the SE_{μ} estimates reflect the scatter of the fifty values due to record-to-record variability. Moreover, the SE_{μ}'s associated to the chord rotation limit states also indicate that the scatter due to record-to-record variability increases with the level of inelastic behaviour associated to the limit state. Furthermore, it is also noted that, due to the issues associated to Eqs. (8.21) and (8.24) previously referred, the limit state probabilities for the shear force limit state of section 1 (beam) have 48 zero values. Therefore, this situation leads to the large value of SE_{μ} presented for the shear force limit state of this section. Finally, it is also referred that some of the lower values of μ_{LS} that are presented in Table 8.1 (e.g. 1.54E-26) have little statistical meaning and could be considered to be equal to zero. Nonetheless, such value are still presented in order to be able to observe their evolution for Cases 2, 3 and 4 which will be analysed in a later Section

Table 8.1. Limit state exceedance probabilities parameters for chord rotation and shear force demands of sections 1 and 2 considering capacities determined according to Case 1.

Demand	LS	Ref. per. = 1 year		Ref. per. = 50 years	
		μ_{LS}	SE_{μ} (%)	μ_{LS}	SE_{μ} (%)
chord rotation+ at section 1	NC	6.16E-07	48.38	2.80E-04	20.57
	SD	1.97E-06	39.32	5.22E-04	18.76
	DL	9.18E-04	14.80	3.27E-02	12.35
chord rotation- at section 1	NC	5.73E-33	100.00	2.09E-09	53.24
	SD	1.54E-26	100.00	9.79E-09	46.27
	DL	9.93E-10	39.47	2.51E-05	21.00
shear force at section 1	NC	3.39E-05	83.12	1.22E-03	79.25
chord rotation at section 2	NC	5.89E-06	86.20	4.56E-04	56.60
	SD	8.76E-06	68.63	7.41E-04	40.84
	DL	2.27E-05	39.77	1.78E-03	24.85
shear force at section 2	NC	1.42E-08	53.58	4.90E-05	25.22

To assess if the obtained limit state probability estimates are reasonably stable and accurate, an approach similar to the one presented in Lupoi *et al.* (2003) was followed. To illustrate the results that were obtained, Figs. 8.8 and 8.9 present the computed evolutions of the limit state probability estimates for an increasing number of samples (three to fifty) randomly ordered, for both sections, reference periods and the considered limit states. The vertical axes of the graphs represent limit state probability estimates while horizontal axes represent the number of samples. To observe the effect of the random order of the samples, results of each section are presented for two different random orders of the samples. Results indicate that for some limit states, estimates involving a number of samples above fifteen are either stable or exhibit small variations. Nonetheless, other limit states exhibit a large variability of the probability estimate with a number of samples near fifty. Still, it is noted that these results are conditioned to a particular ordering of the individual values of the limit state probabilities. Therefore, the results obtained are only indicative. Furthermore, it is also noted that the previously referred number of zero values that occur for the limit state probabilities of the shear force limit state of section 1 (beam) leads to the occurrence of several zero values in the corresponding evolutions of Fig. 8.8.

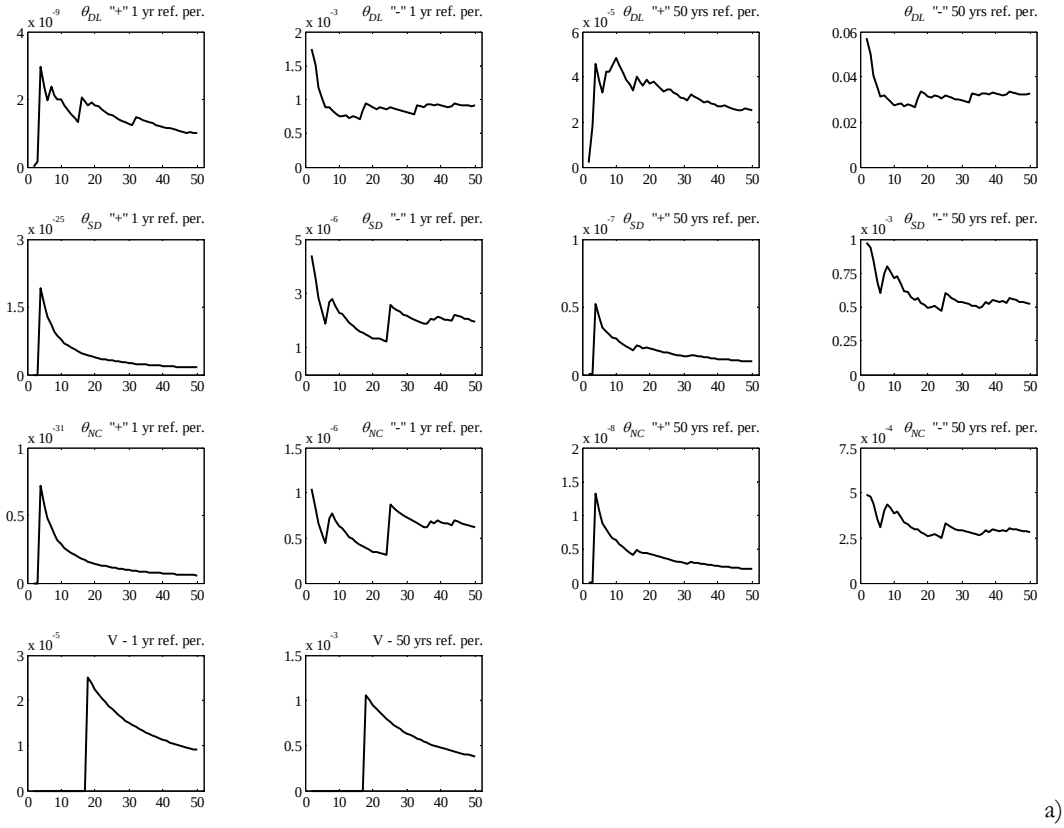

a)

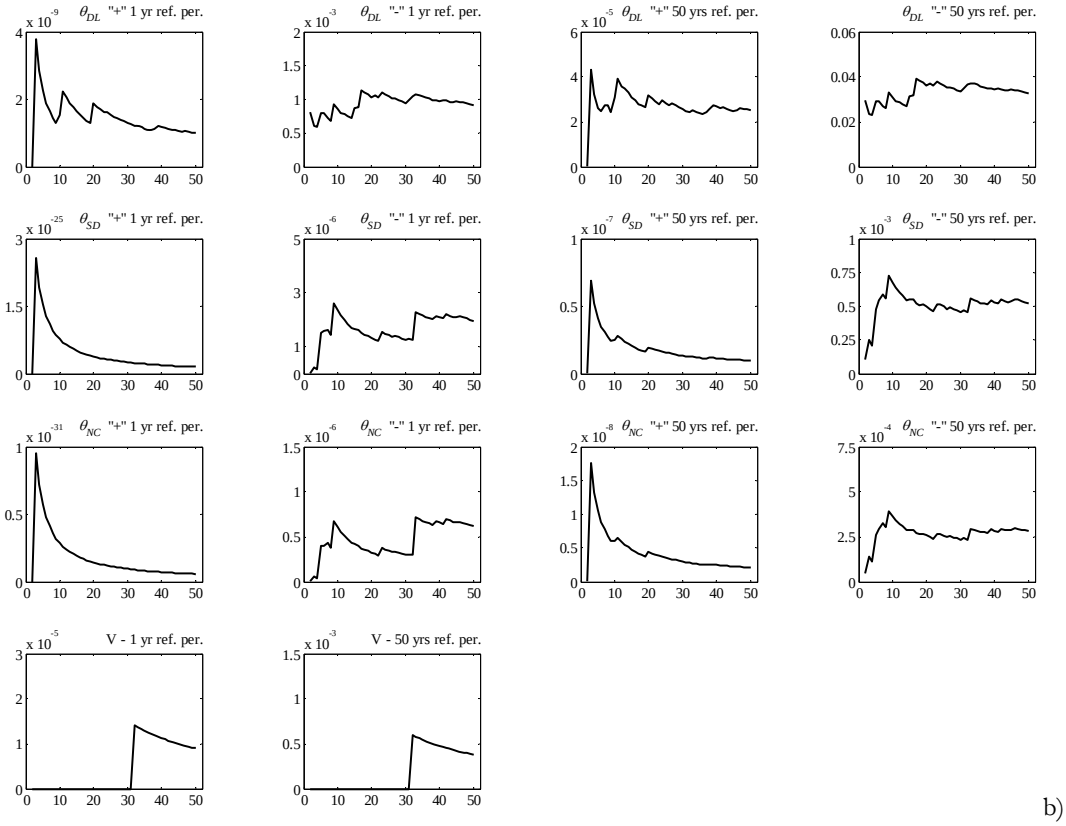

b)

Figure 8.8. Evolution of the limit state probability estimates with increasing number of samples for the chord rotation and shear force limit states of section 1, for the reference periods of 1 year and 50 years, and for two random orders of the samples (a) and (b).

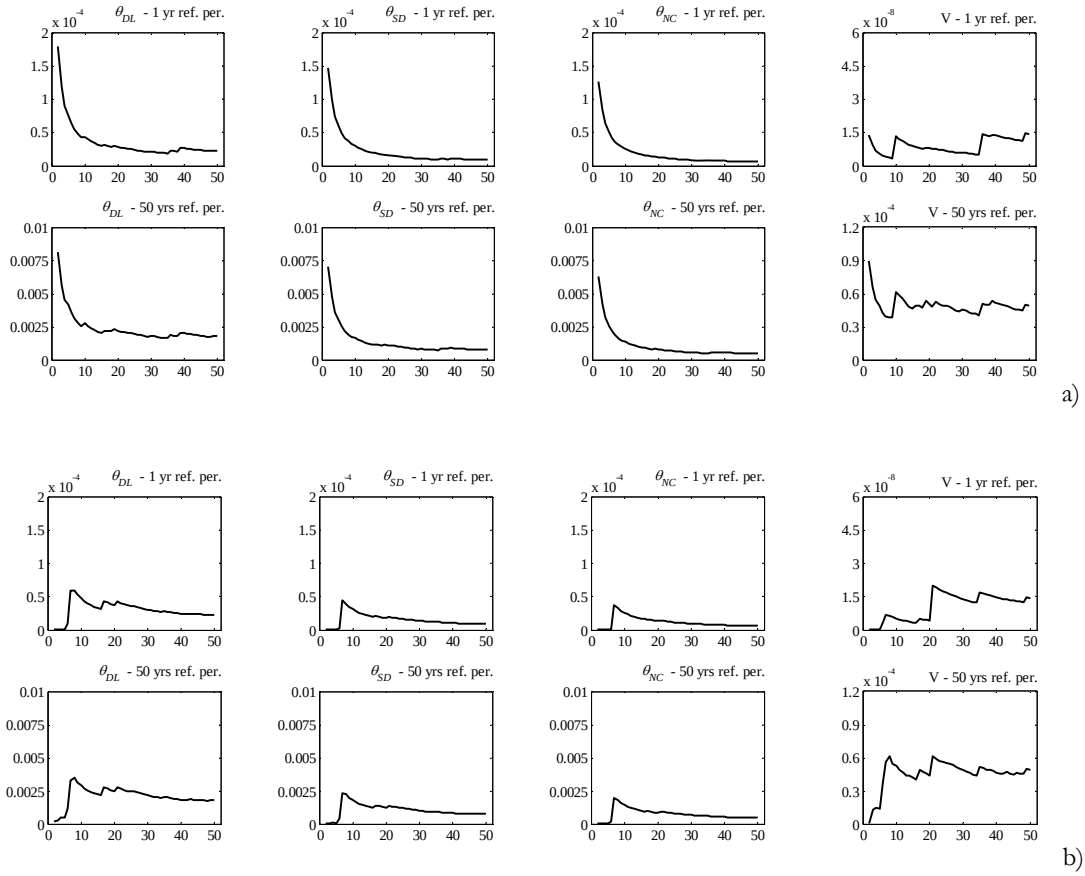

Figure 8.9. Evolution of the limit state probability estimates with increasing number of samples for the chord rotation and shear force limit states of section 2, for the reference periods of 1 year and 50 years, and for two random orders of the samples (a) and (b).

To further assess the effect of the ordering of the samples and of the sample size, fifty combinations of three to forty-nine limit state probabilities were also studied. For each sample size, the average of the estimated SE_μ's over all combinations was computed. Results for both sections, reference periods and for the considered limit states are presented in Figs. 8.10 and 8.11. The vertical axes of the different graphs represent SE_μ expressed as a percentage of μ_{LS} while horizontal axes represent the sample size. As expected, the average standard errors decrease with the increase of sample size. In some cases, such decrease amounts to 50% from samples of size three to forty-nine. However, in other cases, the decrease remains between 25% to 30%. The presented results also indicate that the slope of the decrease varies from one limit state to another. In some cases, for samples of size near twenty, the referred slope is greatly reduced, indicating that SE_μ is stabilizing, while in other cases it remains almost constant up to the size of forty-nine, thus indicating that SE_μ could possibly be further reduced if the sample size was larger.

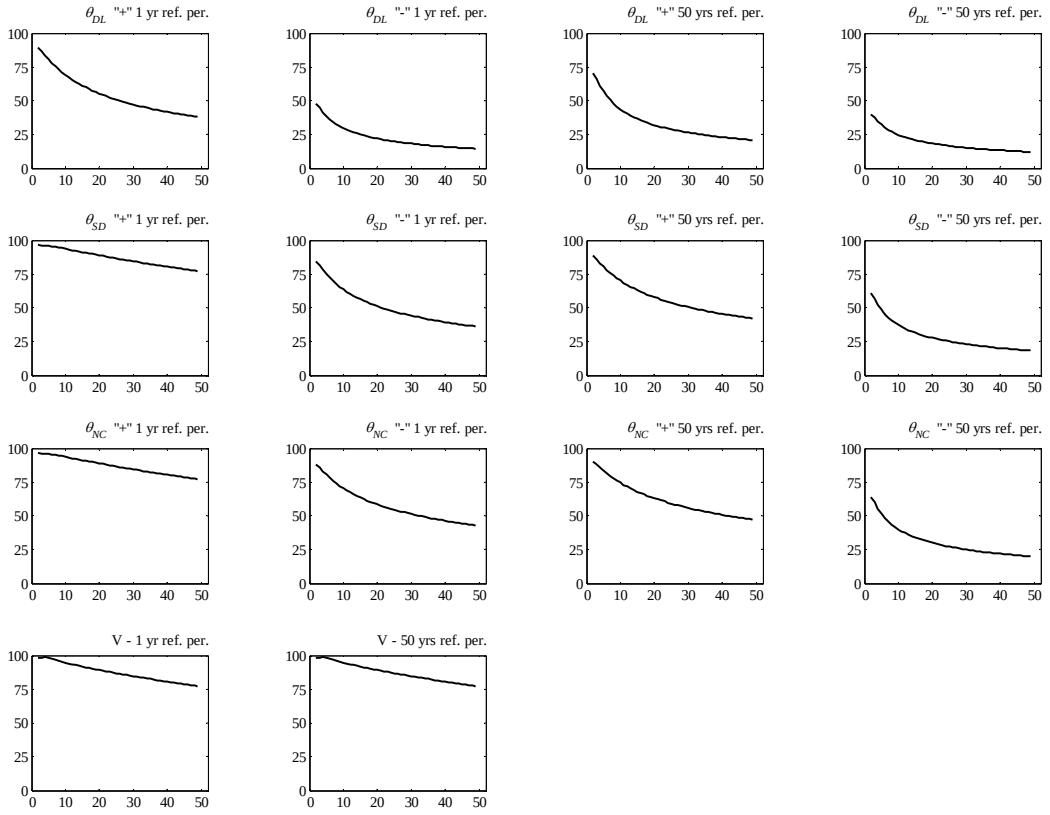

Figure 8.10. Evolution of the average of the SE_μ, expressed as percentages of μ_{LS}, for the chord rotation and shear force limit states of section 1 and the reference periods of 1 year and 50 years.

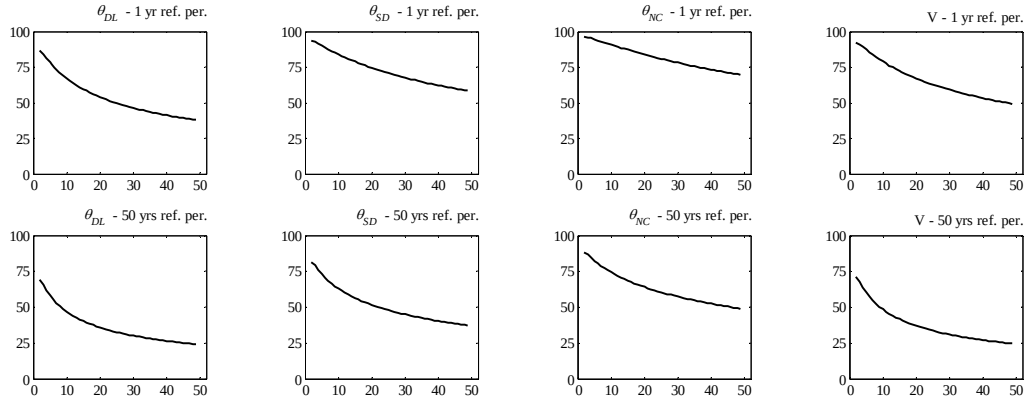

Figure 8.11. Evolution of the average of the SE_μ, expressed as percentages of μ_{LS}, for the chord rotation and shear force limit states of section 2 and the reference periods of 1 year and 50 years.

8.3.1.2.4.2 Limit state probabilities considering deterministic capacities and demand from three IM levels

The application of the proposed procedure for Case 1 was repeated considering the IDA curves fitted using only the three previously referred IM levels (0.03g, 0.15g and 0.30g). After computing the values of μ_{LS} and SE_μ as previously defined for the chord rotation and shear force limit state probabilities, ratios between these and the values presented in Table 8.1 were determined to assess their variations from one case to another. Table 8.2 presents the referred ratios of the limit state exceedance probability values of μ_{LS}

and SE_μ where it can be seen that, for most cases, the parameter ratios exhibit satisfying values. With the exception of a few cases, variations of both μ_{LS} and SE_μ are below 20%. Among these exceptions, reference must be made to some of the results obtained for the chord rotation- of section 1 that exhibit lower ratios. These results occur for the cases that exhibited very low values of the exceedance probability in Table 8.1 and should, therefore, be analysed in light of the comments made to the corresponding results of Table 8.1. An additional note is also made regarding the results obtained for the shear force of section 1 since the lower ratios obtained for this case are a direct consequence of the previously referred applicability issues associated to Eqs. (8.21) and (8.24). Aside from these two situations, the remaining results allow concluding that using three IM levels in the way suggested in Section 8.3.1.1 leads to results that are very close to those obtained when considering all the IM levels (a more accurate approach) with less computational effort.

Table 8.2. Ratios between the limit state exceedance probability results when only three IM levels are considered and those of Table 8.1.

Demand	LS	Ref. per. = 1 year		Ref. per. = 50 years	
		μ_{LS}	SE_μ	μ_{LS}	SE_μ
chord rotation+ at section 1	NC	0.85	0.72	0.99	0.91
	SD	0.92	0.80	0.99	0.94
	DL	0.85	1.07	0.87	1.05
chord rotation- at section 1	NC	0.00	1.00	0.53	0.61
	SD	0.00	1.00	0.62	0.63
	DL	0.83	1.00	1.11	0.81
shear force at section 1	NC	0.67	0.91	0.77	0.87
chord rotation at section 2	NC	1.29	0.99	1.21	0.98
	SD	1.34	1.05	1.22	1.02
	DL	1.28	1.09	1.20	1.01
shear force at section 2	NC	0.93	1.04	0.94	1.03

8.3.1.2.4.3 Limit state probabilities considering random capacities and demand from all IM levels

The results presented in the following are those where the limit state capacities are considered according to Cases 2, 3 and 4, as defined in Section 8.3.1.2.1. In these cases, 2000 limit state capacity values were considered in the calculation of the limit state exceedance probabilities for each ground motion using Eqs. (8.19) to (8.24). For each limit state considered, a total of 100.000 exceedance probabilities were therefore obtained. As for Case 1, parameters μ_{LS} and SE_μ were also computed based on the exceedance probability results of each limit state.

Since, for a given limit state, each one of the 2000 limit state capacity values can be assumed to have a different probability of occurrence, the value of μ_{LS} was then defined by a weighted mean, as suggested in Section 8.3.1. To define the weight of each limit state exceedance probability obtained from a certain capacity value, a statistical distribution was fitted to the 2000 capacity values. Based on the fitted distribution, a random sample of size 1.000.000 was then generated to establish a histogram with bins defined for the original 2000 limit state capacity values. The frequency counts of the bins were then used to define the probability of occurrence of the 2000 capacity values. This procedure was considered to define the limit state exceedance probability $p_{w,LS}$ associated to a given ground motion. The value of μ_{LS} was then defined by the mean of the $p_{w,LS}$ values obtained for all the earthquake records. The values of SE_{μ} that are presented for Cases 2, 3 and 4 were also computed from the $p_{w,LS}$ data in order to obtain values comparable to those presented in Table 8.1. In addition to these parameters, the standard deviations of the limit state exceedance probabilities obtained for Cases 2, 3 and 4 for a given limit state, normalized by the corresponding one obtained for Case 1, are also presented and termed σ_{C2}/σ_{C1}, σ_{C3}/σ_{C1} and σ_{C4}/σ_{C1}. Parameters σ_{C2}, σ_{C3} and σ_{C4}/σ_{C1} were also obtained from the $p_{w,LS}$ values.

The results obtained for Cases 2, 3 and 4 are presented in Tables 8.3, 8.4 and 8.5, respectively, for the previously analysed limit states of sections 1 and 2. Similar to the situation referred in Section 8.3.1.2.4.1, some of the very low and very high values of the parameters in Tables 8.3, 8.4 and 8.5 have little statistical meaning. Nonetheless, these values are still presented in order to be able to observe their evolution between Cases 2, 3 and 4. By comparing the results of Table 8.3 with those of Table 8.1, it can be seen that introducing the variability of the material properties increases the exceedance probability μ_{LS}, especially for limit states exhibiting extremely low probabilities in Table 8.1. With the exception of these extreme situations, the observed increase ranges from a few percents (e.g. for the DL limit state of both sections) to a duplication of the risk or even more (e.g. for the shear force limit state of section 1). With respect to the SE_{μ} results, the values of Table 8.3 are seen to be slightly lower than those of Table 8.1. Still, an exception is observed for the results associated to the shear force limit state of section 1 which decreased significantly. Even though considering the variability of the material properties is expected to increase the dispersion of the results, the SE_{μ} values presented in Table 8.3 appear to contradict this idea. The reason for this situation results from the fact that the SE_{μ} values are normalized by the corresponding value of μ_{LS}. Since μ_{LS} increased from Case 1 to Case 2, the results of SE_{μ} can be misleading. Hence, for a more explicit view of the evolution of the dispersion from Case 1 to Case 2, one should report to the results of parameter σ_{C2}/σ_{C1}. The values of σ_{C2}/σ_{C1} indicate that the variability of the calculated probabilities tends to increase slightly due to the random material properties. However, there are two noticeable exceptions: the shear force limit state of section 1, and the SD and

NC chord rotation limit states of section 1. The former is believed to be connected to the fact that Eqs. (8.21) and (8.24) do not lead to any value of $p_{w,LS}$ that is zero for Case 2. With respect to the latter, the σ_{C2}/σ_{C1} results presented are due to the fact that such limit states were found to have very small standard deviations for Case 1, in addition to the very small probabilities of Table 8.1.

When analysing the results of Tables 8.4 and 8.5 and comparing them to those of Table 8.3, the results of μ_{LS} can be seen to be highly influenced by the introduction of the modelling error of the limit state capacities. The results of Case 3 show a considerable increase of μ_{LS} with respect to those of Case 2. On the other hand, the results of Case 4 exhibit a smaller increase of μ_{LS} with respect to those of Case 3, thus reflecting the lower influence of the randomness of the material properties with respect to that of the modelling error of the capacities. In terms of the results of SE_μ, the results of Case 3 and Case 4 can be seen to be considerably lower than those of Case 2. Again, the reason for this situation results from the fact that the SE_μ values are normalized by the corresponding value of μ_{LS} which increased significantly in Cases 3 and 4. Still, a direct comparison between the SE_μ results of Cases 3 and 4 indicates that the influence of the variability of the material properties remains small. The evolution of the dispersion from Case 1 to Cases 3 and 4 can be seen more explicitly from the results of parameters σ_{C3}/σ_{C1} and σ_{C4}/σ_{C1}. These parameters indicate that the influence of the modelling error of the capacities introduces a considerable amount of variability

Table 8.3. Limit state exceedance probability parameters for chord rotation and shear force demands of sections 1 and 2 considering capacities determined according to Case 2.

Demand	LS	Ref. per. = 1 year			Ref. per. = 50 years		
		μ_{LS}	SE_μ (%)	σ_{C2}/σ_{C1}	μ_{LS}	SE_μ (%)	σ_{C2}/σ_{C1}
chord rotation+ at section 1	NC	6.39E-07	47.74	1.02	2.83E-04	20.50	1.01
	SD	2.04E-06	38.81	1.02	5.28E-04	18.70	1.01
	DL	9.27E-04	14.76	1.01	3.30E-02	12.37	1.01
chord rotation- at section 1	NC	5.82E-21	91.84	9.32E+11	4.98E-09	46.58	2.08
	SD	6.07E-18	79.02	3.12E+08	2.42E-08	39.86	2.13
	DL	1.55E-09	36.74	1.45	2.63E-05	20.72	1.04
shear force at section 1	NC	1.85E-04	10.00	0.66	6.75E-03	9.65	0.67
chord rotation at section 2	NC	6.59E-06	79.46	1.03	5.23E-04	50.79	1.03
	SD	1.11E-05	57.18	1.05	9.10E-04	35.07	1.05
	DL	2.31E-05	39.17	1.00	1.79E-03	24.65	1.00
shear force at section 2	NC	2.07E-08	49.46	1.35	5.22E-05	24.76	1.04

Table 8.4. Limit state exceedance probability parameters for chord rotation and shear force demands of sections 1 and 2 considering capacities determined according to Case 3.

Demand	LS	Ref. per. = 1 year			Ref. per. = 50 years		
		μ_{LS}	SE_{μ} (%)	σ_{C3}/σ_{C1}	μ_{LS}	SE_{μ} (%)	σ_{C3}/σ_{C1}
chord rotation+ at section 1	NC	3.01E-05	13.64	13.80	1.49E-03	10.96	2.84
	SD	7.93E-05	13.51	13.85	3.15E-03	10.18	3.28
	DL	1.86E-03	15.21	2.08	5.77E-02	12.86	1.84
chord rotation- at section 1	NC	7.29E-06	23.20	2.95E+26	1.11E-04	7.38	7.38E+03
	SD	4.49E-05	26.17	7.63E+20	4.95E-04	6.08	6.64E+03
	DL	8.10E-06	12.09	2.50E+3	4.40E-04	9.12	7.61
shear force at section 1	NC	7.01E-04	3.92	0.98	2.28E-02	3.83	0.90
chord rotation at section 2	NC	2.71E-04	8.53	4.56	7.28E-03	6.41	1.81
	SD	7.04E-04	8.93	10.45	1.67E-02	5.71	3.14
	DL	7.78E-05	17.76	1.53	3.81E-03	14.76	1.27
shear force at section 2	NC	4.89E-07	30.96	19.93	1.35E-04	19.35	2.11

Table 8.5. Limit state exceedance probability parameters for chord rotation and shear force demands of sections 1 and 2 considering capacities determined according to Case 4.

Demand	LS	Ref. per. = 1 year			Ref. per. = 50 years		
		μ_{LS}	SE_{μ} (%)	σ_{C4}/σ_{C1}	μ_{LS}	SE_{μ} (%)	σ_{C4}/σ_{C1}
chord rotation+ at section 1	NC	3.33E-05	13.54	15.13	1.59E-03	10.83	2.99
	SD	8.70E-05	13.56	15.25	3.37E-03	10.15	3.49
	DL	1.87E-03	15.23	2.10	5.79E-02	12.83	1.84
chord rotation- at section 1	NC	3.47E-05	24.43	1.48E+27	4.90E-04	7.81	3.44E+04
	SD	1.37E-04	19.33	1.72E+21	1.23E-03	4.53	1.23E+04
	DL	9.36E-06	12.01	2.87E+3	4.81E-04	8.97	8.19
shear force at section 1	NC	7.70E-04	3.67	1.00	2.49E-02	3.59	0.92
chord rotation at section 2	NC	4.34E-04	8.84	7.55	1.08E-02	5.83	2.43
	SD	1.08E-03	9.14	16.35	2.32E-02	5.43	4.16
	DL	7.77E-05	17.73	1.53	3.80E-03	14.75	1.27
shear force at section 2	NC	5.51E-07	30.29	21.98	1.41E-04	19.09	2.18

In the overall, the global analysis of the results presented in Tables 8.1 to 8.5 indicates that considering the uncertainty of the limit state capacities increases significantly

the estimate of the probability of exceedance of the limit states. Furthermore, for the situations that were analysed, the modelling error of the limit state capacity expressions was seen to be the main factor governing both the estimate of the probability of exceedance of the limit state and its variability. With the exception of a few situations, the effects of the variability of the material properties were seen to be relatively small. When comparing results obtained when record-to-record variability was the only source of uncertainty (Case 1) to those where the modelling error was also considered, the effects of the latter were seen, in many cases, to at least duplicate the variability of the probability of exceedance. Therefore, for such cases, the variability introduced by the modelling error can be seen to be, at least, 70% larger than that of the record-to-record variability. Given the significance of the referred modelling error, further research efforts should address the development of alternative formulations for the limit state capacities to obtain expressions providing capacity estimates with less uncertainty.

8.3.2 Methodology 2

Methodology 2 extends the SAC/FEMA method by introducing some modifications that allow overcoming some of the limitations referred in Section 8.1, while maintaining the mathematical tractability of the procedure. Since the linear form in the log-log space of the earthquake hazard assumed by the SAC/FEMA method is one of its main sources of error, one of the proposed modifications involves the use of alternative earthquake hazard fitting functions. In this context, it must be noted that a proposal for an alternative earthquake hazard fitting model has also been presented by Bradley *et al.* (2007). However, this proposal, which takes a hyperbolic form in the log-log space, does not allow for a full analytical treatment of the procedure and involves an approximation in order to obtain a semi-analytical closed form solution for the risk expression (Bradley *et al.*, 2007). In addition to the proposal for an alternative earthquake hazard fitting model, the issue of force-based EDPs is also addressed by developing a new version of the risk assessment method that involves a more adequate demand evolution expression for this type of EDP. Finally, the development of a third approach that involves a second demand evolution expression best suited for force-based EDPs is also addressed. However, the mathematical tractability of this approach is impaired by several issues which are analysed and discussed.

8.3.2.1 A closed form risk assessment method with a new seismic hazard function

The basic assumptions of this new closed form risk assessment method are similar to those of the original SAC/FEMA approach (see Section 8.2). Hence D and C are also assumed to be lognormally distributed random variables referring to a scalar EDP. Also, it

is assumed that demand D can be expressed as a function of the selected IM by an expression similar to Eq. (8.4):

$$D = \left(a \cdot x^{b}\right)\zeta \tag{8.35}$$

where ζ is a lognormal random variable with unit median and dispersion (i.e. a standard deviation of the log of the data) equal to β_D. As for the case of the SAC/FEMA method, the term $a \cdot x^{b}$ can be seen to represent the evolution of the median value $\hat{D}$ of the demand. By rewriting Eq. (8.35) according to

$$\ln\left(D\right) = \ln\left(a\right) + b\ln\left(x\right) + \ln\left(\zeta\right) \tag{8.36}$$

and defining ε as a normal random variable equal to $\ln\left(\zeta\right)$, with zero mean and a standard deviation equal to β_D, the term $\ln\left(x\right)$ can be defined as

$$\ln\left(x\right) = k_1 + k_2\varepsilon \tag{8.37}$$

in which k_1 and k_2 are defined as

$$\begin{cases} k_1 = \dfrac{\ln\left(D\right) - \ln\left(a\right)}{b} \\ k_2 = -\dfrac{1}{b} \end{cases} \tag{8.38}$$

By assuming that, for some reference period under consideration, the seismic hazard function $H\left(x\right)$ can be adequately represented by

$$H\left(x\right) = e^{\alpha_1 \ln\left(x\right)^2 + \alpha_2 \ln\left(x\right) + \alpha_3} \tag{8.39}$$

where α_1, α_2 and α_3 are parameters to be fitted using existing probabilistic seismic hazard data, when replacing the $\ln\left(x\right)$ terms of Eq. (8.39) by Eq. (8.37), one obtains

$$H\left(D\right) = e^{\alpha_1 \left(k_2 \varepsilon + k_1\right)^2 + \alpha_2 \left(k_2 \varepsilon + k_1\right) + \alpha_3} \tag{8.40}$$

which can be rearranged to yield

$$H\left(D\right) = e^{k_3 \varepsilon^2 + k_4 \varepsilon + k_5} \tag{8.41}$$

where k_3, k_4 and k_5 are defined as

$$\begin{cases} k_3 = \dfrac{\alpha_1}{b^2} \\ k_4 = \dfrac{-2\alpha_1\left(\ln(D)-\ln(a)\right)-\alpha_2 b}{b^2} \\ k_5 = \dfrac{\alpha_1 \ln(D)^2 + \alpha_2 b\ln(D) - 2\alpha_1\ln(a)\ln(D) + \alpha_3 b^2 - \alpha_2\ln(a)b + \alpha_1\ln(a)^2}{b^2} \end{cases} \tag{8.42}$$

The hazard function $H(D)$ defined by Eq. (8.41) represents the probability $\Pr(D>d)$ conditioned to the random variable ε, i.e. $\Pr(D>d\,|\,\varepsilon)$. The unconditioned probability $\Pr(D>d)=1-F_D(d)$ can then be obtained by solving:

$$\Pr(D>d) = \int_{-\infty}^{+\infty} \Pr(D>d\,|\,\varepsilon)\cdot f_\varepsilon(\varepsilon)\,d\varepsilon = \int_{-\infty}^{+\infty} e^{k_3\varepsilon^2+k_4\varepsilon+k_5}\cdot\frac{e^{-\frac{\varepsilon^2}{2\beta_D^2}}}{\sqrt{2\pi}\cdot\beta_D}\,d\varepsilon \tag{8.43}$$

The integral defined by Eq. (8.43) can be rearranged to give:

$$\Pr(D>d) = \int_{-\infty}^{+\infty} e^{\frac{2k_5k_6+k_4^2}{2k_6}}\cdot\frac{e^{-\frac{1}{2}\left(\frac{\varepsilon-k_4/k_6}{\sqrt{1/k_6}}\right)^2}}{\sqrt{2\pi}\cdot\beta_D}\,d\varepsilon \tag{8.44}$$

in which k_6 is defined by

$$k_6 = \frac{1}{\beta_D^2} - \frac{2\alpha_1}{b^2} \tag{8.45}$$

The integral defined by Eq. (8.44) can be seen to be equivalent to

$$\Pr(D>d) = \frac{\sqrt{1/k_6}}{\beta_D} e^{\frac{2k_5k_6+k_4^2}{2k_6}}\cdot\int_{-\infty}^{+\infty}\frac{e^{-\frac{1}{2}\left(\frac{\varepsilon-k_4/k_6}{\sqrt{1/k_6}}\right)^2}}{\sqrt{2\pi}\cdot\sqrt{1/k_6}}\,d\varepsilon \tag{8.46}$$

which then simplifies into

$$\Pr(D>d) = \frac{\sqrt{1/k_6}}{\beta_D} e^{\frac{2k_5k_6+k_4^2}{2k_6}} \tag{8.47}$$

since the integral of Eq. (8.46) is that of a normal distribution with mean k_4/k_6 and standard deviation $\sqrt{1/k_6}$, which is equal to one. By replacing the values of k_4, k_5 and k_6 in Eq. (8.47) by those defined in Eqs. (8.42) and (8.45), $\Pr(D>d)$ is then

$$\Pr(D>d) = \frac{b\cdot e^{\frac{2\alpha_1\ln(d)^2+\left(2\alpha_2 b-4\alpha_1\ln(a)\right)\ln(d)+\left(\alpha_2^2-4\alpha_1\alpha_3\right)\beta_D^2+2\alpha_3 b^2-2\alpha_2\ln(a)b+2\alpha_1\ln(a)^2}{2b^2-4\alpha_1\beta_D^2}}}{\sqrt{b^2-2\alpha_1\beta_D^2}} \tag{8.48}$$

The probability of occurrence λ of a given limit state under analysis, i.e. the risk associated to that limit state, can then be obtained according to the classical reliability formulation presented in Eq. (8.1). By considering Eq. (8.48) written according to the following condensed form

$$\Pr\left(D > d\right) = \chi_1 \cdot e^{\chi_2 \ln(d)^2 + \chi_3 \ln(d) + \chi_4} \tag{8.49}$$

where χ_1, χ_2, χ_3 and χ_4 are defined as

$$\begin{cases} \chi_1 = \dfrac{b}{\sqrt{b^2 - 2\alpha_1 \beta_D^2}} \\ \chi_2 = \alpha_1 \left(\dfrac{\chi_1}{b}\right)^2 \\ \chi_3 = \left(\alpha_2 b - 2\alpha_1 \ln(a)\right)\left(\dfrac{\chi_1}{b}\right)^2 \\ \chi_4 = \left[\left(\dfrac{\alpha_2^2}{2} - 2\alpha_1 \alpha_3\right)\beta_D^2 + \alpha_1 \ln(a)^2 - \alpha_2 \ln(a) b + \alpha_3 b^2\right]\left(\dfrac{\chi_1}{b}\right)^2 \end{cases} \tag{8.50}$$

and assuming that C is represented by a lognormal random variable with a mean of the log of the data equal to μ_C and a standard deviation of the log of the data equal to β_C, the value of λ defined by Eq. (8.1) is obtained by solving:

$$\lambda = \int_{-\infty}^{+\infty} \chi_1 \cdot e^{\chi_2 \ln(y)^2 + \chi_3 \ln(y) + \chi_4} \cdot \frac{e^{-\frac{1}{2}\left(\frac{\ln(y) - \mu_C}{\beta_C}\right)^2}}{\sqrt{2\pi} \cdot y \cdot \beta_C} dy \tag{8.51}$$

By considering that $z = \ln(y)$, this integral can be rearranged to give:

$$\lambda = \int_{-\infty}^{+\infty} \chi_1 \cdot e^{\frac{\chi_6^2 - \chi_7 \cdot \chi_5}{2\chi_5}} \cdot \frac{e^{-\frac{1}{2}\left(\frac{z - \chi_6/\chi_5}{\sqrt{1/\chi_5}}\right)^2}}{\sqrt{2\pi} \cdot \beta_C} dz \tag{8.52}$$

where χ_5, χ_6 and χ_7 are defined as

$$\begin{cases} \chi_5 = \dfrac{1}{\beta_C^2} - \dfrac{2\alpha_1}{b^2 - 2\alpha_1 \beta_D^2} \\ \chi_6 = \dfrac{\alpha_2 b - 2\alpha_1 \ln(a)}{b^2 - 2\alpha_1 \beta_D^2} + \dfrac{\mu_C}{\beta_C^2} \\ \chi_7 = \dfrac{\mu_C^2}{\beta_C^2} - \dfrac{\left(\alpha_2^2 - 4\alpha_1 \alpha_3\right)\beta_D^2 + 2\alpha_1 \ln(a)^2 - 2\alpha_2 \ln(a) b + 2\alpha_3 b^2}{b^2 - 2\alpha_1 \beta_D^2} \end{cases} \tag{8.53}$$

The integral defined by Eq. (8.52) can be seen to be equivalent to

$$\lambda = \frac{\chi_1 \cdot \sqrt{1/\chi_5}}{\beta_C} \cdot e^{\frac{\chi_6^2 - \chi_7 \cdot \chi_5}{2\chi_5}} \int_{-\infty}^{+\infty} \cdot \frac{e^{-\frac{1}{2}\left(\frac{z - \chi_6/\chi_5}{\sqrt{1/\chi_5}}\right)^2}}{\sqrt{2\pi} \cdot \sqrt{1/\chi_5}} dz \tag{8.54}$$

which then simplifies into

$$\lambda = \frac{\chi_1 \cdot \sqrt{1/\chi_5}}{\beta_C} \cdot e^{\frac{\chi_6^2 - \chi_7 \cdot \chi_5}{2\chi_5}} \tag{8.55}$$

since the integral of Eq. (8.54) is that of a normal distribution with mean χ_6/χ_5 and standard deviation $\sqrt{1/\chi_5}$, which is equal to one. By replacing the values of χ_5, χ_6 and χ_7 in Eq. (8.55) by those defined in Eq. (8.53), λ is then

$$\lambda = \frac{b \cdot e^{\frac{2\alpha_1 \mu_C^2 + \left(2\alpha_2 b - 4\alpha_1 \ln(a)\right)\mu_C + \left(\alpha_2^2 - 4\alpha_1 \alpha_3\right)\left(\beta_D^2 + \beta_C^2\right) + 2\alpha_1 \ln(a)^2 - 2\alpha_2 \ln(a) b + 2\alpha_3 b^2}{2b^2 - 4\alpha_1\left(\beta_D^2 + \beta_C^2\right)}}}{\sqrt{b^2 - 2\alpha_1\left(\beta_D^2 + \beta_C^2\right)}} \tag{8.56}$$

8.3.2.2 Alternative closed form risk assessment method with a new seismic hazard function and a new demand evolution expression

The alternative closed form risk assessment method that is proposed in the following involves the use of a demand evolution expression that may be more adequate when dealing with force-based EDPs. In this approach, *D* and *C* are assumed to be normally distributed random variables referring to a scalar EDP. Also, it is assumed that demand *D* can be expressed as a function of the selected IM by an expression similar to Eq. (8.15):

$$D = a \ln(x) + b + \varepsilon \tag{8.57}$$

where ε is a normal random variable with zero mean and a standard deviation equal to σ_D. In this case, the term $a \ln(x) + b$ can be seen to represent the evolution of the mean value $\overline{D}$ of the demand. Based on Eq. (8.57), the term $\ln(x)$ can be generally defined as:

$$\ln(x) = k_1 + k_2 \varepsilon \tag{8.58}$$

in which k_1 and k_2 are defined as

$$\begin{cases} k_1 = \dfrac{D - b}{a} \\ k_2 = -\dfrac{1}{a} \end{cases} \tag{8.59}$$

Assuming a seismic hazard function $H(x)$ defined by Eq. (8.39), when replacing the $\ln(x)$ terms by Eq. (8.58), one obtains Eq. (8.40) and, consequently, Eq. (8.41), where k_3, k_4 and k_5 are now defined as

$$\begin{cases} k_3 = \dfrac{\alpha_1}{a^2} \\ k_4 = \dfrac{-2\alpha_1 D + 2\alpha_1 b - \alpha_2 a}{a^2} \\ k_5 = \dfrac{\alpha_1 D^2 - 2\alpha_1 b D + \alpha_2 a D + \alpha_1 b^2 - \alpha_2 a b + \alpha_3 a^2}{a^2} \end{cases} \tag{8.60}$$

The unconditioned probability $\Pr(D > d) = 1 - F_D(d)$ can then be obtained by first conditioning it to the random variable ε and by solving the integral defined by Eq. (8.43), in which β_D should be substituted by σ_D. Using an approach similar to that of the previous case to solve Eq. (8.43), $\Pr(D > d)$ is found to be

$$\Pr(D > d) = \frac{\sqrt{1/k_6}}{\sigma_D} e^{\frac{2k_5 k_6 + k_4^2}{2k_6}} \tag{8.61}$$

in which k_6 is defined by

$$k_6 = \frac{1}{\sigma_D^2} - \frac{2\alpha_1}{a^2} \tag{8.62}$$

By replacing the values of k_4, k_5 and k_6 in Eq. (8.61) by those defined by Eqs. (8.60) and (8.62), $\Pr(D > d)$ is then

$$\Pr(D > d) = \frac{a \cdot e^{\frac{2\alpha_1 d^2 + (2\alpha_2 a - 4\alpha_1 b)d + (\alpha_2^2 - 4\alpha_1 \alpha_3)\sigma_D^2 + 2\alpha_1 b^2 - 2\alpha_2 a b + 2\alpha_3 a^2}{2a^2 - 4\alpha_1 \sigma_D^2}}}{\sqrt{a^2 - 2\alpha_1 \sigma_D^2}} \tag{8.63}$$

By considering Eq. (8.63) written according to the following condensed form

$$\Pr(D > d) = \chi_1 \cdot e^{\chi_2 d^2 + \chi_3 d + \chi_4} \tag{8.64}$$

where χ_1, χ_2, χ_3 and χ_4 are defined as

$$\begin{cases} \chi_1 = \dfrac{a}{\sqrt{a^2 - 2\alpha_1 \sigma_D^2}} \\ \chi_2 = \alpha_1 \left(\dfrac{\chi_1}{a} \right)^2 \\ \chi_3 = \left(\alpha_2 a - 2\alpha_1 b \right) \left(\dfrac{\chi_1}{a} \right)^2 \\ \chi_4 = \left[\left(\dfrac{\alpha_2^2}{2} - 2\alpha_1 \alpha_3 \right) \sigma_D^2 + \alpha_1 b^2 - \alpha_2 a b + \alpha_3 a^2 \right] \left(\dfrac{\chi_1}{a} \right)^2 \end{cases} \tag{8.65}$$

and assuming that C is represented by a normal random variable with mean μ_C and standard deviation equal to σ_C, the value of λ defined by Eq. (8.1) is obtained by solving:

$$\lambda = \int_{-\infty}^{+\infty} \chi_1 \cdot e^{\chi_2 z^2 + \chi_3 z + \chi_4} \cdot \frac{e^{-\frac{1}{2}\left(\frac{z - \mu_C}{\sigma_C} \right)^2}}{\sqrt{2\pi} \cdot \sigma_C} dz \tag{8.66}$$

As for the previous case, solving the corresponding integral yields an expression in the form of Eq. (8.55) in which β_C should be substituted by σ_C, and parameters χ_5, χ_6 and χ_7 are defined as

$$\begin{cases} \chi_5 = \dfrac{1}{\sigma_C^2} - \dfrac{2\alpha_1}{a^2 - 2\alpha_1 \sigma_D^2} \\ \chi_6 = \dfrac{\alpha_2 a - 2\alpha_1 b}{a^2 - 2\alpha_1 \sigma_D^2} + \dfrac{\mu_C}{\sigma_C^2} \\ \chi_7 = \dfrac{\mu_C^2}{\sigma_C^2} - \dfrac{\left(\alpha_2^2 - 4\alpha_1 \alpha_3 \right) \sigma_D^2 + 2\alpha_1 b^2 - 2\alpha_2 a b + 2\alpha_3 a^2}{a^2 - 2\alpha_1 \sigma_D^2} \end{cases} \tag{8.67}$$

By replacing the values of χ_5, χ_6 and χ_7 in Eq. (8.55) by those defined by Eq. (8.67), λ is then

$$\lambda = \frac{a \cdot e^{\frac{2\alpha_1 \mu_C^2 + \left(2\alpha_2 a - 4\alpha_1 b \right) \mu_C + \left(\alpha_2^2 - 4\alpha_1 \alpha_3 \right) \left(\sigma_D^2 + \sigma_C^2 \right) + 2\alpha_1 b^2 - 2\alpha_2 a b + 2\alpha_3 a^2}{2a^2 - 4\alpha_1 \left(\sigma_D^2 + \sigma_C^2 \right)}}}{\sqrt{a^2 - 2\alpha_1 \left(\sigma_D^2 + \sigma_C^2 \right)}} \tag{8.68}$$

8.3.2.3 Tentative development of an additional closed form risk assessment method

The additional closed form risk assessment method that is attempted to be developed in the following involves the use of a demand evolution expression similar to Eq. (8.16) that is believed to be more adequate for force-based EDPs. However, as will be

shown, the mathematical tractability of this approach is impaired by several issues which are analysed and discussed. Proposals trying to overcome these issues are also addressed. In this approach, D and C are also assumed to be normally distributed random variables referring to a scalar EDP.

The proposed approach assumes that demand D can be expressed as a function of the selected IM by:

$$D = a \cdot e^{(-k \cdot x)} + b + \varepsilon \tag{8.69}$$

where ε is a normal random variable with zero mean and a standard deviation equal to σ_D. Variable x can then be defined as:

$$x = \frac{-1}{k} \ln\left(\frac{D - \varepsilon - b}{a}\right) \tag{8.70}$$

By assuming that, for some reference period under consideration, the seismic hazard function $H(x)$ is adequately represented by

$$H(x) = \alpha_1 \cdot e^{\alpha_2 \cdot x} + \alpha_3 \cdot e^{\alpha_4 \cdot x} \tag{8.71}$$

where α_1, α_2, α_3 and α_4 are parameters to be fitted using existing probabilistic seismic hazard data, when replacing the x terms of Eq. (8.71) by Eq. (8.70), one obtains

$$H(D) = \alpha_1 \cdot e^{\frac{-\alpha_2}{k} \ln\left(\frac{D-\varepsilon-b}{a}\right)} + \alpha_3 \cdot e^{\frac{-\alpha_4}{k} \ln\left(\frac{D-\varepsilon-b}{a}\right)} \tag{8.72}$$

which simplifies into

$$H(D) = \alpha_1 \cdot \left(\frac{D - \varepsilon - b}{a}\right)^{-\alpha_2/k} + \alpha_3 \cdot \left(\frac{D - \varepsilon - b}{a}\right)^{-\alpha_4/k} \tag{8.73}$$

The unconditioned probability $\Pr(D > d) = 1 - F_D(d)$ can then be obtained by first conditioning it to the random variable ε and by solving the integral defined by:

$$\Pr(D > d) = \int_{-\infty}^{+\infty} \left[\alpha_1 \cdot \left(\frac{d - \varepsilon - b}{a}\right)^{-\alpha_2/k} + \alpha_3 \cdot \left(\frac{d - \varepsilon - b}{a}\right)^{-\alpha_4/k} \right] \cdot \frac{e^{-\frac{\varepsilon^2}{2\sigma_D^2}}}{\sqrt{2\pi} \cdot \sigma_D} d\varepsilon \tag{8.74}$$

By analysing Eq. (8.74), it can be seen that it is not able to be solved analytically. In an attempt to overcome this situation, alternative formulations were sought to approximate the normal PDF of ε. One of the possibilities pursued was to approximate the PDF of ε by the PDF of a symmetric triangular distribution (Scherer *et al.*, 2003). According to Scherer *et al.* (2003), this approximation allows for suitable mathematical tractability and provides adequate results within 98.5% of the range of the approximated normal PDF. The PDF f_{Tr} of the triangular distribution is defined by Law and Kelton (2000):

$$f_{Tr}(x)=\begin{cases}\dfrac{2(x-u_1)}{(u_3-u_1)(u_2-u_1)} & u_1\le x\le u_2\\[2ex] \dfrac{2(u_3-x)}{(u_3-u_1)(u_3-u_2)} & u_2< x\le u_3\\[2ex] 0 & \textit{otherwise}\end{cases} \tag{8.75}$$

where parameters u_1, u_2 and u_3 are the minimum value, the most likely value (and also the midpoint of the range of the distribution for the symmetric case), and the maximum value, respectively. In order to simulate the required normal distribution, parameters u_1, u_2 and are defined by Scherer *et al.* (2003) as

$$\begin{cases}u_1=-\sqrt{6}\,\sigma_D\\ u_2=0\\ u_3=\sqrt{6}\,\sigma_D\end{cases} \tag{8.76}$$

Therefore, using Eqs. (8.75) and (8.76) to approximate the normal PDF, Eq. (8.74) now becomes

$$\begin{aligned}\Pr(D>d)=&\int_{-\sqrt{6}\,\sigma_D}^{0}\left[\alpha_1\cdot\left(\frac{d-\varepsilon-b}{a}\right)^{-\alpha_2/k}+\alpha_3\cdot\left(\frac{d-\varepsilon-b}{a}\right)^{-\alpha_4/k}\right]\cdot\frac{\sqrt{6}\,\sigma_D+\varepsilon}{6\sigma_D^2}d\varepsilon\ +\\ &\int_{0}^{\sqrt{6}\,\sigma_D}\left[\alpha_1\cdot\left(\frac{d-\varepsilon-b}{a}\right)^{-\alpha_2/k}+\alpha_3\cdot\left(\frac{d-\varepsilon-b}{a}\right)^{-\alpha_4/k}\right]\cdot\frac{\sqrt{6}\,\sigma_D-\varepsilon}{6\sigma_D^2}d\varepsilon\end{aligned} \tag{8.77}$$

After some rearrangements Eq. (8.77) can be written as

$$\begin{aligned}\Pr(D>d)=&\int_{-\sqrt{6}\,\sigma_D}^{0}\left[k_1\cdot(k_2+\varepsilon)^{-\alpha_2/k}+k_3\cdot(k_2+\varepsilon)^{-\alpha_4/k}\right]\cdot(k_4+\varepsilon)d\varepsilon\ +\\ &\int_{0}^{\sqrt{6}\,\sigma_D}\left[k_1\cdot(k_2+\varepsilon)^{-\alpha_2/k}+k_3\cdot(k_2+\varepsilon)^{-\alpha_4/k}\right]\cdot(k_4-\varepsilon)d\varepsilon\end{aligned} \tag{8.78}$$

where k_1, k_2, k_3 and k_4 are given by

$$\begin{cases}k_1=\dfrac{\alpha_1|a|^{\frac{\alpha_2}{k}}}{6\sigma_D^2}\\ k_2=b-d\\ k_3=\dfrac{\alpha_3|a|^{\frac{\alpha_4}{k}}}{6\sigma_D^2}\\ k_4=\sqrt{6}\,\sigma_D\end{cases} \tag{8.79}$$

Since it is known that $a < 0$, the term $|a|$ is considered in Eq. (8.79) instead. Otherwise k_1 and k_2 would have values which are not real numbers. The sign of *a* is then incorporated in the term $k_2 + \varepsilon$.

When analysing Eq. (8.78), it can be shown that its analytical solution exists but will lead to an expression with eight additive terms. Following this step, the integral defined by Eq. (8.1) also needs to be solved in order to obtain the value of λ. It can be shown that such integral is not able to be solved analytically either. In this case, an approximation to the normal PDF of *C* can also be established using the PDF of a symmetric triangular distribution, which enables the referred integral to be solved analytically. Still, such calculations will lead to an expression with thirty-two additive terms, in which some of them have a considerable size. Given the reduced practical applicability of such type of solution, its presentation is omitted herein.

As an alternative attempt to solve Eq. (8.74), the polynomial expansion for the standard normal PDF referred by Mernagh (2006) and defined by

$$f_{poly}(x) = \frac{1}{\sqrt{2\pi}} \sum_{i=0}^{\infty} \frac{(-1)^i x^{2i}}{2^i (i!)} \tag{8.80}$$

was also analysed. This expansion was found to yield accurate results if enough terms are considered. For example, to obtain adequate results for the interval $-2.5 \le x \le 2.5$, the first twelve terms have at least to be considered, thus rendering this alternative of little practical use also within the current context.

Alternatively, the applicability of the normal PDF approximation using a modified cosine distribution was also analysed. This suggestion was first proposed by Raab and Green (1961) for the case of the standard normal PDF and was later revisited by Warsza and Korczynski (2010) which rewrote this approximation for general normal PDFs. For the case of Eq. (8.74), the normal PDF would be approximated by

$$f_{\cos}(x) = \begin{cases} A + A \cdot \cos(2\pi A \cdot x) & -\dfrac{1}{2A} \le x \le \dfrac{1}{2A} \\ 0 & \textit{otherwise} \end{cases} \tag{8.81}$$

where parameter *A* can be related to σ_D by

$$A = \frac{1}{2\sigma_D \sqrt{2\pi}} \tag{8.82}$$

When using the approximation defined by Eq. (8.81) to solve Eq. (8.74), it can be shown that its analytical solution exists but will lead to an expression far too complex to be of use, since it involves the Incomplete Gamma function and complex numbers.

Given the lack of adequacy of the solutions that were found for Eq. (8.74), the development of a risk assessment expression similar to Eqs. (8.56) and (8.68) for the case where demand is represented by Eq. (8.69) was abandoned.

8.3.2.4 Application example

To illustrate the applicability of Eqs. (8.56) and (8.68), the probability of occurrence of several limit states is determined for section 2 of the IRREG6 structure presented in Fig. 8.3. The selected limit states are those of the example presented in Section 8.3.1.2. In this application example, limit state capacities were only considered according to the previously referred Case 4 (see Section 8.3.1.2.1) that includes the variability of the capacity due to both the randomness of the material properties and the modelling error. Furthermore, these limit state probabilities of occurrence were also analysed using the SAC/FEMA method, Eq. (8.9), in order to allow for a direct comparison of the performance of Eqs. (8.56) and (8.68).

To apply these procedures, the hazard curves defined by the SAC/FEMA approach and by the methods proposed herein, Eqs. (8.2) and (8.39), were fitted to the hazard data of the considered seismic scenario. The considered hazard data for the reference periods of one year and fifty years are presented in Figs. 8.8a) and b), respectively, in log-log scale, along with the fitted hazard curves. As expected, the linear form (in log-log scale) of the SAC/FEMA hazard curve proposal only provides an adequate fit over a reduced part of the hazard data, while Eq. (8.39) can be seen to provide an overall much better fit.

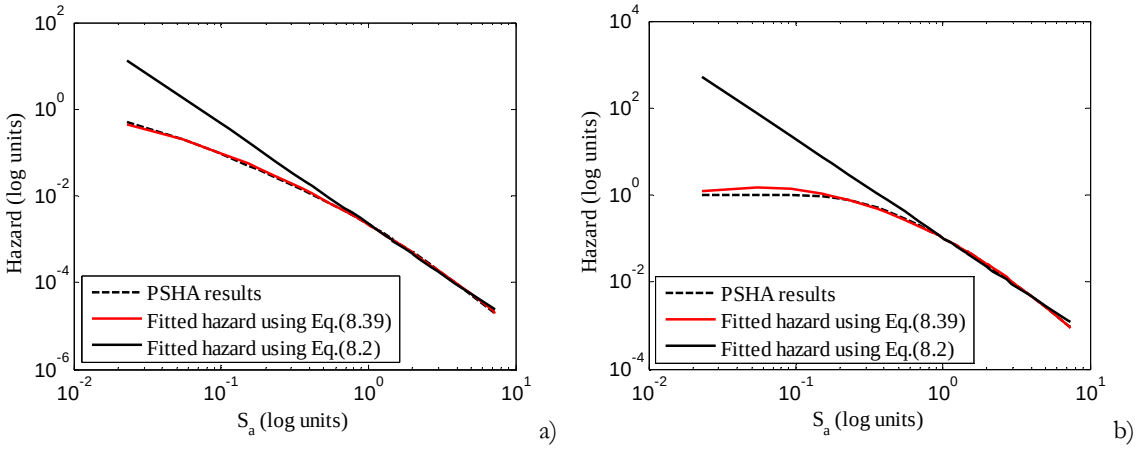

Figure 8.8. Probabilistic seismic hazard analysis (PSHA) results and fitted distribution for a reference period of 1 year (a) and a reference period of 50 years (b) using Eqs. (8.2) and (8.39).

In order to determine the probability of occurrence by Eqs. (8.9), (8.56) and (8.68) for the considered limit states, several demand and capacity parameters must be obtained using the demand data referred in Section 8.3.1.2.3. Namely, the fitting parameters involved

in the evolution of the median value $\hat{D}$ of the demand, Eqs. (8.4) and (8.35), and in the evolution of the mean value $\overline{D}$ of the demand, Eq. (8.57), must be defined. To determine these parameters, $\hat{D}$ and $\overline{D}$ values were computed for each IM level using the demand data obtained from the suite of fifty ground motions presented in Section 8.3.1.2.3. The values of $\overline{D}$ were determined using the logistic M-estimator proposed by Rousseeuw and Verboven (2002) applied to the demand data while the values of $\hat{D}$ were determined using the same estimator applied to the log of the demand data. This estimator was selected based on the findings and recommendations presented in Chapters 6 and 7.

To estimate parameter β_D required for Eqs. (8.9) and (8.56) that represents the dispersion of the demand data, the following situations were considered:

- For the analysis of the DL chord rotation limit state, β_D was considered to be the average of the dispersion of the demand obtained for the first three IM levels. For each IM level, the dispersion was determined by computing the standard deviation of the log of the demand data obtained from the suite of fifty ground motions using the τ-scale truncated standard deviation defined by Yohai and Zamar (1988). This estimator was selected based on the findings and recommendations presented in Chapter 7.

- For the analysis of the SD and NC chord rotation limit states, β_D was considered to be the average of the dispersion of the demand obtained for the last three IM levels. For each IM level, the dispersion was determined as previously referred using the τ-scale truncated standard deviation defined by Yohai and Zamar (1988).

- For the analysis of the NC shear force limit state, β_D was considered to be the average of the dispersion of the demand obtained for all the IM levels. For each IM level, the dispersion was determined as previously referred using the τ-scale truncated standard deviation defined by Yohai and Zamar (1988).

Parameter σ_D, that is required for the analysis of the NC shear force limit state by Eq. (8.68), was considered to be the average of the standard deviation of the demand obtained for all the IM levels. For each IM level, the standard deviation was determined by computing the standard deviation of the demand data obtained from the suite of fifty ground motions using the τ-scale truncated standard deviation proposed by Yohai and Zamar (1988).

The capacity parameters μ_C and β_C required for Eq. (8.56), which represent the mean and the standard deviation of the log of the previously defined Case 4 capacity data, were obtained using the logistic M-estimator proposed by Rousseeuw and Verboven (2002) and the τ-scale truncated standard deviation proposed by Yohai and Zamar (1988),

respectively. For the case of Eq. (8.9), the capacity parameter β_C was obtained using the previous approach while parameter $\hat{C}$ is defined using the relation

$$\hat{C} = e^{\mu_C} \tag{8.83}$$

in which μ_C is also obtained by the previous approach. The capacity parameters μ_C and β_C required for Eq. (8.68), which represent the mean and the standard deviation of the Case 4 capacity data, were obtained using the logistic M-estimator proposed by Rousseeuw and Verboven (2002) and the τ-scale truncated standard deviation proposed by Yohai and Zamar (1988), respectively.

After defining all the required parameters, Eqs. (8.9), (8.56) and (8.68) were applied to determine the probability of occurrence of the referred limit states for section 2. The results obtained for the reference periods of one year and fifty years are presented in Table 8.6 where Methodology 2 refers to the results from the methods proposed herein (Eqs. (8.56) or (8.68), depending on the limit state). As can be observed from these results, the SAC/FEMA yields larger risk values for all the cases analysed. This situation is somehow expected since the SAC/FEMA hazard curve overestimates significantly part of the seismic hazard data (Fig. 8.8). Although some of the SAC/FEMA results could be improved by performing a new fit of the hazard curve (as referred in Section 8.2), such approach was not selected to provide a clear view of the one-to-one application of both methods. Furthermore, by comparing the results of Table 8.6 to those of Table 8.5 for section 2, Methodology 2 can be seen to provide risk results that are very close to the corresponding μ_{LS} values. Therefore, it is considered that such closeness of the risk values validates the applicability of both Methodology 1 and Methodology 2, while indicating that the SAC/FEMA results are expected to generally overestimate risk.

Table 8.6. Risk determined by Methodology 2 and by the SAC/FEMA method, for chord rotation and shear force demands of section 2 considering capacities defined according to Case 4.

Demand	LS	Ref. per. = 1 year		Ref. per. = 50 years	
		Methodology 2	SAC/FEMA	Methodology 2	SAC/FEMA
chord rotation at section 2	NC	4.61E-04	4.90E-03	1.16E-02	1.90E-01
	SD	1.17E-03	2.14E-02	2.54E-02	8.05E-01
	DL	8.65E-05	9.44E-05	4.10E-03	4.53E-03
shear force at section 2	NC	2.03E-06	1.16E-05	9.23E-05	5.98E-04

8.4 Additional comments about the proposed procedures and the reliability of systems

The limit state probability of structural systems, such as buildings or bridges, as a whole is the performance measure that is most closely related to social expectations of safety or serviceability. It is known that the reliability of the structural system is, in most cases, higher than that of its individual components (Moses, 1990; Hendawi and Frangopol, 1994) but to a degree of complex prediction which depends, among other things, on the structural redundancy, configuration and inelastic behaviour of the components.

Although presented for the limit state probability assessment of components such as beams or columns, the proposed methodologies can easily be applied to global measures of structural performance such as maximum inter-storey drift over the height of the structure or storey shear forces (Medina and Krawinkler, 2004). In this case, the limit state probability becomes a measure of global performance instead of a local one, therefore addressing the system reliability problem. However, such approach is an indirect one, since it does not involve the identification of the relevant mechanisms contributing to the system limit state probability, but instead relies on the choice of an adequate demand/damage measure that is efficiently related to the global response. Nevertheless, this approach allows for the evolution of both performance based assessment and performance based design methods towards new directions of much interest (Medina and Krawinkler. 2004; Krawinkler *et al.*, 2006).

When addressing the system reliability problem by the approach which consists in the identification and combination of the relevant mechanisms that contribute to a certain limit state probability, one has to keep in mind the subjectivity of the selection of such mechanisms. In this case, identification of the more significant mechanisms is a task preliminary to risk analysis from which the value of the computed limit state probability value will always be dependent on (Pinto *et al.*, 2004).

In general, the system reliability model is made of single component mechanisms, e.g. the flexural or shear limit state of a beam or column, and of multiple component mechanisms, e.g. soft-storey or beam-sway mechanisms. The latter combine a set of components (beams and/or columns) that must all be in the same state, e.g. yielding, in order to be able to develop the mechanism. In most cases, such mechanisms can be seen as a parallel arrangement of individual components. Although an extensive discussion on how to combine the different mechanism probabilities to obtain the system reliability is beyond the scope of this work, one can suggest the simplification often made that implies independency between the mechanisms (Thoft-Christensen and Murotsu, 1986). Within this approach for the reliability of systems, it can be seen that the proposed procedure addresses the limit state probability of the single component mechanisms. Nonetheless, for the case of multiple component, the proposed procedure may also be used to obtain the limit state probability of the single components for posterior combination to obtain the

limit state probability of the mechanism, e.g. in the case of fully correlated single components (Thoft-Christensen and Murotsu, 1986).

8.5 Conclusions and final remarks

Two methodologies that establish analytical expressions to assess limit state exceedance probabilities of structural components were presented. The definition of these expressions is based on the probabilistic representation of the ground motion hazard and on suitable expressions characterizing the evolution of structural demand for increasing levels of earthquake intensity. In what regards the former, the proposed methodologies adopt different approaches: Methodology 1 uses extreme-type probabilistic distributions for ground motion hazard representation, while Methodology 2 involves an approximate expression that exhibits a clear advantage over the model adopted by the SAC/FEMA method. With respect to the evolution of structural demand with increasing earthquake intensity, distinction is made between deformation-based and force-based structural parameters in the definition of such relations. While the considered functional form for deformation-based demand is founded on the results of existing studies, the proposed force-based demand expressions were defined on the basis of an in-depth analysis of force-based structural demand evolutions, namely of shear force demand. Two functional forms were proposed for shear force demand evolutions: one for smoother evolutions based on a logarithmic function and one for bilinear-type evolutions based on an inverted exponential function. In the context of Methodology 1, the development of analytical expressions for the assessment of limit state exceedance probabilities was able to incorporate both proposals for the shear force demand evolution. On the other hand, the development of expressions in the context of Methodology 2 was not able to account for the bilinear-type evolution.

An application of the proposed methodologies to the assessment of different limit state probabilities of members from a RC structure was presented to illustrate their applicability. The limit states and their corresponding capacities were defined by scalar EDPs (member chord rotation and shear force) according to the proposals found in EC8-3. The application example of Methodology 1 addressed several issues related to the uncertainty of the component limit state capacities. Four different scenarios involving the variability of material properties and/or the modelling error associated to the limit state capacity expressions were analysed. Furthermore, issues related to the probabilistic consistency and computational efficiency of the proposed procedure were also addressed. With respect to Methodology 2, the presented application example only addressed part of the example of Methodology 1 in order to validate the results obtained.

Due to their generalized formulations, the proposed procedures were found suitable to assess the probability of exceedance of any desired component limit state with direct

inclusion of the ground motion hazard information, considering any demand variable and ground motion IM, without the need to compute the fragility curve. Furthermore, the presented application examples illustrated the simplicity of the proposed procedures.

In the overall, the global analysis of the results of the proposed example applications indicated that considering the uncertainty of the limit state capacities increases significantly the estimate of the probability of exceedance of the limit states. Furthermore, for the cases that were analysed, the modelling error of the limit state capacity expressions was seen to be the main factor governing both the estimate of the probability of exceedance of the limit state and its variability. With the exception of a few situations, the effects of the variability of the material properties were found to be small. When comparing results obtained when record-to-record variability was the only source of uncertainty to those where the modelling error was also considered, the effects of the latter were seen, in many cases, to at least duplicate the variability of the probability of exceedance. Therefore, for such cases, the variability introduced by the modelling error was seen to be, at least, 70% larger than that of the record-to-record variability. Given the significance of the referred modelling error, further research efforts should concentrate on developing alternative formulations for the limit state capacities to obtain expressions providing capacity estimates with less uncertainty.

Chapter 9
Probabilistic performance analysis of existing buildings under earthquake loading

9.1 Introduction

Probabilistic seismic safety assessment methods are intrinsic to the conceptual framework established by current Performance-Based Earthquake Engineering (PBEE) methodologies. This framework involves key aspects such as the use of adequate methods of analysis to determine building behaviour and the definition of quantifiable targets to measure performance. In this context, the ATC-63 probabilistic methodology (Kircher and Heintz, 2008; Deierlein *et al.*, 2008; ATC, 2009) for the assessment of building safety against collapse due to earthquake loading is one of the most recent proposals. The methodology involves incremental dynamic analysis (IDA) (Vamvatsikos and Cornell, 2002) and probabilistic procedures to evaluate seismic fragility margins of the building system against collapse and to calibrate appropriate values of design-related parameters such as the behaviour factor and other parameters affecting the response of the building. Although the main objective of this approach is to evaluate the seismic performance of new structures, in order to determine the effectiveness of design rules established by current codes and standards, this probabilistic methodology can also be adapted to assess the safety of existing structures against collapse (ATC, 2009).

With respect to existing constructions, the recent widespread interest in methodologies addressing their assessment and retrofit has led to the development of several normative documents and guidelines for the assessment of their seismic performance (e.g. see ATC, 1996; ASCE, 2003; EC8-3 2005; OPCM 3431, 2005; NZSEE, 2006; ASCE, 2007; NTC, 2008). The assessment methods proposed in these documents consist, essentially, of deterministic approaches involving the evaluation of the seismic response for different limit states which are quantitatively established by limit values of local (member level) demand parameters. Although these methods are expected to be

reliable, since they may include modelling, analysis and verification procedures more detailed than those commonly considered in the design of new structures, a probabilistic validation of such safety assessment approach appears to be essential to observe the adequacy of such procedures. Given these considerations, a probabilistic approach suitable for the evaluation of the seismic safety of existing structures following the concepts which are found in recently developed codes and standards is presented herein.

The proposed probabilistic methodology analyses the seismic safety of a building using global performance metrics to determine if its behaviour conforms to a given limit state. The considered performance metrics are the probability of occurrence λ of the limit state, the corresponding expected loss L_{sc} associated to the repair of the building, and the corresponding number and type of mechanisms that are developed and that establish possible scenarios for the occurrence of that limit state. The term *mechanism* is considered herein as referring to the occurrence of a limit state capacity in one or in a combination of several structural members. The consideration of these assessment parameters can be seen to widen the scope of the limit state definitions proposed in current codes since performance is now controlled using high-level parameters. Furthermore, the simultaneous development of different member or global (system level) limit state mechanisms can also be included. Moreover, it is also possible to use the proposed approach to validate the seismic safety assessment procedures for existing constructions which are available in current standards and codes. By analysing seismic safety according to the assumptions underlying such procedures, it is possible to determine the corresponding values of the referred global performance metrics which are then used to examine the adequacy of the code procedures.

The consideration of λ, L_{sc} and the occurrence of several mechanisms as global performance parameters for a given limit state can be seen to require an update of existing limit state descriptions. Based on some of the limitations identified from interpreting the limit state descriptions of the seismic safety assessment procedures proposed in Part 3 of Eurocode 8 (EC8-3) (EC8-3, 2005), alternative proposals are discussed to establish risk- and cost-related limit state definitions. These alternative proposals are then used to analyse the performance of two reinforced concrete (RC) structures using the proposed methodology and to evaluate the reliability of some of the EC8-3 procedures. It is noted that although EC8-3 is used as a reference, the issues raised by this analysis of the limit states extend beyond this code since similar limit states or performance levels are also considered by other international standards.

9.2 General analysis and interpretation of limit state definitions

The presented methodology addresses the seismic safety assessment of existing structures with respect to limit states other than global collapse. More specifically, the

methodology involves the probabilistic performance analysis of structures considering code-defined limit states which are usually associated to damage control, life safety or near collapse conditions. In order to identify some of the shortcomings about the limit state descriptions established by the seismic safety assessment procedures proposed by existing codes, a discussion addressing their interpretation is presented in the following. Although the limit state definitions considered for this analysis are those presented in EC8-3 (EC8-3, 2005), the issues raised extend beyond this code since other international standards also consider similar limit states or performance levels.

The descriptions of the performance requirements associated to the limit states defined by EC8-3 are initially formulated in qualitative terms and make reference to different damage states which can be related to the global behaviour of the structure (i.e. using a system level approach). Three damage states of increasing severity are established by EC8-3 and the corresponding limit states are termed: Damage Limitation (DL), Significant Damage (SD) and Near Collapse (NC). Although their general descriptions are defined globally at first, the safety verifications required to meet these limit states are established using parameters associated to the behaviour of structural members (i.e. using a local level approach). From Chapter 2, it is recalled that if the member mechanism associated to a given limit state is ductile, the general approach is to check if the member deformation demand is lower than an admissible deformation capacity. In the case where the member mechanism associated to a given limit state is of the brittle type, one has to check if the member capacity in terms of strength is not exceeded by the corresponding demand. The different limit state ductile and brittle mechanism capacities are obtained according to given expressions of empirical or semi-empirical nature defined by EC8-3 (EC8-3, 2005), e.g. see Chapter 2. In general terms, the safety of a given mechanism associated to a certain limit state is accepted when the damage variable ρ associated to the member verifies the condition

$$\rho = \frac{D}{C} \leq 1 \tag{9.1}$$

where D is the member mechanism demand and C is the limit state capacity of the mechanism.

From the point of view of the global safety of the structure, a literal interpretation of the EC8-3 procedures appears to indicate that compliance with a selected limit state is only accepted when all the individual structural members/sections meet their corresponding safety requirement. Depending on the selected limit state, this situation can be seen to be either excessively conservative or permissive. In this context, conservative or permissive states are considered to be referring to situations where the admissible deformation conditions are too low or too high, respectively. An example of a conservative case can be defined when considering the DL limit state, for which the maximum admissible member deformation is the yield chord rotation. In such case, if only one member demand is found

to exceed the yield deformation, and irrespective of which member, the whole building is considered to be nonconforming to this limit state. Based on this interpretation, one can argue that such condition is not easily correlated with a global limit state description that requires *the structure to be only lightly damaged, with structural elements prevented from significant yielding and retaining their strength and stiffness properties* (EC8-3, 2005) and that indicates the possibility of having more than one yielding section. However, the number and type of sections for which this situation is admissible is not able to be inferred from the description.

When analysing the limit state of SD, it is possible to establish another example scenario for which the code interpretation of the limit state might now be seen as too permissive. For a given structure, when comparing the situation where there is only one section with a ρ value above 1.0, along with a number of sections where ρ is in the range 0.85-0.95, with the situation where there is only a significant number of sections with ρ values in the range 0.85-0.95, the safety assessment according to the code proposal implies the latter case to be conforming to the limit state, while the former is not. Based on the description of the SD limit state proposed by EC8-3, which refers, among other aspects, that *the structure will be significantly damaged and likely to be uneconomic to repair* (EC8-3, 2005), one can argue that, given the high values of ρ observed in both situations, their levels of damage are expected to be similar. Therefore, from an economic point of view, both cases could be seen as equivalent.

With respect to the limit state of NC, EC8-3 refers, among other aspects, that *the structure will be heavily damaged, with low residual lateral strength and stiffness* (EC8-3, 2005). Since the structure is expected to remain standing after a severe earthquake, the NC limit refers to a state of the structure that precedes global collapse. However, it is believed that its level of damage renders the building uneconomic to repair. For this limit state, the EC8-3 verification procedure accounts only for failure prevention at the section level and does not contemplate the potential development of global yield mechanisms. Following the definition proposed in Jalayer *et al.* (2007), the development of a yield mechanism corresponds to a situation involving the yielding of several sections (with different levels of inelastic demand) that forms a structural configuration having a significantly reduced lateral stiffness. As can be seen, this type of global structural behaviour fits within the general description of the NC limit state proposed by EC8-3, but the corresponding safety verifications do not refer the possibility of contemplating such mechanisms. With respect to the local failure prevention situation, it is also referred that EC8-3 makes no distinction between column and beam failure. It is seen to be generally accepted (e.g. see Pinto *et al.*, 2004; Deierlein and Haselton, 2005; Jalayer *et al.*, 2007; Fajfar and Dolšek, 2011) that column failure (either by reaching its deformation or shear force capacity) is a more severe scenario than that of beam failure. Hence, the safety assessment results obtained from the

EC8-3 procedure can be considered to be conservative if ρ values above 1.0 only occur on beams.

Given these example situations, it is believed that compliance to a given limit state should be connected to acceptance measures of wider scope that would be able to include different proposals to represent that limit state (e.g. a variable number of accepted sections in yield or a variable range of acceptable damage, depending on the structure) as well as to provide a better correlation with the global behaviour of the structure. A description of a seismic performance assessment methodology of this type is addressed in the following.

9.3 Probabilistic performance analysis methodology

9.3.1 General overview of the methodology

To analyse building performance for a given limit state, the proposed methodology uses the probability of occurrence λ of the limit state, the corresponding loss L_{sc} associated to the repair of the building, and the corresponding number of structural sections n_{LS} where the limit state mechanism occurs. By defining a value for n_{LS}, one establishes a possible scenario for the occurrence of a given limit state. The λ and L_{sc} performance metrics of each of the m_{sc} considered scenarios are then combined to obtain a global performance value representing the expected loss EL over a given reference period of time which can be defined by:

$$EL = \sum_{i=1}^{m_{sc}} \lambda_i \cdot L_{sc,i} \tag{9.2}$$

Finally, the EL value can be compared with an admissible limit EL_{adm} defined by:

$$EL_{adm} = \lambda_{adm} \cdot L_{sc\,adm} \tag{9.3}$$

where λ_{adm} and $L_{sc\,adm}$ are global acceptance thresholds defined for λ and L_{sc}. The value of λ_{adm} can be based on proposals recommended by existing standards and other technical documents (ISO 2394, 1998; JCSS, 2001b; DOE, 2002; Diamantidis and Bazzurro, 2007; ISO 13822, 2010; Vrouwenvelder and Scholten, 2010), while the value of $L_{sc\,adm}$ can be set, for example, by the building owner.

The value of λ is estimated by

$$\lambda = \int_0^{\infty} p_f(x) \cdot \left| \frac{dH(x)}{dx} \right| dx \tag{9.4}$$

where $H(.)$ is the earthquake hazard curve defined in terms of a selected earthquake intensity measure (IM) and $p_f(.)$ is the fragility curve representing the probability of exceeding a given state of performance conditional to a certain value of the IM. The considered formulation of the fragility curve is similar in nature to the IM-based approach referred by Ibarra *et al.* (2002), which is also the basis for the ATC-63 methodology, but it is used for limit states other than collapse. With respect to the expected value of the loss L_{sc}, its quantification is carried out using the storey-based approach proposed by Ramirez and Miranda (2009).

Although the potential total loss due to damage from earthquakes L_{tot} can be formulated in order to include different types of direct costs (costs due to structural damage, to non-structural damage or due to loss of contents) and indirect costs (costs due to business interruption, or due to injuries and fatalities), it is not straightforward to formulate all of them as a function of a unique engineering demand parameter (EDP) in order to simplify the quantification of L_{tot}. For example, depending on the type of non-structural element, damage and costs can be more easily correlated to inter-storey drift or to floor acceleration levels (Foltz, 2004). Furthermore, since most of the indirect costs can be considered to be unique for each building, this situation requires an extensive and updated inventory which may not be available for the seismic safety analysis. In light of these considerations, the use of a simplified loss model that only addresses losses due to structural and non-structural damage, represented by L_{sc}, is suggested instead.

When analysing the evolution of λ and L_{sc} for increasing values of the number of structural sections n_{LS} where a given mechanism occurs (which can be seen as a proxy for the behaviour of the building), it can be seen that λ and L_{sc} have opposite evolution trends (Fig. 9.1). When n_{LS} increases, λ decreases since higher intensity ground motions (with lower probability of occurrence) are required to reach the limit state capacity at a larger number of sections. On the other hand, the value of L_{sc} increases since admitting that a larger number of sections can reach the EDP capacity also leads to higher levels of global building damage. Figure 9.1 also shows the evolution of EL which, as expected, is seen to increase as n_{LS} increases. Based on the value set for the EL_{adm} restriction, it is then possible to establish the admissible building performance which corresponds to the largest value of n_{LS} that conforms with EL_{adm}.

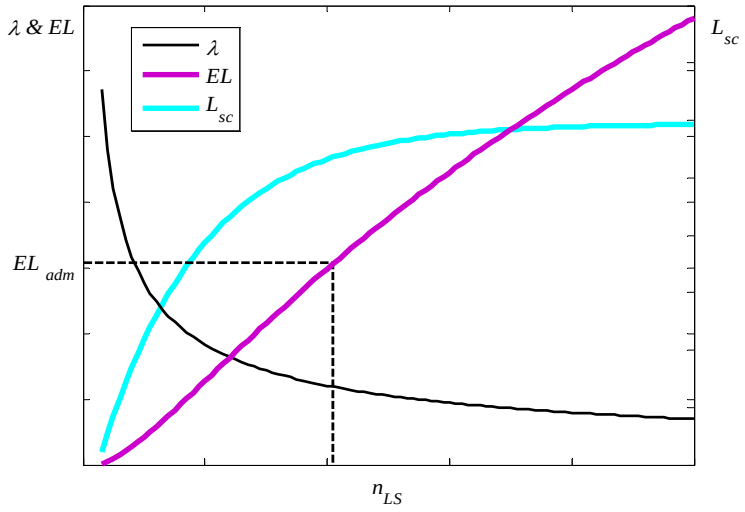

Figure 9.1. Evolution of λ, L_{sc} and EL for increasing values of n_{LS}.

9.3.2 Estimating the limit state fragility curve by using the IM-based approach

Considering that a suitable earthquake hazard curve defined in terms of the selected earthquake IM is available, the quantification of the probability of occurrence λ of a given limit state according to Eq. (9.4) requires the adequate definition of the fragility curve p_f. The determination of p_f involves the characterization of the structural behaviour, usually obtained by the numerical simulation of a detailed mathematical model of the structure subjected to sets of earthquake ground motions scaled for increasing intensities. As previously referred, the fragility curve is estimated by the IM-based approach (Ibarra *et al.*, 2002), which is an efficient procedure that makes use of the IM-capacity concept and can be dated back to the works of Veneziano *et al.* (1983). The IM-based approach defines the fragility curve using a random variable, termed the IM-capacity (IM_C), that represents the ground motion intensity at which a given limit state occurs for the structure under assessment. Several realizations of IM_C associated to the selected limit state can then be obtained by analysing the structure under a set of earthquake records using the IDA procedure (Vamvatsikos and Cornell, 2002) where each record is scaled for increasing intensities until the limit state occurs. The cumulative distribution function (CDF) defined by the statistical distribution of the several IM_C realizations represents the fragility curve of the selected limit state. This fragility curve has been, in many cases (Ibarra and Krawinkler, 2005; Jalayer *et al.*, 2007; Zareian and Krawinkler, 2007; Bradley and Dhakal, 2008; ATC, 2009; Liel *et al.*, 2009; Haselton *et al.*, 2011; Liel *et al.*, 2011), assumed to be well represented by a lognormal CDF which enables it to be written as:

$$p_f(im) = P(IM_C \le IM = im) = \Phi\left(\frac{\ln im - \ln \eta_{IM_C}}{\beta_{IM_C}}\right) \quad (9.5)$$

where $\Phi(.)$ is the normal CDF, and $\ln \eta_{IM_C}$ and β_{IM_C} are the mean and the standard deviation, respectively, of the distribution. In this approach, the value of β_{IM_C} represents the uncertainty in the estimate of IM_C due to several factors, e.g. due to the record-to-record variability of the demand, among others (ATC, 2009).

9.3.3 Estimating the limit state expected loss L_{sc}

As previously referred, the expected value of the loss L_{sc} associated to the occurrence of a given limit state is estimated using the storey-based approach proposed by Ramirez and Miranda (2009). This approach has established loss curves which represent the losses of all the individual components of an entire building storey as a function of a selected EDP, $L_{sc|EDP}$. Different curves have been defined to quantify the losses in structural and non-structural components, and different EDPs are also selected depending on the type of component. To illustrate this type of data, Fig. 9.2 presents $L_{sc|EDP}$ loss curves for structural and inter-storey drift-sensitive non-structural components associated to a typical storey of a mid-rise reinforced concrete interior frame of an office building (adapted from Ramirez and Miranda (2009)). For both cases, the selected EDP was the inter-storey drift ⊿. The presented loss values, which are normalized by the storey replacement cost, can be seen to amount to maximum values close to 25% of the storey cost, for the case of the structural losses, and close to 50% of the storey cost, for those associated to the inter-storey drift-sensitive non-structural components. The remaining losses are assigned to acceleration-sensitive non-structural components (Ramirez and Miranda, 2009).

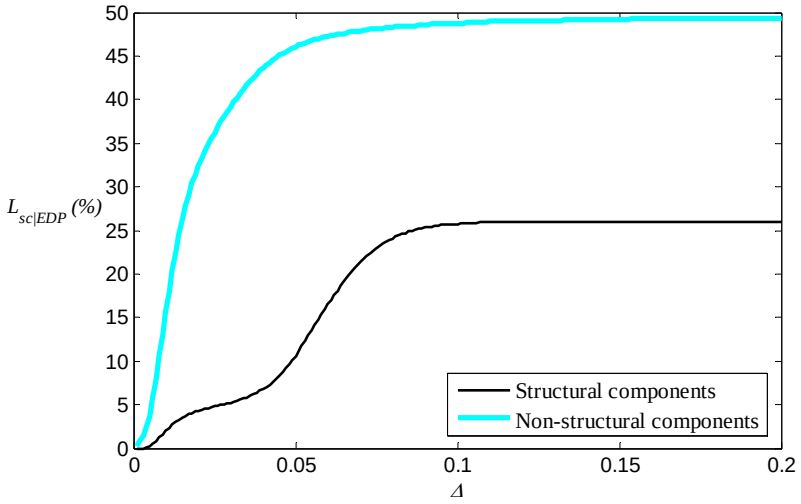

Figure 9.2. Loss curves for structural and inter-storey drift-sensitive non-structural components associated to a typical storey of a mid-rise reinforced concrete interior frame of an office building (adapted from Ramirez and Miranda (2009)).

To quantify the expected loss value associated to the *ith* building storey, $L_{sc,i}$, due to the occurrence of a given limit state, the $L_{sc|EDP,i}$ curve must be combined with the exceedance probability of the selected EDP at the *ith* storey, $P\left(EDP_i > edp_i\right)$. The probabilistic characterization of the *ith* storey EDP can be defined by determining the EDP values corresponding to the several IM_C realizations, EDP_C. The CDF of these EDP_C values represents the fragility curve of the *ith* storey EDP associated to the occurrence of the limit state under analysis, $p_{EDP_{C,i}}$, which can also be assumed to be represented by a lognormal CDF:

$$p_{EDP_{C,i}}\left(edp\right) = P\left(EDP_{C,i} \le EDP = edp\right) = \Phi\left(\frac{\ln edp - \ln \eta_{EDP_{C,i}}}{\beta_{EDP_{C,i}}}\right) \tag{9.6}$$

where $\ln \eta_{EDP_{C,i}}$ and $\beta_{EDP_{C,i}}$ are the mean and the standard deviation, respectively, of the EDP distribution at the *ith* storey. The value of $L_{sc,i}$ can then be obtained by:

$$\begin{aligned} L_{sc,i} &= \int_0^\infty E\left(L_{sc,i} \mid EDP_{C,i}\right) \cdot dP\left(EDP_{C,i} > edp_i\right) = \\ &= \int_0^\infty L_{sc|EDP_{C,i}}\left(x\right) \cdot \left| \frac{d}{dx} \Phi\left(\frac{\ln x - \ln \eta_{EDP_{C,i}}}{\beta_{EDP_{C,i}}}\right) \right| dx \end{aligned} \tag{9.7}$$

in which $L_{sc|EDP_{C,i}}$ represents $L_{sc|EDP,i}$ for the case where the EDP values correspond to those of EDP_C. Finally, the total expected value of the loss L_{sc} associated to the occurrence of the limit state under analysis is obtained by summing the losses of each storey.

Although the values of $L_{sc,i}$ can be obtained by numerical integration of Eq. (9.7), simplified analytical expressions can also be derived to define $L_{sc,i}$. After analysing the $L_{sc|EDP}$ loss curves presented in Fig. 9.2, piecewise linear functions are considered to be adequate enough to represent their shape. Depending on the precision that is required to approximate the $L_{sc|EDP}$ loss curves, and also on the range of inter-storey drift which may govern the performance of a given structure, the curves presented in Fig. 9.2 can be approximated by the linear functions presented in Figs. 9.3 and 9.4. The linear approximations of $L_{sc|EDP_{C,i}}$ proposed in Fig. 9.3 (Option 1) represent a simplified version of the loss curves according to the general expression defined by:

$$L_{sc|EDP_{C,i}}(x) = \begin{cases} A \cdot x & 0 \le x \le \Delta_1 \\ B & x \ge \Delta_1 \end{cases} \tag{9.8}$$

The linear approximations proposed in Fig. 9.4 (Option 2) enable a more realistic representation of the loss curves, namely of the initial branches, and follow the general expression defined by:

$$L_{sc|EDP_{C,i}}(x) = \begin{cases} 0 & 0 \le x \le \Delta_0 \\ A \cdot (x - \Delta_0) & \Delta_0 \le x \le \Delta_1 \\ B \cdot (x - \Delta_1) + A \cdot (\Delta_1 - \Delta_0) & \Delta_1 \le x \le \Delta_2 \\ C & x \ge \Delta_2 \end{cases} \tag{9.9}$$

In both cases, A, B and C represent the slope of the different linear pieces, and Δ_0, Δ_1 and Δ_2 represent the abscissas of the breakpoints.

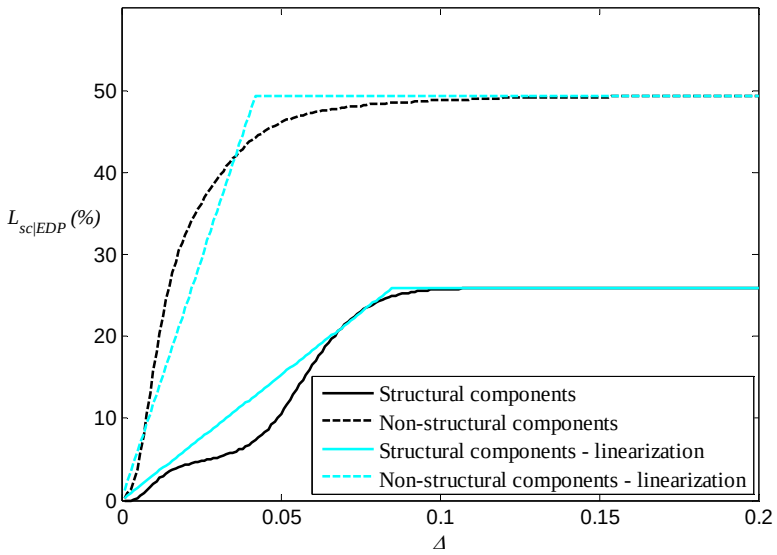

Figure 9.3. Loss curves of Fig. (9.2) and their corresponding piecewise linear approximations using two pieces (Option 1)

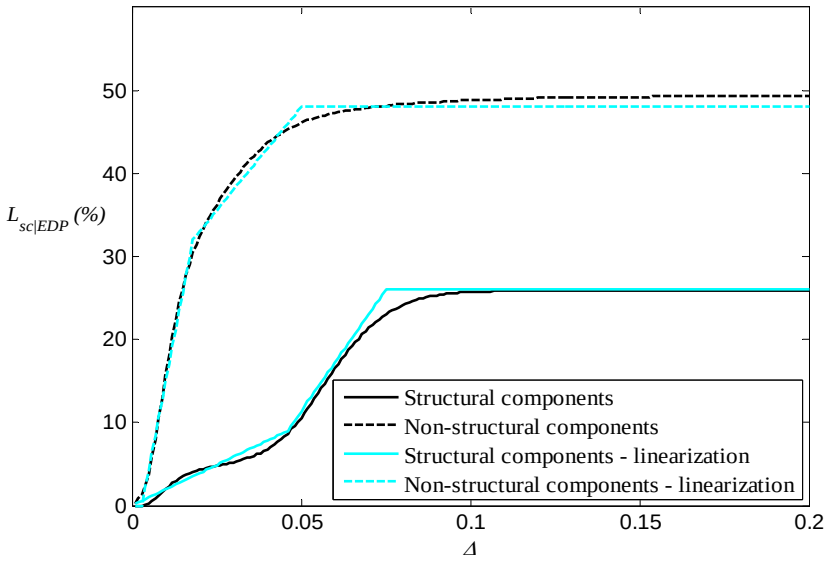

Figure 9.4. Loss curves of Fig. (9.2) and their corresponding piecewise linear approximations using four pieces (Option 2)

After replacing $L_{sc|EDP_{C,i}}$ in Eq. (9.7) with the linear approximations of Eqs. (9.8) and (9.9), integration by parts is then used to solve the corresponding integrals. For the case of Option 1, the following expression is obtained for $L_{sc,i}$:

$$L_{sc,i} = A \cdot e^{\ln \eta_{EDP_{C,i}} + \frac{\beta^2_{EDP_{C,i}}}{2}} \cdot \Phi_a\left(\Delta_1\right) + B \cdot \left[1 - \Phi_b\left(\Delta_1\right)\right] \tag{9.10}$$

where the functions $\Phi_a(.)$ and $\Phi_b(.)$ are given by:

$$\Phi_a\left(x\right) = \Phi\left(\frac{\ln x - \left(\ln \eta_{EDP_{C,i}} + \beta^2_{EDP_{C,i}}\right)}{\beta_{EDP_{C,i}}}\right) \tag{9.11}$$

$$\Phi_b\left(x\right) = \Phi\left(\frac{\ln x - \ln \eta_{EDP_{C,i}}}{\beta_{EDP_{C,i}}}\right) \tag{9.12}$$

The first term of the sum in Eq. (9.10) is the contribution of the first piece of Eq. (9.8) to the integral, which makes use of the following relation (Wolfram|Alpha, 2011):

$$\int e^{-\frac{1}{2}\left(\frac{\ln x - a}{b}\right)^2} dx = -\sqrt{\frac{\pi}{2}} \cdot b \cdot e^{a + \frac{b^2}{2}} erf\left(\frac{a + b^2 - \ln x}{\sqrt{2} \cdot b}\right) + constant \tag{9.13}$$

where $erf(.)$ is the error function (i.e. twice the integral of the normal distribution with zero mean and a variance of 0.5). For the case of Option 2, the following expression is obtained for $L_{sc,i}$, which also uses the relation defined by Eq. (9.13):

$$L_{sc,i} = A \cdot e^{\ln \eta_{EDP_{C,i}} + \frac{\beta^2_{EDP_{C,i}}}{2}} \cdot \left[\Phi_a(\Delta_1) - \Phi_a(\Delta_0)\right] + A \cdot \Delta_0 \cdot \left[\Phi_b(\Delta_0) - \Phi_b(\Delta_2)\right] + B \cdot e^{\ln \eta_{EDP_{C,i}} + \frac{\beta^2_{EDP_{C,i}}}{2}} \cdot \left[\Phi_a(\Delta_2) - \Phi_a(\Delta_1)\right] - (B - A) \cdot \Delta_1 \cdot \left[\Phi_b(\Delta_2) - \Phi_b(\Delta_1)\right] + C\left[1 - \Phi_b(\Delta_2)\right] \quad (9.14)$$

9.3.4 Definition of the limit states

According to the arguments referred in Section 9.2 and to the format of the proposed methodology, an update of the limit state definitions is required. Proposals to define the previously analysed limit states accounting for the issues raised are addressed in the following.

9.3.4.1 The limit state of Damage Limitation

For limit states that follow a general description similar to the one proposed by EC8-3 for the limit state of DL, the fundamental issue requiring a more objective consideration is related to the number of structural sections where yielding is admissible so that the structure under analysis can still be considered to conform to this limit state. An example of such type of approach is the one proposed by the draft code for performance-based seismic design of buildings in Taiwan (Xue *et al.*, 2008) where, for a given limit state, 20% of the members are accepted to be nonconforming to the limit state criterion. However, it is believed that an approach defining a fixed number of admissible yielding sections is as subjective as the example case addressed in Section 9.2 where only one section exceeding the yield deformation would be sufficient to consider the structure to be nonconforming.

Therefore, a conformity condition based on risk and loss criteria is proposed instead which establishes that the occurrence of the limit state can be accepted in a number of scenarios, as long as the corresponding value of EL is not greater than an admissible value $EL_{adm,DL}$. In this case, each scenario corresponds to the situation where a different number n_{DL} of structural sections reaches or exceeds the yield limit. By defining the admissible consequences of reaching this limit state in terms of the $EL_{adm,DL}$, which is a function of the values set for $\lambda_{adm,DL}$ and $L_{sc\,adm,DL}$, the number of admissible yielding sections is set by a more rational decision-making process. Given the type of global structural performance that must be met for the DL limit state, namely the low level of structural damage that is expected, it is suggested that the previously referred simplified loss model could consider the value of $L_{sc\,adm,DL}$ such as to reflect repair costs due to non-structural damage only.

In order to control the level of inelastic behaviour that is admissible at the section level, this definition of the DL limit state can also be associated to additional conditions limiting the ductility demand of beams and/or columns up to a certain specified value that could also be connected to the repair cost. Moreover, if required, it is also possible to associate an additional condition reflecting the global behaviour of the structure, such as a limit value for the admissible inter-storey drift (e.g. 1% as proposed by ASCE (2007)) that, again, can be established based on economic requirements. Another type of global behaviour condition has been proposed by Wang *et al.* (2011) which consists on defining a limit for the reduction of the slope of the IDA curve obtained for a given ground motion. For a limit state similar to the DL limit state, Wang *et al.* (2011) suggest a 10% reduction. Although it is established for a different type of limit state, this condition can be seen to be similar in nature to that which is defined to determine global collapse in methodologies such as the one proposed by ATC-63 (ATC, 2009) where a near 100% reduction of the slope of the IDA curve indicates that global collapse has occurred. However, the reduction value proposed for the DL limit state (10%) is arbitrary and is not able to be objectively connected to the physical state of the structure. Hence, such type of approach is not recommended.

9.3.4.2 The limit state of Significant Damage

For limit states involving conditions similar to those of the EC8-3 SD limit state, the focus of the revised definition proposed herein is related to both the number of structural sections where the corresponding deformation limit can be attained so that the structure can still be considered to conform to this limit state, and to the level of deformation that should be defined for such limit value. As for the DL limit state, a conformity condition based on risk and loss criteria is also proposed which establishes that the occurrence of the limit state can be accepted in a number of scenarios, as long as the corresponding value of EL is not greater than an admissible value $EL_{adm,SD}$. In this case, each scenario corresponds to the situation where a different number n_{SD} of structural sections reaches or exceeds a selected deformation limit d_{lim}. It is believed that d_{lim} should be defined based on economic considerations involving estimates of the expected damage-related costs. The value of $EL_{adm,SD}$ is set as a function of the values defined for $\lambda_{adm,SD}$ and $L_{sc\,adm,SD}$, where the latter should reflect the maximum admissible cost for the repair of the whole structure. Therefore, in terms of the simplified loss model previously referred, $L_{sc\,adm,SD}$ should reflect the admissible value of the repair costs of both the structural and the non-structural elements.

Furthermore, it is also mentioned that, as for the DL limit state, it is also possible to associate an additional condition reflecting the global behaviour of the structure, such as a limit value for the admissible inter-storey drift (e.g. 2% as proposed by ASCE (2007)).

9.3.4.3 The limit state of Near Collapse

With respect to limit states comprising conditions similar to those of the EC8-3 NC limit state, the revised definition proposed herein involves different bounding conditions than those of the previous limit states. Given that, when reaching this limit state, the building is expected to be uneconomic to repair, a bounding condition setting a value for the admissible loss is not considered to be a relevant global performance measure. Hence, the building performance is controlled by limiting the probability of occurrence λ of the limit state to an admissible value $\lambda_{adm,NC}$, and by defining conditions in terms of the number of sections where a given demand/mechanism is accepted. With respect to this last performance measure, when analysing the occurrence of local (section level) mechanisms, distinction must be made between mechanisms occurring in beams and in columns. Given the larger severity of the consequences due to the failure of a column, the occurrence of the NC limit state at a single section is considered to be enough to reflect a nonconforming structure. On the other hand, for beams, it is considered that the limit state capacity of the considered mechanism can occur at several sections. In this case, a nonconforming condition is established when the NC limit state has occurred in all of the beam sections of a given storey.

In addition to the local (section level) analysis of the demand, a global analysis of the building behaviour should be carried out also for this limit state in order to include the influence of the previously referred global yield mechanisms. Existing methodologies identifying the occurrence of such yield mechanisms can be divided in two main types: methodologies tracking the evolution, for increasing levels of the selected IM, of the value of a demand parameter capable of reproducing the global behaviour of the building (Vamvatsikos and Cornell, 2002) or approaches tracking the occurrence of a number of yield mechanisms specified beforehand (Jalayer *et al.*, 2007).

The first type of methodologies is mostly associated to procedures aiming to track the occurrence of global structural collapse such as, for example, the ATC-63 framework (ATC, 2009). Furthermore, the accuracy of this approach can be seen to depend on the adequacy of the relation (i.e. the IDA curve) between the selected EDP (usually the inter-storey drift) and the IM to represent the occurrence of the referred mechanisms. The development of these mechanisms is typically associated to a flatness of the IDA curve representing a very large increase of the EDP for a small increase of the IM which, in turn, indicates that a considerable reduction of the global stiffness of the structure has occurred, e.g. such as when a soft-storey mechanism develops. If the referred flatness does not occur,

the identification of a global mechanism becomes more difficult and some of them might only be identified if deterioration is modelled in the structural analysis (Krawinkler and Lignos, 2009). With respect to the second approach, although the procedure proposed in Jalayer *et al.* (2007) allows the consideration of any type of global mechanism, it has the downside of requiring that all of them must be identified. Given the multitude of possibilities, the adequacy of this approach relies considerably on the opinion and experience of the analyst. Furthermore, this procedure can also be seen to disregard the realistic correlation between the behaviour of the components that are part of the mechanism since it considers that a mechanism occurs when its strongest component begins to yield (Jalayer *et al.*, 2007), i.e. a mechanism is assumed to be formed by a parallel arrangement of fully correlated components. Given the disadvantages of both approaches, an alternative methodology is proposed in the following to identify the occurrence of any type of yield mechanism.

The proposed approach identifies the occurrence of yield mechanisms by assessing the singularity of an equivalent stiffness matrix representing the current state of the building behaviour. This approach is defined by the following steps which are carried out at each time increment of the nonlinear dynamic analysis:

- Step 1 - Check the behaviour state of each structural section to determine if its current loading state is located in a positive or negative post-yield loading branch of the behaviour path. Sections meeting this condition are termed *active yielding sections*. To illustrate the definition of the referred loading branches, Fig. 9.5 presents a generalized force-displacement relation representing different stages of the hysteretic behaviour. In Fig. 9.5, branches 3 and 10 are positive post-yield loading branches, the latter occurring after a negative loading cycle and a positive reloading, while branch 6 is a negative post-yield loading branch.

- Step 2 - If one or more *active yielding sections* are found, an equivalent elastic Euler-Bernoulli stiffness matrix of the structure K_{eq} is formulated with zero-stiffness terms assigned to the flexural terms of those sections.

- Step 3 - If matrix K_{eq} is singular, a situation that represents an unstable structure (Nafday, 2008), the configuration of active yielding sections under consideration is that of a yield mechanism and the corresponding IM value of the ground motion is recorded.

By using such procedure, it is then possible to identify any type of yield mechanism taking into account the correlation of the behaviour between the components forming the mechanism and accounting only for sections actively loaded with post-yield stiffness at each time increment of the analysis.

In addition to the section level and yield mechanisms criteria, it is mentioned that, as for the previous limit states, it is also possible in this case to associate an additional

condition reflecting a lateral deformation limit for the inter-storey drift (e.g. 4% as proposed by ASCE (2007)).

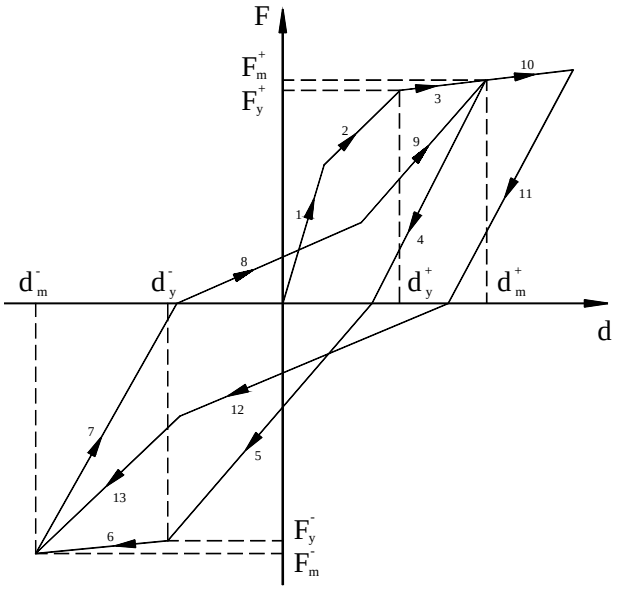

Figure 9.5. Generalized hysteretic force-displacement relation.

9.3.5 Accounting for the uncertainty in the limit state capacities

As referred in Jalayer *et al.* (2007), the uncertainty associated to the modelling of member limit state capacities has a significant contribution to the probability of occurrence λ of a given limit state. Depending on the considered standard, the limit state capacities are seen to be established either by fixed values of a given EDP (e.g. ASCE (2007)) or by expressions of semi-empirical nature (e.g. EC8-3 (2005)) defining the limit values of the referred EDPs. In the former case, the proposed values are expected to be conservative estimates of the real capacity (Haselton, 2006) while in the latter, the average estimates provided by the referred expressions are known to have a large uncertainty (Haselton, 2006; *fib*, 2003a; *fib*, 2003b). In this case, the uncertainty in the limit state capacities can be associated to the modelling error deriving from the proposed capacity formulas as well as to the variability of the mechanical parameters entering those formulas (Jalayer *et al.* 2007).

Among the different methods which are available to account for this uncertainty component (e.g. see Pinto *et al.*, 2004; Jalayer *et al.*, 2007; Liel *et al.*, 2009), the selected approach assumes that limit state capacities C can be modelled according to the following general format:

$$C = \hat{C} \cdot \varepsilon_{UC} \tag{9.15}$$

where $\hat{C}$ is the estimate given by the referred semi-empirical expressions, and ε_{UC} is a lognormal random variable with unit median and a dispersion β_{UC} accounting for the

variability sources previously mentioned. In order to reflect the section-level limit state capacity uncertainty at the system level, i.e. in the uncertainty associated to the estimate of IM_C, the possible correlation between the capacities of different sections must be accounted for. To address this issue, an approach similar to the one proposed by Jalayer *et al.* (2007) is considered herein. Therefore, it is assumed that for a given mechanism (e.g. yield deformation, shear failure) the corresponding limit state capacities of all members are fully correlated. On the other hand, for a given member, the limit state capacities of different mechanisms are considered to be uncorrelated. Given this assumption, the effect of this uncertainty on the estimate of IM_C can be included by sampling different realizations of the individual member capacities using Eq. (9.15) which are then paired with the IDA curves obtained from the considered earthquake ground motions. Therefore, for a given IDA curve, an array of member capacities (i.e. a number of realizations, n_{UC}, of the capacities for each member) is established and each sample of capacities (i.e. one realization of the capacity of each member) will lead to a different realization of the IM_C associated to the limit state under analysis. Using this approach, the quantification of parameters η_{IM_C} and β_{IM_C} which characterize the limit state fragility curve, Eq. (9.5), are now able to account for the uncertainty in the member capacities.

9.3.6 Stepwise description of the proposed methodology

Based on the individual features addressed over the previous sections, the sequence of steps involved in the presented probabilistic methodology for the analysis of building performance is described in the following.

The proposed method assumes that a set of n_{gm} IDA curves with an adequate number of IM levels have been obtained from the analysis of the structure subjected to n_{gm} ground motion records scaled to those IM levels. After selecting the limit state for which the performance of the structure is to be assessed, the following steps must then be carried out:

- Step 1 - Select the mechanism for which seismic safety is going to be analysed for the selected limit state.
- Step 2 - Define a value for n_{UC} (the number of realizations of the capacity of each member) and sample n_{UC} values of ε_{UC} from its distribution.
- Step 3 - Select a value for n_{LS} (the number of structural sections where the limit state mechanism occurs).
- Step 4 - Select a value of ε_{UC} from those sampled in Step 2.

- Step 5 - Select one IDA curve from the set of n_{gm} curves.
- Step 6 - Select the first IM level from the chosen IDA curve.
- Step 7 - Determine $\rho = \dfrac{D}{\hat{C} \cdot \varepsilon_{UC}}$ for all the n_{sec} sections of the structure.
- Step 8 - Determine the number of sections $n_{\rho>1}$ with ρ values larger than 1.0.
- Step 9 - If $n_{\rho>1} < n_{LS}$, select the next IM level and repeat the procedure from Step 7; if $n_{\rho>1} \geq n_{LS}$, record the current IM level, which corresponds to a realization of IM_C (the ground motion intensity at which the limit state scenario occurs), e.g. see Fig. 9.6a), and proceed to the next IDA curve to repeat the procedure from Step 6.
- Step 10 - After going through all the IDA curves, the procedure is repeated from Step 5 for a different value of ε_{UC}, until the whole n_{UC} values have been considered.
- Step 11 - Characterize the limit state fragility curve by Eq. (9.5) based on the different realizations of IM_C, e.g. see Fig. 9.6b).
- Step 12 - Determine the probability of occurrence λ of the limit state by Eq. (9.4).
- Step 13 - Characterize the fragility curves of the selected EDP of each storey for the storey-based loss quantification by Eq. (9.6), e.g. see Fig. 9.6c).
- Step 14 - Determine the expected value of the loss of each storey by Eq. (9.7), or by the simplified approaches defined by Eqs. (9.10) and (9.14).
- Step 15 - Determine the value of the loss L_{sc} of the limit state scenario.

After these steps, the triplet $\left(n_{LS}; \lambda; L_{sc}\right)$ defines a limit state performance scenario. The building performance quantification procedure is then repeated from Step 4 for a different value of n_{LS}. In order to obtain an adequate representation of the building performance evolution for different n_{LS} values, it is suggested that the analysis starts by setting n_{LS} equal to one and that subsequent repetitions of the procedure increase it by single units. The several performance triplets are then combined to obtain EL according to Eq. (9.2). The value of EL is then analysed in light of the limit defined by EL_{adm} to determine which combination of scenarios is admissible for the current limit state.

In a situation where the uncertainty of the member limit state capacities is not considered, the procedure is simplified by considering both n_{UC} and ε_{UC} equal to 1.0 in the necessary steps. Furthermore, additional verifications may be carried out in Step 10 if provisions other than checking the $n_{\rho>1}$ condition are required (e.g. checking the

occurrence of a yield mechanism, of a deformation limit for the inter-storey drift or of a specified limit for the ductility demand of beams and/or columns).

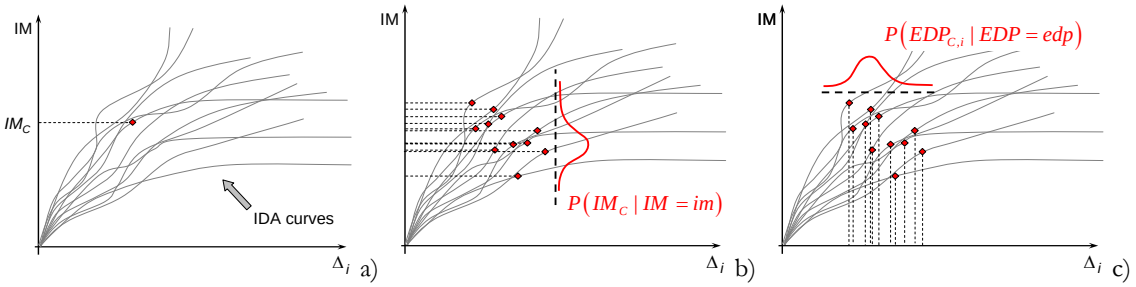

Figure 9.6. Illustration of step 9 (a), of step 11 considering $n_{UC} = 1$ (b) and of step 13 considering $n_{UC} = 1$ and for the *ith* storey (c).

9.4 Example application of the proposed methodology

An application of the proposed methodology is presented in the following addressing the seismic safety assessment of two RC structures for the limit states defined by EC8-3 and involving the modifications presented in Section 9.3.4.

9.4.1 General description of the selected structures

The two selected RC structures are the six-storey RC frames previously referred as REG6 and IRREG6 in Chapter 5. The elevation views of the frames are presented in Figs. 9.7a) and b) along with the column cross section dimensions. All the beams are 0.30×0.50 m^2. Additional information concerning the frame characteristics can be found in Chapter 5 and in Ferracuti *et al.* (2009). Relevant details about the structural modelling, the analysis procedure and the quantification of the demand parameters are discussed in Chapter 5 and are, therefore, omitted herein.

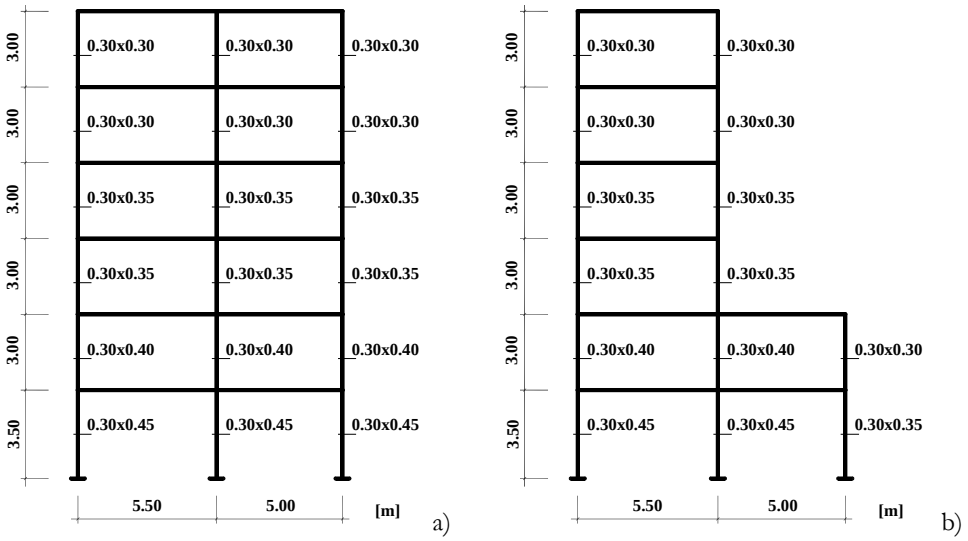

Figure 9.7. Elevation views of the REG6 (a) and of the IRREG6 (b) frames and of their column cross section dimensions.

9.4.2 EC8-3 component capacities and probabilistic modelling of their uncertainty

As mentioned in previous chapters, EC8-3 defines ductile capacities in terms of the admissible DL, SD and NC member chord rotations, while brittle capacities are characterized by the admissible NC shear force. For the quantification of the DL chord rotation capacity θ_{DL}, and assuming that no shear cracking is expected to precede flexural yielding, EC8-3 proposes the following expression

$$\theta_{DL} = \phi_y \cdot \frac{L_s}{3} + 0.0013 \cdot \left(1 + 1.5\frac{h}{L_s}\right) + 0.13 \cdot \phi_y \cdot \frac{d_b \cdot f_y}{\sqrt{f_c}} \tag{9.16}$$

in which ϕ_y is the yield curvature of the member end section, L_s is the shear span, h is the cross section depth, d_b is the mean diameter of the tension reinforcement, f_y is the longitudinal reinforcement yield strength and f_c is the concrete compressive strength. In order to account for the uncertainty in θ_{DL} according to Eq. (9.15), fifty ε_{UC} values are sampled from its distribution, where the dispersion β_{UC} for θ_{DL}, $\beta_{UC,\theta_{DL}}$, is considered to be 0.36 (*fib*, 2003b) which reflects the uncertainty due to the modelling error of Eq. (9.16). The uncertainty due to the variability of the mechanical parameters entering Eq. (9.16) is not taken into account since its effect is considered to be negligible when compared to that of the modelling error (e.g. see Chapter 8).

For the quantification of the NC chord rotation capacity θ_{NC}, the following semi-empirical expression proposed by EC8-3 is considered herein:

$$\theta_{NC} = \frac{1}{\gamma_{el}}\left[\theta_{DL} + \left(\phi_u - \phi_y\right)\cdot L_{pl}\cdot\left(1-\frac{L_{pl}}{2L_s}\right)\right] \tag{9.17}$$

where ϕ_u is the ultimate curvature of the member end section and L_{pl} is the plastic hinge length. The definition of ϕ_u and of L_{pl} depends on the selected confined concrete model (EC8-3, 2005). As referred in Chapter 8, the purpose of factor γ_{el} is to account for the variability of the capacity. In the present application γ_{el} is considered equal to one since the variability of the capacity values is simulated. To account for the uncertainty in θ_{NC} according to Eq. (9.15), fifty ε_{UC} values are sampled from its distribution, where the dispersion β_{UC} for θ_{NC}, $\beta_{UC,\theta_{NC}}$, is considered to be 0.90 (*fib*, 2003b) in order to reflect the uncertainty due to the modelling error of Eq. (9.17). As for the case of θ_{DL}, the uncertainty due to the variability of the mechanical parameters is also not taken into account.

For the case of the SD limit state, EC8-3 states that the corresponding chord rotation capacity θ_{SD} is defined as $\theta_{SD,1} = 0.75\theta_{NC}$. In addition to this case, the performance analysis of the structures for this limit state was also carried out for the situation where a chord rotation capacity $\theta_{SD,2} = 0.85\theta_{SD,1}$ is considered. This additional analysis is performed in order to address the considerations made in Section 9.3.4.2. Since θ_{SD} is a function of θ_{NC}, the uncertainty in θ_{SD} is that of θ_{NC}.

With respect to the shear force capacity V_{NC} for the limit state of NC, EC8-3 proposes the formulation defined by:

$$\begin{aligned} V_{NC} = \frac{1}{\gamma_{el}}\Bigg[&\frac{h-x}{2\cdot L_s}\cdot\min\left(N;0.55\cdot A_c\cdot f_c\right) + \left(1+0.05\cdot\min\left(5;\mu_\Delta^{pl}\right)\right)\cdot \\ &\cdot\left[0.16\cdot\max\left(0.5;100\cdot\rho_{tot}\right)\cdot\left(1-0.16\cdot\min\left(5;\frac{L_s}{h}\right)\right)\cdot\sqrt{f_c}\cdot A_c + V_w\right]\Bigg] \end{aligned} \tag{9.18}$$

where x is the compression zone depth, N is the compressive axial force (equal to zero for tension), A_c is the cross section area taken equal to $b_w\cdot d$ (b_w is the section width and d is the structural depth), ρ_{tot} is the total longitudinal reinforcement ratio, μ_Δ^{pl} is the ratio between the plastic part of the chord rotation demand and the yield chord rotation given by Eq. (9.16), and V_w is the contribution of transverse reinforcement to shear resistance (EC8-3, 2005). To account for the uncertainty in V_{NC} according to Eq. (9.15), fifty ε_{UC} values are sampled from its distribution, where the dispersion β_{UC} for V_{NC}, $\beta_{UC,V_{NC}}$, is considered to be 0.14 (*fib*, 2003a) in order to reflect the uncertainty due to the modelling error of Eq. (9.18).

9.4.3 Seismic demand and hazard scenario

The seismic demand considered for each structure consisted of a suite of fifty real ground motions extracted from the Pacific Earthquake Engineering Research Center NGA database (PEER-NGA, 2009) according to the criteria referred in Chapter 5. Each structure was analysed using a multi-stripe analysis (Jalayer and Cornell, 2009) where the selected ground motions are scaled for increasing values of $S_a(T_1)$ until the selected limit state is attained - $S_a(T_1)$ is the 5% damping spectral acceleration ordinate of the ground motion for the fundamental period of the structure T_1 which is the selected IM and is simply referred to as S_a hereon.

In order to define the earthquake hazard curve $H(x)$ required for Eq. (9.4), seismic hazard data was obtained for the S_a values of the considered structures, and for a reference period of one year, in order obtain results in terms of annual performance of the structures. Details about the selected methodology and the hazard data are referred in Chapter 8. A continuous function $H(x)$ was then defined by fitting a probabilistic complementary cumulative distribution function (CCDF) to the discrete seismic hazard data. This adjustment was performed assuming that the CCDF of a Fréchet distribution (Castillo, 1988) is adequate enough to represent the hazard data (e.g. see Chapter 8). Therefore, the hazard function $H(x)$ is defined by:

$$H(x) = e^{-\left(\frac{x}{\alpha}\right)^{\gamma}} \tag{9.19}$$

where α and γ are the parameters of the CCDF. Figure 9.8 presents the seismic hazard data obtained for the REG6 and the IRREG6 structures, along with the corresponding fitted Fréchet CCDFs.

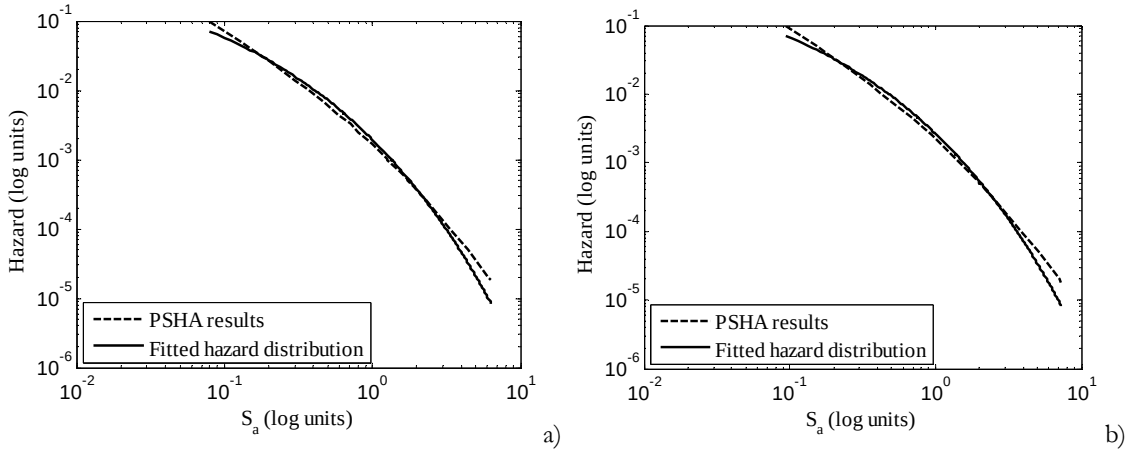

Figure 9.8. Probabilistic seismic hazard analysis (PSHA) results and fitted Fréchet distribution CCDF to the seismic hazard data for the REG6 (a) and IRREG6 structures (b).

9.4.4 Cost analysis data and performance conditions

The expected loss value associated to the *ith* building storey, $L_{sc,i}$, is quantified using the $L_{sc|EDP}$ structural and non-structural loss curves for mid-rise RC interior frames of an office building defined by Ramirez and Miranda (2009). In order to simplify the proposed example applications, only non-structural losses associated to inter-storey drift-sensitive non-structural components are considered herein. The considered loss curves are presented in Fig. 9.9. In addition, the $L_{sc,i}$ values are also determined using the $L_{sc|EDP}$ linear approximations defined by Eqs. (9.8) and (9.9).

With respect to the selected values of the admissible expected losses EL_{adm} defined by Eq. (9.3), values were set for the admissible probability of occurrence of the considered limit states, λ_{adm}, and for their expected repair costs, $L_{sc\,adm}$. For the case of λ_{adm}, it is referred that, for existing structures, current standards and/or available technical documents on the subject do not have definitive proposals on this matter. Therefore, the λ_{adm} values considered herein were defined as a reduction of the target reliability values for new structures proposed by the JCSS (2001b) for a one year reference period and for ultimate limit states. As referred by Diamantidis and Bazzurro (2007), this approach is based on the fact that achieving a higher reliability level in existing structures has a higher cost when compared to that of structures under design. Hence, the λ_{adm} values presented in Table 9.1 were considered for the selected limit states, based on those proposed by the JCSS (2001b) for the higher category of the relative cost of implementing safety measures. These λ_{adm} values are defined for the previously referred reference period of one year and were associated to small, moderate and large risks to life and economic consequences for the limit states of DL, SD and NC, respectively. Along with the values for λ_{adm}, Table 9.1 also presents the corresponding reliability indexes β.

With respect to the selected values for the admissible expected repair costs, $L_{sc\,adm}$, the considered limit values correspond to average repair costs of all the building storeys. Therefore, a value of 10% was assumed for the DL limit state (considering only losses associated to inter-storey drift-sensitive non-structural components) and a value of 25% was assumed for the SD limit state (considering losses associated to inter-storey drift-sensitive non-structural components and losses to structural components). Considering the proposed values of λ_{adm} and $L_{sc\,adm}$ for the limit states of DL and SD, the corresponding values of EL_{adm} set by Eq. (9.3) are then 10^{-4} and 5×10^{-5}, respectively.

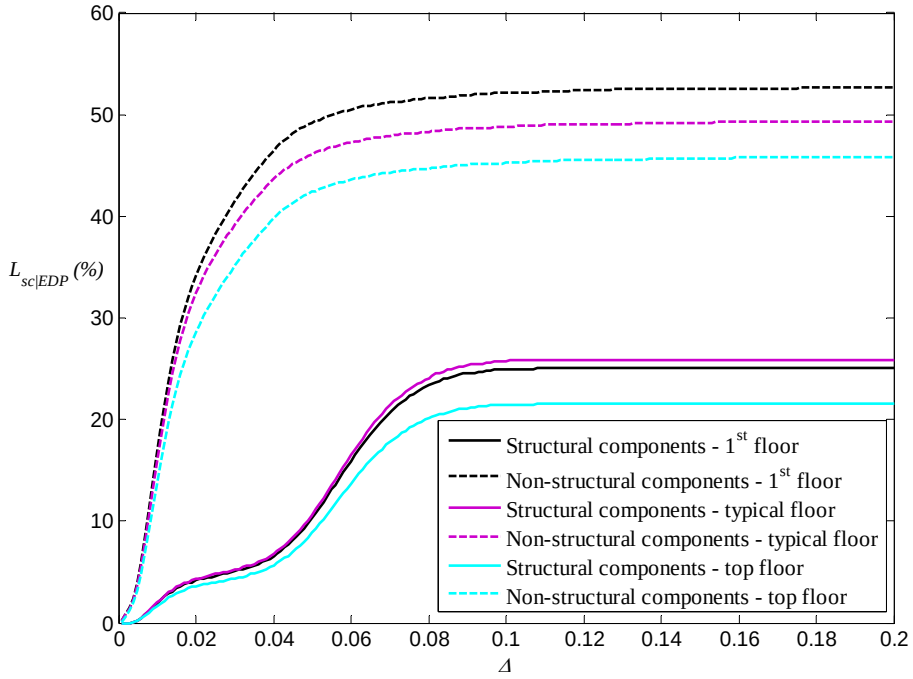

Figure 9.9. Considered loss curves for structural and inter-storey drift-sensitive non-structural components for a mid-rise reinforced concrete interior frame of an office building (adapted from Ramirez and Miranda (2009)).

Table 9.1. Considered values for λ_{adm} for the selected limit states and the corresponding reliability indexes β.

Limit state	λ_{adm}	β
DL	0.001	3.09
SD	0.0002	3.54
NC	0.0001	3.70

9.5 Results of the probabilistic performance analysis

9.5.1 Initial considerations

In order to analyse the applicability of the proposed methodology for performance assessment, results of the probabilistic analysis of the REG6 and the IRREG6 structures for the DL, SD and NC limit states are presented in the following. To emphasize the influence of the modelling error of the selected capacity models, the performance results are presented separately for the situation where the uncertainty of the component capacities is neglected and for the situation where it is accounted for. For the DL limit state, the performance of the structures is analysed considering n_{LS} values of one to six. For the SD limit state, the performance is analysed considering n_{LS} values of one to four instead.

In addition to these results, loss values obtained using the linear approximations of the loss curves are also analysed to observe the accuracy of this approach. Finally, the use of the lognormal distribution to model the fragility curves involved in the performance analysis is addressed to determine the suitability of this common assumption. Results of adequate statistical methods used to test this hypothesis are presented and large-sample situations where the hypothesis is rejected are also discussed.

9.5.2 Results for the DL limit state

Based on the IDA curves obtained for all the considered ground motions, the performance metrics λ and L_{sc} were calculated for n_{LS} values of one to six according to the steps defined in Section 9.3.6. To illustrate the procedure, Fig. 9.10 presents the IDA curves of the REG6 structure considering the inter-storey drift Δ of the third storey as the represented EDP. The third storey was selected since its Δ values are dominant over those of the remaining storeys. The performance points corresponding to the n_{LS} cases one to four of the DL limit state, when the uncertainty of the component capacities is neglected, are also represented. In addition to the IDA curves, Fig. 9.10 also presents the probability density functions (PDFs) of the $S_{a,C}$ realizations (assumed as lognormal distributions) corresponding to the referred performance points of the n_{LS} cases one to four. The CDFs of these distributions are the DL limit state fragility curves $p_{f,n_{LS}=i}$, where *i* stands for the n_{LS} cases one to four, defined by Eq. (9.5). Furthermore, Fig. 9.10 also shows the PDFs of the third storey Δ (assumed as lognormal distributions) which correspond to the referred performance points of the n_{LS} cases one to four, $\Delta_{C,3}$. The CDFs of these distributions are the fragility curves $p_{\Delta_{C,3},n_{LS}=i}$ of the third storey, where *i* stands for the n_{LS} cases one to four, defined by Eq. (9.6). In the current application of the proposed methodology, the mean and the standard deviation of the log of the data required for Eqs. (9.5) and (9.6) were obtained using the logistic M-estimator proposed by Rousseeuw and Verboven (2002) and the τ-scale truncated standard deviation proposed by Yohai and Zamar (1988), respectively. These estimators were selected based on the findings and recommendations presented in Chapters 6 and 7.

From the cloud of performance points corresponding to the n_{LS} cases one to four represented in Fig. 9.10, the $\Delta_{C,3}$ realizations can be seen to range roughly between 0.5% and 1%, which is consistent with the behaviour of the structure that is expected for the DL limit state conditions. By analysing the probability density functions of Fig. 9.10, it is possible to observe the increase of the mean of the lognormal $S_{a,C}$ and $\Delta_{C,3}$ data as n_{LS} increases, which reflects the need for higher earthquake intensities to reach the limit state condition in a larger number of sections. On the other hand, the standard deviation of the

lognormal $S_{a,C}$ and $\Delta_{C,3}$ exhibits a smaller variability across the several n_{LS} values. Furthermore, the represented lognormal distributions can be seen to exhibit low levels of skewness, a fact reflecting the moderate level of dispersion of the data, which exhibits standard deviations of the log of the data between 0.10 and 0.13 for $\Delta_{C,3}$, and between 0.14 and 0.20 for $S_{a,C}$.

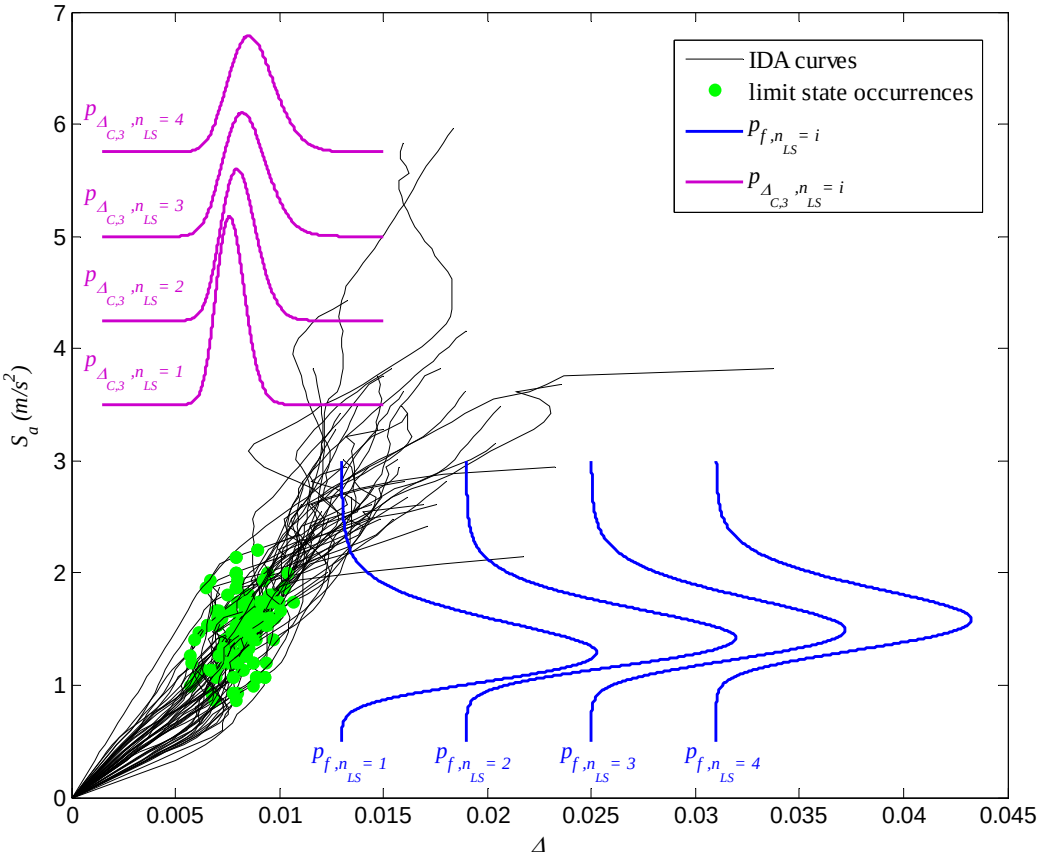

Figure 9.10. IDA curves of the REG6 structure, performance points and probability density functions of the $S_{a,C}$ and $\Delta_{C,3}$ realizations for the n_{LS} cases one to four.

The performance metrics λ and L_{sc} calculated for the REG6 and the IRREG6 structures are presented in Fig. 9.11 for the case where the uncertainty of the component capacities is neglected. In addition to these results, Fig. 9.11 also presents the cumulative sum of EL up to each value of n_{LS} along with the selected value for EL_{adm}. The results of the REG6 and IRREG6 structures indicate that performance scenarios up to n_{LS} equal to six can be seen to lead to acceptable values of EL. This simple comparison emphasizes the importance of using high-level parameters such as λ, L_{sc} and EL to analyse building performance. It is recalled that, according to the interpretation of the code-based limit state definitions presented in Section 9.2, the case where $n_{LS}=1$ corresponds to the scenario implicit in those definitions. Hence, by using EL as a global performance measure (and

accepting the values considered for λ_{adm}, $L_{sc\,adm}$ and therefore EL_{adm}), the proposed methodology is able to establish admissible performance scenarios that go beyond the limitations of the code definitions and allows for a rational decision-making process about the need to retrofit or strengthen a given structure.

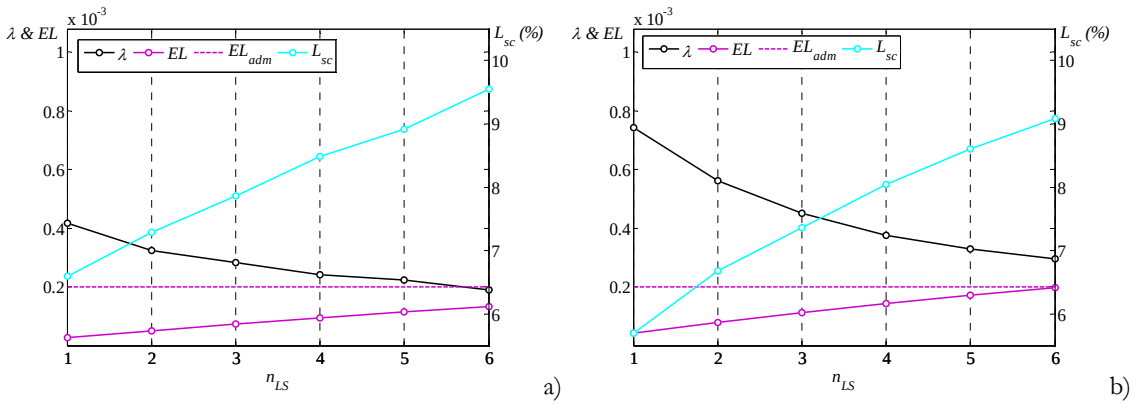

Figure 9.11. Results of the performance analysis of the REG6 (a) and the IRREG6 (b) structures when the uncertainty of the component capacities is neglected.

For a more direct analysis about the influence of the modelling error of the capacity model, the performance results of both structures are presented in Fig. 9.12 for the situation where the uncertainty of the component capacities is neglected and also for the situation where it is accounted for. Parameters λ_{UC}, $L_{sc\,UC}$ and EL_{UC} correspond to the values of λ, L_{sc} and EL obtained when the uncertainty of the component capacities is considered.

From the results presented in Fig. 9.12, allowing for the uncertainty of the component capacities can be seen to increase the risk considerably: the λ_{UC} values are 30% to 75% larger than the λ values. On the other hand, for this limit state, the uncertainty effects on the expected costs are different. For structure REG6, the uncertainty of the component capacities reduces the expected costs: $L_{sc\,UC}$ is, on average, 5% lower than L_{sc}. For structure IRREG6, the uncertainty increases the expected costs for the n_{LS} cases of one to three ($L_{sc\,UC}$ is 6% larger than L_{sc} when $n_{LS}=1$), while there is virtually no difference between $L_{sc\,UC}$ and L_{sc} for the remaining n_{LS} cases. With respect to the performance of the REG6 and the IRREG6 structures, the changes from λ to λ_{UC} and from L_{sc} to $L_{sc\,UC}$ also modify the number of performance scenarios up to which the value of EL is found to be admissible. For REG6, the performance measure EL_{UC} is admissible up to $n_{LS}=5$, while for IRREG6 the performance is only acceptable up to $n_{LS}=3$. Therefore, accounting for the uncertainty in the component capacities can be seen

to have a significant influence on the acceptable performance of the structures, namely due to the significant increase of λ to λ_{UC}.

The differences between λ and λ_{UC} can be explained by the analysis of the limit state fragility curves $p_{f,n_{LS}=i}$ presented in Fig. 9.13a) of the various n_{LS} cases of IRREG6 and for the situations where the uncertainty is and is not considered. When uncertainty is accounted for, the presented fragility curves indicate there is an increase in the variability of the data (i.e. there is a flattening of the curves) as well as a reduction in the median of the data. This reduction ranges from 1% to 5% for IRREG6 and from 10% to 12% for REG6. Such shift in the median values of $S_{a,C}$ has also been reported by Liel *et al.* (2009) and can be seen to be the dominant factor leading to the higher values of λ_{UC} since, according to Eq. (9.4), the higher values of $\left|dH(x)/dx\right|$ have now a larger contribution to λ.

Using a similar reasoning, the fragility curves $p_{\Delta_{C,3},n_{LS}=i}$ of the $\Delta_{C,3}$ realizations of REG6 presented in Fig. 9.13b) (which are similar to those obtained for the remaining storeys) are also able to justify the differences between L_{sc} and $L_{sc\,UC}$. When uncertainty is accounted for, these fragility curves also indicate an increase in the variability of the data and a reduction in the median of the data, which, in this case, ranges from 5% to 9%. For this situation, the shift in the median of the data leads to lower values of $L_{sc\,UC}$ since, according to Eq. (9.7), the lower values of the loss curve have now a larger contribution to the *ith* storey loss. Although these results may seem rather counterintuitive, the reduction in the expected loss is easier to understand when analysing its connection to λ_{UC}. The shift in the median of $S_{a,C}$ that occurs when uncertainty is accounted for indicates there is a significant number of cases where lower values of $S_{a,C}$ lead to the occurrence of the limit state condition, i.e. a significant number of earthquakes with lower IM values are more likely to lead to the occurrence of the limit state condition. Given that, according to the earthquake hazard curve $H(x)$, such lower IM values have a higher probability of occurrence, the risk will increase for this situation. Since the Δ values corresponding to those lower $S_{a,C}$ values are also lower than those obtained when uncertainty is not considered, the corresponding expected losses will decrease.

Although a similar type of behaviour is found in the evolution of the loss data for IRREG6, since the shift in the median Δ of the several storeys only ranges from 1% to 5%, the combined effect of a reduction in the median with that of an increase in the dispersion of the data actually leads to a slight increase in the value of EL_{UC} with respect to that of EL for some n_{LS} cases.

According to Liel *et al.* (2009), the shift in the median can be related to the number of possible failure modes and to the fact that considering the uncertainty or the randomness in the parameters of a given model may lead to the activation of different failure modes.

Furthermore, Liel *et al.* (2009) also refer that structures where a larger number of failure modes are activated tend to be associated with a more significant shift of the median collapse capacity. In the context of the current methodology, the occurrence of the limit state condition at a given section and the $S_{a,C}$ value associated to the occurrence of the limit state play the role of the failure modes and of the collapse capacity, respectively, reported by Liel *et al.* (2009). Hence, for the DL limit state, the number of possible failure modes corresponds to the number of sections where the limit state condition is analysed: sixty sections for REG6 and forty-four for IRREG6. In order to determine if a trend similar to the one reported by Liel *et al.* (2009) is found for the current structures, the percentage of times that the sections where the limit state condition occurs when considering uncertainty are the same as those where it occurs when uncertainty is not considered, represented by $s_{LS} = s_{LS_{UC}}$, is analysed for the n_{LS} cases of one and two. The results of this analysis are presented for each ground motion in Fig. 9.14. By comparing the results obtained for both structures, it can be observed that, for both n_{LS} cases, larger values of $s_{LS} = s_{LS_{UC}}$ occur more times for IRREG6 than for REG6. Even though the differences between the $s_{LS} = s_{LS_{UC}}$ values of both structures are not very large, the results do indicate the existence of a trend similar to that reported by Liel *et al.* (2009).

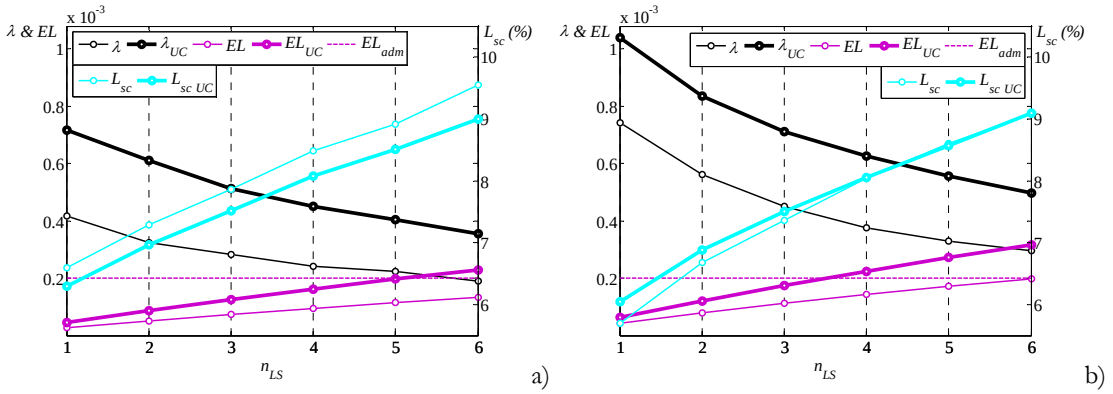

Figure 9.12. Results of the performance analysis of the REG6 (a) and the IRREG6 (b) structures when the uncertainty of the component capacities is neglected and considered also.

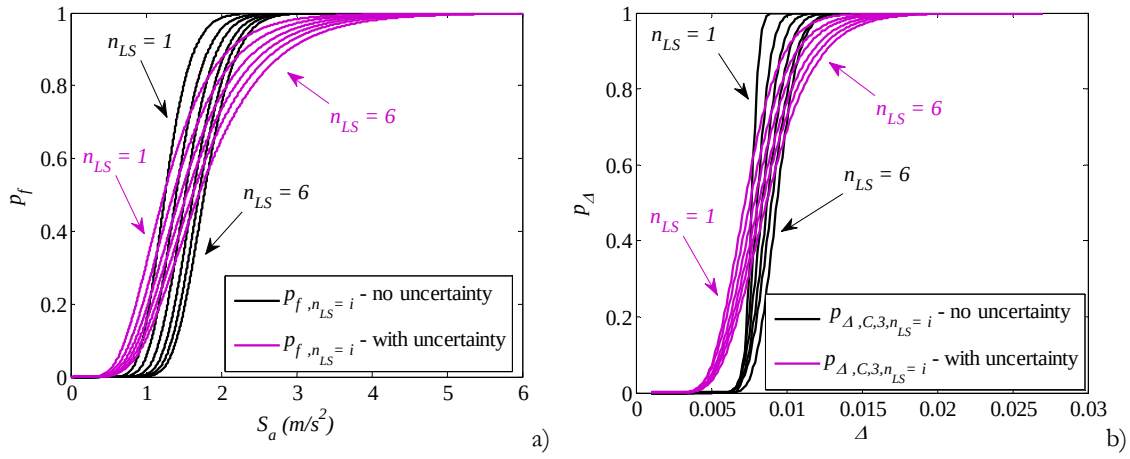

Figure 9.13. Fragility curves of the $S_{a,C}$ realizations for IRREG6 (a) and fragility curves of the $\Delta_{C,3}$ realizations for REG6 (b), with and without the uncertainty of the component capacities and for n_{LS} values of one to six.

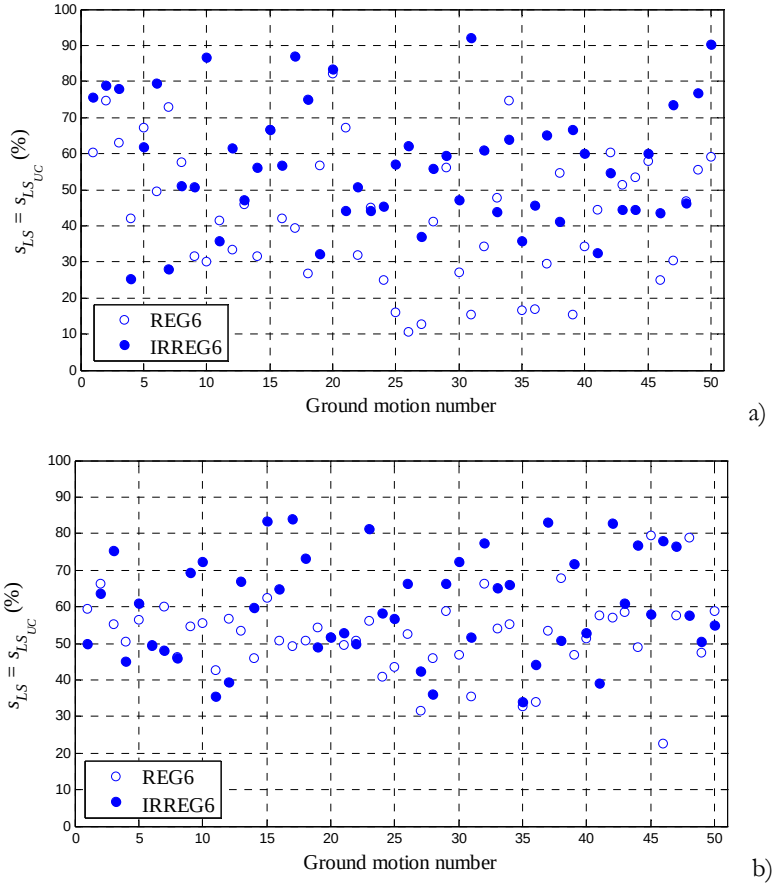

Figure 9.14. Percentage of times that, for a given ground motion, the sections where the limit state condition occurs when considering uncertainty are the same as those where it occurs when uncertainty is not considered, for both structures, and for the cases where n_{LS} is one (a) and two (b).

9.5.3 Results for the SD limit state

The performance metrics λ, L_{sc} and EL obtained for the limit state of SD for the REG6 and the IRREG6 structures are presented in Fig. 9.15 for n_{LS} values of one to four, for the case where the uncertainty of the component capacities is neglected, and considering the chord rotation capacity defined by $\theta_{SD,1}$. Globally, the results of the REG6 and IRREG6 structures indicate that performance scenarios up to n_{LS} equal to four can be seen to lead to acceptable values of EL. However, unlike for the case of the DL limit state, the results of Fig. 9.15 indicate that λ values are globally higher for REG6 than for IRREG6. This situation arises from the fact that, for REG6, larger deformation demands occur at the bottom columns, while for IRREG6 the larger deformation demands are obtained for the columns immediately above the setback. Since the limit state capacity of the bottom columns of REG6 is smaller than that of the IRREG6 third storey columns, REG6 reaches the limit state condition for smaller IM values, thus leading to a larger value of λ.

To analyse the influence of the modelling error of the capacity model, the performance results of both structures are presented in Fig. 9.16 for the situation where the uncertainty of the component capacities is neglected and also for the situation where it is accounted for. As for the DL limit state, λ_{UC}, $L_{sc\,UC}$ and EL_{UC} correspond to the values of λ, L_{sc} and EL obtained when the uncertainty of the component capacities is considered.

From the results presented in Fig. 9.16, including the uncertainty of the component capacities increases the risk considerably: the λ_{UC} values are 50% to 120% larger than the λ values. On the other hand, as observed for the limit state of DL, the influence of the uncertainty on the expected costs has an opposite effect: the $L_{sc\,UC}$ values are 6% to 15% lower than the L_{sc} values. As opposed to what was observed for the DL limit state, accounting for the uncertainty in the component capacities reduces the expected costs of both structures and for all the n_{LS} cases. As referred for the cases of the DL limit state, the increase of λ to λ_{UC} and the reduction from L_{sc} to $L_{sc\,UC}$ reflects the shift of the probabilistic distribution of the data due to the uncertainty, which as the direct effect of reducing the corresponding median values.

As for the DL limit state, accounting for the uncertainty in the component capacities also modifies the number of performance scenarios up to which the value of EL is found to be admissible. For REG6, the performance measure EL_{UC} is only admissible for $n_{LS}=1$, while for IRREG6 the performance is acceptable up to $n_{LS}=3$. Although in this case the performance changes arise from the mixed effects of the increase in the risk and of

the reduction of the expected costs, the significant increase of λ to λ_{UC} is still the governing factor.

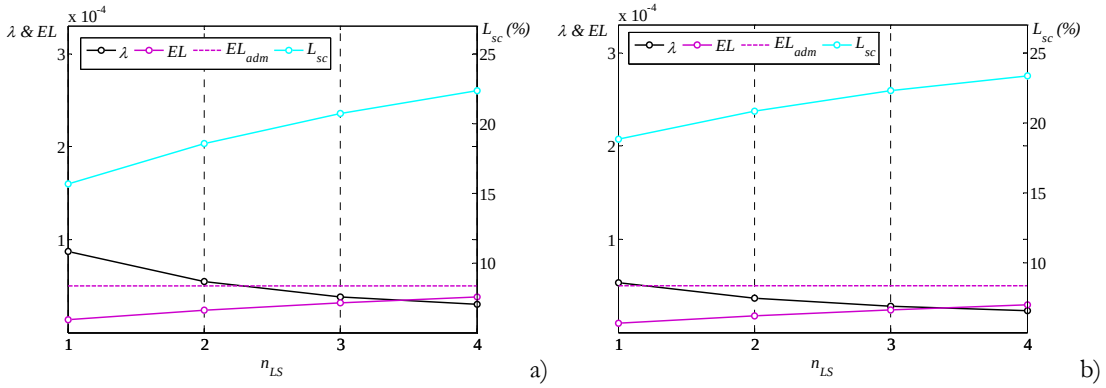

Figure 9.15. Results of the performance analysis of the REG6 (a) and the IRREG6 (b) structures when the uncertainty of the component capacities is neglected, and when the chord rotation capacity is $\theta_{SD,1}$.

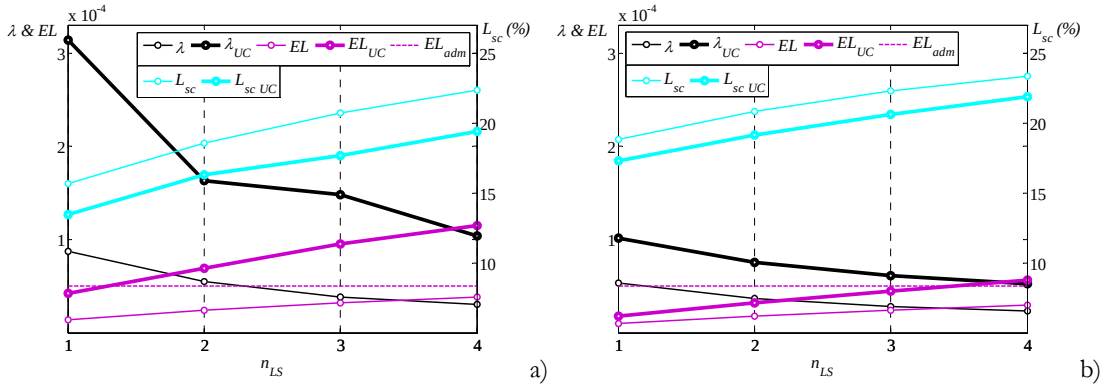

Figure 9.16. Results of the performance analysis of the REG6 (a) and the IRREG6 (b) structures when the uncertainty of the component capacities is neglected and considered also, and when the chord rotation capacity is $\theta_{SD,1}$.

As previously referred, the performance of the REG6 and the IRREG6 structures for this limit state was also carried out for the case where the chord rotation capacities are defined by $\theta_{SD,2}$. This situation was considered in order to analyse the issue referred in Section 9.2 regarding the performance equivalence of the case where a number of sections has ρ values around 0.85-0.95 and the case where only one section has a ρ value of 1.0. These two scenarios are considered to be equivalent if similar $S_{a,C}$ realizations are required to activate them. Since it may be difficult to obtain a scenario with several sections having ρ values around 0.85-0.95 that matches the scenario where only one section has a ρ value of 1.0, the scope of the analysis presented herein is extended. Therefore, scenarios where $n_{SD,2}$ sections have ρ values around 0.85-0.95 are compared to scenarios where

$n_{SD,1} < n_{SD,2}$ sections have a ρ value of 1.0. In order to perform these comparisons, Fig. 9.17 presents the performance results of REG6 and IRREG6 when the uncertainty of the component capacities is considered, and for the cases where the chord rotation capacity is $\theta_{SD,1}$ and $\theta_{SD,2}$. The results of $\lambda_{UC,1}$ and $L_{sc\,UC,1}$ refer to the cases where the chord rotation capacity is $\theta_{SD,1}$, while the results of $\lambda_{UC,2}$ and $L_{sc\,UC,2}$ are those where the chord rotation capacity is $\theta_{SD,2}$. As previously referred, the scenario comparison must be carried out for the n_{LS} cases where $\lambda_{UC,1} \approx \lambda_{UC,2}$, i.e. the performance scenarios for which the distribution of the $S_{a,C}$ realizations considering $\theta_{SD,1}$ or $\theta_{SD,2}$ is roughly the same. For the case of REG6, such similarity is found for $n_{LS} = 2$, when $\theta_{SD,1}$ is considered, and for $n_{LS} = 4$, when $\theta_{SD,2}$ is considered instead. In order to observe this similarity, Fig. 9.18a) presents the fragility curves corresponding to the $S_{a,C}$ realizations of these two scenarios. When comparing the expected costs of these two scenarios, $L_{sc\,UC,2}$ can be seen to be 10% larger than $L_{sc\,UC,1}$. For the case of IRREG6, two sets of scenarios can be seen to be similar. The first set of scenarios is found for $n_{LS} = 1$, when $\theta_{SD,1}$ is considered, and for $n_{LS} = 2$, when $\theta_{SD,2}$ is considered instead. Again, in order to observe the similarity of the scenarios, Fig. 9.18b) presents the fragility curves corresponding to their $S_{a,C}$ realizations. In this case, comparing the expected costs of the two scenarios shows that $L_{sc\,UC,2}$ is only 2% larger than $L_{sc\,UC,1}$. The second set of scenarios is found for $n_{LS} = 2$, when $\theta_{SD,1}$ is considered, and for $n_{LS} = 4$, when $\theta_{SD,2}$ is considered instead. In this case, comparing the expected costs of the two scenarios shows that $L_{sc\,UC,2}$ is about 5% larger than $L_{sc\,UC,1}$.

Based on these results, it is found that, for performance scenarios where the distribution of the $S_{a,C}$ realizations is similar, a lower limit state capacity occurring over a larger number of sections may lead to expected costs which are larger than those of the situation where a higher limit state capacity occurs over a smaller number of sections. Although these results may not be enough to generalize these findings, the observed trend should be further investigated given its potential influence in one of the performance metrics considered in the proposed methodology.

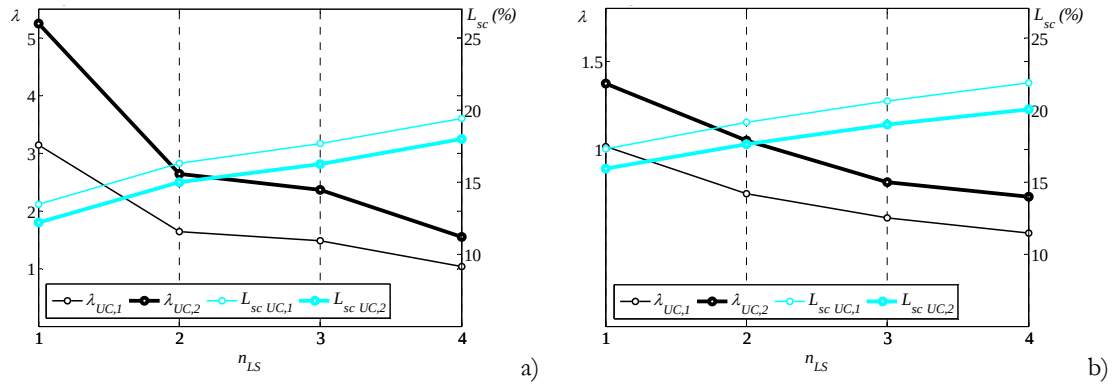

Figure 9.17. Results of the performance analysis of the REG6 (a) and the IRREG6 (b) structures when the uncertainty of the component capacities is considered, and the chord rotation capacity is $\theta_{SD,1}$ and $\theta_{SD,2}$.

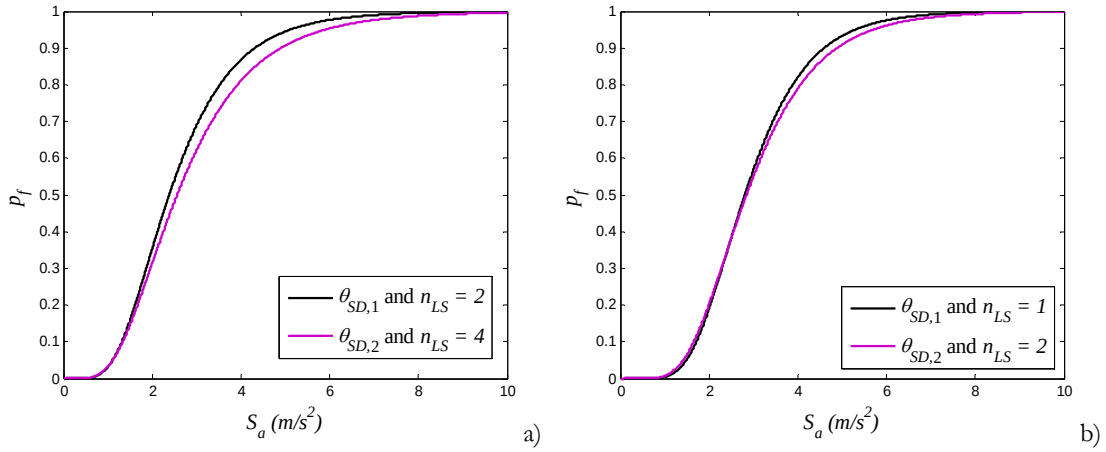

Figure 9.18. Similarity of the fragility curves of the $S_{a,C}$ realizations obtained for different n_{LS} values and when the chord rotation capacity is $\theta_{SD,1}$ and $\theta_{SD,2}$ for REG6 (a) and for IRREG6 (b).

9.5.4 Results for the NC limit state

Given the assumptions established in Section 9.3.4.3, only λ values are presented to analyse the performance of the REG6 and the IRREG6 structures for the limit state of NC. With respect to the limit state conditions also defined in Section 9.3.4.3, it was found that the occurrence of a NC limit state nonconforming condition in all of the beam sections of a given storey was not a governing scenario in any of the cases analysed, both in terms of the rotation capacity θ_{NC} and of the shear force capacity V_{NC}. Furthermore, the occurrence of the shear force capacity V_{NC} in columns was not a governing scenario also. Hence, the NC limit state performance of the structures was governed by the occurrence of the NC rotation capacity in columns and by the development of global yield mechanisms. In order to observe the importance of each of these nonconforming conditions, the following five scenarios were analysed for this limit state:

- Scenario 1 - Only the column rotation demand is controlled and the uncertainty of the rotation capacities is not considered ($S_{\theta_{NC}}$);
- Scenario 2 - Only the column rotation demand is controlled and the uncertainty of the rotation capacities is accounted for ($S_{\theta_{NC,U}}$);
- Scenario 3 - Only the development of global yield mechanisms is controlled (S_{GYM});
- Scenario 4 - Both the column rotation demand and the development of global yield mechanisms are controlled and the uncertainty of the rotation capacities is not considered ($S_{\theta_{NC}} + S_{GYM}$);
- Scenario 5 - Both the column rotation demand and the development of global yield mechanisms are controlled and the uncertainty of the rotation capacities is accounted for ($S_{\theta_{NC,U}} + S_{GYM}$).

Based on the definition of these scenarios, it is reminded that the uncertainty in the development of the global yield mechanisms due to the uncertainty in the value of the yield curvature of the components has not been considered. The λ values which correspond to the performance results of REG6 and IRREG6 for the five scenarios are presented in Table 9.2. The presented results indicate that only scenarios that do not involve the development of global yield mechanisms are able to conform to the condition $\lambda \leq \lambda_{adm} = 0.0001$. As can be observed, when the development of global yield mechanisms is considered, the λ values almost duplicate. This fact clearly emphasizes the importance of considering this type of condition when analysing structural safety and performance under earthquake loading.

When considering the scenario $S_{\theta_{NC}} + S_{GYM}$, the analysis of the results of both structures indicated that the limit state capacity was governed by the rotation demand in a column for only one ground motion. This situation implies that the median of the $S_{a,C}$ realizations has a 0.2% reduction from the scenario S_{GYM} to the scenario $S_{\theta_{NC}} + S_{GYM}$ and that the standard deviations of the log of the $S_{a,C}$ realizations has a reduction of about 2.7%. The latter reduction is the governing factor and leads to the slight decrease of the λ value from S_{GYM} to $S_{\theta_{NC}} + S_{GYM}$. When comparing the scenarios S_{GYM} and $S_{\theta_{NC,U}} + S_{GYM}$, the uncertainty in the rotation capacities plays a larger role and reduces the median of the $S_{a,C}$ realizations by 1.9%. Although there is also a 1.9% reduction of the standard deviations of the log of the $S_{a,C}$ realizations from S_{GYM} to $S_{\theta_{NC,U}} + S_{GYM}$, the shift of the

median is now the governing factor leading to the increase of the λ value from S_{GYM} to $S_{\theta_{NC,U}} + S_{GYM}$.

Table 9.2. Performance results of REG6 and IRREG6 for the NC limit state considered scenarios.

Scenario	λ - REG6	λ - IRREG6
$S_{\theta_{NC}}$	3.13E-5	4.95E-5
$S_{\theta_{NC,U}}$	4.52E-5	7.02E-5
S_{GYM}	1.27E-4	1.91E-4
$S_{\theta_{NC}} + S_{GYM}$	1.26E-4	1.90E-4
$S_{\theta_{NC,U}} + S_{GYM}$	1.33E-4	2.00E-4

With respect to the global yield mechanisms that were found when analysing this limit state, the unpredictability of their configurations and the importance of using a technique such as the one presented in Section 9.3.4.3 should be emphasized. In order to illustrate some of the global yield mechanisms that were found, Fig. 9.19 presents two examples for each structure. Although the cases presented in Figs. 9.19a) and c) ended up being controlled by a familiar mechanism (a soft-storey mechanism), the cases of Figs. 9.19b) and d) are less common. These results indicate clearly that approaches such as the one referred in Jalayer *et al.* (2007) that require the identification of the global yield mechanism configurations may not be practical to use due to the multitude of possibilities.

Finally, it is noted that, for this limit state, the λ values of IRREG6 are again higher than those of REG6. For the $S_{\theta_{NC}}$ and the $S_{\theta_{NC,U}}$ scenarios, this situation occurs since, for this limit state, the contribution of the REG6 upper storeys to the lateral demand is now much more significant, thus reducing the bottom storey demand concentration previously referred. Since, for IRREG6, the larger deformation demands still occur at the columns immediately above the setback, IRREG6 was found to reach the limit state condition for IM values lower than those of REG6, thus leading to higher values of λ. For scenarios where the development of global yield mechanisms governs the performance, IRREG6 was found to reach the limit state condition for IM values lower than those of REG6 since less yielding sections are usually required to develop the referred mechanisms.

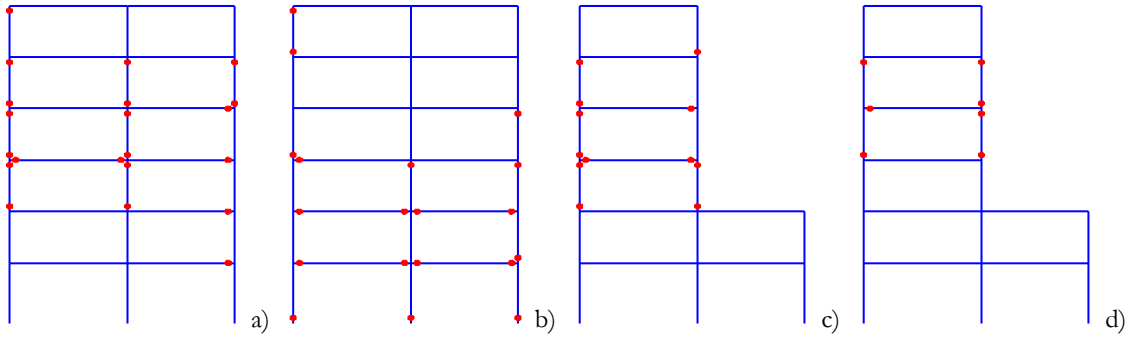

Figure 9.19. Examples of global yield mechanism configurations that were found when analysing the NC limit state.

9.5.5 Loss results obtained using the linear approximations of the loss curves

In order to observe the accuracy of the expected loss estimates obtained using Eqs. (9.10) and (9.14) which involve the linear approximations of the loss curves defined by Eqs. (9.8) (Option 1) and (9.9) (Option 2), respectively, an example application of the proposed formulations is presented. The expected losses of the third storey of the REG6 structure calculated for the several n_{LS} cases of the DL and SD limit states using Eqs. (9.10) and (9.14) are compared herein with the values obtained using the real loss curves. The linear approximations of the loss curves considered for this example are those presented in Figs. 9.3 and 9.4. Table 9.3 presents the results obtained for the DL limit state, while Table 9.4 presents those of the SD limit state. As can be observed, the results obtained with Option 1 for both limit states involve larger relative errors ε. On the other hand, Option 2 is able to capture the real loss value with relative errors below 2%. Although Option 2 performs better, the usefulness of both approaches will depend on the level of accuracy required for a given application and on the level of detail of the available data to define the loss curve.

Table 9.3. Comparison of the losses of the third storey of REG6 for the DL limit state calculated using the real loss curves and the proposed linear approximations, and their relative error ε.

n_{LS}	Real loss (%)	Loss with Option 1 (%) and ε (%)		Loss with Option 2 (%) and ε (%)	
1	9.32	8.74	*(ε = -6.22)*	9.49	*(ε = 1.82)*
2	10.28	9.21	*(ε = -10.41)*	10.34	*(ε = 0.58)*
3	11.02	9.59	*(ε = -12.98)*	11.02	*(ε = 0.00)*
4	11.77	9.96	*(ε = -15.38)*	11.70	*(ε = -0.59)*
5	12.38	10.27	*(ε = -17.04)*	12.25	*(ε = -1.05)*
6	13.04	10.61	*(ε = -18.63)*	12.86	*(ε = -1.38)*

Table 9.4. Comparison of the losses of the third storey of REG6 for the SD limit state calculated using the real loss curves and the proposed linear approximations, and their relative error ε.

n_{LS}	Real loss (%)	Loss with Option 1 (%) and ε (%)		Loss with Option 2 (%) and ε (%)	
1	18.99	16.34	*(ε = -13.95)*	18.78	*(ε =-1.11)*
2	22.94	18.88	*(ε = -17.70)*	22.46	*(ε =-2.09)*
3	24.66	20.34	*(ε = -17.52)*	24.18	*(ε =-1.95)*
4	26.74	21.93	*(ε =-17.99)*	26.21	*(ε =-1.98)*

9.5.6 Analysis of the lognormal distribution hypothesis for the representation of fragility curves

As previously referred, the assumption that the fragility curves involved in the quantification of performance can be adequately modelled by lognormal distributions was also analysed. Although this hypothesis is commonly assumed, the analysis of its validity is seldom found. More specifically, for the case of fragility curves obtained using an IM-based approach such as the one considered in the performance analysis methodology proposed herein, results addressing the validity of the lognormal distribution hypothesis may only be found for the case of collapse assessment, e.g. see (Ibarra and Krawinkler, 2005). Furthermore, such results are based on graphical methods (e.g. cumulative distribution function plots) or based on the use of the Kolmogorov-Smirnov/Lilliefors statistical test (Lilliefors, 1967) usually applied to the log of the data. As discussed in Chapter 5, the use of such procedures to validate this statistical hypothesis for samples of small to moderate sizes is inadequate.

A more efficient approach is, therefore, presented in which the suitability of the lognormal distribution to represent fragility curves is assessed using statistical tests with adequate characteristics. The considered tests were selected according to the results of the benchmark efficiency test presented in Appendix A and were also used in the statistical distribution analyses of structural demand data presented in Chapter 5. In the considered approach, the lognormality assumption is tested by assessing the normality hypothesis of the log of the data. Therefore, the selected tests are best suited to identify non-normal distributions when the data is symmetric. Given the random nature of the data under analysis, the following four tests that have different characteristics and analyse different aspects of the data were selected:

- The β_3^2 normality test based on a polynomial regression proposed by Coin (2008).
- The R_{sJ} normality test focussing on detecting heavier tails proposed by Gel *et al.* (2007).
- The modified measure of kurtosis T_w suggested by Bonett and Seier (2002).

- The *CS* test statistic based on normalized spacings defined by Chen and Shapiro (1995).

Details of the tests are omitted herein but comprehensive descriptions of their formulations and performance are presented in Chapter 5 and Appendix A.

The selected tests were applied to the data samples corresponding to the log of the $S_{a,C}$ realizations and to the log of all the storeys $\measuredangle_{C,i}$ realizations, where *i* stands for the *ith* storey. The considered data samples are those obtained from the analysis of both structures for the various n_{LS} cases of the DL, the SD and the NC limit states. For the case of the SD limit state, data samples obtained considering both cases of the chord rotation capacity (i.e. $\theta_{SD,1}$ and by $\theta_{SD,2}$) were analysed. With respect to the NC limit state, the selected data samples are only those of the $S_{a,C}$ realizations obtained from the scenario where both the column rotation demand and the development of global yield mechanisms are controlled. The total number of analysed samples of $S_{a,C}$ realizations is 30 while that of the $\measuredangle_{C,i}$ realizations is 168, which amounts to a total of 120 and 672 test results, respectively. The analysis of the lognormality hypothesis was first carried out for the cases where the uncertainty of the component capacities is not considered. A second batch of analyses was then carried out for the large-sample situation corresponding to the case where the uncertainty of the component capacities is accounted for.

With respect to the samples where the uncertainty was not considered, the results show that the lognormal distribution hypothesis was accepted in 86.7% of the 120 tests that were carried out on samples of $S_{a,C}$ realizations. For the samples of $\measuredangle_{C,i}$ realizations, the lognormal distribution hypothesis was accepted in 81.1% of the 672 tests. Therefore, these results indicate that the lognormal distribution is suitable for the probabilistic modelling when the data dispersion source is the record-to-record variability of the $S_{a,C}$ realizations and of the $\measuredangle_{C,i}$ realizations.

With respect to the samples where the uncertainty of the component capacities was accounted for, the test results are significantly different. For the samples of $S_{a,C}$ realizations, the lognormal distribution hypothesis was accepted in only 14.2% of the tests, while for the samples of $\measuredangle_{C,i}$ realizations the percentage is even lower. The reason behind such disproportion of results is relatively well known. Most goodness-of-fit tests such as those considered herein are much more sensitive when dealing with larger samples where modest departures from the selected hypothesis are less influential. Since the size of the samples analysed in this case is considerably large (i.e. 2500), the assumption of normality was seen to be rejected for several samples exhibiting only slight imperfections with respect to the theoretical model. To illustrate this situation, Fig. 9.20 presents normal quantile-quantile (*Q-Q*) plots of the log of the REG6 $S_{a,C}$ realizations corresponding to the SD limit state when $n_{LS} = 2$ and $n_{LS} = 3$. Although the two plots are apparently very

similar, as well as visually presenting a good fit to the theoretical model, all four tests rejected the lognormal distribution hypothesis for the sample of Fig. 9.20a), while three of the tests accepted the hypothesis for the sample of Fig. 9.20b). Still, not all samples where the lognormality hypothesis was rejected present such slight deviations. Several of the samples exhibit more pronounced departures from the assumed hypothesis. Figure 9.21 presents two additional examples of normal Q-Q plots of the log of the IRREG6 $\measuredangle_{C,5}$ realizations corresponding to the SD limit state and $n_{LS}=3$, and $S_{a,C}$ realizations corresponding to the DL limit state when $n_{LS}=2$. In these two cases, the tails of the samples exhibit a more pronounced deviation from the assumed theoretical model. Only one test accepted the hypothesis for the sample of Fig. 9.21a), while all four tests rejected the hypothesis for the sample of Fig. 9.21b).

Although the goodness-of-fit results obtained when the uncertainty of the component capacities was not considered seem to be impaired by those obtained for the situation where it is accounted for, the importance of the latter must be interpreted in light of the following. Although visual analysis of the data is far from being an objective method to establish the validity of a given distribution hypothesis, the decision to validate an assumption based on such approach is believed to be acceptable in large sample situations involving small visual departures from the theoretical model, e.g. see Fig. 9.20b). On the other hand, for samples exhibiting more pronounced departures from the assumed hypothesis, such deviations are seen to occur in the tails of the data, especially in the upper tail. In this situation, the influence of using an assumed distribution also depends on the fact that the actual data may have a tail heavier, Fig. 9.21a) or lighter, Fig. 9.21b), than that of the assumed model. Distributions with heavier tails have a larger contribution of data with higher values, while in distributions with light tails the contribution of the higher values is smaller.

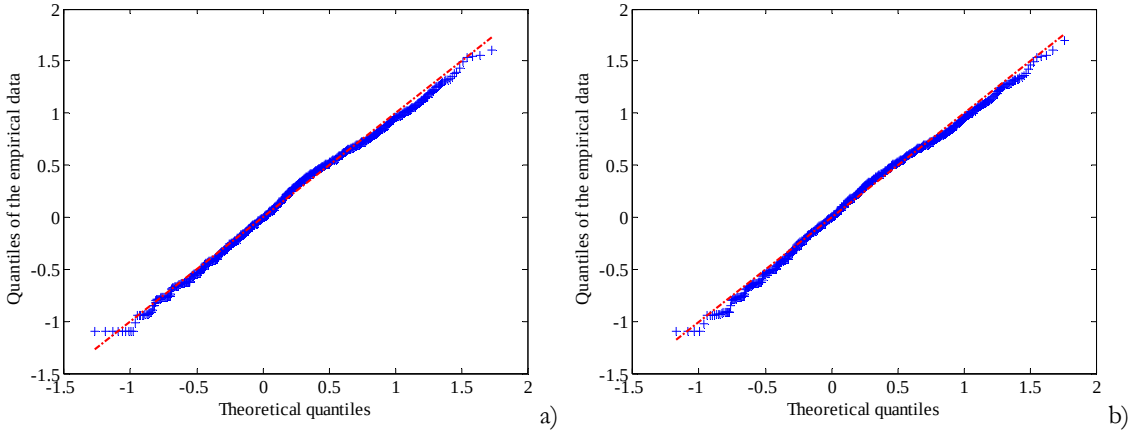

Figure 9.20. Examples of Q-Q plots of the REG6 $S_{a,C}$ realizations for the SD limit state for $n_{LS}=2$ (a) and $n_{LS}=3$ (b), when uncertainty is accounted for.

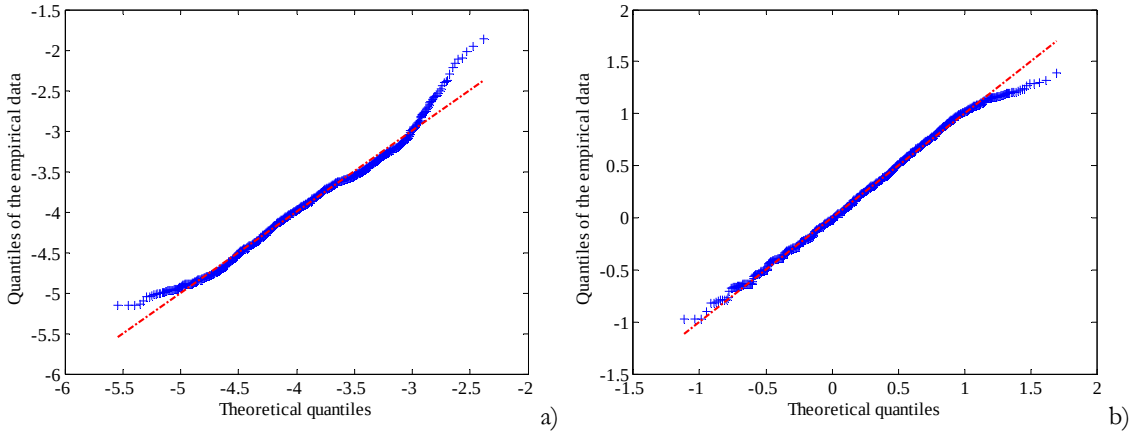

Figure 9.21. Examples of Q-Q plots of the IRREG6 $\perp_{C,5}$ realizations for the SD limit state and $n_{LS} = 3$ (a) and $S_{a,C}$ realizations for the DL limit state and $n_{LS} = 2$ (b), when uncertainty is accounted for.

After a detailed analysis of all the tested samples, it was found that more than 95% of the samples of $S_{a,C}$ realizations have upper tails which are lighter than that of the theoretical model, while more than 95% of the samples of $\perp_{C,i}$ realizations have upper tails which are heavier than that of the theoretical model. Therefore, with respect to the influence of using the lognormal distribution to represent fragility curves instead of using a more data-fitting distribution, the findings indicate that:

- When evaluating Eq. (9.4), larger contributions from the hazard function will be included since the assumed lognormal distribution has a heavier tail than that of the empirical data. Hence, the value of λ calculated using Eq. (9.4) will be overestimated;
- When evaluating Eq. (9.7), the contribution of the higher values of the loss curve will be smaller since the assumed lognormal distribution has a lighter tail than that of the empirical data. Hence, the value of the *ith* storey loss $L_{sc,i}$ calculated using Eq. (9.7) will be underestimated.

In order to estimate the amount of overestimation/underestimation produced by the lognormality assumption, the values of λ and $L_{sc,i}$ of both structures and for all the considered limit states (but only for the cases where the uncertainty of the component capacities is considered) were recalculated using fragility curves that have lighter and heavier tails, respectively, than those of the lognormal fragility assumption. The new values of λ and $L_{sc,i}$ were calculated after switching the normal CDFs of Eqs. (9.5) and (9.7) by fragility curves simulated by the CDF of the Generalized Normal Distribution (GND) (Nadarajah, 2005) defined as:

$$F(x)=\frac{1}{2}\left[1+\frac{\mathrm{sgn}(x-\mu)}{\Gamma(1/\kappa)}\gamma\left(1/\kappa,\left|\frac{x-\mu}{\sqrt{2}\cdot\sigma}\right|^{\kappa}\right)\right] \tag{9.20}$$

where $\mathrm{sgn}(.)$ represents the sign function, $\Gamma(.)$ is the Gamma function and $\gamma(.)$ is the incomplete Gamma function. In order to define fragility functions in agreement with those previously defined by the lognormal distribution, parameters μ and σ must be replaced by $\ln\eta_{IM_C}$ and β_{IM_C}, when evaluating λ, and by $\ln\eta_{EDP_{C,i}}$ and $\beta_{EDP_{C,i}}$, when evaluating $L_{sc,i}$. The simulation of CDFs with different tail weights is regulated by parameter κ, (Nadarajah, 2005). When $\kappa<2$ and $\kappa>2$, the simulated CDFs have tails which are heavier and lighter, respectively, than those of the normal CDF. When $\kappa=2$, Eq. (9.20) represents an exact normal CDF. In order to simulate the light and heavy tails required for the present analysis, κ was considered to be 4.0 and 1.5, respectively. These values were chosen by visually fitting several $S_{a,C}$ and $\Delta_{C,i}$ data distributions over GND Q-Q plots. By comparing the new values of λ and $L_{sc,i}$ with those previously obtained, the following was found:

- The values of λ obtained using the lognormal fragility curves overestimate the risk values obtained using the GND CDFs by 4% to 18%.
- The values of $L_{sc,i}$ obtained using the lognormal fragility curves may underestimate up to 13% the storey loss values obtained using the GND CDFs.

Globally, the results indicate that, when considering fragility curves modelled by the lognormal distribution, the level of error that may be involved is still acceptable. Therefore, based on these results, it is believed that the lognormal distribution is suitable for the probabilistic modelling of the fragility curves of the $S_{a,C}$ realizations and of the $\Delta_{C,i}$ realizations when the variability of the data stems from the record-to-record variability and from the uncertainty of the component capacities. Nonetheless, since this conclusion is based on a limited set of data, additional cases should be analysed in order to generalize this finding.

9.6 Conclusions

A probabilistic methodology was proposed to analyse the seismic performance of existing buildings using global metrics to determine if the behaviour conforms to a given limit state. The considered performance metrics are the probability of occurrence λ of the limit state, the corresponding loss L_{sc} associated to the repair of the building, and the corresponding number n_{LS} and type of mechanisms that occur. Each case of n_{LS}

establishes a scenario corresponding to the occurrence of the limit state. The λ and L_{sc} performance metrics of each considered scenario are then combined to define a global performance value representing the expected loss *EL* associated to that limit state. In order to consider λ, L_{sc} and the occurrence of several scenarios of the mechanisms as global performance parameters, an update of existing limit state descriptions was performed. The limit state descriptions proposed by EC8-3 were analysed and alternative proposals were discussed to establish risk- and cost-related limit state definitions. These proposals were then used to analyse the performance of two RC structures using the proposed methodology for the EC8-3 limit states of DL, SD and NC. Although EC8-3 was used as a reference, the issues raised by this analysis of the limit states extend beyond this code since similar limit states or performance levels are also considered by other international standards.

In order to emphasize the influence of the modelling error of the selected capacity models, the performance assessment results were presented separately for the situation where the uncertainty of the component capacities is neglected and for the situation where it is accounted for. A global analysis of the performance results indicates that, with respect to the situation where the uncertainty of the component capacities is not considered, allowing for such uncertainty increases the risk considerably (e.g. more than duplicating the risk in some cases) while leading to moderate reductions of the expected losses. Such differences were discussed and accounting for the uncertainty of the component capacities was found to produce a shift of the probabilistic distribution of the data. As a direct effect of such shift, there is a reduction in the median of the data, which was found to be the governing factor for the increase and the reduction in the risk and expected loss values. Moreover, such results are seen to disagree with the conventional assumption that accounting for modelling uncertainties has the unique effect of increasing the dispersion of the fragility curves without influencing the median of the data (a fact also disputed by the findings reported by Liel *et al.* (2009)).

In the overall, the proposed methodology was found to be able to determine admissible performance scenarios that go beyond the limitations of the code definitions, which may allow for a rational decision-making process about the need to retrofit or strengthen a given structure. In this context, the performance analysis for the SD limit state showed that, for performance scenarios where the distribution of the $S_{a,C}$ realizations is similar, a lower limit state capacity occurring over a larger number of sections may lead to expected costs which are larger than those of the situation where a higher limit state capacity occurs over a smaller number of sections. Although these results may not be enough to generalize these findings, the observed trend should be further investigated given its potential influence in the assessment of the expected losses. Furthermore, the performance analysis carried out for the NC limit state also emphasized the importance of

considering the potential occurrence of global yield mechanisms, as well as that of having a process able to account for the unpredictability of their configurations.

Additionally, two simplified analytical expressions were also defined to estimate the expected storey loss value. These expressions were established by using different piecewise linear approximations of the structural and non-structural loss curves. The results obtained from these simplified expressions were analysed and the accuracy of one of the proposals was seen to be superior. Still, the usefulness of both approaches will depend on the level of accuracy required for a given application.

Finally, the use of the lognormal distribution to model the fragility curves involved in the performance analysis was also addressed to determine the suitability of this common assumption. Results of adequate statistical methods used to test this hypothesis were presented and large-sample situations where the hypothesis is rejected were also discussed. The results found indicate that the lognormal distribution is suitable for the probabilistic modelling of the fragility curves involved in the proposed methodology when the variability of the data is due to the record-to-record variability. On the other hand, when using the lognormal distribution to model fragility curves in which the variability of the data stems from the record-to-record variability and from the uncertainty of the component capacities, some lack of fit may be involved in the tails of the data. This situation was analysed and simulations were carried out to assess the expected level of error that may occur when considering the lognormal distribution. Since the results obtained indicate that the error is acceptable, the lognormal distribution is also recommended for this situation. Still, additional cases should be analysed in order to generalize this finding.

Chapter 10
Closure

10.1 Conclusions

The present dissertation addressed several topics related to the development and the application of seismic safety assessment methodologies. Although the main observations and conclusions of the work were discussed in each chapter, the most relevant findings alongside important conclusions are presented in the following.

10.1.1 Conclusions regarding the EC8-3 safety assessment methodology

Several aspects of the safety assessment methodology that is proposed in Part 3 of Eurocode 8 (EC8-3) (EC8-3, 2005) were analysed and discussed in order to identify issues that require additional research. After a detailed examination of the difficulties associated to the quantification of the member chord rotation according to the method proposed by EC8-3, several alternatives were analysed. The theoretical based method termed Exact Geometrical Method, combined with corrective alternatives dealing with cases where the abscissa of the point of contraflexure x_{L_s} is ill-defined, is an approach less sensitive to numerical issues that produced adequate results. Moreover, the proposed approximate geometrical method that does not require the quantification of x_{L_s} and considers member drift and nodal rotations for beams and columns was also seen to produce adequate results.

A sensitivity analysis of the EC8-3 limit state capacity models was also carried out with respect to the shear-span L_s in order to validate previous results by Mpampatsikos *et al.* (2008a) which stated that L_s could be generally considered to be $L/2$, where L is the member length. The results presented in Chapter 2 indicated that for $L_s > 0.2L$, the approximation $L_s = L/2$ will yield capacity results with an acceptable accuracy. Moreover,

this approximation was also recommended throughout the whole range of L_s values for the case of the shear force limit state capacity. On the other hand, such recommendation is not applicable to the deformation capacity models since results indicate that L_s values lower than $0.2L$ are more frequent, especially in beams. Therefore, the correct value of L_s should always be computed in this case.

The results obtained from the application of the EC8-3 methodology to assess the seismic safety of two reinforced concrete (RC) structures indicated that linear analysis was not able to be considered. Furthermore, results also indicated that, for structures where seismic design measures were not considered, the applicability of linear analysis might be restricted to the limit state of Damage Limitation (DL) only. Nonetheless, given the potential complexity of the process that verifies if linear analysis is admissible for the case of larger structures, a more practical verification methodology was proposed that allows for a reduction on the number of joints that need to be analysed.

Results obtained from the safety assessment based on nonlinear analyses indicated that DL is the dominant deformation limit state. A similar conclusion was also noted by Mpampatsikos *et al.* (2008b) which also refer that considering the equivalent secant-to-yield stiffness proposed by EC8-3 for this limit state may lead to a significant underestimation of the seismic safety. With respect to the results based on nonlinear dynamic analysis, these revealed that the characteristics of the considered ground motions have a considerable influence on the deformation assessment results. On the other hand, the shear force assessment results can be seen to be much less sensitive to the record characteristics. After exploring different possibilities, it was found that real records having an average response spectrum that matches closely the code spectrum showed a good agreement between their mean demand and that obtained by using artificial accelerograms (the type of records that match more efficiently the EC8-3 requirements) for all the limit states. On the other hand, demand obtained from real records scaled for the 5% damping spectral acceleration ordinate of the ground motion for the fundamental period of the structure $S_a(T_1)$ only exhibited an adequate agreement with that obtained by using artificial accelerograms for the DL limit state. Still, adequate results were obtained for the Significant Damage (SD) and Near Collapse (NC) deformation limit states using an alternative scaling procedure based on a representative inelastic period of the structure.

With respect to the use of pushover analysis, results were seen to be generally on the safe side with respect to those of nonlinear dynamic analysis. Still, more applications should be carried out to determine if this conclusion can be extended to other structures.

To address the consistency and reliability of the safety levels obtained when using the EC8-3 methodology, a probabilistic analysis was carried out to determine fragility values associated to the several limit states analysed. Results of this probabilistic analysis indicated that similar demand-to-capacity (D/C) ratios obtained for different situations may lead to fragility values that may differ considerably. This variability was found to be dependent on

the limit state and on the type of demand (chord rotation or shear force). Nonetheless, the overall results allowed for the definition of estimated ranges for the expected fragility values, given a set of ranges of the D/C ratios. However, the adequacy of these values should be examined within the scope of the general safety format of the EC8-3 procedure, namely in terms of their implications on the system-level safety, and additional applications should be carried out to determine if similar values are obtained for other structures.

In terms of the influence of the selected Knowledge Level (KL) in the assessment results (i.e. by measuring the changes on the limit state capacity values), it was found that going from levels KL1 to KL2 or from KL2 to KL3 produces changes that vary according to the considered limit state. For the case of the deformation-based SD and NC capacity values, these changes were seen to be small, while for the case of the DL and the shear force capacities the variations were seen to be significant in some situations. Hence, from the material characterization point of view, the need for an increase in knowledge about their properties must be carefully thought out due to the increase in work, costs and on-site difficulties that may be implied.

To gain a more comprehensive understanding about the influence of the information that is required to define the KLs and about the reliability of the corresponding Confidence Factor (CF) values, a more detailed review of the EC8-3 procedures was carried out. This analysis indicated that only the uncertainty related to the materials is adequately reflected in the quantification of the EC8-3 safety measures. Therefore, the reliability of the CFs was assessed using a probabilistic framework focussing the influence of the characterization of material properties where the essential features are the number of material tests and the existence of prior knowledge. The presented study uses the concrete compressive strength to analyse the CFs but conclusions for other materials and other material properties were also inferred from the results. For cases where the normal and the lognormal distribution assumptions are considered to represent the statistical distribution of the selected material property, the probabilistic framework that was defined to obtain the CF values depends only on the coefficient of variation (CoV) of the material property. Hence, the proposed expressions can be applied to the properties of other materials of interest for which these statistical distribution assumptions are acceptable.

Results obtained when the existence of prior knowledge is not considered indicated that the EC8-3 proposed CFs are more consistent with the assumption of known variance. Moreover, the KL1 and KL2 CFs were believed to be adequate, assuming that the selected confidence levels are satisfactory. With respect to KL3, the EC8-3 proposed CF is not met by any of the cases studied. Nonetheless, the known variance assumption is also selected since it leads to lower values of the CF. For this case, a CF value of 1.08 is seen to be more adequate to the assumptions made in the study. Furthermore, it was observed that if the EC8-3 minimum number of tests are met, and assuming a maximum CoV of 20% for the concrete compressive strength, the CF values could be significantly reduced for buildings

higher than three-storeys (e.g. from 1.35 to 1.14, for KL1, and from 1.20 to 1.08, for KL2). Similarly, the EC8-3 proposed CF for KL2 and the proposed value of 1.08 for KL3 was seen to agree also with the unknown variance hypothesis for buildings higher than three-storeys, even assuming a value for the sample CoV as high as 40%. For the case of KL1, this situation can only be attained if the maximum sample CoV is reduced to 32%.

Results for the case where the existence of prior knowledge is considered were only obtained for the situation where the material property under analysis follows a normal distribution. By using a Bayesian framework, the results obtained lead to the conclusion that when the prior knowledge and the new test data are in agreement, the necessary CF decreases, when compared to the value obtained in the absence of prior knowledge. Nonetheless, the CF value obtained for KL3 is still larger than the value proposed by EC8-3. In addition, the case of combining different sources of testing data was also addressed considering the same Bayesian framework, as it is a special case of the situation where prior knowledge exists. Results of this analysis indicate that combining different types of tests leads to CF values that are lower than those obtained in the first part of the proposed study for all KLs.

10.1.2 Conclusions addressing the probabilistic characterization of the demand under earthquake loading

The goodness-of-fit results obtained by analysing structural demand distributions using appropriate statistical methods indicated that the lognormal distribution is suitable for the probabilistic modelling of the curvature, of the chord rotation and of the inter-storey drift demands. With respect to the shear force demand, the results indicated that both the normal and the lognormal distributions have the same potential to model its probabilistic distribution. Still, the results obtained for the shear force were not found to be entirely satisfactory, either due to the occurrence of demand distributions with very low levels of dispersion in yielding elements or, in other cases, due to the occurrence of a larger number of outlying observations. With respect to the type of intensity measure (IM), $S_a\left(T_1\right)$ was seen to be generally more adequate than the peak ground acceleration (PGA) to obtain demand distributions compatible with the selected distribution hypotheses.

Furthermore, the goodness-of-fit results obtained also emphasized the influence of outlying observations that were seen to occur in several situations. Therefore, it was found that adequate robust methods should be used to determine the distribution parameters in order to minimize their effects. In this context, the results obtained from the analysis of the statistical performance of robust estimators to compute central value estimates of structural demand distributions indicated that estimators $T_{Hub,3}$, $T_{Ham,2}$, $T_{Ham,3}$, $T_{Tuk,3}$ and T_{log} (see Chapter 6 for their description) are recommended for samples of size between fifty and

fifteen. On the other hand, for samples of smaller size, estimators $\overline{x}_{0.08-HQ1}$ and $\overline{x}_{0.12-HQ1}$ (see Chapter 6 for their description) are recommended instead. With respect to the effects of the selected IMs, $S_a(T_1)$ and PGA, on the efficiency of these estimators, no definite trend was observed as their efficiencies are similar irrespective of the IM. Although such results indicate that these estimators are fit to be considered under various conditions of the variability of the demand, further IMs should be analysed to confirm this conclusion. In addition, reference is made to the performance results obtained for the median, a widely used estimator in performance-based earthquake engineering (PBEE) methodologies. The results obtained for the median pointed out the inadequate performance of this estimator in all cases analysed, when compared to that of the recommended estimators. Therefore, it is suggested that in future PBEE applications, central values estimates of seismic demand should be obtained by one of these estimators instead.

In order to define a complete probabilistic model for the structural demand data that was found to follow a lognormal or a normal distribution, the characterization of the dispersion of the data using robust estimators was also addressed. This analysis resulted in the definition of combinations of robust central value and dispersion estimators found to be more adequate to define the referred probabilistic models. After analysing the statistical performance of several combinations, it was found that, for larger sample sizes (e.g. larger than fifteen), combinations involving $T_{Hub,3}$ or T_{log} as the central value estimator and with τ_s as the dispersion estimator (see Chapter 7 for its description) should be used. On the other hand, for samples of smaller sizes (e.g. lower than fifteen), combinations involving $\overline{x}_{0.08-HQ1}$ or T_{log} as the central value estimator and with $s_{t,3}$ as the dispersion estimator (see Chapter 7 for its description) are suggested instead. As for the previous results obtained for the central value estimators, no definite trend was observed regarding the effects of the selected IMs, $S_a(T_1)$ and PGA, on the efficiency of the dispersion estimators.

10.1.3 Conclusions associated to the development of methodologies for seismic risk assessment

The methodologies (Methodology 1 and Methodology 2) that were proposed for the seismic risk assessment of building components involved the development of analytical closed form expressions for the quantification of limit state exceedance probabilities. The development of these expressions was achieved by introducing original contributions for the probabilistic representation of the ground motion hazard and by defining suitable expressions characterizing the evolution of structural demand for increasing levels of earthquake intensity. Methodology 1 has proposed the use of extreme-type probabilistic distributions to represent ground motion hazard, while Methodology 2 involves an

approximate expression that exhibited a clear advantage over the model adopted by the SAC/FEMA method. With respect to the evolution of structural demand with increasing earthquake intensity, two proposals were made for force-based demand evolutions, namely for shear force demand: one for smoother evolutions based on a logarithmic function and one for bilinear-type evolutions based on an inverted exponential function. Within the scope of developing Methodology 1, both proposals for the shear force demand evolution were able to be incorporated. On the other hand, the development of Methodology 2 was not able to account for the bilinear-type evolution.

Due to their generalized formulations, the proposed procedures were found suitable to assess the probability of exceedance of component limit states without obtaining the fragility curve. Furthermore, the presented application examples illustrated the simplicity of the proposed procedures. The analysis of the results of the example applications indicated that the uncertainty of the limit state capacities increases significantly the estimate of the probability of exceedance of the limit states. Furthermore, for the cases that were analysed, the modelling error of the limit state capacity expressions was seen to be the main factor governing both the estimate of the probability of exceedance of the limit state as well as its variability.

The probabilistic methodology that was proposed to analyse the seismic performance of existing buildings for a given limit state uses global performance metrics to determine the admissibility of building behaviour. These performance metrics are the probability of occurrence of the limit state, the corresponding expected loss associated to the repair of the building, and the corresponding number and type of mechanisms that are developed, which establish possible scenarios for the occurrence of that limit state. Furthermore, the development of the proposed methodology has involved limit state definitions adapted from those proposed by EC8-3 in order to extend their scope and establish risk- and cost-related limit state definitions.

Results obtained from applying the proposed methodology to case-study examples indicated that the methodology was able to establish admissible performance scenarios that go beyond the limitations of the code definitions, which may allow for a rational decision-making process about the need to retrofit or strengthen a given structure. In this context, the performance analysis for the SD limit state showed that, for performance scenarios where the distribution of the IM-capacities (i.e. the distribution of the ground motion intensities at which a given limit state occurs for the structure under assessment) is similar, a lower limit state capacity occurring over a larger number of sections may lead to expected costs which are larger than those of the situation where a higher limit state capacity occurs over a smaller number of sections. Although these results may not be enough to generalize these findings, the observed trend should be further investigated given its potential influence in the assessment of the expected losses. Furthermore, the performance analysis carried out for the NC limit state also emphasized the importance of considering the

potential occurrence of global yield mechanisms, as well as that of having a process able to account for the unpredictability of their configurations.

The results of the considered application example also emphasized the influence of the modelling error of the capacity models. The performance results indicated that, with respect to the situation where the uncertainty of the component capacities was not considered, allowing for such uncertainty increases the risk considerably (e.g. more than duplicating the risk in some cases) while leading to moderate reductions of the expected losses. Accounting for the uncertainty of the component capacities was found to produce a shift of the probabilistic distribution of the data. As a direct effect of such shift, there is a reduction in the median of the data, which was found to be the governing factor for the increase and the reduction in the risk and expected loss values. Moreover, such results were seen to disagree with the conventional assumption that accounting for the modelling uncertainties has the unique effect of increasing the dispersion of the fragility curves without influencing the median of the data (a fact also disputed by the findings reported by Liel *et al.* (2009)).

Within the scope of this methodology, two simplified analytical expressions were also defined to estimate the expected storey loss value. These expressions were established by using different piecewise linear approximations of the structural and non-structural loss curves. Based on the results obtained from these simplified expressions, the accuracy of one involving more linear branches was found to be superior. Still, the usefulness of both approaches will depend on the level of accuracy required for a given application.

Finally, the use of the lognormal distribution to model the fragility curves involved in the performance analysis was also addressed to determine the suitability of this common assumption. Results of adequate statistical methods used to test this hypothesis were presented and large-sample situations where the hypothesis is rejected were also discussed. The lognormal distribution was found to be suitable for the probabilistic modelling of the fragility curves involved in the proposed methodology when the variability of the data is due to the record-to-record variability. On the other hand, if the variability of the data stems from the record-to-record variability and from the uncertainty of the component capacities, the lognormal distribution may present some lack of fit in the tails of the data. Simulations were carried out to assess the expected level of error that may occur when considering the lognormal distribution under this situation and the results obtained indicated that the error was acceptable.

10.2 Recommendations for future research

The course of this research raised several questions that were not addressed in this thesis. In this context, some topics requiring further analysis are referred in the following:

- An in-depth analysis of the surveying procedures proposed in EC8-3 should be carried out. The practicability of the procedures must be addressed based on real-case applications, namely examine aspects such as the percentage of structural members that need to be checked and the number of material samples that need to be analysed. A more clear relation should also be established between the amount and the quality of the information that is obtained by performing more detailed and intrusive surveys and the corresponding losses implied by those operations;

- In order to assist in the structural survey procedures, guidelines defining specific characteristics of the structures and construction practice according to the period of their construction should be established at the national level. This historical information would facilitate the survey of older structures for which design data is seldom available, allowing also to reduce the number of intrusive survey operations;

- Specific studies involving Bayesian analysis and real data obtained from different types of material tests should be developed in order to include the various sources of uncertainty inherent to the characterization of a given material property. Such uncertainty should then be reflected in the statistical definition of the CF;

- Given the analysis presented in Chapter 4 along with results from other existing studies (e.g. Franchin *et al.*, 2010), a revision of the CF concept proposed by EC8-3 should be further analysed. In particular, the possibility of defining a CF that would incorporate more objectively the influence of several sources of uncertainty (both aleatory and epistemic) should be envisaged, for example, by considering a CF that affects the capacity parameter instead of the material properties, similar to the CF concept proposed by ASCE (2007);

- Given the importance of the modelling error of the limit state capacity expressions proposed in EC8-3, further research should address the development of alternative formulations providing a more adequate fitting to the available experimental results;

- Studies similar to the one presented in Chapter 5 for the characterization of the type of statistical distribution for structural demand should be carried out for other relevant engineering demand parameters (EDPs). In particular, the assumption that the probabilistic distribution of the peak floor acceleration follows a lognormal distribution (Miranda and Aslani, 2003) should be further examined;

- For situations where the distribution of the EDP under analysis is seen to exhibit a significant number of outlying observations, additional studies should address the possibility of using statistical distributions other than the normal and the lognormal to characterize its probabilistic distribution. Given the nature of the Ex-Gaussian distribution, a distribution obtained from the convolution of a normal distribution and an exponential distribution, and its ability to capture the behaviour of more

extreme observations (Luce, 1986), its applicability to model the probabilistic distribution of certain EDPs should be investigated;

- Studies similar to those presented in Chapters 6 and 7 for the characterization of the central value an the dispersion of structural demand should be carried out for other relevant EDPs (e.g. the peak floor acceleration) and further IMs should be analysed in order to determine if this parameter influences the performance of the estimators;

- In the context of Methodology 2 (see Chapter 8), an alternative expression should be examined for the bilinear-type evolution of the shear force for increasing levels of the earthquake intensity to obtain a risk assessment expression also for this case. A suggestion is made to analyse the adequacy of approximating the shear force evolution using a piecewise linear function;

- In order to establish a full probabilistic model for structural demand, the effects of the uncertainty in the structural modelling parameters and of the randomness of the material properties must be examined. In particular, assumptions regarding the type of probabilistic distribution of the demand when these effects are included must be analysed. Furthermore, variations on both the central value and the dispersion of the demand resulting from these effects must also be characterized with respect to the case where the record-to-record variability of the demand is the only source of uncertainty. It should be noted that variations in the central value due to the inclusion of other sources of uncertainty are particularly important (e.g. see Chapter 9) and specific procedures should be developed to include them in methodologies such as the one proposed in ATC (2009);

- The methodology proposed in Chapter 9 to analyse the seismic performance of existing buildings should be improved in order to include the quantification of the losses for acceleration-sensitive non-structural components.

Appendix A
An empirical power comparison of univariate goodness-of-fit tests for normality

A.1 Introduction

There is a multitude of statistical models and procedures which rely on the validity of a given data hypothesis, being the normality of the data assumption one of the most commonly found in statistical studies. As observed in many econometric models and in research on applied economics, following the normal distribution assumption blindly may affect the accuracy of inference and estimation procedures, in both cross-sectional and time series datasets (Costa *et al.*, 2005). The evaluation of this distributional assumption has been addressed, for example, in Min (2007) where the conditional normality assumption in the sample selection model applied to housing demand is examined, or in Liesenfeld and Jung (2000) and Herbst (2007) where the normality assumption has been addressed in the context of stock market data, a type of data that has been found to be typically heavy-tailed (Gel and Gastwirth, 2008; Nematollahi and Tafakori, 2007). The analysis of the normality hypothesis can also be found in the characterization of error terms in the context of regression analysis models applied to economic time-series (Giles, 2007; Dufour *et al.*, 1998; Thadewald and Büning, 2007), to probit models (Wilde, 2008) or to other types of time series (Önder and Zaman, 2005; Quddus, 2008). In medical research the assumption of normality is also very common (Shoder and Himmelmann, 2006; Sürücü and Koç, 2007) but the suitability of this assumption must also be verified with adequate statistical tests as, for example, in the case of the variability of gene expression data (Mathur and Dolo, 2008) or in the case of assessing the effectiveness of new treatments using clinical trials (Tsong *et al.*, 2007). Similarly, the normality hypothesis considered in the field of quality control (Vännman and Albing, 2007; Muttlak and Al-Sabah, 2003; Madan *et al.*, 2008) also needs verification, namely when using techniques based on Shewhart control charts that are based on the normality assumption (Oakland, 2008). In addition, it can be seen that the

lognormality assumption, which is frequent in many science fields, e.g. see Limpert *et al.* (2001) and the several references presented in Chapter 5, can also be examined by testing the normality hypothesis after the logarithmic transformation of the data (Halley and Inchausti, 2002; Bengtsson *et al.*, 2005; Singh *et al.*, 1997).

The definition of adequate normality tests can, therefore, be seen to be of much importance since the acceptance or rejection of the normality assumption of a given dataset plays a central role in numerous research fields. As such, the problem of testing normality has gained considerable importance in both theoretical and empirical research and has led to the development of a large number of goodness-of-fit tests to detect departures from normality. Given the importance of this subject and the widespread development of normality tests over the years, comprehensive descriptions and power comparisons of such tests have also been the focus of attention, thus helping the analyst in the choice of suitable tests for his particular needs. Examples of such comprehensive reviews on the effectiveness of many normality tests towards a wide range of non-normality alternatives may be found, for example, in Shapiro (1968), Stephens (1974), Pearson *et al.* (1977), D'Agostino and Stephens (1986), Baringhaus *et al.* (1989), Gan and Koehler (1990), Royston (1991), Landry and Lepage (1992), Seier (2002), Thode (2002), Farrel and Rogers-Stewart (2006), Henderson (2006), Yazici and Yolacan (2007) and in the references cited therein. Since the tests that have been developed are based on different characteristics of the normal distribution, it can be seen from these comparison studies, that their power to detect departures from normality can be significantly different depending on the nature of the non-normality.

Furthermore, although the referred comparison studies have been appearing over the years, it is worth mention that some of the more recent ones, e.g. Farrel and Rogers-Stewart (2006) and Yazici and Yolacan (2007), do not include several interesting and more recently developed tests. Moreover, power results presented in Yazici and Yolacan (2007) appear to contradict those resulting from previous studies. A further comparison of normality tests, such as the one proposed herein, can therefore be considered to be of foremost interest.

An extensive simulation study is presented herein to estimate the power of thirty-three tests aiming to assess the validity of the univariate normality assumption of a data set. The selected tests include a group of well established normality tests as well as more recently developed ones. Section A.2 presents a general description of the normality tests selected for the study, while Section A.3 discuses, for some of the considered tests, the adequacy of the asymptotical critical values when compared to the empirical ones. The effects on the power of the tests due to the sample size, the selected significance level and the type of alternative distribution are also considered in the proposed study. The study is carried out for various sample sizes n and considering several significance levels α. With respect to the considered alternative distributions, the study considers a number of statistical distributions which are categorized into three sets. The first set includes several

types of symmetric non-normal distributions, the second set includes several types of asymmetric distributions and the third set comprises a number of modified normal distributions with various shapes. Section A.4 presents a more detailed description of the distributions included in these three sets. Section A.5 presents the simulation approach considered in the study and the power results of the normality tests for the different alternative distribution sets, which are then discussed in Section A.6. Finally, conclusions and recommendations resulting from the study are provided in Section A.7.

A.2 Goodness-of-fit tests for normality

The selected normality tests are considered for testing the composite null hypothesis for the case where both location and scale parameters, μ and σ, respectively, are unknown. Normality test formulations differ according to the different characteristics of the normal distribution they focus. The goodness-of-fit tests considered in the proposed study are grouped into four general categories and a brief review of each test is presented herein.

In the following review, it is considered that $x_1, x_2, ...x_n$ represent a random sample of size n, $x_{(1)}, x_{(2)}, ...x_{(n)}$ represent the order statistics of that sample, $\overline{x}$, s^2, $\sqrt{b_1}$ and b_2 are the sample mean, variance, skewness and kurtosis, respectively, given by

$$\overline{x} = n^{-1}\sum_{i=1}^{n} x_i \; ; \; s^2 = (n-1)^{-1}\sum_{i=1}^{n}(x_i - \overline{x})^2 \tag{A.1}$$

$$\sqrt{b_1} = m_3 / (m_2)^{3/2} \; ; \; b_2 = m_4 / (m_2)^2 \tag{A.2}$$

where the *jth* central moment m_j is defined by

$$m_j = n^{-1}\sum_{i=1}^{n}(x_i - \overline{x})^j \; ; \tag{A.3}$$

A.2.1 Tests based on the empirical distribution function

A.2.1.1 The Kolmogorov-Smirnov test modified by Lilliefors

Lilliefors (Lilliefors, 1967) proposed a modification of the Kolmogorov-Smirnov test for normality when the mean and the variance are unknown, and must be estimated from the data. The test statistic *K-S* is defined as

$$K\text{-}S = \max_{1 \le i \le n}\left[\Phi(x_i; \overline{x}; s^2) - (i-1)/n \; ; \; i/n - \Phi(x_i; \overline{x}; s^2)\right] \tag{A.4}$$

where $\Phi\left(x_i;\overline{x};s^2\right)$ is the cumulative distribution function of the normal distribution with parameters estimated from the data. The normality hypothesis of the data is then rejected for large values of *K-S*. Although the competitiveness of this test has been contested in several comparison studies (e.g. see D'Agostino and Stephens (1986), Gan and Koehler 1990)), it is considered in the proposed study due to its large availability in commercial software and also due to the recent performance results presented in Yazici and Yolacan (2007) which contradict the aforementioned about *K-S*.

A.2.1.2 The Anderson-Darling test

Anderson and Darling (Anderson and Darling, 1952) proposed a test statistic AD of the form

$$AD = n\int_{-\infty}^{\infty}\left[F_n(x)-\Phi(x)\right]^2\psi(x)\,dF(x) \tag{A.5}$$

where $F_n(x)$ is the empirical distribution function (EDF), $\Phi(x)$ is the cumulative distribution function of the standard normal distribution and $\psi(x)$ is a weight function given by $\left[\Phi(x)\cdot\left(1-\Phi(x)\right)\right]^{-1}$. It can be seen (Anderson and Darling, 1954) that AD can be written has

$$AD = -n-\frac{1}{n}\sum_{i=1}^{n}(2i-1)\left[\ln(p_i)+\ln\left(1-p_{n+1-i}\right)\right] \tag{A.6}$$

where the p_i values are given by $\Phi\left(z_{(i)}\right)$, with $z_{(i)}=\left(x_{(i)}-\overline{x}\right)\Big/s$. In order to increase its power when μ and σ are estimated from the sample, a modification factor has been proposed for AD (Stephens, 1974) resulting in the new statistic AD*:

$$AD^* = AD\left(1+0.75/n+2.25/n^2\right) \tag{A.7}$$

The normality hypothesis of the data is then rejected for large values of the test statistic.

A.2.1.3 The Zhang-Wu Z_C and Z_A tests

Zhang and Wu (Zhang and Wu, 2005) recently proposed test statistics Z_C and Z_A of the general form

$$Z = \int_{-\infty}^{\infty}2n\left\{F_n(x)\ln\left(\frac{F_n(x)}{F_0(x)}\right)+\left(1-F_n(x)\right)\ln\left(\frac{1-F_n(x)}{1-F_0(x)}\right)\right\}dw(x) \tag{A.8}$$

where $F_0(x)$ is a hypothetical distribution function completely specified and $w(x)$ is a weight function. When $dw(x)$ is considered to be $\left[1/F_0(x)\right]\cdot\left[1/\left(1-F_0(x)\right)\right]dF_0(x)$ and $F_0(x)$ is $\Phi(x)$, the test statistic Z_C is obtained (Zhang and Wu, 2005)

$$Z_C = \sum_{i=1}^{n}\left[\ln\frac{\left(1/\Phi\left(z_{(i)}\right)-1\right)}{(n-0.5)/(i-0.75)-1}\right]^2 \tag{A.9}$$

In the case where $dw(x)$ is considered to be $\left[1/F_n(x)\right]\cdot\left[1/\left(1-F_n(x)\right)\right]dF_n(x)$, the test statistic Z_A is then obtained (Zhang and Wu, 2005)

$$Z_A = -\sum_{i=1}^{n}\left[\frac{\ln\Phi\left(z_{(i)}\right)}{n-i+0.5}+\frac{\ln\left[1-\Phi\left(z_{(i)}\right)\right]}{i-0.5}\right] \tag{A.10}$$

For both tests, the normality hypothesis of the data is rejected for large values of the test statistic. Zhang and Wu (Zhang and Wu, 2005) have also proposed another test statistic, Z_K, which is not included it in the proposed study, as results presented in (Zhang and Wu, 2005) indicate that Z_C and Z_A are generally more powerful than Z_K.

A.2.1.4 The Glen-Leemis-Barr test

Glen, Leemis and Barr (Glen *et al.*, 2001) recently proposed a test statistic based on the quantiles of the order statistics. Given the relation between the order statistics and the EDF, this test was included in this category. The Glen-Leemis-Barr test statistic P_s is given by

$$P_s = -n-\frac{1}{n}\sum_{i=1}^{n}\left[(2n+1-2i)\ln\left(p_{(i)}\right)+(2i-1)\ln\left(1-p_{(i)}\right)\right] \tag{A.11}$$

where $p_{(i)}$ are the elements of the vector p containing the quantiles of the order statistics sorted in ascending order. Following the proposal in (Glen *et al.*, 2001), the elements of p can be obtained by defining vector u, with elements sorted in ascending order and given by $u_{(i)} = \Phi\left(z_{(i)}\right)$. Considering that $u_{(1)}, u_{(2)}, \ldots u_{(n)}$ represent the order statistics of a sample taken from a Uniform distribution $U(0;1)$, their quantiles, which correspond to the elements of p, can be determined knowing that $u_{(i)}$ follows a Beta distribution $B(i;n-i+1)$ (D'Agostino and Stephens, 1986). The normality hypothesis of the data is rejected for large values of the test statistic.

A.2.2 Tests based on measures of the moments

A.2.2.1 The D'Agostino-Pearson K^2 test

D'Agostino and Pearson (D'Agostino and Pearson, 1973) proposed the test statistic K^2 that combines normalizing transformations of skewness and kurtosis, $Z\left(\sqrt{b_1}\right)$ and $Z(b_2)$, respectively. The statistic K^2 is given by $\left[Z\left(\sqrt{b_1}\right)\right]^2+\left[Z(b_2)\right]^2$, in which the transformed skewness $Z\left(\sqrt{b_1}\right)$ is obtained by (D'Agostino *et al.*, 1990)

$$Z\left(\sqrt{b_1}\right)=\ln\left(Y/c+\sqrt{\left(Y/c\right)^2+1}\right)\Big/\sqrt{\ln(w)} \tag{A.12}$$

with Y, c and w obtained by

$$Y=\sqrt{b_1}\cdot\sqrt{\frac{(n+1)(n+3)}{6(n-2)}};\ w^2=-1+\sqrt{2\beta_2-1};\tag{A.13}$$

$$\beta_2=\frac{3\left(n^2+27n-70\right)(n+1)(n+3)}{(n-2)(n+5)(n+7)(n+9)};\ c=\sqrt{2/\left(w^2-1\right)}\tag{A.14}$$

and the transformed kurtosis $Z(b_2)$ is obtained by (D'Agostino *et al.*, 1990)

$$Z(b_2)=\left[\left(1-\frac{2}{9A}\right)-\sqrt[3]{\frac{1-2/A}{1+y\sqrt{2/(A-4)}}}\right]\sqrt{\frac{9A}{2}};\tag{A.15}$$

with A and y obtained by

$$A=6+\frac{8}{\sqrt{\beta_1}}\left(\frac{2}{\sqrt{\beta_1}}+\sqrt{1+\frac{4}{\beta_1}}\right);\ \sqrt{\beta_1}=\frac{6\left(n^2-5n+2\right)}{(n+7)(n+9)}\sqrt{\frac{6(n+3)(n+5)}{n(n-2)(n-3)}}\tag{A.16}$$

$$y=\frac{b_2-3(n-1)/(n+1)}{24n(n-2)(n-3)\Big/\left[(n+1)^2(n+3)(n+5)\right]}\tag{A.17}$$

The normality hypothesis of the data is rejected for large values of the test statistic. Furthermore, according to (D'Agostino *et al.*, 1990), the statistic K^2 is approximately chi-squared distributed with two degrees of freedom.

A.2.2.2 The Jarque-Bera test

The Jarque-Bera test is a popular goodness-of-fit test in the field of economics. It has been first proposed by Bowman and Shenton (Bowman and Shenton, 1975) but is mostly

known from the proposal of Jarque and Bera (Jarque and Bera, 1980). The test Statistic *JB* is defined by

$$JB = \frac{n}{6}\left(b_1 + \frac{\left(b_2 - 3\right)^2}{4} \right) \tag{A.18}$$

The normality hypothesis of the data is rejected for large values of the test statistic. In addition, according to Bowman and Shenton (1975), it can be seen that *JB* is asymptotically chi-squared distributed with two degrees of freedom.

A.2.2.3 The Doornik-Hansen test

Various modifications of the Jarque-Bera test have been proposed over the years in order to increase its efficiency. For example, Urzúa (1996) introduced a modification consisting of a different standardization process for b_1 and b_2, though Thadewald and Büning (2007) showed that such modification did not improve the power of the original formulation. A less known formulation is that of Doornik and Hansen (2008) which suggest the use of the transformed skewness according to Eq. (A.12) and the use of a transformed kurtosis according to the proposal in Bowman and Shenton (1977). The statistic of the Doornik-Hansen test *DH* is thus given by $\left[Z\left(\sqrt{b_1}\right) \right]^2 + \left[z_2 \right]^2$, in which the transformed kurtosis z_2 is obtained by (Doornik and Hansen, 2008)

$$z_2 = \left[\left(\frac{\xi}{2a} \right)^{1/3} - 1 + \frac{1}{9a} \right] \left(9a\right)^{1/2} \tag{A.19}$$

with ξ and a obtained by

$$\xi = \left(b_2 - 1 - b_1\right) 2k \,;\; k = \frac{\left(n+5\right)\left(n+7\right)\left(n^3 + 37n^2 + 11n - 313\right)}{12\left(n-3\right)\left(n+1\right)\left(n^2 + 15n - 4\right)} \tag{A.20}$$

$$a = \frac{\left(n+5\right)\left(n+7\right)\left[\left(n-2\right)\left(n^2 + 27n - 70\right) + b_1 \cdot \left(n-7\right)\left(n^2 + 2n - 5\right) \right]}{6\left(n-3\right)\left(n+1\right)\left(n^2 + 15n - 4\right)} \tag{A.21}$$

The normality hypothesis of the data is rejected for large values of the test statistic and, according to (Doornik and Hansen, 2008), *DH* is also approximately chi-squared distributed with two degrees of freedom.

A.2.2.4 The Gel-Gastwirth robust Jarque-Bera test

Gel and Gastwirth (Gel and Gastwirth, 2008) recently proposed a robust version of the Jarque-Bera. Stemming from the fact that sample moments are, among other things, known to be sensitive to outliers, see e.g. Henderson (2006), Gel and Gastwirth have proposed a modification of *JB* that uses a robust estimate of the dispersion in the skewness and kurtosis definitions given in Eq. (A.2) instead of the second order central moment m_2. The selected robust dispersion measure is the average absolute deviation from the median and leads to the following statistic of the robust Jarque-Bera test *RJB* given by

$$RJB = \frac{n}{6}\left(\frac{m_3}{J_n^3}\right)^2 + \frac{n}{64}\left(\frac{m_4}{J_n^4} - 3\right)^2 \tag{A.22}$$

with J_n obtained by

$$J_n = \frac{\sqrt{\pi/2}}{n}\sum_{i=1}^{n}\left|x_i - M\right| \tag{A.23}$$

in which M is the sample median. The normality hypothesis of the data is rejected for large values of the test statistic and, according to Gel and Gastwirth (2008), *RJB* asymptotically follows the chi-square distribution with two degrees of freedom.

A.2.2.5 The Hosking L-moments based test

Given the several disadvantages associated with the use of central moments (Henderson, 2006; Hoskings, 1990; Hoskings, 1992; Ulrych *et al.*, 2000), Hosking (Hoskings, 1990) advocated the use of linear combinations of the order statistics instead, termed L-moments, which are less affected by sample variability and, therefore, are more robust to outliers and better for making inferences about an underlying probability distribution. Hosking (Hoskings, 1990) has shown the *rth* order sample L-moment can be estimated by

$$l_r = \sum_{k=0}^{r-1} p^*_{r-1,k} \cdot b_k \tag{A.24}$$

where $p^*_{r,k}$ and b_k are obtained by

$$p^*_{r,k} = (-1)^{r-k}\binom{r}{k}\binom{r+k}{k};\ b_k = n^{-1}\sum_{i=1}^{n}\frac{(i-1)(i-2)\ldots(i-k)}{(n-1)(n-2)\ldots(n-k)}x_{(i)} \tag{A.25}$$

Based on the second, third and fourth sample L-moments, which have similarities with the corresponding central moments, Hosking (Hoskings, 1990) also defines new measures of skewness and kurtosis, termed L-skewness τ_3 and L-kurtosis τ_4, and given by

$$\tau_3 = l_3/l_2\,,\ \tau_4 = l_4/l_2 \tag{A.26}$$

The value of τ_3 is bounded between -1 and 1 for all distributions and is close to 0 for the normal distribution, while the value of τ_4 is ≤ 1 for all distributions and is close to 0.1226 for the normal distribution. As referred in (Hoskings, 1990), Hosking as suggested that normality could be tested based on τ_3 and τ_4 according the following statistic T_{Lmom}

$$T_{Lmom} = \frac{\tau_3 - \mu_{\tau_3}}{\mathrm{var}(\tau_3)} + \frac{\tau_4 - \mu_{\tau_4}}{\mathrm{var}(\tau_4)} \tag{A.27}$$

where μ_{τ_3} and μ_{τ_4} are the mean of τ_3 and τ_4, and $\mathrm{var}(\tau_3)$ and $\mathrm{var}(\tau_4)$ are their corresponding variances. The values of μ_{τ_3}, μ_{τ_4}, $\mathrm{var}(\tau_3)$ and $\mathrm{var}(\tau_4)$ can be obtained by simulation. Nonetheless, μ_{τ_3} and μ_{τ_4} are expected to be close to 0 and 0.1226, and Hosking (Hoskings, 1990) provides an approximation for $\mathrm{var}(\tau_3)$. For the case of $\mathrm{var}(\tau_4)$ there is no approximation currently available. Details concerning the values of these parameters considered in this study are presented in Section A.5. The normality hypothesis of the data is rejected for large values of T_{Lmom}, which is also approximately chi-squared distributed with two degrees of freedom according to Henderson (2006).

A.2.2.6 The Hosking test based on trimmed L-moments

Although L-moments exhibit some robustness towards outliers in the data, as previously referred, they may still be affected by extreme observations (Elamir and Seheult, 2003). A robust generalization of the sample L-moments has, therefore, been formulated by Elamir and Seheult (Elamir and Seheult, 2003) leading to the development of trimmed L-moments. The proposed formulation for the trimmed L-moments allows for both symmetric and asymmetric trimming of the smallest and largest sample observations. For the case of normality testing suggested herein, only symmetric trimming is considered.

Considering an integer symmetric trimming level *t*, Elamir and Seheult (Elamir and Seheult, 2003) have shown the *rth* order sample trimmed L-moment $l_r^{(t)}$ can be estimated by

$$l_r^{(t)} = \frac{1}{r}\sum_{i=t+1}^{n-t}\left\{\frac{\sum_{k=0}^{r-1}\left[(-1)^k\binom{r-1}{k}\binom{i-1}{r+t-1-k}\binom{n-i}{t+k}\right]}{\binom{n}{r+2t}}\right\}x_{(i)} \tag{A.28}$$

Based on the second, third and fourth sample trimmed L-moments, Elamir and Seheult (Elamir and Seheult, 2003) also define new measures of skewness and kurtosis, termed TL-skewness $\tau_3^{(t)}$ and TL-kurtosis $\tau_4^{(t)}$, given by

$$\tau_3^{(t)} = l_3^{(t)} / l_2^{(t)},\ \tau_4^{(t)} = l_4^{(t)} / l_2^{(t)} \tag{A.29}$$

Based on these new measures, the following test, similar to that given by Eq. (A.27), is considered in the present study:

$$T_{TL\_mom}{}^{(t)} = \frac{\tau_3^{(t)} - \mu_{\tau_3}^{(t)}}{\mathrm{var}\left(\tau_3^{(t)}\right)} + \frac{\tau_4^{(t)} - \mu_{\tau_4}^{(t)}}{\mathrm{var}\left(\tau_4^{(t)}\right)} \tag{A.30}$$

where, for a selected trimming level *t*, $\mu_{\tau_3}^{(t)}$ and $\mu_{\tau_4}^{(t)}$ are the mean of $\tau_3^{(t)}$ and $\tau_4^{(t)}$, and $\mathrm{var}\left(\tau_3^{(t)}\right)$ and $\mathrm{var}\left(\tau_4^{(t)}\right)$ are their corresponding variances. As for the previous test, the values of $\mu_{\tau_3}^{(t)}$, $\mu_{\tau_4}^{(t)}$, $\mathrm{var}\left(\tau_3^{(t)}\right)$ and $\mathrm{var}\left(\tau_4^{(t)}\right)$ can be obtained by simulation. Details concerning the values of these parameters considered in this study are presented in Section A.5.

Three versions of this test are considered in the proposed study, which correspond to symmetric trimming levels *t* of 1, 2 and 3. For each test, the normality hypothesis of the data is rejected for large values of the statistic $T_{TL\_mom}{}^{(t)}$.

A.2.2.7 The Bontemps-Meddahi tests

Bontemps and Meddahi (Bontemps and Meddahi, 2005) recently proposed a family of normality tests based on moment conditions known as the Stein equations and their relation with Hermite polynomials. The test statistics are developed using the generalized method of moments approach (Hansen, 1982) associated to Hermite polynomials, which leads to test statistics that are robust against parameter uncertainty. The general expression of the test family is thus given by

$$BM_{3-p} = \sum_{k=3}^{p} \left(\frac{1}{\sqrt{n}} \sum_{i=1}^{n} H_k\left(z_i\right) \right)^2 \tag{A.31}$$

where $z_i = \left(x_i - \bar{x}\right)/s$ and $H_k(.)$ represents the *kth* order normalized Hermite polynomial having the general expression given by the following recursive formulation

$$\forall i > 1,\ H_i(u) = \frac{1}{\sqrt{i}}\left[u \cdot H_{i-1}(u) - \sqrt{i-1} \cdot H_{i-2}(u) \right],\ H_0(u) = 1,\ H_1(u) = u \tag{A.32}$$

It can be seen from Eq. (A.31) that a number of different tests can be obtained by assigning different values to p, which represents the maximum order of the considered normalized Hermite polynomials. Based on the results presented in Bontemps and Meddahi (2005), two different tests are considered in the study presented herein. Following the terminology provided in Eq. (A.31), these tests are termed BM_{3-4} and BM_{3-6}. In both cases, the normality hypothesis of the data is rejected for large values of the test statistic and, according to Bontemps and Meddahi (2005), the general BM_{3-p} family of tests asymptotically follows the chi-square distribution with p-2 degrees of freedom.

A.2.2.8 The Brys-Hubert-Struyf *MC-LR* test

Brys, Hubert and Struyf (Brys *et al.*, 2008) have proposed a goodness-of-fit test based on robust measures of skewness and tailweight. The considered robust measure of skewness is the medcouple *MC* (Brys *et al.*, 2003; Brys *et al.*, 2004) defined as

$$MC = \underset{x_{(i)} \le m_F \le x_{(j)}}{med} h\left(x_{(i)}, x_{(j)}\right) \tag{A.33}$$

where *med* stands for the median, m_F is the sample median and the kernel function h is given by

$$h\left(x_{(i)}, x_{(j)}\right) = \frac{\left(x_{(j)} - m_F\right) - \left(m_F - x_{(i)}\right)}{x_{(i)} - x_{(j)}} \tag{A.34}$$

and for which a fast computation algorithm is provided in Brys *et al.* (2004). For the case where $x_{(i)} = x_{(j)} = m_F$, h is then set by

$$h\left(x_{(i)}, x_{(j)}\right) = \begin{cases} 1 & i > j \\ 0 & i = j \\ -1 & i < j \end{cases} \tag{A.35}$$

The left medcouple (LMC) and the right medcouple (RMC) are the considered robust measures of left and right tail weight (Brys *et al.*, 2006), respectively, and are defined by

$$LMC = -MC\left(x < m_F\right);\ RMC = MC\left(x > m_F\right) \tag{A.36}$$

The test statistic $T_{MC\text{-}LR}$ is then defined by

$$T_{MC-LR} = n\left(w - \omega\right)^t \cdot V^1 \cdot \left(w - \omega\right) \tag{A.37}$$

in which w is set as $[MC, LMC, RMC]^t$, and ω and V are obtained based on the influence function of the estimators in w (Brys *et al.*, 2004, Brys *et al.*, 2006). For the case of a normal distribution ω and V are defined as (Brys *et al.*, 2008)

$$\omega = [0, 0.199, 0.199]^t \; ; \; V = \begin{bmatrix} 1.25 & 0.323 & -0.323 \\ 0.323 & 2.62 & -0.0123 \\ -0.323 & -0.0123 & 2.62 \end{bmatrix} \tag{A.38}$$

The normality hypothesis of the data is rejected for large values of $T_{MC\text{-}LR}$ and, according to Brys *et al.* (2007), it is suggested that $T_{MC\text{-}LR}$ approximately follows the chi-square distribution with three degrees of freedom.

A.2.2.9 The Bonett-Seier test

Bonett and Seier (Bonett and Seier, 2002) have suggested a modified measure of kurtosis for testing normality, which is based on a modification of Geary's proposal (Geary, 1936). The test statistic of the new kurtosis measure T_w is thus given by:

$$T_w = \sqrt{n+2} \cdot \left(\hat{\omega} - 3\right) \Big/ 3.54 \tag{A.39}$$

in which $\hat{\omega}$ is set by

$$\hat{\omega} = 13.29 \left[\ln \sqrt{m_2} - \ln \left(n^{-1} \sum_{i=1}^{n} \left| x_i - \bar{x} \right| \right) \right] \tag{A.40}$$

The normality hypothesis of the data is rejected for both small and large values of T_w using a two-sided test and, according to (Bonett and Seier, 2002), it is suggested that T_w approximately follows a standard normal distribution.

A.2.2.10 The Brys-Hubert-Struyf-Bonett-Seier joint test

Considering that the Brys-Hubert-Struyf *MC-LR* test is, mainly, a skewness associated test and that the Bonett-Seier proposal is a kurtosis based test, a joint test, termed $T_{MC\text{-}LR}$-T_w, considering both these measures is proposed herein for testing normality. This joint test attempts to make use of the two referred focused tests in order to increase the power to detect different kinds of departure from normality. This joint test is proposed herein based on the assumption that the individual tests can be considered independent. This assumption is based on a simulation of the two statistics considering 200000 samples of size 100 drawn from a standard normal distribution that yielded a correlation coefficient of approximately -0.06. In order to control the overall Type I error at the nominal level a,

the normality hypothesis of the data is rejected for the joint test when rejection is obtained for either one of the two individual tests for a significance level of $\alpha/2$.

A.2.2.11 The Cabaña-Cabaña tests

Cabaña and Cabaña (Cabaña and Cabaña, 2003) have recently proposed four families of normality tests based on transformed empirical processes. Two test families are of the Kolmogorov-Smirnov type while the other two are of the Cramér-von Mises type. One family of each type of test focuses on changes on skewness and the other one is sensitive to changes in kurtosis. Considering the results provided in Cabaña and Cabaña (2003), the power of the Kolmogorov-Smirnov type tests is seen to be very similar to that of the Cramér-von Mises type tests. Therefore, only the Kolmogorov-Smirnov type tests were selected in the proposed study, as their implementation complexity is comparatively lower than that of the Cramér-von Mises type tests.

The test statistics proposed in Cabaña and Cabaña (2003) are based on the definition of approximate transformed estimated empirical processes (ATEEP) sensitive to changes in skewness or kurtosis. The proposed ATEEP sensitive to changes in skewness is defined as:

$$w_{S,\ell}(x) = \Phi(x)\cdot \bar{H}_3 - \phi(x)\cdot \sum_{j=1}^{\ell} \frac{1}{\sqrt{j}} H_{j-1}(x)\cdot \bar{H}_{j+3} \tag{A.41}$$

where ℓ is a dimensionality parameter, $\phi(x)$ is the probability density function of the standard normal distribution, $H_j(.)$ represents the *jth* order normalized Hermite polynomial given by Eq. (A.32) and $\bar{H}_j$ is the *jth* order normalized mean of the Hermite polynomial defined as

$$\bar{H}_j = \frac{1}{\sqrt{n}} \sum_{i=1}^{n} H_j(x_i) \tag{A.42}$$

The proposed ATEEP sensitive to changes in kurtosis is defined as:

$$\begin{aligned} w_{K,\ell}(x) = &-\phi(x)\cdot \bar{H}_3 + \left[\Phi(x) - x\cdot\phi(x)\right]\cdot \bar{H}_4 - \\ &\phi(x)\cdot \sum_{j=2}^{\ell} \left(\sqrt{\frac{j}{j-1}} H_{j-2}(x)\cdot H_j(x) \right)\cdot \bar{H}_{j+3} \end{aligned} \tag{A.43}$$

According to Cabaña and Cabaña (2003), the dimensionality parameter ℓ ensures the test is consistent against alternative distributions differing from the normal distribution having the same mean and variance in at least one moment of order not greater than $\ell+3$.

The Kolmogorov-Smirnov type test statistics sensitive to changes in skewness and in kurtosis, $T_{S,\ell}$ and $T_{K,\ell}$, respectively, are defined as

$$T_{S,\ell} = \max\left|w_{S,\ell}(x)\right|;\ T_{K,\ell} = \max\left|w_{K,\ell}(x)\right| \tag{A.44}$$

For both cases, the normality hypothesis of the data is rejected for large values of the test statistic. Based on results presented in Cabaña and Cabaña (2003), parameter ℓ was considered to be 5.

A.2.3 Regression and correlation tests

A.2.3.1 The Shapiro–Wilk test

The Shapiro and Wilk W statistic (Shapiro and Wilk, 1965) is a well-established and powerful test of normality. The statistic W represents the ratio of two estimates of the variance of a normal distribution and is obtained by

$$W = \frac{\left(\sum_{i=1}^{n} a_i \cdot x_{(i)}\right)^2}{n \cdot m_2} \tag{A.45}$$

where the vector of weights a is obtained by $(a_1,...,a_n) = m \cdot V^{-1} \cdot \left(m \cdot V^{-1} \cdot V^{-1} \cdot m^t\right)^{-0.5}$, in which m and V are the mean vector and covariance matrix of the order statistics of the standard normal distribution. The computation of the vector of weights a considered herein is defined according to the improved algorithm presented by Royston (1995) which considers the methodology described in Royston (1992) and Royston (1993a). Given the definition of W, it is intuitive to observe the normality hypothesis of the data is rejected for small values of W. In order to simplify the application of this test, transformations g have been defined in Royston (1993a) for different sample sizes such that $g(W)$ approximately follows a standard normal distribution.

A.2.3.2 The Shapiro–Francia test

Since explicit values of m and V are not readily available and the computation of V^{-1} is time consuming for large samples, Shapiro and Francia (Shapiro and Francia, 1972) have proposed a modification of the Shapiro–Wilk test, hereon termed W_{SF}, based on the fact that, for large samples, the samples observations can be treated as being independent. In this context, Shapiro and Francia suggested to replace V^{-1} by an identity matrix, which

leads to a vector of weights a defined as $m \cdot \left(m \cdot m^t \right)^{-0.5}$. The computation of the W_{SF} test considered herein is defined according to the procedure proposed in Royston (1993b). Similarly to the W test, the normality hypothesis of the data is rejected for small values of W_{SF}. As for the previous test, transformations g have also been defined in Royston (1993a) for different sample sizes such that $g\left(W_{SF}\right)$ approximately follows a standard normal distribution.

A.2.3.3 The Rahman-Govindarajulu modification of the Shapiro–Wilk test

Rahman and Govindarajulu (Rahman and Govindarajulu, 1997) have proposed a modification to the Shapiro–Wilk test, hereon termed W_{RG}, which is simpler to compute and relies on a new definition of the weights a using the approximations to m and V suggested in Mosteller (1946) and Blom (1958). According to these proposals, each element a_i of the new vector of weights becomes

$$a_i = -(n+1)(n+2)\phi(m_i)\left[m_{i-1}\phi(m_{i-1}) - 2m_i\phi(m_i) + m_{i+1}\phi(m_{i+1}) \right] \tag{A.46}$$

where it is assumed that $m_0\phi(m_0) = m_{n+1}\phi(m_{n+1}) = 0$. With this modification, the new test statistic W_{RG} assigns larger weights to the extreme order statistics than the original W test, which has been seen to result in higher power against short tailed alternative distributions (Rahman and Govindarajulu, 1997; Bai and Chen, 2003). As for the original W test, the normality hypothesis of the data is rejected for small values of W_{RG}.

A.2.3.4 The D'Agostino *D* test

D'Agostino (D'Agostino, 1971) proposed the D test statistic as an extension of the Shapiro–Wilk test. The D'Agostino proposal eliminates the need to define the vector of weights a of the Shapiro–Wilk test and is obtained by

$$D = \frac{\sum_{i=1}^{n} \left(i - (n+1)/2 \right) \cdot x_{(i)}}{n^2 \cdot \sqrt{m_2}} \tag{A.47}$$

The normality hypothesis of the data is rejected for both small and large values of D using a two-sided test.

A.2.3.5 The Filliben correlation test

Filliben (Filliben, 1975) described the probability plot correlation coefficient *r* as a test for normality. The correlation coefficient is defined between the sample order statistics and the estimated median values of the theoretical order statistics.

Considering that $m_{(1)}, m_{(2)}, ...m_{(n)}$ represent the estimated median values of order statistics from a Uniform distribution $U(0;1)$, each $m_{(i)}$ is obtained by

$$m_{(i)} = \begin{cases} 1-0.5^{(1/n)} & i=1 \\ (i-0.3175)/(n+0.365) & 1<i<n \\ 0.5^{(1/n)} & i=n \end{cases} \tag{A.48}$$

upon which the estimated median values of the theoretical order statistics can be obtained using the transformation $M_{(i)} = \Phi^{-1}\left(m_{(i)}\right)$. The correlation coefficient *r* is then defined as

$$r = \frac{\sum_{i=1}^{n} x_{(i)} \cdot M_{(i)}}{\sqrt{\sum_{i=1}^{n} M_{(i)}^2} \cdot \sqrt{(n-1)\cdot s^2}} \tag{A.49}$$

leading to the rejection of the normality hypothesis of the data for small values of *r*.

A.2.3.6 The Chen–Shapiro test

Chen and Shapiro (Chen and Shapiro, 1995) introduced an alternative test statistic *CS* based on normalized spacings and defined as

$$CS = \frac{1}{(n-1)\cdot s} \sum_{i=1}^{n-1} \frac{x_{(i+1)} - x_{(i)}}{M_{i+1} - M_i} \tag{A.50}$$

in which M_i is the *ith* quantile of a standard normal distribution obtained by $\Phi^{-1}\left[(i-0.375)/(n+0.25)\right]$. Since a close relation between *CS* and the Shapiro-Wilk test has been shown to exist (Bai and Chen, 2003), their performance is expected to be similar also. According to (Chen and Shapiro, 1995), the normality hypothesis of the data is rejected for small values of *CS*.

A.2.3.7 The Zhang *Q* tests

Zhang (Zhang, 1999) introduced the Q test statistic based on the ratio of two unbiased estimators of standard deviation, q_1 and q_2, and given by $Q = \ln\left(q_1/q_2\right)$. The estimators q_1 and q_2 are obtained by $q_1 = \sum_{i=1}^{n} a_i x_{(i)}$ and $q_2 = \sum_{i=1}^{n} b_i x_{(i)}$ where the ith order linear coefficients a_i and b_i result from

$$a_i = \left[\left(u_i - u_1\right)\left(n-1\right)\right]^{-1}, \; for\; i \neq 1; \; a_1 = \sum_{i=2}^{n} a_i \tag{A.51}$$

$$b_i = \begin{cases} -b_{n-i+1} = \left[\left(u_i - u_{i+4}\right)\left(n-4\right)\right]^{-1} & i = 1,...,4 \\ \left(n-4\right)^{-1} \cdot \left[\left(u_i - u_{i+4}\right)^{-1} - \left(u_{i-4} - u_i\right)^{-1}\right] & i = 5,...,n-4 \end{cases} \tag{A.52}$$

where the *ith* expected value of the order statistics of a standard normal distribution, u_i, is defined by $\Phi^{-1}\left[\left(i-0.375\right)/\left(n+0.25\right)\right]$. According to Zhang (1999), Q is less powerful against negatively skewed distributions. Therefore, Zhang (Zhang, 1999) has also proposed the alternative statistic Q^* by switching the *ith* order statistics $x_{(i)}$ in q_1 and q_2 by $x^*_{(i)} = -x_{(n-i+1)}$. Based on the definition of both Q and Q^*, the normality hypothesis of the data is rejected for both small and large values of the statistic using a two-sided test.

In addition to these two tests, Zhang (Zhang, 1999) has also proposed a joint test Q-Q^*, stemming from the fact that Q and Q^* are approximately independent. Therefore, for the case of the joint test Q-Q^*, the normality hypothesis of the data is rejected at the significance level *a* when rejection is obtained for either one of the two individual tests for a significance level of $\alpha/2$.

According to Zhang (1999), both Q and Q^* approximately follow a normal distribution. However, Hwang and Wei (Hwang and Wei, 2007) have proven otherwise and state that the performance of these tests is better when based on their empirical distribution. Since the joint test has shown to be more powerful than the individual tests (Zhang, 1999; Hwang and Wei, 2007), the joint test Q-Q^* is the primary choice for the proposed study. Nonetheless, the Q test is also included for comparison purposes.

A.2.3.8 The del Barrio-Cuesta-Albertos-Matrán-Rodríguez-Rodríguez quantile correlation test

A novel approach for normality testing based on the L_2-Wasserstein distance has been proposed by del Barrio, Cuesta-Albertos, Matrán and Rodríguez-Rodríguez (del Barrio *et al.*, 1999; Krauczi, 2007). The *BCMR* test statistic is defined by

$$BCMR = \frac{m_2 - \left[\sum_{i=1}^{n} x_{(i)} \cdot \int_{(i-1)/n}^{i/n} \Phi^{-1}(t)\,dt\right]^2}{m_2} \tag{A.53}$$

where, according to del Barrio *et al.* (1999), the numerator represents the squared L_2-Wasserstein distance. The normality hypothesis of the data is rejected for large values of the test statistic.

A.2.3.9 The β_3^2 Coin test

Coin (Coin, 2008), has recently proposed a normality test based on a polynomial regression focused on detecting symmetric non-normal alternative distributions. According to Coin (2008), the analysis of standard normal Q-Q plots of different symmetric non-normal distributions suggests that fitting a model of the type:

$$z_{(i)} = \beta_1 \cdot \alpha_i + \beta_3 \cdot \alpha_i^3 \tag{A.54}$$

where β_1 and β_3 are fitting parameters and α_i represent the expected values of standard normal order statistics, leads to values β_3 different from zero when in presence of symmetric non-normal distributions. Therefore, Coin (Coin, 2008) suggests the use of β_3^2 as a statistic for testing normality, thus rejecting the normality hypothesis of the data for large values of β_3^2. As suggested in Coin (2008), the values of α_i are obtained using the approximations provided in Royston (1982).

A.2.4 Other tests

A.2.4.1 The Epps-Pulley test

Epps and Pulley (Epps and Pulley, 1983; BS 2846-7, 1997) have proposed a test statistic T_{EP} based on the following weighted integral

$$T_{EP} = \int_{-\infty}^{\infty} \left|\phi_n(t) - \hat{\phi}_0(t)\right|^2 dG(t) \tag{A.55}$$

where $\phi_n(t)$ is the empirical characteristic function given by $n^{-1}\sum_{j=1}^{n}\exp\left(itx_j\right)$, $\hat{\phi}_0(t)$ is the sample estimate of the characteristic function of the normal distribution given by $\exp\left(it\bar{x} - 0.5m_2t^2\right)$ and $G(t)$ is an adequate function chosen according to several

considerations (Epps and Pulley, 1983). By setting $dG(t) = g(t)dt$ and selecting $g(t) = \sqrt{m_2/2\pi} \cdot \exp\left(-0.5 m_2 t^2\right)$ the following statistic can be obtained (Epps and Pulley, 1983).

$$T_{EP} = 1 + \frac{n}{\sqrt{3}} + \frac{2}{n}\sum_{k=2}^{n}\sum_{j=1}^{k-1} e^{\frac{-\left(x_j - x_k\right)^2}{2m_2}} - \sqrt{2}\sum_{j=1}^{n} e^{\frac{-\left(x_j - \bar{x}\right)^2}{4m_2}} \tag{A.56}$$

for which the normality hypothesis of the data is rejected when large values of T_{EP} are obtained. To simplify the use of this test by eliminating the need for tables of percentage points of T_{EP}, an approximation to the limit distribution of T_{EP} has been presented in Henze (1990).

A.2.4.2 The Martinez-Iglewicz test

Martinez and Iglewicz (Martinez and Iglewicz, 1981) have proposed a normality test based on the ratio of two estimators of variance, where one the estimators is the robust biweigth scale estimator S_b^2

$$S_b^2 = \frac{n \cdot \sum_{|\tilde{z}_i|<1} \left(x_i - M\right)^2 \left(1 - \tilde{z}_i^2\right)^4}{\left[\sum_{|\tilde{z}_i|<1} \left(1 - \tilde{z}_i^2\right)\left(1 - 5\tilde{z}_i^2\right)\right]^2} \tag{A.57}$$

where M is the sample median, $\tilde{z}_i = \left(x_i - M\right)/\left(9A\right)$, with A being the median of $\left|x_i - M\right|$, and when $\left|\tilde{z}_i\right| > 1$, $\tilde{z}_i$ is set to 0. The Martinez-Iglewicz test statistic I_n is then given by

$$I_n = \frac{\sum_{i=1}^{n}\left(x_i - M\right)^2}{\left(n-1\right)\cdot S_b^2} \tag{A.58}$$

for which the normality hypothesis of the data is rejected for large values of I_n.

A.2.4.3 The Gel-Miao-Gastwirth test

Gel, Miao and Gastwirth (Gel *et al.*, 2007) have recently proposed a directed normality test which focuses on detecting heavier tails and outliers of symmetric distributions. The test is based on the ratio of the standard deviation and on the robust measure of dispersion J_n defined in Eq. (A.23). The normality test statistic R_{sJ} is therefore

given by $R_{sJ} = s/J_n$ which should tend to one under a normal distribution. According to Gel *et al.*, (2007), the normality hypothesis of the data is rejected for large values of R_{sJ} and the statistic $\sqrt{n}\left(R_{sJ}-1\right)$ is seen to asymptotically follow the normal distribution $N\left(0;\pi/2-1.5\right)$. However, it has been empirically found that rejecting the normality hypothesis using a two-sided test extends the range of application of this test, namely to light-tailed distributions, without a significant reduction of its power towards heavy-tailed distributions.

Given its enhanced behaviour, the two-sided test is the primary choice for the proposed study. Nonetheless, a detailed power comparison of the two-sided test with the one-sided test, hereon termed $R_{sJ,1}$, is also presented.

A.3 Comparison of empirical and asymptotical critical values

For many normality tests, the sampling distributions of their corresponding statistics are intractable, for both finite and large sample situations. Nonetheless, in cases where such limit distribution can be approximated, it is of interest to determine how close the simulated percentile values of such distributions are to the corresponding asymptotic values and how fast is the convergence to such values. The tests presented in the previous Section for which the limit distribution has been examined in previous studies are referred herein. Reference to previous works on the adequacy of such limit distributions is also made when available. For the remaining cases, comparison results from this study clarifying the suitability of their asymptotical critical values are presented herein. For a given test, the referred results correspond to the comparison of the asymptotical critical values to the empirical ones based on 1000000 samples drawn from the standard normal distribution, for five sample sizes n (n = 25, n = 50, n = 100, n = 200 and n = 500) and considering several significance levels α.

The matter of the limit distribution has been previously addressed for statistics *BCMR*, *D*, $T_{S,\ell}$, $T_{K,\ell}$, T_{EP}, *JB*, *RJB*, *W*, W_{SF}, R_{sJ}, *DH*, K^2, T_{Lmom}, BM_{3-4}, BM_{3-6}, $T_{MC\text{-}LR}$ and T_w. Furthermore, as stated before, a limit distribution was also proposed for statistics *Q* and *Q**, but was rejected based on the subsequent studies (Hwang and Wei, 2007).

According to Krauczi (2007), the asymptotic distribution of *BCMR* can be obtained numerically by computing its characteristic function and performing a numerical inversion. The convergence of the numerically simulated critical values to those obtained by the asymptotic distribution is very slow and the use of the asymptotic critical values generally yields conservative results (i.e. the normality hypothesis is rejected more times when considering the asymptotical values than when using the simulated ones) for sample sizes as low as 10. Hence, the use of asymptotic critical values is not recommended for this test.

With respect to the *D* statistic, a standardized version can be defined in order to transform *D* into a standard normal variable (D'Agostino, 1971; D'Agostino, 1972). Nonetheless, studies have shown that, even for a sample size of 1000, the percentiles of this new standard statistic do not converge to those of the standard normal distribution and exhibit asymmetric behaviour (Thode, 2002). Hence, there is evidence of low convergence to the asymptotic distribution and the use of empirical critical values is recommended. For the case of statistics $T_{S,\ell}$ and $T_{K,\ell}$, the theoretical basis of their limit distribution is addressed in Cabaña and Cabaña (2003) but a closed analytical expression is not available. Nonetheless, through some refined numerical analysis, the asymptotic critical percentiles were determined and compared to those obtained through simulation. Despite the relative proximity of the asymptotic and simulated values, the latter are seen to be more conservative and their use is recommended for a more accurate performance of these tests (Cabaña and Cabaña, 2003). With respect to the limit distribution of T_{EP}, a numerical definition of the first four moments of the referred distribution as well as approximations to the limit distribution, obtained by fitting members of the Johnson and of the Pearson system of distributions, can be found in Henze (1990). By comparing the upper percentiles given by the approximated limit distributions with those simulated numerically, it can be observed that for moderate sample sizes ($n \geq 50$) the simulated upper percentiles are very close to the asymptotic values and convergence to these values is seen to be rather fast. Furthermore, a transformation to normality of T_{EP} that enables the use of standard normal percentiles to apply the test is also proposed. Nonetheless, it should be noted that, in either case, for smaller sample sizes, the use of numerically simulated critical values is recommended. According to results presented for *JB* in Thadewald and Büning (2007), for $a \geq 0.05$ the normality hypothesis is rejected more times when considering the simulated values than when using the asymptotical ones, especially for small sample sizes, while for $a < 0.05$ the pattern is not as definite. Figure A.1a) presents the comparison of the *JB* asymptotical critical values to the empirical ones, which leads to conclude that, in the overall, the chi-squared distribution approximation of the limit distribution does not work well, even for large sample sizes, and that the speed of convergence is slow. Thus, for a meaningful application of *JB*, empirical critical values have to be used (Thadewald and Büning, 2007). Similar results were also reported for *RJB* in Gel and Gastwirth (2008), where it is concluded that the asymptotic chi-squared approximation of critical values is not accurate enough in small to moderate sized samples. Figure A.1b) presents the comparison of the *RJB* asymptotical critical values to the empirical ones where it can be seen that the asymptotical approximation is inadequate, even for large sample sizes, and that the speed of convergence is also slow. Hence, the use of empirical critical values is also recommended for *RBJ*. The problem of finding the limit distribution of *W* and W_{SF} has been addressed over the years by several researchers using different approaches (Royston, 1993a; Leslie *et al.*, 1986; Verril and Johnson, 1988; Sen, 2002; del Barrio *et al.*, 2005).

Special emphasis is given to Verril and Johnson (1988) where their asymptotic null distributions are derived and are seen to be identical, though convergence to their critical values is seen to be very slow. As previously referred, transformations *g* have been defined in Royston (1993a) for different sample sizes such that $g(W)$ and $g(W_{SF})$ have an approximately standard normal distribution. According to this approximation, the normality hypothesis is rejected if the transformed variable is larger than the upper percentile of the standard normal distribution. As can be seen from the results presented in Figs. A.1c) and d) for both tests, the transformed statistics have empirical critical values very close to the standard normal percentiles. Hence, these transformations to normality and the use of critical values obtained from the standard normal distribution are recommended for practical use of these tests. With respect to R_{sJ}, although the statistic $\sqrt{n}\left(R_{sJ}-1\right)$ asymptotically follows the normal distribution as previously referred, observation of Fig. A.1e) shows that the asymptotical critical values differ from the empirical ones, the latter being more conservative. In the overall, the empirical values can be seen to exhibit an asymmetric distribution and a slow convergence towards the asymptotical values. Hence, the use of empirical critical values is recommended for R_{sJ}. Similar conclusions can be drawn from Fig. A.1f) for the case of T_w. Nonetheless, empirical and asymptotical critical values of T_w are closer and the speed of convergence is higher than that of R_{sJ}. For the case of *DH*, results presented in Fig. A.1g) show that, for $a \geq 0.05$, the asymptotical and empirical critical values are very close and that convergence is fast. On the other hand, for $a < 0.05$ the empirical critical values are more conservative. Similar conclusions can be drawn from the results of test K^2 presented in Fig. A.1h), although convergence to the asymptotical values is slower for this test, especially for $a < 0.05$. Thus, for *DH* and K^2, the use of asymptotical critical values is recommended for $a \geq 0.05$, while empirical ones should be used for $a < 0.05$. For the case of T_{Lmom}, results presented in Fig. A.1i) show that the asymptotical and the empirical critical values are very close and that convergence is very fast for all significance levels. Hence, the use of asymptotical critical values is recommended for this test. For the case of tests BM_{3-4} and BM_{3-6}, results presented in Figs. A.1j) and k) show an overall low agreement between asymptotical and empirical critical values. In general, the speed of convergence is slow and convergence does not appear to increase with sample size, especially for BM_{3-4}. Hence, for an adequate application of these tests, empirical critical values have to be used. Finally, with respect to $T_{MC\text{-}LR}$, results presented in Fig. A.1l) show that, although the convergence speed is slow, the empirical critical values are close to the asymptotical ones. Nevertheless, the use of empirical critical values is recommended for an adequate use of this test.

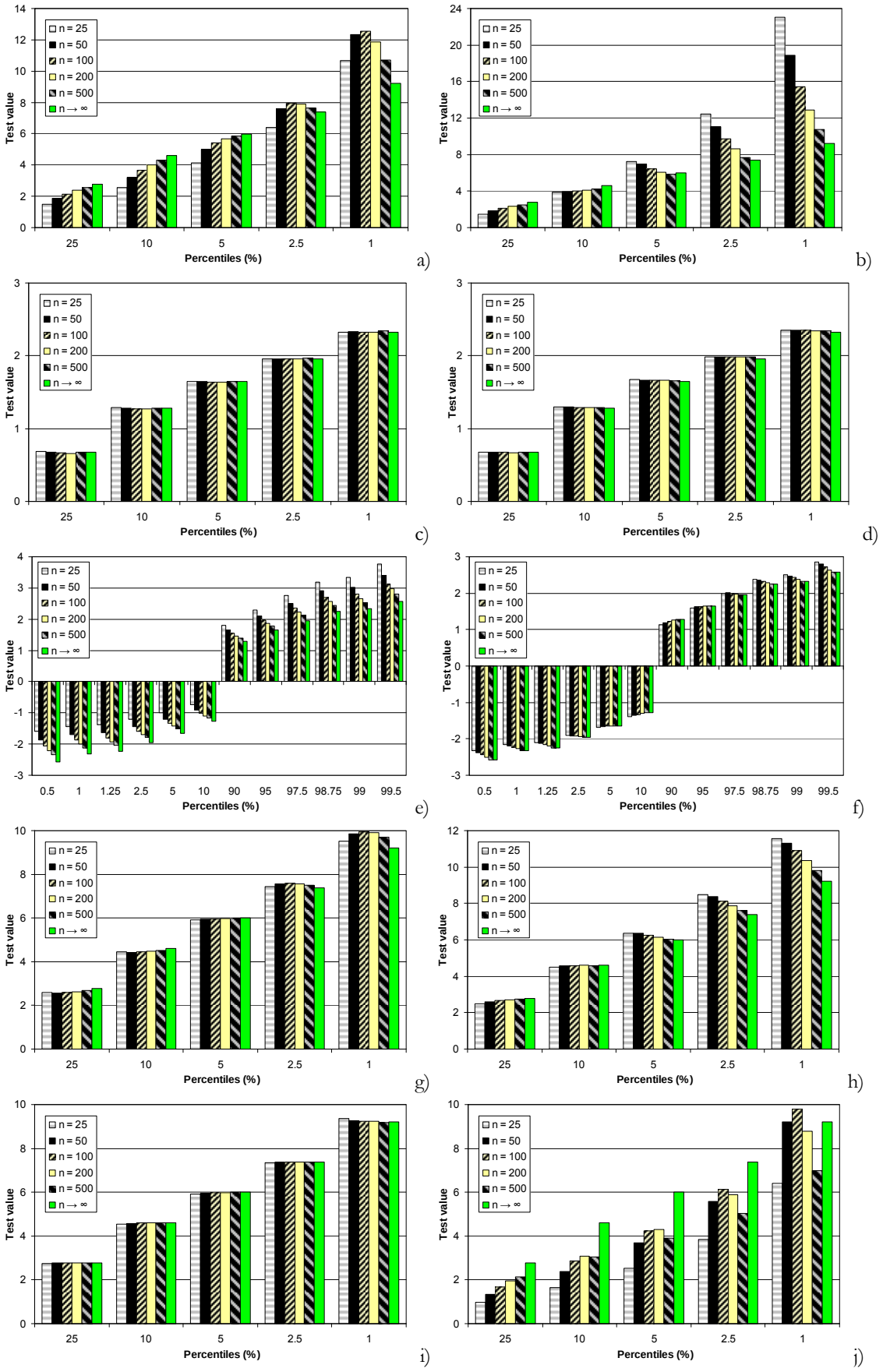

Figure A.1. Comparison of empirical and asymptotical critical values for *JB* (a), *RJB* (b), *W* (c), W_{SF} (d), R_{sJ} (e), T_w (f), *DH* (g), K^2 (h), T_{Lmom} (i), BM_{3-4} (j), BM_{3-6} (k) and $T_{MC\text{-}LR}$ (l).

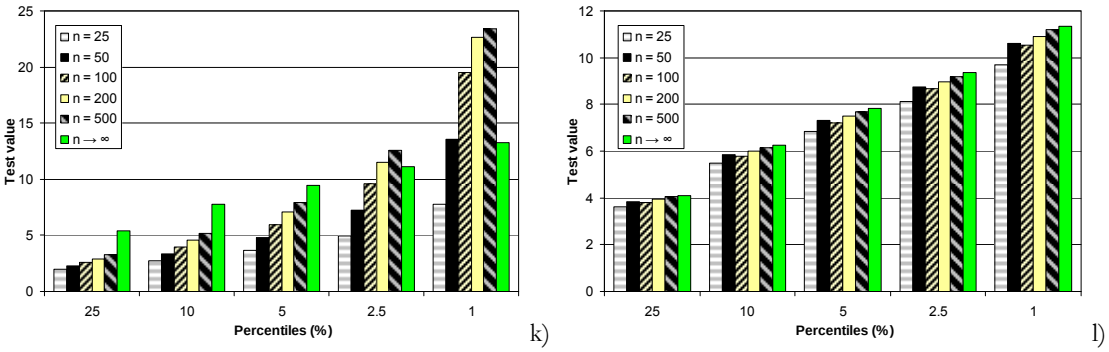

k) l)

Figure A.1 (continued). Comparison of empirical and asymptotical critical values for *JB* (a), *RJB* (b), *W* (c), W_{SF} (d), R_{sJ} (e), T_w (f), *DH* (g), K^2 (h), T_{L_mom} (i), BM_{3-4} (j), BM_{3-6} (k) and $T_{MC\text{-}LR}$ (l).

A.4 Statistical distributions considered in the simulation study

As previously referred, the simulation study considers a number of statistical distributions over which the performance of the presented normality tests is to be assessed. The selected alternative distributions were chosen in order to be a representative set exhibiting different values of important properties such as skewness and kurtosis, as found in available power studies. These alternative distributions are categorized into three sets. The first set includes several types of symmetric distributions, the second set includes several types of asymmetric distributions and the third set comprises a number of modified normal distributions with various shapes. A brief description of these distributions is presented in the following.

A.4.1 Symmetric distributions

The considered symmetric distributions are:

- Three cases of the Beta(*a*,*b*) distribution, where *a* and *b* are the shape parameters, defined as Beta(0.5;0.5), Beta(1;1) and Beta(2;2).

- Three cases of the Cauchy(*t*,*s*) distribution, where *t* and *s* are the location and scale parameters, respectively, defined as Cauchy(0;0.5), Cauchy(0;1) and Cauchy(0;2);

- One case of the Laplace(*t*,*s*) distribution, where *t* and *s* are the location and scale parameters, respectively, defined as Laplace(0;1);

- One case of the Logistic(*t*,*s*) distribution, where *t* and *s* are the location and scale parameters, respectively, defined as Logistic(2;2);

- Four cases of the t-Student(ν) distribution, where ν is the number of degrees of freedom, defined as t(1), t(2), t(4) and t(10);

- Five cases of the Tukey(λ) distribution, where λ is the shape parameter, defined as Tukey(0.14), Tukey(0.5), Tukey(2), Tukey(5) and Tukey(10);

- One case of the normal distribution, corresponding to the standard normal distribution defined as $N(0;1)$. This distribution is included in order to confirm the nominal significance levels.

A.4.2 Asymmetric distributions

The considered asymmetric distributions are:

- Four cases of the Beta(a,b) distribution, defined as Beta(2;1), Beta(2;5), Beta(4;0.5) and Beta(5;1);

- Four cases of the chi-squared(ν) distribution, where ν is the number of degrees of freedom, defined as $\chi^2(1)$, $\chi^2(2)$, $\chi^2(4)$ and $\chi^2(10)$;

- Six cases of the Gamma(a,b) distribution, where a and b are the shape and scale parameters, respectively, defined as Gamma(2;2), Gamma(3;2), Gamma(5;1), Gamma(9;1), Gamma(15;1) and Gamma(100;1);

- One case of the Gumbel(t,s) distribution, where t and s are the location and scale parameters, respectively, defined as Gumbel(1;2);

- One case of the lognormal(t,s) distribution, where t and s are the location and scale parameters, respectively, defined as LN(0;1);

- Four cases of the Weibull(a,b) distribution, where a and b are the scale and shape parameters, respectively, defined as Weibull(0.5;1), Weibull(1;2), Weibull(2;3.4) and Weibull(3;4).

A.4.3 Modified normal distributions

The considered modified normal distributions are:

- Six cases of the standard normal distribution truncated at *a* and *b* Trunc(*a*;*b*), where *a* and *b* are the lower and upper truncations points, respectively, defined as Trunc(-1;1), Trunc(-2;2), Trunc(-3;3), Trunc(-2;1), Trunc(-3;1) and Trunc(-3;2);

- Nine cases of a location-contaminated standard normal distribution, hereon termed LoConN(*p*;*a*), consisting of randomly selected observations with probability *1-p* drawn from a standard normal distribution and with probability *p* drawn from a normal distribution with mean *a* and standard deviation 1. The selected cases are defined as LoConN(0.3;1), LoConN(0.4;1), LoConN(0.5;1), LoConN(0.3;3), LoConN(0.4;3), LoConN(0.5;3), LoConN(0.3;5), LoConN(0.4;5) and LoConN(0.5;5);

- Nine cases of a scale-contaminated standard normal distribution, hereon termed ScConN(*p*;*b*), consisting of randomly selected observations with probability *1-p* drawn from a standard normal distribution and with probability *p* drawn from a normal distribution with mean 0 and standard deviation *b*. The selected cases are defined as ScConN(0.05;0.25), ScConN(0.10;0.25), ScConN(0.20;0.25), ScConN(0.05;2), ScConN(0.10;2), ScConN(0.20;2), ScConN(0.05;4), ScConN(0.10;4) and ScConN(0.20;4);

- Twelve cases of a mixture of normal distributions, hereon termed MixN(*p*;*a*;*b*), consisting of randomly selected observations with probability *1-p* drawn from a standard normal distribution and with probability *p* drawn from a normal distribution with mean *a* and standard deviation *b*. The selected cases are defined as MixN(0.3;1;0.25), MixN(0.4;1;0.25), MixN(0.5;1;0.25), MixN(0.3;3;0.25), MixN(0.4;3;0.25), MixN(0.5;3;0.25), MixN(0.3;1;4), MixN(0.4;1;4) , MixN(0.5;1;4), MixN(0.3;3;4), MixN(0.4;3;4) and MixN(0.5;3;4);

- Five cases of standard normal distributions with outliers, hereon termed Nout1 to Nout5, consisting of observations drawn from a standard normal distribution where some of the values are randomly replaced by extreme observations. The extreme observations are separated into upper and lower extreme observations, x^*_{up} and x^*_{low}, respectively. An observation x^*_{up} is defined as $x_{q3} + k \cdot IQR$, where IQR represents the inter-quartile range of the standard normal distribution, x_{q3} is the *75%* quartile of the standard normal distribution and *k* is a selected constant. An observation x^*_{low} is defined as $x_{q1} - k \cdot IQR$, where x_{q1} is the *25%* quartile of the standard normal distribution. The distribution Nout1 has one extreme observation x^*_{up} with $k = 2$, the distribution Nout2 has one extreme observation x^*_{up} with $k = 3$, the distribution Nout3 has two extreme observations x^*_{up} with

$k = 2$ and $k = 3$, the distribution Nout4 has one extreme observation x^*_{up} and one extreme observation x^*_{low} both with $k = 2$ and the distribution Nout5 has two extreme observations x^*_{up} and two extreme observations x^*_{low}, with $k = 2$ and $k = 3$. This set of distributions was specifically considered in order to identify which normality tests are less sensitive to extreme observations that may be present in an underlying normal data sample.

A.5 Simulation study and power results

An extensive simulation study is presented in the following to estimate the power of the selected normality tests. The effects on the power of the tests due to the sample size, the selected significance level and the type of alternative distribution are considered in the simulation study. The study is carried out for three sample sizes ($n = 25$, $n = 50$ and $n = 100$) and considering significance levels α of 0.10, 0.05, 0.025 and 0.01.

Although critical values or limiting distributions of the tests statistics are available for some of the tests considered herein, critical values for each sample size under consideration were, nonetheless, derived empirically for each test for the considered nominal significance levels, before carrying out the power study. These critical values were based on 1000000 samples drawn from the standard normal distribution. In addition to the referred critical values, the values of μ_{τ_3}, μ_{τ_4}, $\mathrm{var}(\tau_3)$ and $\mathrm{var}(\tau_4)$, for the Hosking L-moments based test, and the values of $\mu^{(t)}_{\tau_3}$, $\mu^{(t)}_{\tau_4}$, $\mathrm{var}\left(\tau_3^{(t)}\right)$ and $\mathrm{var}\left(\tau_4^{(t)}\right)$, for the Hosking trimmed L-moments based test, were also determined for each sample size by simulation from 1000000 samples drawn from the standard normal distribution. For the latter test, the parameters were obtained for each of the previously referred trimming levels t of 1, 2 and 3. The values resulting from this empirical evaluation are presented in Table A.1. As can be seen, the values of μ_{τ_3} and of $\mu^{(t)}_{\tau_3}$ for the different trimming levels are very close to zero, and are considered to be zero in the subsequent power study.

Since complete lists of the simulated power values of the several normality tests, for the different sample sizes and significance levels represent a prohibitive amount of data, only a sample of these results, considered to be representative of the general trend of results, is presented herein. Hence, Tables A.2 to A.10 present the power results for the symmetric, asymmetric and modified normal distribution sets, considering samples sizes of 25, 50 and 100 and a significance level α of 0.05. Within the symmetric and asymmetric sets, distributions are ordered according to their skewness ($\sqrt{\beta_1}$) and kurtosis (β_2) values while for the modified normal distributions set this ordering is performed for each group of distributions. To complement these results, Tables A.11 and A.12 and Fig. A.2 present

the average power results of the different tests over each distribution set and for significance levels α of 0.05 and 0.10. For Fig. A.2, the numbering of the tests is defined according to Table A.13. In the definition of the average powers, the N(0;1) distribution case is not considered for the case of symmetric distributions and distributions Nout1 to Nout5 are also not considered for the modified normal distributions case. The format of the performance results of Tables A.11 and A.12 is defined such that power values above 75% are in bold and values between 50% and 75% are in italic.

Table A.1. Empirical values of μ_{τ_3}, μ_{τ_4}, $\mathrm{var}(\tau_3)$, $\mathrm{var}(\tau_4)$, $\mu_{\tau_3}^{(t)}$, $\mu_{\tau_4}^{(t)}$, $\mathrm{var}(\tau_3^{(t)})$ and $\mathrm{var}(\tau_4^{(t)})$.

Sample size n		μ_{τ_3}	μ_{τ_4}	$\mathrm{var}(\tau_3)$	$\mathrm{var}(\tau_4)$
25		-1.3015e-5 *	1.2383e-1	8.8038e-3	4.9295e-3
50		-2.5783e-5 *	1.2321e-1	4.0493e-3	2.0802e-3
100		7.9729e-6 *	1.2291e-1	1.9434e-3	9.5785e-4
Sample size n	Trimming level t	$\mu_{\tau_3}^{(t)}$	$\mu_{\tau_4}^{(t)}$	$\mathrm{var}(\tau_3^{(t)})$	$\mathrm{var}(\tau_4^{(t)})$
25	1	2.8032e-5 *	6.7077e-2	8.1391e-3	4.2752e-3
	2	3.0692e-5 *	4.4174e-2	8.6570e-3	4.2066e-3
	3	2.0512e-5 *	3.3180e-2	9.5765e-3	4.4609e-3
50	1	-3.7182e-5 *	6.4456e-2	3.4657e-3	1.5699e-3
	2	-1.4220e-5 *	4.0389e-2	3.3818e-3	1.3301e-3
	3	8.5138e-6 *	2.8224e-2	3.3813e-3	1.1823e-3
100	1	-1.7081e-5 *	6.3424e-2	1.6064e-3	6.8100e-4
	2	-1.4710e-5 *	3.9030e-2	1.5120e-3	5.4207e-4
	3	-3.5160e-6 *	2.6645e-2	1.4547e-3	4.5107e-4

* these values are considered to be zero in the remaining of the power study.

Table A.2. Empirical power results for symmetrical distributions (α = 0.05, n = 25).

Distribution	$\sqrt{\beta_1}$	β_2	K-S	*AD**	Z_c	Z_a	P_s	K^2	*JB*	*DH*	*RJB*	T_{Lmom}	$T_{TLmom}^{(1)}$	$T_{TLmom}^{(2)}$	$T_{TLmom}^{(3)}$	$BM_{3\text{-}4}$	$BM_{3\text{-}6}$	$T_{MC\text{-}LR}$
Beta(0.5;0.5)	0	1.50	41.1	**75.9**	**90.5**	**85.0**	**75.8**	*69.4*	0.5	*62.1*	0.2	**83.7**	38.9	18.1	10.8	0.0	0.0	45.8
Beta(1;1)	0	1.80	12.1	22.9	32.3	22.2	22.8	23.9	0.1	13.2	0.1	28.1	9.4	5.3	4.4	0.0	0.0	12.9
Tukey(2)	0	1.80	12.0	23.1	32.5	22.4	23.0	24.0	0.2	13.4	0.1	28.4	9.4	5.2	4.4	0.0	0.0	13.0
Tukey(0.5)	0	2.08	6.3	8.1	8.2	5.2	8.0	6.4	0.2	3.2	0.2	7.8	4.8	4.0	4.0	0.1	0.1	7.4
Beta(2;2)	0	2.14	5.7	6.7	6.6	4.2	6.7	5.0	0.3	2.6	0.3	6.2	4.4	3.9	4.0	0.1	0.1	6.8
Tukey(5)	0	2.90	13.6	13.3	4.0	4.4	13.4	2.4	2.9	4.9	7.0	9.6	25.1	23.7	19.9	1.9	2.0	5.3
Tukey(0.14)	0	2.97	5.0	4.9	4.7	4.8	4.9	4.7	4.7	4.7	4.8	4.9	4.8	4.7	4.7	4.6	4.6	4.9
N(0;1)	0	3.00	5.0	5.1	5.0	5.0	5.1	5.0	5.0	5.0	5.0	5.0	4.8	4.7	4.7	5.0	5.0	4.9
t(10)	0	4.00	7.6	9.4	11.4	11.2	9.5	13.0	13.9	13.4	14.2	11.2	6.1	5.5	5.2	13.8	13.9	4.8
Logistic(0;2)	0	4.20	9.1	11.8	13.6	13.6	11.9	15.8	17.0	16.7	17.9	14.1	7.2	6.2	5.7	16.6	16.8	4.8
Tukey(10)	0	5.38	**95.4**	**96.2**	*71.9*	**80.6**	**96.2**	*51.6*	*58.8*	*68.4*	**89.3**	**92.7**	**98.3**	**96.9**	**93.7**	41.2	44.7	*55.7*
Laplace(0;1)	0	6.00	25.8	32.3	28.7	29.9	32.8	32.5	35.3	36.6	41.7	38.1	22.5	16.4	13.0	32.1	32.9	5.4
t(4)	0	∞	19.7	26.1	28.6	28.8	26.4	32.0	34.0	33.9	36.0	30.4	11.0	8.0	6.9	32.6	33.2	4.9
t(2)	0	∞	*52.5*	*61.3*	*59.7*	*61.0*	*61.6*	*62.7*	*65.1*	*66.1*	*69.3*	*65.9*	29.1	16.6	12.4	*61.5*	*62.5*	6.6
t(1)	0	∞	**90.6**	**93.5**	**90.7**	**91.9**	**93.7**	**90.7**	**92.1**	**93.0**	**95.0**	**94.7**	*74.1*	*51.3*	38.8	**88.9**	**89.7**	17.0
Cauchy(0;0.5)	-	-	**90.7**	**93.6**	**90.7**	**91.9**	**93.7**	**90.7**	**92.1**	**93.1**	**95.0**	**94.8**	*74.0*	*51.1*	38.6	**88.9**	**89.8**	17.0
Cauchy(0;1)	-	-	**90.8**	**93.5**	**90.6**	**91.8**	**93.6**	**90.6**	**92.0**	**92.9**	**94.9**	**94.6**	*74.2*	*51.3*	38.6	**88.9**	**89.7**	17.1
Cauchy(0;2)	-	-	**90.7**	**93.4**	**90.6**	**91.8**	**93.5**	**90.6**	**92.0**	**92.9**	**94.8**	**94.6**	*73.9*	*51.1*	38.5	**88.9**	**89.7**	17.1

Table A.2. (continued) Empirical power results for symmetrical distributions (α = 0.05, n = 25).

Distribution	$\sqrt{\beta_1}$	β_2	T_w	$T_{MC\text{-}LR}$-T_w	$T_{S,l}$	$T_{K,l}$	*W*	W_{SF}	W_{RG}	*D*	*r*	*CS*	*Q*	*Q-Q**	*BCMR*	β_3^2	T_{EP}	I_n	$R_{s,l}$
Beta(0.5;0.5)	0	1.50	*67.7*	*67.6*	3.3	5.7	**86.5**	*65.5*	**96.1**	3.9	*60.9*	**88.7**	*61.5*	**86.0**	**82.4**	**90.5**	*63.2*	0.8	*60.1*
Beta(1;1)	0	1.80	30.8	25.6	1.1	3.0	28.2	11.2	*51.3*	14.3	9.3	32.0	20.5	24.0	23.2	44.0	18.0	0.2	29.1
Tukey(2)	0	1.80	30.9	25.7	1.1	3.0	28.4	11.4	*51.4*	14.3	9.5	32.3	20.8	24.2	23.4	44.0	18.3	0.2	29.2
Tukey(0.5)	0	2.08	13.5	11.0	0.8	2.4	7.9	2.8	17.9	11.0	2.3	9.3	6.5	6.4	6.2	13.4	6.5	0.3	13.3
Beta(2;2)	0	2.14	11.3	9.4	0.8	2.5	6.4	2.4	14.5	9.8	2.0	7.6	5.5	5.2	5.0	10.5	5.5	0.4	11.2
Tukey(5)	0	2.90	11.2	8.8	3.3	12.5	7.3	8.0	5.6	6.3	8.1	6.6	2.4	2.0	7.4	7.8	7.5	10.0	11.1
Tukey(0.14)	0	2.97	4.8	4.7	4.8	4.9	4.8	4.8	4.8	4.8	4.8	4.8	4.7	4.6	4.8	4.8	4.9	4.8	4.8
N(0;1)	0	3.00	5.0	4.8	5.0	5.0	5.0	5.0	5.0	5.1	5.0	5.0	5.0	4.9	5.0	5.0	5.0	5.0	5.0
t(10)	0	4.00	9.4	8.0	12.5	10.1	10.8	12.8	6.8	10.6	13.0	10.4	9.2	11.1	11.5	11.3	9.9	13.0	9.5
Logistic(0;2)	0	4.20	11.9	9.6	14.9	12.1	13.2	15.9	7.7	13.2	16.2	12.6	10.9	13.2	14.1	14.3	12.1	16.3	11.9
Tukey(10)	0	5.38	**83.8**	**90.4**	48.8	*50.9*	**89.0**	**91.7**	*72.5*	**89.7**	**91.9**	**87.2**	37.9	46.7	**89.9**	**82.2**	**80.4**	14.7	**95.5**
Laplace(0;1)	0	6.00	34.4	28.2	30.0	25.3	30.9	36.9	17.1	33.8	37.5	29.2	19.7	27.1	32.8	36.3	30.7	33.2	35.7
t(4)	0	∞	26.8	22.8	29.9	24.4	28.4	32.8	17.9	29.5	33.2	27.3	19.8	28.0	29.8	30.3	26.8	27.5	27.4
t(2)	0	∞	*61.8*	*57.0*	*58.9*	*51.3*	*61.4*	*66.2*	47.4	*64.0*	*66.6*	*60.1*	39.2	*57.9*	*63.0*	*63.9*	*61.2*	31.9	*63.4*
t(1)	0	∞	**92.8**	**91.3**	**88.0**	**82.0**	**92.6**	**94.2**	**86.0**	**93.8**	**94.3**	**92.0**	*64.9*	**88.4**	**93.1**	**92.9**	**92.7**	11.2	**94.3**
Cauchy(0;0.5)	-	-	**92.9**	**91.5**	**88.2**	**82.0**	**92.6**	**94.2**	**86.0**	**93.8**	**94.3**	**92.0**	*64.9*	**88.5**	**93.1**	**92.9**	**92.7**	11.1	**94.3**
Cauchy(0;1)	-	-	**92.8**	**91.5**	**88.0**	**82.1**	**92.5**	**94.1**	**85.9**	**93.7**	**94.2**	**91.9**	*64.7*	**88.4**	**93.0**	**92.8**	**92.6**	11.2	**94.3**
Cauchy(0;2)	-	-	**92.8**	**91.4**	**87.9**	**82.0**	**92.4**	**94.0**	**85.9**	**93.7**	**94.2**	**91.8**	*64.8*	**88.5**	**93.0**	**92.8**	**92.5**	11.1	**94.3**

Table A.3. Empirical power results for symmetrical distributions (α = 0.05, n = 50).

Distribution	$\sqrt{\beta_1}$	β_2	K-S	*AD**	Z_c	Z_a	P_s	K^2	*JB*	*DH*	*RJB*	T_{Lmom}	$T_{TLmom}^{(1)}$	$T_{TLmom}^{(2)}$	$T_{TLmom}^{(3)}$	$BM_{3\text{-}4}$	$BM_{3\text{-}6}$	$T_{MC\text{-}LR}$
Beta(0.5;0.5)	0	1.50	**80.0**	**99.1**	**100.0**	**100.0**	**99.2**	**99.5**	38.8	**97.6**	0.0	**99.6**	**82.2**	*51.3*	30.9	0.0	0.0	*69.8*
Beta(1;1)	0	1.80	26.0	*57.6*	**82.6**	**79.4**	*57.9*	**77.8**	0.8	45.7	0.0	*70.5*	25.9	11.7	7.3	0.0	0.0	19.0
Tukey(2)	0	1.80	26.0	*57.7*	**82.7**	**79.5**	*58.1*	**77.8**	0.8	46.0	0.0	*70.7*	26.0	11.8	7.5	0.0	0.0	19.0
Tukey(0.5)	0	2.08	9.8	17.2	24.3	20.2	17.4	28.8	0.1	8.7	0.0	23.1	8.9	5.5	4.6	0.0	0.0	8.6
Beta(2;2)	0	2.14	8.2	13.3	17.4	14.3	13.4	21.4	0.1	6.0	0.0	17.3	7.4	5.0	4.3	0.0	0.0	7.7
Tukey(5)	0	2.90	23.6	24.9	4.1	3.5	25.2	0.8	1.1	1.7	6.3	13.2	44.4	45.2	40.1	0.2	0.2	7.7
Tukey(0.14)	0	2.97	5.0	4.9	4.4	4.6	4.9	4.3	4.3	4.4	4.4	4.8	4.8	4.8	4.8	4.1	4.1	5.0
N(0;1)	0	3.00	5.0	5.0	5.0	5.0	5.0	5.1	5.0	5.1	5.0	5.0	4.8	4.9	4.9	5.1	5.1	5.0
t(10)	0	4.00	8.8	12.0	16.2	14.6	12.1	17.9	20.5	19.9	21.2	14.5	7.1	6.1	5.7	19.9	20.0	4.7
Logistic(0;2)	0	4.20	11.3	15.9	19.7	18.0	16.0	22.2	25.8	25.2	27.4	19.6	9.1	7.3	6.5	24.1	24.4	4.8
Tukey(10)	0	5.38	**100.0**	**100.0**	**94.9**	**97.4**	**100.0**	*66.0*	**78.9**	**84.7**	**99.3**	**99.8**	**100.0**	**100.0**	**99.9**	42.6	46.2	**83.6**
Laplace(0;1)	0	6.00	43.2	*54.6*	45.6	45.4	*55.2*	48.8	*55.5*	*56.8*	*65.6*	*61.7*	41.4	29.6	23.0	47.5	48.3	7.2
t(4)	0	∞	30.6	42.1	46.0	44.1	42.5	49.3	*54.0*	*54.0*	*56.9*	47.4	16.7	10.6	8.6	*50.4*	*50.9*	5.4
t(2)	0	∞	**77.8**	**85.9**	**84.0**	**84.1**	**86.1**	**85.2**	**88.1**	**88.7**	**91.1**	**88.8**	*53.2*	29.4	20.2	**84.0**	**84.6**	9.4
t(1)	0	∞	**99.4**	**99.7**	**99.3**	**99.5**	**99.7**	**99.2**	**99.5**	**99.6**	**99.8**	**99.8**	**96.8**	**83.4**	*66.9*	**98.7**	**98.9**	34.2
Cauchy(0;0.5)	-	-	**99.4**	**99.7**	**99.4**	**99.5**	**99.7**	**99.3**	**99.6**	**99.6**	**99.8**	**99.8**	**96.8**	**83.4**	*66.9*	**98.8**	**98.9**	34.2
Cauchy(0;1)	-	-	**99.4**	**99.7**	**99.3**	**99.5**	**99.7**	**99.2**	**99.5**	**99.6**	**99.8**	**99.8**	**96.8**	**83.4**	*66.9*	**98.8**	**98.9**	34.2
Cauchy(0;2)	-	-	**99.4**	**99.7**	**99.3**	**99.4**	**99.7**	**99.2**	**99.5**	**99.6**	**99.8**	**99.8**	**96.8**	**83.4**	*67.0*	**98.8**	**98.9**	34.1

Table A.3. (continued) Empirical power results for symmetrical distributions (α = 0.05, n = 50).

Distribution	$\sqrt{\beta_1}$	β_2	T_w	$T_{MC\text{-}LR}$-T_w	$T_{S,I}$	$T_{K,I}$	W	W_{SF}	W_{RG}	D	r	CS	Q	Q-Q*	$BCMR$	β_3^2	T_{EP}	I_n	$R_{s,J}$
Beta(0.5;0.5)	0	1.50	**96.4**	**95.7**	14.4	5.9	**99.9**	**99.2**	**100.0**	11.8	**98.8**	**100.0**	**94.1**	**99.9**	**99.9**	**100.0**	**97.7**	0.1	**93.2**
Beta(1;1)	0	1.80	*64.7*	*56.0*	2.3	2.3	*74.9*	46.2	**93.8**	*56.3*	40.6	**80.6**	*55.5*	*69.2*	*68.7*	**90.7**	*54.3*	0.0	*62.2*
Tukey(2)	0	1.80	*64.8*	*55.9*	2.3	2.4	*75.0*	46.4	**93.8**	*56.1*	40.8	**80.8**	*55.4*	*69.4*	*68.8*	**90.7**	*54.5*	0.0	*62.3*
Tukey(0.5)	0	2.08	29.2	22.6	0.8	1.6	20.8	7.3	45.5	36.4	5.8	26.0	14.3	14.9	16.7	40.8	16.5	0.0	28.7
Beta(2;2)	0	2.14	23.7	18.2	0.7	1.5	15.2	5.0	35.9	30.0	3.9	19.3	11.0	11.0	12.0	31.1	12.6	0.0	23.0
Tukey(5)	0	2.90	19.8	15.0	1.9	16.9	13.0	10.7	13.7	7.2	10.5	11.8	1.1	0.8	11.9	5.4	9.5	9.7	20.0
Tukey(0.14)	0	2.97	4.7	4.7	4.4	4.5	4.6	4.5	4.9	4.5	4.5	4.6	4.5	4.2	4.6	4.6	4.9	4.5	4.7
N(0;1)	0	3.00	5.1	4.9	5.0	5.0	5.0	5.0	5.0	5.1	5.0	5.0	5.1	5.0	5.0	5.0	5.0	5.1	5.1
t(10)	0	4.00	13.7	11.2	16.3	16.0	15.5	18.8	7.4	16.1	19.2	14.2	12.0	15.3	16.6	17.1	12.5	20.8	13.8
Logistic(0;2)	0	4.20	18.7	15.2	19.6	19.1	19.5	24.0	8.5	21.3	24.5	17.7	14.0	18.1	21.0	22.9	16.4	27.2	18.8
Tukey(10)	0	5.38	**98.6**	**99.7**	*64.7*	*60.5*	**99.7**	**99.7**	**97.9**	**99.5**	**99.8**	**99.5**	33.6	36.3	**99.7**	**97.0**	**98.2**	10.6	**100.0**
Laplace(0;1)	0	6.00	*62.9*	*55.0*	41.5	40.1	*52.1*	*59.2*	26.7	*59.9*	*60.0*	48.4	26.9	37.6	*54.4*	*60.9*	*51.5*	*54.9*	*63.9*
t(4)	0	∞	47.1	41.5	43.5	42.6	46.8	*52.7*	27.4	*51.1*	*53.3*	44.3	29.2	42.5	48.8	*52.1*	42.9	44.7	47.6
t(2)	0	∞	**88.6**	**85.8**	**79.5**	**77.8**	**86.4**	**89.2**	*72.1*	**89.4**	**89.4**	**84.8**	*55.3*	**78.7**	**87.3**	**89.3**	**85.9**	33.3	**88.8**
t(1)	0	∞	**99.8**	**99.7**	**98.4**	**97.5**	**99.7**	**99.8**	**98.6**	**99.8**	**99.8**	**99.6**	**78.8**	**98.0**	**99.7**	**99.7**	**99.7**	2.9	**99.8**
Cauchy(0;0.5)	-	-	**99.8**	**99.7**	**98.4**	**97.5**	**99.7**	**99.8**	**98.7**	**99.8**	**99.8**	**99.6**	**78.6**	**98.1**	**99.7**	**99.7**	**99.7**	2.8	**99.8**
Cauchy(0;1)	-	-	**99.8**	**99.7**	**98.4**	**97.4**	**99.6**	**99.8**	**98.6**	**99.8**	**99.8**	**99.6**	**78.9**	**98.1**	**99.7**	**99.7**	**99.7**	2.8	**99.8**
Cauchy(0;2)	-	-	**99.8**	**99.7**	**98.3**	**97.4**	**99.6**	**99.7**	**98.6**	**99.8**	**99.8**	**99.6**	**78.7**	**98.1**	**99.7**	**99.7**	**99.7**	2.9	**99.8**

Table A.4. Empirical power results for symmetrical distributions ($\alpha = 0.05$, $n = 100$).

Distribution	$\sqrt{\beta_1}$	β_2	K-S	*AD**	Z_c	Z_a	P_s	K^2	*JB*	*DH*	*RJB*	T_{Lmom}	$T_{TLmom}^{(1)}$	$T_{TLmom}^{(2)}$	$T_{TLmom}^{(3)}$	$BM_{3\text{-}4}$	$BM_{3\text{-}6}$	$T_{MC\text{-}LR}$
Beta(0.5;0.5)	0	1.50	**99.4**	**100.0**	**100.0**	**100.0**	**100.0**	**96.8**	**100.0**	**100.0**	*62.8*	**100.0**	**99.3**	**88.4**	*67.1*	0.0	0.0	**93.4**
Beta(1;1)	0	1.80	*58.7*	**95.0**	**99.9**	**99.9**	**95.2**	**99.7**	*74.4*	**95.2**	0.8	**97.7**	*59.2*	28.6	16.0	0.0	0.0	32.3
Tukey(2)	0	1.80	*58.8*	**95.0**	**99.9**	**100.0**	**95.2**	**99.7**	*74.4*	**95.3**	0.8	**97.7**	*59.4*	28.6	16.2	0.0	0.0	32.2
Tukey(0.5)	0	2.08	19.5	42.7	*70.9*	*70.5*	43.3	**75.7**	8.9	38.5	0.0	*56.8*	19.7	9.8	6.6	0.0	0.0	11.3
Beta(2;2)	0	2.14	15.0	31.9	*55.6*	*55.0*	32.3	*63.0*	4.6	26.4	0.0	44.4	15.1	7.9	5.8	0.0	0.0	9.6
Tukey(5)	0	2.90	44.8	*51.9*	16.4	11.3	*52.7*	0.4	0.4	0.5	6.9	22.2	*72.7*	**76.1**	*71.5*	0.0	0.0	16.0
Tukey(0.14)	0	2.97	4.9	4.9	3.9	4.2	4.9	3.9	3.8	3.9	4.0	4.7	4.9	4.9	4.9	3.4	3.4	5.0
N(0;1)	0	3.00	5.0	5.0	5.0	5.0	5.0	5.0	5.0	5.0	5.0	5.0	4.8	4.8	4.8	5.0	5.1	4.9
t(10)	0	4.00	10.8	16.2	23.6	19.4	16.3	26.0	30.8	29.5	31.9	19.8	8.4	6.7	6.1	28.7	28.4	5.0
Logistic(0;2)	0	4.20	15.6	24.0	29.7	25.0	24.2	33.3	39.5	38.5	42.4	29.6	12.3	8.7	7.3	35.0	34.6	5.3
Tukey(10)	0	5.38	**100.0**	**100.0**	**100.0**	**100.0**	**100.0**	**89.4**	**96.4**	**97.6**	**100.0**	**100.0**	**100.0**	**100.0**	**100.0**	43.0	41.0	**98.3**
Laplace(0;1)	0	6.00	*70.4*	**82.6**	*69.5*	*68.9*	**83.0**	*72.1*	**80.0**	**80.7**	**88.8**	**87.4**	*70.2*	*53.2*	41.3	*66.4*	*65.5*	13.1
t(4)	0	∞	49.0	*65.2*	*68.7*	*65.5*	*65.6*	*72.0*	**77.4**	**77.4**	**80.4**	*70.6*	27.6	15.0	11.0	*71.3*	*70.7*	6.9
t(2)	0	∞	**95.9**	**98.5**	**97.7**	**97.7**	**98.5**	**98.0**	**98.8**	**98.9**	**99.3**	**99.0**	**82.1**	*50.7*	32.5	**97.0**	**96.8**	17.1
t(1)	0	∞	**100.0**	**100.0**	**100.0**	**100.0**	**100.0**	**100.0**	**100.0**	**100.0**	**100.0**	**100.0**	**100.0**	**98.7**	**91.6**	**100.0**	**100.0**	*65.2*
Cauchy(0;0.5)	-	-	**100.0**	**100.0**	**100.0**	**100.0**	**100.0**	**100.0**	**100.0**	**100.0**	**100.0**	**100.0**	**100.0**	**98.7**	**91.6**	**100.0**	**100.0**	*65.1*
Cauchy(0;1)	-	-	**100.0**	**100.0**	**100.0**	**100.0**	**100.0**	**100.0**	**100.0**	**100.0**	**100.0**	**100.0**	**100.0**	**98.7**	**91.5**	**100.0**	**100.0**	*65.3*
Cauchy(0;2)	-	-	**100.0**	**100.0**	**100.0**	**100.0**	**100.0**	**100.0**	**100.0**	**100.0**	**100.0**	**100.0**	**100.0**	**98.6**	**91.4**	**100.0**	**100.0**	*65.0*

Table A.4. (continued) Empirical power results for symmetrical distributions ($\alpha = 0.05$, $n = 100$).

Distribution	$\sqrt{\beta_1}$	β_2	T_w	$T_{MC\text{-}LR}$-T_w	$T_{S,l}$	$T_{K,l}$	W	W_{SF}	W_{RG}	D	r	CS	Q	Q-Q*	$BCMR$	β_3^2	T_{EP}	I_n	$R_{s,l}$
Beta(0.5;0.5)	0	1.50	**100.0**	**100.0**	*71.0*	7.8	**100.0**	**100.0**	**100.0**	37.0	**100.0**	**100.0**	**100.0**	**100.0**	**100.0**	**100.0**	**100.0**	0.0	**99.9**
Beta(1;1)	0	1.80	**94.2**	**90.5**	15.8	2.6	**99.6**	**96.5**	**100.0**	**95.6**	**95.0**	**99.8**	**95.9**	**99.6**	**99.3**	**100.0**	**94.3**	0.0	**93.6**
Tukey(2)	0	1.80	**94.3**	**90.5**	15.7	2.5	**99.6**	**96.5**	**100.0**	**95.5**	**95.1**	**99.8**	**95.8**	**99.6**	**99.3**	**100.0**	**94.3**	0.0	**93.6**
Tukey(0.5)	0	2.08	*59.1*	48.5	2.5	1.3	*60.4*	32.3	**88.3**	**79.6**	27.5	*69.7*	40.9	46.2	*53.6*	**86.0**	45.6	0.0	*58.5*
Beta(2;2)	0	2.14	49.0	39.2	1.7	1.2	45.7	21.1	**78.1**	*70.6*	17.4	*55.2*	30.4	33.2	39.2	**75.1**	34.3	0.0	48.6
Tukey(5)	0	2.90	38.9	31.7	1.4	27.2	37.8	25.1	*53.1*	9.8	23.6	39.1	2.6	1.8	32.8	3.1	15.2	8.4	39.4
Tukey(0.14)	0	2.97	4.7	4.7	4.3	4.0	4.3	4.1	4.8	4.4	4.1	4.3	4.1	3.8	4.2	4.4	4.8	4.2	4.8
N(0;1)	0	3.00	5.0	4.9	5.0	5.0	5.0	5.0	4.9	5.0	5.0	5.0	5.1	4.9	5.0	5.0	5.0	5.0	5.0
t(10)	0	4.00	21.1	17.1	20.6	23.2	23.1	28.0	8.4	25.7	28.6	20.4	15.7	20.8	24.7	27.1	17.1	32.6	21.3
Logistic(0;2)	0	4.20	31.7	25.6	25.3	27.8	30.7	36.9	10.7	36.4	37.6	27.1	18.4	24.7	32.7	38.1	25.1	44.1	31.7
Tukey(10)	0	5.38	**100.0**	**100.0**	**91.0**	*70.5*	**100.0**	**100.0**	**100.0**	**100.0**	**100.0**	**100.0**	24.3	21.6	**100.0**	**99.9**	**100.0**	4.4	**100.0**
Laplace(0;1)	0	6.00	**90.2**	**86.3**	*57.3*	*56.9*	**79.7**	**84.1**	48.8	**87.2**	**84.7**	**75.8**	36.5	*50.7*	**81.1**	**86.1**	**80.1**	*74.7*	**90.6**
t(4)	0	∞	*73.5*	*68.2*	*59.8*	*63.1*	*71.2*	**76.3**	44.8	**77.6**	**76.9**	*67.8*	41.8	*60.1*	*72.9*	**78.1**	*66.7*	*61.3*	*73.6*
t(2)	0	∞	**99.2**	**98.8**	**94.7**	**94.6**	**98.6**	**99.0**	**93.8**	**99.3**	**99.1**	**98.2**	*73.1*	**93.6**	**98.7**	**99.2**	**98.5**	24.9	**99.2**
t(1)	0	∞	**100.0**	**100.0**	**100.0**	**99.9**	**100.0**	**100.0**	**100.0**	**100.0**	**100.0**	**100.0**	**89.3**	**99.9**	**100.0**	**100.0**	**100.0**	0.3	**100.0**
Cauchy(0;0.5)	-	-	**100.0**	**100.0**	**100.0**	**99.9**	**100.0**	**100.0**	**100.0**	**100.0**	**100.0**	**100.0**	**89.2**	**99.9**	**100.0**	**100.0**	**100.0**	0.2	**100.0**
Cauchy(0;1)	-	-	**100.0**	**100.0**	**100.0**	**100.0**	**100.0**	**100.0**	**100.0**	**100.0**	**100.0**	**100.0**	**89.3**	**99.9**	**100.0**	**100.0**	**100.0**	0.2	**100.0**
Cauchy(0;2)	-	-	**100.0**	**100.0**	**100.0**	**100.0**	**100.0**	**100.0**	**100.0**	**100.0**	**100.0**	**100.0**	**89.3**	**99.9**	**100.0**	**100.0**	**100.0**	0.3	**100.0**

Table A.5. Empirical power results for asymmetrical distributions (α = 0.05, n = 25).

Distribution	$\sqrt{\beta_1}$	β_2	K-S	*AD**	Z_c	Z_a	P_s	K^2	*JB*	*DH*	*RJB*	T_{Lmom}	$T_{TLmom}^{(1)}$	$T_{TLmom}^{(2)}$	$T_{TLmom}^{(3)}$	$BM_{3\text{-}4}$	$BM_{3\text{-}6}$	$T_{MC\text{-}LR}$
Beta(4;0.5)	-1.79	6.35	**89.5**	**97.9**	**99.2**	**99.6**	**97.7**	**76.3**	**83.4**	**95.7**	**75.1**	**98.2**	*64.2*	*62.6*	*62.2*	49.8	*51.0*	*73.8*
Beta(5;1)	-1.18	4.20	47.0	*69.3*	**78.1**	**83.3**	*68.4*	43.3	48.3	*64.9*	39.2	*70.5*	24.5	23.0	22.5	26.0	26.5	28.7
Beta(2;1)	-0.57	2.40	22.1	34.3	40.5	43.6	33.8	11.9	8.5	25.6	5.7	34.6	11.9	10.3	9.9	2.6	2.6	16.9
Weibull(3;4).	-0.09	2.75	4.8	4.6	4.0	4.0	4.6	3.2	2.8	3.2	2.8	4.1	4.5	4.6	4.6	2.5	2.5	5.1
Weibull(2;3.4)	0.05	2.71	4.5	4.3	3.6	3.5	4.3	3.0	2.4	2.8	2.4	3.6	4.4	4.6	4.6	2.3	2.3	5.2
Gamma(100;1)	0.20	3.06	5.5	5.8	6.2	6.2	5.8	6.2	6.2	5.8	6.0	5.9	4.9	4.9	4.9	6.0	5.9	5.2
Gamma(15;1)	0.52	3.40	9.4	11.4	13.5	13.7	11.3	12.4	12.9	11.2	11.7	11.6	6.4	6.3	6.1	10.6	10.5	6.1
Beta(2;5)	0.60	2.88	13.7	18.6	21.3	23.3	18.3	11.9	11.8	14.7	9.3	17.4	7.8	7.5	7.4	7.1	7.1	9.0
Weibull(1;2)	0.63	3.25	12.0	15.7	19.3	20.6	15.5	14.3	14.5	14.1	12.1	15.4	6.7	6.6	6.5	10.7	10.6	7.6
Gamma(9;1)	0.67	3.67	12.3	15.9	18.9	19.6	15.7	16.6	17.3	15.5	15.6	16.1	7.3	7.0	6.8	13.7	13.7	6.9
χ2(10)	0.89	4.20	18.5	25.5	30.4	31.9	25.1	24.7	26.1	25.0	22.9	25.6	9.6	9.1	8.9	19.2	19.2	8.6
Gamma(5;1)	0.89	4.20	18.5	25.5	30.3	31.9	25.2	24.8	26.3	25.0	23.1	25.7	9.8	9.2	8.9	19.2	19.2	8.6
Gumbel(1;2)	1.14	5.40	24.5	33.6	38.7	40.2	33.2	33.6	35.4	33.8	32.2	34.3	12.6	11.5	11.0	26.5	26.7	9.5
χ2(4)	1.14	6.00	39.8	*57.1*	*64.8*	*68.8*	*56.4*	46.2	49.8	*56.2*	43.4	*57.7*	19.4	17.9	17.3	33.3	33.7	17.4
Gamma(3;2)	1.15	5.00	27.9	40.2	46.8	49.9	39.6	35.3	37.7	39.6	32.9	40.4	13.6	12.6	12.2	26.1	26.2	11.9
Gamma(2;2)	1.41	6.00	39.6	*57.1*	*64.7*	*68.8*	*56.3*	46.3	49.9	*56.1*	43.6	*57.6*	19.4	17.8	17.2	33.4	33.8	17.5
χ2(2)	2.00	9.00	*69.4*	**87.6**	**92.3**	**94.7**	**87.0**	*68.3*	*73.6*	**85.3**	*66.0*	**88.3**	39.5	36.7	35.9	48.8	49.7	40.2
Weibull(0.5;1)	2.00	9.00	*69.4*	**87.4**	**92.2**	**94.6**	**86.8**	*68.4*	*73.6*	**85.3**	*66.0*	**88.2**	39.4	36.7	36.0	48.9	49.8	40.3
χ2(1)	2.83	15.00	**95.2**	**99.3**	**99.7**	**99.9**	**99.2**	**87.8**	**92.2**	**98.3**	**87.5**	**99.4**	*74.6*	*73.0*	*72.8*	*67.2*	*68.5*	**79.8**
LN(0;1)	6.18	113.90	**88.0**	**96.0**	**97.5**	**98.2**	**95.8**	**87.4**	**90.5**	**95.4**	**86.9**	**96.3**	*62.2*	*57.5*	*56.5*	*72.3*	*73.3*	*51.0*

Table A.5. (continued) Empirical power results for asymmetrical distributions (α = 0.05, n = 25).

Distribution	$\sqrt{\beta_1}$	β_2	T_w	$T_{MC\text{-}LR}$-T_w	$T_{S,I}$	$T_{K,I}$	W	W_{SF}	W_{RG}	D	r	*CS*	Q	*Q-Q**	*BCMR*	β_3^2	T_{EP}	I_n	$R_{s,J}$
Beta(4;0.5)	-1.79	6.35	21.3	*71.5*	**89.7**	39.4	**99.1**	**98.2**	**99.4**	**76.8**	**98.0**	**99.2**	*50.3*	**99.8**	**99.0**	14.5	**96.4**	39.7	*50.6*
Beta(5;1)	-1.18	4.20	10.8	24.6	*60.1*	18.6	**78.3**	*71.2*	**80.1**	31.5	*69.8*	**79.2**	23.7	**82.7**	**76.7**	8.0	*69.5*	34.8	18.2
Beta(2;1)	-0.57	2.40	13.7	16.7	15.4	1.4	40.8	27.8	*52.0*	6.2	25.9	42.9	2.5	49.7	37.4	15.5	34.0	6.1	11.5
Weibull(3;4).	-0.09	2.75	4.7	4.7	3.2	3.0	4.2	3.4	5.5	4.4	3.3	4.4	3.5	3.8	4.0	4.0	4.5	3.0	4.7
Weibull(2;3.4)	0.05	2.71	4.8	4.9	2.8	3.3	3.8	3.0	5.4	4.6	2.9	4.1	3.5	3.6	3.6	4.0	4.1	2.6	4.8
Gamma(100;1)	0.20	3.06	5.2	5.1	6.4	5.7	6.1	6.1	5.8	5.6	6.1	6.1	5.1	5.8	6.1	5.2	6.0	5.7	5.3
Gamma(15;1)	0.52	3.40	6.4	6.5	14.7	9.1	13.3	13.1	11.4	8.7	12.9	13.2	8.5	10.8	13.4	5.9	12.9	10.1	7.2
Beta(2;5)	0.60	2.88	7.1	8.3	18.2	11.8	21.9	17.3	24.5	7.6	16.6	22.5	25.5	18.9	20.7	5.6	20.9	8.2	7.4
Weibull(1;2)	0.63	3.25	6.8	7.4	18.7	10.4	19.2	16.9	19.0	9.3	16.5	19.5	17.6	15.8	18.7	5.4	18.0	10.2	7.7
Gamma(9;1)	0.67	3.67	7.3	7.5	20.5	11.4	18.8	18.1	16.2	11.1	17.9	18.7	11.8	14.8	18.7	6.3	18.2	13.2	8.6
χ2(10)	0.89	4.20	9.1	9.9	31.8	15.9	30.4	28.7	27.0	16.1	28.3	30.3	20.2	23.2	30.1	7.3	29.0	19.1	11.9
Gamma(5;1)	0.89	4.20	9.1	9.9	31.8	15.9	30.4	28.8	27.0	16.1	28.4	30.3	20.3	23.2	30.1	7.4	29.1	19.2	11.9
Gumbel(1;2)	1.14	5.40	12.9	13.4	41.3	20.7	38.9	37.8	33.8	23.4	37.5	38.7	21.8	29.4	38.8	11.2	37.7	25.7	17.5
χ2(4)	1.14	6.00	15.0	19.8	*61.0*	28.3	*65.1*	*60.6*	*63.7*	34.0	*59.8*	*65.5*	*60.1*	*58.2*	*64.2*	11.1	*60.7*	34.8	23.0
Gamma(3;2)	1.15	5.00	11.6	13.9	46.5	21.8	47.1	43.9	44.2	24.0	43.2	47.3	36.6	37.6	46.5	9.0	44.5	27.0	16.7
Gamma(2;2)	1.41	6.00	14.9	19.8	*60.8*	28.3	*65.0*	*60.6*	*63.5*	34.1	*59.7*	*65.5*	*60.1*	*58.1*	*64.1*	11.1	*60.6*	34.9	23.2
χ2(2)	2.00	9.00	23.6	42.7	**84.9**	42.6	**92.4**	**89.1**	**92.9**	*60.7*	**88.4**	**92.8**	**95.9**	**94.3**	**91.8**	17.2	**87.3**	44.5	41.8
Weibull(0.5;1)	2.00	9.00	23.9	42.8	**85.1**	42.7	**92.3**	**89.0**	**92.8**	*60.7*	**88.3**	**92.6**	**95.8**	**94.3**	**91.6**	17.6	**87.2**	44.3	41.7
χ2(1)	2.83	15.00	39.4	**82.2**	**97.4**	*58.0*	**99.7**	**99.4**	**99.8**	**89.0**	**99.3**	**99.8**	**100.0**	**100.0**	**99.7**	30.9	**98.6**	27.6	*70.9*
LN(0;1)	6.18	113.90	*50.7*	*67.3*	**95.4**	*61.7*	**97.6**	**96.6**	**97.5**	**84.6**	**96.3**	**97.7**	**97.6**	**97.2**	**97.4**	43.6	**96.1**	30.6	*72.5*

Table A.6. Empirical power results for asymmetrical distributions (α = 0.05, n = 50).

Distribution	$\sqrt{\beta_1}$	β_2	K-S	*AD**	Z_c	Z_a	P_s	K^2	*JB*	*DH*	*RJB*	T_{Lmom}	$T_{TLmom}^{(1)}$	$T_{TLmom}^{(2)}$	$T_{TLmom}^{(3)}$	$BM_{3\text{-}4}$	$BM_{3\text{-}6}$	$T_{MC\text{-}LR}$
Beta(4;0.5)	-1.79	6.35	**99.9**	**100.0**	**100.0**	**100.0**	**100.0**	**98.9**	**99.7**	**100.0**	**97.3**	**100.0**	**96.4**	**96.6**	**96.6**	*67.8*	*68.8*	**95.6**
Beta(5;1)	-1.18	4.20	**81.4**	**96.7**	**99.2**	**99.8**	**96.2**	**77.3**	**85.0**	**96.7**	*70.4*	**97.7**	*58.0*	*56.9*	*56.4*	35.5	36.1	*53.0*
Beta(2;1)	-0.57	2.40	45.7	*72.2*	**85.2**	**91.8**	*71.4*	29.0	20.0	*67.9*	8.5	**77.8**	30.6	25.4	23.5	0.7	0.7	29.5
Weibull(3;4).	-0.09	2.75	5.1	5.1	3.7	4.1	5.0	3.1	1.8	2.7	1.8	4.4	4.8	4.8	4.9	1.4	1.4	5.4
Weibull(2;3.4)	0.05	2.71	4.7	4.6	3.6	3.9	4.5	3.3	1.6	2.3	1.6	4.0	4.4	4.5	4.5	1.5	1.5	5.2
Gamma(100;1)	0.20	3.06	6.3	6.9	7.7	7.8	6.9	7.5	7.6	7.1	7.3	7.2	5.4	5.4	5.4	6.6	6.6	5.2
Gamma(15;1)	0.52	3.40	14.2	18.7	23.2	24.4	18.2	20.1	21.1	20.4	18.9	19.9	8.7	8.6	8.5	14.4	14.4	7.2
Beta(2;5)	0.60	2.88	25.7	39.6	49.1	*58.6*	38.6	21.9	22.3	39.8	15.7	43.0	15.0	14.2	13.8	7.1	7.0	13.4
Weibull(1;2)	0.63	3.25	20.8	31.0	41.0	47.6	30.0	25.7	26.5	33.8	21.3	33.8	11.5	11.2	11.1	14.2	14.1	10.4
Gamma(9;1)	0.67	3.67	20.4	28.6	35.5	37.9	27.9	29.2	31.0	31.8	27.4	30.8	11.7	11.5	11.3	19.7	19.7	8.9
χ2(10)	0.89	4.20	33.6	48.6	*58.1*	*62.5*	47.5	44.9	48.1	*53.8*	42.2	*51.8*	18.4	17.9	17.8	28.7	28.8	13.0
Gamma(5;1)	0.89	4.20	33.2	48.4	*57.8*	*62.3*	47.3	44.7	47.9	*53.5*	41.9	*51.6*	18.4	17.9	17.7	28.5	28.6	13.0
Gumbel(1;2)	1.14	5.40	43.8	*60.3*	*67.6*	*70.4*	*59.3*	*58.4*	*61.7*	*65.0*	*56.8*	*63.4*	24.8	23.4	22.8	40.4	40.6	14.9
χ2(4)	1.14	6.00	*69.9*	**89.1**	**94.8**	**97.1**	**88.2**	**77.3**	**82.4**	**91.6**	*73.9*	**91.3**	44.1	43.0	42.8	49.6	50.0	32.4
Gamma(3;2)	1.15	5.00	*51.4*	*72.2*	**81.4**	**86.1**	*70.8*	*62.6*	*67.1*	**77.0**	*59.1*	**75.5**	29.4	28.5	28.3	39.2	39.4	20.5
Gamma(2;2)	1.41	6.00	*69.9*	**89.3**	**94.8**	**97.1**	**88.4**	**77.4**	**82.4**	**91.8**	*73.9*	**91.4**	44.3	43.2	42.9	49.5	49.9	32.6
χ2(2)	2.00	9.00	**96.1**	**99.7**	**99.9**	**100.0**	**99.6**	**95.4**	**97.6**	**99.7**	**93.3**	**99.8**	**79.0**	**78.6**	**78.7**	*69.4*	*70.1*	*70.2*
Weibull(0.5;1)	2.00	9.00	**96.2**	**99.7**	**100.0**	**100.0**	**99.6**	**95.4**	**97.6**	**99.7**	**93.3**	**99.8**	**79.1**	**78.7**	**78.8**	*69.5*	*70.2*	*70.2*
χ2(1)	2.83	15.00	**100.0**	**100.0**	**100.0**	**100.0**	**100.0**	**99.8**	**100.0**	**100.0**	**99.4**	**100.0**	**98.6**	**98.8**	**98.8**	**86.8**	**87.5**	**97.5**
LN(0;1)	6.18	113.90	**99.5**	**100.0**	**100.0**	**100.0**	**100.0**	**99.5**	**99.8**	**100.0**	**99.3**	**100.0**	**94.7**	**94.3**	**94.4**	**91.3**	**91.8**	**82.6**

Table A.6. (continued) Empirical power results for asymmetrical distributions (α = 0.05, n = 50).

Distribution	$\sqrt{\beta_1}$	β_2	T_w	$T_{MC\text{-}LR}$-T_w	$T_{S,l}$	$T_{K,l}$	W	W_{SF}	W_{RG}	D	r	CS	Q	Q-Q*	$BCMR$	β_3^2	T_{EP}	I_n	$R_{s,l}$
Beta(4;0.5)	-1.79	6.35	30.5	**95.0**	**99.8**	*70.2*	**100.0**	**100.0**	**100.0**	**96.7**	**100.0**	**100.0**	*68.8*	**100.0**	**100.0**	16.1	**100.0**	49.4	*73.8*
Beta(5;1)	-1.18	4.20	11.5	45.6	**92.0**	38.2	**99.2**	**98.0**	**99.4**	*53.2*	**97.7**	**99.3**	33.0	**99.8**	**99.0**	8.8	**96.1**	*58.4*	24.3
Beta(2;1)	-0.57	2.40	25.7	32.3	34.1	1.0	**84.2**	*69.7*	**92.3**	6.7	*66.6*	**86.8**	0.8	**94.5**	**81.2**	40.4	*71.9*	5.0	18.3
Weibull(3;4).	-0.09	2.75	4.9	5.0	2.8	2.1	4.2	2.9	6.8	4.8	2.7	4.7	2.7	3.7	3.8	4.0	5.1	1.8	4.9
Weibull(2;3.4)	0.05	2.71	5.3	5.2	2.4	1.9	3.9	2.5	6.8	5.4	2.4	4.4	3.7	3.8	3.5	4.3	4.4	1.5	5.3
Gamma(100;1)	0.20	3.06	5.4	5.3	8.3	5.2	7.7	7.6	6.8	5.9	7.5	7.6	5.7	6.7	7.7	5.3	7.4	6.6	5.5
Gamma(15;1)	0.52	3.40	7.1	7.6	26.7	9.8	23.6	22.4	19.6	11.2	22.1	23.5	14.2	16.8	23.4	6.3	21.6	14.7	8.2
Beta(2;5)	0.60	2.88	9.1	12.3	40.4	10.0	*50.2*	39.6	*56.0*	8.2	37.7	*52.4*	*62.2*	49.3	47.7	9.3	44.6	9.9	8.4
Weibull(1;2)	0.63	3.25	7.7	9.5	39.1	10.3	41.5	35.0	42.3	11.8	33.8	42.7	43.4	35.6	40.0	6.6	35.7	14.7	8.4
Gamma(9;1)	0.67	3.67	8.6	9.6	39.7	13.4	36.2	34.0	31.2	15.7	33.4	36.2	22.7	25.1	35.9	7.1	33.2	20.9	10.6
χ2(10)	0.89	4.20	11.5	14.4	*60.7*	19.8	*59.2*	*55.1*	*54.7*	25.4	*54.3*	*59.5*	43.5	44.1	*58.4*	8.8	*54.2*	32.3	16.0
Gamma(5;1)	0.89	4.20	11.4	14.4	*60.4*	19.6	*58.9*	*55.0*	*54.4*	25.1	*54.1*	*59.3*	43.3	43.8	*58.2*	8.7	*54.0*	32.0	15.8
Gumbel(1;2)	1.14	5.40	19.3	21.8	*71.8*	29.1	*69.0*	*66.7*	*62.7*	39.4	*66.1*	*68.9*	42.3	*50.4*	*68.7*	15.8	*65.4*	43.8	27.1
χ2(4)	1.14	6.00	21.4	34.8	**91.9**	37.4	**94.9**	**92.3**	**94.8**	*56.8*	**91.7**	**95.3**	**95.8**	**93.9**	**94.4**	14.3	**90.7**	*57.1*	35.4
Gamma(3;2)	1.15	5.00	15.8	22.5	**80.0**	28.3	**82.1**	**77.8**	**80.4**	39.9	**76.8**	**82.7**	**75.4**	*72.4*	**81.2**	11.3	**76.3**	45.8	24.3
Gamma(2;2)	1.41	6.00	21.4	35.0	**91.9**	37.5	**95.0**	**92.4**	**94.9**	*56.7*	**91.8**	**95.4**	**95.8**	**93.9**	**94.5**	14.4	**90.8**	*57.1*	35.2
χ2(2)	2.00	9.00	37.5	*73.2*	**99.5**	*56.7*	**99.9**	**99.8**	**100.0**	**87.5**	**99.8**	**100.0**	**100.0**	**100.0**	**99.9**	24.6	**99.5**	*60.9*	*64.5*
Weibull(0.5;1)	2.00	9.00	37.4	*73.4*	**99.5**	*56.7*	**99.9**	**99.8**	**100.0**	**87.6**	**99.8**	**100.0**	**100.0**	**100.0**	**99.9**	24.5	**99.6**	*60.8*	*64.5*
χ2(1)	2.83	15.00	*63.0*	**98.4**	**100.0**	**76.7**	**100.0**	**100.0**	**100.0**	**99.4**	**100.0**	**100.0**	**100.0**	**100.0**	**100.0**	47.6	**100.0**	21.6	**92.1**
LN(0;1)	6.18	113.90	**77.2**	**93.4**	**100.0**	**84.3**	**100.0**	**100.0**	**100.0**	**98.4**	**100.0**	**100.0**	**100.0**	**100.0**	**100.0**	*67.1*	**100.0**	23.3	**93.3**

Table A.7. Empirical power results for asymmetrical distributions (α = 0.05, n = 100).

Distribution	$\sqrt{\beta_1}$	β_2	K-S	*AD**	Z_c	Z_a	P_s	K^2	*JB*	*DH*	*RJB*	T_{Lmom}	$T_{TLmom}^{(1)}$	$T_{TLmom}^{(2)}$	$T_{TLmom}^{(3)}$	$BM_{3\text{-}4}$	$BM_{3\text{-}6}$	$T_{MC\text{-}LR}$
Beta(4;0.5)	-1.79	6.35	**100.0**	**100.0**	**100.0**	**100.0**	**100.0**	**100.0**	**100.0**	**100.0**	**100.0**	**100.0**	**100.0**	**100.0**	**100.0**	**85.5**	**84.7**	**100.0**
Beta(5;1)	-1.18	4.20	**99.4**	**100.0**	**100.0**	**100.0**	**100.0**	**99.8**	**99.9**	**100.0**	**98.7**	**100.0**	**92.3**	**91.9**	**91.6**	48.3	47.3	**86.0**
Beta(2;1)	-0.57	2.40	**81.8**	**98.3**	**99.9**	**100.0**	**98.0**	**90.0**	**84.8**	**98.5**	34.7	**99.0**	*65.6*	*56.1*	*51.8*	0.0	0.0	*56.2*
Weibull(3;4).	-0.09	2.75	5.9	6.3	4.4	5.7	6.3	4.0	1.5	3.2	1.4	5.8	5.4	5.4	5.4	0.6	0.6	5.6
Weibull(2;3.4)	0.05	2.71	4.9	5.2	4.5	5.5	5.2	4.8	1.4	2.6	1.2	5.1	4.7	4.5	4.5	1.1	1.2	5.3
Gamma(100;1)	0.20	3.06	7.7	8.9	10.3	10.5	8.7	10.0	10.2	9.8	9.8	9.4	6.1	6.1	6.1	7.6	7.5	5.6
Gamma(15;1)	0.52	3.40	23.9	33.9	42.5	45.3	32.7	36.6	38.6	41.0	35.0	38.0	14.4	14.1	14.1	20.0	19.8	10.2
Beta(2;5)	0.60	2.88	*50.0*	**75.9**	**90.5**	**96.2**	*74.2*	*56.6*	*59.4*	**83.4**	38.7	**82.3**	32.4	30.2	29.4	6.4	6.3	24.7
Weibull(1;2)	0.63	3.25	39.2	*61.1*	**79.6**	**88.2**	*59.0*	*53.2*	*56.3*	*72.5*	44.3	*68.5*	22.6	21.9	21.7	18.9	18.6	17.1
Gamma(9;1)	0.67	3.67	36.9	*53.1*	*64.1*	*68.3*	*51.5*	*54.2*	*57.2*	*62.9*	*51.4*	*58.6*	21.9	21.5	21.4	28.1	27.8	14.4
χ2(10)	0.89	4.20	*59.6*	**80.6**	**89.6**	**92.8**	**79.0**	**78.0**	**81.6**	**88.4**	*74.4*	**85.2**	37.6	36.9	36.9	41.6	41.0	24.4
Gamma(5;1)	0.89	4.20	*59.7*	**80.7**	**89.7**	**92.8**	**79.2**	**78.3**	**81.8**	**88.6**	*74.7*	**85.3**	37.8	37.3	37.1	41.5	41.0	24.5
Gumbel(1;2)	1.14	5.40	*73.2*	**89.0**	**93.4**	**94.7**	**88.0**	**88.6**	**90.7**	**93.6**	**87.2**	**91.8**	49.8	48.4	48.0	*58.6*	*57.9*	29.6
χ2(4)	1.14	6.00	**95.3**	**99.8**	**100.0**	**100.0**	**99.7**	**99.1**	**99.5**	**99.9**	**97.9**	**99.9**	**80.1**	**79.9**	**79.9**	*69.3*	*68.5*	*63.0*
Gamma(3;2)	1.15	5.00	**82.3**	**96.5**	**99.1**	**99.7**	**95.8**	**94.1**	**95.9**	**98.6**	**91.2**	**97.8**	*59.7*	*59.3*	*59.2*	*56.3*	*55.4*	41.8
Gamma(2;2)	1.41	6.00	**95.3**	**99.8**	**100.0**	**100.0**	**99.7**	**99.1**	**99.5**	**99.9**	**98.0**	**99.9**	**80.0**	**79.9**	**79.9**	*69.3*	*68.5*	*62.8*
χ2(2)	2.00	9.00	**100.0**	**100.0**	**100.0**	**100.0**	**100.0**	**100.0**	**100.0**	**100.0**	**100.0**	**100.0**	**98.9**	**99.0**	**99.0**	**88.1**	**87.5**	**95.6**
Weibull(0.5;1)	2.00	9.00	**100.0**	**100.0**	**100.0**	**100.0**	**100.0**	**100.0**	**100.0**	**100.0**	**100.0**	**100.0**	**98.9**	**98.9**	**98.9**	**88.1**	**87.5**	**95.7**
χ2(1)	2.83	15.00	**100.0**	**100.0**	**100.0**	**100.0**	**100.0**	**100.0**	**100.0**	**100.0**	**100.0**	**100.0**	**100.0**	**100.0**	**100.0**	**97.7**	**97.5**	**100.0**
LN(0;1)	6.18	113.90	**100.0**	**100.0**	**100.0**	**100.0**	**100.0**	**100.0**	**100.0**	**100.0**	**100.0**	**100.0**	**100.0**	**100.0**	**100.0**	**99.1**	**99.0**	**98.9**

Table A.7. (continued) Empirical power results for asymmetrical distributions (α = 0.05, n = 100).

Distribution	$\sqrt{\beta_1}$	β_2	T_w	$T_{MC\text{-}LR}$-T_w	$T_{S,I}$	$T_{K,I}$	*W*	W_{SF}	W_{RG}	*D*	*r*	*CS*	*Q*	*Q-Q**	*BCMR*	β_3^2	T_{EP}	I_n	$R_{s,J}$
Beta(4;0.5)	-1.79	6.35	45.6	**99.9**	**100.0**	**93.3**	**100.0**	**100.0**	**100.0**	**100.0**	**100.0**	**100.0**	**85.4**	**100.0**	**100.0**	18.7	**100.0**	*56.9*	**93.3**
Beta(5;1)	-1.18	4.20	12.2	**80.8**	**99.9**	*65.0*	**100.0**	**100.0**	**100.0**	**80.8**	**100.0**	**100.0**	44.5	**100.0**	**100.0**	10.7	**100.0**	**84.2**	34.3
Beta(2;1)	-0.57	2.40	48.4	*62.5*	*72.5*	0.5	**99.9**	**99.2**	**100.0**	7.0	**98.9**	**99.9**	0.3	**100.0**	**99.8**	**82.2**	**97.8**	3.8	31.6
Weibull(3;4).	-0.09	2.75	5.8	5.7	2.8	1.3	5.3	3.1	9.5	6.0	2.8	6.3	2.3	4.3	4.6	5.1	6.6	1.0	5.8
Weibull(2;3.4)	0.05	2.71	6.9	6.0	2.5	1.1	4.6	2.5	9.5	7.7	2.3	5.7	5.3	4.6	3.9	6.2	5.1	0.8	6.8
Gamma(100;1)	0.20	3.06	5.4	5.5	12.3	4.7	10.6	10.2	8.8	6.3	10.1	10.5	7.1	8.1	10.5	5.3	9.9	7.4	5.6
Gamma(15;1)	0.52	3.40	7.8	10.0	49.9	12.1	44.3	41.4	37.2	14.8	40.7	44.4	25.1	26.8	43.8	6.7	39.3	21.6	9.5
Beta(2;5)	0.60	2.88	13.0	22.0	**79.1**	8.1	**89.9**	**81.8**	**92.8**	8.3	**79.8**	**91.7**	**97.0**	**92.8**	**88.3**	19.3	**80.1**	11.8	10.0
Weibull(1;2)	0.63	3.25	8.5	14.7	*73.6*	11.4	**79.1**	*71.1*	**80.6**	14.3	*69.3*	**81.1**	**85.7**	**77.2**	**77.5**	9.2	*67.0*	20.8	8.9
Gamma(9;1)	0.67	3.67	9.9	14.2	*70.4*	18.0	*65.9*	*62.0*	*59.7*	23.0	*61.1*	*66.4*	42.5	43.3	*65.2*	7.8	*59.6*	32.4	13.3
χ2(10)	0.89	4.20	14.4	24.4	**90.6**	28.8	**90.3**	**87.3**	**88.0**	40.0	**86.6**	**90.8**	**76.6**	*74.4*	**89.7**	10.2	**84.8**	*50.7*	21.8
Gamma(5;1)	0.89	4.20	14.4	24.4	**90.6**	28.8	**90.4**	**87.4**	**88.1**	40.1	**86.8**	**90.9**	**76.4**	*74.2*	**89.8**	10.1	**85.0**	*51.0*	22.1
Gumbel(1;2)	1.14	5.40	29.6	38.8	**95.5**	45.6	**94.3**	**93.1**	**91.5**	*62.3*	**92.8**	**94.4**	*68.9*	**75.1**	**94.1**	22.9	**91.8**	*66.0*	42.2
χ2(4)	1.14	6.00	31.7	*64.6*	**99.9**	*56.4*	**100.0**	**99.9**	**100.0**	**82.7**	**99.9**	**100.0**	**100.0**	**100.0**	**100.0**	18.8	**99.8**	**79.2**	*54.2*
Gamma(3;2)	1.15	5.00	21.8	42.2	**98.5**	42.5	**99.1**	**98.4**	**99.0**	*63.1*	**98.2**	**99.3**	**98.7**	**97.7**	**99.0**	13.7	**97.4**	*69.0*	36.4
Gamma(2;2)	1.41	6.00	31.5	*64.4*	**99.9**	*56.1*	**100.0**	**99.9**	**100.0**	**82.7**	**99.9**	**100.0**	**100.0**	**100.0**	**100.0**	18.6	**99.8**	**79.3**	*54.0*
χ2(2)	2.00	9.00	*57.7*	**96.8**	**100.0**	**80.2**	**100.0**	**100.0**	**100.0**	**99.1**	**100.0**	**100.0**	**100.0**	**100.0**	**100.0**	35.6	**100.0**	*71.8*	**87.2**
Weibull(0.5;1)	2.00	9.00	*57.5*	**96.7**	**100.0**	**80.3**	**100.0**	**100.0**	**100.0**	**99.0**	**100.0**	**100.0**	**100.0**	**100.0**	**100.0**	35.6	**100.0**	*71.8*	**87.2**
χ2(1)	2.83	15.00	**86.6**	**100.0**	**100.0**	**95.5**	**100.0**	**100.0**	**100.0**	**100.0**	**100.0**	**100.0**	**100.0**	**100.0**	**100.0**	*69.3*	**100.0**	14.8	**99.5**
LN(0;1)	6.18	113.90	**95.6**	**99.9**	**100.0**	**98.2**	**100.0**	**100.0**	**100.0**	**100.0**	**100.0**	**100.0**	**100.0**	**100.0**	**100.0**	**88.9**	**100.0**	14.6	**99.6**

Table A.8. Empirical power results for normal modified distributions (α = 0.05, n = 25).

Distribution	$\sqrt{\beta_1}$	β_2	K-S	*AD**	Z_c	Z_a	P_s	K^2	*JB*	*DH*	*RJB*	T_{Lmom}	$T_{TLmom}^{(1)}$	$T_{TLmom}^{(2)}$	$T_{TLmom}^{(3)}$	$BM_{3\text{-}4}$	$BM_{3\text{-}6}$	$T_{MC\text{-}LR}$
Trunc(-3;1)	-0.55	2.78	10.7	14.8	18.4	20.4	14.6	10.1	9.3	11.3	7.1	14.1	6.1	5.9	6.0	6.1	6.0	8.3
Trunc(-2;1)	-0.32	2.27	8.3	11.0	12.0	11.3	10.8	5.3	1.9	6.0	1.5	9.8	5.3	5.1	5.1	0.8	0.8	7.9
Trunc(-3;2)	-0.18	2.65	4.7	4.6	4.0	3.8	4.6	3.1	2.4	2.6	2.3	3.8	4.4	4.4	4.5	2.1	2.1	5.3
Trunc(-1;1)	0	1.94	7.5	12.2	16.1	9.9	12.1	12.1	0.1	5.7	0.1	13.9	5.6	4.0	3.9	0.0	0.0	8.7
Trunc(-2;2)	0	2.36	4.3	4.2	3.2	2.5	4.1	2.0	0.5	1.5	0.6	3.0	4.1	4.3	4.4	0.3	0.3	5.3
Trunc(-3;3)	0	2.84	4.8	4.5	3.7	3.8	4.5	3.2	3.0	3.4	3.2	4.1	4.6	4.7	4.6	2.8	2.8	5.0
LoConN(0.5;5)	0	1.51	**78.7**	**92.0**	**84.1**	*71.6*	**92.0**	*73.8*	0.8	*72.0*	0.8	**84.2**	**84.4**	*70.1*	*53.7*	0.0	0.0	*52.3*
LoConN(0.5;3)	0	2.04	15.3	19.4	15.5	10.7	19.4	13.4	0.5	8.1	0.4	17.1	14.4	9.8	7.4	0.2	0.2	13.0
LoConN(0.5;1)	0	2.92	4.9	4.8	4.6	4.6	4.8	4.4	4.3	4.4	4.3	4.6	4.6	4.6	4.7	4.3	4.3	5.0
LoConN(0.4;1)	0.04	2.93	4.9	4.8	4.6	4.7	4.8	4.5	4.4	4.4	4.4	4.6	4.6	4.7	4.6	4.4	4.4	5.1
LoConN(0.3;1)	0.06	2.96	5.0	4.9	4.7	4.8	4.9	4.7	4.6	4.6	4.6	4.8	4.7	4.7	4.8	4.5	4.5	5.0
LoConN(0.4;3)	0.23	2.14	18.0	22.4	17.2	13.6	22.2	11.1	1.6	10.6	1.4	17.6	15.7	12.2	10.8	0.6	0.5	13.8
LoConN(0.4;5)	0.32	1.65	**81.3**	**93.1**	**85.3**	**75.2**	**93.1**	*60.2*	4.1	**75.4**	3.9	**82.4**	**84.8**	*72.7*	*59.9*	0.2	0.2	*57.0*
LoConN(0.3;3)	0.46	2.47	23.8	29.0	21.9	20.6	28.8	9.4	6.7	16.6	6.5	20.6	19.2	18.3	17.6	2.4	2.4	13.9
LoConN(0.3;5)	0.67	2.13	**86.6**	**95.2**	**88.7**	**83.5**	**95.2**	38.6	21.1	**82.7**	20.9	**82.0**	**84.8**	**78.7**	*72.1*	2.2	2.4	*56.8*
ScConN(0.05;0.25)	0	3.14	5.6	5.8	5.4	5.5	5.8	5.8	6.2	6.3	6.8	6.1	6.0	6.0	5.8	6.1	6.2	4.7
ScConN(0.10;0.25)	0	3.29	7.1	7.3	6.4	6.5	7.4	7.2	7.9	8.0	9.4	8.2	8.4	8.1	7.5	7.5	7.7	4.4
ScConN(0.20;0.25)	0	3.64	12.7	13.6	9.5	10.0	13.9	11.2	12.6	13.3	16.9	15.5	16.4	14.3	12.1	11.4	11.7	4.6
ScConN(0.05;2)	0	3.97	7.0	8.7	10.9	10.7	8.8	12.0	12.5	11.9	12.2	9.7	5.2	5.0	4.9	12.6	12.7	5.0
ScConN(0.10;2)	0	4.43	8.6	11.4	15.0	14.6	11.5	16.8	17.7	16.8	17.6	13.3	5.8	5.3	5.1	17.8	18.0	5.0
ScConN(0.20;2)	0	4.68	10.6	14.8	18.6	18.5	15.0	21.4	22.9	22.2	23.5	18.1	7.0	5.8	5.4	22.4	22.8	4.9
ScConN(0.20;4)	0	9.75	*52.3*	*65.1*	*64.1*	*66.5*	*65.5*	*66.6*	*70.1*	*71.5*	*74.5*	*69.6*	26.3	13.2	9.9	*64.0*	*65.7*	6.9
ScConN(0.10;4)	0	12.75	37.1	47.5	*52.7*	*52.8*	47.8	*55.3*	*57.0*	*56.4*	*57.6*	*50.9*	12.7	7.4	6.5	*55.3*	*56.0*	5.7
ScConN(0.05;4)	0	13.55	23.6	30.5	35.5	35.1	30.6	37.4	38.2	37.2	38.0	32.4	7.4	5.6	5.4	38.2	38.4	5.3
MixN(0.5;1;0.25)	-1.02	3.87	*72.6*	**79.1**	*66.9*	*69.4*	**79.0**	39.8	45.9	*62.5*	45.1	*71.2*	*63.9*	*60.8*	*58.3*	20.9	21.5	38.8
MixN(0.4;1;0.25)	-0.78	3.34	*53.3*	*60.4*	48.8	*50.9*	*60.2*	24.6	27.5	43.1	25.3	*51.4*	45.0	42.7	40.8	12.8	13.0	31.3
MixN(0.3;1;0.25)	-0.57	3.03	32.2	37.5	30.4	31.8	37.3	14.7	14.8	24.7	12.4	31.0	25.3	23.4	22.0	7.9	8.0	21.0
MixN(0.5;3;0.25)	-0.46	1.78	**94.9**	**96.8**	**96.4**	**94.2**	**96.6**	*56.2*	8.6	**78.3**	6.4	**93.9**	**88.7**	**80.7**	*72.6*	0.7	0.7	*69.8*
MixN(0.4;3;0.25)	-0.16	1.67	**79.4**	**86.9**	**85.6**	**77.9**	**86.3**	*55.9*	1.2	*52.9*	0.8	**76.3**	*69.6*	*54.4*	43.5	0.1	0.1	*57.1*
MixN(0.3;3;0.25)	0.12	1.81	*52.6*	*68.3*	*65.0*	*51.5*	*67.2*	35.7	0.8	31.0	0.9	46.4	45.7	34.6	29.3	0.1	0.1	48.7
MixN(0.5;1;4)	0.44	5.21	47.6	*55.5*	38.3	42.7	*56.1*	38.1	42.5	46.7	*55.3*	*57.9*	46.7	33.6	25.8	32.9	34.3	10.2
MixN(0.4;1;4)	0.56	6.17	*56.6*	*67.1*	*52.0*	*57.1*	*67.7*	*51.8*	*56.6*	*60.8*	*69.0*	*70.5*	48.4	31.7	23.6	44.7	46.7	10.6
MixN(0.3;1;4)	0.7	7.58	*60.2*	*71.8*	*62.8*	*67.1*	*72.3*	*63.4*	*67.9*	*71.0*	**76.9**	**75.9**	42.1	24.8	18.1	*56.6*	*58.8*	9.6
MixN(0.5;3;4)	0.96	4.37	*65.1*	*72.2*	*56.7*	*60.0*	*72.3*	41.5	46.8	*55.1*	*50.8*	*65.6*	*59.1*	*54.2*	*50.6*	25.9	26.7	27.7
MixN(0.4;3;4)	1.21	5.29	**75.9**	**83.3**	*71.1*	*74.5*	**83.4**	*59.3*	*64.9*	*70.1*	*69.9*	**80.0**	*66.4*	*57.7*	*52.1*	38.7	40.2	27.7
MixN(0.3;3;4)	1.52	6.76	**79.1**	**86.9**	**80.5**	**83.1**	**87.0**	*74.5*	**78.9**	**80.7**	**83.2**	**87.0**	*63.2*	49.7	42.6	*54.7*	*56.6*	23.3
Nout1	0	3.00	10.0	13.9	26.1	24.6	14.2	34.4	37.3	31.5	34.9	20.5	6.2	5.4	5.2	41.0	40.9	5.2
Nout2	0	3.00	29.6	*57.1*	**91.1**	**86.2**	*57.5*	**95.8**	**96.6**	**92.9**	**94.2**	*64.7*	6.4	5.5	5.3	**98.2**	**98.1**	5.4
Nout3	0	3.00	43.2	*64.5*	*74.3*	**75.9**	*64.6*	**85.9**	**87.4**	*72.0*	**85.9**	**75.7**	17.2	8.7	7.5	**79.1**	**79.0**	6.8
Nout4	0	3.00	8.6	15.3	7.3	15.2	16.5	9.9	19.7	50.0	30.8	26.1	7.4	5.6	5.1	22.7	28.5	4.6
Nout5	0	3.00	32.3	*50.8*	10.9	31.3	*52.3*	10.2	24.2	*74.6*	*63.6*	*73.5*	29.7	8.2	5.9	12.4	18.2	4.7

Table A.8. (continued) Empirical power results for normal modified distributions (α = 0.05, n = 25).

Distribution	$\sqrt{\beta_1}$	β_2	T_w	$T_{MC\text{-}LR}$-T_w	$T_{S,I}$	$T_{K,I}$	W	W_{SF}	W_{RG}	D	r	CS	Q	Q-Q*	$BCMR$	β_3^2	T_{EP}	I_n	$R_{s,J}$
Trunc(-3;1)	-0.55	2.78	7.2	7.9	12.8	4.0	18.4	13.8	22.1	6.8	13.1	19.2	5.6	19.0	17.1	6.4	16.1	6.0	7.4
Trunc(-2;1)	-0.32	2.27	9.7	9.0	3.6	1.0	12.2	6.3	21.2	7.1	5.7	13.5	1.8	13.6	10.5	10.0	11.0	1.5	9.3
Trunc(-3;2)	-0.18	2.65	4.7	4.8	3.0	3.7	4.2	3.1	6.1	4.8	3.0	4.5	3.6	3.7	3.8	3.7	4.5	2.4	4.9
Trunc(-1;1)	0	1.94	19.3	15.5	0.7	2.5	14.1	4.8	30.8	13.6	3.9	16.6	11.3	11.8	11.1	25.0	9.6	0.2	18.7
Trunc(-2;2)	0	2.36	5.7	5.3	1.1	3.0	3.5	1.7	7.2	6.0	1.5	4.0	3.3	3.1	2.9	4.5	3.7	0.8	5.8
Trunc(-3;3)	0	2.84	4.5	4.4	3.5	4.1	4.0	3.5	4.8	4.2	3.5	4.1	3.9	3.6	3.8	4.1	4.3	3.5	4.4
LoConN(0.5;5)	0	1.51	**88.4**	**89.7**	5.1	8.3	**87.4**	*71.3*	**94.0**	1.5	*67.4*	**89.7**	27.4	35.9	**84.7**	*73.4*	**84.6**	2.1	*64.0*
LoConN(0.5;3)	0	2.04	30.0	25.3	1.6	2.8	16.4	7.4	28.5	8.6	6.4	18.9	8.8	9.6	13.9	19.6	14.6	0.6	26.5
LoConN(0.5;1)	0	2.92	4.8	4.8	4.4	4.6	4.6	4.4	5.0	4.9	4.4	4.7	4.7	4.5	4.5	4.6	4.7	4.3	4.8
LoConN(0.4;1)	0.04	2.93	4.9	4.8	4.5	4.8	4.7	4.5	5.0	4.9	4.5	4.7	4.7	4.5	4.7	4.8	4.8	4.4	4.9
LoConN(0.3;1)	0.06	2.96	4.9	4.8	4.9	5.2	4.8	4.7	5.0	4.9	4.7	4.8	4.8	4.7	4.7	4.8	4.9	4.6	4.9
LoConN(0.4;3)	0.23	2.14	23.8	21.3	5.1	10.7	19.1	10.4	29.4	7.1	9.3	21.2	14.9	10.9	16.7	15.8	19.2	1.9	19.8
LoConN(0.4;5)	0.32	1.65	*73.8*	**80.2**	19.3	33.2	**89.1**	**75.8**	**94.3**	5.0	*72.5*	**90.9**	45.5	39.6	**86.7**	*59.5*	**87.8**	7.2	46.7
LoConN(0.3;3)	0.46	2.47	11.8	13.7	15.1	24.2	25.7	18.6	31.2	6.3	17.6	26.8	18.8	13.3	23.8	8.5	29.6	7.3	9.9
LoConN(0.3;5)	0.67	2.13	39.6	*58.4*	*51.8*	*68.1*	**92.5**	**85.0**	**94.9**	21.5	**83.1**	**93.4**	*55.2*	45.7	**91.3**	29.7	**93.7**	25.8	27.2
ScConN(0.05;0.25)	0	3.14	5.6	5.0	6.0	6.2	5.6	6.1	4.6	5.6	6.2	5.4	5.3	5.3	5.7	6.2	5.7	6.8	5.5
ScConN(0.10;0.25)	0	3.29	7.4	6.1	7.3	7.8	6.7	7.9	4.5	6.8	8.1	6.3	5.8	6.0	7.0	8.0	6.9	9.2	7.3
ScConN(0.20;0.25)	0	3.64	14.5	10.9	10.9	12.1	11.1	14.0	5.8	11.8	14.3	10.2	7.7	8.5	12.0	14.6	11.5	16.5	14.5
ScConN(0.05;2)	0	3.97	8.7	7.7	11.4	9.6	10.2	11.4	7.3	10.0	11.5	10.0	8.9	10.9	10.6	9.8	9.1	10.9	8.7
ScConN(0.10;2)	0	4.43	11.5	9.9	15.7	12.5	14.0	16.1	8.9	13.7	16.3	13.5	11.6	14.8	14.7	13.5	12.0	15.4	11.8
ScConN(0.20;2)	0	4.68	15.1	12.3	19.9	15.0	17.6	21.1	10.2	17.8	21.5	17.0	14.4	18.3	18.8	18.2	15.7	20.8	15.5
ScConN(0.20;4)	0	9.75	*64.3*	*58.8*	*60.9*	49.2	*66.5*	*72.0*	47.4	*69.5*	*72.5*	*65.0*	42.7	*60.6*	*68.4*	*66.4*	*65.5*	43.7	*66.4*
ScConN(0.10;4)	0	12.75	47.4	43.5	*51.5*	43.4	*51.9*	*55.6*	39.5	*52.8*	*55.9*	*51.1*	35.0	*51.7*	*53.2*	49.8	48.9	33.3	48.5
ScConN(0.05;4)	0	13.55	30.5	28.0	35.4	30.9	34.3	36.6	26.9	34.3	36.8	33.9	23.4	35.4	35.2	32.4	31.4	22.9	31.0
MixN(0.5;1;0.25)	-1.02	3.87	16.2	35.1	*58.3*	13.4	*74.2*	*72.2*	*68.7*	40.3	*71.5*	*74.2*	20.7	42.9	*74.1*	14.2	**76.3**	37.7	32.3
MixN(0.4;1;0.25)	-0.78	3.34	13.1	26.8	38.1	7.4	*55.4*	*51.3*	*52.5*	20.9	*50.3*	*55.9*	12.1	31.9	*54.8*	9.6	*56.6*	26.1	18.3
MixN(0.3;1;0.25)	-0.57	3.03	11.7	18.8	21.2	4.3	34.5	29.9	34.7	10.0	28.9	35.3	7.3	21.5	33.5	7.6	34.5	14.4	12.0
MixN(0.5;3;0.25)	-0.46	1.78	**81.8**	**91.6**	13.3	1.0	**96.8**	**91.1**	**98.6**	14.5	**89.5**	**97.5**	4.0	**87.2**	**96.0**	*65.9*	**84.5**	7.0	*55.9*
MixN(0.4;3;0.25)	-0.16	1.67	*70.7*	**78.4**	3.0	5.5	**86.6**	*72.2*	**93.0**	2.4	*68.7*	**88.6**	8.2	*63.9*	**84.0**	*70.4*	*63.6*	2.1	*56.5*
MixN(0.3;3;0.25)	0.12	1.81	39.3	*53.3*	4.2	20.2	*67.0*	47.3	**78.7**	1.4	43.6	*69.9*	13.7	33.7	*62.8*	*50.1*	45.6	1.7	30.6
MixN(0.5;1;4)	0.44	5.21	46.8	41.0	37.3	39.1	47.2	*54.1*	27.9	48.8	*54.7*	44.6	19.5	30.0	49.4	46.8	49.1	43.4	*53.2*
MixN(0.4;1;4)	0.56	6.17	*58.6*	*52.5*	48.8	44.3	*60.8*	*67.7*	39.1	*63.4*	*68.3*	*58.3*	25.8	42.3	*63.1*	*58.8*	*62.7*	47.6	*65.0*
MixN(0.3;1;4)	0.7	7.58	*65.7*	*60.1*	*59.0*	47.6	*69.1*	**75.1**	47.8	*71.9*	**75.7**	*67.0*	31.6	*54.4*	*71.1*	*66.3*	*70.1*	47.4	*71.2*
MixN(0.5;3;4)	0.96	4.37	22.5	32.0	*56.6*	46.7	*65.5*	*66.5*	*54.9*	44.6	*66.3*	*64.6*	27.7	35.0	*66.2*	23.2	*69.0*	40.7	39.8
MixN(0.4;3;4)	1.21	5.29	36.1	43.6	*70.7*	*51.6*	**78.7**	**80.7**	*67.1*	*64.3*	**80.7**	**77.6**	32.2	47.3	**79.5**	35.7	**81.4**	45.3	*59.1*
MixN(0.3;3;4)	1.52	6.76	*53.6*	*56.2*	**79.4**	*53.5*	**85.2**	**87.4**	*74.2*	**78.5**	**87.5**	**84.2**	34.6	*60.4*	**86.1**	*50.7*	**86.8**	43.9	*73.9*
Nout1	0	3.00	14.7	10.8	29.4	5.9	21.1	28.6	8.0	19.5	29.4	20.0	6.1	26.1	23.7	21.1	15.2	30.2	14.8
Nout2	0	3.00	*59.3*	47.8	**89.5**	*59.5*	**83.8**	**91.2**	*50.8*	**82.6**	**91.6**	**82.7**	7.7	**93.1**	**86.8**	*66.4*	*62.5*	*74.5*	*61.3*
Nout3	0	3.00	46.0	35.1	**84.1**	7.5	*73.7*	**80.0**	49.7	*67.3*	**80.5**	*71.2*	12.5	*58.5*	**76.0**	44.1	*72.4*	*69.3*	*53.9*
Nout4	0	3.00	31.4	22.4	3.8	6.2	10.8	24.2	0.8	29.8	26.1	9.3	20.6	16.0	14.5	*57.9*	13.8	42.2	28.7
Nout5	0	3.00	*74.6*	*62.1*	5.7	35.5	29.7	*50.6*	3.2	*64.7*	*53.1*	24.4	23.0	15.6	35.8	**91.2**	43.4	*72.1*	*70.9*

Table A.9. Empirical power results for normal modified distributions (α = 0.05, n = 50).

Distribution	$\sqrt{\beta_1}$	β_2	K-S	*AD**	Z_c	Z_a	P_s	K^2	*JB*	*DH*	*RJB*	T_{Lmom}	$T_{TLmom}^{(1)}$	$T_{TLmom}^{(2)}$	$T_{TLmom}^{(3)}$	$BM_{3\text{-}4}$	$BM_{3\text{-}6}$	$T_{MC\text{-}LR}$
Trunc(-3;1)	-0.55	2.78	19.3	31.5	45.8	*58.1*	30.5	18.4	16.6	31.2	11.1	35.7	10.5	9.6	9.4	5.6	5.5	11.2
Trunc(-2;1)	-0.32	2.27	14.5	24.8	35.6	41.2	24.4	16.2	2.0	19.1	1.1	28.7	9.3	7.5	7.1	0.1	0.1	10.1
Trunc(-3;2)	-0.18	2.65	5.2	5.4	4.7	5.4	5.4	4.0	1.9	2.8	1.8	5.0	4.5	4.6	4.7	1.1	1.1	5.4
Trunc(-1;1)	0	1.94	14.0	31.0	*53.6*	48.5	31.3	*51.7*	0.1	20.3	0.0	42.0	12.7	6.5	4.9	0.0	0.0	10.9
Trunc(-2;2)	0	2.36	4.7	5.5	5.3	4.5	5.5	5.9	0.1	1.8	0.1	5.2	4.4	4.3	4.3	0.0	0.0	5.4
Trunc(-3;3)	0	2.84	4.7	4.4	2.9	3.4	4.4	2.4	1.8	2.4	2.0	3.9	4.7	4.7	4.7	1.2	1.3	5.0
LoConN(0.5;5)	0	1.51	**99.3**	**100.0**	**99.6**	**98.9**	**100.0**	**99.4**	43.6	**98.1**	0.2	**99.9**	**99.9**	**99.5**	**98.1**	0.0	0.0	*67.7*
LoConN(0.5;3)	0	2.04	31.7	44.4	34.4	29.8	44.8	43.4	0.3	20.3	0.1	47.4	39.0	27.8	20.4	0.1	0.1	17.9
LoConN(0.5;1)	0	2.92	4.9	4.8	4.4	4.6	4.8	4.3	3.9	4.1	3.9	4.6	4.6	4.7	4.7	3.9	3.9	5.1
LoConN(0.4;1)	0.04	2.93	5.0	4.9	4.6	4.8	4.9	4.5	4.1	4.3	4.0	4.7	4.7	4.7	4.7	4.1	4.0	5.1
LoConN(0.3;1)	0.06	2.96	5.1	5.1	4.9	5.0	5.1	4.8	4.6	4.6	4.5	5.0	4.8	4.8	4.8	4.5	4.5	5.1
LoConN(0.4;3)	0.23	2.14	37.0	49.2	37.0	33.8	49.4	33.9	1.9	26.4	0.9	46.2	40.6	31.6	26.2	0.2	0.2	22.7
LoConN(0.4;5)	0.32	1.65	**99.4**	**100.0**	**99.6**	**99.2**	**100.0**	**96.5**	*51.0*	**98.6**	3.3	**99.8**	**99.9**	**99.4**	**98.1**	0.0	0.0	**83.9**
LoConN(0.3;3)	0.46	2.47	47.7	*59.3*	43.9	43.8	*59.1*	19.1	11.4	40.1	8.6	48.3	45.2	42.6	41.3	1.0	1.0	25.4
LoConN(0.3;5)	0.67	2.13	**99.7**	**100.0**	**99.8**	**99.6**	**100.0**	**87.2**	*74.4*	**99.4**	31.8	**99.7**	**99.9**	**99.6**	**99.1**	0.3	0.3	**91.7**
ScConN(0.05;0.25)	0	3.14	6.1	6.2	5.6	5.3	6.2	5.9	6.7	6.5	7.7	6.6	6.8	6.8	6.6	6.4	6.4	4.6
ScConN(0.10;0.25)	0	3.29	8.9	9.1	6.7	6.3	9.2	7.4	9.0	8.8	11.7	10.1	11.2	10.8	10.2	8.0	8.1	4.6
ScConN(0.20;0.25)	0	3.64	20.0	21.6	11.5	11.0	22.0	13.0	16.2	16.5	24.4	23.9	27.6	24.8	21.2	13.0	13.3	5.9
ScConN(0.05;2)	0	3.97	7.6	10.3	16.3	14.6	10.3	17.3	18.7	17.9	18.3	11.7	5.4	5.1	5.0	19.3	19.3	5.0
ScConN(0.10;2)	0	4.43	10.1	15.0	23.5	21.2	15.1	25.2	27.9	26.9	27.6	17.6	6.4	5.6	5.4	27.9	28.1	5.0
ScConN(0.20;2)	0	4.68	13.7	21.4	29.1	26.7	21.6	32.1	36.4	35.8	37.4	25.6	8.8	6.6	6.0	34.6	35.0	5.1
ScConN(0.20;4)	0	9.75	**78.0**	**89.0**	**89.2**	**89.7**	**89.2**	**89.6**	**92.9**	**93.4**	**94.5**	**90.8**	46.5	21.3	14.3	**86.6**	**87.7**	8.9
ScConN(0.10;4)	0	12.75	*56.7*	*70.2*	**78.0**	**76.6**	*70.4*	**79.4**	**81.6**	**81.2**	**81.5**	*71.9*	18.9	9.4	7.8	**80.4**	**80.7**	5.9
ScConN(0.05;4)	0	13.55	35.3	47.1	*57.5*	*55.3*	47.2	*58.7*	*60.3*	*59.5*	*59.8*	48.3	9.1	6.2	5.7	*60.7*	*60.8*	5.2
MixN(0.5;1;0.25)	-1.02	3.87	**96.4**	**98.2**	**89.5**	**91.6**	**98.2**	*69.5*	**76.8**	**84.7**	*72.2*	**94.5**	**95.7**	**95.5**	**95.2**	24.6	25.2	*74.3*
MixN(0.4;1;0.25)	-0.78	3.34	**85.3**	**90.3**	*72.7*	**75.7**	**90.3**	44.6	*51.5*	*68.3*	42.6	**81.5**	**83.3**	**83.2**	**82.5**	14.1	14.3	*60.7*
MixN(0.3;1;0.25)	-0.57	3.03	*60.5*	*68.0*	48.4	*51.4*	*67.9*	24.9	26.5	44.6	19.0	*57.6*	*56.4*	*55.8*	*54.2*	8.5	8.5	37.3
MixN(0.5;3;0.25)	-0.46	1.78	**100.0**	**100.0**	**100.0**	**100.0**	**100.0**	**94.6**	*62.8*	**97.7**	6.4	**99.9**	**99.8**	**98.9**	**96.9**	0.2	0.2	*73.4*
MixN(0.4;3;0.25)	-0.16	1.67	**99.2**	**99.8**	**99.7**	**99.6**	**99.8**	**92.3**	23.8	**85.1**	0.2	**97.4**	**96.7**	**88.7**	**77.7**	0.0	0.0	*69.6*
MixN(0.3;3;0.25)	0.12	1.81	**90.9**	**97.2**	**96.2**	**93.7**	**96.8**	**75.5**	6.7	*61.5*	0.3	**79.9**	**82.7**	*69.0*	*58.7*	0.0	0.0	**78.5**
MixN(0.5;1;4)	0.44	5.21	**77.8**	**85.9**	*59.6*	*64.6*	**86.3**	*55.7*	*64.3*	*65.8*	**81.5**	**86.1**	**81.5**	*65.9*	*52.6*	43.3	44.8	21.9
MixN(0.4;1;4)	0.56	6.17	**85.8**	**93.3**	**77.6**	**82.0**	**93.5**	*73.6*	**81.1**	**82.4**	**92.4**	**94.3**	**82.0**	*60.6*	45.8	*60.0*	*61.9*	22.4
MixN(0.3;1;4)	0.7	7.58	**87.3**	**94.6**	**88.4**	**90.7**	**94.8**	**86.5**	**91.6**	**92.3**	**96.4**	**96.0**	*72.9*	46.4	33.3	**76.4**	**78.2**	17.8
MixN(0.5;3;4)	0.96	4.37	**92.7**	**96.0**	**80.8**	**84.2**	**96.0**	*67.4*	*73.3*	**75.3**	**77.6**	**90.7**	**93.1**	**91.5**	**90.0**	31.9	32.8	*56.6*
MixN(0.4;3;4)	1.21	5.29	**97.1**	**98.9**	**92.6**	**94.5**	**98.9**	**85.8**	**89.3**	**88.6**	**93.3**	**97.6**	**95.8**	**92.2**	**89.2**	*50.0*	*51.4*	*57.4*
MixN(0.3;3;4)	1.52	6.76	**97.5**	**99.2**	**97.3**	**98.1**	**99.2**	**95.4**	**96.8**	**96.0**	**98.6**	**99.2**	**92.4**	**83.5**	**77.6**	*71.0*	*72.6*	49.3
Nout1	0	3.00	7.6	9.7	21.1	17.1	9.8	25.4	31.1	26.4	28.7	14.1	5.7	5.2	5.1	36.7	36.7	5.0
Nout2	0	3.00	19.2	40.1	**97.7**	**89.6**	40.5	**98.3**	**99.1**	**98.0**	**97.3**	46.5	5.7	5.3	5.1	**99.9**	**99.9**	5.1
Nout3	0	3.00	34.6	*62.8*	**93.1**	**88.1**	*62.3*	**97.3**	**98.1**	**94.5**	**96.9**	*72.8*	10.3	7.0	6.5	**98.4**	**98.4**	5.7
Nout4	0	3.00	7.5	13.6	10.4	15.3	14.5	12.7	29.7	*50.1*	33.8	20.3	6.7	5.4	5.1	34.0	35.0	4.8
Nout5	0	3.00	42.2	**78.6**	*67.0*	**80.9**	**80.2**	*74.8*	**94.5**	**99.0**	**96.0**	**86.7**	17.0	7.0	5.7	**92.7**	**93.6**	5.1

Table A.9. (continued) Empirical power results for normal modified distributions (α = 0.05, n = 50).

Distribution	$\sqrt{\beta_1}$	β_2	T_w	$T_{MC\text{-}LR}$-T_w	$T_{S,I}$	$T_{K,I}$	W	W_{SF}	W_{RG}	D	r	CS	Q	Q-Q*	$BCMR$	β_3^2	T_{EP}	I_n	$R_{s,J}$
Trunc(-3;1)	-0.55	2.78	9.8	11.5	27.5	7.1	45.1	33.1	*53.9*	7.8	31.1	48.0	4.9	*57.8*	42.1	12.2	34.7	6.3	9.0
Trunc(-2;1)	-0.32	2.27	18.6	16.0	6.1	0.3	33.6	17.3	*55.3*	14.8	15.1	38.3	1.2	46.1	29.0	28.7	26.5	0.5	16.9
Trunc(-3;2)	-0.18	2.65	5.6	5.3	3.2	3.3	5.2	3.2	9.3	6.3	3.0	5.9	2.5	4.6	4.6	4.9	5.6	1.3	5.7
Trunc(-1;1)	0	1.94	42.9	34.3	1.1	1.8	44.7	19.2	**75.7**	*50.7*	15.7	*52.1*	33.7	39.0	37.8	*69.8*	29.3	0.0	41.4
Trunc(-2;2)	0	2.36	9.1	7.4	0.7	2.0	5.1	1.7	14.5	12.6	1.4	6.7	4.8	4.4	4.0	10.0	5.1	0.1	9.1
Trunc(-3;3)	0	2.84	4.2	4.4	2.8	2.9	3.5	2.7	5.2	3.8	2.6	3.8	3.2	2.9	3.2	3.5	4.3	2.3	4.3
LoConN(0.5;5)	0	1.51	**99.5**	**99.8**	16.6	7.4	**99.9**	**99.3**	**100.0**	0.8	**99.0**	**99.9**	46.3	*61.2*	**99.8**	**98.4**	**99.9**	0.3	**90.1**
LoConN(0.5;3)	0	2.04	*62.4*	*54.3*	2.0	1.7	37.7	20.7	*54.8*	26.6	17.9	43.2	14.5	16.6	33.7	46.8	38.3	0.1	*57.2*
LoConN(0.5;1)	0	2.92	4.9	4.8	4.2	4.2	4.6	4.1	5.4	4.8	4.1	4.7	4.6	4.5	4.4	4.5	4.7	3.8	4.9
LoConN(0.4;1)	0.04	2.93	5.0	5.0	4.4	4.4	4.8	4.4	5.3	4.9	4.3	4.9	4.9	4.6	4.6	4.6	4.9	4.0	4.9
LoConN(0.3;1)	0.06	2.96	5.0	4.8	4.8	4.7	5.0	4.8	5.3	5.0	4.7	5.1	5.0	4.8	4.9	4.8	5.1	4.5	4.9
LoConN(0.4;3)	0.23	2.14	47.5	43.7	11.1	12.1	42.1	26.3	*56.5*	17.0	23.6	46.8	24.5	18.7	38.5	36.8	45.8	0.7	38.0
LoConN(0.4;5)	0.32	1.65	**92.4**	**98.2**	*59.2*	46.1	**99.9**	**99.5**	**100.0**	3.9	**99.3**	**99.9**	*68.3*	*64.3*	**99.8**	**90.2**	**99.9**	3.8	*61.7*
LoConN(0.3;3)	0.46	2.47	17.8	24.7	35.3	33.6	*52.9*	41.2	*60.0*	6.9	38.9	*55.5*	30.2	21.9	*50.2*	15.7	*61.3*	6.6	11.9
LoConN(0.3;5)	0.67	2.13	*52.2*	**88.7**	**93.2**	**89.5**	**100.0**	**99.8**	**100.0**	30.3	**99.8**	**100.0**	**76.6**	*68.5*	**99.9**	*51.6*	**100.0**	31.3	27.8
ScConN(0.05;0.25)	0	3.14	6.4	5.5	6.0	6.6	5.8	6.5	4.3	5.8	6.6	5.4	5.2	5.2	6.0	6.5	5.9	7.9	6.3
ScConN(0.10;0.25)	0	3.29	10.5	8.2	7.5	8.6	7.7	9.3	4.3	8.2	9.5	6.9	5.5	5.7	8.1	9.6	7.8	12.0	10.4
ScConN(0.20;0.25)	0	3.64	26.4	20.1	12.0	14.7	16.0	19.7	6.6	18.8	20.2	13.8	7.7	8.3	17.0	20.7	16.3	25.2	26.6
ScConN(0.05;2)	0	3.97	11.7	10.1	15.8	15.9	14.8	17.1	8.3	14.6	17.3	14.1	12.2	16.1	15.6	14.2	10.7	16.9	11.6
ScConN(0.10;2)	0	4.43	17.1	14.4	22.3	22.2	21.7	25.5	10.6	21.9	25.9	20.3	16.6	22.6	23.0	21.7	15.8	25.8	17.4
ScConN(0.20;2)	0	4.68	24.9	20.3	27.3	26.3	28.0	33.8	12.3	30.3	34.4	25.9	20.0	26.7	30.0	31.3	22.5	36.2	24.9
ScConN(0.20;4)	0	9.75	**90.6**	**88.1**	**80.3**	**75.7**	**91.1**	**93.5**	*74.6*	**93.3**	**93.7**	**89.7**	*59.3*	**79.5**	**91.9**	**92.3**	**89.8**	*51.9*	**91.0**
ScConN(0.10;4)	0	12.75	*72.9*	*69.6*	*73.0*	*73.2*	**77.1**	**80.2**	*61.3*	**78.4**	**80.4**	**75.9**	*53.7*	**75.5**	**78.2**	**76.8**	*71.5*	44.5	*73.5*
ScConN(0.05;4)	0	13.55	49.9	46.5	*54.4*	*55.4*	*55.6*	*58.6*	43.1	*55.8*	*58.8*	*54.6*	38.1	*57.0*	*56.7*	*54.0*	48.2	34.3	*50.1*
MixN(0.5;1;0.25)	-1.02	3.87	18.0	*68.1*	**86.9**	23.5	**96.0**	**95.8**	**91.3**	*65.3*	**95.7**	**95.8**	24.4	45.8	**96.1**	16.1	**96.9**	*59.3*	47.5
MixN(0.4;1;0.25)	-0.78	3.34	15.7	*53.9*	*66.2*	12.6	**84.1**	**82.6**	**77.0**	33.6	**81.9**	**84.1**	13.6	33.9	**84.2**	9.9	**86.2**	42.5	21.9
MixN(0.3;1;0.25)	-0.57	3.03	17.0	34.5	39.3	7.3	*59.7*	*55.7*	*54.3*	12.6	*54.5*	*60.4*	7.9	23.8	*59.4*	8.6	*62.0*	20.2	13.7
MixN(0.5;3;0.25)	-0.46	1.78	**98.7**	**99.8**	23.8	0.3	**100.0**	**100.0**	**100.0**	18.2	**100.0**	**100.0**	3.4	**99.3**	**100.0**	**93.1**	**99.6**	7.3	*74.9*
MixN(0.4;3;0.25)	-0.16	1.67	**94.2**	**98.5**	5.7	5.0	**99.8**	**99.2**	**99.9**	1.3	**98.9**	**99.9**	10.2	**93.0**	**99.8**	**97.2**	**95.8**	0.7	**86.2**
MixN(0.3;3;0.25)	0.12	1.81	*62.9*	**82.0**	14.7	32.2	**97.4**	**92.3**	**98.8**	1.1	**90.7**	**98.0**	19.0	*64.9*	**96.6**	**83.9**	**85.4**	0.3	46.8
MixN(0.5;1;4)	0.44	5.21	**78.0**	*74.5*	49.2	49.3	**77.1**	**81.7**	*50.3*	**80.0**	**82.2**	*73.5*	19.9	33.1	**78.5**	*72.3*	**79.4**	*64.8*	**85.0**
MixN(0.4;1;4)	0.56	6.17	**88.9**	**86.6**	*63.7*	*56.8*	**89.4**	**92.2**	*67.4*	**91.7**	**92.5**	**87.0**	28.3	49.3	**90.3**	**85.7**	**90.9**	*61.9*	**93.3**
MixN(0.3;1;4)	0.7	7.58	**93.3**	**91.4**	**76.0**	*65.5*	**93.8**	**95.8**	**77.7**	**95.7**	**95.9**	**92.4**	38.4	*67.1*	**94.5**	**92.1**	**94.5**	*55.7*	**95.3**
MixN(0.5;3;4)	0.96	4.37	31.0	*59.5*	**79.4**	49.5	**91.6**	**92.3**	**81.3**	*72.4*	**92.3**	**90.8**	24.9	35.7	**92.0**	32.6	**93.7**	*62.0*	*63.6*
MixN(0.4;3;4)	1.21	5.29	*56.0*	**75.4**	**89.1**	*54.9*	**97.6**	**98.1**	**91.7**	**91.1**	**98.1**	**97.2**	30.5	*51.4*	**97.8**	*53.0*	**98.4**	*57.7*	**86.5**
MixN(0.3;3;4)	1.52	6.76	**81.1**	**88.4**	**93.8**	*64.3*	**99.0**	**99.3**	**95.5**	**97.8**	**99.3**	**98.7**	37.0	*69.5*	**99.1**	*73.8*	**99.2**	46.7	**96.2**
Nout1	0	3.00	11.2	8.8	21.3	5.5	16.0	23.1	4.5	14.8	23.9	14.1	5.7	20.3	18.3	18.1	10.4	27.0	11.3
Nout2	0	3.00	*54.6*	43.1	**89.6**	**91.0**	**91.1**	**96.6**	42.9	**86.9**	**96.9**	**89.3**	6.8	**98.9**	**93.6**	*69.1*	42.7	**87.4**	*55.2*
Nout3	0	3.00	*59.2*	47.9	**92.2**	*68.7*	**88.8**	**94.0**	*53.5*	**85.6**	**94.4**	**86.0**	10.1	**91.3**	**90.9**	*68.5*	*69.8*	**88.2**	*62.3*
Nout4	0	3.00	28.0	20.3	3.5	4.8	12.9	28.4	0.5	35.1	30.5	9.9	20.7	13.3	17.3	*57.8*	14.2	*51.5*	27.0
Nout5	0	3.00	**91.9**	**85.7**	31.1	21.6	**78.2**	**92.5**	13.3	**97.1**	**93.5**	*70.5*	**77.8**	*65.8*	**84.0**	**99.5**	**83.4**	**95.7**	**91.0**

Table A.10. Empirical power results for normal modified distributions (α = 0.05, n = 100).

Distribution	$\sqrt{\beta_1}$	β_2	K-S	*AD**	Z_c	Z_a	P_s	K^2	*JB*	*DH*	*RJB*	T_{Lmom}	$T_{TLmom}^{(1)}$	$T_{TLmom}^{(2)}$	$T_{TLmom}^{(3)}$	$BM_{3\text{-}4}$	$BM_{3\text{-}6}$	$T_{MC\text{-}LR}$
Trunc(-3;1)	-0.55	2.78	38.2	*67.3*	**91.0**	**97.6**	*65.1*	47.4	47.6	*74.9*	28.1	*74.7*	21.2	18.5	17.7	3.9	3.8	18.9
Trunc(-2;1)	-0.32	2.27	30.3	*58.5*	**86.7**	**93.3**	*57.6*	*55.1*	19.7	*62.0*	2.4	*67.2*	19.7	14.1	12.6	0.0	0.0	15.6
Trunc(-3;2)	-0.18	2.65	6.3	7.6	9.2	13.0	7.5	7.1	2.2	5.4	1.8	8.3	5.0	5.0	5.0	0.2	0.2	5.6
Trunc(-1;1)	0	1.94	31.1	*72.0*	**97.3**	**97.7**	*72.5*	**94.9**	32.4	*71.9*	0.0	**82.6**	29.8	12.8	7.7	0.0	0.0	15.8
Trunc(-2;2)	0	2.36	6.0	9.1	16.8	16.9	9.2	19.7	0.3	5.0	0.0	11.4	5.2	4.4	4.3	0.0	0.0	5.4
Trunc(-3;3)	0	2.84	4.7	4.5	2.6	3.5	4.5	2.3	1.1	1.9	1.3	3.9	4.6	4.7	4.7	0.2	0.2	4.9
LoConN(0.5;5)	0	1.51	**100.0**	**100.0**	**100.0**	**100.0**	**100.0**	**97.3**	**100.0**	**100.0**	**84.5**	**100.0**	**100.0**	**100.0**	**100.0**	0.0	0.0	**82.3**
LoConN(0.5;3)	0	2.04	*64.2*	**81.9**	*69.4*	*66.5*	**82.4**	**82.5**	22.7	*56.6*	0.1	**86.6**	**78.0**	*64.0*	*51.5*	0.0	0.0	28.3
LoConN(0.5;1)	0	2.92	4.8	4.8	4.4	4.9	4.9	4.4	3.6	3.9	3.5	4.7	4.7	4.6	4.7	3.6	3.6	5.0
LoConN(0.4;1)	0.04	2.93	5.0	4.9	4.5	4.9	4.9	4.5	3.8	4.1	3.7	4.7	4.8	4.8	4.8	3.8	3.8	5.1
LoConN(0.3;1)	0.06	2.96	5.3	5.3	5.0	5.4	5.2	4.9	4.6	4.8	4.6	5.2	5.0	5.0	5.0	4.3	4.3	5.1
LoConN(0.4;3)	0.23	2.14	*70.7*	**85.5**	*72.1*	*70.3*	**85.8**	*74.2*	27.7	*65.0*	1.4	**85.4**	**79.2**	*67.8*	*58.7*	0.0	0.0	44.8
LoConN(0.4;5)	0.32	1.65	**100.0**	**100.0**	**100.0**	**100.0**	**100.0**	**99.4**	**100.0**	**100.0**	*61.1*	**100.0**	**100.0**	**100.0**	**100.0**	0.0	0.0	**97.1**
LoConN(0.3;3)	0.46	2.47	**81.5**	**91.5**	**78.6**	**78.5**	**91.4**	*58.3*	47.9	**79.0**	20.7	**86.0**	**82.3**	**79.2**	**77.7**	0.4	0.4	*52.8*
LoConN(0.3;5)	0.67	2.13	**100.0**	**100.0**	**100.0**	**100.0**	**100.0**	**100.0**	**100.0**	**100.0**	**85.4**	**100.0**	**100.0**	**100.0**	**100.0**	0.0	0.0	**99.9**
ScConN(0.05;0.25)	0	3.14	6.8	7.0	5.7	5.1	7.0	6.1	7.4	7.0	9.1	7.5	8.1	8.2	8.0	6.7	6.7	4.6
ScConN(0.10;0.25)	0	3.29	12.4	12.8	7.3	6.2	13.0	8.4	11.0	10.2	15.6	14.0	16.9	16.4	15.3	8.8	8.7	5.3
ScConN(0.20;0.25)	0	3.64	35.4	39.2	15.2	13.9	39.7	17.0	22.9	22.4	38.1	41.0	49.2	45.4	39.5	15.1	14.8	10.2
ScConN(0.05;2)	0	3.97	8.3	12.5	24.9	20.6	12.6	25.6	28.4	27.3	27.6	14.3	5.6	5.2	5.1	29.5	29.4	5.0
ScConN(0.10;2)	0	4.43	12.2	20.4	36.1	30.4	20.5	37.9	42.7	41.6	42.2	23.6	7.2	5.9	5.6	42.4	42.0	5.1
ScConN(0.20;2)	0	4.68	19.6	33.0	44.8	39.3	33.2	48.6	*55.7*	*55.0*	*56.8*	38.3	11.5	7.6	6.6	*50.9*	*50.2*	5.4
ScConN(0.20;4)	0	9.75	**96.1**	**99.1**	**99.2**	**99.2**	**99.1**	**99.3**	**99.6**	**99.7**	**99.7**	**99.2**	*73.2*	34.1	19.6	**98.0**	**97.8**	12.9
ScConN(0.10;4)	0	12.75	**79.5**	**90.2**	**95.0**	**94.0**	**90.3**	**95.4**	**96.4**	**96.3**	**96.3**	**90.1**	29.5	11.6	8.7	**95.9**	**95.7**	6.4
ScConN(0.05;4)	0	13.55	*51.7*	*67.3*	**80.5**	**77.7**	*67.4*	**81.0**	**82.6**	**82.1**	**82.0**	*66.3*	11.1	6.6	6.0	**83.1**	**83.0**	5.3
MixN(0.5;1;0.25)	-1.02	3.87	**100.0**	**100.0**	**99.5**	**99.7**	**100.0**	**95.7**	**96.9**	**97.0**	**96.3**	**99.9**	**100.0**	**100.0**	**100.0**	30.2	29.6	**98.0**
MixN(0.4;1;0.25)	-0.78	3.34	**99.3**	**99.7**	**94.1**	**95.4**	**99.7**	**80.8**	**84.2**	**88.5**	**76.3**	**98.0**	**99.3**	**99.4**	**99.3**	16.3	16.1	**91.8**
MixN(0.3;1;0.25)	-0.57	3.03	**90.5**	**94.3**	*73.4*	**76.5**	**94.3**	*53.0*	*56.0*	*68.8*	39.9	**86.6**	**89.8**	**90.4**	**89.6**	9.3	9.2	*65.3*
MixN(0.5;3;0.25)	-0.46	1.78	**100.0**	**100.0**	**100.0**	**100.0**	**100.0**	**99.6**	**99.8**	**100.0**	**94.0**	**100.0**	**100.0**	**100.0**	**100.0**	0.1	0.1	**82.7**
MixN(0.4;3;0.25)	-0.16	1.67	**100.0**	**100.0**	**100.0**	**100.0**	**100.0**	**99.3**	**96.3**	**99.3**	45.4	**100.0**	**100.0**	**99.7**	**97.9**	0.0	0.0	**83.9**
MixN(0.3;3;0.25)	0.12	1.81	**99.9**	**100.0**	**100.0**	**100.0**	**100.0**	**97.5**	**77.1**	**92.7**	3.7	**98.3**	**99.1**	**96.2**	**90.8**	0.0	0.0	**95.3**
MixN(0.5;1;4)	0.44	5.21	**97.7**	**99.3**	**87.5**	**90.6**	**99.3**	**81.1**	**88.5**	**88.0**	**97.7**	**99.1**	**98.7**	**93.1**	**83.0**	*57.3*	*56.2*	*53.2*
MixN(0.4;1;4)	0.56	6.17	**99.2**	**99.9**	**97.2**	**98.2**	**99.9**	**94.5**	**97.5**	**97.4**	**99.7**	**99.9**	**98.5**	**88.7**	*73.7*	**77.3**	**76.2**	*51.7*
MixN(0.3;1;4)	0.7	7.58	**99.2**	**99.9**	**99.4**	**99.6**	**99.9**	**98.9**	**99.7**	**99.7**	**100.0**	**99.9**	**95.1**	*73.9*	*55.1*	**92.1**	**91.5**	36.9
MixN(0.5;3;4)	0.96	4.37	**99.9**	**100.0**	**97.8**	**98.5**	**100.0**	**92.8**	**94.4**	**93.0**	**96.8**	**99.6**	**99.9**	**99.9**	**99.8**	40.9	40.1	**90.6**
MixN(0.4;3;4)	1.21	5.29	**100.0**	**100.0**	**99.8**	**99.9**	**100.0**	**99.0**	**99.3**	**98.7**	**99.8**	**100.0**	**100.0**	**99.8**	**99.6**	*64.5*	*63.3*	**91.8**
MixN(0.3;3;4)	1.52	6.76	**100.0**	**100.0**	**100.0**	**100.0**	**100.0**	**99.9**	**100.0**	**99.9**	**100.0**	**100.0**	**99.7**	**98.5**	**96.9**	**86.9**	**86.0**	**85.0**
Nout1	0	3.00	6.3	7.4	12.8	10.8	7.4	15.0	20.2	17.0	19.5	9.8	5.4	5.1	5.0	23.0	22.7	5.1
Nout2	0	3.00	12.0	22.2	**99.4**	**87.0**	22.4	**98.6**	**99.5**	**99.0**	**97.5**	28.6	5.3	5.0	5.0	**100.0**	**100.0**	5.1
Nout3	0	3.00	22.1	44.3	**98.5**	**90.8**	43.3	**99.0**	**99.6**	**98.8**	**98.6**	*53.8*	7.2	6.0	5.7	**99.9**	**100.0**	5.3
Nout4	0	3.00	6.6	10.2	8.6	9.8	10.6	12.3	28.0	37.8	28.3	14.0	5.9	5.1	4.9	32.6	27.1	4.9
Nout5	0	3.00	35.2	**80.5**	**96.9**	**96.6**	**82.2**	**98.7**	**99.9**	**100.0**	**99.6**	**79.1**	10.2	6.1	5.5	**100.0**	**99.9**	5.0

Table A.10. (continued) Empirical power results for normal modified distributions (α = 0.05, n = 100).

Distribution	$\sqrt{\beta_1}$	β_2	T_w	$T_{MC\text{-}LR}$-T_w	$T_{S,l}$	$T_{K,l}$	W	W_{SF}	W_{RG}	D	r	CS	Q	Q-Q^*	$BCMR$	β_3^2	T_{EP}	I_n	$R_{s,J}$
Trunc(-3;1)	-0.55	2.78	15.0	19.3	*59.2*	12.2	**88.9**	**78.4**	**93.3**	7.8	**75.9**	**91.3**	3.2	**98.0**	**86.8**	26.1	*69.4*	6.5	12.2
Trunc(-2;1)	-0.32	2.27	37.7	32.1	15.7	0.1	**81.4**	*59.4*	**95.3**	31.1	*54.7*	**86.4**	1.7	**94.9**	**76.7**	*71.8*	*61.2*	0.1	33.2
Trunc(-3;2)	-0.18	2.65	7.7	6.7	4.9	3.4	9.3	4.7	18.9	9.8	4.2	11.4	1.6	11.1	7.9	9.0	8.5	0.6	7.6
Trunc(-1;1)	0	1.94	**77.7**	*68.7*	5.5	1.7	**92.9**	*73.1*	**99.6**	**92.4**	*67.7*	**96.0**	**83.0**	**92.3**	**89.5**	**98.8**	*72.2*	0.0	**77.2**
Trunc(-2;2)	0	2.36	17.0	12.4	0.8	1.6	12.5	3.7	38.4	30.4	2.8	17.6	11.3	10.5	9.5	30.0	9.5	0.0	17.1
Trunc(-3;3)	0	2.84	4.4	4.4	2.4	1.9	3.3	2.1	5.8	3.9	2.0	3.8	2.8	2.7	2.9	3.2	4.4	1.4	4.3
LoConN(0.5;5)	0	1.51	**100.0**	**100.0**	*74.2*	8.8	**100.0**	**100.0**	**100.0**	1.5	**100.0**	**100.0**	*71.1*	**87.1**	**100.0**	**100.0**	**100.0**	0.0	**99.3**
LoConN(0.5;3)	0	2.04	**92.8**	**88.9**	6.9	1.3	**75.2**	*58.6*	**85.2**	*70.1*	*54.5*	**80.3**	24.3	30.3	*72.3*	**82.8**	**78.7**	0.0	**90.6**
LoConN(0.5;1)	0	2.92	5.0	4.9	4.1	4.0	4.5	4.0	5.6	5.0	3.9	4.8	4.6	4.5	4.3	4.6	4.8	3.3	5.1
LoConN(0.4;1)	0.04	2.93	5.0	4.9	4.5	4.0	4.6	4.1	5.7	4.9	4.0	4.9	4.9	4.6	4.5	4.6	4.9	3.5	5.0
LoConN(0.3;1)	0.06	2.96	4.9	4.9	5.3	4.2	5.2	4.8	5.7	4.9	4.8	5.3	5.3	4.8	5.1	4.7	5.4	4.2	5.0
LoConN(0.4;3)	0.23	2.14	**78.6**	**77.4**	37.1	18.3	**79.5**	*65.9*	**86.9**	38.6	*62.5*	**83.5**	38.4	32.2	**77.1**	*70.5*	**84.5**	0.1	*64.5*
LoConN(0.4;5)	0.32	1.65	**99.4**	**100.0**	**99.0**	*71.7*	**100.0**	**100.0**	**100.0**	3.4	**100.0**	**100.0**	**87.0**	**86.6**	**100.0**	**99.6**	**100.0**	1.2	**78.4**
LoConN(0.3;3)	0.46	2.47	29.1	49.3	**75.8**	*51.5*	**87.5**	**80.2**	**89.7**	7.3	**78.4**	**89.2**	44.5	35.0	**86.2**	32.6	**92.7**	5.4	14.2
LoConN(0.3;5)	0.67	2.13	*69.7*	**99.7**	**100.0**	**99.3**	**100.0**	**100.0**	**100.0**	47.1	**100.0**	**100.0**	**90.7**	**86.4**	**100.0**	**80.6**	**100.0**	34.5	27.9
ScConN(0.05;0.25)	0	3.14	7.9	6.5	6.2	6.8	6.3	7.1	4.3	6.6	7.3	5.7	5.1	5.1	6.5	7.1	6.3	9.3	7.9
ScConN(0.10;0.25)	0	3.29	16.9	12.9	7.8	9.3	9.8	11.6	4.6	11.3	11.9	8.3	5.5	5.6	10.2	11.9	9.9	16.1	16.8
ScConN(0.20;0.25)	0	3.64	49.3	40.6	13.9	16.9	26.7	30.7	10.5	33.2	31.3	23.0	7.7	8.5	27.6	31.1	27.4	39.1	49.6
ScConN(0.05;2)	0	3.97	16.0	13.5	21.0	24.6	22.2	26.0	9.6	21.8	26.4	20.6	17.2	24.1	23.6	21.7	13.2	26.2	16.0
ScConN(0.10;2)	0	4.43	26.4	22.3	29.7	34.5	33.4	39.3	13.1	35.1	39.9	30.5	23.7	33.4	35.5	35.5	22.0	41.2	26.5
ScConN(0.20;2)	0	4.68	41.3	35.0	35.7	40.2	44.8	*52.2*	17.0	*50.7*	*53.1*	40.6	27.2	37.2	47.3	*52.1*	35.4	*57.9*	41.5
ScConN(0.20;4)	0	9.75	**99.4**	**99.1**	**95.8**	**93.9**	**99.5**	**99.6**	**96.2**	**99.7**	**99.7**	**99.3**	*74.8*	**91.7**	**99.5**	**99.6**	**99.2**	*57.7*	**99.4**
ScConN(0.10;4)	0	12.75	**92.5**	**91.0**	**90.4**	**93.2**	**94.7**	**95.8**	**85.0**	**95.4**	**95.9**	**94.0**	*73.3*	**92.5**	**95.1**	**95.1**	**91.1**	*51.1*	**92.8**
ScConN(0.05;4)	0	13.55	*72.2*	*69.0*	*74.8*	**79.3**	**78.8**	**81.2**	*63.9*	**79.0**	**81.5**	**77.6**	*57.1*	**79.5**	**79.7**	**77.9**	*68.5*	43.9	*72.1*
MixN(0.5;1;0.25)	-1.02	3.87	18.8	**97.0**	**99.2**	37.0	**100.0**	**100.0**	**99.7**	**90.3**	**100.0**	**100.0**	29.3	44.1	**100.0**	19.2	**100.0**	**82.1**	*68.6*
MixN(0.4;1;0.25)	-0.78	3.34	19.3	**89.1**	**92.6**	19.3	**98.9**	**98.7**	**96.4**	*55.5*	**98.7**	**98.8**	15.6	32.1	**98.9**	9.9	**99.1**	*65.3*	26.9
MixN(0.3;1;0.25)	-0.57	3.03	26.3	*63.1*	*68.7*	10.5	**88.3**	**86.9**	**80.3**	18.3	**86.3**	**88.3**	8.7	22.3	**88.4**	9.3	**90.0**	28.7	15.7
MixN(0.5;3;0.25)	-0.46	1.78	**100.0**	**100.0**	*53.4*	0.1	**100.0**	**100.0**	**100.0**	26.7	**100.0**	**100.0**	4.1	**100.0**	**100.0**	**99.8**	**100.0**	6.8	**87.9**
MixN(0.4;3;0.25)	-0.16	1.67	**99.8**	**100.0**	29.0	7.2	**100.0**	**100.0**	**100.0**	1.0	**100.0**	**100.0**	15.0	**99.8**	**100.0**	**100.0**	**100.0**	0.1	**98.8**
MixN(0.3;3;0.25)	0.12	1.81	**87.1**	**94.9**	*56.0*	*60.5*	**100.0**	**100.0**	**100.0**	2.9	**100.0**	**100.0**	27.2	**94.5**	**100.0**	**98.9**	**99.7**	0.0	*69.0*
MixN(0.5;1;4)	0.44	5.21	**97.1**	**97.1**	*66.8*	*56.5*	**97.6**	**98.2**	**86.7**	**98.0**	**98.3**	**96.7**	22.1	38.5	**97.8**	**93.0**	**98.1**	**80.7**	**99.0**
MixN(0.4;1;4)	0.56	6.17	**99.5**	**99.5**	**83.7**	*68.5*	**99.7**	**99.8**	**96.1**	**99.8**	**99.8**	**99.5**	32.6	*58.4*	**99.7**	**98.5**	**99.8**	*72.1*	**99.9**
MixN(0.3;1;4)	0.7	7.58	**99.9**	**99.8**	**93.7**	**83.2**	**99.9**	**99.9**	**98.3**	**100.0**	**99.9**	**99.8**	45.5	**78.7**	**99.9**	**99.7**	**99.9**	*62.9*	**99.9**
MixN(0.5;3;4)	0.96	4.37	44.7	**92.7**	**94.9**	49.1	**99.8**	**99.8**	**98.5**	**94.8**	**99.8**	**99.8**	19.4	35.6	**99.8**	48.8	**99.9**	**81.6**	**87.5**
MixN(0.4;3;4)	1.21	5.29	**78.7**	**98.0**	**98.5**	*61.3*	**100.0**	**100.0**	**99.9**	**99.7**	**100.0**	**100.0**	24.3	*55.1*	**100.0**	*74.9*	**100.0**	*67.7*	**98.8**
MixN(0.3;3;4)	1.52	6.76	**97.1**	**99.7**	**99.6**	**81.5**	**100.0**	**100.0**	**100.0**	**100.0**	**100.0**	**100.0**	31.6	**77.7**	**100.0**	**92.6**	**100.0**	*50.5*	**100.0**
Nout1	0	3.00	8.5	7.1	13.7	2.8	11.1	15.6	3.0	10.5	16.2	9.2	5.5	9.3	12.5	13.7	7.9	20.0	8.6
Nout2	0	3.00	40.6	30.7	**81.7**	**97.2**	**93.4**	**98.2**	25.6	**81.0**	**98.5**	**90.8**	6.0	**99.9**	**95.9**	*63.2*	23.4	**91.8**	40.5
Nout3	0	3.00	*53.5*	42.6	**90.7**	**93.0**	**93.9**	**97.9**	43.3	**88.2**	**98.2**	**90.9**	7.9	**99.1**	**95.8**	*74.4*	49.7	**94.9**	*54.9*
Nout4	0	3.00	20.2	14.7	3.9	4.6	10.9	23.6	0.3	29.3	25.6	7.3	11.8	5.5	14.4	46.5	11.0	47.4	19.9
Nout5	0	3.00	**93.6**	**89.0**	41.1	**84.1**	**96.0**	**99.4**	19.1	**99.7**	**99.6**	**92.2**	**97.0**	**95.9**	**97.9**	**99.9**	**87.6**	**99.2**	**93.3**

Table A.11. Average empirical power results by distribution type for all sample sizes (α = 0.05).

Distribution	Sample size	K-S	AD^*	Z_c	Z_a	P_s	K^2	JB	DH	RJB	T_{Lmom}	$T_{TLmom}^{(1)}$	$T_{TLmom}^{(2)}$	$T_{TLmom}^{(3)}$	$BM_{3\text{-}4}$	$BM_{3\text{-}6}$	$T_{MC\text{-}LR}$
Symmetric	25	39.3	45.1	44.4	43.6	45.2	41.5	35.4	41.8	38.9	47.0	33.4	24.6	20.2	32.9	33.5	14.5
	50	49.9	*57.9*	*60.0*	*59.0*	*58.1*	*58.6*	45.1	*55.2*	45.4	*60.6*	47.9	38.4	31.3	39.3	39.7	22.8
	100	*61.3*	*71.1*	*72.7*	*71.6*	*71.2*	*72.3*	*64.1*	*69.5*	*54.0*	*72.3*	*60.6*	*51.4*	44.3	43.8	43.5	35.6
Asymmetric	25	36.1	45.3	49.2	*50.9*	44.9	37.3	39.4	43.8	35.4	45.6	22.0	20.8	20.4	27.3	27.6	22.1
	50	*52.3*	*62.2*	*66.8*	*69.2*	*61.6*	*55.8*	*57.5*	*63.7*	*52.6*	*63.9*	39.4	38.7	38.4	37.9	38.2	33.9
	100	*67.9*	**76.8**	**80.6**	**82.1**	**76.2**	*74.9*	**75.6**	**79.6**	*70.1*	**78.7**	*56.8*	*55.9*	*55.6*	49.2	48.7	48.5
Modified Normal	25	35.9	41.3	37.7	36.7	41.3	29.0	21.3	34.2	22.6	38.8	30.7	25.6	22.4	15.6	16.0	19.0
	50	50.0	*55.0*	*52.7*	*53.1*	*55.1*	46.8	36.4	49.0	31.0	*54.4*	46.0	41.1	38.0	20.5	20.9	28.9
	100	*59.9*	*65.8*	*66.5*	*66.6*	*65.7*	*62.9*	*56.9*	*63.9*	47.7	*66.6*	*56.4*	*51.8*	48.7	25.6	25.4	40.9

Table A.11. (continued) Average empirical power results by distribution type for all sample sizes ($\alpha = 0.05$).

Distribution	Sample size	T_w	$T_{MC\text{-}LR}$-T_w	$T_{S,I}$	$T_{K,I}$	W	W_{SF}	W_{RG}	D	r	CS	Q	Q-Q*	$BCMR$	$\beta_3{}^2$	T_{EP}	I_n	$R_{s,J}$
Symmetric	25	45.3	43.2	33.1	31.5	45.5	43.5	44.4	40.0	43.1	45.6	30.5	40.6	45.0	48.5	42.1	11.6	45.8
	50	*60.7*	*57.4*	40.3	40.1	*60.1*	*56.6*	*60.1*	*55.2*	*55.9*	*60.6*	42.5	*52.4*	*59.4*	*64.8*	*56.2*	12.8	*60.4*
	100	*73.9*	*70.6*	*50.6*	46.0	*73.6*	*70.6*	*72.4*	*71.7*	*70.0*	*74.0*	*55.1*	*62.1*	*72.8*	**76.3**	*69.2*	15.0	*73.8*
Asymmetric	25	14.9	23.9	44.3	22.5	48.2	45.5	48.1	30.4	45.0	48.5	38.0	46.1	47.6	12.0	45.8	22.1	22.9
	50	21.6	35.4	*62.0*	30.4	*65.5*	*62.5*	*65.2*	41.8	*61.9*	*65.9*	*52.7*	*61.7*	*64.9*	17.3	*62.5*	30.9	31.8
	100	30.2	48.7	**76.9**	41.4	**78.7**	**76.9**	**78.2**	*51.8*	**76.5**	**79.1**	*65.8*	*73.9*	**78.3**	24.7	**76.2**	40.4	41.2
Modified Normal	25	29.3	31.2	23.5	19.5	40.0	37.5	38.1	22.0	36.9	40.2	16.8	27.4	39.6	27.6	38.3	16.9	28.8
	50	42.3	47.2	35.0	26.1	*55.2*	*52.9*	*53.1*	32.9	*52.5*	*55.5*	22.2	38.4	*54.8*	42.4	*53.8*	22.2	42.0
	100	*53.7*	*61.0*	*50.2*	33.8	*67.9*	*65.7*	*66.4*	43.8	*65.1*	*68.2*	28.9	49.9	*67.6*	*55.4*	*65.4*	27.8	*53.2*

Table A.12. Average empirical power results by distribution type for all sample sizes ($\alpha = 0.10$).

Distribution	Sample size	K-S	AD*	Z_c	Z_a	P_s	K^2	JB	DH	RJB	T_{Lmom}	$T_{TLmom}{}^{(1)}$	$T_{TLmom}{}^{(2)}$	$T_{TLmom}{}^{(3)}$	$BM_{3\text{-}4}$	$BM_{3\text{-}6}$	$T_{MC\text{-}LR}$
Symmetric	25	46.3	*51.8*	*52.0*	*50.8*	*51.9*	49.8	42.8	49.3	43.1	*53.6*	40.5	31.9	27.2	38.0	38.7	22.6
	50	*56.9*	*64.3*	*66.3*	*65.0*	*64.5*	*65.6*	*58.6*	*62.5*	48.9	*66.4*	*54.5*	45.4	38.5	43.6	44.4	31.8
	100	*68.3*	**76.3**	**78.0**	**76.8**	**76.5**	**76.8**	*74.0*	*75.0*	*68.3*	**76.8**	*66.5*	*57.5*	*50.9*	48.0	48.5	44.0
Asymmetric	25	44.4	*52.2*	*56.6*	*57.3*	*51.9*	45.7	*50.2*	*51.3*	43.8	*52.9*	30.8	29.9	29.6	34.2	34.5	31.0
	50	*58.9*	*67.0*	*71.8*	*73.0*	*66.5*	*63.7*	*66.9*	*68.7*	*59.9*	*68.8*	47.3	46.6	46.4	44.0	44.5	42.4
	100	*72.1*	**78.8**	**82.2**	**82.8**	**78.3**	**79.0**	**80.1**	**81.0**	**77.1**	**80.4**	*62.7*	*61.9*	*61.6*	*53.5*	*53.6*	*55.5*
Modified Normal	25	44.3	48.7	46.3	45.6	48.7	39.6	35.9	43.0	29.3	47.0	39.2	34.6	31.6	21.4	21.9	27.3
	50	*56.3*	*60.8*	*60.1*	*60.1*	*60.8*	*56.1*	*53.3*	*56.7*	38.8	*60.7*	*52.4*	47.7	44.8	26.1	26.7	37.1
	100	*65.2*	*70.2*	*71.3*	*71.0*	*70.1*	*69.5*	*68.2*	*69.6*	*62.2*	*70.9*	*61.2*	*56.9*	*54.1*	30.7	31.0	47.5

Table A.12. (continued) Average empirical power results by distribution type for all sample sizes ($\alpha = 0.10$).

Distribution	Sample size	T_w	$T_{MC\text{-}LR}$-T_w	$T_{S,I}$	$T_{K,I}$	W	W_{SF}	W_{RG}	D	r	CS	Q	Q-Q*	$BCMR$	$\beta_3{}^2$	T_{EP}	I_n	$R_{s,J}$
Symmetric	25	*52.2*	49.6	38.6	36.8	*52.6*	*50.4*	*51.3*	46.1	49.9	*52.7*	37.7	47.6	*52.2*	*55.6*	49.9	15.7	*52.4*
	50	*66.8*	*63.1*	47.1	44.9	*66.5*	*63.3*	*65.4*	*62.0*	*62.6*	*66.7*	49.9	*59.1*	*65.8*	*70.1*	*63.3*	16.2	*66.5*
	100	**78.5**	**75.4**	*59.2*	*51.1*	**78.9**	**76.3**	**76.3**	**76.4**	**75.7**	**79.0**	*61.7*	*67.9*	**78.3**	**79.6**	*74.7*	17.9	**78.5**
Asymmetric	25	21.6	31.8	*53.7*	29.1	*56.2*	*53.5*	*56.1*	37.5	*53.0*	*56.4*	45.8	*53.5*	*55.6*	18.7	*54.0*	29.5	29.6
	50	28.5	43.1	*69.6*	36.2	*71.5*	*69.0*	*71.2*	47.9	*68.5*	*71.9*	*59.8*	*67.8*	*71.0*	24.4	*69.1*	37.9	38.3
	100	37.1	*55.8*	**81.4**	45.5	**82.0**	**80.6**	**81.9**	*57.1*	**80.3**	**82.4**	*70.9*	**78.2**	**81.7**	31.8	**80.3**	46.3	47.3
Modified Normal	25	36.7	39.2	31.9	25.6	48.0	46.3	45.6	28.8	45.8	48.1	24.1	36.0	47.8	36.0	47.0	22.5	36.3
	50	48.9	*54.0*	44.6	32.3	*61.6*	*59.4*	*59.4*	39.4	*58.9*	*61.8*	29.9	47.0	*61.2*	49.7	*60.3*	27.1	48.5
	100	*59.3*	*65.8*	*59.6*	40.0	*72.1*	*70.8*	*70.2*	49.7	*70.3*	*72.2*	36.5	*56.9*	*71.9*	*61.2*	*70.1*	32.1	*58.7*

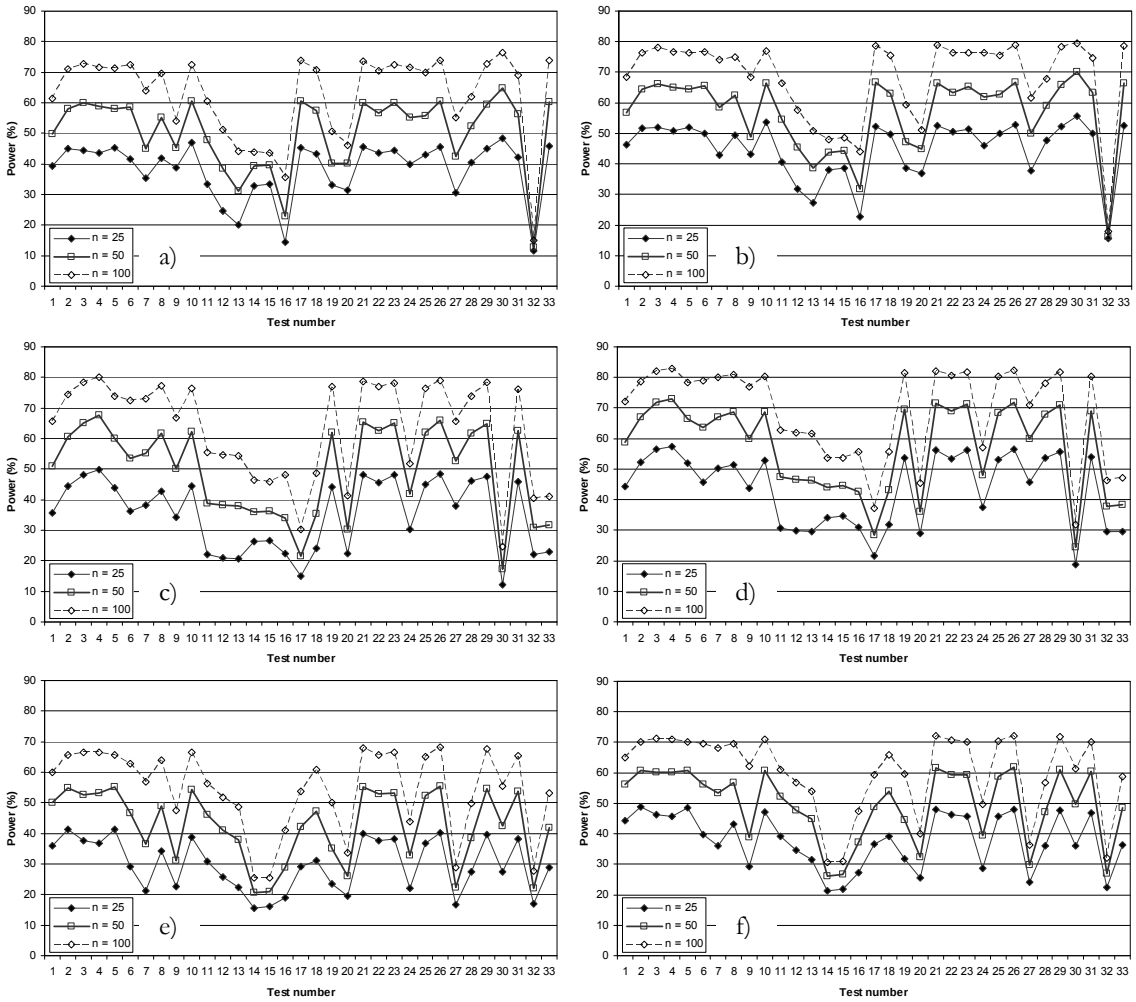

Figure A.2. Average empirical power results, for all sample sizes, for the symmetric distributions with $\alpha = 0.05$ (a) and $\alpha = 0.10$ (b); for the asymmetric distributions with $\alpha = 0.05$ (c) and $\alpha = 0.10$ (d); for the modified normal distributions with $\alpha = 0.05$ (e) and $\alpha = 0.10$ (f).

Table A.13. Numbering of the tests.

Test	K-S	AD^*	Z_c	Z_a	P_s	K^2	JB	DH	RJB	T_{Lmom}	$T_{TLmom}^{(1)}$	$T_{TLmom}^{(2)}$	$T_{TLmom}^{(3)}$	$BM_{3\text{-}4}$	$BM_{3\text{-}6}$	$T_{MC\text{-}LR}$
Test number	1	2	3	4	5	6	7	8	9	10	11	12	13	14	15	16

Test	T_w	$T_{MC\text{-}LR}$-T_w	$T_{S,l}$	$T_{K,l}$	W	W_{SF}	W_{RG}	D	r	CS	Q	Q-Q^*	$BCMR$	β_3^2	T_{EP}	I_n	$R_{s,J}$
Test number	17	18	19	20	21	22	23	24	25	26	27	28	29	30	31	32	33

A.6 Discussion of the results

A summary of the power results is presented in the following comprising several different levels of comparison. A preliminary general assessment of the results is presented based on the values of $\sqrt{\beta_1}$ and β_2. Then, comparisons are performed by type of normality test, by type of simulated distribution, by sample size and also considering the totality of results. An additional comparison is also performed with respect to the outlier sensitivity of the tests, by specifically addressing the power results obtained for the Nout1 to Nout5 distributions.

Regarding the influence of $\sqrt{\beta_1}$ and β_2, it is observed that when their corresponding values are near those of the normal distribution, none of the tests produces significant power results. With respect to symmetric distributions, most of the tests are seen to yield better performance when β_2 is either significantly lower or higher than 3. In terms of asymmetric distributions, the influence of $\sqrt{\beta_1}$ appears to be slightly larger than that of β_2 over the power of the tests. In general terms, the power of the tests appears to increase with skewness increase. With respect to the modified normal distributions, the influence of $\sqrt{\beta_1}$ and β_2 is not easily identified due to the additional influence of the considered level of contamination.

In terms of the selected normality tests based on the EDF, with the exception of *K-S*, the remaining tests generally exhibit similar power over the range of selected distributions. In general, the powers of AD^* and P_s are very similar while those of Z_C and Z_A are closer to each other. For the case of the symmetric distributions, and disregarding *K-S*, there is no clear advantage of one test over the others as their relative performance varies according to sample size and significance level. On the other hand, for the asymmetric distributions, Z_C and Z_A are best, with Z_A presenting a slight edge over Z_C. For the modified normal distributions AD^* and P_s are better when sample size decreases, while for the larger sample size again all tests except *K-S* yield similar results.

In terms of the selected normality tests based on measures of the moments, T_w, T_{Lmom} and K^2 generally exhibit better performance for the symmetric distributions. Nonetheless, T_{Lmom} is best when sample size decreases and K^2 loses more power for the smaller sample size, for which tests such as $T_{MC\text{-}LR}$-T_w and *DH* present similar or slightly better power. For the case of asymmetric distributions, *DH*, T_{Lmom} and $T_{S,\ell}$ are seen to have better power, with *DH* being somewhat better when the sample size is larger while T_{Lmom} is slightly better for smaller n. For the modified normal distributions, T_{Lmom}, *DH* and K^2 appear to be the best choices. Nonetheless, for smaller n, $T_{MC\text{-}LR}$-T_w presents, in some cases, better performance than K^2.

In terms of regression and correlation tests, β_3^2, *CS* and *W* exhibit better performance for the case of symmetric distributions, with β_3^2 showing an increasing relative power towards the other two tests as *n* decreases. For the asymmetric distributions, *CS* and *W* are generally better, with W_{RG} and *BCMR* closely following with similar power, while for the modified normal distributions, *CS*, *W* and *BCMR* present the best performance.

When considering all the normality tests for the selected alternative symmetric distributions, β_3^2, *CS*, T_w and R_{sJ} are generally better, with β_3^2 having a slight edge over the others. For smaller sample sizes β_3^2 is still the best choice and T_{L_mom} also shows good power, with *CS*, *W*, T_w and R_{sJ} close behind. A similar analysis for the case of asymmetric distributions shows that Z_A, Z_C, *CS* and *W* appear to be the best choices, with relative performance depending on the selected sample size and significance level. For the modified normal distributions, *CS*, *BCMR* and *W* are generally better although, as *n* decreases, *AD**, P_s and also T_{L_mom} become more significant.

To allow for a more clear view of the individual power results of the best tests identified for each distribution set, Fig. A.3 presents their corresponding power results for the selected distributions of each set, a significance level α of 0.05 and a sample size of 50. Similar relative trends were observed for the other significance levels and sample sizes.

When considering all the normality tests against all the non-normal alternative distributions, but excluding the Nout1 to Nout5 distributions, it can be seen that, for the smaller sample size, *CS*, *W* and *BCMR* are generally the best choices, though Z_A, Z_C, T_{L_mom}, W_{RG} , *AD** and P_s follow closely. For the sample size of 50, *CS*, *W* and Z_A are better, with *BCMR*, Z_C, W_{RG} and T_{L_mom} also following closely. For the larger sample size, *CS*, *W* and *BCMR* are again the best choices with close performances of Z_A, Z_C and W_{RG}. Considering the whole range of sample sizes, *CS*, *W* and *BCMR* emerge as the best choices, although tests such as Z_A, Z_C, W_{RG}, T_{L_mom}, *AD**, P_s, W_{SF} and T_{EP} also show an overall comparable average power.

When analysing the power results for the Nout1 to Nout5 distributions, the main objective is not to find tests that reject the normality hypothesis as many times as possible. Instead, the search is for tests whose power is close to the nominal significance level, therefore implying a low sensitivity to outliers. Observation of the power results of all the normality tests against these distributions leads to conclude that $T_{MC\text{-}LR}$, $T_{TL\_mom}^{(3)}$ and $T_{TL\_mom}^{(2)}$ are the best choices over the complete set of selected normal distributions with outliers. Nonetheless, it is noted that both $T_{TL\_mom}^{(1)}$ and Q also have a low sensitivity to few outliers, i.e. a single outlier or two outliers defined as one lower and one upper extreme observations.

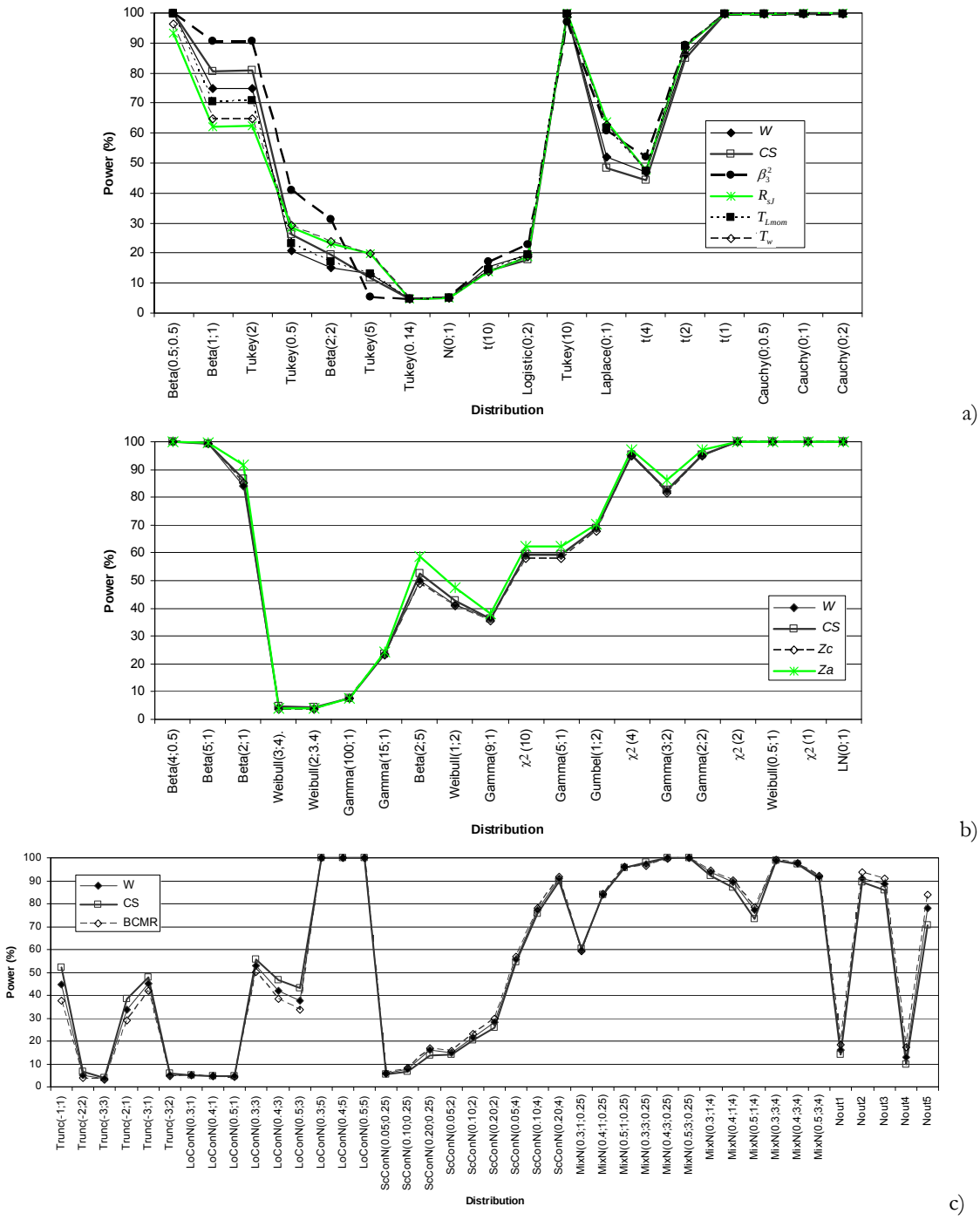

Figure A.3. Power of the best tests for with α = 0.05, a sample size of 50, and for the symmetric distributions (a), for the asymmetric distributions (b) and for the modified normal distributions (c).

With respect to the power of the proposed joint test $T_{MC\text{-}LR}$-T_w, observation of the power of this test for the different distributions shows an advantage over the performance of the individual tests for the asymmetric and modified normal distributions, excluding the Nout1 to Nout5 distributions. For the symmetric distributions, the individual test T_w is generally better than $T_{MC\text{-}LR}$-T_w.

As previously referred, a comparison of the two-sided R_{sJ} test with the one-sided version $R_{sJ,1}$ was carried out for each distribution set in order to verify the advantages of the

former. Fig. A.4 presents the corresponding power results for a significance level α of 0.05 and a sample size of 100. Similar relative trends were observed for the other significance levels and sample sizes. When comparing R_{sJ} to $R_{sJ,1}$, the former can be seen to extend the range of application of this test, namely to light-tailed distributions, without a significant reduction of its power towards heavy-tailed distributions. Therefore, when the nature of the non-normality is unknown R_{sJ} is considered to be more adequate than $R_{sJ,1}$.

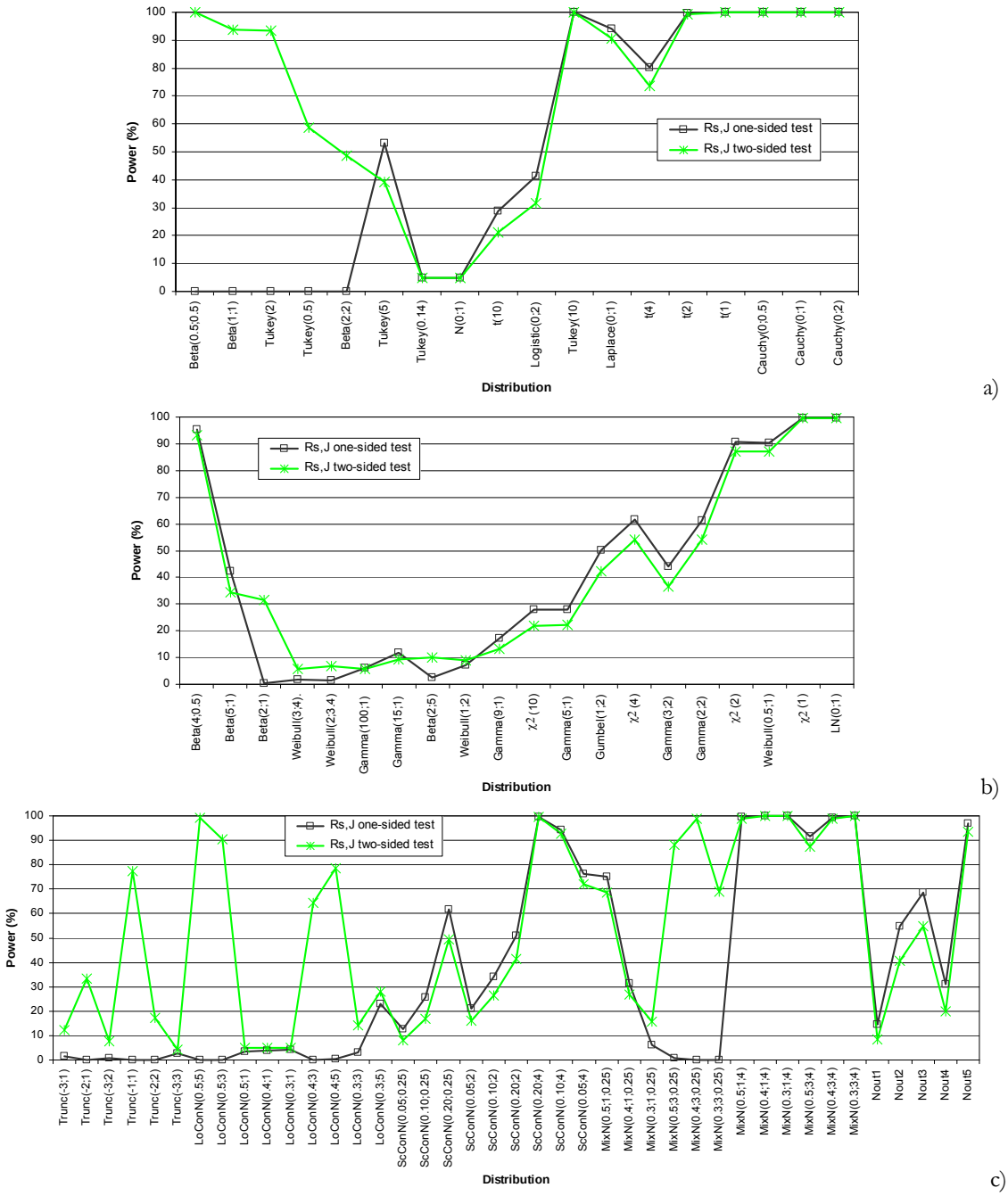

Figure A.4. Comparison of power of tests R_{sJ} and $R_{sJ,1}$ for with α = 0.05, a sample size of 100, and for the symmetric distributions (a), for the asymmetric distributions (b) and for the modified normal distributions (c).

Finally, a last remark on the performance obtained for the tests *K-S*, *JB*, *D* and *W* and corresponding comparison with results available in Yazici and Yolacan (2007). Considering the common sample size and significance level, results presented herein do not corroborate the findings in Yazici and Yolacan (2007) but are in much larger agreement with results of other previous studies referenced herein.

A.7 Concluding remarks

A comprehensive power comparison of existing tests for normality has been performed in the presented study. Given the importance of this subject and the widespread development of normality tests, comprehensive descriptions and power comparisons of such tests are of considerable interest. Since recent comparison studies do not include several interesting and more recently developed tests, a further comparison of normality tests, such as the one presented herein, is considered to be of foremost interest.

The study addresses the performance of thirty-three normality tests, for various sample sizes *n*, considering several significance levels α and for a number of symmetric, asymmetric and modified normal distributions.

General recommendations stemming from the analysis of the power of the selected tests indicate the best choices for normality testing are β_3^2, *CS*, T_w and R_{sJ} for symmetric distributions, Z_A, Z_C, *CS* and *W* for asymmetric distributions and *CS*, *BCMR* and *W* for modified normal distributions, excluding normal distributions with outliers. For this latter case, the tests $T_{MC\text{-}LR}$, $T_{TL\_mom}^{(3)}$ and $T_{TL\_mom}^{(2)}$ are recommended since they exhibit less sensitivity to outliers. When the nature of the non-normality is unknown, the tests *CS*, *W* and *BCMR* appear to be the best choices.

References

A

ACI 228.1R-03 (2003) In-place methods to estimate concrete strength. American Concrete Institute, Farmington Hills, Michigan, USA.

Aguiar, B., Veiga, V. and Oliveira, P. (2003) Statistical analysis of compressive strength of concrete specimens. *Proceedings of the International Conference on the Performance of Construction Materials in the New Millennium*. Cairo, Egypt.

Ambraseys, N., Simpson, K. and Bommer, J. (1996) Prediction of horizontal response spectra in Europe. *Earthquake Engineering and Structural Dynamics* **25**(4), 371-400.

Anderson, T. and Darling, D. (1952) Asymptotic theory of certain "goodness-of-fit" criteria based on stochastic processes. *Annals of Mathematical Statistics* **23**(2), 193-212.

Anderson, T. and Darling, D. (1954) A test of goodness of fit. *Journal of the American Statistical Association* **49**(268), 765-769.

Ang, A. and Tang, W. (1984) *Probability concepts in engineering: emphasis on applications to civil and environmental engineering*. Wiley, NewYork, USA.

Aoshima, M. and Govindarajulu, Z. (2002) Fixed-width confidence interval for a lognormal mean. *International Journal of Mathematics and Mathematical Sciences* **29**(3), 143-153.

Arêde, A. and Pinto, A. (1996) Reinforced concrete global section modelling: definition of skeleton curves. Special Publication Nº.I.96.36. Institute for Systems, Informatics and Safety, Joint Research Center, Ispra, Italy.

ARUP (2010) GB Oxfam Haiti Earthquake Response: An ARUP Assignment Report.

ASCE (2003) Seismic evaluation of existing buildings (ASCE/SEI 31-03). American Society of Civil Engineers, Reston, Virginia, USA.

ASCE (2007) Seismic rehabilitation of existing buildings (ASCE/SEI 41-06). American Society of Civil Engineers, Reston, Virginia, USA.

Aslani, H. and Miranda, E. (2005) Probability-based seismic response analysis. *Engineering Structures* **27**(8), 1151-1163.

Aslani, H. (2005) Probabilistic earthquake loss estimation and loss disaggregation in buildings. *PhD Thesis*, Stanford University, Stanford, California, USA.

ATC (1985) ATC-13 Earthquake damage evaluation data for California. Applied Technology Council, Redwood City, California, USA.

ATC (1996) ATC 40 Seismic evaluation and retrofit of concrete buildings. Applied Technology Council, Redwood City, California, USA.

ATC (2009) ATC-63 Quantification of building system performance and response parameters. Applied Technology Council, Redwood City, California, USA.

Athanassiadou, C. (2008) Seismic performance of R/C plane frames irregular in elevation. *Engineering Structures* **30**(5), 1250-1261.

Au, S. and Beck, J. (2003) Subset simulation and its application to seismic risk based on dynamic analysis. *Journal of Engineering Mechanics* **129**(8), 901-917.

B

Bai, Z. and Chen, L. (2003) Weighted W test for normality and asymptotics a revisit of Chen–Shapiro test for normality. *Journal of Statistical Planning and Inference* **113**(2), 485-503.

Baker, J. (2005) Vector-valued ground motion intensity measures for probabilistic seismic. demand analysis. *PhD Thesis*, Stanford University, Stanford, California, USA.

Baker, J. and Cornell, C.A. (2008) Uncertainty propagation in probabilistic loss estimation. *Structural Safety* **30**(3), 236-252.

Baringhaus, L., Danschke, R. and Henze, N. (1989) Recent and classical tests for normality - a comparative study. *Communications in Statistics - Simulation and Computation* **18**(1), 363-379.

Bartlett, F. (1997) Precision of in-place concrete strengths predicted using core strength correction factors obtained by weighted regression analysis. *Structural Safety* **19**(4), 397-410.

Bartlett, F. and MacGregor, J. (1994) Assessment of concrete strength in existing structures. Structural Engineering Report No. 198. University of Alberta, Canada.

Bartlett, F. and MacGregor, J. (1995) Equivalent specified concrete strength from core test data. *Concrete International* **17**(3), 52-58.

Bartlett, F. and MacGregor, J. (1999) Variation of in-place concrete strength in structures. *ACI Materials Journal* **96**(2), 261-270.

Bengtsson, M., Ståhlberg, A., Rorsman, P. and Kubista, M. (2005) Gene expression profiling in single cells from the pancreatic islets of Langerhans reveals lognormal distribution of mRNA levels. *Genome Research* **15**(10), 1388–1392.

Bertero, R. and Bertero, V. (2004) Performance-based seismic engineering: development and application of a comprehensive conceptual approach to the design of buildings. In *Earthquake Engineering: From Engineering Seismology to Performance-Based Engineering*, Bozorgnia, Y. and Bertero, V. (editors). CRC Press, Boca Raton, Florida, USA.

Bickel, D. and Frühwirth, R. (2006) On a fast, robust estimator of the mode: Comparisons to other robust estimators with applications. *Computational Statistics and Data Analysis* **50**(12), 3500-3530.

Bilham, R. (2006) Harry Fielding Reid medal citation for Nicholas Ambrasey. *Seismological Research Letters* **77**(4), 487-489.

Biskinis, D. (2007) Deformations of concrete members at yielding and ultimate. *PhD Thesis*, University of Patras, Greece (in Greek).

Blom, G. (1958) *Statistical Estimates and Transformed Beta Variables*. Wiley, NewYork, USA.

Bonett, D. and Seier, E. (2002) A test of normality with high uniform power. *Computational Statistics and Data Analysis* **40**(3), 435-445.

Bontemps, C. and Meddahi, N. (2005) Testing normality: a GMM approach. *Journal. of Econometrics* **124**(1), 149-186.

Bowman, K. and Shenton, L. (1975) Omnibus test contours for departures from normality based on √b1 and b2. *Biometrika* **62**(2), 243-250.

Bowman, K. and Shenton, L. (1977) A bivariate model for the distribution of √b1 and b2. *Journal of the American Statistical Association* **72**(357), 206-211

Bradley, B. and Dhakal, R. (2008) Error estimation of closed-form solution for annual rate of structural collapse. *Earthquake Engineering and Structural Dynamics* **37**(15), 1721-1737.

Bradley, B. and Lee, D. (2010) Accuracy of approximate methods of uncertainty propagation in seismic loss estimation. *Structural Safety* **32**(1), 13-24.

Bradley, B., Dhakal, R., Cubrinovski, M., Mander, J. and MacRae, G. (2007) Improved seismic hazard model with application to probabilistic seismic demand analysis. *Earthquake Engineering and Structural Dynamics* **36**(14), 2211-2225.

BRI (2001a) Standard for Seismic Evaluation of Existing Reinforced Concrete Buildings. Building Research Institute, Japan Building Disaster Prevention Association, Tokyo, Japan.

BRI (2001b) Technical Manual for Seismic Evaluation of Existing Reinforced Concrete Buildings. Building Research Institute, Japan Building Disaster Prevention Association, Tokyo, Japan.

Brys, G., Hubert, M. and Struyf, A. (2003) A comparison of some new measures of skewness. In *Developments in Robust Statistics, ICORS 2001*, Dutter, R., Filzmoser, P., Gather, U. and Rousseeuw, P. (editors). Springer, Berlin, Germany.

Brys, G., Hubert, M. and Struyf, A. (2004) A robust measure of skewness. *Journal of Computational and Graphical Statistics* **13**(4), 996-1017.

Brys, G., Hubert, M. and Struyf, A. (2006) Robust measures of tail weight. *Computational Statistics and Data Analysis* **50**(3), 733-759.

Brys, G., Hubert, M. and Struyf, A. (2008) Goodness-of-fit tests based on a robust measure of skewness. *Computational Statistics* **23**(3), 429–442.

BS 2846-7 (1997) Guide to statistical interpretation of data. Part 7: Tests for departure from normality. British Standards Institution, London, England, UK.

Bungey, J. and Millard, S. (1996) *Testing of Concrete in Structures, 3rd Ed.* Blackie Academic & Professional, London, England, UK.

Buratti, N., Stafford, P. and Bommer, J. (2011) Earthquake accelerogram selection and scaling procedures for estimating the distribution of drift response. *Journal of Structural Engineering* **137**(3), 345-358.

C

Cabaña, A. and Cabaña, E. (2003) Tests of normality based on transformed empirical processes. *Methodology and Computing in Applied Probability* **5**(3), 309-335.

Campos Costa, A., Sousa, M., Carvalho, A. (2008) Seismic zonation for Portuguese National Annex of Eurocode 8. *Proceedings of the 14th World Conference on Earthquake Engineering*. Beijing, China.

Carvalho, E., Coelho, E. and Campos Costa, A. (1999) Preparation of the full-scale tests on reinforced concrete frames - Characteristics of the test specimens, materials and testing conditions. ICONS report, Innovative Seismic Design Concepts for New and Existing Structures, European TMR Network, Laboratório Nacional de Engenharia Civil, Lisbon, Portugal.

Castillo, E. (1988) *Extreme value theory in engineering*. Academic Press, New York, USA.

CEB (1996) RC frames under earthquake loading. Bulletin nº 231, Comité Euro-International du Béton. Thomas Telford, London, England, UK.

Chao, B., Gross, R. and Han, Y.-B. (1996) Seismic excitation of the polar motion, 1977-1993. *Pure and Applied Geophysics* **146**(3), 407-419.

Chen, L. and Shapiro, S. (1995) An alternative test for normality based on normalized spacings. *Journal of Statistical Computation and Simulation* **53**(3), 269-287.

Chopra, A. and Goel, R. (2001) Direct displacement-based design: Use of inelastic vs. elastic design spectra. *Earthquake Spectra* **17**(1), 47-64.

Chouw, N., Hao, H. and Goldsworthy, H. (2011) Some observations of damage in the 22nd February Christchurch earthquake. Earthquake Reconnaissance Report. Australian Earthquake Engineering Society.

Chrysostomou, C. (2005) A pilot application of Eurocode 8 for the seismic assessment and retrofit of a real building. *Proceedings of the International Conference "250th Anniversary of the 1755 Lisbon Earthquake"*. Lisbon, Portugal.

Clifton, C., Bruneau, M., Fussell, A., Leon, R. and MacRae, G. (2011) Steel Building Damage From The Christchurch Earthquake Series of 2010 and 2011. Technical Report. Royal Commission of Inquiry into Building Failure Caused by the Canterbury Earthquakes, Department of Internal Affairs, Christchurch, New Zealand.

Coin, D. (2008) A goodness-of-fit test for normality based on polynomial regression. *Computational Statistics and Data Analysis* **52**(4), 2185-2198.

Cornell, C.A. and Krawinkler, H. (2000) Progress and challenges in seismic performance assessment. *PEER Center News* **3**(2).
http://peer.berkeley.edu/news/2000spring/performance.html (Accessed May 2010)

Cornell, C.A., Jalayer, F., Hamburger R. and Foutch, D. (2002) The probabilistic basis for the 2000 SAC/FEMA steel moment frame guidelines. *Journal of Structural Engineering* **128**(4), 526-533.

Costa, A. and Campos Costa, A. (1987) Force-displacement hysteretic model adequate to the seismic analysis of structures. Technical Report, Núcleo de Dinâmica Aplicada, Laboratório Nacional de Engenharia Civil, Lisbon, Portugal (in Portuguese).

Costa, M., Cavaliere, G. and Iezzi, S. (2005) The role of the normal distribution in financial markets. In *New Developments in Classification and Data Analysis*, Vichi, M., Monari, P., Mignani, S. and Montanari, A. (editors). Springer, Berlin, Germany.

D

D'Agostino, R. and Stephens, M. (1986) *Goodness-of-fit Techniques*. Marcel Dekker, Inc., New York, USA.

D'Agostino, R. (1971) An omnibus test of normality for moderate and large size samples. *Biometrika* **58**(2), 341-348.

D'Agostino, R. (1972) Small sample probability points for the D test of normality. *Biometrika* **59**(1), 219-221.

D'Agostino, R. and Pearson, E. (1973) Tests for departure from normality. Empirical results for the distributions of b2 and √b1. *Biometrika* **60**(3), 613-622.

D'Agostino, R., Belanger, A. and D'Agostino Jr., R. (1990) A suggestion for using powerful and informative tests of normality. *The American Statistician* **44**(4), 316-321.

Day, K. (1999) *Concrete Mix Design, Quality Control and Specification, 2nd Ed.* Spon Press, London, England, UK.

Decanini, L., Liberatore, L. and Mollaioli, F. (2003) Characterization of displacement demand for elastic and inelastic SDOF systems. *Soil Dynamics and Earthquake Engineering* **23**(6), 455-471.

Deierlein G. (2004) Overview of a comprehensive framework for earthquake performance assessment. In *Performance-based seismic design: Concepts and implementation: Proceedings of the International Workshop, Bled, Slovenia, 28 June-1 July 2004*, Fajfar, P. and Krawinkler, H. (editors). PEER report 2004/05. Bled, Slovenia.

Deierlein, G. and Haselton, C. (2005) Benchmarking the collapse safety of code-compliant reinforced concrete moment frame building systems. *ATC/JSCA US-Japan Workshop on Improvement of Structural Design and Construction Practices, Proceedings of an International Workshop*. Kobe, Japan.

Deierlein, G., Liel, A., Haselton, C. and Kircher, C. (2008) ATC-63 methodology for evaluating seismic collapse safety of archetype buildings. *Proceedings of the ASCE-SEI Structures Congress*. Vancouver, Canada.

del Barrio, E., Cuesta-Albertos, J., Matrán, C. and Rodríguez-Rodríguez, J. (1999) Tests of goodness of fit based on the L_2-Wasserstein distance. *The Annals of Statistics* **27**(4), 1230-1239.

del Barrio, E., Giné, E. and Utzet, F. (2005) Asymptotics for L2 functionals of the empirical quantile process, with applications to tests of fit based on weighted Wasserstein distances. *Bernoulli* **11**(1), 131-189.

Delgado, R., Costa, A., Arêde, A., Vila Pouca, N., Guedes, J., Romão, X., Delgado, P. and Rocha, P (2010) Ongoing research on seismic safety assessment. *Bulletin of Earthquake Engineering* 8(1), 181-199.

Dennis, J. and Welsch, R. (1978) Techniques for nonlinear least squares and robust regression. *Communications in Statistics - Simulation and Computation* **7**(4), 345-359

Der Kiureghian, A. (1996) Structural reliability methods for seismic safety assessment: A review. *Engineering Structures* **18**(6), 412-426.

Diamantidis, D. and Bazzurro, P. (2007) Safety acceptance criteria for existing structures. *Workshop on Risk Acceptance and Risk Communication*. Stanford, California, USA.

Dimitri, V. and Stewart, M. (2002) Safety factors for assessment of existing structures. *Journal of Structural Engineering* **128**(2), 258-265.

Ditlevsen, O. and Madsen, H. (1996) *Structural Reliability Methods*. John Wiley & Sons, Chichester, England, UK.

DOE (2002) Natural Phenomena Hazards Design and Evaluation Criteria for Department of Energy Facilities. DOE-STD-1020-2002. U.S. Department of Energy, Washington D.C., Maryland, USA.

Doornik, J. and Hansen, H. (2008) An omnibus test or univariate and multivariate normality. *Oxford Bulletin of Economics and Statistics* **70**(s1), 927-939.

Drezner, Z., Turel, O. and Zerom, D. (2010) A modified Kolmogorov-Smirnov test for normality. *Communications in Statistics - Simulation and Computation* **39**(4), 693-704.

Drysdale, R. (1973) Variation of concrete strength in existing buildings. *Magazine of Concrete Research* **25**(85), 201-207.

Dufour, J-M., Farhat, A., Gardiol, L. and Khalaf, L. (1998) Simulation-based finite sample normality tests in linear regressions. *The Econometrics Journal* **1**(1), 154-173.

Dymiotis, C. and Gutlederer, B. (2002) Allowing for uncertainties in the modelling of masonry compressive strength. *Construction and Building Materials* **16**(8), 443-452.

Dymiotis, C, Kappos, A. and Chryssanthopo, M. (1999) Seismic reliability of RC frames with uncertain drift and member capacity. *Journal of Structural Engineering* **125**(9), 1038-1047.

E

Eberhard, M., Baldridge, S., Marshall, J. and Rix, G. (2010) USGS/EERI Advance Reconnaissance Team Report: The Mw 7.0 Haiti Earthquake. United States Geological Survey, United States Department of the Interior, USA.

EC2-1 (2004) ENV 1992-1. Eurocode 2: Design of Concrete Structures - Part 1: General rules for buildings. European Committee for Standardization, Brussels, Belgium.

EC8-1 (2004) ENV 1998-1. Eurocode 8: Design of structures for earthquake resistance - Part 1: General rules, seismic actions and rules for buildings. European Committee for Standardization, Brussels, Belgium.

EC8-1 (2010) NP ENV 1998-1. Portuguese National Annex to Eurocode 8: Design of structures for earthquake resistance - Part 1: General rules, seismic actions and rules for buildings. Instituto Português da Qualidade, Lisbon, Portugal.

EC8-3 (2005) ENV 1998-3. Eurocode 8: Design of structures for earthquake resistance - Part 3: Assessment and retrofitting of buildings. European Committee for Standardization, Brussels, Belgium.

Elamir, E. and Seheult, A. (2003) Trimmed L-moments. *Computational Statistics and Data Analysis* **43**(3), 299-314.

Elefante, L. (2009) Dealing with uncertainties in the assessment of existing RC buildings. *PhD Thesis*, Università degli Studi di Napoli Federico II, Naples; Italy.

Elnashai, A., Gencturk, B., Kwon, O.-S., Al Qadi, I., Hashash, Y., Roesler, J., Kim, S., Jeong, S.-H., Dukes, J. and Valdivia, A. (2010) The Maule (Chile) Earthquake of February 27, 2010: Consequence Assessment and Case Studies. Mid-America Earthquake (MAE) Center Report Series, CD-Release 10-04.

El-Shaarawi, A. and Lin, J. (2007) Interval estimation for log-normal mean with applications to water quality. *Environmetrics* **18**(1), 1-10.

EN 13791 (2007) Assessment of in-situ compressive strength in structures and precast concrete components. European Committee for Standardization, Brussels, Belgium.

Epps, T. and Pulley, L. (1983) A test for normality based on the empirical characteristic function. *Biometrika* **70**(3), 723-726.

EERI (2011) The M 6.3 Christchurch, New Zealand, Earthquake of February 22, 2011. EERI Special Earthquake Report. Earthquake Engineering Research Institute, Oakland, California, USA.

F

Fajfar, P. and Dolšek, M. (2011) A practice-oriented estimation of the failure probability of building structures. *Earthquake Engineering and Structural Dynamics* DOI: 10.1002/eqe.1143.

Faria, R., Vila Pouca, N. and Delgado, R. (2002) Seismic behaviour of a R/C wall: Numerical simulation and experimental validation. *Journal of Earthquake Engineering* **6**(4), 473-498

Farrell, P. and Rogers-Stewart, K. (2006) Comprehensive study of tests for normality and symmetry: extending the Spiegelhalter test. *Journal of Statistical Computation and Simulation* **76**(9), 803-816.

FEMA 273 (1997) Guidelines for the seismic rehabilitation of buildings. National Earthquake Hazard Reduction Program. Federal Emergency Management Agency, Washington D.C., Maryland, USA.

FEMA 274 (1997) Commentary for the seismic rehabilitation of buildings. National Earthquake Hazard Reduction Program. Federal Emergency Management Agency, Washington D.C., Maryland, USA.

FEMA 310 (1998) Handbook for the seismic evaluation of buildings - A prestandard. National Earthquake Hazard Reduction Program. Federal Emergency Management Agency, Washington D.C., Maryland, USA.

FEMA 350 (2000) Recommended seismic design criteria for new steel moment-frame buildings. Developed by the SAC Joint Venture for the Federal Emergency Management Agency, Washington D.C., Maryland, USA.

FEMA 356 (2000) Prestandard and commentary for the seismic rehabilitation of buildings. Federal Emergency Management Agency, Washington D.C., Maryland, USA.

Ferracuti, B., Pinho, R., Savoia, M. and Francia, R. (2009) Verification of displacement-based adaptive pushover through multi-ground motion incremental dynamic analyses. *Engineering Structures* **31**(8), 1789-1799.

Ferreira, M. (2012) Seismic risk in urban systems. *PhD Thesis*, Higher Technical Institute, Technical University of Lisbon, Lisbon, Portugal (in Portuguese).

fib (2003a) Seismic assessment and retrofit of reinforced concrete buildings. Bulletin nº24, Fédération Internationale du Béton. Lausanne, Switzerland.

fib (2003b) Displacement-based seismic design of reinforced concrete buildings. Bulletin nº25, Fédération Internationale du Béton. Lausanne, Switzerland.

fib (2006) Retrofitting of concrete structures by externally bonded FRPs, with emphasis on seismic applications. Bulletin nº35, Fédération Internationale du Béton. Lausanne, Switzerland.

Filippou, F. and Fenves, G. (2004) Methods of analysis for earthquake-resistant structures. In *Earthquake Engineering: From Engineering Seismology to Performance-Based Engineering*, Bozorgnia, Y. and Bertero, V. (editors). CRC Press, Boca Raton, Florida, USA.

Filliben, J. (1975) The probability plot correlation coefficient test for normality. *Technometrics* **17**(1), 111-117.

Foltz, R. (2004) Estimating seismic damage and repair costs. *Proceedings of the 2004 Earthquake Engineering Symposium for Young Researchers.* Charleston, South Carolina, USA.

Franchin, P. (2004) Reliability of uncertain inelastic structures under earthquake excitation. *Journal of Engineering Mechanics* **130**(2), 180-191.

Franchin, P., Pinto, P.E. and Rajeev, P. (2008) Assessing the adequacy of a single Confidence Factor in accounting for epistemic uncertainty. In *Valutazione e riduzione della vulnerabilità sismica di edifici esistenti in cemento armato*, Cosenza, E., Manfredi, G. and Monti, G. (editors). Polimetrica s.a.s. International Scientific Publisher, Monza, Italy.

Franchin, P., Pinto P.E. and Rajeev, P. (2009) Confidence in the confidence factor. *Convegno Finale del Progetto ReLuis-DPC*. Naples, Italy.

Franchin, P., Pinto, P.E. and Rajeev, P. (2010) Confidence factor? *Journal of Earthquake Engineering* **14**(7), 989-1007.

G

Gan, F. and Koehler, K. (1990) Goodness-of-fit tests based on P–P probability plots. *Technometrics* **32**(3), 289-303.

Geary, R. (1936) Moments of the ratio of the mean deviation to the standard deviation for normal samples. *Biometrika* **28**(3/4), 295-307.

Gel, Y. and Gastwirth, J. (2008) A robust modification of the Jarque–Bera test of normality. *Economics Letters* **99**(1), 30–32.

Gel, Y., Miao, W. and Gastwirth, J. (2007) Robust directed tests of normality against heavy-tailed alternatives. *Computational Statistics and Data Analysis* **51**(5), 2734-2746.

Giles, D. (2007) Spurious regressions with time-series data: further asymptotic results. *Communications in Statistics - Theory and Methods* **36**(5), 967-979.

Giovenale, P., Cornell, C.A. and Esteva, L. (2004) Comparing the adequacy of alternative ground motion intensity measures for the estimation of structural responses. *Earthquake Engineering and Structural Dynamics* **33**(8), 951-979.

Glen, A., Leemis, L. and Barr, D. (2001) Order statistics in goodness-of-fit testing. *IEEE Transactions on Reliability* **50**(2), 209-213.

Goda, K., Hong, H. and Lee, C. (2009) Probabilistic characteristics of seismic ductility demand of SDOF systems with Bouc-Wen hysteretic behaviour. *Journal of Earthquake Engineering* **13**(5), 600-622.

Goulet, C., Haselton, C., Mitrani-Reiser, J., Beck, J., Deierlein, G., Porter, K. and Stewart, J. (2007) Evaluation of the seismic performance of a code-conforming reinforced-concrete frame building: from seismic hazard to collapse safety and economic losses. *Earthquake Engineering and Structural Dynamics* **36**(13), 1973-1997.

Gurenko, E. (2011) Developing catastrophe and weather risk markets in the EU: prerequisites for success. *Proceedings of the Conference "Prevention and Insurance of Natural Catastrophes"*. Brussels, Belgium.

H

H2 (2005) *Handbook 2 - Reliability backgrounds*. Leonardo da Vinci Pilot Project CZ/02/B/F/PP-134007, Development of skills facilitating implementation of Eurocodes. European Commission. Brussels, Belgium

Hadjian, A. (2002) A general framework for risk-consistent seismic design. *Earthquake Engineering and Structural Dynamics* **31**(3), 601-626.

Halley, J. and Inchausti, P. (2002) Lognormality in ecological time series. *Oikos* **99**(3), 518-530.

Hampel, F. (1971) A general qualitative definition of robustness. *The Annals of Mathematical Statistics,* **42**(6) 1887-1896.

Hampel, F. (1973) Robust estimation: A condensed partial survey. *Probability Theory and Related Fields* **27**(2), 87-104

Hampel, F., Ronchetti, E., Rousseeuw, P. and Stahel, W. (1986). *Robust Statistics: The Approach Based on Influence Functions*. Wiley, New York, USA.

Hancock, J., Watson-Lamprey, J., Abrahamson, N., Bommer, J., Markatis, A., Mccoy, E. and Mendis, R. (2006) An improved method of matching response spectra of recorded earthquake ground motion using wavelets. *Journal of Earthquake Engineering* **10**(1), 67-89.

Hansen, L. (1982) Large sample properties of generalized method of moments estimators. *Econometrica* **50**(4), 1029-1054.

Haselton, C. (2006) Assessing seismic collapse safety of modern reinforced concrete moment frame buildings. *PhD Thesis*, Stanford University, Stanford, California, USA.

Haselton, C. and Baker, J. (2006) Ground motion intensity measures for collapse capacity prediction: Choice of optimal spectral period and effect of spectral shape. *Proceedings of the 8th National Conference on Earthquake Engineering*. San Francisco, California, USA.

Haselton, C., Liel, A., Deierlein, G., Dean, B. and Chou, J. (2011) Seismic collapse safety of reinforced concrete buildings. I: Assessment of ductile moment frames. *Journal of Structural Engineering* **137**(4), 481-491.

Haukaas, T. (2003) Finite element reliability and sensitivity analysis of hysteretic degrading structures. *PhD Thesis*, University of California, Berkeley, California, USA.

Hendawi, S. and Frangopol, D. (1994) System reliability and redundancy in structural design and evaluation. *Structural Safety* **16**(1-2), 47-71

Henderson, A. (2006) Testing experimental data for univariate normality. *Clinica Chimica Acta* **366**(1/2), 112-129.

Henze, N. (1990) An approximation to the limit distribution of the Epps-Pulley test statistic for normality. *Metrika* **37**(1), 7-18.

Herbst, A. (2007) Lunacy in the stock market – What is the evidence? *Journal of Bioeconomics* **9**(1), 1-18.

Hill, N. and Padmanabhan, A. (1991) Some adaptive robust estimators which work with real data. *Biometrical Journal* **33**(1), 81-101

Hindo, K. and Bergstrom, W. (1985) Statistical evaluation of the in-place compressive strength of concrete. *Concrete International* **7**(2), 44-48.

Hoaglin, D., Mosteller, F. and Tukey, J. (editors) (1983) *Understanding robust and exploratory data analysis*. Wiley, New York, USA.

Hogg, R. (1974) Adaptive robust procedures: A partial review and some suggestions for future applications and theory. *Journal of the American Statistical Association* **69**(348), 909-923

Hogg, R. (1982) On adaptive statistical inferences. *Communications in Statistics - Theory and Methods* **11**(22), 2531-2542

Hosking, J. (1990) L-moments: analysis and estimation of distributions using linear combinations of order statistics. *Journal of the Royal Statistical Society, Series B* **52**(1), 105-124.

Hosking, J. (1992) Moments or L-moments? An example comparing two measures of distributional shape. *The American Statistician* **46**(3), 186-189.

Huber P. (1981) *Robust Statistics*. Wiley, New York, USA.

Hwang, Y. and Wei, P. (2007) A remark on the Zhang omnibus test for normality. *Journal of Applied Statistics* **34**(2), 177-184.

I

IAEA (2006) Chernobyl´s Legacy: Health, Environmental and Socio-economic Impacts and Recommendations to the Governments of Belarus, the Russian Federation and Ukraine. International Atomic Energy Agency, Vienna, Austria.

Ibarra, L. and Krawinkler, H. (2005) Global collapse of frame structures under seismic excitations. PEER Report 2005/06. Pacific Earthquake Engineering Research Center, Berkeley, California, USA.

Ibarra, L., Medina, R. and Krawinkler, H. (2002) Collapse assessment of deteriorating SDOF systems. *Proceedings of the 12th European Conference on Earthquake Engineering*. London, England, UK.

Iervolino, I., Maddaloni, G. and Cosenza, E. (2008) Eurocode 8 compliant real record sets for seismic analysis of structures. *Journal of Earthquake Engineering* **12**(1), 54-90.

Iman, R. and Conover, W. (1982) A distribution-free approach to inducing rank correlation among input variables. *Communications in Statistics B* **11**(3), 311-334.

ISO 12491 (1997) Statistical methods for quality control of building materials and components. International Organization for Standardization. Geneva, Switzerland.

ISO 13822 (2010) Bases for design of structures - Assessment of existing structures. International Organization for Standardization. Geneva, Switzerland.

ISO 2394 (1998) General principles on reliability for structures. International Organization for Standardization. Geneva, Switzerland.

J

Jalayer, F. and Cornell, C.A. (2000) Technical framework for probability-based demand and capacity factor (DCFD) seismic formats. PEER Report 2003/08. Pacific Earthquake Engineering Research Center, Berkeley, California, USA.

Jalayer, F. and Cornell, C.A. (2009) Alternative nonlinear demand estimation methods for probability-based seismic assessments. *Earthquake Engineering and Structural Dynamics* **38**(8), 951-972.

Jalayer, F., Franchin, P. and Pinto, P.E. (2007) A scalar damage measure for seismic reliability analysis of RC frames. *Earthquake Engineering and Structural Dynamics* **36**(13), 2059-2079.

Jalayer, F., Elefante, L., Iervolino, I. and Manfredi, G. (2011) Knowledge-based performance assessment of existing RC buildings. *Journal of Earthquake Engineering* **15**(3), 362-389.

Jarque, C. and Bera, A. (1980) Efficient tests for normality, homoscedasticity and serial independence of regression residuals. *Economics Letters* **6**(3), 255-259.

JCSS (2001a) Probabilistic Model Code - Part 3: Resistance models. Joint Committee on Structural Safety.

JCSS (2001b) *Probabilistic Assessment of Existing Structures*. Joint Committee on Structural Safety. RILEM Publications S.A.R.L, Bagneux, France.

Johnson, N., Kotz, S. and Balakrishnan, N. (1994) *Continuous Univariate Distributions, Vol. 1*. Wiley, New York, USA.

K

Kappos, A., Chryssanthopoulos, M. and Dymiotis, C. (1999) Uncertainty analysis of strength and ductility of confined reinforced concrete members. *Engineering Structures* **21**(2), 195-208.

Kato, H., Tajiri, S. and Mukai, T. (2010) Preliminary Reconnaissance Report of the Chile Earthquake 2010. Building Research Institute, Japan Building Disaster Prevention Association, Tokyo, Japan.

Kennedy, R. and Short, S. (1994) Basis for seismic provisions of DOE-STD-1020. UCRLCR-111478 and BNL-52418. Lawrence Livermore National Laboratory and Brookhaven National Laboratory. Livermore, California, USA.

Keselman, H., Wilcox, R., Lix, L., Algina, J., Fradette, K. (2007) Adaptive robust estimation and testing. *British Journal of Mathematical and Statistical Psychology* **60**(2), 267-293.

Kircher, C. and Heintz, J. (2008) Overview and key concepts of the ATC-63 methodology. *Proceedings of the ASCE-SEI Structures Congress*. Vancouver, Canada.

Kiureghian, A. (2005) Non-ergodicity and PEER's framework formula. *Earthquake Engineering and Structural Dynamics* **34**(13), 1643-1652.

Krauczi, É. (2007) A study of the quantile correlation test for normality. *Test* **18**(1), 156-165.

Krawinkler, H. (1997) Research issues in performance based seismic engineering. In *Seismic design methodologies for the next generation of codes, Proceedings of the International Workshop on Seismic Design Methodologies for the Next Generation of Codes*, Fajfar, P and Krawinkler, H. (editors). A. A. Balkema, Rotterdam, the Netherlands.

Krawinkler, H. and Lignos, D. (2009) How to predict the probability of collapse of non-ductile building structures. In *Seismic Risk Assessment and Retrofitting: With special emphasis on existing low rise structures*, Alper Ilki, A., Karadogan, F., Pala, S. and Yuksel, E. (editors). Springer, New York, USA.

Krawinkler, H., Zareian, F., Medina, R. and Ibarra, L. (2006) Decision support for conceptual performance-based design. *Earthquake Engineering and Structural Dynamics* **35**(1), 115-133.

Krinitzsky, E. (1993) Earthquake probability in engineering: Part 1. The use and misuse of expert opinion. *Engineering Geology* **33**(4), 257-288.

Krishnamoorthy, K. and Mathew, T. (2003) Inferences on the means of lognormal distributions using generalized p-values and generalized confidence intervals. *Journal of statistical planning and inference* **115**(1), 103-121.

Kuhn, B., Lukic, A., Nussbaumer, A., Gunther, H.-P., Helmerich, R., Herion, S., Kolstein, M., Walbridge, S., Androic, B., Dijkstra, O. and Bucak, O. (2008) Assessment of existing steel structures: Recommendations for estimation of remaining fatigue life. Joint Report Prepared under the JRC–ECCS Eurocode 3 Cooperation Agreement. Office for Official Publications of the European Communities, Luxembourg.

Kurama, Y. and Farrow, K. (2003) Ground motion scaling methods for different site conditions and structure characteristics. *Earthquake Engineering and Structural Dynamics* **32**(15), 2425-2450.

Kwon, O.-S. and Elnashai, A. (2006) The effect of material and ground motion uncertainty on the seismic vulnerability curves of RC structure. *Engineering Structures* **28**(2), 289-303.

Kwon, O.-S. and Elnashai, A. (2007) Probabilistic seismic assessment of structure, foundation and soil interacting systems. Newmark Structural Engineering Laboratory Report Series 004, 2007-12. University of Illinois, Urbana-Champaign, Illinois, USA.

L

Landry, L. and Lepage, Y. (1992) Empirical behavior of some tests for normality. *Communications in Statistics - Simulation and Computation* **21**(4), 971-999.

Law, A. and Kelton, D. (2000) *Simulation modeling and analysis*. McGraw-Hill, New York, USA.

Lawless, J. (1982) *Statistical Models and Methods for Lifetime Data, 2nd Ed.* Wiley, New York, USA.

Lax, D. (1985) Robust estimators of scale: finite-sample performance in long-tailed symmetric distributions. *Journal of the American Statistical Association* **80**(391), 736-741.

Leonowicz Z., Karvanen J., Shishkin S. (2005) Trimmed estimators for robust averaging of event-related potentials. *Journal of Neuroscience Methods* **142**(1), 17-26.

Leslie, J., Stephens, M. and Fotopoulos, S. (1986) Asymptotic distribution of the Shapiro-Wilk W for testing for normality. *Annals of Statistics* **14**(4), 1497-1506.

LessLoss (2006) LessLoss - Risk Mitigation for Earthquakes and Landslides. Applications of probabilistic seismic assessment methods to selected case studies. Technical Report nº 78, Integrated Research & Development Project of the European Commission, Sixth Framework Programme, Contract No. GOCE-CT-2003-505448.

Liel, A., Haselton, C., Deierlein, G. and Baker, J. (2009). Incorporating modeling uncertainties in the assessment of seismic collapse risk of buildings. *Structural Safety* **31**(2), 197-211.

Liel, A., Haselton, C. and Deierlein, G. (2011) Seismic collapse safety of reinforced concrete buildings. II: Comparative assessment of nonductile and ductile moment frames. *Journal of Structural Engineering* **137**(4), 492-502.

Liesenfeld, R. and Jung, R. (2000) Stochastic volatility models: conditional normality versus heavy-tailed distributions. *Journal of Applied Econometrics* **15**(2), 137-160.

Lilliefors, H. (1967) On the Kolmogorov-Smirnov test for normality with mean and variance unknown. *Journal of the American Statistical Association* **62**(318), 399-402.

Limpert, E., Stahel, W. and Abbt, M. (2001) Log-normal distributions across the sciences: keys and clues. *BioScience* **51**(5), 341-352.

Luce, R. (1986) *Response times*. Oxford University Press, New York, USA.

Luco, N. and Bazzurro, P. (2004) Effects of earthquake record scaling on nonlinear structural response. Report for PEER Center Lifelines Program - Task 1G00, Pacific Earthquake Engineering Research Center, Berkeley, California, USA.

Luco, N. and Cornell, C.A. (2007) Structure-specific scalar intensity measures for near-source and ordinary earthquake ground motions. *Earthquake spectra* **23**(2), 357-392.

Lupoi, A., Franchin, P. and Schotanus, M. (2003) Seismic risk evaluation of RC bridge structures. *Earthquake Engineering and Structural Dynamics* **32**(8), 1275-1290.

Lupoi, G., Lupoi, A. and Pinto, P.E. (2002) Seismic risk assessment of RC structures with the "2000 SAC/FEMA" method. *Journal of Earthquake Engineering* **6**(4), 499-512.

M

Mackie, K. and Stojadinovic, B. (2007) Performance-based seismic bridge design for damage and loss limit states. *Earthquake Engineering and Structural Dynamics* **36**(13), 1953-1971.

Madan, A., Borckardt, J. and Nash, M. (2008) A parametric control chart adjustment for handling serial dependence in health care quality data. *Quality Management in Health Care* **17**(2), 154-161.

Markatou, M., Horowitz, J. and Lenth, R. (1995) Robust scale estimation based on the empirical characteristic function. *Statistics and Probability Letters*, **25**(2), 185-192.

Maronna, R. and Zamar, R. (2002) Robust estimates of location and dispersion of high-dimensional datasets. *Technometrics* **44**(4), 307-317.

Maronna, R., Martin, D. and Yohai, V. (2006) *Robust Statistics - Theory and Methods*. Wiley, New York, USA.

Martinez, J. and Iglewicz, B. (1981) A test for departure from normality based on a biweight estimator of scale. *Biometrika* **68**(1), 331-333.

Masi, A., Vona, M. and Manfredi, V. (2008) A parametric study on RC existing buildings to compare different analysis methods considered in the European seismic code (EC8-3). *Proceedings of the 14th World Conference on Earthquake Engineering*. Beijing, China.

Mathur, S. and Dolo, S. (2008) A new efficient statistical test for detecting variability in the gene expression data. *Statistical Methods in Medical Research* **17**(4), 405-419.

Matlab (2008) The MathWorks, Inc. http://www.mathworks.com/ (Accessed May 2011)

Medina, R. and Krawinkler, H. (2004) Seismic demands for nondeteriorating frame structures and their dependence on ground motions. PEER Report 2003/15. Pacific Earthquake Engineering Research Center, Berkeley, California, USA.

Melchers, R. (1999) *Structural reliability: analysis and prediction, 2nd Ed.* Wiley, New York, USA.

Melchers, R. (2001) Assessment of existing structures - Approaches and research. *Journal of Structural Engineering* **127**(4), 406-411.

Mernagh, M. (2006) The Mernagh Expansion to approximate standard normal distributions. *Proceedings of the 26th Conference on Applied Statistics in Ireland (CASI 2006)*. Killarney, Ireland.

Min, I. (2007) A nonparametric test of the conditional normality of housing demand. *Applied Economics Letters* **14**(2), 105-109.

Miranda, E. and Aslani, H. (2003) Building-specific loss estimation methodology. PEER Report 2003/03. Pacific Earthquake Engineering Research Center, Berkeley, California, USA.

Mitrani-Reiser, J. (2007) An ounce of prevention: probabilistic loss estimation for performance-based earthquake engineering. *PhD Thesis*. California Institute of Technology, Pasadena, California, USA.

Mojsilovic, N. and Faber, M. (2008) Probabilistic model framework for the design of structural masonry. *Proceedings of the International Conference of the Engineering Mechanics Institute (EM08)*. Minneapolis, USA.

Montgomery, D. and Runger, G. (2003) *Applied Statistics and Probability for Engineers, 3rd Ed.* Wiley, New York, USA.

Monti, G. and Alessandri, S. (2009) Application of Bayesian techniques to material strength evaluation and calibration of confidence factors. *Proceedings of the Convegno Finale del Progetto ReLuis-DPC*. Naples, Italy.

Moses, F. (1990) New directions and research needs in system reliability. *Structural Safety* **7(**2-4), 93-100.

Mosteller, F. (1946) On some useful 'inefficient' statistics. *Annals of Mathematical Statistics* **17**(4), 377-408.

Mpampatsikos, V., Nascimbene, R. and Petrini, L. (2008a) A critical review of the R.C. frame existing building assessment procedure according to Eurocode 8 and Italian seismic code. *Journal of Earthquake Engineering* **12**(S1), 52-82.

Mpampatsikos, V., Nascimbene, R. and Petrini, L. (2008b) Some considerations about the eurocode 8 R.C. frame building assessment procedure. *Proceedings of the 14th World Conference on Earthquake Engineering*, Beijing, China.

Muttlak, H. and Al-Sabah, W. (2003) Statistical quality control based on ranked set sampling. *Journal of Applied Statistics* **30**(9), 1055-1078.

N

Nadarajah, S. (2005) A generalized normal distribution. *Journal of Applied Statistics* **32**(7), 685-694.

Nafday, A. (2008) System safety metrics for skeletal structures. *Journal of Structural Engineering* **134**(3), 499-504.

NASA (2011) Japan Quake May Have Shortened Earth Days, Moved Axis. Jet Propulsion Laboratory, National Aeronautics and Space Administration, Pasadena, California, USA. http://www.nasa.gov/topics/earth/features/japanquake/earth20110314.html (Accessed December 2011)

Nematollahi, A. and Tafakori, L. (2007) On comparison of the tail index of heavy tail distributions using Pitman's measure of closeness. *Applied Mathematical Sciences* **1**(19), 909-914.

Neville, A. (1996) *Properties of Concrete, 4th Ed.* Wiley, New York, USA.

NGDC (2011) Significant Earthquake Database. National Geophysical Data Center. National Environmental Satellite, Data and Information Service, National Oceanic & Atmospheric Administration, Boulder, Colorado, USA.
http://www.ngdc.noaa.gov/hazard/ (Accessed December 2011)

NZSEE (2006) Assessment and improvement of the structural performance of buildings in earthquake. Recommendations of a NZSEE Study Group on Earthquake Risk Buildings. New Zealand Society for Earthquake Engineering, New Zealand.

NTC (2008) Norme Tecniche per le Costruzioni. Decreto del Ministero delle infrastrutture, Supplemento Ordinario n.30 alla Gazzetta Ufficiale della Repubblica italiana n.29 del 4/02/2008, Italy (in Italian).

O

Oakland, J. (2008) *Statistical Process Control, 6th Ed.* Butterworth-Heinemann, England, UK.

Önder, A. and Zaman, A. (2005) Robust tests for normality of errors in regression models. *Economics Letters* **86**(1), 63-68.

OPCM 3274 (2003) Primi elementi in material di criteri generali per la classificazione sismica del territorio nazionale e di normative tecniche per le costruzioni in zona sismica. Ordinanza del Presidente del Consiglio dei Ministri nº 3274/2003, Supplemento Ordinario n.72 alla Gazzetta Ufficiale della Repubblica italiana n.105 del 8/5/2003, e successive modifiche ed integrazioni, Italy (in Italian).

OPCM 3431 (2005) Ulteriori modifiche ed integrazioni all'Ordinanza n.3274 del 20/3/2003, recante 'Primi elementi in materia di criteri generali per la classificazione sismica del territorio nazionale e di normative tecniche per le costruzioni in zona sismica'. Ordinanza del Presidente del Consiglio dei Ministri nº 3431/2005, Supplemento Ordinario n.85 alla Gazzetta Ufficiale della Repubblica italiana n.107 del 10/5/2005, Italy (in Italian).

Otani, S. (1999) Disaster mitigation engineering: the Kobe earthquake disaster. *Proceedings of the Japan Society for the Promotion of Science Seminar on Engineering in Japan*. London, UK.

P

Padgett, J., Nielson, B. and DesRoches, R. (2008) Selection of optimal intensity measures in probabilistic seismic demand models of highway bridge portfolios. *Earthquake Engineering and Structural Dynamics* **37**(5), 711-725.

Pearson, E., D'Agostino, R. and Bowman, K. (1977) Tests for departure from normality: comparison of powers. *Biometrika* **64**(2), 231-246.

PEER-NGA (2009) Pacific Earthquake Engineering Research Center: NGA Database. http://peer.berkeley.edu/nga/ (Accessed April 2010).

Pennacchi P. (2008) Robust estimate of excitations in mechanical systems using M-estimators - Theoretical background and numerical applications. *Journal of Sound and Vibration* **310**(4-5), 923-946

Pennecchi, F., Callegaro, L. (2006) Between the mean and the median: the Lp estimator. *Metrologia* **43**(3), 213-219.

Pinto, P.E. (2001) Reliability methods in earthquake engineering. *Progress in Structural Engineering and Materials* **3**(1), 76-85.

Pinto, P.E. and Franchin, P. (2008) Assessing existing buildings with Eurocode 8 Part 3: a discussion with some proposals. *Background documents for the "Eurocodes: Background and applications" workshop*. Brussels, Belgium.

Pinto, P.E., Giannini, R. and Franchin, P. (2004) *Seismic reliability analysis of structures*. IUSS Press, Istituto Universitario di Studi Superiori di Pavia, Pavia, Italy.

Pomonis, A., Kappos, A., Karababa, F. and Panagopoulos, G. (2011) Seismic Vulnerability and Collapse Probability Assessment of Buildings in Greece. In *Human Casualties in Earthquakes: Progress in Modelling and Mitigation*, Spence, R. So, E. and Scawthorn, C. (editors). Springer, Berlin, Germany.

Porter, K. (2003) An overview of PEER's performance-based earthquake engineering methodology. *Proceedings of the Ninth International Conference on Applications of Statistics and Probability in Civil Engineering*. San Francisco, California.

Priestley, M.J.N. (2003) *Myths and Fallacies in Earthquake Engineering, Revisited. The Mallet Milne Lecture*. IUSS Press, Istituto Universitario di Studi Superiori di Pavia, Pavia, Italy.

Q

Quddus, M. (2008) Time series count data models: An empirical application to traffic accidents. *Accident Analysis and Prevention* **40**(5), 1732-1741.

R

Raab, D. and Green, E. (1961) A cosine approximation to the normal distribution. *Psychometrika* **26**(4), 447-450.

Rahman, M. and Govindarajulu, Z. (1997) A modification of the test of Shapiro and Wilk for normality. *Journal of Applied Statistics* **24**(2), 219-235.

Ramirez, C. and Miranda, E. (2009) Building-specific loss estimation methods & tools for simplified performance-based earthquake engineering. Report Nº 171. John A. Blume earthquake engineering research center. Stanford University. Stanford, California, USA.

Randal, J. (2008) A reinvestigation of robust scale estimation in finite samples. *Computational Statistics and Data Analysis* **52**(11), 5014-5021.

Reed, J. and Stark, D. (1996) Hinge estimators of location: Robust to asymmetry. *Computer Methods and Programs in Biomedicine* **49**(1), 11-17.

RMS (2010) The 2010 Maule, Chile Earthquake: Lessons and Future Challenges. Report. Risk Management Solutions, San Francisco, California, USA.

Rocha, P., Delgado, P., Costa, A. and Delgado, R. (2004) Seismic retrofit of RC frames. *Computers and Structures* **82**(17-19), 1523-1534.

Rodrigues, H. (2005) Development and calibration of numerical models for the seismic analysis of buildings. *MSc Thesis*, Faculty of Engineering of the University of Porto, Porto, Portugal (in Portuguese).

Rojas, F., Lew, M. and Naeim, F. (2010) An overview of building codes and standards in Chile at the time of the 27 February 2010 offshore Maule, Chile earthquake. *The Structural Design of Tall and Special Buildings* **19**(8), 853-865.

Romão, X. (2002) New models for the seismic design of structures. *MSc Thesis*, Faculty of Engineering of the University of Porto, Porto, Portugal (in Portuguese).

Romão, X., Guedes, J., Costa, A. and Delgado, R. (2008) Analytical evaluation of structural component limit state probabilities. *Bulletin of Earthquake Engineering* **6**(2), 309–333.

Romão, X., Delgado, R. and Costa, A. (2010a) Practical aspects of demand and capacity evaluation of RC members in the context of EC8-3. *Earthquake Engineering and Structural Dynamics* **39**(5), 473-499.

Romão, X., Guedes, J., Costa, A. and Delgado, R. (2010b) A comparative application of different EC8-3 procedures for the seismic safety assessment of existing structures. *Bulletin of Earthquake Engineering* **8**(1), 91-118.

Romão, X., Delgado, R. and Costa, A. (2010c) An empirical power comparison of univariate goodness-of-fit tests for normality. *Journal of Statistical Computation and Simulation* **80**(5), 545-591.

Romão, X., Costa, A. and Delgado, R. (2011) Assessment of the statistical distributions of structural demand under earthquake loading. *Journal of Earthquake Engineering* **15**(5), 724-753.

Romão, X., Gonçalves, R., Costa, A. and Delgado, R. (2012a) Evaluation of the EC8-3 confidence factors for the characterization of concrete strength in existing structures. *Materials and Structures* (submitted for publication).

Romão, X., Costa, A. and Delgado, R. (2012b) Statistical characterization of structural demand under earthquake loading. Part 1: Robust estimation of the central value of the data. *Journal of Earthquake Engineering*, DOI:10.1080/13632469.2012.669514.

Romão, X., Costa, A. and Delgado, R. (2012c) Statistical characterization of structural demand under earthquake loading. Part 2: Robust estimation of the dispersion of the data. *Journal of Earthquake Engineering*, DOI:10.1080/13632469.2012.669515.

Rousseeuw, P. (1984) Least median of squares regression. *Journal of the American Statistical Association* **79**(388), 871-880.

Rousseeuw, P. and Croux, C. (1993) Alternatives to the median absolute deviation. *Journal of the American Statistical Association* **88**(424), 1273-1283.

Rousseeuw, P. and Katrien van Driessen, K. (1999) A fast algorithm for the minimum covariance determinant estimator. *Technometrics* **41**(3), 212-223

Rousseeuw, P. and Leroy, A. (1988) A robust scale estimator based on the shortest half. *Statistica Neerlandica* **42**(2), 103-116.

Rousseeuw, P. and Verboven, S. (2002) Robust estimation in very small samples. *Computational Statistics and Data Analysis* **40**(4), 741-758

Royston, J. (1982) Algorithm AS 177: Expected normal order statistics (exact and approximate). *Applied Statistics* **31**(2), 161-165.

Royston, P. (1991) Estimating departure from normality. *Statistics in Medicine* **10**(8), 1283-1293.

Royston, P. (1992) Approximating the Shapiro-Wilk W-test for non-normality. *Statistics and Computing* **2**(3), 117-119.

Royston, P. (1993a) A toolkit for testing for non-normality in complete and censored samples. *The Statistician* **42**(1), 37-43.

Royston, P. (1993b) A pocket-calculator algorithm for the Shapiro-Francia test for non-normality: an application to Medicine. *Statistics in Medicine* **12**(2), 181-184.

Royston, P. (1995) Remark AS R94: A remark on Algorithm AS 181: The W test for normality. *Applied Statistics* **44**(4), 547-551.

Ruiz-Garcia, J. and Miranda, E. (2010) Probabilistic estimation of residual drift demands for seismic assessment of multi-story framed buildings. *Engineering Structures* **32**(1), 11-20.

S

Sasani, M. and Der Kiureghian, A. (2001) Seismic fragility of RC structural walls: displacement approach. *Journal of Structural Engineering* **127**(2), 219-228.

Sawilowsky, S. (2002) A measure of relative efficiency for location of a single sample. *Journal of Modern Applied Statistical Methods* **1**(1), 52-60.

Scherer, W., Pomroy, T. and Fuller, D. (2003) The triangular density to approximate the normal density: decision rules-of-thumb. *Reliability Engineering and System Safety* **82**(3), 331-341.

Schoder, V., Himmelmann, A. and Wilhelm, K. (2006) Preliminary testing for normality: some statistical aspects of a common concept. *Clinical and Experimental Dermatology* **31**(6), 757-761.

Schotanus, M., Franchin, P., Lupoi, A. and Pinto, P.E. (2004) Seismic fragility analysis of 3D structures. *Structural Safety* **26**(4), 421-441.

Schueremans, L. (2001) Probabilistic evaluation of structural unreinforced masonry. *PhD Thesis*, Katholieke Universiteit Leuven, Leuven, Belgium.

Seier, E. (2002) Comparison of tests for univariate normality. *Interstat* **January**. Available at http://interstat.statjournals.net/YEAR/2002/articles/0201001.pdf.

Sen, P. (2002) Shapiro–Wilk-type goodness-of-fit tests for normality: asymptotics revisited. In *Goodness-of-fit Tests and Model Validity*, Huber-Carol, C., Balakrishnan, N., Nikulin, M. and Mesbah, M. (editors). Birkhäuser, Boston, USA.

Shapiro, S. and Francia, R. (1972) An approximate analysis of variance test for normality. *Journal of the American Statistical Association* **67**(337), 215-216.

Shapiro, S. and Wilk, M. (1965) An analysis of variance test for normality (complete samples). *Biometrika* **52**(3/4), 591-611.

Shapiro, S., Wilk, M. and Chen, H. (1968) A comparative study of various tests for normality. *Journal of the American Statistical Association* **63**(324), 1343-1372.

Shen, H. (2003) Nonparametric regression for problems involving lognormal distributions. *PhD Thesis*, University of Pennsylvania, Pennsylvania, USA.

Scherer, W., Pomroy, T. and Fuller, D. (2003) The triangular density to approximate the normal density: decision rules-of-thumb. *Reliability Engineering and System Safety* **82**(3), 331-341.

Shinozuka, M., Feng, M., Lee, J. and Naganuma, T. (2000) Statistical analysis of fragility curves. *Journal of Engineering Mechanics* **126**(12), 1224-1231.

Shome, N. and Cornell, C.A. (1999) Probabilistic seismic demand analysis of nonlinear structures. Report RMS-35, Reliability of Marine Structures Program. Stanford University. Stanford, California, USA.

Shome, N., Cornell, C.A., Bazzurro, P. and Carballo, I. (1998) Earthquakes, records and nonlinear responses. *Earthquake Spectra* **14**(3), 469-500.

Singh, A., Singh, A. and Engelhardt, M. (1997) The lognormal distribution in environmental applications. EPA/600/S-97/006. Environmental Protection Agency, Washington D.C., USA.

Singhal, A. and Kiremidjian, A. (1998) Bayesian updating of fragilities with application to RC frames. *Journal of Structural Engineering* **124**(8), 922-929.

Skokan, M. and Hart, G. (2008) Reliability-based performance-based design: learning from Allin Cornell. *The Structural Design of Tall and Special Buildings* **17**(6), 1031-1050.

Song, J. and Ellingwood, B. (1999) Seismic reliability of special moment steel frames with welded connections. *Journal of Structural Engineering* **125**(4), 357-371.

Song, J., Kang, W-H., Kim, K. and Jung, S. (2010) Probabilistic shear strength models for reinforced concrete beams without shear reinforcement. *Structural Engineering and Mechanics* **34**(1), 15-38.

Sousa, M. and Oliveira, C. (1996) Hazard mapping based on macroseismic data considering the influence of geological conditions. *Natural Hazards* **14**(2), 207-225.

Spence, R. and So, E. (2009) Estimating shaking-induced casualties and building damage for global earthquake events. Technical Report. NEHRP Grant number 08HQGR0102.

Sposito, V. (1990) Some properties of Lp-estimators. In *Robust Regression. Analysis and Applications*, Lawrence, K. and Arthur, J. (editors). Marcel Dekker, New York, USA.

Staudte, R. and Sheather, S. (1990) *Robust Estimation and Testing*. John Wiley & Sons, New York, USA.

Stephens, M. (1974) EDF statistics for goodness of fit and some comparisons. *Journal of the American Statistical Association* **69**(347), 730-737.

Stephenson, F. (2003) Harold Jeffreys Lecture 2002: Historical eclipses and Earth's rotation. *Astronomy & Geophysics* **44**(2), 22-27.

Stewart M. (1995) Workmanship and its influence on probabilistic models of concrete compressive strength. *ACI Materials Journal* **92**(4), 361-372.

Stewart, J., Chiou, S., Bray, J., Graves, R., Somerville, P. and Abrahamson, N. (2001) Ground motion evaluation procedures for performance-based design. PEER Report 2001/09. Pacific Earthquake Engineering Research Center, Berkeley, California, USA.

Stigler, S. (1977) Do robust estimators work with real data? *The Annals of Statistics* **5**(6), 1055-1098 — with discussion.

Sürücü, B. and Koç, E. (2007) Assessing the validity of a statistical distribution: some illustrative examples from dermatological research. *Clinical and Experimental Dermatology* **33**(3), 239-242.

T

Taghavi-Ardakan, S. (2006) Probabilistic seismic assessment of floor acceleration demands in multi-story buildings. *PhD Thesis*, Stanford University, Stanford, California, USA.

Tanner, J. and Carboni, A. (2011) Performance of Masonry Buildings in the 2010 Chile (Maule) Earthquake. *Proceedings of the 11th North American Masonry Conference.* Minneapolis, Minnesota, California, USA.

Thadewald, T. and Büning, H. (2007) Jarque-Bera test and its competitors for testing normality - a power comparison. *Journal of Applied Statistics* **34**(1), 87-105.

Thode, H. (2002) *Testing for Normality*. Marcel Dekker, Inc., New York, USA.

Thoft-Christensen, P. and Murotsu, Y. (1986) *Application of Structural Systems Reliability Theory*. Springer Verlag, Berlin, Germany.

Tiku, M. and Sürücü, B. (2009) MMLEs are as good as M-estimators or better. *Statistics and Probability Letters* **79**(7), 984-989.

Tothong, P. and Luco, N. (2007) Probabilistic seismic demand analysis using advanced ground motion intensity measures. *Earthquake Engineering and Structural Dynamics* **36**(13), 1837-1860.

Tsong, Y., Zhang, J. and Levenson, M. (2007) Choice of δ noninferiority margin and dependency of the noninferiority trials. *Journal of Biopharmaceutical Statistics* **17**(2), 279-288.

Tumidajski, P., Fiore, L., Khodabocus, T., Lachemi, M. and Pari, R. (2006) Comparison of Weibull and Normal distributions for concrete compressive strengths. *Canadian Journal of Civil Engineering* **33**(10), 1287-1292.

U

Ulrych, T., Velis, D., Woodbury, A. and Sacchi, M. (2000) L-moments and C-moments. *Stochastic Environmental Research and Risk Assessment* **14**(1), 50-68.

Urzúa, C. (1996) On the correct use of omnibus tests for normality. *Economics Letters* **53**(3), 247-251.

USGS (2009) FAQs - Measuring Earthquakes. United States Geological Survey, United States Department of the Interior, USA. http://earthquake.usgs.gov/learn/faq/?faqID=33 (Accessed December 2011).

V

Vallander, S. (1974) Calculation of the Wasserstein distance between probability distributions on the line. *Theory of Probability and its Applications* **18**(4), 784-786.

Vamvatsikos, D. and Cornell, C.A. (2002) Incremental dynamic analysis. *Earthquake Engineering Structural Dynamics* **31**(3), 491-514.

van der Vaart, A. (1998) *Asymptotic Statistics*. Cambridge University Press, Cambridge, England, UK.

Vännman, K. and Albing, M. (2007) Process capability indices for one-sided specification intervals and skewed distributions. *Quality and Reliability Engineering International* **23**(6), 755-765.

Varum, H. (1997) Numerical model for the seismic analysis of reinforced concrete plane frames. *MSc Thesis*, Faculty of Engineering of the University of Porto, Porto, Portugal (in Portuguese).

Veneziano D., Casciati F. and Faravelli L. (1983) Method of seismic fragility for complicated systems. *Proceedings of the 2nd Specialist Meeting on Probabilistic Methods in Seismic Risk Assessment for NPP*. Committee on Safety of Nuclear Installations (CSNI), Livermore, California, USA.

Verrill, S. and Johnson, R. (1988) Tables and large-sample distribution theory for censored-data correlation statistics for testing normality. *Journal of the American Statistical Association* **83**(404), 1192-1197.

Vrouwenvelder, T. and Scholten, N. (2010) Assessment criteria for existing structures. *Structural Engineering International* **20**(1), 62-65.

W

Wang, Q., Shi, Q. and Men, J. (2011) Seismic performance evaluation of SRC frames based on incremental dynamic analysis. *Advanced Materials Research* **163-167**, 4331-4335.

Warsza, Z. and Korczynski, M. (2010) Shifted up cosine function as unconventional model of probability distribution. *Journal of Automation, Mobile Robotics & Intelligent Systems* **4**(1), 49-55.

Watson-Lamprey, J. and Abrahamson, N. (2006) Selection of ground motion time series and limits on scaling. *Soil Dynamics and Earthquake Engineering* **26**(5), 477-482.

Wilcox, R. (2005) *Introduction to Robust Estimation and Hypothesis Testing, 2nd Ed.* Academic Press, San Diego, California, USA.

Wilde, J. (2008) A simple representation of the Bera–Jarque–Lee test for probit models. *Economics Letters* **101**(2), 119-121.

Wísniewski, D. (2007) Safety formats for the assessment of concrete bridges: with special focus on precast concrete. *PhD Thesis*, University of Minho, Portugal.

Wolfram|Alpha (2011) Wolfram Alpha LLC.
http://www.wolframalpha.com/input/?i=integrate+exp%28-%28%28%28ln%28x%29-a%29%2Fb%29^2%29%2F2%29 (Accessed September 2011).

Wong, W., Chiew, S. and Ho, N. (1993) Evaluation of in-situ test data from existing concrete structures. In *Proceedings of the symposium concrete 2000 – economic and durable construction through excellence, vol. 2*, Dhir, R. and Jones, M. (editors). Spon Press, London, England, UK.

Wu, J. and Lindell, M. (2004) Housing reconstruction after two major earthquakes: the 1994 Northridge earthquake in the United States and the 1999 Chi-Chi earthquake in Taiwan. *Disasters* **28**(1), 63-81.

X

Xie, M., Yang, Z. and Gaudoin, O. (2000) More on the mis-specification of the shape parameter with Weibull-to-exponential transformation. *Quality and Reliability Engineering International* **16**(4), 281-290.

Xue, Q., Wua, C.-W., Chena, C.-C. and Chena, K.-C. (2008) The draft code for performance-based seismic design of buildings in Taiwan. *Engineering Structures* **30**(6), 1535-1547.

Y

Yang, Z., Xie, M. and Wong, A. (2007) A unified confidence interval for reliability-related quantities of two-parameter Weibull distribution. *Journal of Statistical Computation and Simulation* **77**(5), 365-378.

Yazici, B. and Yolacan, S. (2007) A comparison of various tests of normality. *Journal of Statistical Computation and Simulation* **77**(2), 175-183.

Yohai, V. and Zamar, R. (1988) High breakdown-point estimates of regression by means of the minimization of an efficient scale. *Journal of the American Statistical Association* **83**(402), 406-413.

Z

Zareian, F. and Krawinkler, H. (2007) Assessment of probability of collapse and design for collapse safety. *Earthquake Engineering and Structural Dynamics* **36**(13), 1901-1914.

Zhang, J. and Wu, Y. (2005) Likelihood-ratio tests for normality. *Computational Statistics and Data Analysis* **49**(3), 709-721.

Zhang, P. (1999) Omnibus test of normality using the Q statistic. *Journal of Applied Statistics* **26**(4), 519-528.

Zhou, X.-H. and Gao, S. (1997) Confidence intervals for the log-normal mean. *Statistics in Medicine* **16**(7), 783-790.

Zou, G., Huo C. and Taleban, J. (2009) Simple confidence intervals for lognormal means and their differences with environmental applications. *Environmetrics* **20**(2), 172-180.

This thesis was written using Monotype Garamond fonts, a digital version of the typefaces created by the French printer Jean Jannon in 1621, which, until 1926, were believed to be the work of the 16th century master punchcutter Claude Garamond.